ISSN 0021-9673

VOL. 627 NOS. 1 + 2 DECEMBER 25, 1992

COMPLETE IN ONE ISSUE

JOURNAL OF CHROMATOGRAPHY

INCLUDING ELECTROPHORESIS AND OTHER SEPARATION METHODS

ELSEVIER

JOURNAL OF CHROMATOGRAPHY

INCLUDING ELECTROPHORESIS AND OTHER SEPARATION METHODS

Scope. The *Journal of Chromatography* publishes papers on all aspects of **chromatography, electrophoresis** and related methods. Contributions consist mainly of research papers dealing with chromatographic theory, instrumental developments and their applications. The section *Biomedical Applications*, which is under separate editorship, deals with the following aspects: developments in and applications of chromatographic and electrophoretic techniques related to clinical diagnosis or alterations during medical treatment; screening and profiling of body fluids or tissues related to the analysis of active substances and to metabolic disorders; drug level monitoring and pharmacokinetic studies; clinical toxicology; forensic medicine; veterinary medicine; occupational medicine; results from basic medical research with direct consequences in clinical practice. In *Symposium volumes*, which are under separate editorship, proceedings of symposia on chromatography, electrophoresis and related methods are published.

Submission of Papers. The preferred medium of submission is on disk with accompanying manuscript (see *Electronic manuscripts* in the Instructions to Authors, which can be obtained from the publisher, Elsevier Science Publishers B.V., P.O. Box 330, 1000 AH Amsterdam, Netherlands). Manuscripts (in English; *four* copies are required) should be submitted to: Editorial Office of *Journal of Chromatography*, P.O. Box 681, 1000 AR Amsterdam, Netherlands, Telefax (+31-20) 5862 304, or to: The Editor of *Journal of Chromatography, Biomedical Applications*, P.O. Box 681, 1000 AR Amsterdam, Netherlands. Review articles are invited or proposed in writing to the Editors who welcome suggestions for subjects. An outline of the proposed review should first be forwarded to the Editors for preliminary discussion prior to preparation. Submission of an article is understood to imply that the article is original and unpublished and is not being considered for publication elsewhere. For copyright regulations, see below.

Publication. The *Journal of Chromatography* (incl. *Biomedical Applications*) has 40 volumes in 1993. The subscription prices for 1993 are:

J. Chromatogr. (incl. *Cum. Indexes, Vols. 601–650*) + *Biomed. Appl.* (Vols. 612–651):
Dfl. 8520.00 plus Dfl. 1320.00 (p.p.h.) (total *ca.* US$ 5927.75)

J. Chromatogr. (incl. *Cum. Indexes, Vols. 601–650*) only (Vols. 623–651):
Dfl. 7047.00 plus Dfl. 957.00 (p.p.h.) (total *ca.* US$ 4821.75)

Biomed. Appl. only (Vols. 612–622):
Dfl. 2783.00 plus Dfl. 363.00 (p.p.h.) (total *ca.* US$ 1895.25).

Subscription Orders. The Dutch guilder price is definitive. The US$ price is subject to exchange-rate fluctuations and is given as a guide. Subscriptions are accepted on a prepaid basis only, unless different terms have been previously agreed upon. Subscriptions orders can be entered only by calender year (Jan.–Dec.) and should be sent to Elsevier Science Publishers, Journal Department, P.O. Box 211, 1000 AE Amsterdam, Netherlands, Tel. (+31-20) 5803 642, Telefax (+31-20) 5803 598, or to your usual subscription agent. Postage and handling charges include surface delivery except to the following countries where air delivery via SAL (Surface Air Lift) mail is ensured: Argentina, Australia, Brazil, Canada, China, Hong Kong, India, Israel, Japan*, Malaysia, Mexico, New Zealand, Pakistan, Singapore, South Africa, South Korea, Taiwan, Thailand, USA. *For Japan air delivery (SAL) requires 25% additional charge of the normal postage and handling charge. For all other countries airmail rates are available upon request. Claims for missing issues must be made within three months of our publication (mailing) date, otherwise such claims cannot be honoured free of charge. Back volumes of the *Journal of Chromatography* (Vols. 1–611) are available at Dfl. 230.00 (plus postage). Customers in the USA and Canada wishing information on this and other Elsevier journals, please contact Journal Information Center, Elsevier Science Publishing Co. Inc., 655 Avenue of the Americas, New York, NY 10010, USA, Tel. (+1-212) 633 3750, Telefax (+1-212) 633 3764.

Abstracts/Contents Lists published in Analytical Abstracts, Biochemical Abstracts, Biological Abstracts, Chemical Abstracts, Chemical Titles, Chromatography Abstracts, Clinical Chemistry Lookout, Current Awareness in Biological Sciences (CABS), Current Contents/Life Sciences, Current Contents/Physical, Chemical & Earth Sciences, Deep-Sea Research/Part B: Oceanographic Literature Review, Excerpta Medica, Index Medicus, Mass Spectrometry Bulletin, PASCAL-CNRS, Pharmaceutical Abstracts, Referativnyi Zhurnal, Research Alert, Science Citation Index and Trends in Biotechnology.

US Mailing Notice. *Journal of Chromatography* (ISSN 0021-9673) is published weekly (total 58 issues) by Elsevier Science Publishers (Sara Burgerhartstraat 25, P.O. Box 211, 1000 AE Amsterdam, Netherlands). Annual subscription price in the USA US$ 5927.75 (subject to change), including air speed delivery. Application to mail at second class postage rate is pending at Jamaica, NY 11431. **USA POSTMASTERS**: Send address changes to *Journal of Chromatography*, Publications Expediting, Inc., 200 Meacham Avenue, Elmont, NY 11003. Airfreight and mailing in the USA by Publication Expediting.

See inside back cover for Publication Schedule, Information for Authors and information on Advertisements.

0021-9673/92/$05.00

This issue is printed on acid-free paper.

Printed in the Netherlands

VOL. 627, NOS. 1+2 JOURNAL OF CHROMATOGRAPHY DECEMBER 25, 1992

CONTENTS

(Abstracts/Contents Lists published in Analytical Abstracts, Biochemical Abstracts, Biological Abstracts, Chemical Abstracts, Chemical Titles, Chromatography Abstracts, Current Awareness in Biological Sciences (CABS), Current Contents/Life Sciences, Current Contents/Physical, Chemical & Earth Sciences, Deep-Sea Research/Part B: Oceanographic Literature Review, Excerpta Medica, Index Medicus, Mass Spectrometry Bulletin, PASCAL-CNRS, Referativnyi Zhurnal, Research Alert and Science Citation Index)

(Continued overleaf)

Contents (continued)

JOURNAL OF CHROMATOGRAPHY

VOL. 627 (1992)

JOURNAL of CHROMATOGRAPHY

INCLUDING ELECTROPHORESIS AND OTHER SEPARATION METHODS

ELSEVIER

AMSTERDAM — LONDON — NEW YORK — TOKYO

0021-9673/92/$05.00

Printed in the Netherlands

Journal of Chromatography, 627 (1992) 1–16
Elsevier Science Publishers B.V., Amsterdam

CHROM. 24 553

Review

O-(2,3,4,5,6-Pentafluorophenyl)methylhydroxylamine hydrochloride: a versatile reagent for the determination of carbonyl-containing compounds

Devon A. Cancilla

Department of Chemistry, University of Western Ontario, London, Ontario N6A 5B7 (Canada)

Shane S. Que Hee

Department of Environmental Health Sciences, UCLA School of Public Health, 10833 Le Conte Avenue, Los Angeles, CA 90024-1772 (USA)

(First received June 11th, 1992; revised manuscript received August 10th, 1992)

ABSTRACT

A review on the use of O-(2,3,4,5,6-pentafluorophenyl)methylhydroxylamine hydrochloride (PFBHA) for the determination of carbonyl-containing compounds is presented. PFBHA has been used in the determination of such diverse compounds as thromboxane B_2, prostaglandins, amygdalin and a variety of other aldehydes, ketones and acids. PFBHA has been used for the determination of these compounds found in water, blood, urine, air and even clothing. The review covers literature referenced in *Chemical Abstracts* from 1975, when PFBHA was first synthesized, through March 1992.

CONTENTS

Correspondence to: D. A. Cancilla, National Laboratory for Environmental Testing, Canada Centre for Inland Waters, 867 Lakeshore Road, Box 5050, Burlington, Ontario L7R 4A6, Canada (present address).

0021-9673/92/$05.00

1. INTRODUCTION

O-Substituted derivatives of hydroxylamine are useful reagents for the determination of carbonyl-containing compounds. Of particular importance is the fluorine-containing O-substituted hydroxylamine O-(2,3,4,5,6-pentafluorophenyl)methylhydroxylamine hydrochloride (Fig. 1). This compound has appeared in the literature by the name of O-(2,3,4,5,6-pentafluorobenzyl)hydroxylamine hydrochloride or pentafluorobenzyloxylamine and has been abbreviated as PFBHA, PFBOA and PFBHOX. PFBHA (CAS Registry No. 57981-02-9), as it is referred to in this review, has been used as a derivatizing agent in a wide variety of biomedical and environmental investigations.

PFBHA, like hydroxylamine, reacts with carbonyl functional groups to produce the corresponding oximes (Fig. 2). Oxime formation is pH dependent and proceeds readily in both aqueous and organic solutions. The oximes are easily extracted into organic solvents, with unreacted PFBHA being removed through acidic washings. The oximes can be separated by gas chromatography (GC) and analyzed with a variety of detectors. Electron-capture detection (ECD) is particularly sensitive for the determination of these pentafluoro oxime derivatives.

PFBHA has been used in the determination of such diverse compounds as thromboxane B2, prostaglandins, amygdalin and formaldehyde. It has also been used in the determination of aldehydes, ketones and acids found in water, blood, urine, air and even clothing. This review will discuss the methodologies for the use of PFBHA in the determination of a variety of compounds using gas chromatography–mass spectrometry (GC–MS), GC-flame ionization detection (FID) or GC–ECD. This review covers literature referenced in *Chemical Abstracts* from 1975, when PFBHA was first synthesized, through March 1992.

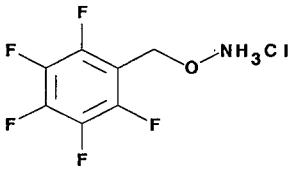

Fig. 1. O-(2,3,4,5,6-Pentafluorophenyl)methylhydroxylamine hydrochloride (PFBHA).

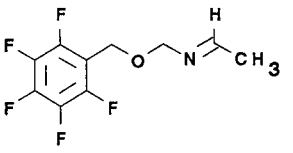

I

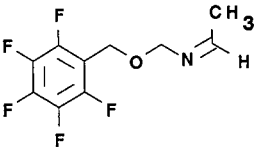

II

Fig. 2. (I) *E* and (II) *Z* geometrical isomers of acetaldehyde O-[(pentafluorophenyl)methyl] oxime.

2. NOMENCLATURE OF PFBHA DERIVATIVES OF CARBONYL-CONTAINING COMPOUNDS

As Fig. 2 indicates, the presence of three different groups around the carbon-nitrogen double bond produces geometrical isomers. The *E*/*Z* method of nomenclature will be used to describe specific geometrical isomers. In this system, functional groups about the double bond are prioritized [1], with the *Z* isomer containing the highest priority groups on the same side of the double bond. The *E* isomer contains the two highest priority groups on opposite sides of the double bond.

3. SYNTHESIS AND INITIAL USE OF PFBHA

The synthesis and use of PFBHA was first described in a series of papers by three groups of researchers in 1975 and early 1976. In the first paper, Koshy *et al.* [2] at Upjohn used PFBHA to form monooximes of 3,17- and 20-keto steroids and dioximes of 3,17- and 3,20-diketo steroids. Although their experimental section indicated that PFBHA was synthesized at the Upjohn Research Laboratories and acknowledged Dr. G. A. Youngdale for the synthesis, the actual synthetic method was not described. In 1975, Nambara *et al.* [3] also described both the synthesis and use of PFBHA for the analysis of 17-keto steroids.

Youngdale's synthetic method was published in

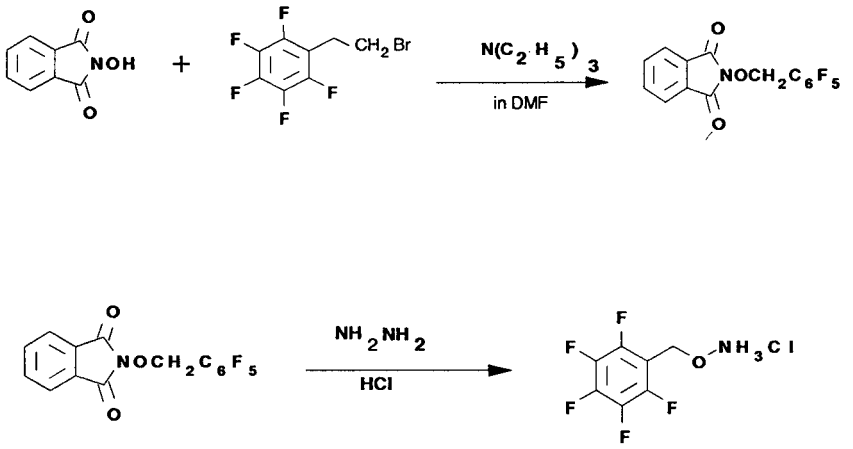

Fig. 3. Youngdale's [4] synthetic method for PFBHA.

1976 [4], although it had been accepted for publication in early 1975. The method, described as a modification of methods developed by McKay *et al.* [5] for the synthesis of O-substituted oxyamines, is shown in Fig. 3. Except for a few differences, such as molar amounts used and choice of solvents, the method described by Nambara *et al.* is essentially the same. None of the investigators included spectroscopic data in support of the structure or purity of PFBHA or the oximes.

The general approach for the determination of steroids by both the Koshy and Nambara groups was to react the specific steroid in a solution of pyridine containing excess of PFBHA at elevated temperatures (60–65°C) for either 30 or 60 min. Time and temperature conditions or PFBHA and steroid concentrations were not optimized. The Koshy group removed the pyridine under nitrogen and redissolved the oxime in cyclohexane. This solution was then washed once with distilled water, dried with sodium sulfate and analyzed by GC–FID, GC–ECD or GC–MS. Further experiments were performed using thin-layer chromatography (TLC). The hydroxy functional groups were not derivatized. The method was used only for standards in pyridine and was not extended to detect steroids in biological matrices.

After initial oxime formation in the PFBHA pyridine solution, the Nambara group used 0.1 *M* HCl, 0.1 *M* NaOH and water washings followed by treatment with hexamethyldisilane and trimethylchlorosilane. Pyridine was removed and the samples redissolved in hexane for analysis by GC–ECD or GC–FID. Individual samples in pyridine were prepared in this manner. The method was then used to determine levels of dehydroepiandrosterone added to human plasma.

A number of interesting and significant conclusions were reached in these initial papers, perhaps the most important being the demonstration of the existence of geometrical isomers by the Koshy group. Using TLC and longer GC columns, both geometrical isomers of testosterone and 7α,17α-dimethyl-19-nortestosterone were isolated and detected after reaction with PFBHA. Except for this demonstration, however, the optimized analytical conditions necessary to separate any of the other possible steroid oxime *E*/*Z* isomers were not described. GC determination of the various steroid oxime derivatives used the unresolved isomers. As little as 5 pg of the unresolved testosterone oxime were detected with GC–ECD. Detected amounts of other steroids ranged from 50 to 200 pg, with detector response ranging from $1.54 \cdot 10^4$ C/mol for andosterone to $9.60 \cdot 10^4$ C/mol for progesterone.

Koshy *et al.* further demonstrated the stability of the oxime derivatives in milligram or microgram amounts by determining recovered amounts after solvent partitioning (GC–FID) and TLC separation (^{3}H-labeled scintillation spectrometry), again using testosterone and 7α,17α-dimethyl-19-nortestosterone. Recovery was quantitative for solvent

partitioning and was between 85 and 97% by TLC.

Nambara *et al.* focused primarily on the 17-keto steroids because the 11-keto steroids failed to react with PFBHA under the described experimental conditions. Through a series of spiking experiments, they found that 84.5% of the spiked dehydroepiandrosterone in human plasma could be recovered as the oxime. It was further suggested that PFBHA was added to biological material to remove ketones in these matrices.

These papers were important for demonstrating that PFBHA could be used for the determination of steroids through formation of their oximes. The oximes were found to be easily separated and detected by GC–ECD and were stable under a variety of analytical conditions. This early work had its limitations; none of the groups synthesized or characterized pure oximes to be used as analytical standards, optimized the reaction conditions, or measured steroid levels in actual biological samples. Nonetheless, these investigators presented an important new derivatizing agent and demonstrated that PFBHA had the potential to be an extremely useful analytical agent.

4. BIOLOGICAL APPLICATIONS OF PFBHA

4.1. Prostaglandins and thromboxanes

The need of researchers to detect submicrogram levels of prostaglandins and thromboxane B_2 in biological matrices soon provided another use for PFBHA. These methods are listed in Table 1. In 1977, Fitzpatrick *et al.* [6] demonstrated that PFBHA could be used to form the pentafluorobenzyl oxime (PFB oxime) of prostaglandins (PGs) and thromboxane B_2 (TX).

PG and TX were isolated from washed platelets and processed through a three-step derivatization which included methyl esterification and oxime formation. Samples were analyzed using either GC–ECD or GC–MS.

Although no analytical data were supplied, TX was reported to be recovered nearly quantitatively (90%) from washed platelets. The TX methyl ester PFB oxime was then formed and extracted quantitatively with two hexane washings. A number of PGs (PGA_2, PGB_2, PGE_2 and PGD_2) were resolved and were clearly separable from the geometrical isomers of TX, although those of PGs could

TABLE 1

SUMMARY OF PFBHA METHODS FOR THE DETERMINATION OF PROSTAGLANDINS AND THROMBOXANES

Compound type	Matrix type	Detection method	Chromatographic method	Ref.
Mono- and diketo steroids	Pyridine	ECD, FID, MS	Packed column GC, TLC	2
Mono- and diketo steroids	Pyridine, plasma	ECD, FID	Packed column GC	3
Prostaglandins, Thromboxane	Platelets	ECD, MS	Packed column GC	6
Prostaglandins, Thromboxane	Platelets	UV(254 nm), ECD	C_{18} liquid chromatography, packed column GC	7
Prostaglandins, Thromboxane	Cell preparations (Balb 3T3, Balb 3T12)	ECD	Capillary GC	8
Prostaglandins, Thromboxane	Mouse peritoneal macrophage cells	MS	Capillary GC	9,10
Prostaglandins	Blood	ECD	Capillary GC	11
Prostaglandins, Thromboxane	Semen, rat aorta, dog serum, trout gill	ECD	Capillary GC	12
Prostaglandins	Phosphate buffer, fetal calf serum, lung fibroblasts, plasma	ECD	Capillary GC	13
Prostaglandins	Pyridine	NCI-MS	Capillary GC	14

not be separated. Peak-height ratios of the *E*/*Z* isomers of TX varied by only ±5%, providing a rough qualitative assurance measure; any deviation beyond this was claimed to result from co-eluting and interfering peaks.

Derivatization reproducibility experiments for the TX methyl ester PFB oxime at the 50–375-ng level ranged from ±11 to ±42%. This poor reproducibility was attributed to both the labile nature of TX and to difficulties associated with carrying out three successive derivatizations on nanogram amounts of material.

In a subsequent paper, the Fitzpatrick group [7] expanded upon its earlier work by demonstrating that PGs and TX could be determined with liquid chromatographic (LC) separation using a 254-nm fixed-wavelength detector. Modifications in the derivatization procedure included formation of the PFB oximes of PG PFB esters and methyl esters. The oximes of the PFB esters were detected at between 60 ng (15-methyl-PGB_2) and 930 ng (PGE_2). The oximes of the methyl esters could not be adequately detected. In parallel experiments, the *p*-nitrobenzyl oximes of both the methyl and PFB esters were detected at significantly lower concentrations than the PFB oxime. LC separation of the PGs allowed resolution of geometrical isomers in some instances.

Derivatization reproducibility, as determined by GC–ECD, did not improve from that reported in earlier work for either the TX or PG derivatives [6]. The methyl ester PFB oximes were more sensitive to detection by GC–ECD than the PFB ester–PFB oximes of the prostaglandins. Detection limits were between 15 and 300 pg for the methyl ester PFB oximes and between 30 and 400 pg for the PFB ester–PFB oximes. The *E*/*Z* isomers of the methyl ester oximes were chromatographically separated.

Better separation of prostaglandins was achieved by Fitzpatrick *et al.* [8] through the use of glass capillary GC–ECD. Samples were methyl esterified as described earlier [7] and, after treatment with pyridine containing of excess PFBHA, were washed with water at pH 3.0. Prostaglandin and thromboxane methyl ester oximes were then converted into trimethysilyl ethers. A 1-μl volume of the final derivative was used for analysis by GC–ECD. The detector was equipped with a tee to supply a make-up gas flow, which was found to be optimum at about 15 ml/min [helium–argon (90:10)]. The detector response decreased logarithmically with increasing make-up flow-rate and a fixed column flow-rate (helium) of 22.5 ml/min. Derivative separation and detection equaled or exceeded that found for packed column GC–ECD. The methyl ester PFB oxime trimethysilyl ethers of PGD_2, PGE_2 TXB_2 and 6-keto-$PGF_{1\alpha}$ were not completely resolved, although the *E*/*Z* isomers of the oximes were distinguished. Using this method, 100 pg of PGH_2 were detected at a signal-to-noise ratio of 20:1. These methods were used to monitor metabolic profiles of PGH_2 in cell preparations.

Rosello and co-workers [9,10] demonstrated the use of capillary GC–MS for the determination of the major metabolites of the cyclooxygenase pathway of arachidonic acid from mouse peritoneal macrophage cells using methyl ester–PFB oxime–butylboronate–TMS derivatives of TXB_2 and 6-keto-$PGF_{1\alpha}$. This involved a four-step derivatization,

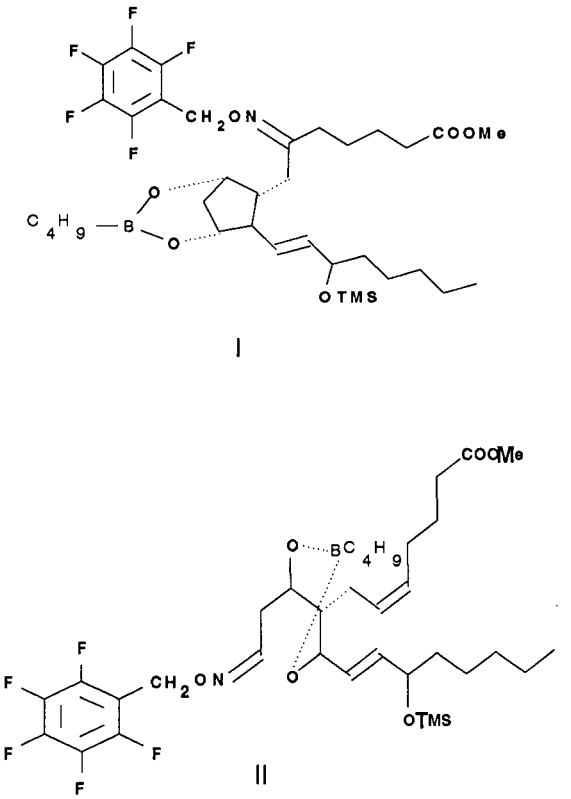

Fig. 4. PFBO–NBB–TMS–Me derivatives of (I) 6-keto-$PGF_{1\alpha}$ and (II) TXB_2.

beginning with esterification followed by oximation with PFBHA, boronation and silylation. Fig. 4 shows the resulting PFBO–NBB–TMS–Me derivatives of the 6-keto-$PGF_{1\alpha}$ and TXB_2. Samples were chromatographed using glass capillary columns.

The *E*/*Z* isomers were easily resolved, as were various PGs and TX mixtures. The PFB–NBB–TMS–Me derivatives generally showed better chromatographic separation than the PFB–TMS–Me derivatives. The *E*/*Z* isomers of 6-keto-$PGF_{1\alpha}$ co-eluted under these conditions, although they could be separated using less polar OV-1 or OV-101 stationary phases. A characteristic loss of M − 197 (attributed to loss of $C_6F_5CH_2O$) was noted in the mass spectra of the derivatives of 6-keto-$PGF_{1\alpha}$ and TXB_2.

In a lengthy procedure, Christ-Hazelhof and Nugteren [11] used the PFB derivative of 6-oxo-$PGF_{1\alpha}$, a hydrolysis product of prostacyclin, to determine prostacyclin (PGI_2) levels in blood.

Recoveries using this multi-step process were reported to be between 57 and 60%. No prostacyclin was detected in normal human venous peripheral whole blood or blood plasma or in samples taken during and after hyperventilation, indicating that prostacyclin is not a normally circulating hormone. Ten micrograms of sodium prostacyclinate in 2.5 ml of saline infused into one arm vein of a male volunteer for 5 min were detected in whole blood samples drawn from the other arm at 2, 3, 4, 5, 7, 9, and 11 min. Results from this experiment produced levels of 400 pg of prostacyclin per milliliter of whole blood. This showed the half life of infused prostacyclin to be between 2 and 4 min.

Optimized GC–ECD conditions for the analysis of PG and TX as their PFB–TMS derivatives were described by Mai *et al.* [12]. Using the method of Fitzpatrick *et al.* [7], PGs and TX were esterified, oximated and silylated. Samples were detected by ^{63}NiECD or GC–MS using selective ion monitoring (SIM) (no ions were specified). Glass columns were either 2.8 m × 0.32 cm I.D. or 4.7 m × 0.32 cm I.D. The suitabilities of ten separate stationary phases were tested, with 3% SE-30, 3% OV-1, 3% SP-2100 and 3% SP2100 providing the best general separations for PG pentafluorobenzyl derivatives. Capillary columns were necessary to achieve the best separations.

Column temperatures were optimized using a 2.8 m × 0.32 cm I.D. 3% OV-101 glass column and the PGE_2–PFBO–PFBE–TMS derivative. Optimum chromatographic resolution was achieved by holding the column at 270°C for 10 min, then programming to 285°C at 5°C/min. It appears that no effort was made to optimize the injector temperature, which was reported as 270°C. The detector response was found to increase with increasing detector temperature, with the highest sensitivity achieved at 350°C. Argon–methane (90:10) carrier gas at a flow-rate of 16 ml/min offered the best detector response. As a general rule, decreases in response were observed with increasing flow-rates, and poor separations were achieved at low flow-rates. Plotting ECD response against the amounts of PG used for derivatization provided calibration graphs which showed the same overall trends as those observed by Fitzpatrick *et al.* [8] using glass capillary column GC–ECD. Relative response factors on two separate columns of fourteen PGs using 1a,1b-dibromo-$PGF_{1\alpha}$ as internal standard are reported. The ratios of the *E*/*Z* isomers of the nine PFB oxime PFB ester TMS ether derivatives were reported as the ratio of the peak area of the first peak to the second peak. No attempt was made to assign configurations to specific peaks or to observe the effects of various operating conditions on the ratios.

Rosenfeld *et al.* [13] demonstrated a method for the solid-phase sample preparation for PGs using PFBHA as an oximation agent. XAD-2, a styrene–divinylbenzene cross-linked polymeric macroreticular resin, was used as the sorbent for PGE_2 from various biological samples (phosphate buffer, biological incubate–10% fetal calf serum and human lung fibroblasts and human plasma).

TLC using silica gel plates and a toluene–ethyl acetate–methanol (55:45:2.5, v/v/v) of ^{14}C-labeled and authentic PGE_2 derivatives was used to obtain reaction yields. The yields were calculated to be 73 ± 4% (buffer) and 54 ± 9% (plasma). Total radiolabel recovery was 85% from all matrices. Incomplete reaction products such as oximation, esterification or unreacted PGE_2 accounted for the remaining detected products and were attributed to matrix affects. It was questioned whether proteins containing sulfhydryl groups caused the lowered recovery. Reaction of PGE_2 in an aqueous solution containing physiological concentrations of added

serum albumin gave recoveries (63 ± 5%) similar to those for buffered solutions, however, indicating other causes. The *E*/*Z* isomers could be separated using TLC and GC. The *Z* isomer was assigned to the minor GC peak, although no supporting spectral evidence was provided to confirm this assignment. Linear calibration graphs from 25 to 250 ng/ml were obtained using a 1–2-μl volume of the derivatized sample with GC–ECD and on-column injection.

In summary, a significant amount of research has been focused on the isolation and detection of PGs and TXs from biological matrices using PFBHA. Usually, multi-step derivatizations are required to prepare these compounds for analysis. PFBHA has been used for reaction of the carbonyl functional groups of these compounds to form the resulting oxime. Generally, *E*/*Z* isomers of these compounds are formed and can be separated by TLC, HPLC and GC. Recovery and reproducibility from the multi-step derivatizations varied in the different studies, ranging from 63% to 90%. The detection limits were reported to be in the range 25–50 ng and the derivatization reproducibility was 42%.

GC–ECD has been shown to be the most sensitive method for the determination of the PFB oxime derivatives. SIM-MS can approach the sensitivity of ECD, although a significant amount of work remains to be done on determination of the actual detection limits. The addition of two electron-capturing groups, the PFB oxime and the PFB ester, did not lower detection limits. Generally, these double derivatives had limits of detection much poorer than those for the single derivatives. This trend was also observed in a study by Waddell *et al.* [14] using GC–negative-ion chemical ionization mass spectrometry (GC–NICI-MS). The fragmentation patterns of various PFB oxime derivatives of 6-oxo-$PGF_{1\alpha}$ were studied using methane as the reagent gas, an ionizer temperature of 200°C and an ion source pressure of 27 Pa. Two fragment ions, of *m*/*z* 178 $[C_7F_4H_2O]^-$ and *m*/*z* 196 $[C_7F_5HO]^-$, were found to carry most of the total ion current for the PFB oxime, methyl ester, tris-TMS derivative of 6-oxo-$PGF_{1\alpha}$. The limit of detection for the *m*/*z* 686 ion $[M-C_3H_{10}SiOF]^-$ was reported to be 800 pg on-column.

4.2. Determination of other metabolic products and drugs

PFBHA has been successfully used for the determination of a number of drugs and metabolic products in plasma, urine, feces and tissue (Table 2). Park *et al.* [15] detected arildone (Fig. 5), an anti-

TABLE 2

SUMMARY OF PFBHA METHODS FOR THE DETERMINATION OF METABOLIC PRODUCTS AND DRUGS

Compound type	Matrix type	Detection method	Chromatographic method	Ref.
Arildone	Urine, plasma	ECD	Capillary GC	15
Geranylgeranylacetone	Serum	MS	Packed column GC	16
Acetone, Acetoacetic acid	Urine	FID	Packed column GC	17
4-Hydroxynonenal	Rat heart, liver, adrenal, testis	NCI-MS	Capillary GC	18
Monosaccharides	Pyridine	FID, MS	Packed column GC	19
Aldehydes, ketones, oxo acids	Water, urine, plasma, amniotic fluid	FID, MS	Capillary GC	20
Acetaldehyde	Blood	ECD	Packed column GC	21
Aldehydes, ketones, oxo acids	Urine, plasma, amniotic fluid	MS	Capillary GC	22
Aldehydes, ketones, oxo acids	Urine, plasma, amniotic fluid	MS	Capillary GC	23
trans-4-Hydroxy-2-nonenal (HNE)	Platelets, monocytes, plasma, oxidized low-density lipoprotein	NCI-MS	Capillary GC	24
2,5-hexanedione	Urine, serum	FID, ECD	Capillary GC	25
Indole-3-pyruvate	Tomato shoots	ECD, MS	Capillary GC	26

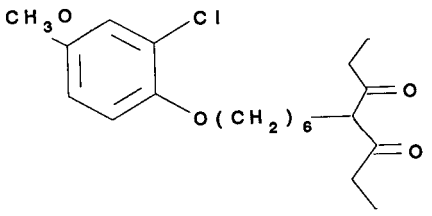

Fig. 5. Arildone, 4-[6-(2-chloro-4-methoxyphenoxy)hexyl]-3,5-heptanedione).

viral agent, in urine and plasma using packed column GC–ECD. Linear dynamic ranges of 10–120 ng/ml for plasma and 2.5–20 ng/ml in urine were achieved. The minimum quantifiable level of the oxime derivative of arildone was 1.4 ± 0.2 ng/ml in urine and 6.4 ± 0.1 ng/ml in plasma. The precision was 5.5% in urine and 6.4% in plasma.

A number of problems were reported in the derivatization of arildone, a diketone. Generally, mixed *E*/*Z* isomers could not be resolved using the short packed column and all quantification was done on the co-eluting isomer peaks. Further, the column required conditioning by injection of high concentrations of derivatives prior to injection of samples.

The anti-ulcer drug geranylgeranylacetone (GGA) [16] was determined in human serum using GC–MS. Generally, 1 ml of serum was used and a multi-step clean-up was required before oxime derivatization could be undertaken.

GC–MS of the derivatives showed four peaks attributed to the formation of *E*/*Z* isomers from each of the *cis*/*trans* isomers (*cis*/*trans* about internal double bonds) of GGA. Although no other spectral evidence was provided, the *E* isomer of the *cis*-GGA starting isomer was assigned by its spectrum showing the more intense *m*/*z* 320 ion (eight times that in the spectrum for the *Z* isomer). The formation ratio of isomers was almost constant, which provided an opportunity to use SIM for quantification of the *m*/*z* 320 ion of the *E* isomer. The linear dynamic range was 1–1000 ng/ml, with a variation of less than 5%. Experiments with different concentrations of PFBHA showed that the optimum formation of the GGA oxime was achieved using 5 mg of PFBHA per 0.2 ml pyridine.

Kobayashi *et al.* [17] demonstrated a GC method for the determination of acetone and acetoacetic acid in urine. It was reported that acetoacetic acid underwent rapid decomposition in acidic media to yield acetone. Linear calibration graphs in the range 17–862 μmol/l for acetone and 20–980 μmol/l for acetoacetic acid were obtained for urine samples spiked with the analytes and diluted ten-fold. Reproducibilities for identical sample solutions containing 345 μmol/l of acetone and 490 μmol/l of acetoacetic acid were 1.7% and 2.0% (n = 5), respectively. The absolute sensitivity for acetone was 3.45 μmol/l for acetone and 10 μmol/l for acetoacetic acid.

4-Hydroxynonenal was detected at the 10–100-pg level from the heart, liver, adrenal and testis of rats using NCI-MS [18]. The reaction was carried out in the presence of a buffer (pH 7.0); no evidence was provided, however, to demonstrate that this was the optimum pH under which oximes could be formed and extracted. Samples were analyzed using GC–NICI-MS. Ammonia was the reagent gas and NICI mass spectra were obtained by SIM using the ion of *m*/*z* 152. A comparison between isomer intensity ratios of oximes extracted from rat livers and those from authentic standards showed that the two were equivalent. NICI-SIM-MS was between 20 and 100 times more sensitive than electron impact (EI)-MS; the most abundant ion in this method was *m*/*z* 200.

The optimum conditions necessary for the determination of the PFB oxime–acetyl ester derivatives of neutral monosaccharides were studied by Biondi *et al.* [19]. Conditions of solvent type, reaction time and temperature were examined, but other factors, such as pH, extraction number, PFBHA concentration and chromatographic conditions, were not investigated. Reaction of PFBHA in pyridine for 20 min at 80°C was found to provide the optimum conditions for oxime formation. Incomplete derivatization occurred when other solvent combinations were used, as demonstrated by the appearance of extra peaks in the chromatograms. No information was provided on experiments to optimize the chromatographic conditions, although the optimized conditions were described (180°C for 4 min, then increased at 5°C/min to 240°C and held for 10 min, injector temperature 270°C and detector temperature 240°C).

Recovery studies were performed using milligram amounts of glucose to form the Ac–PFB–Gl derivative. Excess of PFBHA was removed by passing the reaction mixture through a Bond Elut SCX sul-

phonated silica column which was reported to retain PFBHA selectively. The MS of the O-PFB oxime acetates of frucose, arabinose, xylose, glucose, galactose and mannose were provided. Common to all spectra was the base peak at m/z 181, which was attributed to the $C_7H_2F_5$ ion. Recoveries were reported to be between 87 and 95% for the 10-nmol range and between 94 and 98% for the 100-nmol range. No decrease in peak heights was observed for derivatives stored at room temperature for 2 days.

Hoffmann and Sweetman [20] reported on the oxime–TMS ester derivatives of approximately twenty physiologically important aldehydes, ketones and oxo acids. Aqueous samples were used for initial method development, which was then generalized for use with urine, plasma and amniotic fluid.

Silicic acid column clean-up of samples to remove unreacted PFBHA and unwanted artifacts was described as an important step in the reaction procedure. It was reported that PFBHA reacted with silylating reagents to produce corresponding PFB–TMS derivatives as byproducts which could be chromatographed. This could be an obvious source of problems if chromatographic retention times overlapped with the analytes of interest. The E/Z isomers of many of the analytes were observed as double chromatographic peaks, with the second peak generally much more prominent than the first and increasing with increasing complexity of the R group. Succinylacetone yielded four product peaks which were attributed to all possible E/Z combinations resulting from the existence of two oxo groups. Relative standard deviations of between 15 and 78% were observed for samples between 0.20 and 0.01 μmol and between 2 and 7% for samples between 1.00 and 0.5 μmol. This would indicate that determinations of levels below 0.02 μmol could prove difficult using GC–FID.

A method for the determination of acetaldehyde in blood using PFBHA derivatization and GC–ECD was described by Tomita *et al.* [21]. Blood samples spiked with 3 and 9 μM acetaldehyde were recovered at 94.7 and 99.8%, respectively. Samples spiked with 9 μM acetaldehyde and 20 μM ethanol showed a recovery of 96.8%. The detection limit was about 1 μM. Samples containing ethanol had to be extracted within 2 min, as ethanol formed acetaldehyde under these analytical conditions. A further complication was that samples spiked with both acetaldehyde and ethanol and left at 26°C before work-up showed a significant decline in the amount of acetaldehyde recovered over time, with levels disappearing within 60 min.This was attributed to the binding of acetaldehyde to erythrocytes or plasma proteins and the resulting oxidation of acetaldehyde by aldehyde dehydrogenase. Another problem was noted with the high background levels of formaldehyde present in blank and spiked samples.

This was one of the first reports using lowered temperatures (ice-bath temperatures) instead of elevated temperatures for the formation of the PFB oxime derivative. Despite the obvious problem of acetaldehyde loss, relatively high recoveries were achieved at these low temperatures. One defect of the study was that the effects of temperature on the formation of the acetaldehyde oxime were not fully addressed. ECD temperatures were also generally lower than those reported as being optimum for oxime derivatives.

In a continuation of their earlier work, Hoffmann *et al.* [22] described the batchwise isolation of the oximes of aldehydes, ketones and oxo acids through the use of liquid partition chromatography. This method was used to isolate these derivatives from urine, plasma and amniotic fluid samples. Oxime formation and chromatographic conditions were as described in their earlier work [20]. An interesting variation on the earlier method was the addition of 20 μl of a 2.5 g/l rosolic acid solution as a pH indicator. After initial reaction with PFBHA at a pH of 3.5, the pH was adjusted to between 7 and 8, as indicated by the rosolic acid color change. After lyophilization, pH adjustment and liquid partition chromatography, the eluate was titrated with 10 mmol/l NaOH in methanol. Titration to the endpoint of red rosolic acid provided a measure of the total organic acid content of each sample. Mass spectrometry of the PFBHA derivatives showed that the pentafluorotropylium ion $[C_6F_5CH_2]^+$ at m/z 181 was the most or second-most intense ion generated from all the oxo acids, aldehydes and ketones analyzed. This ion was then used for the quantification of the various oxime derivatives by SIM-MS.

Hoffmann and Sweetman [23] provided EI mass spectral data for a number of oxo acids, aldehydes

and ketones from biological samples. These samples included amniotic fluid, plasma and urine.

A method for the determination of the lipid peroxidation product *trans*-4-hydroxy-2-nonenal (HNE) in platelets, monocytes, plasma and oxidized low-density lipoprotein in the low ng/ml range was developed by Selley *et al.* [24]. Samples were analyzed by GC–NCI-MS using deuterated HNE as the internal standard. HPLC was performed using a C_{18} reversed-phase column to separate *E*/*Z* isomers of the HNE oxime derivative, so that proton nuclear magnetic resonance (NMR) studies of the isomers could be undertaken. Synthetic PFB oximes of HNE were prepared and NMR spectroscopy performed on the separated isomers. Except for the assignment of the formyl proton adjacent to oxime (δ 7.70 for the *Z* isomer and δ 7.04 for the *E* isomer), no further NMR data were provided. This method did allow the assignment of the larger and later eluting peak by HPLC as the *E* isomer (Fig. 6). The *E*/*Z* isomers of the PFB oxime TMS ether showed significantly different relative ion abundances by NCI-MS using ammonia as the reagent gas. The *E*/*Z* ratios were calculated to be 1:0.25 for *m*/*z* 303, 1:0.26 for *m*/*z* 373 and 1:3.32 for *m*/*z* 333, indicating important MS differences between the geometrical isomers.

Kezic and Monster [25] published a note on the determination of 2,5-hexanedione (25HD), a metabolite of *n*-hexane, in urine and serum by GC–FID and GC–ECD. Three isomer peaks were observed for the oxime of 25HD. Detection limits were reported to be 4 μg/l with ECD and 50 μg/l with FID. The precision was 3.8% using ECD and 4.5% with FID, with linearity ranges of 4–100 μg/l for ECD and 0.05–10 mg/l for FID. 25HD could be detected in the serum and urine of individuals exposed to 180 mg/m^3 of *n*-hexane. No quantitative results were reported, although blank urine contained 6.4 ± 2.6 μg/l of background 25HD.

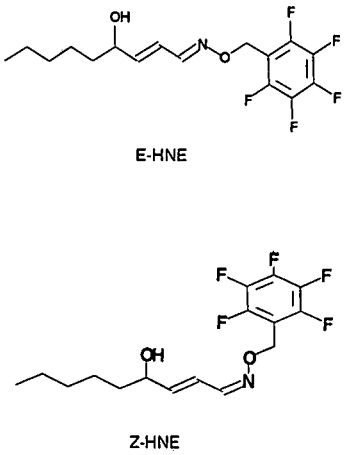

Fig. 6. *E* and *Z* isomers of the PFBHA oxime derivative of *trans*-4-hydroxy-2-nonenal (HNE).

In a study to determine if indole-3-pyruvate (IPyA) is an intermediate in the biosynthesis of indole-3-acetic acid from tryptophan in tomato shoots, a method for the measurement and detection of IPyA using PFBHA derivatization and MS detection was developed [26]. Analysis was performed using GC–ECD or GC–MS. PFB–IPyA methyl ester could be detected by GC–ECD at a level of 50 pg from calibration graphs and at levels between 8.4 and 10.3 ng gf. wt. from plant tissue as compared with tritiated standards. No information was provided on the possible formation of isomers.

PFBHA can be used for a wide range of biological applications. The solubility of PFBHA in various biological fluids and its reactivity over a wide pH range make it a highly desirable derivatizing agent. Excess of reagent can be removed through column chromatography or acid washing. Many of the aldehydes studied formed *E*/*Z* isomers which posed varying levels of difficulty relative to resolution and quantification. Most researchers stated that the ratio of the isomers was stable, but few groups provided sufficient data to support this claim.

4.3. PFBHA as a tool for indirect measurements: enzymatic reactions

A number of researchers have exploited the ease with which PFBHA can be used in aqueous solutions to monitor enzymatic reactions (Table 3). PFBHA was used to derivatize specific carbonyl compounds produced as products from these reactions. In 1981, Kawai *et al.* [27] showed that PFBHA could be used to monitor amygdalin concentrations in aqueous solutions by determination of benzaldehyde formed as a result of the enzymatic hydrolysis of amygdalin by β-glucosidase. Determination of the derivatives was carried out using either packed or capillary column GC–FID or GC–ECD. Solutions were buffered at pH 4.8 to achieve

TABLE 3

SUMMARY OF PFBHA METHODS FOR THE ANALYSIS OF ENZYMATIC REACTIONS

Compound type	Matrix type	Detection method	Chromatographic method	Ref.
Benzaldehyde	Aqueous solutions	ECD, FID	Packed column GC	27
Formaldehyde, Methoxyphenoxy-acetaldehyde	Aqueous solutions	FID, MS	Packed column GC	28
Formaldehyde	Aqueous solution	FID, ECD	Packed column GC	29
Formaldehyde	Aqueous solution	FID	Packed column GC	30
Formaldehyde	Catalaze–hydrogen peroxide aqueous solution	ECD	Packed column GC	31

both optimum β-glucosidase activity and oxime formation. No experimental results were described showing how this value was achieved. Separation of *E*/*Z* isomers was not achieved using the chromatographic conditions described.

PFBHA oximes of formaldehyde and methoxyphenoxyacetaldehyde (MPA) formed from the periodate oxidation of guaiacol glyceryl ether (GGE) were used for the GC determination of GGE in aqueous solutions [28]. Samples were analyzed by GC–FID using packed glass columns (3% XE-60). Experiments on the effect of pH on oxime formation showed that formaldehyde and MPA oximes formed over the pH range 3–6. However, lower yields were achieved as the pH approached 6. MS of the MPA oxime showed a base peak at *m*/*z* 123. *E*/*Z* isomers of the MPA oxime were observed.

A methanol–catalase system was described by Kobayashi and Kawai [29] for the GC determination of hydrogen peroxide. This system is based on the reaction of hydrogen peroxide and methanol to produce formaldehyde in the presence of catalase and the subsequent formation of the PFBHA–formaldehyde oxime.

Experiments to optimize pH, reaction period, catalase concentration, methanol concentration and the effect of reducing agents were performed using 30 μg of hydrogen peroxide. These experiments showed that pH between 3 and 8, catalase concentrations above 100 U, methanol concentrations between 8.0 and 30% (for 30 μg of hydrogen peroxide) and reaction times between 40 and 120 min could be used. L-Ascorbic acid was used to test the effect of the reducing compound on the system. It was found that there was no significant effect with 5–45 μg per 3 ml of sample solution containing 30 μg of hydrogen peroxide.

Calibration graphs were found to be linear in the range 1.5–60 μg of hydrogen peroxide in 2.0 ml of aqueous solution with FID and 0.006–1.2 μg for ECD. Correlation coefficients for the calibration graphs were 0.9996 for FID and 0.9995 for ECD. Relative standard deviations were 1.39% with FID and 1.28% with ECD. The detection limit for hydrogen peroxide was reported to be 0.001 μg/ml. Blank values were found to be high, corresponding to about 0.05 μg of hydrogen peroxide. Apparently the system was not calibrated using pure analytical standards of the PFB–formaldehyde oxime. Therefore, the reported values for detection limits and calibration represent relative values. Further, no evidence was provided to determine whether formaldehyde had formed from the reaction of hydrogen peroxide and any naturally occurring organics in the aqueous matrix.

In a continuation of this work, Kobayashi and Kawai used the formation of aldehyde products and subsequent PFB oxime formation as a method for the determination of two other enzymatic reactions. In the first system, monoamine oxidase activity was measured [30], while the second was an assay for glucose in serum using measurements of the formaldehyde produced from the glucose oxidase–catalase system [31].

In the glucose oxidase–catalase system [31], a pH between 5 and 6 gave an optimum yield of the PFB oxime. This pH range was important not only for oxime formation but also for glucose oxidase and

catalase activity. The effects of enzyme concentration, methanol concentration, reaction time and reducing compounds were studied; no attempt was made, however, to optimize PFBHA concentrations. Recoveries with glucose-spiked serum were calculated to be 102 ± 2.7%. Although linearity was achieved in the range 20–100 μg, no detection limit was reported for the method. Blank values were reported to be negligible using FID, although the earlier paper indicated high background levels using ECD [24].

The assay of monoamine oxidase [30] took advantage of a similar production of hydrogen peroxide from the initial enzymatic step and the subsequent reaction of hydrogen peroxide with methanol in the presence of catalase to form formaldehyde. The procedure is similar to that used in the other systems, with PFBHA being added to the solution to react with formaldehyde. Although six different amines were used as substrates in the reaction, no indication was given as to possible aldehyde formation and subsequent interference from these products. The precision of the method using these substrates varied between 5.9 and 2.9%. Blank values were again found to be high using ECD.

Because PFBHA is soluble in aqueous solution, it has been found to be a useful reagent for the analysis of enzymatic byproducts. PFBHA was added to solutions containing enzymes and substrates and could effectively scavenge the resulting aldehyde byproducts, with the PFBHA oximes being readily extracted into hexane. The high background levels of formaldehyde in aqueous solutions appears to be a problem common throughout the literature for the analysis of formaldehyde using PFBHA. Work to ruggedize these methods, including an analysis of the effects of many reagents and the use of pure standards to determine absolute recoveries and instrumental response, needs to be undertaken.

5. ENVIRONMENTAL APPLICATIONS OF PFBHA

PFBHA has been used in a wide variety of environmental applications, many of which involve the analysis of contaminants found in aqueous systems (Table 4). This is due, in part, to the ease with which PFBHA reacts with carbonyl compounds and the increased sensitivity to ECD that these PFB oxime derivatives display. In developing methods for the determination of carbonyl compounds as indicators of enzymatic reactions, Kobayashi and co-workers explored oxime formation of lower molecular mass carbonyls in aqueous systems (see section 4.3). This work laid the foundation for environmental appli-

TABLE 4

SUMMARY OF PFBHA METHODS FOR ENVIRONMENTAL APPLICATIONS

Compound type	Matrix type	Detection method	Chromatographic method	Ref.
Aldehydes, ketones	Aqueous solution	FID	Packed column GC	33
α-Keto acids	Aqueous solution	FID, ECD	Packed column GC	34
Formaldehyde	Clothes	ECD	Capillary GC	35
Benzophenone	River water, sea water, sediment	ECD	Capillary GC	36
Formaldehyde	Air	ECD	Capillary GC	37
Formaldehyde	Air	ECD	Capillary GC	38
Aldehydes	Exhaust gas	FTD	Capillary GC	39
Aliphatic aldehydes	River water, sea water	FTD	Capillary GC	40
Aldehydes, ketones	Ozonated water	ECD, MS	Packed column GC	41
Aldehydes, ketones	Ozonated water	ECD, MS	Capillary GC	42
Aldehydes	Ozonated water	MS	Capillary GC	43, 44

cations. Some of this work was described by Kobayashi and Kawai [32] in a review describing fluorine-containing reagents for the GC determination of carbonyl compounds.

In the initial work, Kobayashi *et al.* [33] studied the reaction of PFBHA with a series of thirteen aldehydes and ketones. Samples were analyzed by GC–FID using 2-m packed columns. Four different stationary phases were utilized, each using a different isothermal temperature for elution. Linear calibrations were obtained between 1 and 50 μg for formaldehyde, acetaldehyde, isobutyraldehyde and diethyl ketone. The reproducibility of the method was found to be 1.48% using isobutyraldehyde. No indication of the reproducibility or the concentrations of other analytes was provided, nor were the effects of the different columns or column temperatures on the method reported.

The reaction was found to be "complete" for aldehydes after 20 min at room temperature, after which the measured values were constant. The effect of reaction temperature was explored using diethyl ketone. Increasing temperature provided only a moderate improvement. It was stated that PFB–isobutyraldehyde oxime was stable when stored at room temperature for a few days.

In a continuation of this work, Kobayashi *et al.* [34] extended the use of PFBHA to the determination of α-keto acids in aqueous solutions. Samples of 1.0 ml, containing eight acids, were analyzed using 0.5 ml of PFBHA at 1.0 mg/ml and a reaction time of 30 min. Other conditions were identical with those used above [27], except that samples were also derivatized with diazomethane. *E*/*Z* isomers were detected and the main peak was used for quantification. It was noted that the ratio of the peak area of the second peak to that of the first became smaller with increasing complexity of the R group in the α-keto acid, with the ratio being reversed for α-ketoisovaleric acid and α-keto-β-methyl-*n*-valeric acid. Nonetheless, it was believed that the ratios of the *E*/*Z* isomers were sufficiently constant for the main peak to be used for analysis.

The reaction was optimum at pH values between 2 and 5 and with a reaction time of 30 min. The extent of extraction of oxime derivatives increased with increasing acidity of the medium. A linear relative response was achieved for the α-keto acids studied in the range 0.2–1.0 μmol in 1.0 ml of aqueous solution, although different slopes were reported, indicating unequal response factors.

In another report on the use of PFBHA for the determination of formaldehyde, Kobayashi *et al.* [35] detected trace amounts (0.80–198.6 ppm) of formaldehyde in clothes. Finely chopped clothes were extracted with water at 40°C for 1 h. After reaction, the mixtures were saturated with sodium chloride, acidified with sulfuric acid and extracted with hexane. GC–ECD was used for separation and detection. It was reported that 5 ppb of formaldehyde in water were detectable.

Benzophenone was determined in water and sediment using PFBHA derivatization and GC–ECD [36]. Benzophenone was extracted from water into *n*-hexane and then purified by silica gel column chromatography and treatment with sulfuric acid. The purified benzophenone was derivatized with PFBHA and determined by GC–ECD. Spiked samples of river water, sea water and sediment were analyzed with recoveries of 70 ± 11, 64 ± 12 and 66 ± 8%, respectively.

Nishikawa *et al.* [37] measured formaldehyde in air by passing 1 l/min of air through distilled water. The free formaldehyde was then reacted with PFBHA. A volume of 0.2 ml of an aqueous solution of PFBHA (0.5 mg/ml) was used for the derivatizations, with a 40-min reaction time at room temperature. The PFBHA–formaldehyde oximes were determined by GC–ECD. The detection limit was 2 ng with a recovery of 94 ± 4%.

Woelfel *et al.* [38] developed a method for the measurement of formaldehyde in workspace air. Using active or passive sampling in aqueous solutions, PFBHA was used to derivatize free formaldehyde. The PFBHA–formaldehyde oxime was then extracted into hexane and determined by GC–ECD. A detection limit of 1 ng/ml was achieved.

In a method developed by Nishikawa *et al.* [39], formaldehyde, acetaldehyde, propionaldehyde and butyraldehyde were detected in exhaust gas and thermal degradation emissions at 14, 10, 67 and 38 ppb, respectively. Gas samples of 2–30 l were collected using impingers connected in series. The impingers contained 10 ml of an ethanol solution containing PFBHA at 0.3 mg/ml. Capillary GC with flame thermionic detection (FTD) was used for analysis.

Baba *et al.* [40] analyzed river and sea waters for

saturated and α-unsaturated aliphatic aldehydes using PFBHA derivatization. Water samples of 500 ml were analyzed by GC with a 5% phenyl–methylsilicone fused-silica capillary column equipped with a flame thermionic detector.

Butyraldehyde, isobutyraldehyde, crotonaldehyde and methacrolein were determined by this method. Recoveries ranged between 77 and 110% with a relative standard deviation of 2.6 and 9.7% for pure water samples spiked at levels between 1 and 4 μg/l. The detection limits were between 0.6 and 0.9 μg/l. Recoveries from river water varied between 90 and 96% and from sea water between 86 and 94%. Full-scan mass spectra of the derivatives were provided.

Yamada and Somiya [41] demonstrated the formation of a series of aldehydes and ketones from ozonized water using PFBHA derivatization and GC–ECD or GC–MS. GC–ECD and GC–MS were performed using 3 m × 3 mm I.D. packed glass columns of OV-17 on Chromosorb W AW DMCS (80–100 mesh). It was shown that formaldehyde, glyoxal and methylglyoxal were major carbonyl by-products in ozonized water. No information was provided on the detection limits of this method, however, although calibration graphs were generated. Dissolved ozone interfered with the PFBHA reaction. Mass spectra for the PFBHA oximes of acetaldehyde and methylglyoxal were provided, both showing a base peak at m/z 181.

Glaze *et al.* [42] modified Yamada and Somiya's method [41] through the use of capillary column chromatography, the addition of sodium thiosulfate prior to derivatization with PFBHA, the use of a 2-h reaction time and GC–SIM-MS. Detection limits for seventeen aldehydes were determined, ranging between 1.7 μg/l for formaldehyde to 5.1 μg/l for glyoxal. Two of the seventeen aldehydes detected were methylglyoxal and acrolein. High blank levels of formaldehyde were reported, indicating a potential problem with its determination. Full-scan mass spectra of the seventeen aldehydes and acetone were provided.

In a continuation of this work, Cancilla and coworkers [43, 44] addressed the problem of quantification through the synthesis and spectroscopic characterization of a series of straight-chain aldehydes as their PFBHA oximes. Purified oximes were used as analytical standards to determine the absolute instrumental response, recoveries and reaction efficiencies for the use of PFBHA derivatization for the determination of aldehydes in water. MS, NMR, IR and UV data were reported for the oximes of formaldehyde, acetaldehyde, *n*-heptanal, *n*-decanal and the dialdehyde glyoxal.

Conditions of pH, temperature, extraction number and acid type were optimized. It was reported that matrix effects should be considered when determining aldehydes by PFBHA derivatization, that excess of PFBHA must be present and that pure analytical standards should be utilized in quantification studies. Formation of the monoglyoxal derivative was demonstrated using reaction conditions commonly in use for aldehyde detection in ozonized water. This derivative could be mistaken for the PFBHA–acetone or PFBHA–propanal derivatives by MS.

6. INSECTICIDAL PFBHA OXIMES

Although this review concerns the use of PFBHA as a derivatizing agent for the trace determination of carbonyl compounds, it should be noted that other applications for PFBHA have been developed. One such application is the formation of insecticidal PFB oximes [45–49]. The cited papers describe the physiological effects of some of these compounds and provide spectral data, such as NMR, which would be useful to investigators interested in pursuing various aspects of PFBHA oxime formation for analytical applications. Johnson *et al.* [46] described the separation of geometric isomers by HPLC. Holan *et al.* [47] reported proton NMR studies of the E/Z isomers of various oxime O-ether insecticides and the effect of polar solvents on E/Z ratios.

7. CONCLUSIONS

PFBHA has proved to be a valuable derivatizing agent for the analysis of carbonyl-containing compounds, particularly aldehydes. The ease of oxime formation over a wide pH range and the solubility of PFBHA in aqueous solutions have allowed PFBHA to be used for the determination of aldehydes in a variety of biological and environmental matrices. Much work remains to be done to explore other matrices and to optimize the conditions under

which PFBHA can used as an analytical agent.

The effects of chromatographic and analytical conditions on E/Z ratios of the PFB oximes have not been fully explored. The possibility of changing E/Z ratios under different analytical conditions brings into question the accurate quantification of the PFB oximes. This is particularly true if only one isomer peak is used for quantification, as different analytical conditions may cause different isomer ratios to be favored. The use of high resolution capillary columns has generally made the separation of E/Z isomers easier to achieve than the use of packed columns, allowing for changing isomer ratios to be more easily observed. With dicarbonyl species such as glyoxal or succinylacetone, E/Z isomerism occurs from oxime formation with both carbonyl groups, increasing the number of possible isomers. The existence of multiple isomers makes it essential to understand better the thermodynamic and kinetic behavior of the various isomers under a variety of analytical conditions. Analytical conditions include the effect of pH, solvent type, reaction time and temperature. Instrumental conditions include injector temperatures, column type and temperature and detector response. The lack of commercially available PFB oxime standards has slowed progress of PFB oxime studies in these areas. However, PFB oximes are easily prepared in the laboratory in milligram or greater amounts. Therefore, research into the use of PFB oximes should employ analytical standards.

The continued reaction of PFBHA with aldehydes in organic solvents could pose significant problems to researchers involved in the detection of aldehydes in the environment. This is particularly true for the more volatile aldehydes such as formaldehyde and acetaldehyde, two aldehydes commonly found in air. Another important consideration is the proper storage of PFBHA and its working solutions. Because of the ease with which PFBHA reacts with carbonyl compounds, it can easily become contaminated through the formation of oximes. This, in turn, may lead researchers inadvertently to add already formed oximes to the mixtures under analysis. For this reason, the effect of different storage conditions on pure PFBHA and the working solutions made with PFBHA should be studied. Recrystallization of PFBHA may be required before use to obtain solutions free of oximes.

A number of other fluorinated reagents have been developed for the determination of carbonyl containing compounds. Pentafluorophenylhydrazine (PFPH) is one such reagent found to be useful for a wide variety of applications. Kobayashi and Kawai [32] provided one of the earlier reviews on the use of this reagent and reported that PFB oximes are generally more easily formed than PFPH hydrazones. Further, PFB oximes were found to be much more volatile and amenable to GC separation. Both types of derivatizing agents produced E/Z isomers, reacted readily at room temperature in aqueous solution and produced derivatives which were easily extracted into organic solvents.

Because PFBHA is such a versatile reagent, there is little doubt that analytical applications using PFBHA will continue to be developed. This is particularly true in areas where there is a need to determine carbonyl containing compounds as derivatives which are stable under a variety of conditions, which form rapidly, are chromatographed easily and are detected at low concentrations.

REFERENCES

1 J. D. Roberts and M. C. Caserio, *Basic Principles of Organic Chemistry*, Benjamin, Menlo Park, CA, 1977.
2 K. T. Koshy, D. G. Kaiser and A. L VanDerSlik, *J. Chromatogr. Sci.*, 13 (1975) 97.
3 T. Nambara, K. Kigasawa, T. Iwata and M. Ibuki, *J. Chromatogr.*, 114 (1975) 81.
4 G. A. Youngdale, *J. Pharm. Sci.*, 65 (1976) 625.
5 S. G. McKay, D. L. Garmaise, G. Y. Paris and S. Gelblum, *Can. J. Chem.*, 38 (1960) 343.
6 F. A. Fitzpatrick, R. R. Gorman and M. A. Wynalda, *Prostaglandins*, 13 (1977) 201.
7 F. A. Fitzpatrick, M. A. Wynalda and D. G. Kaiser, *Anal. Chem.*, 49 (1977) 1032.
8 F. A. Fitzpatrick, D. A. Stringfellow, J. Maclouf and M. Rigaud, *J. Chromatogr.*, 177 (1979) 51.
9 J. Rosello, E. Gelpi, M. Rigaud, J. Durand and J. C. Breton, *Biomed. Mass Spectrom.*, 8 (1981) 149.
10 J. Rosello, E. Gelpi, M. Rigaud and J. C. Breton, *J. High Resolut. Chromatogr. Chromatogr. Commun.*, 4 (1981) 437.
11 R. Christ-Hazelhof and D. H. Nugteren, *Prostaglandins*, 22 (1981) 739.
12 J. Mai, S. K. Goswami, G. Bruckner and J. E. Kinsella, *J. Chromatogr.*, 230 (1982) 15.
13 J. M. Rosenfeld, M. Mureika-Russell and M. Love, *J. Chromatogr.*, 489 (1989) 263.
14 K. A. Waddell, I. A. Blair and J. Wellby, *Biomed. Mass Spectrom.*, 10 (1983) 83.
15 G. B. Park, P. Erdtmansky, M. P. Kullberg and J. Edelson, *J. Chromatogr.*, 222 (1981) 213.

16 M. Tanaka, J. Hasegawa, J. Tsutsumi and T. Fujita, *J. Chromatogr.*, 231 (1982) 301.
17 K. Kobayashi, M. Okada, Y. Yasuda and S. Kawai, *Clin. Chim. Acta*, 133 (1983) 223.
18 F. J. G. M. van Kuijk, D. W. Thomas, R. J. Stephens and E. A. Dratz, *Biochem. Biophys. Res. Commun.*, 139 (1986) 144.
19 P. A. Biondi, F. Manca, A. Negri, C. Secchi and M. Montana, *J. Chromatogr.*, 411 (1987) 275.
20 G. Hoffmann and L. Sweetman, *J. Chromatogr.*, 421 (1987) 336.
21 M. Tomita, I. Ijiri, K. Shimosato and S. Kawai, *J. Chromatogr.*, 414 (1987) 454.
22 G. Hoffmann, S. Aramaki, E. Blum-Hoffmann, W. L. Nyhan and L. Sweetman, *Clin. Chem.*, 35 (1989) 587.
23 G. F. Hoffmann and L. Sweetman, *Clin. Chim. Acta*, 199 (1991) 273.
24 M. L. Selley, M. R. Bartlett, J. A. McGuiness, A. J. Hapel, N. G. Ardlie and M. J. Lacey, *J. Chromatogr.*, 488 (1989) 329.
25 S. Kezic and A. C. Monster, *J. Chromatogr.*, 563 (1991) 199.
26 T. P. Cooney and H. M. Nonhebel, *Biochem. Biophys. Res. Commun.*, 162 (1989) 761.
27 S. Kawai, K. Kobayashi and Y. Takayama, *J. Chromatogr.*, 210 (1981) 342.
28 K. Kobayashi, M. Okamoto and S. Kawai, *Yakugaku Zasshi*, 102 (1982) 1095.
29 K. Kobayashi and S. Kawai, *J. Chromatogr.*, 245 (1982) 339.
30 K. Kobayashi and S. Kawai, *J. Chromatogr.*, 274 (1983) 313.
31 K. Kobayashi and S. Kawai, *J. Chromatogr.*, 275 (1983) 394.
32 K. Kobayashi and S. Kawai, *Ann. Proc. Gifu Coll. Pharm.*, 32 (1983) 15.
33 K. Kobayashi, M. Tanaka and S. Kawai, *J. Chromatogr.*, 187 (1980) 413.
34 K. Kobayashi, E. Fukui, M. Tanaka and S. Kawai, *J. Chromatogr.*, 202 (1980) 93.
35 K. Kobayashi, O. Mitsuyoshi and K. Satoshi, *Bunseki Kagaku*, 30 (1981) 76.
36 K. Ozaki, H. Mukai and H. Murayama, *Niigatta-ken Kogai Kenkyusho Kenkyu Hokoku*, 6 (1982) 27.
37 H. Nishikawa, Y. Takahara, H. Mori and T. Hayakawa, *Taiki Osen Gakkaishi*, 19 (1984) 387.
38 G. Woelfel, J. Mueller and K. H. Schaller, *Staub-Reinhalt. Luft*, 45 (1985) 550.
39 H. Nishikawa, T. Hayakawa and T. Sakai, *Bunseki Kagaku*, 36 (1987) 381.
40 K. Baba, S. Ishikawa, Y. Hanada, Y. Uchimura, S. Sueta and K. Kido, *Bunseki Kagaku*, 37 (1988) 519.
41 H. Yamada and I. Somiya, *Ozone Sci. Eng.*, 11 (1989) 127.
42 W. H. Glaze, M. Koga and D. Cancilla, *Environ. Sci. Technol.*, 23 (1989) 838.
43 D. A. Cancilla, *Ph.D. Dissertation*, University of California, Los Angeles, 1991.
44 D. A. Cancilla, R. Barthel, C. C. Chou and S. S. Que Hee, *J. Assoc. Off. Anal. Chem.*, 75 (1992) 842.
45 Commonwealth Scientific and Industrial Research Organization, *Jpn. Kokai Tokkyo Koho JP*, 57 185 255 (1982); AU Appl. 81/8653.
46 W. M. P. Johnson, D. F. O'Keefe and K. Rihs, *J. Chromatogr.*, 291 (1984) 449.
47 G. Holan, W. M. P. Johnson and C. T. Virgona, *Pestic. Sci.*, 15 (1984) 361.
48 G. Holan, W. M. P. Johnson, D. F. O'Keefe, G. L. Quint, K. Rihs, T. H. Spurling, R. Walser, C. T. Virgona, C. Frelin, M. Lazdunski, G. Johnson and S. Chen Chow, *R. Soc. Chem. Spec. Publ.*, 53 (1985) 114.
49 M. D. Leibowitz, J. R. Schwarz, G. Holan and B. Hille, *J. Gen. Physiol.*, 90 (1987) 75.

Journal of Chromatography, 627 (1992) 17–22
Elsevier Science Publishers B.V., Amsterdam

CHROM. 24 573

Retention model of multiple eluent ion chromatography

A priori estimations of analyte capacity factor and peak intensity

Atsushi Yamamoto

Toyama Institute of Health, 17-1, Nakataikoyama, Kosugi-machi, Toyama 939-03 (Japan)

Kazuichi Hayakawa

Faculty of Pharmaceutical Sciences, Kanazawa University, 13-1, Takara-machi, Kanazawa 920 (Japan)

Akinobu Matsunaga and Eiichi Mizukami

Toyama Institute of Health, 17-1, Nakataikoyama, Kosugi-machi, Toyama 939-03 (Japan)

Motoichi Miyazaki

Faculty of Pharmaceutical Sciences, Kanazawa University, 13-1, Takara-machi, Kanazawa 920 (Japan)

(First received May 15th, 1992; revised manuscript received August 19th, 1992)

ABSTRACT

In multiple eluent ion chromatography, the analyte elution behaviour still remains unclear. In this work, the inter-eluent selectivity coefficient was accurately determined by re-interpreting Hoover's model. Obtaining the inter-eluent selectivity coefficient was greatly simplified by introducing the concept of an "inter-eluent separation factor". From the coefficients obtained, analyte capacity factors in polyprotic eluent systems can be estimated *a priori*. Moreover, this new factor permits the calculation of eluent species with different charges and, through stoichiometric simulation of the chromatogram, makes possible the *a priori* estimation of analyte peak intensities.

INTRODUCTION

In ion chromatography (IC), the retention time and the peak intensity of an analyte have been dominated by the eluent composition and its concentration. Usually, optimum conditions for analyte separation and detection are determined experimentally each time the elution conditions change. If the retention time and the peak intensity of target analyte can be calculated *a priori*, then analysis can be greatly simplified and estimation of the composition of unknown peaks made possible.

The selectivity coefficient between an analyte and the eluent can be defined theoretically for a given ion-exchange equilibrium [1]. When the analyte and the eluent ion are both composed of a single species under fixed conditions, not only can the analyte capacity factor be estimated *a priori* [2,3], but also the peak intensity after simple stoichiometric treat-

Correspondence to: A. Yamamoto, Toyama Institute of Health, 17-1, Nakataikoyama, Kosugi-machi, Toyama 939-03, Japan.

0021-9673/92/$05.00

ment [4,5]. However, multi-component eluents are generally used in IC, *e.g.*, carbonate–hydrogencarbonate and phthalate–hydrogenphthalate eluents for suppressed and non-suppressed IC, respectively, and hence the analyte behaviour becomes complicated.

Hoover [6] proposed the use of an "inter-eluent selectivity coefficient", in which there is a constant selectivity coefficient between every pair of active eluent species, in order to solve this problem. Jenke and Pagenkopf [7] applied this concept to non-suppressed IC using a low-capacity ion-exchange column, but they could not correctly obtain the inter-eluent selectivity coefficient. Kuwamoto and co-workers [8,9] tried to omit this coefficient from their equations, thus avoiding the difficulties involved in calculating it. However, the elution mechanism in multi-eluent systems cannot be calculated without the inter-eluent selectivity coefficient.

In this paper, we define a new "inter-eluent separation factor" as a method for easily calculating the inter-eluent selectivity coefficient. The use of stoichiometric analysis together with the coefficients obtained permitted the elution and detection behaviour of an analyte in a multi-species eluent to be determined.

THEORY

Experimental observations were made using a diprotic organic acid as the eluent. We have already reported that the equilibrium in Fig. 1 holds, in an anion-exchange column, for an eluent acid, EH_2, that dissociates into EH^- and E^{2-}, with K_{e1} and K_{e2} as its first and second acid dissociation constants, respectively [4]. From Hoover's model, all of the exchange sites are occupied by eluent anions.

$$[Cap] = 2[E^{2-}]_s + [EH^-]_s \quad (1)$$

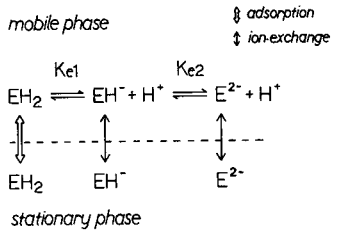

Fig. 1. Equilibrium diagram of eluent acid in the column.

where [Cap] is the anion-exchange capacity and the subscripts m and s represent existence in the mobile and stationary phase, respectively. If we assume that these eluent ions establish the equilibrium shown in eqn. 2, the inter-eluent selectivity coefficient, X_{21}, for this reaction is defined as in eqn. 3:

$$[E^{2-}]_m + 2[EH^-]_s \rightleftharpoons 2[EH^-]_m + [E^{2-}]_s \quad (2)$$

$$X_{21} = [E^{2-}]_s[EH^-]_m^2/[E^{2-}]_m[EH^-]_s^2 \quad (3)$$

This coefficient is considered to be a constant on condition that the eluent ionic strength is very low, because the contributions of the activity of ionic species to the calculation are negligible.

We can define the inter-eluent separation factor, R_E, as

$$R_E = [E^{2-}]_s[EH^-]_m/[E^{2-}]_m[EH^-]_s \quad (4)$$

Unlike the inter-eluent selectivity coefficient, this factor varies with change in eluent concentration and/or pH. However, it can be regarded as a constant when the eluent conditions are fixed, and substitution of eqn. 3 into eqn. 4 gives

$$R_E = X_{21}[EH^-]_s/[EH^-]_m \quad (5)$$

Solution of eqns. 1 and 3 for $[EH^-]_s$ and substitution into eqn. 5 gives

$$R_E = [H^+]\{(1 + 8X_{21}K_{e2}[Cap]/[H^+][EH^-]_m)^{1/2} - 1\}/4K_{e2} \quad (6)$$

When the analyte anion, S^-, is a monoprotic acid, the selectivity coefficients between this anion and differently charged eluent ions are K_{11} and K_{12}, respectively:

$$K_{11} = [S^-]_s[EH^-]_m/[S^-]_m[EH^-]_s \quad (7)$$

$$K_{12} = [S^-]_s^2[E^{2-}]_m/[S^-]_m^2[E^{2-}]_s \quad (8)$$

If the undissociated analyte, SH, and the column packing material do not interact at all, then the following ralationship between the experimental capacity factor, k'_{ex}, and the capacity factor of dissociated analyte, k'_{s^-}, holds:

$$k'_{ex} = [S^-]_s\phi/([SH]_m + [S^-]_m) = K_{s1}k'_{s^-}/([H^+] + K_{s1}) \quad (9)$$

where K_{s1} is the acid dissociation constant of the analyte and ϕ is the phase ratio of the column. The ratio of eluent species in the stationary phase

becomes, according to eqn. 4,

$$[E^{2-}]_s/[EH^-]_s = R_E K_{e2}/[H^+] \quad (10)$$

Solution of eqns. 1 and 10 for $[EH^-]_s$ and substitution into eqn. 7 gives

$$K_{11}\phi = k'_{s-}[EH^-]_m(2R_E K_{e2} + [H^+])/[Cap][H^+] \quad (11)$$

Since eqn. 11 is first order for $K_{11}\phi$ and R_E, they can be easily calculated using the value of k'_{s-} obtained from eqn. 9. From eqns. 3, 7 and 8, the following relationship holds between K_{11} and K_{12}:

$$X_{21} = K_{11}^2/K_{12} \quad (12)$$

Consequently, the selectivity coefficients determined in the above way include the phase ratio. The introduction of R_E obtained enables X_{21} to be calculated according to eqn. 6. As R_E is a function of $[EH^-]_m$, eqn. 11 implies that there is not a linear relationship between log k' and the logarithm of the eluent concentration in a multiple eluent IC system even if [Cap] is constant.

Next we deal in an analogous manner with polyprotic acid analytes. When differently charged analyte ions are treated as different ionic species, similarly in the case of the eluent, there are two by i kinds of selectivity coefficients, K_{i1} and K_{i2}, made between the analyte (i dissociation steps) and eluent (two dissociation steps). The capacity factor of each charged analyte, k'_{si-}, are determined by the following equations.

$$k'_{ex} = \left[\sum_{n=1}^{i} k'_{sn-}[H^+]^{i-n}\left(\prod_{l=1}^{n} K_{sl}\right)\right] \Bigg/ \left[[H^+]^i + \sum_{n=1}^{i} [H^+]^{i-n}\left(\prod_{l=1}^{n} K_{sl}\right)\right] \quad (13)$$

$$k'_{si-} = R_E^{i-2} K_{i1} k'_{s2-}/X_{21}^{i-1} K_{22} \quad (14)$$

where K_{sl} is the lth acid dissociation constant of the analyte. By using the value of X_{21} obtained experimentally for the monoprotic analyte, the values of these inter-eluent selectivity coefficients can be calculated by eqns. 13 and 14.

All of the selectivity coefficients can be calculated in the same manner as described above. By using these coefficients, the elution behaviour of analyte can be calculated in a diprotic eluent system, *i.e.*, the changes of each eluent species fraction in the stationary phase, according as the analyte fraction changes, can be calculated. Dividing eqn. 7 by eqn. 8 gives

$$\Delta[E^{2-}]_s/\Delta[EH^-]_s = K_{11}\phi k'_{s-}\Delta[E^{2-}]_m/K_{12}\phi^2\Delta[EH^-]_m = \Delta[E^{2-}]_m R_E/\Delta[EH^-]_m \quad (15)$$

where Δ means the change of the bracketed species fraction. As the amount of analyte relative to that of the eluent is negligible in the overall stoichiometry of the stationary phase, the following equation applies:

$$\sum_{n=1}^{i} n\Delta[S^{n-}]_s = \Delta[EH^-]_s + 2\Delta[E^{2-}]_s \quad (16)$$

Using eqns. 15 and 16, the simulation of chromatogram using the diprotic eluent system can be performed stoichiometrically.

In the case of a triprotic eluent system, the calculation of these coefficients is very complicated. All the selectivity coefficients, K_{ij}, of the triprotic analyte to be used as an eluent must first be calculated in mono- and/or diprotic eluent systems, where j represents the charge of the eluent. The inter-eluent selectivity coefficients of this triprotic acid eluent, X_{ij}, are determined by the following equation:

$$X_{ij} = K_{ij}/K_{jj}^i \quad (17)$$

EXPERIMENTAL

The IC system consisted of a Shimadzu (Kyoto, Japan) LC-5A pump, a Rheodyne (Cotati, CA, USA) Model 7125 injector, a Shimadzu SPD-6AV UV–visible detector and a Shimadzu Chromatopac C-R4A integrator.

Chromatographic separation of anions was performed on a 5 cm × 4.6 mm I.D. column packed with low-capacity anion exchangers (Tosoh, Tokyo, Japan, TSK gel IC-Anion-PW, 0.03 mequiv./ml) maintained at 25°C. Phthalic acid eluents of various concentrations and pH values were delivered at 0.8 ml/min. Helium purging was performed to prevent atmospheric carbon dioxide from dissolving in the eluent at higher pH values. The detection wavelength was adjusted so that the absorbance of the eluent was approximately unity. The column void volume was determined from the front peak by injecting sodium hydroxide solution.

Chromatographic simulations were run on an

NEC (Tokyo, Japan) PC-9801 RA personal computer as described previously [4].

RESULTS AND DISCUSSION

The capacity factors of the four analytes at various phthalate concentrations and pH values are summarized in Table I. The equations in the theoretical section hold, as the ion-exchange capacity is constant. The IC-Anion-PW column used in this work was packed with a strongly basic anion-exchange resin of the quaternary ammonium salt type and its capacity is negligibly affected by altering the pH value of the eluent. In practice, there was not a significant change in the capacity for eluents of pH 4–6. Consequently, the value of the inter-eluent selectivity coefficient was calculated from the elution data for chloride anion, completely dissociated species, in the pH range mentioned above. Other coefficients were determined by using this coefficient. Four diprotic analyte selectivity coefficients were calculated from eqns. 13 and 14. Introduction of the concept of an "inter-eluent separation factor" enabled these values to be calculated accurately and readily. The calculated coefficients are shown in Table II.

TABLE I

CAPACITY FACTORS OF ANALYTES

Phthalate concentration (10^{-3} M)	pH	Capacity factor			
		Lactate	Chloride	Phosphate	Malate
0.5	3.95	8.45	24.8	–	45.6
	4.50	7.06	15.6	7.58	56.9
	5.9[a]	3.50	7.39	6.35	38.7
	6.4[a]	2.92	6.26	9.10	31.5
	7.1[a]	3.00	6.40	16.2	33.2
0.7	3.95	6.89	19.5	–	32.8
	4.49	5.73	12.7	6.15	39.0
	5.18	3.79	7.96	4.00	33.8
	6.4[a]	2.74	5.83	7.10	25.0
	7.1[a]	2.68	5.66	13.2	24.5
1.0	3.41	4.48	26.0	12.4	16.3
	3.95	5.47	15.1	7.71	22.7
	4.49	4.84	10.5	5.12	27.9
	5.19	3.15	6.48	3.27	22.8
	5.9[a]	2.47	5.21	3.95	19.3
	6.4[a]	2.26	4.81	5.04	17.4
	7.1[a]	2.26	4.81	8.91	17.2
1.5	3.41	3.54	18.0	9.17	10.7
	3.98	4.24	10.8	5.82	14.2
	4.51	3.79	8.00	3.94	18.0
	5.18	2.58	5.21	2.63	14.7
	5.9[a]	2.05	4.28	2.94	13.0
	6.5[a]	1.85	3.91	3.57	11.3
	7.0[a]	1.80	3.83	5.63	11.3
2.0	3.41	2.92	13.9	7.19	8.06
	3.98	3.60	8.89	–	10.8
	4.49	3.21	6.54	3.25	13.1
	5.19	2.23	4.58	2.27	11.3
	5.9[a]	1.78	3.74	2.45	9.82
	6.5[a]	1.53	3.38	3.02	8.38
	7.1[a]	1.54	3.29	4.28	8.22

[a] Helium purging.

TABLE II

SELECTIVITY COEFFICIENTS AND THEIR STANDARD DEVIATIONS FOR HOOVER'S MODEL

Analyte	$K_{11}\phi$	$K_{12}\phi^2$	$K_{21}\phi^a$	$K_{22}\phi$	X_{21}
Chloride	1.29 ± 0.07	1.49	–	–	1.12 ± 0.18
Lactate	0.68 ± 0.04	0.41	–	–	
Phosphate	0.61	0.33	1.68	1.50 ± 0.43	
Malate	0.69	0.43	1.48	1.32 ± 0.09	

[a] $K_{21} = K_{22}X_{21}$.

The relationhips between calculated (using the coefficients obtained) and observed analyte capacity factors show good linearity. The correlation coefficients and relative standard deviations (in parentheses) for lactate, chloride, phosphate and malate were 0.996 (6.5%), 0.994 (5.3%), 0.998 (2.8%) and 0.990 (6.1%), respectively. An example with a 1 m*M* phthalate eluent is shown in Fig. 2. The solid lines represent the calculated capacity factors and the symbols the observed values. The small discrepancies for lactate in the low-pH region can be attributed to the adsorption of its undissociated form and those for diprotic analytes in the high-pH region to the decrease in the ion-exchange capacity of the column. However, it should be noted that the *a priori* calculation of a polyprotic analyte capacity factor is possible even if both analyte and phthalate eluent are dissociated in the form of mixed charges.

As there was good agreement between the calculated and observed values, chromatographic simulation was carried out based on eqns. 15 and 16. The observed and simulated peak areas as a function of pH in a 1 m*M* phthalate eluent for the diprotic analytes malate and phosphate show good agreement, as can be seen in Fig. 3. The above findings show that the *a priori* estimation of analyte capacity factors and peak intensities is possible over a wide range of eluent pH. This calculation is considered to be practicable in polyprotic analyte and eluent systems. Consequently, these coefficients are useful in cases where the optimum conditions are to be established for multiple eluent IC.

If $\Delta[H^+]$ in the analyte zone is negligibly small, eqn. 15 can be rewritten as follows:

$$\Delta[E^{2-}]_s/\Delta[EH^-]_s = 2K_{e2}^2 R_E/([H^+]^2 + 4K_{e2}[H^+]) \quad (18)$$

Eqn. 18 implies that the ratio of the changes of eluent species fraction in the stationary phase is constant regardless of the analyte species. The value of $\Delta[E^{2-}]_s/\Delta[EH^-]_s$ in eqn. 18 is smaller than that of

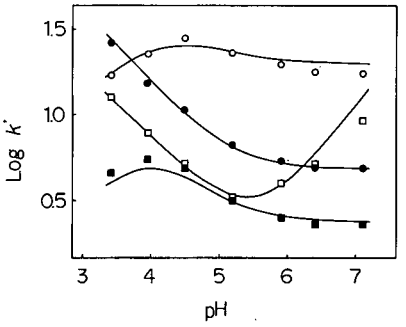

Fig. 2. Comparison of calculated capacity factors (solid lines) with observed values for malate (○), chloride (●), phosphate (□) and lactate (■).

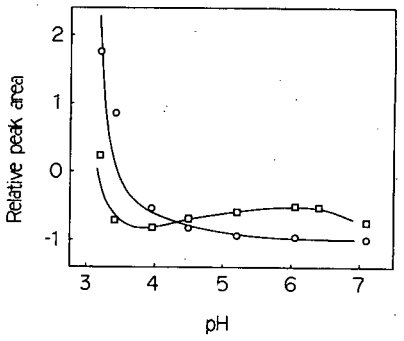

Fig. 3. Comparison of simulated relative peak areas (solid lines) with observed values for malate (○) and phosphate (□).

$[E^{2-}]_s/[EH^-]_s$ in eqn. 10. As far as the phthalate eluent is concerned, the results of the calculation show that this value is close to that of $[E^{2-}]_m/[EH^-]_m$, that is, there is no great difference between the ratio of eluent species participating in the elution of the analyte and that present in the mobile phase. This means that there is not a large difference in elution power between the two eluent species.

Overall, it can be concluded that the selectivity coefficients, based on the modified Hoover model, can be obtained accurately and readily by introducing the concept of an "inter-eluent separation factor". All equations are simplified when this new factor is used. Moreover, the use of the coefficients obtained reveals the behaviour of multiple eluents in the stationary phase and makes the *a priori* estimation of analyte peak intensity possible through stoichiometric simulation of the chromatogram.

REFERENCES

1 R. W. Grimshaw and C. E. Harland, *Ion-Exchange: Introduction to Theory and Practice*, Chemical Society, London, 1975.
2 P. Jandera and J. Churacek, *J. Chromatogr.*, 91 (1974) 207.
3 D. T. Gjerde, G. Schmuckler and J. S. Fritz, *J. Chromatogr.*, 187 (1980) 35.
4 A. Yamamoto, A. Matsunaga, M. Ohto, E. Mizukami, K. Hayakawa and M. Miyazaki, *J. Chromatogr.*, 482 (1989) 145.
5 H. Sato, *Anal. Chem.*, 62 (1990) 1576.
6 T. B. Hoover, *Sep. Sci. Technol.*, 17 (1982) 295.
7 D. R. Jenke and G. K. Pagenkopf, *Anal. Chem.*, 56 (1984) 88.
8 M. Maruo, N. Hirayama and T. Kuwamoto, *J. Chromatogr.*, 481 (1989) 315.
9 N. Hirayama and T. Kuwamoto, *J. Chromatogr.*, 508 (1990) 51.

Journal of Chromatography, 627 (1992) 23–35
Elsevier Science Publishers B.V., Amsterdam

CHROM. 24 549

Rapid breakthrough measurement of void volume for field-flow fractionation channels

J. Calvin Giddings, P. Stephen Williams and Maria Anna Benincasa*

Field-Flow Fractionation Research Center, Department of Chemistry, University of Utah, Salt Lake City, UT 84112 (USA)

(First received May 4th, 1992; revised manuscript received August 5th, 1992)

ABSTRACT

A peak breakthrough technique is described and evaluated for measuring the void volume of field-flow fractionation (FFF) channels, particularly those used for flow FFF. This technique uses a high-molecular-mass macromolecular or particulate probe that can be displaced rapidly by flow through the FFF channel with minimal transverse diffusion. The particles that emerge first are those carried through the entire length near the channel centerline at the apex of the parabolic flow profile. These particles generate a sharp breakthrough profile. The measured breakthrough time is two thirds of the void time, thus making it possible to calculate both the void time and the associated void volume. This method, although applicable to all FFF channels (and capable of extension to open tubes), is particularly useful for flow FFF because conventional low-molecular-mass void probes can diffuse into the permeable walls and thus distort void measurements. The theoretical basis of the breakthrough technique and an explanation for the sharpness of the breakthrough front are given. A method for compensating for deviations from perfect sharpness is developed in which the breakthrough time is identified with the time needed to reach 85–88% of the breakthrough peak maximum. Preliminary experimental results are shown using various protein probes in four different FFF channel systems.

INTRODUCTION

The void volume V^0 (or, equivalently, the void time t^0) is a critical parameter in field-flow fractionation (FFF) whose value must be established in order to derive molecular mass and particle size information from FFF retention measurements [1–4]. In principle, V^0 and t^0 are simple to measure: they can be equated to the experimental retention volume and time, respectively, of a component that is unaffected by applied external fields. Such a component will ordinarily be distributed fairly evenly over the channel cross-section and its observed average velocity will equal the mean velocity of the carrier fluid in the FFF channel. The component should thus emerge from the channel (and be detected) after a volume of carrier approximately equal to the volume of the empty space, or void volume, is displaced through the channel. Hence V^0 should be obtainable in two ways: either as the measured "sweep" or "retention" volume of a non-retained component peak or as the physical volume of the FFF channel. As FFF channels generally have a simple rectangular geometry, the physical or geometrical volume can be calculated in terms of channel dimensions, provided that the latter are accurately known. In this case, the two volumes (inert retention volume and geometrical volume) can be compared for self-consistency and thus for assurance that an accurate V^0 is available. (A very small difference, usually $<1\%$, in the two volumes can be induced by edge effects [5].) Once V^0 is known, t^0 can be calculated by means of the simple relationship

$$V^0 = \dot{V}t^0 \tag{1}$$

where $\dot{V}$ is the volumetric flow-rate of carrier liquid flowing through the channel.

Correspondence to: J. C. Giddings, Field-Flow Fractionation Research Center, Department of Chemistry, University of Utah, Salt Lake City, UT 84112, USA.

* Present address: Via Ugo de Carolis 83, 00136 Rome, Italy.

0021-9673/92/$05.00

The dual approach noted above for obtaining V^0 is commonly employed in sedimentation and thermal FFF. However, the dual strategy has several weaknesses when applied to flow FFF channels [3,4]. First, and most important, the low-molecular-mass components that are most often used to probe the void volume are small enough in molecular dimensions that they generally penetrate into the semipermeable membrane used for the accumulation wall. When the upper (or depletion) wall is permeable, as is usual, they can also partition into this wall. Thus, at worst, the non-retained component will be lost through the membrane and fail to appear at the detector and, at best, the component will be delayed by virtue of its partitioning into stagnant pore space which will yield an erroneous result. Losses through the membrane can be minimized by eliminating the cross-flow during void peak migration, but then the component is more likely to partition into the larger pores of the depletion wall. A void probe of larger molecular size can be used to avoid membrane partitioning, but the pore space of the depletion wall (usually consisting of a flat slab of frit with micrometer-sized pores) can still be readily penetrated unless very large probes are used. If one does proceed to micrometer-sized probes, then hydrodynamic lift forces will influence their retention. Also, any increase in the size of the probe molecule or particle will slow its diffusion and thus increase the run time necessary to obtain a sharp and meaningful void peak.

The geometrical volume of flow FFF channels is also subject to uncertainty. In addition to the error in volume associated with the small geometrical uncertainties common to most FFF channels, flow FFF systems are generally constructed with a compressible membrane used for the accumulation wall [3,4]. As this membrane is clamped in place beneath a spacer of well characterized thickness, the uncompressed portion of the membrane protrudes into the channel space, occupying some of the volume that would normally be part of the void volume. This protrusion reduces the channel thickness w (and thus V^0) as illustrated in Fig. 1. Unless the degree of compression is well characterized, the actual thickness of the channel will not be known and thus V^0 will be undetermined. The uncertainty introduced by membrane compression makes it desirable to use thin and relatively incompressible membranes wherever possible. Many commercial membranes (one exception is noted below) are, however, subject to considerable compression, making the geometrical V^0 difficult to ascertain.

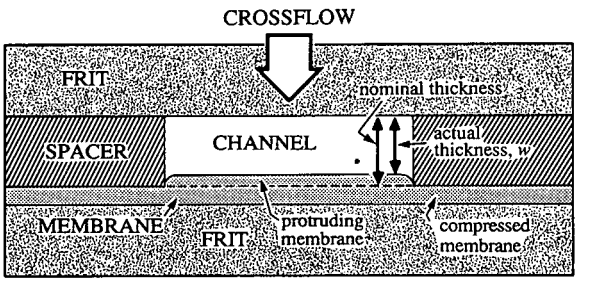

Fig. 1. Schematic cross-section (perpendicular to flow axis) of flow FFF channel showing effect of protruding membrane on channel thickness.

In order to improve void peak measurements in flow FFF (and perhaps also in other forms of FFF), it is useful to examine the flow profile over the channel thickness and its role in void peak transport. The flow profile is, of course, parabolic as illustrated in Fig. 2. Thus entrained molecules or particles will be carried along at a velocity $v(x)$ that differs from one position (expressed in terms of the distance x from the accumulation wall) to another along the transverse coordinate of the channel. If each molecule of a void probe stayed in its initial streamline, then the probe molecules would elute at widely different times because of their different velocities. In order to obtain a compact void peak, the flow velocity must be sufficiently slow that each probe molecule can diffuse numerous times across the channel in order to experience a statistical mix of all velocity vectors. However, this extended diffusion process, of necessity, brings the probe molecules to the channel walls where they may suffer unwanted retardation by the pores in the wall as described

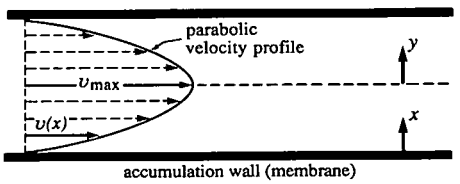

Fig. 2. Edge view of flow FFF channel showing parabolic flow velocity profile.

above. Hence the goals of obtaining a sharp and statistically meaningful void peak and of avoiding wall interactions are largely contradictory.

In view of the above contradiction, it is useful to examine the possibility of working at the other extreme where probe molecules have little opportunity for transverse diffusion before they are swept through the channel. In the limit of ultrafast flow or negligible diffusion, each probe will stay with its original streamline. The first probe molecules to appear will be those travelling at the centerline of the channel, which coincides with the apex of the parabola (see Fig. 2). In principle, the timing of these early arrivals, coupled with the assumption that the flow is parabolic, fully characterizes the fluid motion in the channel and the associated void time. This can be seen as follows.

The parabolic flow profile in an FFF channel with a rectangular cross-section of high aspect ratio can be expressed by [6]

$$v(x) = 6\langle v\rangle\left[\frac{x}{w} - \left(\frac{x}{w}\right)^2\right] \tag{2}$$

where $\langle v\rangle$ is the average cross-sectional velocity. At the center of the channel ($x/w = 0.5$), velocity v reaches a maximum value given by

$$v_{max} = \frac{3}{2}\langle v\rangle \tag{3}$$

This equation shows that the fastest probe molecules are traveling at a velocity 1.5 times greater than the average fluid velocity. Hence the time of first appearance, or breakthrough time t_b, of probe molecules will precede the void time t^0, which corresponds to the elution time of probe molecules sampling all streamlines, according to the relationship

$$t_b = \frac{2}{3}t^0 \tag{4}$$

Similarly, in view of the proportionality between time and volume, the measured breakthrough volume V_b will relate to V^0 according to

$$V_b = \frac{2}{3}V^0 \tag{5}$$

Thus, the measurement of t_b or V_b leads directly to the corresponding void parameter t^0 or V^0.

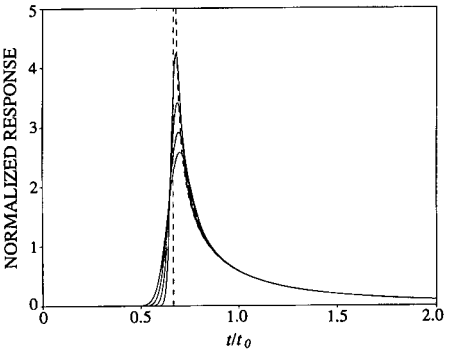

Fig. 3. Ideal peak profile (dashed curve) showing abrupt breakthrough in the zero diffusion limit, $\tau^0 \to 0$, and results of its convolution with Gaussian band spreading function for which $\sigma_t/t^0 = 0.02$, 0.03, 0.04 and 0.05.

We note that early peaks, eluting before t_0 or V^0, have been described previously in the FFF literature, but they have not been proposed as a means for determining V^0. "Leading peaks" resulting from incomplete relaxation in flow FFF were shown to precede V^0 in 1977 [7]. In discussing these peaks it was pointed out that non-diffusing particles traveling in the most rapid streamlines would elute after 67% of the void volume had been pumped into the channel. Similar peaks eluting prior to V^0 in sedimentation FFF were described in the early 1980s [8,9].

Ideally, the detector signal for a breakthrough peak will rise abruptly (see eqn. 11 and Fig. 3) at time $t = t_b$, thus giving an unequivocal measure of t_b. In practice, the abrupt rise is moderated by various non-idealities including longitudinal diffusion, finite detector response time, channel imperfections, channel end effects, finite sample size and peak broadening in the dead volume of inlet and outlet tubing and in the detector cell. We note that the dead volume must be subtracted from the experimental breakthrough volume to yield a meaningful V_b.

In addition, it is impossible to generate infinite flow-rates or to find probes with zero diffusivities to make this breakthrough procedure work perfectly. The criterion for workability, providing the above non-idealities are reduced to a minimum, can be formulated in terms of the dimensionless time given by

$$\tau = 4Dt/w^2 \tag{6}$$

where D is the diffusion coefficient of the probe material and t is the time elapsed from sample introduction. As the time required to diffuse from the center of the channel to one wall is given approximately by $t_D = w^2/8D$, the dimensionless time τ may be defined alternatively in the following terms:

$$\tau = t/2t_D \tag{7}$$

The dimensionless void time τ_0 is then given by

$$\tau^0 = \frac{4Dt^0}{w^2} = \frac{t^0}{2t_D} \tag{8}$$

This parameter is a convenient measure of the ability of probe molecules or particles to sample all stream velocities during migration through the channel. Effective sampling by means of multiple diffusive excursions requires that $\tau^0 \gg 1$. Our proposed method requires that τ^0 be kept small relative to unity such that excursions across streamlines are minimized rather than maximized. The most practical approach to achieving low τ^0 values involves the dual strategy of increasing the flow-rate in order to reduce t^0 and of choosing macromolecular or colloidal probes for which D is small.

In this study we utilize a number of proteins as probes. The diffusion coefficients and the t_D values for various proteins in a channel of typical thickness, $w = 254$ μm, are given in Table I. These t_D values range from about 2 to 11 min. These values would be four times less in a twofold thinner channel, $w = 127$ μm. Larger t_D values, if desired, could be readily obtained using colloidal latex (see later). There is no strict need for the probe material to be monodisperse and its diffusion coefficient need not be accurately known.

It is clear that the best results using the above approach will be obtained when $\tau^0 \ll 1$. However, the degree to which τ^0 must fall below unity in practice must be determined by further work. Our preliminary results (see below) suggest that τ^0 values up to 0.5, and possibly higher, can be used to obtain consistent V^0 values. We note that there are specific characteristics of the parabolic flow profile that make the criterion $\tau^0 \ll 1$ less demanding than might be expected. Specifically, the maximum of a parabolic flow profile is rather blunt, which means that a probe molecule starting at the channel centerline can diffuse a considerable fraction of channel thickness w before becoming entrained in low velocity streamlines. This is seen best by converting eqn. 2 to the form

$$\frac{v}{v_{max}} = 1 - \left(\frac{2y}{w}\right)^2 \tag{9}$$

where y (which replaces x) is the distance from the centerline (see Fig. 2). This can be rearranged to

$$\frac{2y}{w} = \left(1 - \frac{v}{v_{max}}\right)^{1/2} \tag{10}$$

Eqn. 10 can be utilized as follows. If we decide that the probe molecule must stay within a central lamina of such thickness ($2y$) that the flow velocity maintains at least 90% of its maximum velocity ($v/v_{max} = 0.9$), then eqn. 8 shows that the probe can undertake diffusive excursions that extend across almost 32% of the channel ($2y/w = 0.32$). If, more rigorously, we require that all stream velocities in the lamina be within 5% of the maximum, then $2y/w = 0.22$. A lamina containing only 1% velocity variation still leaves 10% of the channel available for diffusive displacement.

The fact that the velocity drops off only modestly as one moves away from the centerline is a great advantage to the present method of void volume determination. The first advantage, as implied above, is that probe molecules can undergo finite diffusional displacements without losing their value as breakthrough probes. Second, since the lamina in which flow velocities have only a negligible departure from

TABLE I

DIFFUSION COEFFICIENTS, D, AND DIFFUSION TIMES, $t_D = w^2/8D$, FOR SODIUM BENZOATE AND VARIOUS PROTEINS IN A 0.0254 cm THICK FFF CHANNEL AT 20°C

Probe	$D \cdot 10^7$ (cm^2/s)[a]	t_D (s)
Sodium benzoate	83.0	9.7
Ovalbumin	7.8	100
Hemoglobin	6.7	120
α-Globulin	5.2	160
γ-Globulin	4.0	200
Horse fibrinogen	1.2	670

[a] From *Handbook of Biochemistry* (CRC, 1978), except for sodium benzoate, for which D was taken from ref. 25.

the maximum velocity is fairly thick, it contains a substantial fraction of all the probe molecules initially introduced into the channel. This large breakthrough population, emerging almost simultaneously, will obviously simplify detection and measurement. More specifically, the sudden breakthrough will lead to an abrupt rise to a peak maximum in the detector signal $S(t/t^0)$, followed by a rapid drop and finally by a slowly attenuating tail representing the elution of probe molecules carried by the slower streamlines. It can be shown (see Appendix) that the ideal normalized peak profile (in the zero diffusion limit) is given by

$$S(t/t^0) = \frac{(t^0/t)^2}{(9 - 6t^0/t)^{1/2}} \tag{11}$$

which has unit area on the dimensionless time scale t/t^0. This function is valid for time $t > 2t^0/3$ and approaches infinity as $t \to 2t^0/3$. A plot of $S(t/t^0)$ is shown as a dashed line in Fig. 3.

The approach described here is equally applicable to the determination of the internal volumes of uniform straight tubes. In tubes of circular cross-section the velocity of fluid at the center line is twice the mean fluid velocity, which results in an ideal breakthrough time equal to half the void time. Ordinarily the tube should be straight because curvature gives rise to secondary flows, particularly important at high flow-rates. The secondary flows will mix the probe particles or molecules from the various regions of the tube cross-section. (Some weaker secondary flows will also be encountered in curved FFF channels.) Sampling of the various stream velocities by the probe species is thereby enhanced and the ideal sharp breakthrough curve degraded. (In order to counteract secondary flow effects in curved tubes the flow-rate would need to be limited, thus requiring that the probe species have an unusually low diffusion coefficient to keep τ_0 small.) This enhanced secondary mixing and that induced at transition points in the flow path explain why the full dead volume of connecting tubes and fittings, rather than some fraction of this dead volume, is subtracted from observed volumes in our determination of FFF channel void volumes.

The published literature concerning breakthrough curves for straight tubes of circular cross-section is far more extensive than for parallel-plate systems (see, *e.g.*, refs. 10–37). Studies were initiated by Taylor [10,11] and Aris [12], who derived the asymptotic solution for $\tau \gg 1$, where $\tau = Dt/R^2$ with R being the internal radius of the tube. Later studies were concerned mainly with the theoretical prediction and experimental observation of breakthrough curves at lower τ^0, where $\tau^0 = Dt^0/R^2$. The general behavior is well established. When $\tau^0 \ll 1$ the ideal normalized breakthrough curve for an eluted sample is described by (see Appendix)

$$S(t/t^0) = \frac{1}{2}\left(\frac{t^0}{t}\right)^2 \tag{12}$$

an equation valid when $t/t^0 > 1/2$. [We note that most studies to date have utilized on-tube detection which results in $S(t/t^0)$ decaying with $1/t$; see Caro [14] and Lighthill [15].] As τ^0 increases, the tail predicted by eqn. 12 becomes truncated because the longer residence time allows those sample components entrained in streamlines adjacent to the walls to diffuse into faster streams and elute earlier. This tendency is aided by the fact that the time for elution is greatest for these components and the shear rate of the carrier is greatest at the wall. The latter point tells us that if a particle or molecule moves a relatively small distance away from the wall it will encounter considerably faster fluid velocities. For $\tau^0 \approx 0.05$, a distinct shoulder appears on the trailing side of the breakthrough curve. For still larger τ^0, the curve takes on a bimodal form, provided system non-idealities do not mask the effect. The leading peak is due to the fast elution of material near the center of the tube and the trailing peak is due to material diffusing inward from the wall. The second peak tends to build close to the true void time as τ^0 increases. At $\tau^0 \approx 0.5$, the leading peak has a much reduced presence in the overall elution curve, and at $\tau^0 \approx 1$ the curve already is fairly well approximated by the predicted high τ asymptotic peak whose elution is centered about t^0.

Parallel-plate FFF systems are likely to exhibit a similar variation in breakthrough curve behavior at comparable dimensionless times. For instance, the effective longitudinal dispersion coefficient in tube flow was predicted [17] to reach a constant level at $\tau \approx 0.5$. In parallel-plate systems the dispersion coefficient is likewise predicted [38] to approach a constant value at $\tau \approx 0.5$. Monte Carlo simulations [39] of particle migrations in parallel-plate systems support qualitative similarity with tube flow sys-

tems. At $\tau^0 = 0.15$, the predicted breakthrough curve exhibits a sharp front and a shoulder on the trailing side. At $\tau^0 = 0.67$, a single peak was predicted with a maximum slightly preceding the theoretical void time. For intermediate τ^0, we might expect a gradual transformation which may or may not pass through a bimodal stage. The parallel-plate system results in a t_b of $2t^0/3$ as opposed to $t^0/2$ for tubular flow. The material eluting in the central region will not be as well separated from that which samples a wider range of velocity and elutes closer to t^0.

It is reasonable to suppose that provided $\tau^0 \lesssim 0.1$ for both parallel-plate and tube flow, the leading part of the breakthrough curve will correspond closely with the ideal $\tau^0 = 0$ curve. For our purposes we are not concerned with the form of the trailing portion of the elution curve.

It was mentioned earlier that, in practice, the abrupt rise in the ideal elution profile will be moderated by various non-idealities of the system. These non-idealities can be modeled by convoluting the ideal curve with a Gaussian function representing the combination of band spreading effects. The non-idealities will differ from system to system and we therefore expect the standard deviation (σ_t) for the Gaussian band spreading function to vary significantly between systems. Fig. 3 shows the results of convolution of the ideal curve for a parallel-plate system (dashed line) with Gaussian functions for which $\sigma_t/t^0 = 0.02, 0.03, 0.04$ and 0.05. As σ_t/t^0 increases, the initial rise is seen to become less steep and the peak maximum is displaced to higher t/t^0. Thus the breakthrough point becomes more difficult to identify. Fig. 3 shows that a significant error will be incurred if breakthrough is identified with the peak maximum. A still larger error will be found by equating the breakthrough time with the time of the initial observed rise of the signal. However, we observe that each of the convoluted curves appears to intersect the ideal vertical breakthrough (dashed) line found at $t/t^0 = 2/3$ at a fairly constant fraction of its maximum height. We may be able to exploit this property to determine void times and void volumes accurately even for non-ideal breakthrough curves.

To explore the above possibility in more detail, the ideal profile was convoluted with a set of Gaussian functions with σ_t/t^0 ranging from 0.004 to 0.10. The relative heights of the points of intersection with the ideal breakthrough line at $t/t^0 = 2/3$ were obtained. These are plotted in Fig. 4 as h_b/h_{max} *versus* σ_t/t^0, where h_b is the height of each curve at $t/t^0 = 2/3$ and h_{max} is the maximum height of each respective curve. The value of h_b/h_{max} increases from around 0.84 for $\sigma_t/t^0 = 0.004$ up to 0.88 at $\sigma_t/t^0 = 0.10$. Examination of typical elution profiles for non-retained, low-diffusing materials suggests that σ_t/t^0 is generally much less than 0.05 (see Figs. 3, 7, 8 and 9) and we can therefore assume that h_b/h_{max} will fall in the narrow range between 0.84 and 0.86.

The final objective, of course, is to determine the breakthrough value, $t_b = (2/3)t^0$, and hence t^0 and V^0. For small σ_t/t^0 the convoluted result differs from the ideal curve to only a small extent. The initial rise remains relatively steep and consequently the value deduced for t_b will be insensitive to the value assumed for h_b/h_{max}. Therefore, if we need to select a best overall value for h_b/h_{max} for some range of σ_t/t^0, we might expect that the favorable choice would correspond to h_b/h_{max} for the upper limit for the range of σ_t/t^0. Discrete values for h_b/h_{max} of 0.84, 0.85, 0.86, 0.87 and 0.88 were examined with regard to their accuracy in the determination of t_b, and hence t^0 and V^0. Fig. 5 shows the percentage error realized for each of these discrete values as σ_t/t^0 ranges from 0 to 0.1. As expected, if the range of interest for σ_t/t^0 extends to 0.10, then the best overall value for h_b/h_{max} is close to 0.88. If σ_t/t^0 is expected to lie below 0.05 (as we have suggested), then the best overall value will be close to 0.86. In the latter case the error in determination of void volume is pre-

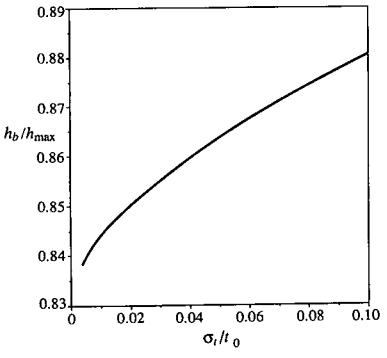

Fig. 4. Plot of h_b/h_{max} *versus* σ_t/t^0 of a Gaussian band spreading function convoluted with the ideal breakthrough curve.

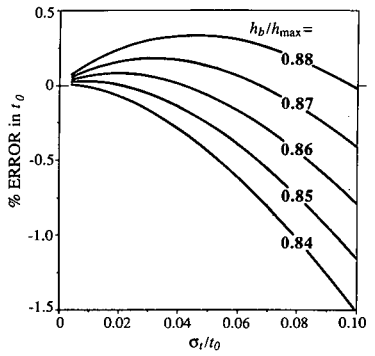

Fig. 5. Percentage error in determined t^0 as a function of σ_t/t^0 for band spreading function for each of the assumed values of h_b/h_{max}: 0.84, 0.85, 0.86, 0.87 and 0.88.

dicted to be less than 0.1% for any σ_t/t^0 less than 0.05.

Some of the experiments we report below involve the introduction of sodium benzoate as a relatively fast diffusing probe. For rapidly diffusing species the general long-time asymptotic solution obtained by Krishnamurthy and Subramanian [38] for an infinite parallel-plate system is expected to be applicable. This solution may be transformed to the following normalized function describing the predicted elution curve:

$$S(t/t^0) = \frac{t^0}{\sqrt{2\pi}\,\sigma_t}\left(\frac{t^0}{t}\right)^{1/2} \exp\left[-\frac{t^0}{t}\cdot\frac{(t^0-t)^2}{2\sigma_t^2}\right] \quad (13)$$

where

$$\sigma_t = w\left(\frac{t^0}{105D}\right)^{1/2} \quad (14)$$

Eqn. 13 requires only that $t^0D/w^2 \gg 1/8$ or $\tau^0 \gg 1/2$.

EXPERIMENTAL

Experimental measurements of void volumes were undertaken using four different channel structures. The channels were constructed by sandwiching a Teflon spacer between two wall elements. The volume cut out of the spacer constitutes the channel void volume. We designate the tip-to-tip length of the cutout section as L_{tt}, the thickness as w and the breadth as b.

To construct Channel I, the spacer was sandwiched between two transparent glass plates. The cutout dimensions are $L_{tt} = 22.5$, $w = 0.0254$ and $b = 2.0$ cm. The geometrical void volume is 0.99 ml (this is less than the product bwL_{tt} because the ends of the channel volume are tapered). Channel II is almost identical with Channel I ($L_{tt} = 22.0$, $b = 2.0$ cm) except that the spacer thickness w is 0.0127 cm and the geometrical V^0 is 0.48 ml.

Channel III is identical with Channel II except that a membrane was layered over the bottom glass wall. The membrane is Celgard 2400 from Hoechst-Celanese (Charlotte, NC, USA).

Channel IV is a conventional flow FFF channel [3,40] in which the walls are flat permeable frits. The bottom (accumulation) wall was covered by the Celgard 2400 membrane. In this case, $L_{tt} = 27.7$, $w = 0.0254$, $b = 2.0$ cm and the geometrical V^0 is 1.27 ml. For this channel, the inlet and outlet crossflow lines were joined together to prevent any displacement of liquid by crossflow during the run.

Each channel was connected by 0.787 mm I.D. tubing to an injection tee at the inlet end and the detector cell at the outlet. The inlet and outlet dead volumes were typically *ca.* 48 and *ca.* 62 μl, respectively.

Flow through the above channels was generated by an in-house syringe pump for most measurements and a Model 110B HPLC pump from Beckman Instruments (Berkeley, CA, USA) for the remaining measurements. The carrier liquid in all instances was 0.02% (w/w) sodium azide in doubly distilled, deionized water. Various proteins (listed in the tables) were used as the breakthrough probes. The proteins were complemented by a low-molecular-mass probe, sodium benzoate. All probes were injected by syringe into the inlet tubing next to the channel. The sample volumes injected were in the range 10–20 μl. The peaks were detected by a Model SPD-6A variable-wavelength detector from Shimadzu (Kyoto, Japan) with an 8-μl cell.

RESULTS AND DISCUSSION

All void volume determinations reported in Tables II–VI were based on the assumption that the sum of the dead time t_d and the breakthrough time t_b corresponds to the point on the elution curve front where $h = 0.86\,h_{max}$. Fig. 6 illustrates the interpreta-

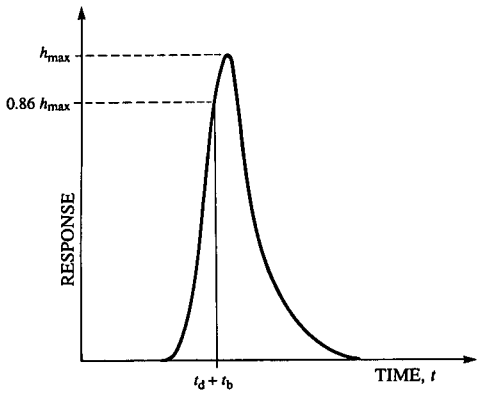

Fig. 6. Interpretation of elution curve for sample probe for which $\tau^0 < 0.1$.

tion of the elution curve for a sample probe for which $\tau^0 < 0.1$. A perpendicular is dropped to the time axis from a point on the front of the peak corresponding to 0.86 of the peak height h_{max}. The dead time t_d ($= V_d/\dot{V}$) is subtracted from the time recorded at the foot of the perpendicular to obtain the breakthrough time t_b. This subtraction is necessary because run time is measured from the time of sample injection. The void time t^0 is obtained from t_b simply by multiplying by 3/2, and the void volume is then given by eqn. 1. The reported V^0 values represent the means for several repeat runs, and standard deviations σ in V^0, where reported, were determined from a minimum of five such repeat runs. The dimensionless void times τ_0 in all tables were calculated according to nominal geometric channel dimensions.

TABLE II

VOID VOLUMES, V^0, WITH STANDARD DEVIATIONS, σ, DETERMINED FOR CHANNEL I (ASSUMING $h_b/h_{max} = 0.86$) WITH VARIOUS PROTEIN PROBES AT THE INDICATED FLOW-RATES AND DIMENSIONLESS VOID TIMES, τ^0, CALCULATED ACCORDING TO NOMINAL GEOMETRICAL DIMENSIONS

Probe	$\dot{V} = 0.55$ ml/min		$\dot{V} = 1.44$ ml/min		
	τ^0	V^0 (ml)	τ^0	V^0 (ml)	σ (ml)
Ovalbumin	0.52	1.02	0.20	1.00	0.018
Hemoglobin	0.45	1.02	0.17	0.98	–
α-Globulin	0.35	1.02	0.13	0.99	–
γ-Globulin	0.27	1.03	0.10	0.99	0.005
Horse fibrinogen	0.080	0.98	0.030	0.98	0.013

TABLE III

VOID VOLUMES, V^0, WITH STANDARD DEVIATIONS, σ, DETERMINED FOR CHANNEL II (ASSUMING $h_b/h_{max} = 0.86$) WITH VARIOUS PROTEIN PROBES AT $\dot{V} = 0.58$ ml/min AND VALUES FOR τ^0 CALCULATED ACCORDING TO NOMINAL DIMENSIONS

Probe	τ^0	V^0 (ml)	σ (ml)
Ovalbumin	0.96	0.65	0.012
Hemoglobin	0.83	0.63	0.024
γ-Globulin	0.49	0.53	0.044
Horse fibrinogen	0.15	0.45	0.019

The results for determination of V^0 for Channel I are listed in Table II. The protein probes were eluted at channel flow-rates $\dot{V}$ of 0.55 and 1.44 ml/min. The dead volume for the connecting tubing was calculated to be 0.105 ml. The overall agreement between the results is seen to be excellent, and all are close to the geometrical volume of 0.99 ml. Even the experiments with ovalbumin at $\dot{V} = 0.55$ ml/min, for which $\tau^0 \doteq 0.52$, yield a value for V^0 in good agreement with determinations using more slowly diffusing probes. It appears that at least in this instance, where the channel has impermeable glass walls, the condition $\tau^0 \ll 1$ may be relaxed considerably.

Table III shows the results obtained for Channel II. In this instance both w and the geometrical volume (0.48 ml) are reduced by a factor of 2

TABLE IV

VOID VOLUMES, V^0, WITH STANDARD DEVIATIONS, σ, DETERMINED FOR CHANNEL II (ASSUMING $h_b/h_{max} = 0.86$) USING SODIUM BENZOATE AT THE INDICATED FLOW-RATES AND VALUES FOR τ^0 CALCULATED ACCORDING TO NOMINAL DIMENSIONS

$\dot{V}$ (ml/min)	τ^0	V^0 (ml)	σ (ml)
0.51	12.0	0.69	0.014
0.97	6.1	0.66	0.021
4.24	1.4	0.57	0.013

compared with Channel I. The dead volume was calculated to be 0.100 ml. Any uncertainty in the dead volume will therefore have a larger influence on the accuracy of determined V^0 values for Channel II than for Channel I. Horse fibrinogen, for which $\tau^0 = 0.15$ at $\dot{V} = 0.58$ ml/min, yields a value for V^0 of 0.45 ml, which is close to the geometrical volume. The result for γ-globulin is slightly higher at 0.53 ml, which is reasonable even though $\tau^0 = 0.49$. Hemoglobin and ovalbumin yield still higher V^0 values, as expected considering the relatively high τ^0 for these runs. (The high τ^0 values are a consequence of the reduced channel thickness w. These τ^0 values could be reduced and accuracy improved by using more slowly diffusing probes, as explained later.)

Sodium benzoate was also introduced as a probe for Channel II. Three flow-rates, 0.51, 0.97 and 4.24 ml/min, were employed for which $\tau^0 = 12.0$, 6.1 and 1.4, respectively. The results for the determination of V^0, using the method employed for protein probes, are given in Table IV. The V^0 values determined in this way are higher than the true V^0, as expected for $\tau^0 > 1$. We note that as τ_0 is allowed to increase, the peak maximum (when adjusted for the dead time $t_d = V_d/\dot{V}$, where V_d is the total dead volume) is expected to approach the void time t^0 (see eqn. 13). The relative width of the elution peak will at the same time decrease because molecules have more time to sample all stream velocities. This effect is apparent by rearranging eqn. 14 as follows:

$$\frac{\sigma_t}{t^0} = \frac{w}{(105t^0D)^{1/2}} = \frac{2}{(105\tau^0)^{1/2}} \quad (15)$$

The net result is that the point corresponding to 0.86 h_{max} will approach t^0 (corrected for t_d) for large τ^0, rather than (2/3)t^0 as expected for small τ^0. The assumption of high τ^0 behavior would yield V^0 values equal to two third of the volumes listed in Table IV. For example, the experiments corresponding to $\tau^0 = 12$ would yield $V^0 = 0.46$ ml if high τ^0 asymptotic behavior is assumed. This value of 0.46 ml is in good agreement with the result obtained at small τ^0 with horse fibrinogen, 0.45 ml, and is close to the geometrical volume of 0.48 ml. The highest flow-rate, for which $\tau^0 = 1.4$, yields a value of $V^0 = 0.57$ ml (assuming low τ^0 behavior with $h_b/h_{max} = 0.86$). This is higher than the probable true value for V^0 and lower than the value obtained for $\tau^0 = 12.0$, which suggests intermediate behavior in which both diffusion and convection contribute significantly to transport. Such intermediate behavior, although of theoretical interest, is clearly not desirable for void volume determinations.

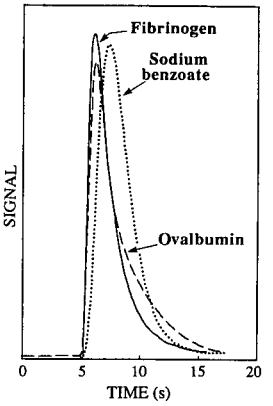

Fig. 7. Elution profiles for fibrinogen, ovalbumin and sodium benzoate sample probes injected into Channel III at a flow-rate $\dot{V}$ of 4.18 ml/min.

Fig. 7 shows typical overlayed elution curves for horse fibrinogen, ovalbumin and sodium benzoate samples injected into Channel III with a flow-rate of 4.18 ml/min. The τ^0 values were calculated to be 0.021, 0.13 and 1.4, respectively. The protein probes yield peaks that rise sharply at the front and then tail. The tails are not as extended as predicted by the plots for $\tau^0 = 0$ shown in Fig. 3. This is expected, as we explained earlier, since material will diffuse out of the regions close to the walls into faster fluid streams. The fibrinogen and ovalbumin peaks yield V^0 values of 0.45 and 0.46 ml, respectively, based on the breakthrough approach. The peak for sodium benzoate is more symmetrical and the peak maximum is retarded relative to the others. The low τ^0 breakthrough approach yields $V^0 = 0.57$ ml while the high τ^0 peak maximum approach yields $V^0 = 0.42$ ml. The former value is in good agreement with the result obtained for Channel II with sodium benzoate at $\tau^0 = 1.4$. Again, this suggests intermediate behavior since the results bracket the probable true V^0.

In Fig. 8 we show typical overlayed elution curves for horse fibrinogen, hemoglobin and sodium benzoate injected into Channel III once more, but at a reduced flow-rate of 0.55 ml/min. The τ^0 values are

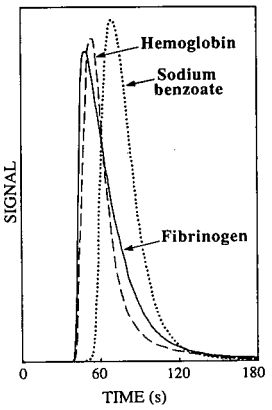

Fig. 8. Peak profiles for fibrinogen, hemoglobin and sodium benzoate in Channel III with $\dot{V} = 0.55$ ml/min.

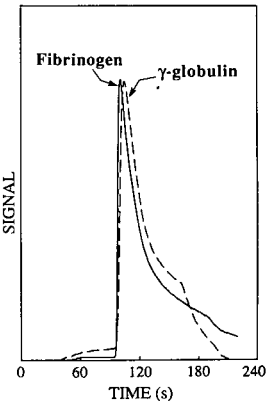

Fig. 9. Breakthrough profiles for fibrinogen and γ-globulin eluted from flow FFF channel (Channel IV) at $\dot{V} = 0.58$ ml/min.

increased relative to those in Fig. 7 by a factor of *ca.* 8, being 0.16, 0.87 and 11.0, respectively. The peak for fibrinogen rises abruptly as with the higher flow-rate, but that for hemoglobin is apparently influenced by the diffusive component to transport. The rise is less abrupt and the peak maximum is slightly retarded. The peak for sodium benzoate is more symmetric and relatively narrower than that obtained at the higher flow-rate. The reduction in relative peak width is in agreement with the prediction of eqn. 15. The dead volume of 0.103 ml (applicable to this channel) requires subtraction of a dead time t_d of 11 s. The benzoate peak maximum, eluting at 68 s, yields a void time of 57 s and thus a void volume of 0.52 ml (assuming high τ^0 behavior). Fibrinogen, on the other hand, yields a void volume of 0.46 ml (assuming low τ^0 behavior), in excellent agreement with results obtained at two other flow-rates as reported in Table V. The higher apparent V^0 for sodium benzoate may reflect diffusion into stationary fluid in membrane pores. The void volumes for Channel III determined with other protein probes at flow-rates of 1.42 and 4.18 ml/min are also given in Table V. The consistency of the results lends credence to our approach. The experimental void volume is determined to be 0.46 ml, which is just slightly smaller than the geometrical volume of 0.48 ml. The polypropylene membrane (Celgard 2400) used in this channel has an uncompressed thickness of only 25 μm. About 5 μm compression, with consequent protrusion of the uncompressed membrane into the channel, would be required to

TABLE V

VOID VOLUMES, V^0, WITH STANDARD DEVIATIONS, σ, DETERMINED FOR CHANNEL III (ASSUMING $h_b/h_{max} = 0.86$) WITH VARIOUS PROTEIN PROBES AT THE TWO INDICATED FLOW-RATES AND VALUES FOR τ^0 CALCULATED ACCORDING TO NOMINAL DIMENSIONS

Probe	$\dot{V} = 1.42$ ml/min			$\dot{V} = 4.18$ ml/min		
	τ^0	V^0 (ml)	σ (ml)	τ^0	V^0 (ml)	σ (ml)
Ovalbumin	0.39	0.47	0.007	0.13	0.46	0.004
Hemoglobin	–	–	–	0.11	0.47	0.009
γ-Globulin	0.20	0.46	0.006	0.068	0.45	0.012
Horse fibrinogen	0.060	0.46	0.005	0.021	0.46	0.004

TABLE VI

VOID VOLUMES, V^0, WITH STANDARD DEVIATIONS, σ, DETERMINED FOR CHANNEL IV (ASSUMING h_b/h_{max} = 0.86) WITH VARIOUS PROTEIN PROBES AT $\dot{V}$ = 0.58 ml/min AND VALUES FOR τ^0 CALCULATED ACCORDING TO NOMINAL DIMENSIONS

Probe	τ^0	V^0 (ml)	σ (ml)
Ovalbumin	0.64	1.31	–
α-Globulin	0.42	1.30	0.016
γ-Globulin	0.33	1.31	0.009
Horse fibrinogen	0.098	1.28	0.017

explain the difference. However, small uncertainties in channel breadth, dead volume effects, etc., may contribute to the small discrepancy.

Overlayed elution curves for horse fibrinogen and γ-globulin obtained with Channel IV at a flow-rate of 0.58 ml/min are shown in Fig. 9. The τ^0 values were calculated to be 0.098 and 0.33, respectively. The peaks are seen to rise abruptly, as observed in the previous cases. However, the trailing edges of the peaks are drawn out and distorted, probably owing to the diffusion of protein into the pores of the frits. Although the trailing edges of the peaks may be distorted by the porous walls, the leading edges appear (and according to theory should be) normal as a consequence of the fact that protein molecules starting near the channel centerline do not have sufficient time during the run to reach the walls and engage in partitioning into the pores. Void volumes determined for Channel IV with protein probes at a flow-rate of 0.58 ml/min are listed in Table VI. The agreement of the average experimental V^0 of 1.30 ml with the geometrical volume of 1.27 ml is fairly good. This suggests that the thin polypropylene (Celgard 2400) membrane does not give rise to significant compressibility problems associated with some ultrafiltration membranes that have been used in flow FFF systems [3,4].

CONCLUSIONS

The results of this study demonstrate that the void volume of FFF-like channels can be measured with reasonable consistency and accuracy based on the breakthrough time of a probe component that undergoes minimal transverse diffusion during elution. The constraint on diffusion is given by $\tau^0 \ll 1$, where τ_0 is the dimensionless ratio of the void time to twice the diffusion time as given by eqn. 8. The criterion $\tau^0 \ll 1$ can be fulfilled by using high flow-rates and/or probes with low diffusion coefficients (in more concrete and practical terms, this criterion can be stated as $\tau^0 < 0.1$).

In the studies reported we used a variety of protein molecules as probes because these high-molecular-mass components have low diffusion coefficients, in the range 10^{-6}–10^{-7} cm^2/s. For these probes in a typical 254-μm thick channel, the diffusion time is roughly 1–10 min. The requirement that $\tau^0 \ll 1$ therefore means that the void time t^0 and the breakthrough time t_b should be much smaller than these diffusion times, thus being forced down to values in extreme cases of no more than a few seconds. Although some of our results were obtained in this time frame and showed reasonable consistency, it is likely that better results could be obtained for most experimental systems (including our own) employing longer experimental times that would be less disturbed by various time constants of the system and small errors in the measurement of injection time and breakthrough time. The demand for such high-speed measurement could be most simply relaxed by using probes of even lower diffusivity. Perhaps most suitable would be polystyrene latex beads, which are available in a great range of sizes above 0.1 μm diameter. For example, a latex bead of diameter 0.436 μm at 25°C has a diffusion coefficient $D = 1.00 \cdot 10^{-8}$ cm^2/s, which is from one to two orders of magnitude less than the D values of the proteins used in this study. As shown by eqn. 8, the smaller D would allow (but not require) an increase by the same factor in t^0 without violating the condition $\tau^0 \ll 1$.

The optimum size of latex void probes would have to be established by additional experiments. We note that above *ca.* 0.5 μm diameter, hydrodynamic lift forces begin to play an important role in particle transport along the transverse axis of the channel [41]. These forces exert the greatest influence on particles close to the channel walls but, in principle, because of channel symmetry, do not disturb the trajectories of particles at the channel centerline that generate the breakthrough signal. Hence whereas lift forces may significantly alter the ideal elution profile

of Fig. 3, they may have little influence on the validity of breakthrough measurements. It may therefore be possible to use breakthrough probes exceeding 1 μm diameter. Whether or not this is actually feasible and whether there is any practical advantage of such large probes over submicrometer-size latex probes can only be answered by further experimentation.

SYMBOLS

b	Channel breadth
D	Diffusion coefficient
h_b	Height of void peak at $t = t_b$
h_{max}	Maximum height of void peak
L_{tt}	Tip-to-tip channel length
r	Radial distance from tube center
R	Internal tube radius
$S(t/t^0)$	Detector signal as function of t/t^0
t	Time
t_b	Breakthrough time
t_d	Dead time ($= V_d/\dot{V}$)
t_D	Diffusion time
t^0	Channel void time
$\langle v \rangle$	Mean fluid velocity
v_{max}	Maximum fluid velocity
$v(x)$	Velocity of flow vector at position x
$\dot{V}$	Channel flow-rate
V_b	Breakthrough volume
V_d	Dead volume
V^0	Channel void volume
w	Channel thickness
x	Distance from accumulation wall
y	Distance from channel centerline
σ_t	Standard deviation of Gaussian band spreading function
τ	Dimensionless time ($= 4Dt/w^2$ for parallel-plate systems, or Dt/R^2 for circular tubes)
τ^0	Dimensionless void time ($= 4Dt^0/w^2$ for parallel-plate systems, or Dt^0/R^2 for circular tubes)

ACKNOWLEDGEMENTS

This work was supported by Public Health Service Grant GM10851-35 from the National Institutes of Health. Supplementary support was provided by the industrially suponsored Technology Transfer Program of the Field-Flow Fractionation Research Center.

APPENDIX

A derivation of the ideal response curve for a non-retained pulse input to a parallel-plate channel, assuming negligible diffusion, is given below. In this derivation it is assumed that the sample is initially evenly distributed across the channel thickness, that the sample molecules do not migrate in a direction perpendicular to flow (by diffusion or any other means) and that the velocity of each molecule corresponds to that of the fluid occupying the same position relative to the walls. The ideal response assumes linear detector response and does not include any contribution to band spreading due to extra-channel effects.

The detector will respond to the mass per unit volume (or concentration) of solute eluted from the channel outlet. When the channel flow-rate is constant this will be proportional to the mass eluted per unit time. The elution time t for an element of fluid at a position x/w is given by

$$t = \frac{L}{v(x/w)} = \frac{L}{6\langle v \rangle \frac{x}{w}\left(1 - \frac{x}{w}\right)} \tag{A1}$$

where L is the channel length. From eqn. A1 it may be shown that

$$\left|\frac{d(x/w)}{dt}\right| = \frac{t^0}{6t^2\left(1 - \frac{2t^0}{3t}\right)^{1/2}} \tag{A2}$$

where it is required that $t > (2/3)t^0$.

The response therefore has the following proportionality:

$$\text{detector response} \propto \frac{\delta m}{\delta t} = \frac{\delta m}{\delta(x/w)}\left|\frac{\delta(x/w)}{\delta t}\right| \tag{A3}$$

where δm is the small element of mass that elutes in the small time interval δt, and as the sample is assumed to be uniformly distributed across the channel thickness, *i.e.*, $\delta m/\delta(x/w)$ must be constant, it follows that in the limit of $\delta t \to 0$ we have

$$\text{detector response} \propto \left|\frac{d(x/w)}{dt}\right| \tag{A4}$$

For convenience the response may be normalized to unit area for the dimensionless time scale of t/t^0. We obtain

$$S(t/t^0) = \frac{(t^0/t)^2}{(9 - 6t^0/t)^{1/2}} \tag{A5}$$

where $S(t/t^0)$ is the normalized response and it is again required that $t/t^0 > 2/3$.

The ideal response for a non-retained pulse input to a straight tube of circular cross-section is derived similarly. The elution time t for an element of fluid at a radial distance r from the center of the tube is given by

$$t = \frac{L}{v(r/R)} = \frac{L}{2\langle v\rangle\left[1 - \left(\frac{r}{R}\right)^2\right]} \quad \text{(A6)}$$

where R is the internal radius of the tube and L is its length. From eqn. A6 we see that for $t > t^0/2$

$$\frac{dr/R}{dt} = \frac{t^0}{4t^2\left(1 - \frac{t^0}{2t}\right)^{1/2}} \quad \text{(A7)}$$

In the case of an input pulse uniformly distributed across the tube cross-section, we have $\delta m/\delta(r/R) \propto r/R = [1 - t^0/(2t)]^{1/2}$. It follows that for elution of the sample from the tube

$$\text{detector response} \propto \frac{t^0}{4t^2} \quad \text{(A8)}$$

Normalizing this result to unit area on the t/t^0 scale, we obtain

$$S(t/t^0) = \frac{1}{2}\left(\frac{t^0}{t}\right)^2 \quad \text{(A9)}$$

where it is required that $t/t^0 > 1/2$. For $t/t^0 \leqslant 1/2$, $S(t/t^0) = 0$.

REFERENCES

1 J. C. Giddings, G. C. Lin and M. N. Myers, *J. Colloid Interface Sci.*, 65 (1978) 67.
2 J. C. Giddings, G. C. Lin and M. N. Myers, *J. Liq. Chromatogr.*, 1 (1978) 1.
3 S. K. Ratanathanawongs and J. C. Giddings, in T. Provder (Editor), *Particle Size Distribution II: Assessment and Characterization (ACS Symposium Series*, No. 472), American Chemical Society, Washington, DC, 1991, Ch. 15.
4 J. C. Giddings, S. K. Ratanathanawongs, B. N. Barman, M. H. Moon, G. Liu, B. L. Tjelta and M. E. Hansen, in H. Bergna (Editor), *Colloid Chemistry of Silica (Advances in Chemistry Series*, No. 234), American Chemical Society, Washington, DC, in press.
5 J. C. Giddings and M. R. Schure, *Chem. Eng. Sci.*, 42 (1987) 1471.
6 J. C. Giddings, *Unified Separation Science*, Wiley, New York, 1991.
7 F. J. Yang, M. N. Myers and J. C. Giddings, *Anal. Chem.*, 49 (1977) 659.
8 J. J. Kirkland, W. W. Yau, W. A. Doerner and J. W. Grant, *Anal. Chem.*, 52 (1980) 1944.
9 C. H. Dilks, Jr., W. W. Yau and J. J. Kirkland, *J. Chromatogr.*, 315 (1984) 45.
10 G. Taylor, *Proc. R. Soc. London, Ser. A*, 219 (1953) 186.
11 G. Taylor, *Proc. R. Soc. London, Ser. A*, 225 (1954) 473.
12 R. Aris, *Proc. R. Soc. London, Ser. A*, 235 (1956) 67.
13 H. R. Bailey and W. B. Gogarty, *Proc. R. Soc. London, Ser. A*, 269 (1962) 352.
14 C. G. Caro, *J. Physiol.*, 185 (1966) 501.
15 M. J. Lighthill, *J. Inst. Math. Its Appl.*, 2 (1966) 97.
16 V. Ananthakrishnan, W. N. Gill and A. J. Barduhn, *AIChE J.*, 11 (1965) 1063.
17 W. N. Gill and V. Ananthakrishnan, *AIChE J.*, 13 (1967) 801.
18 W. N. Gill and R. Sankarasubramanian, *Proc. R. Soc. London, Ser. A*, 316 (1970) 341.
19 W. N. Gill and R. Sankarasubramanian, *Proc. R. Soc. London, Ser. A*, 322 (1971) 101.
20 H. Bate, S. Rowlands, J. A. Sirs and H. W. Thomas, *Br. J. Appl. Phys. (J. Phys. D)*, 2 (1969) 1447.
21 J. S. Yu, *J. Appl. Mech.*, 43 (1976) 537.
22 J. S. Yu, *J. Appl. Mech.*, 46 (1979) 750.
23 W. N. Gill and R. S. Subramanian, *J. Appl. Mech.*, 47 (1980) 975.
24 J. S. Yu, *J. Appl. Mech.*, 48 (1981) 217.
25 M. J. E. Golay and J. G. Atwood, *J. Chromatogr.*, 186 (1979) 353.
26 J. G. Atwood and M. J. E. Golay, *J. Chromatogr.*, 218 (1981) 97.
27 K. P. Mayock, J. M. Tarbell and J. L. Duda, *Sep. Sci. Technol.*, 15 (1980) 1285.
28 B. Andersson and T. Berglin, *Proc. R. Soc. London, Ser. A*, 377 (1981) 251.
29 J. T. Vanderslice, K. K. Stewart, A. G. Rosenfeld and D. J. Higgs, *Talanta*, 28 (1981) 11.
30 J. E. Houseworth, *J. Fluid Mech.*, 142 (1984) 289.
31 C. N. Trumbore, M. Grehlinger, M. Stowe and F. M. Kelleher, *J. Chromatogr.*, 322 (1985) 443.
32 S. C. Chikwendu, *Int. J. Eng. Sci.*, 24 (1986) 1031.
33 J. S. Vrentas and C. M. Vrentas, *AIChE J.*, 34 (1988) 1423.
34 T. Korenaga, F.-H. Shen, H. Yoshida and T. Takahashi, *Anal. Chim. Acta*, 214 (1988) 97.
35 T. Korenaga, F. Shen and T. Takahashi, *AIChE J.*, 34 (1989) 1395.
36 A. Shankar and A. M. Lenhoff, *AIChE J.*, 35 (1989) 2048.
37 A. Shankar and A. M. Lenhoff, *J. Chromatogr.*, 556 (1991) 235.
38 S. Krishnamurthy and R. S. Subramanian, *Sep. Sci.*, 12 (1977) 347.
39 M. R. Schure, *Anal. Chem.*, 60 (1988) 1109.
40 J. C. Giddings, M. N. Myers, K. D. Caldwell and S. R. Fisher, *Methods Biochem. Anal.*, 26 (1980) 79.
41 P. S. Williams, T. Koch and J. C. Giddings, *Chem. Eng. Commun.*, 111 (1992) 121.

Journal of Chromatography, 627 (1992) 37–41
Elsevier Science Publishers B.V., Amsterdam

CHROM. 24 582

Correlation of the eluting strengths of solvents in adsorption chromatography with solvatochromic parameters

Dean C. Luehrs and David J. Chesney

Department of Chemistry, Michigan Technological University, Houghton, MI 49931 (USA)

Kalpana A. Godbole

Department of Mathematical Sciences, Michigan Technological University, Houghton, MI 49931 (USA)

(First received July 7th, 1992; revised manuscript received August 25th, 1992)

ABSTRACT

The Snyder measure of solvent eluting strength (ε^0) in adsorption chromatography correlates well with the molecular dipolarity/polarizability (π^*), hydrogen bond acidity (α), and hydrogen bond basicity (β) solvatochromic parameters. In addition, the δ correction term to π^* is a minor influence but statistically significant. There is also a good correlation with a combination of the donor number and acceptor number parameters. These correlations indicate that both acidic and basic sites on the alumina interact with the eluting solvent.

INTRODUCTION

The ε^0 scale of Snyder has been used for many years as a measure of solvent eluting strength in adsorption chromatography [1–3]. By the use of solvatochromic parameters in other areas of chromatography, it has been possible to find correlations which permit the estimation of retention times under a given set of conditions. In addition, often information is gained about the process not otherwise available such as the relative importance of dispersion and hydrogen bonding interactions in gas chromatography [4–13]. Krygowski *et al.* [14] reported a good correlation of ε^0 for alumina with the $E_T(30)$ parameter and a modified β (hydrogen bond basicity) parameter for 28 solvents. However, as pointed out by Park and Carr [15], the $E_T(30)$ parameter is a composite parameter of the Kamlet–Taft parameters π^* (molecular dipolarity/polarizability) and α (hydrogen bond acidity), so it is not truly a measure of a single specific solvent characteristic which complicates chemical interpretation of the results. Park and Carr [15] thoroughly studied the correlation of ε^0 values for 23 solvents with both alumina and silica as solid phases. It was indicated that for alumina, ε^0 depends on the π^* parameter, the α hydrogen bond donor (HBD), and the β hydrogen bond acceptor (HBA) parameters of Kamlet and co-workers [11–13]. In addition, there was a slight dependence on the δ polarizability correction term. However, the ratio of solvents to parameters used was not as high as desirable for firm statistical reliability [16]. Therefore, this study was initiated with the object of including as many solvents as possible in the correlation using the most recent measurements of solvent parameters as well

Correspondence to: D. C. Luehrs, Department of Chemistry, Michigan Technological University, Houghton, MI 49931, USA.

0021-9673/92/$05.00

as a very recently published methodology of reliably estimating values of solvatochromic parameters if values for closely related solvents are available [17]. It was possible to collect values for 37 solvents which greatly increases the confidence of the results as compared to the results of Park and Carr for 23 solvents [15]. Another advantage of this study is that solvents with a wider range of ε^0 and π^* were included which should also improve the statistical reliability of the results.

RESULTS

The P' solvent parameter of Snyder [18] ranks the relative eluting strength of solvents in bonded-phase partition chromatography. Although applied in completely different chromatographic modes, the relative order of the ε^0 and P' scales is similar enough to suggest a relationship.

However, when the ε^0 parameter is regressed against the P' parameter to test for a possible relationship, the result is $\varepsilon^0 = (0.127 \pm 0.012)P'$; $r = 0.877$, $s = 0.07$, $n = 34$. This indicates some correlation of the two scales but not an identity by any means.

Next the data for ε^0 were fitted to the general linear solvation energy relationship (LSER) equation of Kamlet and co-workers [11–13], $XYZ = XYZ_0 + s(\pi^* + d\delta) + a\alpha + b\beta$, where π^* is a measure of the solvent polarity/polarizability, α is a measure of the HBD strength of the solvent, and β is a measure of the HBA strength of the solvent. The δ is an index parameter which is 1.0 for aromatic solvents, 0.5 for polychlorinated aliphatic solvents, and 0.0 for other aliphatic solvents. The δ term attempts to correct for situations where the effects of solvent polarizability are different from the effects on the π^* probe. Multiple linear regression for those solvents for which data were available or the solvatochromic parameters could be reliably estimated gave $\varepsilon^0 = (0.563 \pm 0.040)(\pi^* - 0.16\delta) + (0.272 \pm 0.056)\alpha + (0.394 \pm 0.049)\beta$; $R = 0.970$, $s = 0.07$, $n = 37$ (see Fig. 1). The constant term was not significantly different from zero at the 90% confidence level. In addition, since many correlations have been observed where the molar volume, V, is significant [19–22], the dependence of ε^0 on V was tested and found to be statistically not significant.

It is observed that there is an approximately equal dependence of ε^0 on π^* and α. This explains the success of Krygowski *et al.* [14] in correlating ε^0 with the $E_T(30)$ parameter of Dimroth and Reichardt [23] and β since $E_T(30)$ has a similar dependence on π^* and α [11]. Furthermore, the β HBA parameter is known to be highly correlated with the donor number, DN, of Gutmann [11–13,24] and the acceptor number [25], AN, of Gutmann is known to also be correlated with a linear combination of π^* and α [11–13]. The AN and DN are still used by many workers, especially in Europe. In order to compare the effectiveness of the Kamlet–Taft and the Gutmann set of parameters, we carried out a correlation of ε^0 with a linear combination of DN

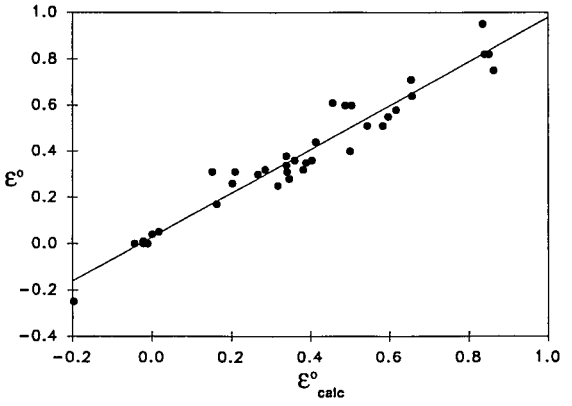

Fig. 1. Correlation of ε^0 with $0.563(\pi^* - 0.16\delta) + 0.272\alpha + 0.394\beta$.

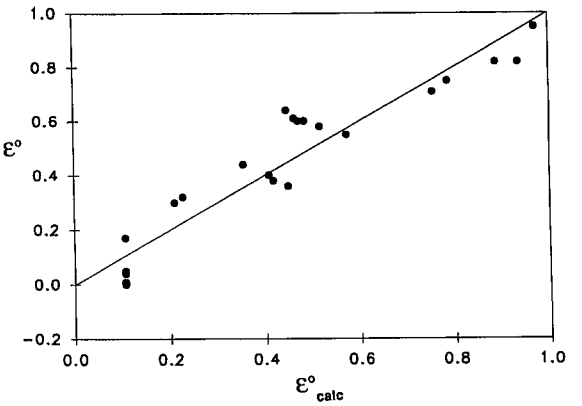

Fig. 2. Correlation of ε^0 with 0.0148AN + 0.0132DN + 0.11.

TABLE I

ε^0 VALUES AND SOLVATOCHROMIC PARAMETERS

ε^0 Values are from refs. 1, 2 and 15. π^*, α and β values are from refs. 12 and 30.

Compound	ε^0	π^*	α	β	δ	ε^0_{calc}
(1) Pentane	0.00	−0.08	0.00	0.00	0.0	−0.05
(2) Hexane	0.00	−0.04	0.00	0.00	0.0	−0.02
(3) Heptane	0.00	−0.02	0.00	0.00	0.0	−0.01
(4) Isooctane	0.01	−0.04	0.00	0.00	0.0	−0.02
(5) Cyclohexane	0.04	0.00	0.00	0.00	0.0	0.00
(6) Cyclopentane	0.05	0.03	0.00	0.00	0.0	0.02
(7) Carbon tetrachloride	0.17	0.29	0.00	0.00	0.5	0.16
(8) Toluene	0.30	0.55	0.00	0.11	1.0	0.27
(9) 1-Chloropropane	0.31	0.37	0.00	0.00	0.0	0.21
(10) Chlorobenzene	0.31	0.71	0.00	0.07	1.0	0.34
(11) Benzene	0.32	0.59	0.00	0.10	1.0	0.28
(12) Bromoethane	0.34	0.60	0.00	0.00	0.0	0.34
(13) Triethylamine	0.36	0.14	0.00	0.71	0.0	0.36
(14) Diethyl ether	0.38	0.27	0.00	0.47	0.0	0.34
(15) Chloroform	0.36	0.58	0.44	0.00	0.5	0.40
(16) Methylene chloride	0.40	0.82	0.30	0.00	0.5	0.50
(17) 1,2-Dichloroethane	0.44	0.81	0.00	0.00	0.5	0.41
(18) Tetrahydrofuran	0.51	0.58	0.00	0.55	0.0	0.54
(19) Acetonitrile	0.55	0.75	0.19	0.31	0.0	0.60
(20) 2-Butanone	0.51	0.67	0.06	0.48	0.0	0.58
(21) *p*-Xylene	0.26	0.43	0.00	0.12[a]	1.0	0.20
(22) Fluoroalkanes	−0.25	−0.35	0.00	0.00	0.0	−0.20
(23) Acetone	0.58	0.72	0.08	0.48	0.0	0.61
(24) Ethyl acetate	0.60	0.55	0.00	0.45	0.0	0.49
(25) Methyl acetate	0.60	0.60	0.00	0.42	0.0	0.50
(26) Nitromethane	0.64	0.85	0.22	0.30[a]	0.0	0.66
(27) Pyridine	0.71	0.87	0.00	0.64	1.0	0.65
(28) Dimethyl sulfoxide	0.75	1.00	0.00	0.76	0.0	0.86
(29) 2-Propanol	0.82	0.48	0.76	0.95	0.0	0.85
(30) 1-Propanol	0.82	0.52	0.78	0.85[a]	0.0	0.84
(31) Methanol	0.95	0.60	0.93	0.62	0.0	0.84
(32) Diisopropyl ether	0.28	0.27	0.00	0.49	0.0	0.35
(33) 2-Chloropropane	0.31	0.27	0.00	0.00	0.0	0.15
(34) Di-*n*-butyl ether	0.25	0.24	0.00	0.46	0.0	0.32
(35) Bromobenzene	0.32	0.79	0.00	0.06	1.0	0.38
(36) Iodobenzene	0.35	0.81	0.00	0.05	1.0	0.39
(37) Dioxane	0.61	0.55	0.00	0.37	0.0	0.46

[a] Estimated.

and AN. Correlations of solvent effects with a combination of the AN and DN have been done occasionally [25–27] although the usual practice is to do a correlation with only one of these parameters at a time. Multiple linear regression gave: $\varepsilon^0 = 0.11 \pm 0.03 + (0.0148 \pm 0.0019)$AN $+ (0.0132 \pm 0.0021)$ DN; $r = 0.949$, $s = 0.10$, $n = 24$ (see Fig. 2). All the ε^0 values and solvent parameters used in this study are given in Tables I and II.

DISCUSSION

The results of multiple linear regression using the LSER equation indicate that ε^0 has a substantial dependence on the π^* polarity/polarizability parameter as well as the α HBD and the β HBA parameters. There is a very small but statistically significant dependence on the δ polarizability index parameter. Because of the nature of the probe used

TABLE II

ε^0 VALUES AND ACCEPTOR AND DONOR NUMBERS

ε^0 Values are from refs. 1, 2 and 15. AN and DN values are from refs. 24 and 25.

Compound	ε^0	AN	DN	ε^0_{calc}
(1) Pentane	0.00	0.0[a]	0.0[a]	0.11
(2) Hexane	0.00	0.0[a]	0.0[a]	0.11
(3) Heptane	0.00	0.0[a]	0.0[a]	0.11
(4) Isooctane	0.01	0.0[a]	0.0[a]	0.11
(5) Cyclohexane	0.04	0.0[a]	0.0[a]	0.11
(6) Cyclopentane	0.05	0.0[a]	0.0[a]	0.11
(7) Carbon tetrachloride	0.17	0.0	0.0[a]	0.11
(8) Toluene	0.30	7.0[a]	0.0[a]	0.21
(9) Benzene	0.32	8.2	0.0	0.23
(10) Chloroform	0.36	23.1	0.0[a]	0.45
(11) Ether	0.38	3.9	19.2	0.42
(12) Methylene chloride	0.40	20.4	0.0[a]	0.41
(13) 1,2-Dichloroethane	0.44	16.7	0.1	0.35
(14) Acetone	0.58	12.5	17.0	0.52
(15) Ethyl acetate	0.60	9.3	17.1	0.47
(16) Methyl acetate	0.60	10.7	16.5	0.48
(17) Dioxane	0.61	10.8	14:8	0.46
(18) Nitromethane	0.64	20.5	2.7	0.45
(19) Pyridine	0.71	14.2	33.1	0.75
(20) Dimethyl sulfoxide	0.75	19.3	29.8	0.79
(21) 2-Propanol	0.82	33.6	21.5[a]	0.89
(22) 1-Propanol	0.82	37.3	21.0[a]	0.94
(23) Methanol	0.95	41.5	19.0	0.97
(24) Acetonitrile	0.55	18.9	14.1	0.57

[a] Estimated.

to measure π^* and the way the index parameter is defined, d, the coefficient of δ in the LSER equation, is never positive. Values of the coefficient of δ are always found to be in the range 0.00 to -0.40. A value of the coefficient between -0.3 and -0.4 indicates the absence of any dispersion interaction. The value of -0.16, obtained in the correlation in this study, indicates a moderate polarizability or dispersion interaction of the solvent with the alumina [28].

The results in this study turned out to be drastically different from the situation in bonded-phase chromatography where only polarity interactions are significant in determining the solvent eluting strength [9]. The substantial coefficients of π^*, α and β in the correlation of ε^0 parameter with the solvatochromic parameters indicate that polarity/polarizability, HBD, and HBA are each of importance in the adsorption of the solvent to alumina and thus its strength as an eluting solvent in adsorption chromatography. Both acidic and basic sites on the alumina must be interacting with the solvent molecule which is consistent with the behavior of activated alumina as a catalyst [29]. In contrast, adsorption on activated carbon depends on π^*, β, and the molar volume of the solvent but not on the α HBD parameter indicating that activated carbon has acidic sites but no basic sites of importance [20]. The study of Park and Carr [15] showed that adsorption on silica was similar to adsorption on alumina except that basic sites on the silica are not significant.

It was interesting that the multiple linear correlations of ε^0 with the pair of parameters AN and DN was virtually as good as the multiple linear correlation with π^*, α and β. Ordinarily, a correlation using a smaller number of parameters is much preferred, but in this case, since AN has been shown to be a composite parameter depending on both π^* and α, it is considered that the correlation with π^*, α

and β gives clearer chemical information than the correlation with AN and DN or the correlation with $E_T(30)$ and β carried out by Krygowski *et al.* [14] and Park and Carr [15].

In general, the results of this study with the larger number of solvents fully confirm the earlier work of Park and Carr [15]. The coefficients of π^*, δ, α and β are the same as those obtained by Park and Carr [15] at the 90% level of confidence. A minor difference is that the constant term XYZ_0 was not statistically different from zero in this study whereas with the smaller data set of Park and Carr [15] it was small yet statistically different from zero.

It was not realistic to assume beforehand, as Krygowski *et al.* [14] did, that polarity, HBD, and HBA ability of the solvent would each be significant in adsorption chromatography. It is unusual for as many terms of the LSER equation to be statistically different from zero as was the case in this study [11–13].

REFERENCES

1 B. L. Karger, L. R. Snyder and Cs. Horváth, *An Introduction to Separation Science*, Wiley, New York, 1973, Ch. 13.
2 L. R. Snyder, *J. Chromatogr.*, 23 (1966) 388.
3 L. R. Snyder, *J. Chromatogr.*, 16 (1964) 55.
4 J.-L.M. Abboud, R. W. Taft and M. J. Kamlet, *J. Chem. Res., Synop.*, (1984) 98.
5 P. C. Sadek, P. W. Carr, M. R. Doherty, M. J. Kamlet, R. W. Taft and M. H. Abraham, *Anal. Chem.*, 57 (1985) 2971.
6 B. P. Johnson, M. G. Khaledi and J. G. Dorsey, *Anal. Chem.*, 58 (1986) 2354.
7 M. H. Abraham, G. J. Bruist, P. L. Grellier, R. A. McGill, R. M. Doherty, M. J. Kamlet, R. W. Taft and S.G. Maroldo, *J. Chromatogr.*, 409 (1987) 15.
8 S. C. Rutan, P. W. Carr and R. W. Taft, *J. Phys. Chem.*, 93 (1989) 4292.
9 D. C. Luehrs, D. J. Chesney and K. A. Godbole, *J. Chromatogr. Sci.*, 29 (1991) 463.
10 J. Li and P. W. Carr, *13th Annual Minnesota Chromatography Forum, May 6–8, 1991, Bloomington, MN*, paper No. 2.
11 M. J. Kamlet, J.-L. M. Abboud and R.W. Taft, *Prog. Phys. Org. Chem.*, 13 (1981) 485.
12 M. J. Kamlet, J.-L. M. Abboud, M. H. Abraham and R.W. Taft, *J. Org. Chem.*, 48 (1983) 2877.
13 R. W. Taft, J.-L. M. Abboud, M. J. Kamlet and M. H. Abraham, *J. Solution Chem.*, 14 (1985) 153.
14 T. M. Krygowski, J. P. Radomski, A. Rzeszowiak, P. K. Wrona and C. Reichardt, *Tetrahedron*, 37 (1981) 119.
15. J. H. Park and P. W. Carr, *J. Chromatogr.*, 465 (1989) 123.
16 M. H. Abraham, P. L. Grellier, J.-L. M. Abboud, R. M. Doherty and R. W. Taft, *Can. J. Chem.*, 66 (1988) 2673.
17 J. P. Hickey and D. R. Passino-Reader, *Environ. Sci. Technol.*, 25 (1991) 1753.
18 L. R. Snyder, *J. Chromatogr. Sci.*, 16 (1978) 223.
19 Y. Marcus, M. J. Kamlet and R. W. Taft, *J. Phys. Chem.*, 92 (1988) 3613.
20 M. J. Kamlet, R. M. Doherty, M. H. Abraham and R. W. Taft, *Carbon*, 23 (1985) 549.
21 R. D. Cramer, III, *J. Am. Chem. Soc.*, 102 (1980) 1837.
22 C. Silipo and A. Vittoria, in C. Hansch, P. G. Sammes, J. B. Taylor and C. A. Ramsden (Editors), *Comprehensive Medicinal Chemistry*, Vol. 4, Pergamon, New York, 1990, Ch. 18.4.
23 C. Reichardt, *Solvents and Solvent Effects in Organic Chemistry*, VCH, Weinheim, 2nd ed., 1988, Ch. 7.
24 V. Gutmann, *Coordination Chemistry in Non-Aqueous Solvents*, Springer, Wein, 1968, Ch. II.
25 A. J. Parker, U. Mayer, R. Schmid and V. Gutmann, *J. Org. Chem.*, 43 (1978) 1843.
26 W. G. Jackson, G. A. Lawrence, P. A. Kay and A. M. Sargeson, *Aust. J. Chem.*, 35 (1982) 1561.
27 U. Mayer, *Monatsh. Chem.*, 109 (1978) 775.
28 R. W. Taft and M. J. Kamlet, *Inorg. Chem.*, 22 (1983) 250.
29 G. MacZura, K. P. Goodboy and J. J. Koen, in M. Grayson (Editor), *Kirk-Othmer Encyclopedia of Chemical Technology*, Vol. 2, Wiley, New York, 1978, p. 218.
30 J. E. Brady and P. W. Carr, *J. Phys. Chem.*, 89 (1985) 1813.

Journal of Chromatography, 627 (1992) 43–50
Elsevier Science Publishers B.V., Amsterdam

CHROM. 24 594

Determination of Stokes radii and molecular masses of sodium hyaluronates by Sepharose gel chromatography

Eiji Shimada and Go Matsumura

School of Pharmaceutical Sciences, Showa University, 1-5-8, Hatanodai, Shinagawa-ku, Tokyo 142 (Japan)

(First received April 10th, 1992; revised manuscript received August 25th, 1992)

ABSTRACT

On the basis of available volumes (K_{av}) of a chondroitin sulphate fraction and some proteins with known Stokes radii (R) in Sepharose (6B, 4B and 2B) gel chromatography, it was found that Ogston's equation correlating K_{av} with R was also applicable to Sepharose gel in addition to the Sephadex gel previously examined. Therefore, R values for sodium hyaluronate samples were determined in a similar manner to that already described for R values for hyaluronate oligosaccharides by Sephadex gel chromatography, using bovine serum albumin as a standard of known size and the radius (2.5 nm) of an agarose chain forming the gel networks. The molecular masses (M) of these samples, estimated from their intrinsic viscosities according to Mark–Houwink equations, were in the range $3.9 \cdot 10^4$–$3.0 \cdot 10^5$. Their Stokes radii determined by gel chromatography were in the range 5.9–14.4 nm. A simple relationship of $R = 0.030\ M^{1/2}$ was maintained for the hyaluronates with M below $1.3 \cdot 10^5$ (R = 11 nm). The plots of R against $M^{1/2}$ gave $R = 4.82 + 0.0175\ M^{1/2}$ for M above $1.3 \cdot 10^5$. By use of these relationships, the molecular mass of hyaluronate can be determined from its Stokes radius under the experimental conditions.

INTRODUCTION

In a previous paper [1] we presented a method for determining the Stokes radius (R) of a substance by use of its available volume (K_{av}) in Sephadex gel chromatography. The method is based on Ogston's equation [2]. Taking the natural logarithm of the equation gives

$$\log K_{av} = -\pi L (R + r)^2 \quad (1)$$

where, for Sephadex gel, L is the total concentration of the dextran chain expressed in length per unit volume and r is the radius of a dextran chain. K_{av} was calculated from the relationship determined by Laurent and Killander [3]:

$$K_{av} = (V_e - V_0)/(V_t - V_0) \quad (2)$$

where V_e is elution volume, V_0 is void volume and V_t is total bed volume. The term K_{av} is hereafter denoted K.

When substances A and B are chromatographed on the same Sephadex gel, the following relationship is derived from eqn.1:

$$\log K(B)/\log K(A) = \{[R(B) + r]/[R(A) + r]\}^2 \quad (3)$$

where K(A), K(B) and R(A), R(B) are available volumes and Stokes radii of A and B, respectively. It is emphasized that a complicated factor, L, in eqn. 1 is eliminated in the above ratio. If r is independent of the type of Sephadex, log K(B)/log K(A) will be constant for any Sephadex gel.

When a substance A is chromatographed on two types of Sephadex (m and n), another relationship is derived from eqn. 1 on the assumption that R(A) and r in gel m are identical with those in gel n:

$$\log K_n(A)/\log K_m(A) = L_n/L_m \quad (4)$$

This equation suggests that the ratio log K_m(A)/log K_n(A) is determined by the dextran concentrations in gels m and n.

Correspondence to: E. Shimada, School of Pharmaceutical Sciences, Showa University, 1-5-8, Hatanodai, Shinagawa-ku, Tokyo 142, Japan.

0021-9673/92/$05.00

The validity of eqns. 3 and 4, as described previously [1], was verified by gel chromatography of a series of even-numbered hyaluronate oligosaccharides on Sephadex G-25, -50 and -75. Therefore, we could determine the Stokes radius of hyaluronate oligosaccharide, R(B), using an equation obtained directly from eqn. 3:

$$R(\mathrm{B}) = R(\mathrm{A})\,[\log K(\mathrm{B})/\log K(\mathrm{A})]^{1/2} + r\{[\log K(\mathrm{B})/\log K(\mathrm{A})]^{1/2} - 1\} \quad (5)$$

where A is a substance with known Stokes radius such bovine serum albumin, and r is 0.2 nm [1,4].

We are interested in the conformation of hyaluronic acid of high molecular mass, which is generally excluded from Sephadex gels, and we therefore tried to examine whether Ogston's model is applicable to Sepharose gels, which can include the glycosaminoglycan of larger molecular size. As the usefulness of Ogston's equation was also evidenced by means of Sepharose (6B, 4B and 2B) gel filtration of some materials with known molecular sizes, R values for hyaluronate fractions covering a molecular mass range from $4 \cdot 10^4$ to $3 \cdot 10^5$ were calculated according to eqn. 5, using 2.5 nm as the radius of a straight agarose chain constituting Sepharose gel.

In this paper, we describe a method for determining the Stokes radii of sodium hyaluronates by Sepharose gel chromatography and discuss the relationships between their molecular sizes and masses.

EXPERIMENTAL

Materials

For the determination of the Stokes radius of hyaluronate by gel chromatography, it is necessary to obtain a fraction characterized by limited molecular size or mass ranges. These fractions were prepared in the following way from purified sodium hyaluronate (rooster comb) provided by Seikagaku Kogyo. The given hyaluronate had a relatively low molecular mass and was included in Sepharose 2B gel as shown by the dashed curve in Fig. 1.

Part (0.2 g) of the hyaluronate was dissolved in 20 ml of 0.2 M sodium chloride and 2-ml aliquots were chromatographed on a column (100 × 2 cm I.D.) of Sepharose 2B equilibrated with the above salt solution. The eluate was divided into four fractions (1, 2, 3 and 4), as indicated in Fig. 1, in ten identical runs. The molecular size distributions of the four

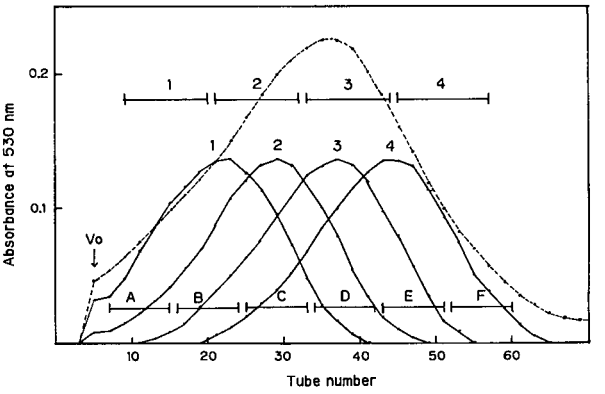

Fig. 1. Gel chromatograms of a hyaluronate preparation and several fractions obtained from it on Sepharose 2B. Samples of 20 mg of a sodium hyaluronate preparation were dissolved in 2 ml of 0.2 M sodium chloride solution and fractionated on a column (100 x 2 cm I.D.) of Sepharose 2B (dashed curve). The column eluents were divided into four fractions (1–4) as indicated. Each rechromatographic pattern of fractions 1–4 on the same column is also given (solid curve). In this instance, samples of 10 mg of a fraction were applied. These column eluents were divided into six fractions (A–F) on the basis of elution volume. All the hyaluronate samples were chromatographed with 0.2 M sodium chloride solution and fractions of 3 ml were analysed for uronic acid. The elution volume of Blue Dextran 2000, V_0, was 86 ml.

fractions were checked by rechromatography on the same column. Their elution profiles, illustrated by solid curves in Fig. 1, were still broad, so these hyaluronates were further fractionated into six fractions (A, B, C, D, E and F in Fig. 1) after rechromatography. Fractions B and E were further rechromatographed under the same conditions mentioned above; B was subdivided into three fractions (B-1, -2 and -3) and E into four fractions (E-1, -2, -3 and -4). Finally, each pooled fraction was lyophilized after dialysis against distilled water. Fraction F was not used in this experiment because of its trace amounts.

In order to obtain a chondroitin sulphate fraction with limited molecular sizes, commercial chondroitin sulphate A (Seikagaku Kogyo) was fractionated with a Sephadex G-200 column (57 x 2 cm I.D.), essentially according to the procedure of Wasteson [5]. The sulphated glcosaminoglycan (150 mg) was dissolved in 9 ml of 0.2 M sodium chloride solution and each 1.5 ml portion was applied to the column, which was eluted with the above salt solution. The eluate was divided into five groups. The corresponding fractions from six separate runs were

pooled, dialysed against distilled water and then lyophilized. The major fraction among them was employed to examine its Stokes radius.

Several proteins with known Stokes radii were also used, namely bovine serum albumin (BSA) (Sigma), soybean trypsin inhibitor and 75% clottable bovine fibrinogen (Miles Labs.), cytochrome *c* (Boehringer) and γ-globulin (United States Biochemical); their molecular radii are 3.49 [6], 2.26 [3], 10.6 [7], 1.64 [3] and 5.55 [3] nm, respectively.

Gel chromatography

Gel filtration for the determination of K was performed on Sephadex G-200 and Sepharose 6B, 4B and 2B (Pharmacia) at room temperature, using 0.01 M sodium phosphate buffer (pH 7.4) containing 0.15 M sodium chloride as the eluent, which was chosen by taking into account Wasteson's comment: on Sephadex G-200 or Sepharose 6B gel chromatography of chondroitin sulphate fractions, he emphasized that the ionic strength of the eluent was an important factor affecting their elution positions and patterns especially at low ionic strength, and recommended 0.2 M sodium chloride solution as an adequate eluent. Chromatographic columns (54–57 × 2 cm I.D.) were fitted with a sintered-glass filter disc at the bottom to facilitate the measurement of the total bed volume, V_t. The samples (1 mg for proteins and 2 mg for glycosaminoglycans) were applied in 1 ml of the buffer described above. Column eluents were collected in 2-ml fractions.

Blue Dextran 2000 (Pharmacia) of concentration 10 mg/ml was used to determine the void volume, V_0, of a given column.

Analytical methods

Hyaluronate and chondroitin sulphate samples in column eluents were detected by the method of Bitter and Muir [8]. Proteins and blue dextran were determined by absorbance measurements at 230 and 620 nm, respectively.

Molecular mass

The mass-average molecular masses (M) of hyaluronate samples were calculated from their intrinsic viscosities, $[\eta]$ (100 ml/g), according to the Mark–Houwink relationships based on the mass-average molecular mass of hyaluronic acid determined by sedimentation equilibrium described in a previous paper [9], in which the plots of log $[\eta]$ against log M suggested two linear regions below and above $[\eta] = 4.9$ corresponding to $M = 1.5 \cdot 10^5$, and therefore $[\eta] = 3.0 \cdot 10^{-6} \cdot M^{1.20}$ was used for lower $[\eta]$ and $[\eta] = 5.7 \cdot 10^{-4} \cdot M^{0.76}$ for higher values. Viscosity measurements were performed at 37°C on the glycosaminoglycan samples (E-1–4, D, C, B-1–3 and A) dialysed against 0.2 M sodium phosphate buffer (pH 7.3) with a Cannon–Manning semi-micro viscometer using 0.5 ml of the sample solution. Hyaluronic acid concentrations were calculated from the uronic acid value, using glucuronolactone as a standard, by multiplication by an experimental factor of 2.39. In order to determine intrinsic viscosities, one concentration analysis [9] using the equation $[\eta] = [2(\eta_{sp} - \log \eta_{rel})]^{1/2}/c$ derived from the combination of both equations of Huggins and Kraemer was employed. Mean $[\eta]$ values of the two concentrations (2 and 1 mg/ml for E series, 0.7 and 0.35 mg/ml for D and C, 0.5 and 0.25 mg/ml for the other fractions) are listed in Table II. Each error was less than 1%.

RESULTS AND DISCUSSION

Gel chromatography of glycosaminoglycans and proteins

Representative elution profiles of various substances on a Sepharose 2B column are given in Fig. 2. In spite of repeated fractionation by rechromatography, a series of fractions of hyaluronate still covered a wide range of molecular sizes compared with the chondroitin sulphate fraction (ChS) and commercial proteins. However, further fractionation of these hyaluronate samples (A, B-1–3, C, D and E-1–4) was not done.

Relationships between log K values for glycosaminoglycans and proteins on three types of Sepharose

Hyaluronate fractions (E-1, -2 and -3), a chondroitin sulphate fraction (ChS) and five proteins (fibrinogen, γ-globulin, BSA, trypsin inhibitor and cytochrome *c*) were separately chromatographed on Sepharose 6B, 4B and 2B, respectively. Available volumes (K) of the nine substances on each Sepharose type and log K ratios based on BSA are presented in Table I. The ratios of log K to log K(BSA) for a given substance on the three Sepharose gels

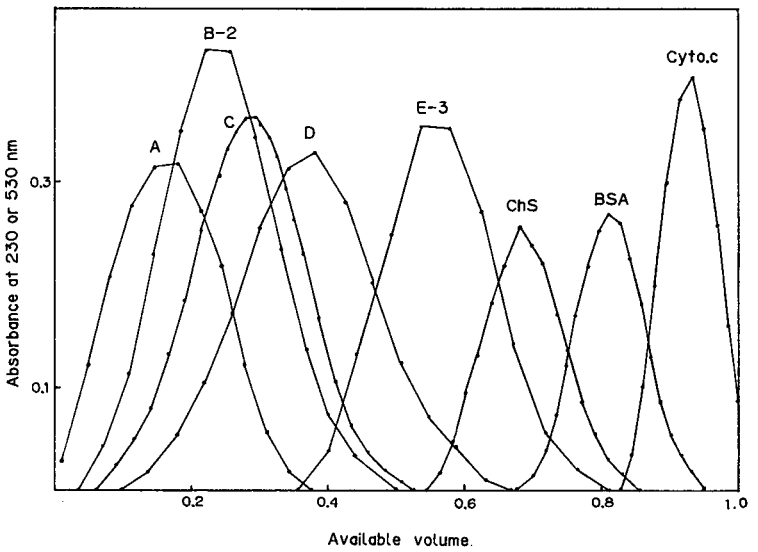

Fig. 2. Available volumes (K) of glycosaminoglycans and proteins on Sepharose 2B. Hyaluronate samples (A, B-2, C, D and E-3), a chondroitin sulphate fraction (ChS), BSA and cytochrome c (Cyto.c) were separately chromatographed on a column (54–57 × 2 cm I.D.) of Sepharose 2B. Fractions of 2 ml per tube were collected. Glycosaminoglycans were detected by the carbazole reaction and proteins by the absorbance at 230 nm.

agreed well with each other but were clearly distinct from those on Sephadex G-200. The results suggest a difference between the values of r(agarose) and r(dextran). Log K ratios of a given substance on Sepharose 2B, 4B and 6B are also shown in Table I. Mean values ± S.D. for log K_{2B}/log K_{4B}, log K_{2B}/log K_{6B} and log K_{4B}/log K_{6B} were 0.74 ± 0.02, 0.46 ± 0.01 and 0.62 ± 0.02, respectively. The constancy of the various log K ratios listed in Table I indicates that Ogston's model is applicable to Sepharose gel chromatography.

On the basis of eqn. 1, we obtain

$$(-\log K)^{1/2} = (\pi L)^{1/2} (R + r) \quad (6)$$

This equation implies that the plots of $(-\log K)^{1/2}$ against Stokes radius (R) should give a straight line for a given Sepharose gel and these lines reflecting agarose concentrations of the gels should intersect at one point on the abscissa, the absolute value of the intersection representing the radius of the agarose chain (r). We have already demonstrated the validity of Ogston's model in Sephadex gel chromatography. Therefore, the values of $(-\log K)^{1/2}$ from the data on Sephadex G-200 in Table I were plotted against the Stokes radii obtained from the literature (see Experimental); 5.5 nm as R(ChS) was determined according to eqn. 5, by a combination of 2.3 = log K(ChS)/log K(BSA) in Table I, R(BSA) = 3.49 nm and r(dextran) = 0.20 nm. As can be seen in Fig. 3, these plots suggested a straight line crossing at a point −0.2 nm on the abscissa, with the exception of γ-globulin. On the other hand, the data for six samples with known Stokes radii on Sepharose gels (Table I) were similarly plotted in Fig. 3, where we utilized 2.5 nm for r(agarose) estimated by Laurent [10]. Three points corresponding to chondroitin sulphate, BSA and trypsin inhibitor appeared to lie on a straight line, which intersected at a point −2.5 nm on the abscissa, for any Sepharose gel examined. Judging from the linearity of these points and the satisfactory value of the intercept, it seems reasonable to conclude that Ogston's equation is applicable to substances that do not interact with Sepharose gel grains. Fig. 3 shows that the estimated Stokes radii of cytochrome c, γ-globulin and fibrinogen are smaller than their reference values. Although the reason for this deviation is unknown, there is a possibility that they interact with the gel grains to retard their elution.

The notation 2B′ in Fig. 3 indicates a different lot of Sepharose 2B. The available volumes of a sample on the two lots differed from each other but the log

TABLE I

RELATIONSHIPS BETWEEN LOG K VALUES FOR GLYCOSAMINOGLYCANS AND PROTEINS ON SEPHAROSE 6B, 4B AND 2B

K values for a chondroitin sulphate fraction (ChS) and four proteins on Sephadex G-200 are also given for comparison.

Sample	2B		4B		6B		G-200		$\log K_{2B}/\log K_{4B}$	$\log K_{2B}/\log K_{6B}$	$\log K_{4B}/\log K_{6B}$
	K	Ratio[a]	K	Ratio	K	Ratio	K	Ratio			
E-1	0.32	5.1	0.21	5.2	0.08	5.3			0.73	0.45	0.62
E-2	0.45	3.6	0.35	3.5	0.17	3.7			0.76	0.45	0.59
E-3	0.54	2.8	0.43	2.8	0.25	2.9			0.73	0.44	0.61
Fibrinogen	0.62	2.1	0.51	2.2	0.35	2.2			0.71	0.44	0.64
ChS	0.68	1.7	0.60	1.7	0.43	1.8	0.08	2.3	0.75	0.46	0.61
γ-Globulin	0.76	1.2	0.69	1.2	0.56	1.2	0.15	1.8	0.74	0.47	0.64
BSA	0.80	1.0	0.74	1.0	0.62	1.0	0.34	1.0	0.74	0.47	0.63
Trypsin inhibitor	0.87	0.62	0.83	0.62	0.73	0.66	0.63	0.43	0.75	0.44	0.59
Cytochrome *c*	0.93	0.33	0.91	0.31	0.86	0.32	0.75	0.27	0.77	0.48	0.63

[a] Log K ratio based on that of BSA.

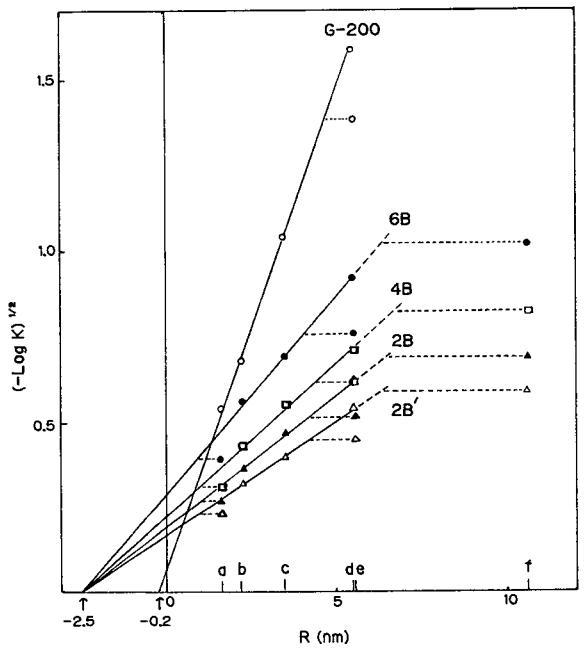

Fig. 3. Relationship between available volume (K) and Stokes radius (R) of chondroitin sulphate and protein samples on Sephadex or Sepharose gel chromatography. The plots of $(-\log K)^{1/2}$ against R are shown with the use of K values in Table I. On the abscissa, a (1.64 nm), b (2.26), c (3.49), d (5.5), e (5.55) and f (10.6) indicate R values in the literature for cytochrome c, trypsin inhibitor, BSA, a chondroitin sulphate fraction (ChS), γ-globulin and fibrinogen, respectively. Sephadex G-200 and Sepharose 6B, 4B and 2B were employed; 2B′ indicates a different lot.

K ratios based on BSA agreed well. The mean ± S.D. for $\log K_{2B}/\log K'_{2B}$ of the six samples in Fig. 3 was 1.37 ± 0.04, indicating a constant value. The observations seem to reflect the difference in agarose concentration. Similar results for $\log K$ ratios had been obtained in previous work by use of different lots of Sephadex G-15 [1].

Determination of Stokes radii of hyaluronates

Sodium hyaluronate fractions were chromatographed on a Sepharose gel column as described in the text and their Stokes radii (R) were estimated from eqn. 5 with a combination of R(BSA) = 3.49 nm and r(agarose) = 2.5 nm. R values for these fractions are summarized in Table II, together with data for the available volume (K), the intrinsic viscosity ($[\eta]$), the molecular mass (M) and the number of repeating disaccharide units (N).

Relationship of Stokes radius with molecular mass or viscosity

In order to evaluate the relationship between molecular size and chain length, the ratio of R to $N^{1/2}$ was useful (Table II). As can be seen in Table II, a constant ratio (0.60) of R to $N^{1/2}$ is observed, indicating that the Stokes radius is proportional to the square root of the number of disaccharide repeating units. In other words, R is proportional to $M^{1/2}$. This relationship is illustrated in Fig. 4 (closed circles). These plots are approximated by two linear regions below and above R = 11 nm corresponding to $M = 1.3 \cdot 10^5$. Such a downward tendency appears to reflect the downward break observed in the double logarithmic plot of $[\eta]$ against M for hyaluronic acid [9,11,12]. Cleland and Wang [11] explained the conformational change of hyaluronic acid at $M \approx 10^5$ in terms of a worm-like chain or non-Gaussian behaviour of short chains at lower molecular masses and a flexible chain or Gaussian behaviour of long chains at higher molecular masses. The equation for each line (Fig. 4) calculated by a linear least-squares method was $R = 0.030\ M^{1/2}$ for the former and $R = 0.0175\ M^{1/2} + 4.82$ for the latter. The results can be used to determine the molecular mass of hyaluronic acid from its Stokes radius estimated by Sephadex or Sepharose gel chromatography. This method has the advantage that calibration with hyaluronic acid of known molecular mass is not necessary. Fraction A had the highest molecular mass of $3 \cdot 10^5$ among the hyaluronate fractions examined and its K value was 0.17 on Sepharose 2B. Under the experimental conditions, an upper limit of M for hyaluronate measurable by gel filtration on Sepharose 2B may be $4 \cdot 10^5$, by assuming K(hyaluronate) = 0.10 and K(BSA) = 0.80.

Using the data in Table II, the relationship between R and $[\eta]$ of hyaluronic acid was investigated. The open circles in Fig. 4 are for R plotted against $[\eta]^{1/3}$. The reason for the choice of the exponent 1/3 is that intrinsic viscosity is related to the hydrodynamic volume (V_h) for spheres by $[\eta]$ = constant · (V_h/M), in which V_h is proportional to R^3. These plots gave a straight line with a correlation coefficient of 0.999. Although the molecular mass of hyaluronic acid with an appropriate size can be estimated from the R value determined by the method described in the text, the relationship among R, $[\eta]$ and M seems not to be simple for the glycosaminoglycan and remains to be elucidated.

It will also be useful to discuss our data from the standpoint of the resolution concept in size-exclusion chromatography (SEC) of polymers [13], by the use of measurable column parameters. On the assumption that each peak in Fig. 2 is approximated by a Gaussian function, standard deviations (σ) calculated for cytochrome *c*, BSA, and nine hyaluronate fractions including four (E-1, E-2, B-1 and B-3) not shown in Fig. 2 were 5.0, 6.1, and 10.0 ± 0.9 ml (mean ± S.D.), respectively. Higher values of σ for the glycosaminoglycan fractions than those for single molecular species such as protein standards are due to broad molecular mass distributions of the polymer. For BSA given in Fig. 2, the number of theoretical plates, $(V_R/\sigma)^2$, where V_R (peak retention volume) in ref. 13 corresponds to V_e (elution volume) in the text, was about 600, which was very low compared with, for instance, the plate numbers of toluene (2700–24 500) obtained using high-speed SEC by use of various types of column packings [14]. The low value appears to reflect an inherent property in a soft gel such as Sepharose. The relationship between the molecular mass of a polymer (M) and its elution volumes (V_R or V_e) is known as the SEC calibration graph [13], and this is expressed by

$$\log_{10} M = \log_{10} D_1 - (D_2 / 2.303) V_R \quad (7)$$

where D_1 and D_2 are constants. Therefore, the molecular masses of sodium hyaluronates (Table II) were plotted against their elution volumes, which were estimated by use of K values, except for E-4 (Table II) and V_0 = 52 ml found for a Sepharose 2B column (55.1 × 2 cm I.D., V_t = 173 ml). These plots were approximated by a straight line. The equation calculated by a linear least-squares method was $\log_{10} M = 6.52 - 0.015 V_R$, with a correlation coefficient 0.990. Hence, D_2 was 0.035. This small value can be ascribed to the narrow molecular mass range of hyaluronic acids separable on a Sepharose 2B column. The specific resolution R_{sp} ($= 0.58/\sigma D_2$) of the above column using D_2 = 0.035 and σ = 10.0 ml was 1.66, which means that the difference in elution volume is about 6.8 σ (68 ml) for a pair of peaks having a decade of molecular mass difference. The molecular mass accuracy (M^*), that is, the error averaged for $\overline{M}_n^*$ {$= \exp[-(\sigma D_2)^2/2] - 1$} and $\overline{M}_w^*$ {$= \exp[(\sigma D_2)^2/2 - 1$} was 6.1%, where $\overline{M}_n^*$ ($\overline{M}_w^*$) is defined as the relative number- (mass-) average molecular mass error [14]. As the error is caused by column dispersion alone, it is expected to decrease with the decrease in the molecular mass distribution of each polymer fraction.

Apart from the resolution concept of SEC, we speculate here on an error in M originating from the assumed error in the measurement of V_e. If V_e to give K in Table II has an error of 2 ml (volume per tube), the error for each K becomes about ± 0.02. On the basis of the resulting K values and a fixed K (0.80) of BSA, R and then M were recalculated. The

TABLE II

PHYSICO-CHEMICAL DATA FOR SODIUM HYALURONATES

Sample	K	$[\eta]$ (100 ml/g)	M^b ($\times 10^{-4}$)	N^c	R (nm)	$R/N^{1/2}$
E-4	0.39[a]	0.96	3.9	97	5.9	0.60
E-3	0.54	1.67	6.1	152	7.5	0.61
E-2	0.45	2.56	8.8	219	8.9	0.60
D	0.36	3.57	11.6	289	10.4	0.61
E-1	0.32	4.13	13.1	327	11.1	0.61
C	0.28	5.08	15.8	394	11.8	0.60
B-3	0.27	5.33	16.8	419	12.0	0.59
B-2	0.23	6.44	21.5	536	12.9	0.56
B-1	0.21	6.91	23.6	589	13.4	0.55
A	0.17	8.34	30.2	753	14.4	0.52

[a] K(E-4) was obtained by gel chromatography on Sepharose 6B and R(E-4) was calculated by use of K(BSA) = 0.62 given in Table I. The other K values were obtained by gel filtration on Sepharose 2B and their R values were calculated with the use of K(BSA) = 0.80.

[b] M is the mass-average molecular mass determined by sedimentation equilibrium.

[c] Number of repeating disaccharide units. N was obtained by dividing M by the average molecular mass of the unit (401 g/mol).

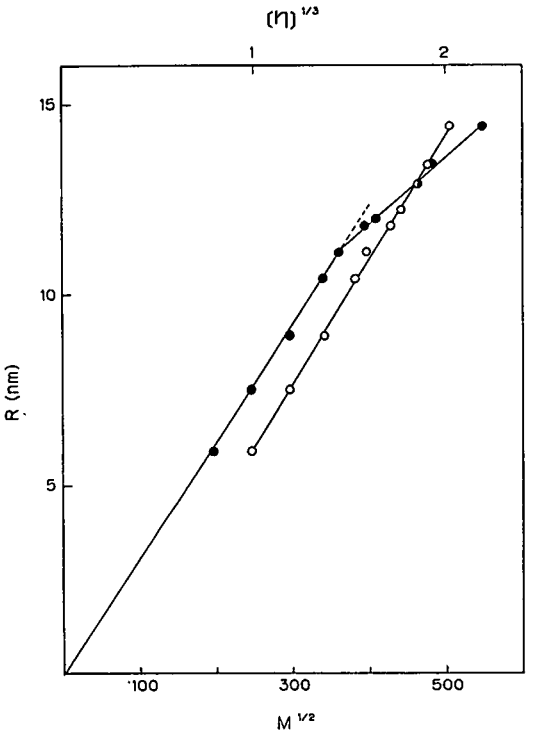

Fig. 4. Relationship between Stokes radius (R) and (●) molecular mass (M) and (○) intrinsic viscosity ([η]) of hyaluronate samples.

assumed error in the molecular mass increased with increase in M. It was approximately ± 6% and ± 10% for samples E-3 and A, respectively.

The most suitable terms (σ, D_2, R_{sp} and M^*) to express the column resolution in SEC of polymers have mainly been discussed in the field of high-speed or high-performance SEC. Therefore, it is interesting that these terms can be estimated from the chromatograms obtained using Sepharose gel filtration with a low flow-rate. These factors established in rapid SEC could also be utilized in the field of slow SEC such as Sephadex or Sepharose gel chromatography to obtain numerous data from SEC.

REFERENCES

1 E. Shimada and G. Matsumura, *J. Chromatogr.*, 472 (1989) 145.
2 A. G. Ogston, *Trans. Faraday Soc.*, 54 (1958) 1754.
3 T. C. Laurent and J. Killander, *J. Chromatogr.*, 14 (1964) 317.
4 L. M. Siegel and K. J. Monty, *Biochim. Biophys. Acta*, 112 (1966) 346.
5 A. Wasteson, *Biochem. J.*, 122 (1971) 477.
6 J. M. Creeth, *Biochemistry*, 51 (1952) 10.
7 S. Shulman, *J. Am. Chem. Soc.*, 75 (1953) 5846.
8 J. Bitter and H. Muir, *Anal. Biochem.*, 4 (1962) 330.
9 E. Shimada and G. Matsumura, *J. Biochem. (Tokyo)*, 78 (1975) 513.
10 T. C. Laurent, *Biochim. Biophys. Acta*, 136 (1967) 199.
11 R. L. Cleland and J. L. Wang, *Biopolymers*, 9 (1970) 799.
12 R. L. Cleland, *Biopolymers*, 23 (1984) 647.
13 W. W. Yau, J. J. Kirkland and D. D. Bly, *Modern Size-Exclusion Liquid Chromatography*, Wiley-Interscience, New York, 1979, Ch. 4.
14 W. W. Yau, J. J. Kirkland, D. D. Bly and H. J. Stoklosa, *J. Chromatogr.*, 125 (1976) 219.

Journal of Chromatography, 627 (1992) 51–61
Elsevier Science Publishers B.V., Amsterdam

CHROM. 24 584

"Paralogs", sorbent families for protein separations

Kálmán Benedek*, Andrea Várkonyi**, Betsy Hughes, Karen Zabel** and Lawrence M. Kauvar

Terrapin Technologies, Inc., 750-H Gateway Boulevard, South San Francisco, CA 94080 (USA)

(First received October 15th, 1991; revised manuscript received July 21st, 1992)

ABSTRACT

Novel peptide-based (paralog) sorbents are evaluated with respect to performance, reproducibility and reusability in a 96-well test plate screening format, and to utility in protein separations. The results demonstrate that this approach to constructing sorbents provides a new and generally applicable set of tools for separating proteins.

INTRODUCTION

Liquid chromatography produces physical separations by exploiting differences in affinity of dissolved analytes for a stationary phase [1]. In conventional single-mode chromatography, such as ion-exchange or hydrophobic interaction chromatography, the differential affinities of analytes is relatively small.

Higher differential affinities can be achieved by using specific antibodies or other affinity sorbents. High affinity can be a drawback for chromatography, however, because it often renders impossible the recovery of bound analytes under mild conditions which would preserve bioactivity [2] and because it eliminates moderately related variants that may be of interest. Further, the use of strong elution conditions, effectively creating a binary on/off mechanism, eliminates the opportunity to identify microheterogeneities by the traditional chromatographic process in which numerous partitioning events take place between the stationary and mobile phases.

An antibody's high specificity for its target protein relative to accompanying contaminants is attributable to (i) the molecular scale mixture of separation modes provided by the polypeptide recognition site (paratope), and (ii) the rigidity of the binding environment due to the framework structure of immunoglobulins [3]. This rigidity contributes to high binding affinities and probably accounts for difficulties in eluting bound proteins in active form. Even in the case of ion exchangers, rigid spatial localization of the binding moieties can irreversibly distort the structure of the bound protein [4].

Molecular scale multi-mode sorbents for protein separation can be created by coupling short peptides to a solid support [5,6]. Systematic diversification of sorbent characteristics can be achieved by manipulating multiple properties of the ligands described by parameters drawn from the protein structure literature [7].

The use of short peptide-based ligands as paratope analogues, or "paralogs", overcomes in principle drawbacks inherent in high-affinity sorbents while retaining the desirable feature of providing specificities that are distinct from those available in single-mode sorbents. Unlike most previous mixed-

Correspondence to: L. M. Kauvar, Terrapin Technologies, Inc., 750-H Gateway Boulevard, South San Francisco, CA 94080, USA.

* Present address: Amgen, Thousand Oaks, CA, USA.

** Present address: UCSF Medical School, San Francisco, CA, USA.

0021-9673/92/$05.00

mode sorbents (see ref. 8, where random co-polymers of amino acids as a chromatographic matrix are described. Polysorb MP-3 (Interaction Chemicals) is a mixed-mode polymeric sorbent containing both C_{18} and sulfonic acid moieties. Several varieties of Cibacron-Blue attached to DEAE- or CM-agarose are available, *e.g.* from Bio-Rad.) which combine modes at a level equivalent to bulk mixing of single mode sorbents, paralogs combine modes at the molecular size scale where binding actually occurs. Chemically synthesized paralogs may also contain non-peptide constituents which, in principle, allow the creation of specificities not possible with antibodies.

Previous assessment of paralog sorbents has been by examination of the patterns of proteins the sorbents bind, using a yeast extract as the source material and sodium dodecyl sulfate (SDS) gel electrophoresis as the analytical tool [7,9]. The qualitative conclusions from these experiments were that a variety of proteins can bind to a particular sorbent, that the same protein (or more accurately, SDS gel band) can bind to a variety of sorbents, and that the pattern of relative binding strengths to the different sorbents is characteristic of each protein, just as is true for single-mode sorbents such as DEAE-cellulose.

For the present study, a set of paralog sorbents, selected to mimic existing sorbents with varying degrees of fidelity [9], were studied in greater detail and used to establish general operating guidelines for handling these novel reagents.

EXPERIMENTAL

Reagents

DEAE-Cellulose (DEAE), CM-cellulose (CM), yeast extract, phenylmethylsulfonyl fluoride (PMSF) and all single proteins were purchased from Sigma (St. Louis, MO, USA). Affi-Gel 10 was purchased from Bio-Rad (Richmond, CA, USA). Paralog sorbents were synthesized at Terrapin Technologies (South San Francisco, CA, USA). Paralog sorbents each consist of a single paralog peptide coupled to N-hydroxy-succinimide activated agarose (Affi-Gel 10) at a particular loading density, generally *ca.* 4 μmol/ml sorbent settled bed volume (SBV) unless otherwise indicated. The coupling of paralogs to the agarose support was performed, with minor modifications, according to the manufacturer's recommendation. After completion of the coupling reaction, the remaining non-attached paralog was quantitated by HPLC. The difference between the initial peptide amount in the reaction mixture and the amount present post-coupling, after washing the beads, was considered to be covalently attached to the agarose sorbent. All peptides were synthesized by Multiple Peptide Systems (La Jolla, CA, USA), Advanced Chemtech (Louisville, KY, USA) or Coast Scientific Products (La Jolla, CA, USA).

A slurry of each sorbent was placed in replicate wells of a membrane-bottomed (flow-through) 96-well test plate (Silent Monitor, Pall Biosupport Corporation, Glen Cove, NY, USA) effectively creating miniature "columns" of 150 μl SBV. The wells of such sorbent plates were filled with storage buffer and the plates sealed and refrigerated until further use.

Collection plates (Falcon) were pretreated with Tween-20 to block protein adsorption to the plastic surfaces. The protein contents in the flow-through and retained-eluted fractions were determined using the Bio-Rad protein assay, adapted to the 96-well plate format; absorbances were read in a Vmax Plate Reader using SOFTmax software for curve fitting (Molecular Devices, Menlo Park, CA, USA). Homologous protein was used to generate a standard curve for each protein.

Paralog structures

The properties of the side chains of the various paralogs are summarized in Table I. An N-terminal amino acid spacer is present in all cases, the free amino group of which is used for coupling to the sorbent. With the exception of P3 and P7, this residue is α-aminoisobutyric acid (aib); for P3 and P7, it is 2-aminobutyric acid (2ab). In all cases, the C-terminus is capped with an amide group. Hydrophobic amino acids used (phenylalanine, alanine, valine) are D-isomers. Positive (ornithine), negative (aspartate) and neutral hydrophilic residues (serine) have the shortest length side chains readily available. Intra-chain cyclization is via a disulfide bond between two cysteine residues.

Using the standard three letter codes for the amino acids, along with the abbreviations noted above, the structures of the paralogs used in this study are

TABLE I

PARALOG STRUCTURES

Short peptides attached to a solid support allow proteins to bind to the sorbent through a controlled mixture of binding modes. Side chain properties (positive or negative, hydrophilic or hydrophobic) for sorbents that mimic conventional ion exchangers to varying degrees are illustrated. Internal cyclization via disulfide bonds are also indicated.

Paralog sorbent	Charge structure	Paralog sorbent	Charge structure
P1	+++++	P6	-----
P2	++OO++	P7	Δ----Δ
P3	Δ++++Δ	P8	Δ-++-Δ
P4	ΔO++OΔ	P9	H--OO+
P5	-H+++O	P10	HHOHH

as follows: P1 = aib–Orn–Orn–Orn–Orn–Orn; P2 = aib–Orn–Orn–Ser–Ser–Orn–Orn; P3 = 2ab–Cys–Orn–Orn–Orn–Orn–Cys; P4 = aib–Cys–Ser–Orn–Orn–Ser–Cys; P5 = aib–Asp–Ala–Orn–Orn–Orn–Ser; P6 = aib–Asp–Asp–Asp–Asp–Asp; P7 = 2ab–Cys–Asp–Asp–Asp–Asp–Cys; P8 = aib–Cys–Asp–Orn–Orn–Asp–Cys; P9 = aib–Phe–Asp–Asp–Ser–Ser–Orn; P10 = aib–Tyr–Ala–Gly–Ala–Tyr.

Buffers

The standard buffer used for preparing the sorbent slurries and sample loading was 10 m*M* Tris–HCl, pH 7.5, 1 m*M* EDTA (TE). The standard elution buffer was 10 m*M* Tris–HCl, pH 7.5, 1 m*M* EDTA, 1000 m*M* NaCl (TEN-1000). In fractionation experiments, we used TE- and NaCl-based elution buffers where the NaCl concentrations (m*M*) are indicated by the number following TEN-. For long-term storage of the sorbent plates, 2% glycerol and 0.01% sodium azide in TE was used. All reagents and steps were at room temperature.

Chromatography in the 96-well test plate format

The storage buffer was removed from the sorbent plate by centrifugation into an empty 96-well plate. The columns were washed with 200 μl TE three times. Centrifugation steps to drain the plates were performed on a Beckman TJ-6 centrifuge (Beckman Instruments, Fullerton CA, USA), equipped with 96-well test plate carriers, at 750 *g* (*ca.* 2000 rpm) for 2 min. The columns were then equilibrated in TE by the addition of 200 μl TE and incubation for 15 min. Excess buffer was again removed by centrifugation.

For binding profile experiments, 50 μl of a purified protein solution (1 mg/ml in TE buffer) were loaded onto each column in the sorbent plate. The plate was incubated at room temperature for 15 min to allow adsorption of the sample to the chromatographic sorbents, after which 50 μl of TE was added to each well and the buffer and unbound sample collected by centrifugation into a 96-well plate. An additional 50 μl TE were added to each well and removed by centrifugation into the same collection plate. This microplate then contained *ca.* 150 μl of unbound or flow-through (FT) protein fraction.

Proteins bound to the chromatographic sorbents were typically eluted by the addition of 75-μl TEN-1000 to each column and equilibration for 15 min at room temperature. The eluted proteins were collected into a second pretreated microplate by centrifugation. A second 75-μl TEN-1000 equilibration and elution step was performed, collecting into the same plate. These samples are the TEN-1000 retained-eluted (RE) fraction. The plates were washed with 6 *M* urea and re-equilibrated in TE prior to loading the next protein samples.

Affinity binding constant measurement

Equal volumes (200 μl) of a bovine serum albumin (BSA) solution series at varying concentrations (2.5, 5.0, 10.0, 20.0 and 50.0 mg/ml) were loaded onto 80-μl SBV "columns" of DEAE and 200-μl SBV "columns" of paralog sorbents P3 and P4 at a ligand density of *ca.* 14 μmol/ml SBV. After incubation for 15 min, the sorbents were washed with TE buffer to remove the non-adsorbed BSA. The adsorbed BSA was then eluted with TEN-1000 buffer and the protein concentration of the fraction determined. Adsorption isotherms were constructed and affinity binding constants calculated by Scatchard analysis [10].

Yeast extract prefractionation

Yeast extract, a whole cell acetone lysate, was dissolved in TE (180 mg solid in 2 ml buffer) with 10 μl of freshly prepared 50 m*M* PMSF added as a

protease inhibitor. After centrifugation at 10 000 *g* for 10 min, the sample solution was loaded on a 5-ml SBV DEAE-cellulose column and washed with 80 ml loading buffer. The adsorbed proteins were eluted with approximately 100 ml TEN-200 buffer, dialyzed against distilled water and lyophilized. This protein mixture was then used as starting material for further fractionation experiments comparing the performance of DEAE-cellulose and selected paralog sorbents, again using the microplate format for sequential step gradient elutions. For these experiments, all fractions were collected, dialyzed, lyophilized and then analyzed by SDS-polyacrylamide gel (10%) electrophoresis (PAGE) [11] using silver staining [12] as the visualization technique.

RESULTS

As detailed in the Experimental section, we developed a protocol that allows rapid evaluation of the adsorption characteristics of a large number of sorbents in parallel experiments. The key to this technique is use of a flow-through 96-well test plate, a device orginally developed for immunochemistry assays on large numbers of parallel samples and thus well adapted for efficient processing using tools such as multi-channel pipettors and 96-well plate readers. We selected BSA for our standard protein because of its widespread occurrence in the biotechnology industry, as a contaminant in fermentation products and assays, and as a stabilizer in drug formulations.

Diversification of sorbent characteristics was created by starting with a homopolymer of an amino acid and then substituting amino acids with other properties for particular positions [9]. Variations in ligand structure were tested which involve the absolute number and the spacing of substitutions as well as the extent to which the substitution differs in properties from the dominant monomer. A third parameter which was varied was stabilization of the backbone conformation by an intramolecular cross-link.

The paralogs examined in this paper were chosen to deviate to varying extents from traditional single-mode exchangers (Table I). Paralog sorbents P1, P2, P3, P4 and P5 represent new anion-exchange-like sorbents, designed to deviate from DEAE-cellulose to varying extents. Paralog sorbents P6 and P7 are designed to be cation-exchanger variants that deviate from CM-cellulose. P8 and P9 are mixed property sorbents and P10 is a hydrophobic paralog sorbent. Complete structures are provided in the Experimental section above. Ethanolamine-blocked Affi-Gel 10 (AFG) served as a "negative control".

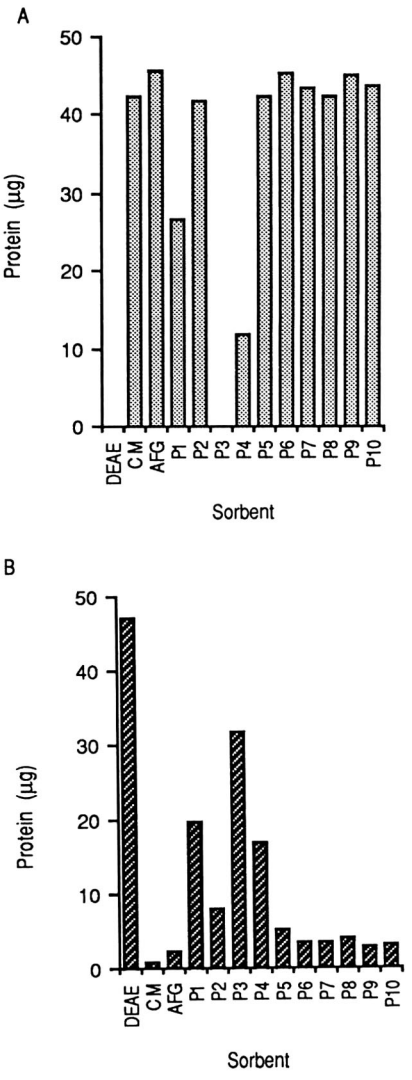

Fig. 1. Binding profile of BSA on a sorbent plate. (A) amount of BSA in the flow-through fraction (FT); (B) retained and eluted (RE) fraction. The sorbent plate contains DEAE- and CM-cellulose, and Affi-Gel control (AFG), and ten different sorbents prepared by coupling paralogs to Affi-Gel 10.

Protein binding profiles

The test protocol was designed to provide basic information on the adsorption, elution and recovery profile of single proteins. The two step protocol provided the amount of material which does not bind to the paralog sorbents and the amount of material which can be eluted from the columns under such conditions that maximum recovery is expected. The protein concentration in the FT and the RE fractions allow calculation of the mass balance of the procedure. Similarly, activity balance and/or composition analysis can be performed on the fractions.

The characteristic binding profile of BSA to the paralog sorbents is shown in Fig. 1. For comparison, the binding profile includes the adsorption of BSA to DEAE-cellulose, CM-cellulose and ethanolamine-blocked Affi-Gel (AFG). The amounts of BSA in the FT and the RE fractions for each sorbent are shown in Fig. 1A and B, respectively. Under these experimental conditions, DEAE-cellulose and paralog sorbents P1, P3, and P4 bind a significant amount of protein while CM-cellulose and the control AFG do not bind BSA.

Reproducibility of the protein binding profile protocol

Since the sorbent plate is not a standard chromatography format, we evaluated the plate-to-plate reproducibility. A 50-μg amount of BSA was loaded into each well and eluted according to the standard protocol. Using three different sorbent plates, we calculated the amount of protein in the FT and the RE fractions (Table II). The average relative standard deviation for the FT and RE fractions with significant protein content was *ca.* 15%. The mass balance averaged to 88% of starting material for all sorbents.

Reusability of the sorbent plates

Since short peptides are not subject to denaturation, it should be possible to regenerate the sorbents by stripping all bound proteins with a strong denaturant. To test this expectation, the sorbents from the previous experiment were treated with 6 *M* urea, re-equilibrated in TE, and tested again for their ability to bind BSA. A total of five binding/elution/regeneration cycles were performed on three different sorbent plates. Typical results, from one plate, are diagrammed in Fig. 2 in a three-dimensional

TABLE II

PLATE-TO-PLATE REPRODUCIBILITY

The BSA screening profile against the paralog sorbents illustrated in Table I provides the micrograms of total protein recovered in the flow-through and retained fractions, out of 50 μg applied. All sorbents have high % protein recovery except P3 and P4, the sorbents which have the highest affinity for BSA. The results for three plates were averaged for each determination.

Sorbent	Flow-through			Retained-eluted			Total protein		
	Average	S.D.	Recovery (%)	Average	S.D.	Recovery (%)	Average	S.D.	Recovery (%)
DEAE	0.0	0.0	0	47.3	4.4	95	47.3	4.4	95
CM	42.2	9.2	84	0.8	0.9	2	43.0	8.5	86
AFG	45.6	2.8	91	2.2	1.9	4	47.8	4.7	96
P1	26.7	2.6	53	19.7	1.6	39	46.4	3.8	93
P2	41.8	2.5	84	8.0	0.8	16	49.7	1.7	99
P3	0.0	0.0	0	31.7	1.7	63	31.7	1.7	63
P4	11.9	6.5	24	16.8	3.5	34	28.7	8.3	57
P5	42.3	2.6	85	5.0	1.3	10	47.3	2.6	95
P6	45.2	1.5	90	3.5	1.8	7	48.7	1.6	97
P7	43.3	3.5	87	3.5	3.0	7	46.8	6.4	94
P8	42.3	3.2	85	4.1	3.2	8	46.4	6.3	93
P9	45.2	3.3	90	3.0	1.3	6	48.2	4.5	96
P10	43.8	8.0	88	3.1	0.7	6	46.9	7.3	94

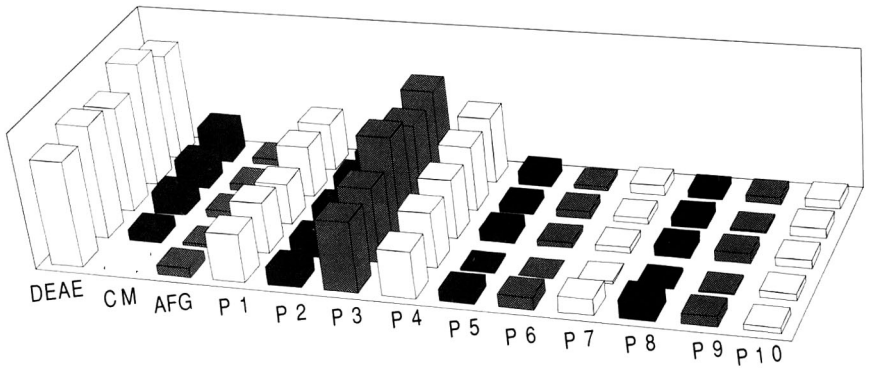

Fig. 2. Reusability of the sorbent plates. BSA retained and eluted profiles on a sorbent plate, determined as in Fig. 1, are conserved through five cycles of screening and sorbent regeneration.

bar-chart which displays the BSA binding profile on a panel of sorbents across five successive cycles.

Protease resistance of the paralog sorbents

A concern regarding re-use of paralog sorbents is the inherent protease sensitivity of peptide ligands. The paralog sorbents examined here have both N and C termini blocked; they also incorporate several non-standard amino acids. To test the efficacy of these features in hindering proteolysis, the BSA binding capacity of fresh paralog sorbents was compared to that of sorbents incubated with 1 mg/ml trypsin solution for 30 min. The acitivity of the trypsin solution was confirmed in parallel experiments by observing release into solution of dye from azocoll, an insoluble dye–protein conjugate [13]. After removing the trypsin, washing the sorbents with 6 *M* urea and re-equilibrating the sorbent plate in TE buffer, we repeated the BSA binding experiment. The amount of BSA bound was comparable to that shown in Table II indicating that at least those paralog sorbents which bind BSA are resistant to proteolysis. During a different set of experiments, we saw that trypsin treatment of plates used many times with a variety of proteins helped to restore the BSA binding characteristics, presumably by degrading irreversibly bound protein (data not shown).

Binding profiles of a panel of single proteins

After establishing the reproducibility of operations with BSA, we used the standard protocol to determine the binding profile of several other commercially available purified single proteins. The binding experiments were performed at least three times for each protein. Periodically, BSA was run on the plates as a quality assurance marker. The BSA profiles were similar to Table II providing additional evidence for reusability of the plates. Fig. 3 displays the binding profile of several proteins on DEAE-cellulose, CM-cellulose, blocked Affi-Gel, and the paralog sorbents. For this figure, the results are presented as a transformed bar chart in which the height of the bars have been transferred into gray scale values. We established five levels on the gray scale, which correspond to <5, 5–15, 15–25, 25–35 and >35 μg adsorbed protein out of the 50 μg applied. Fig. 3 thus allows data for all three parameters to be easily visualized: 13 sorbents $\times$ 10 proteins $\times$ 5 qualitative adsorption values.

Measurement of the affinity binding constant

The binding affinity of BSA for two paralog sorbents was determined in TE buffer using standard Scatchard analysis [10]. The results (Fig. 4) indicate that the sorbents provide binding strengths comparable to traditional ion-exchange resins, *ca.* 10^4 M^{-1}, a range that also characterizes low to moderate affinity antibodies [14]. The affinity of protein–paralog interactions is thus in the range which is typically used for chromatographic resolution of similar proteins by repeated differential partitioning, a process not generally possible in the on/off step elution mode of traditional affinity chromatography using high-affinity ligands.

At a ligand density of 14 μmol/ml of paralog sor-

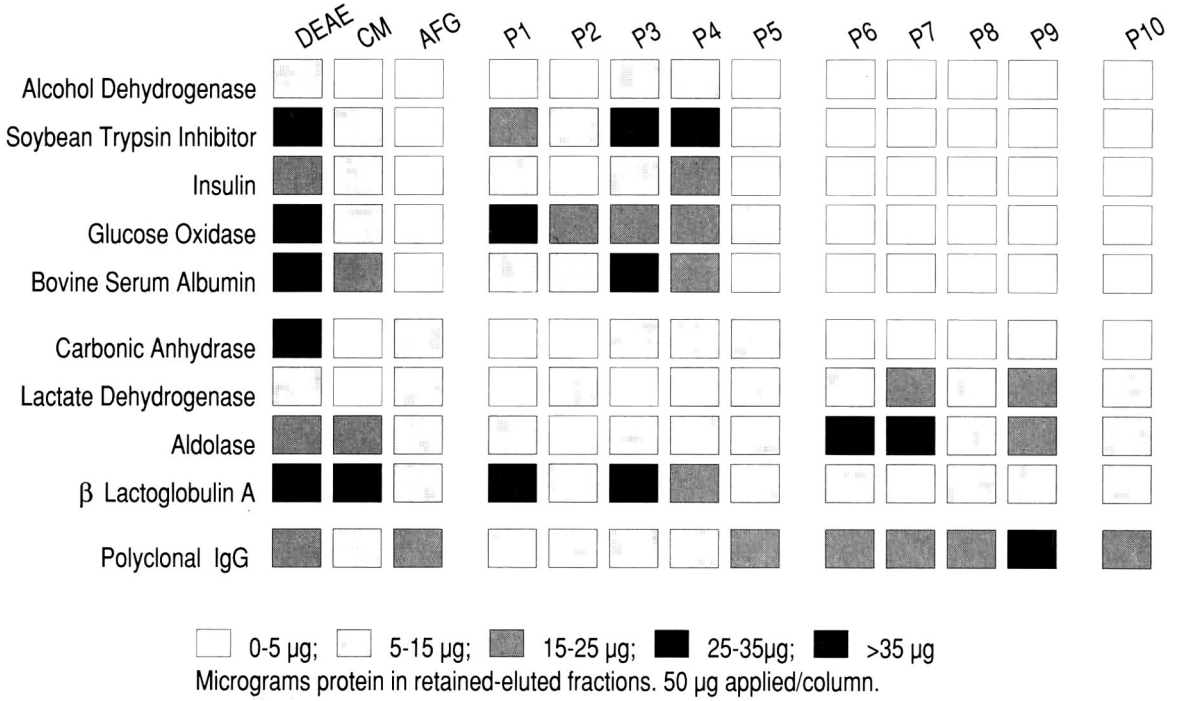

Fig. 3. Comparative binding profiles of single proteins. The squares represent the amount of protein retained on the sorbents: the darker the square, the more protein retained and eluted from the sorbent; in all cases, 50 μg of protein was applied.

bent, the capacity of P3 for BSA is about 13% the capacity of a comparable amount of DEAE-cellulose, in reasonable accord with the fact that the number of positive charges is about 9% that of DEAE-cellulose. Independently prepared batches of paralog sorbents, with constant amount of paralog put into the coupling reaction, yielded sorbents with equal ligand densities to within the accuracy of the determination. For these experiments, the amount of ligand conjugated to the solid support was estimated from the difference between ligand added to the conjugation reaction and ligand recovered free in solution following the reaction. As a functional test, two independently prepared batches of P4 were used to generate BSA binding profiles, with the results matching to within the precision of the determination. A second pair of sorbents using paralog P4 was also prepared with half the amount of ligand put into the coupling reaction resulting in approximately half the amount of ligand attached to the solid phase; the maximal binding for BSA to these sorbents was reduced appoximately by half compared to the higher ligand density sorbent.

Application of paralog sorbents to sequential fractionation of a complex protein mixture

Differential binding profiles of proteins is expected to aid in protein purification. To further examine the utility of the novel sorbents in a model protein fractionation system, a complex mixture of yeast proteins was first fractionated on DEAE-cellulose using a steep NaCl gradient. The protein fractions were eluted with 0, 20, 50, 80, 100 and 140 m*M* NaCl in TE buffer. The 80 m*M* NaCl fraction was then dialyzed against TE. Following a commonly practiced protein purification strategy, that fraction was then re-fractionated on DEAE using a shallower NaCl gradient (10, 20, 30, 40, 50, 60, 70, 80, 90 and 100 m*M* NaCl) to provide higher resolution. In parallel, other aliquots of the same fraction were chromatographed on paralog sorbents P3 and P4, anion-exchange variants. The use of a flow-through microplate, following the protocol described above for single protein profile determinations, helped to insure that these parallel processing steps were conducted under identical conditions. Three wells of each sorbent were used, and fractions pooled, to

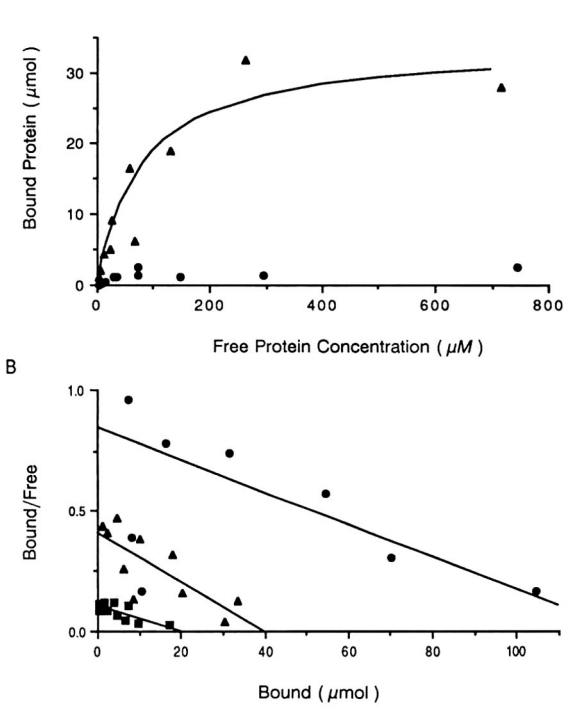

Fig. 4. Adsorption isotherm of BSA on DEAE-cellulose, P3 and P4. (A) specific BSA binding, in μmol, on sorbent P3 (▲) and a blank Affi-Gel control (●). (B) Scatchard analysis of these data along with comparable data for P4 (■) and DEAE (●) (▲ = P3). The paralog ligand density on the sorbents was 14 μmol/ml SBV. The calculated affinity constants for BSA binding are: $1 \cdot 10^4\ M^{-1}$ (P3), $5 \cdot 10^3\ M^{-1}$ (P4), $7 \cdot 10^3\ M^{-1}$ (DEAE). The maximal binding in the DEAE case is 2.5 × larger than the graph shows because a 40% smaller settled bed volume of DEAE sorbent was used than in the paralog cases.

provide enough capacity for the sequential fractionation experiments.

The SDS-PAGE analysis of the resulting fractions are provided in Fig. 5. A constant proportion of each fraction was loaded onto the gel, thus resulting in certain lanes being overloaded with regard to optimal staining for visualization of individual bands but allowing clear visualization of the differences in overall binding between the various fractions. The differences in selectivity between DEAE and the paralog sorbents are clearly illustrated in Fig. 5B. The ionic strength necessary for the elution of the protein mixtures is lower on the paralog sorbents than on DEAE-cellulose. The composition differences of the coresponding fractions (*e.g.* same ionic strength) collected from P3 and P4 are also distinct.

To further compare the utility of the differing selectivities provided by the family of paralog sorbents, we selected the 50 m*M* NaCl fraction from the secondary separation on P3 and, following dialysis against TE, subjected it to a tertiary fractionation on sorbent P4. Similarly, the 50 m*M* NaCl fraction from P4 was applied to P3. The proteins in these tertiary fractionation steps on both paralog sorbents were eluted with a salt gradient containing 30, 40, 50 and 80 m*M* NaCl steps. The SDS-PAGE analysis of these fractions are displayed in Fig. 5C. It is evident that the composition of the analogous fractions are significantly different. These observations indicate that consecutive purification steps on different paralog sorbents can provide favorable selectivity for a variety of proteins.

DISCUSSION

The availability of sorbents that deviate to varying extents in binding properties from conventional ion-exchangers is expected to be of general utility in protein purification due simply to the differences themselves, quite apart from the absolute specificity that the sorbents offer, because the differences allow sequential separation of a variety of contaminants. The data provided here show, for both individual purified proteins and for the many different proteins in a yeast extract, that one protein's binding affinity to each member of a panel of paralog sorbents is largely uncorrelated with the binding affinity of other proteins for each member of the same panel. By contrast, conventional sorbents of the same "type", such as anion exchangers of strong, medium, and weak varieties, show a high degree of correlation in binding pattern to the panel of one protein compared to other proteins, with essentially all analytes binding more tightly to the strong form at a given pH.

Because paralogs differ in both character of binding motifs and their spatial distribution, individual proteins were expected to show less uniformity in their binding profiles across a panel of paralog sorbents than against a panel of sorbents differing in only one parameter. The experiments reported here document the validity of this hypothesis and thereby establish the generalized applicability of the pa-

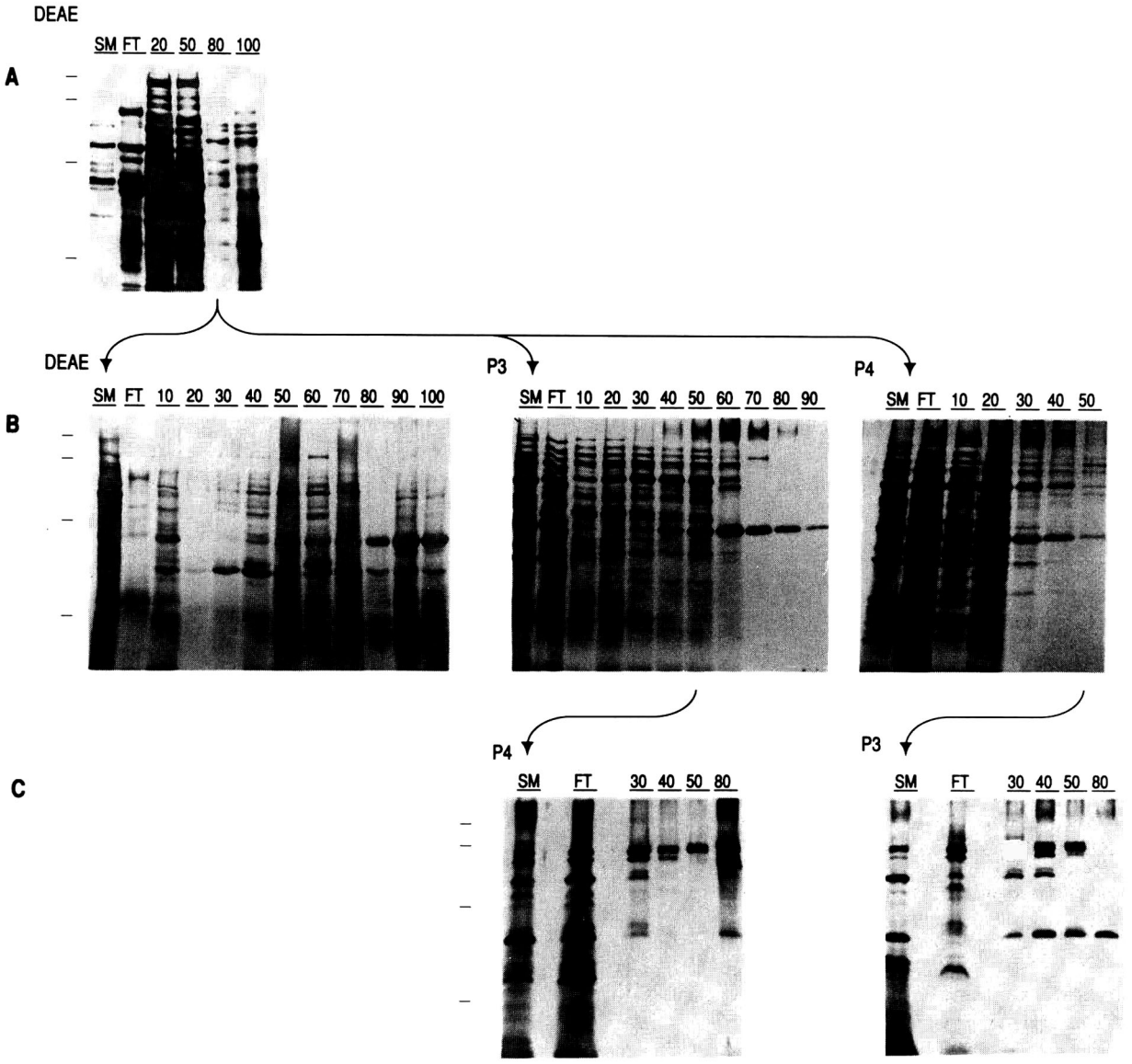

Fig. 5. Fractionation of a yeast cell lysate by sequential purification. First lanes are the starting material (SM), second lanes are the flow-through fractions (FT) and the numbers over the remaining lanes indicate the NaCl concentration (m*M*) of the elution buffer. SDS-PAGE (10%) and silver staining was used to visualize the fractionated protein patterns. Equal-sized aliquots of each fraction were loaded on the gel, resulting in some overloading of lanes for fractions with very high protein contents. Molecular mass markers (Bio-Rad, pre-stained) are M_r 80 000, 49 500, 32 500 and 18 500. (A) Primary fractionation of yeast proteins on DEAE-cellulose sorbent. (B) Secondary fractionation of yeast proteins on DEAE-cellulose, P3 and P4; (C) Tertiary fractionation of yeast proteins on sequentially run paralog sorbents. The 50 m*M* eluate on P3 from (B) was loaded onto P4; likewise, the 50 m*M* eluate on P4 from (B) was loaded onto P3.

ralog concept. By providing molecular scale combinations of known single-mode separations, analogous to that furnished by antibody binding sites (paratopes), paralogs allow a wide range of separation characteristics useful for distinguishing proteins. The set studied here mimics conventional ion

exchangers to varying degrees. Additional sets can in principle also be produced, centered on other structural motifs. Such reagents offer a number of advantages in purification optimization. First, the selectivity differences between family members is a valuable parameter by itself as in traditional affinity chromatography. Second, the moderate affinity allows gradient elution, providing additional utility analogous to traditional uni-modal chromatography. Further, since the ionic strength necessary for the elution is low, properly selected sorbents can be applied in sequence without prior desalting of the sample. These desirable operating charactersistics of the paralog sorbents should reduce the losses in yield and activity generally associated with other sequential purification schemes.

The novel properties of the anion exchanger paralogs are more evident in the experiments reported here than for the cation exchangers in part because many of the test proteins also bind to the blocked Affi-Gel, most likely due to free carboxylic acid residues which remain exposed on the final sorbents. These excess carboxylic acid groups are attributable to the manufacturing procedure of Affi-Gel 10.

While providing some of the selectivity characteristics of antibodies, paralogs can be treated with strongly denaturing buffers without the loss of activity encountered with antibodies, and can be used without the introduction into the purified protein of macromolecular contaminants resulting from degradation and leaching of the antibody off the support. Theoretically, other regeneration conditions compatible with peptide and agarose chemistry may also be used, such as guanidine hydrochloride, sodium thiocyanate, 0.2 *M* propionic acid, methanol, or a variety of detergents. We note, however, that the efficiency of regeneration and the stability of these unique sorbents might be different when more complex protein mixtures are used than those tested here. Therefore, the reuseability should be directly established for such samples.

The standard screening protocol described here used only one arbitrarily selected buffer, with pH and ionic strength conditions chosen to correspond to a frequently applied protein purification condition. We anticipate that other conditions would provide additional diversity in the binding profiles. The sorbent plate format allows not only rapid evaluation of numerous sorbents under identical mobile phase conditions, but also evaluation of a single sorbent under a variety of mobile phase conditions. The effects of ionic strength, counter-ion type, organic modifiers, and pH on the adsorption of a single protein or of a protein mixture can thus be conveniently measured.

CONCLUSIONS

A wide range of protein purification and characterization applications should benefit from the development of families of diverse sorbents with properties intermediate between existing sorbents [15]. The sorbent design strategy illustrated here provides one route to building such an array. Another example of the same concept is the recently introduced panel of sorbents derivatized with individually synthesized textile dyes, a panel that provides some additional selectivity over the previous sorbents derivatized with the mixture of dyes known as Cibacron Blue [16]. The utility of any such panel of sorbents is augmented when combined with a convenient format for their rapid evaluation, such as the flow-through microplate used here. More broadly, interactions between short peptides and macromolecules have become an area of increasing interest due to work in immunology [3], drug design [17], and through intriguing observations of particular peptides binding to particular proteins [6,18]. The results reported here establish the immediate feasibility of studying such peptide-macromolecule interactions by use of simple chromatographic procedures that provide highly sensitive indications of differential affinity.

ACKNOWLEDGEMENTS

We thank Carol Topp for feedback throughout the project as well as editorial and artistic aid in production of the manuscript. This work was supported in part by a Small Business Innovative Research Grant (ISI-9022271) from the US National Science Foundation.

REFERENCES

1 K. Benedek and J. K. Swadesh, in G. W. Fong and S. K. Lam (Editors), *HPLC in the Pharmaceutical Industry*, Marcel Dekker, New York, 1991, Ch. 11, p. 241.

2 S. Ohlson, A. Lundblad and D. Zopf, *Anal. Biochem.*, 169 (1989) 204.
3 E. D. Getzoff, J. A. Tainer, R. A. Lerner and H. M. Geysen, *Adv. Immunol.*, 43 (1988) 1.
4 W. Muller, *J. Chromatogr.*, 510 (1990) 133.
5 G. Fassina and I. M. Chaiken, *Adv. Chromatogr.*, 27 (1987) 247.
6 G. W. Welling, T. Geurts, J. van Gorkum, R. A. Damhof and J. W. Drijfhout, *J. Chromatogr.*, 512 (1990) 337.
7 L. M. Kauvar, P. Y. K. Cheung, R. H. Gomer and A. A. Fleischer, *BioTechniques*, 8 (1990) 204; L. Kauvar, US Pat., 4 963 263 (1990).
8 H. Kiniwa, US Pat., 4 694 044 (1987).
9 L. M. Kauvar, in T. Kline (Editor), *Handbook of Affinity Chromatography*, Marcel Dekker, New York, 1992, Ch. 3, in press.
10 G. Scatchard, *Ann. N.Y. Acad. Sci.*, 51 (1949) 660.
11 U. K. Laemmli, *Nature (London)*, 227 (1970) 680.
12 H. Blum, H. Beier and H. J. Gross, *Electrophoresis*, 8 (1987) 93.
13 R. Chavira, T. J. Burnett and J. H. Hageman, , *Anal. Biochem.*, 136 (1984) 446.
14 D. Zopf and S. Ohlson, *Nature (London)*, 346 (1990) 87.
15 F. E. Regnier, *Science (Washington, D.C.)*, 238 (1987) 319.
16 S. J. Burton, S. B. McLoughlin, C. V. Stead and C. R. Lowe, *J. Chromatogr.*, 435 (1988) 127.
17 M. Mutter, *Trends Biochem. Sci.*, 13 (1988) 260.
18 M. Z. Atassi, in M. Inouye and R. Sarma (Editors), *Protein Engineering*, Academic Press, New York, 1986, p. 125.

Journal of Chromatography, 627 (1992) 63–73
Elsevier Science Publishers B.V., Amsterdam

CHROM. 24 575

Characterization of sugar oligomers by on-line high-performance anion-exchange chromatography–thermospray mass spectrometry

R. A. M. van der Hoeven and W. M. A. Niessen

Division of Analytical Chemistry, Center for Bio-Pharmaceutical Sciences, University of Leiden, P.O. Box 9502, 2300 RA Leiden (Netherlands)

H. A. Schols

Department of Food Science, Wageningen Agricultural University, Bomenweg 2, 6703 HD Wageningen (Netherlands)

C. Bruggink

Dionex BV, P.O. Box 9338, 4801 LH Breda (Netherlands)

A. G. J. Voragen

Department of Food Science, Wageningen Agricultural University, Bomenweg 2, 6703 HD Wageningen (Netherlands)

J. van der Greef

Division of Analytical Chemistry, Center for Bio-Pharmaceutical Sciences, University of Leiden, P.O. Box 9502, 2300 RA Leiden (Netherlands)

(First received June 15th, 1992; revised manuscript received August 19th, 1992)

ABSTRACT

The on-line coupling of high-performance anion-exchange chromatography and thermospray mass spectrometry via an anion-micromembrane suppressor and a booster pump is described. The system was applied to the analysis of homologous series of oligosaccharides. Among others, the mass spectrometric detection of β-1,4-xylose oligomers up to degree of polymerization (DP) 25 is demonstrated. Further, the system was used in the analysis of more complex oligosaccharide samples, containing mixed oligomers of hexoses, pentoses and uronic acids. In such samples oligomers up to DP 10 can be detected. The potential use of this approach in the characterization of oligosaccharides obtained from (enzymic) degradation of plant cell wall oligosaccharides is discussed.

INTRODUCTION

High-performance anion-exchange chromatography (HPAEC) is a powerful method for the separation of sugars [1–5]. The technique is widely used in the analysis of food for sugars and in the characterization of sugar oligomers obtained by (enzymic) deg-

Correspondence to: W. M. A. Niessen, Division of Analytical Chemistry, Center for Bio-Pharmaceutical Sciences, University of Leiden, P.O. Box 9502, 2300 BA Leiden, Netherlands.

0021-9673/92/$05.00

radation of glycoproteins and plant cell wall polysaccharides. One of the problems with HPAEC, especially in the latter fields of application where in most instances no standards are available, is the difficulty of predicting the elution order of heterogeneous sugar oligomers. Further, a full characterization of sugar oligomers requires the determination of the sugar composition and the sugar linkage positions. In these respects, the abilities of mass spectrometry (MS), especially in an on-line combination with HPAEC, are expected to be extremely useful. However, the solvent conditions generally used in the HPAEC of sugar oligomers are not compatible with on-line MS detection. The problems with the high salt concentrations of the mobile phase, *e.g.*, 0.1 mol/l sodium hydroxide and a gradient of 0–0.5 mol/l sodium acetate, as used in the separation of sugar oligomers, have already been solved for conductivity detectors in ion chromatography by the introduction of a micromembrane suppressor [4–7], which efficiently replaces either cations or anions by protons or hydroxyl ions. An anion micromembrane suppressor (AMMS) can be used in combination with HPAEC in sugar analysis to remove the excess sodium ions. On-line desalting with an AMMS prior to fraction collection for off-line fast atom bombardment MS or ^{1}H NMR analysis has been described by Basa and Spellman [4]. Simpson *et al.* [7] demonstrated that with an AMMS the sodium concentration can be decreased from 0.1 mol/l to a level compatible with on-line thermospray mass spectrometry. The system was applied to analyse for mono- and diamino sugars [7]. Next, coupling of ion-exchange chromatography to MS via a micromembrane suppressor was described for ionspray [8] and particle-beam [9] interfaces.

In this paper, the coupling of HPAEC to thermospray MS via an AMMS is described for the characterization of sugar oligomers. The technology as already described by Simpson *et al.* [7] was applied without many changes. However, the application range has been significantly widened, especially in terms of the maximum degree of polymerization of the oligosaccharides analysed [degree of polymerization (DP) = 2 by Simpson *et al.* [7] and DP > 10 in this work] and the maximum allowable sodium concentrations in the mobile phase (0.1 mol/l by Simpson *et al.* [7] and up to 0.4 mol/l in this work). Attention is mainly focused on the characterization of the HPAEC–MS system by means of analyses for homologous non-branched sugar oligomers. An example of the HPAEC–MS analysis of a more complex sample obtained by enzymic degradation of plant cell wall polysacchsrides is also described. The applicability of HPAEC–MS in the latter field is discussed in more detail elsewhere [10].

EXPERIMENTAL

Apparatus

The general experimental set-up for HPAEC–MS with a thermospray interface is similar to that used by Simpson *et al.* [7]. The total system consisted of a Dionex (Sunnyvale, CA, USA) DX-300 chromatography system, a Kratos (Manchester, UK) Spectroflow 400 LC pump, acting as booster pump, and a Finnigan MAT (San José, CA, USA) TSQ-70 mass spectrometer equipped with a Finnigan MAT thermospray interface. A schematic diagram of the set-up is given in Fig. 1.

The Dionex DX-300 chromatography system consisted of an EDM-2 solvent degas unit, an AGP pump module and an LCM-3 chromatography module, containing a Rheodyne (Cotati, CA, USA) Model 9126 injector (25-μl loop), a pulsed electrochemical detector with gold electrode and two AMMS-II micromembrane suppressors in series, regenerated with 10–15 ml/min of 0.15 mol/l sul-

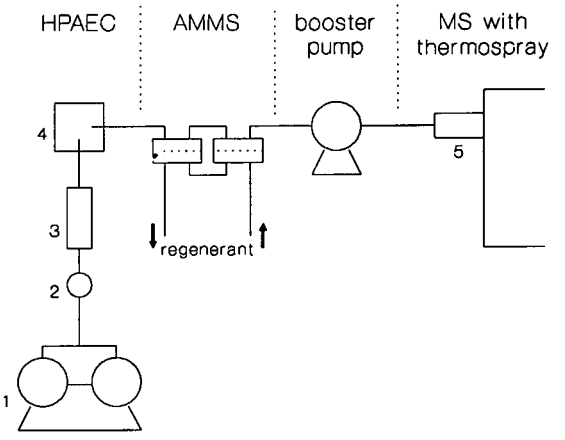

Fig. 1. Schematic diagram of the experimental set-up. 1 = AGP pump module; 2 = injection valve with 25-μl loop; 3 = 250 mm × 4 mm I.D. CarboPac PA1 column; 4 = electrochemical detector; 5 = thermospray interface.

phuric acid delivered by a Chem/Tech Iwaki (Lowell, MA, USA) Model EP B15 pump. The effluent from the AMMS was mixed with 1 ml/min of 0.1 mmol/l aqueous sodium acetate and delivered to the thermospray interface by means of the booster pump. The thermospray interface was operated in the positive-ion mode [scanning over the range m/z = 150–1500 or with multiple ion detection (MID) at 3–5 s per scan] with a block temperature of 350°C, a vaporizer temperature of 100°C and a repeller potential of 50 V.

Ion-moderated partition chromatography was performed using a Spectra-Physics (San José, CA, USA) Model SP8800 pump in combination with a Model SP8800 autosampler, a column oven and a Winner Integration Software package. The effluent was monitored using a Shodex Model SE 61 refractive index detector (Showa Denka, Tokyo, Japan).

Chromatography

In HPAEC, a Dionex CarboPac PA1 column (250 mm × 4 mm I.D.) was used. Gradient elution was performed using mixtures of 0.1 mol/l sodium hydroxide (solvent A) and 1 mol/l sodium acetate in 0.1 mol/l sodium hydroxide (solvent B). The flow-rate was 1 ml/min. The gradient programmes used are given in Table I.

In ion-moderated partition chromatography, a Aminex (Bio-Rad Labs., Richmond, CA, USA) HPX-22H column (300 mm × 7.8 mm I.D.) was used with 5 mmol/l sulphuric acid as the mobile phase at a flow-rate of 0.2 ml/min at 85°C. Glucose and xylose were used as standards for the determination of the mass percentages of α-,4-glucose and β-1,4-xylose oligomers, respectively.

TABLE I

GRADIENT PROGRAMME FOR THE SAMPLES ANALYSED

CarboPac PA1 column. Solvent A: 0.1 mol/l sodium hydroxide. Solvent B: 1 mol/l sodium acetate in 0.1 mol/l sodium hydroxide. Flow-rate: 1 ml/min. Each programme ends with a washing step consisting of a linear gradient up to 100% B in 5 min and a re-equilibration step of 15 min at 0% B.

Sample	Gradient programme (%B in A)
α-1,4-Glucose	0–30% B in 40 min
α-1,5-Arabinose	0% B for 5 min, 0–40% B in 28 min
β-1,4-Xylose	0–5% B in 5 min, 5–30% B in 40 min
Pectin digest	0% B for 5 min, 0–30% B in 21 min
Arabinoxylan digest	0–30% B in 30 min

Samples

All monomeric sugars were obtained from commercial sources. Maltodextrins (α-1,4-glucose oligomers, MD-25) were obtained from Roquette (Lille, France). The α-1,5-arabinose oligomers were prepared by degrading a linear arabinan with pure enzymes as described by Voragen *et al.* [11]. Acetylated β-1,4-xylose oligomers were isolated from birchwood by steam extraction and were kindly provided by Dr. J. Puls (Institute of Wood Chemistry and Chemical Technology of Wood, BFH, Hamburg, Germany). A pectin digest was obtained by incubation of a pectic polysaccharide fraction with Pectinex Ultra SP (Novo Ferment, Basle, Switzerland). Arabinoxylan oligomers were isolated by chromatography over Bio-Gel P2 after incubation of wheat arabinoxylan with endoxylanase [12].

RESULTS AND DISCUSSION

HPAEC–MS coupling

The most important aspect of coupling HPAEC and MS via a thermospray interface is the proper functioning of the AMMS. With the present set-up, where two AMMS systems are used in series, the sodium ions could be removed sufficiently to allow thermospray MS detection as long as the sodium concentration in the mobile phase did not exceed 0.4 mol/l. Otherwise, significant salt deposits will occur in the ion source, which hampers further analysis. When higher sodium concentrations are required in the gradient programme, such as in the washing procedure performed after each run, the HPAEC system was generally disconnected from the mass spectrometer as soon as the 0.4 mol/l sodium limit was exceeded (corresponding to 30% solvent B in solvent A). As a result, the maximum degree of polymerization that can be determined by HPAEC–MS is limited, the extent depending on the type of sugar oligomers. Given the gradient programmes in Table I, the percentage of solvent B and the sodium concentration in the mobile phase at which a particular oligomer elutes are plotted in Fig. 2 as a function of DP for homologous oligomers of α-1,4-glucose, α-1,5-arabinose and β-1,4-xylose.

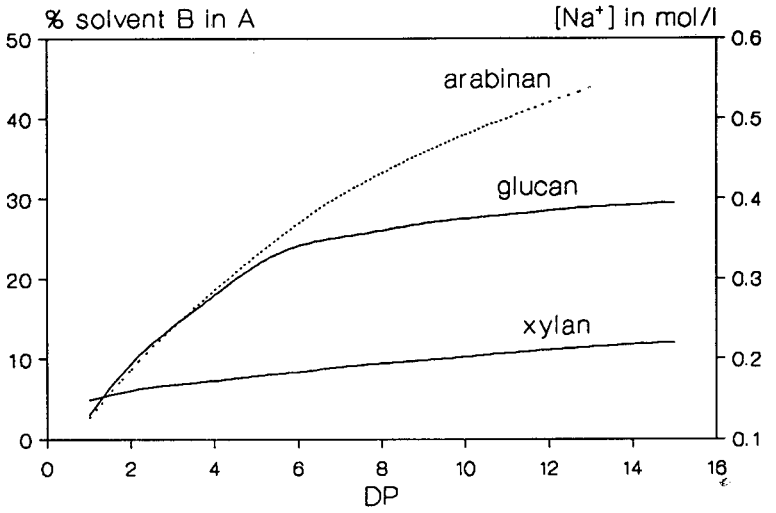

Fig. 2. Plot of the percentage of solvent B and the sodium acetate concentration at which a particular oligomer elutes as a function of the degree of polymerization for oligomers of α-1,4-glucose, α-1,5-arabinose and β-1,4-xylose. For conditions, see Table I.

The data handling, especially after the analysis of unknown samples, is elaborate. As a result of the significant background signal from sodium acetate cluster ions, especially with sodium concentrations between 0.2 and 0.4 mol/l, no peaks are generally detected in the total ion current chromatograms. Therefore, mass chromatograms must be constructed for the known m/z values of series of oligomers and searched for the presence of peaks. In practice, with the type of samples analysed, the searching can be performed using a limited number of m/z values. It must be emphasized that poor total ion current chromatograms are frequently found in LC–thermospray MS.

Mass spectra of oligosaccharides

Intact oligosaccharides can be studied by thermospray MS via ionization with akali metal ions, *e.g.*, sodium or lithium, but not in the presence of the commonly used ammonium acetate [13,14]. This is also possible using the solvent system obtained after desalting by AMMS in HPAEC–MS. The mass spectra of the sugar oligomers under these conditions are dominated by the presence of strong sodiated molecules at $m/z = M_r + 23$, while with higher DP values doubly charged disodiated molecules are observed at $m/z = (M_r + 46)/2$. No fragmentation is observed.

The peak positions in the mass spectra of homologous sugar oligomers are readily predictable, as subsequent members in a series differ by either 132 (pentose units) or 162 (hexose units) for singly charged ions, and 66 or 81, respectively, for doubly charged ions. From the mass spectrum obtained under these conditions no discrimination is possible between various isomeric sugars, *e.g.*, the pentoses xylose and arabinose or the hexoses glucose and galactose.

α-1,4-Glucose oligomers

Previously, reversed-phase LC–MS data for α-1,4-glucose oligomers up to DP = 10 have been reported [14]. In that work, it was primarily the sensitivity, badly influenced by the peak broadening owing to the separation of the sugar anomers, which prevented the observation of peaks at higher DP values. With HPAEC–MS the same sample of α-1,4-glucose oligomers (MD-25, 25 μg injected) was analysed. Glucose oligomers could be detected up to DP = 6. Oligomers with higher DP values were not detected owing to a lack of sensitivity, the low concentration of the higher oligomers and the high sodium concentration necessary for the elution of these oligomers (*cf.*, Fig. 2).

The response of the first oligomer in the series (glucose) is significantly lower than that of the dimer and trimer. Whereas in the reversed-phase LC–MS experiments the observed peak areas of the first

three oligomers are in the proportions *ca.* 10:5:2, in HPAEC–MS it is 5:10:8 for the monomer, dimer and trimer, respectively. From ion-moderated partition chromatography with refractive index detection it was calculated that the MD-25 sample contains *ca.* 14% monomer, 10% dimer and 9% trimer. The decrease in response in the HPAEC–MS experiments can be attributed to losses of the small monomers in the AMMS system, although experiments with a single AMMS performed by Dionex indicated losses of only *ca.* 20% for the monomers [15]. However, an unexpected low response for the monomeric sugar was observed with the other samples analysed also (see, for instance, the data on xylose oligomers discussed below).

Significant additional peak broadening in HPAEC–MS is expected owing to the large dead volume between the electrochemical detector and mass spectrometer, *i.e.*, two AMMS-II systems, each with 40 μl dead volume, the pump head of the booster pump and the necessary tubings and connections. The peak broadening in terms of peak standard deviation (measured at 0.6 of the peak height) was evaluated for the glucose dimer and trimer from the α-1,4-glucose sample. Peak standard deviations of *ca.* 6 and 7.7 s were observed in the chromatogram with the electrochemical detector and in the mass chromatograms, respectively, yielding an effective peak standard deviation of the dead volume of *ca.* 4.8 s (assuming independence of peak standard deviations). In general, no significant decrease in resolution due to the additional peak broadening was experienced.

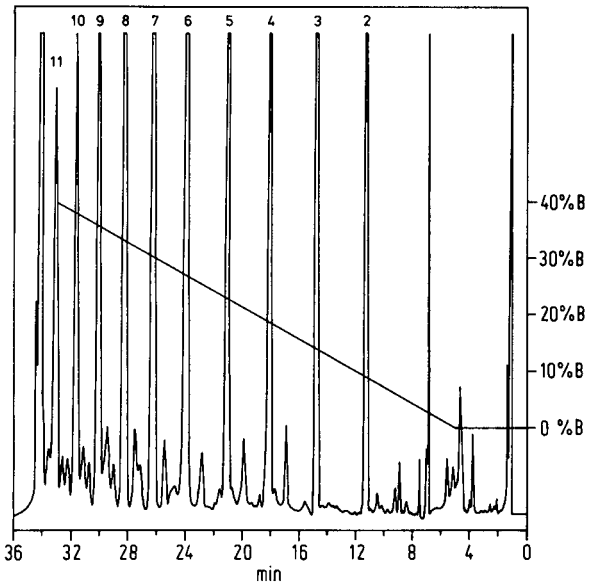

Fig. 3. HPAEC of α-1,5-arabinose oligomers monitored with electrochemical detection. The gradient programme is indicated (*cf.*, Table I); for other experimental conditions, see text.

α-1,5-Arabinose oligomers

The chromatogram of α-1,5-arabinose oligomers, as obtained with electrochemical detection, is given in Fig. 3; the gradient programme is also indicated. In this particular chromatogram, arabinose oligomers were detected up to DP = 11. By extending the gradient programme to 50% B, oligomers of higher DP values can also be detected. In the HPAEC–MS of this α-1,5-arabinose sample, oligomers could be detected up to DP = 9 (using MID). At low DP values, only singly charged ions are detected, whereas at DP values exceeding 5 an increasing intensity of doubly charged ions is observed. The relative intensities of singly and doubly charged ions as a function of the DP value for the α-1,5-arabinose oligomers are shown in Fig. 4. The response for the arabinose oligomers with DP > 5, based on summed peak areas of singly and doubly charged ions, is fairly constant. From the gradient programme indicated in Fig. 3, it can be concluded that DP = 7 is eluting at 30% B (0.4 mol/l sodium in the mobile phase), whereas DP = 8 and 9 are eluting at even higher sodium concentrations.

β-1,4-Xylose oligomers

While the study of oligomers with high DP values is hampered by the required sodium acetate concentration in the mobile phase with α-1,4-glucose and α-1,5-arabinose oligomers, this is not the case with β-1,4-xylose oligomers. The latter elute at significantly lower sodium acetate concentrations, as demonstrated in Fig. 2. Therefore, it must be possible to detect oligomers with higher DP values and thus with higher *m/z* ratios.

A series of mass chromatograms reconstructed from the full-scan data for the *m/z* values of the doubly charged ions of DP = 12–17 are given in Fig. 5. In full-scan acquisition (*m/z* = 150–1500 with 5 s per scan), xylose oligomers could be detected up to DP = 16 as doubly charged ions at *m/z* = 1088.

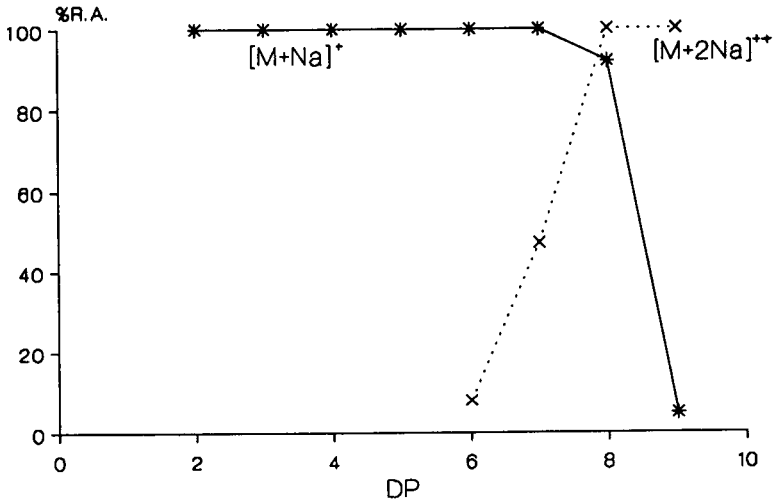

Fig. 4. Relative intensities of the $[M + Na]^+$ and $[M + 2Na]^{2+}$ ions of α-1,5-arabinose oligomers as a function of the degree of polymerization. R.A. = Relative abundance.

For xylose oligomers and for other pentose oligomers the singly charged ions have odd m/z ratios and the doubly charged ions even m/z ratios.

In MID, using various groups of 5–10 ions and stepping from one appropriate group to another during elution, the peak shapes and signal-to-noise ratios significantly improve. As a result, detection of xylose oligomers up to DP = 25 (molecular mass 3318) is now achievable. The peak of the doubly charged ion of DP = 25, still having an acceptable signal-to-noise ratio, is found at m/z = 1682. A series of mass chromatograms demonstrating the detection of these large oligomers is shown in Fig. 6. At high DP values the separation of the various

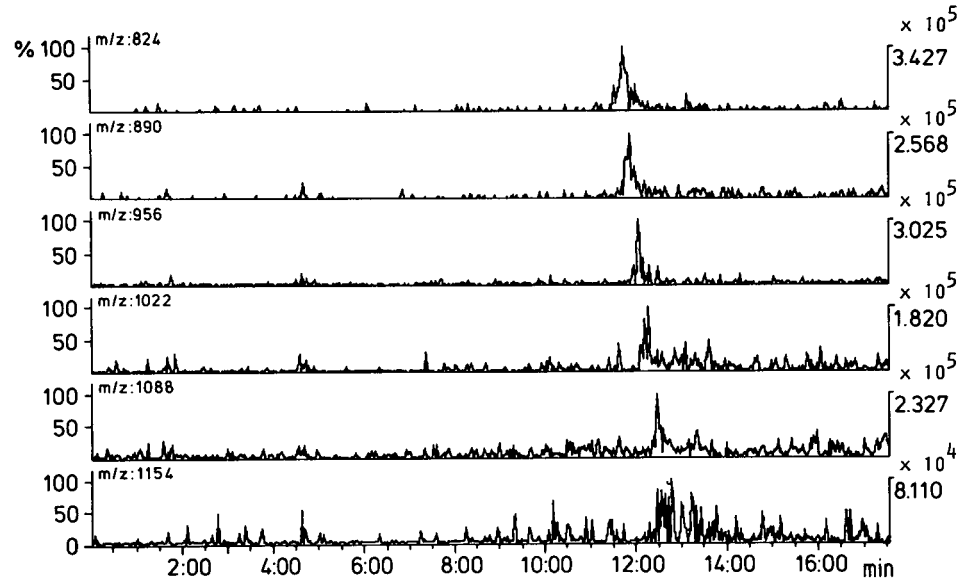

Fig. 5. HPAEC–MS of β-1,4-xylose oligomers. Mass chromatograms of doubly charged ions for DP = 12–17 reconstructed from full-scan acquisition (m/z = 150–1500 with 5 s per scan). Right-hand abscissa is ion intensity in arbitrary units. For conditions, see text.

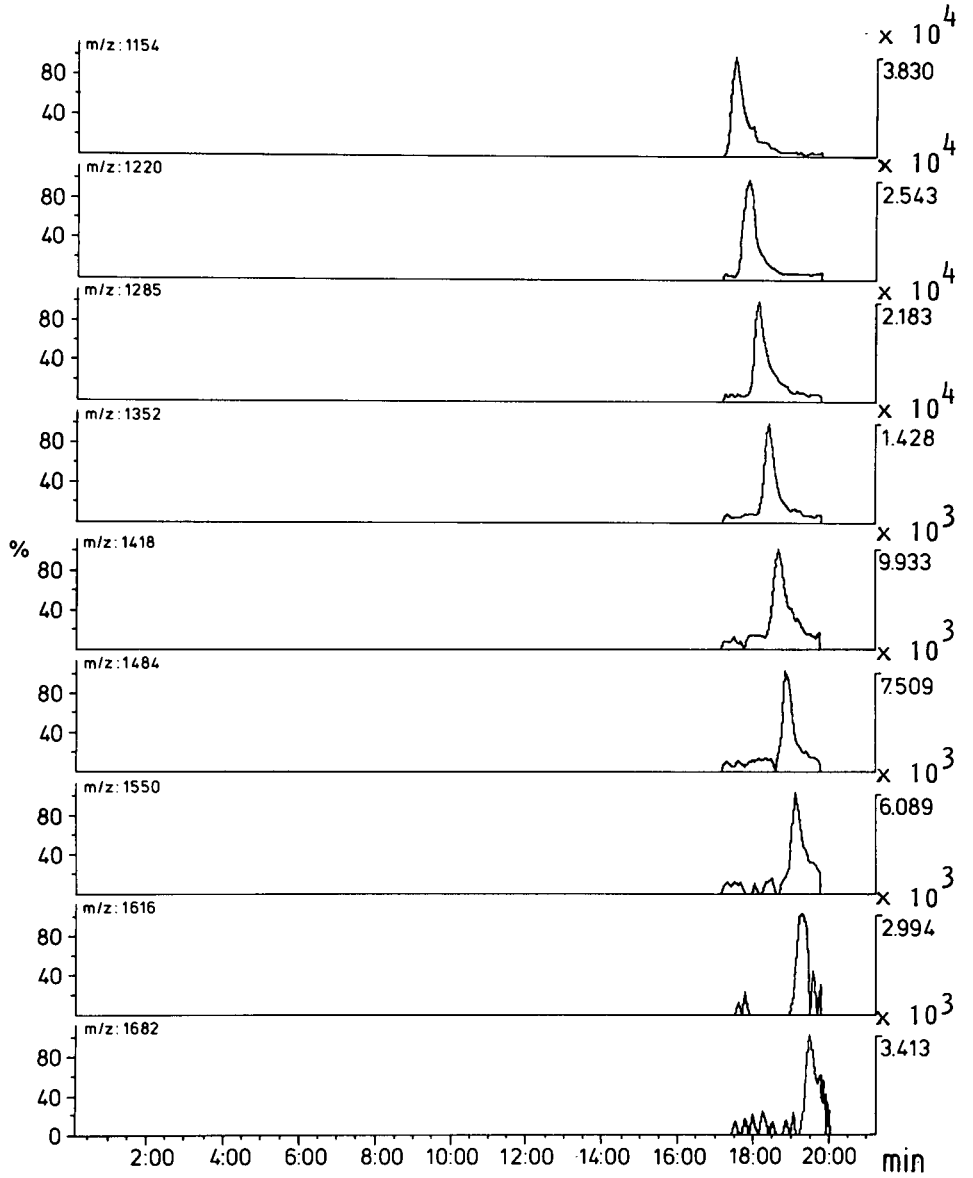

Fig. 6. HPAEC–MS of β-1,4-xylose oligomers. Mass chromatograms of doubly charged ions for DP = 17–25 obtained by multiple ion detection. Right-hand abscissa is ion intensity in arbitrary units.

peaks under the present chromatographic conditions is rather poor, but the peaks are readily distinguishable as a result of the selectivity of MS detection. A good chromatographic separation of the peaks of the xylose oligomers under the conditions used was observed with electrochemical detection only up to DP = 18.

From these data, it may be concluded that the response in thermospray MS appears to be sufficient also for the larger sugar oligomers (DP > 10). However, in order to allow HPAEC–MS detection of higher oligomers other than xylans, more attention must be paid to the efficient removal of the sodium ions from the column effluent prior to

thermospray MS. In that way the range of applicability of the HPAEC–MS approach can be expanded.

In the experiments with β-1,4-xylose oligomers, it was found that singly charged ions could be detected up to DP = 11, whereas doubly charged ions could be detected from DP = 5 upwards. The peak areas observed for singly and doubly charged ions are plotted as a function of the DP value (from 5 to 25) in Fig. 7a. This plot provides information on the relative importance of singly and doubly charged ions to the total peak area observed. Fig. 7a not only demonstrates the growing importance of the doubly charged ions with increasing DP value, but also provides information of the decrease in response as a function of DP. However, the decrease in response as a function of DP, which earlier was found to be large for α-1,4-glucose oligomers [14], is more readily evaluated by plotting the peak area per mass percentage or the peak area per mole of each individual xylose oligomer injected (Fig. 7b). These plots were constructed by using data on the actual composition of the β-1,4-xylose sample as obtained from an ion-moderated partition separation with refractive index detection, using xylose as a stan-

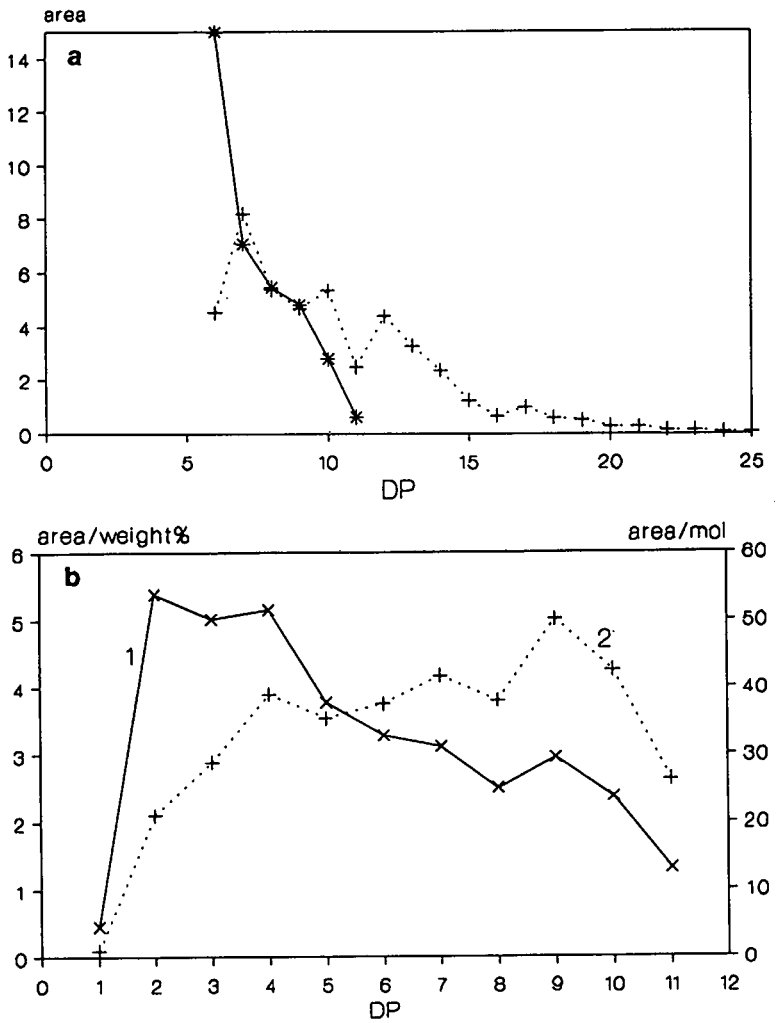

Fig. 7. (a) Peak areas (in arbitrary units) of singly charged (* = $[M + Na]^+$) and doubly charged ions (+ = $[M + 2Na]^{2+}$) (arbitrary units) in the MID run with β-1,4-xylose oligomers as a function of the DP value. (b) Peak area (in arbitrary units) per mass percentage (1) and peak area per mole (2) (both in arbitrary units) for DP = 1–11 oligomers of β-1,4-xylose in HPAEC–MS.

dard. It can be concluded that (i) the monomer is very efficiently lost in the AMMS, as it is present in the sample in a threefold excess over the dimer, (ii) the decrease in response in the peak area per mass percentage plot is approximately fivefold between DP 2 and 10, which is less than observed with α-1,4-glucose oligomers (fifteenfold between DP 2 and 10 [14]), and (iii) the response in peak area per mole is fairly constant between DP 4 and 10.

Heterogeneous oligosaccharides

In practice, the most interesting applications of the HPAEC–MS combination are in the characterization of complex mixtures of heterogeneous oligo-

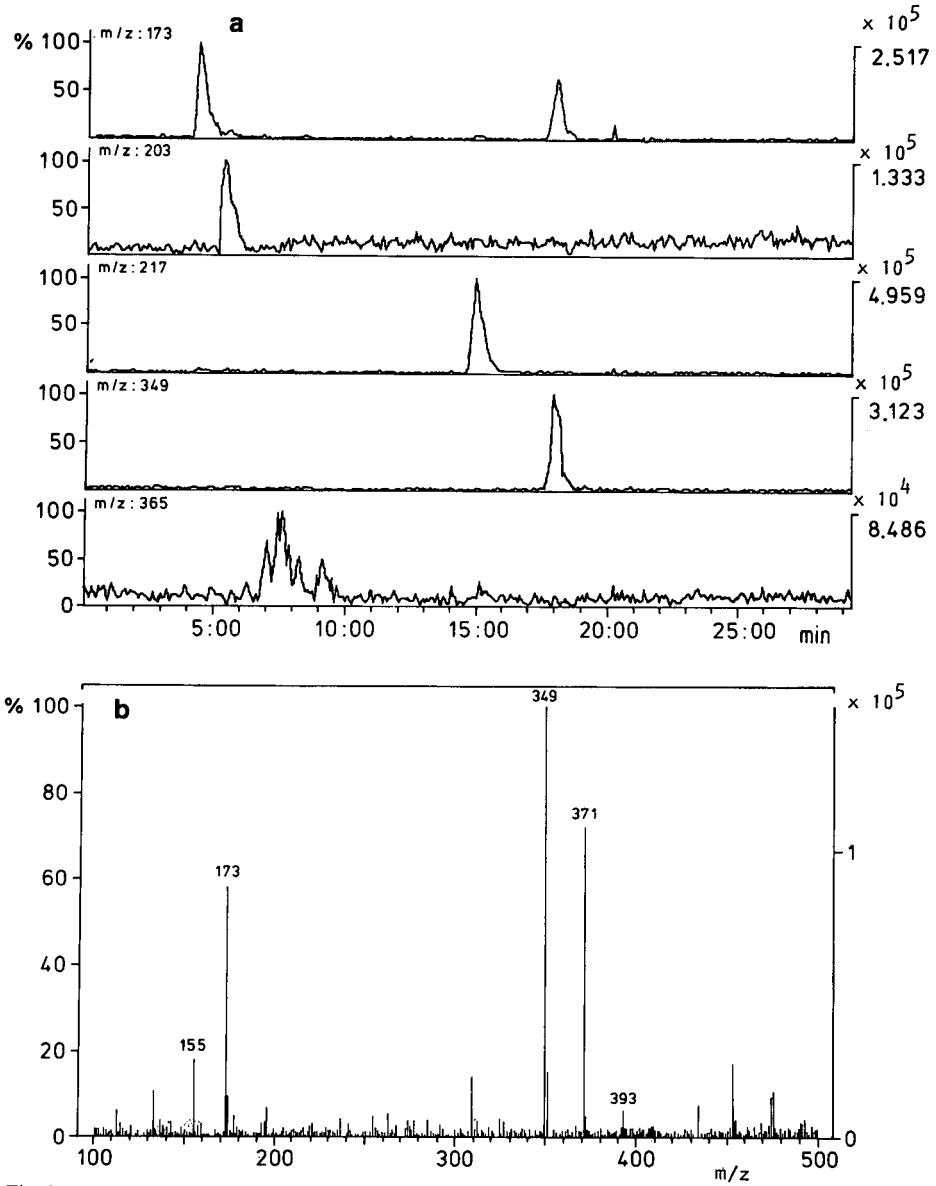

Fig. 8. (a) Mass chromatograms of the peaks detected in the pectin digest. For gradient programme, see Table I. (b) Mass spectrum of GalA–Xyl. Right-hand abscissa is ion intensity in arbitrary units.

saccharides. The ability to give rapid relative molecular mass information on-line with the separation of the various sample constituents is extremely helpful in the evaluation of enzymic behaviour and in the determination of the sugar composition of mixtures from the enzymic degradation of plant cell wall oligosaccharides. The HPAEC–MS method was developed in our laboratory for this field of application.

A digest of pectin was known to contain various monomeric sugars, *i.e.*, rhamnose, arabinose, galactose and galacturonic acid, in addition to an unknown dimer, most likely GalA–Xyl. The sample was analysed by HPAEC–MS. The mass chromatograms are shown in Fig. 8a. Peaks were detected with the m/z values expected for the monomeric sugars present, *i.e.*, (in order of elution) $m/z = 173$ for arabinose, $m/z = 203$ for galactose and $m/z = 217$ for galacturonic acid, while rhamnose was not detected as it was present in a low concentration and probably lost in the AMMS. Further, two dimeric species were found, *i.e.*, a hexose dimer at $m/z = 365$, which is most likely Gal_2 as deduced from its chromatographic behaviour, and at $m/z = 349$ for a uronic acid–pentose dimer, probably GalA–Xyl. The mass spectrum of GalA–Xyl is shown in Fig. 8b. Exceptionally, fragmentation owing to the loss of GalA with charge retention of the Xyl was observed in this spectrum. Further, some features of the mass spectra of uronic acids can be deduced. Uronic acids generally show two strong peaks, *i.e.*, a base peak due to the sodiated acid at $m/z = M_r + 23$ and a peak due to the sodiated sodium salt at $m/z = M_r + 45$. In polyuronic acids a series of sodiated sodium salt peaks can be observed. In some instances, a peak due to the loss of water from the sodiated acid is also observed (not in this instance).

An arabinoxylan sample was treated with endoxylanase and subsequently fractionated using Bio-Gel P2. One of the fractions, expected to contain hexamers of arabinose and xylose, was analysed by HPAEC–MS. In the sample two monomer peaks were found at $m/z = 173$, most likely due to xylose and arabinose; and two pentamer and two hexamer peaks at $m/z = 701$ and $m/z = 428$ and 833, respectively. Different pentamers and hexamers have been isolated and fully characterized by NMR [12]. Interestingly, the elution order of the latter four peaks is pentamer, hexamer, pentamer and hexamer. This example indicates the power of the on-line HPAEC–MS approach in elucidating the elution order of oligosaccharides in anion-exchange chromatography, where often unexpected orders are observed. Obviously, a next and highly desirable step is the elucidation of structural differences between the two pentamers and the two hexamers. The use of tandem mass spectrometry in this respect is currently under investigation.

As indicated before, the peaks of the oligomers present must be searched for by mass chromatography in the non-informative total ion current chromatograms. This can be considered a drawback, although the number of m/z values to be reconstructed is limited in the type of samples analysed in the present field of application. More extensive applications of HPAEC–MS to oligosaccharide mixtures obtained by enzymic degradation of plant cell wall polysaccharides are described elsewhere [10].

CONCLUSIONS

HPAEC–MS is a powerful technique in the characterization of oligosaccharides in mixtures. The method is fast and straightforward. Although at present only molecular mass information is obtained, this already is often very useful in combination with the available knowledge of the cell wall polysaccharides and in the evaluation of the action of enzymes and enzyme mixtures on plant cell wall material. The range of oligomers (DP values) that can be analysed depends greatly on the sugar composition. With β-1,4-xylose, oligomers up to DP = 25 could be observed. With heterogeneous sugar oligomers, compounds with DP values up to 10 are generally amenable to HPAEC–MS. In practice, the sample amounts used are 1–100 μg in a 25-μl injection volume (exact amounts in enzymic digests are unknown).

REFERENCES

1 R. E. Reim and R. M. VanEffen, *Anal. Chem.*, 58 (1986) 3203.
2 M. R. Hardy, R. R. Townsend and Y. C. Lee, *Anal. Biochem.*, 170 (1988) 54.
3 R. R. Townsend, M. R. Hardy, O. Hindsgaul and Y. C. Lee, *Anal. Biochem.*, 174 (1988) 459.
4 L. J. Basa and M. W. Spellman, *J. Chromatogr.*, 499 (1990) 205.

5 Y. C. Lee, *Anal. Biochem.*, 189 (1990) 151.
6 J. Stillian, *LC Mag.*, 3 (1985) 802.
7 R. C. Simpson, C. C. Fenselau, M. R. Hardy, R. R. Townsend, Y. C. Lee and R. J. Cotter, *Anal. Chem.*, 62 (1990) 248.
8 J. J. Conboy, J. D. Henion, M. W. Martin and J. A. Zweigenbaum, *Anal. Chem.*, 62 (1990) 800.
9 J. Hsu, *Anal. Chem.*, 64 (1992) 434.
10 W. M. A. Niessen, R. A. M. van der Hoeven, J. van der Greef, H. A. Schols, G. Lucas-Lokhorst, A. G. J. Voragen and C. Bruggink, *Rapid Commun. Mass Spectrom.*, 6 (1992) 474.
11 A. G. J. Voragen, H. A. Schols, M. F. Searle-van Leeuwen, G. Beldman and F. M. Rombouts, *J. Chromatogr.*, 370 (1986) 113.
12 H. Gruppen, R. A. Hoffmann, F. J. M. Kormelink, A. G. J. Voragen, J. P. Kamerling and J. F. G. Vliegenthart, *Carbohydr. Res.*, 233 (1992) 45.
13 W. M. A. Niessen, R. A. M. van der Hoeven and J. van der Greef, *Org. Mass Spectrom.*, 27 (1992) 341.
14 W. M. A. Niessen, R. A. M. van der Hoeven, J. van der Greef, H. A. Schols and A. G. J. Voragen, *Rapid Commun. Mass Spectrom.*, 6 (1992) 197.
15 C. Bruggink, Dionex, Breda, Netherlands, unpublished results, 1992.

Journal of Chromatography, 627 (1992) 75–86
Elsevier Science Publishers B.V., Amsterdam

CHROM. 24 565

Resolution of carboxylic acid enantiomers by high-performance liquid chromatography with peroxyoxalate chemiluminescence detection

Toshimasa Toyo'oka, Mumio Ishibashi and Tadao Terao

Division of Drugs, National Institute of Hygienic Sciences, 1-18-1 Kamiyoga, Setagaya-ku, Tokyo 158 (Japan)

(First received June 16th, 1992; revised manuscript received August 17th, 1992)

ABSTRACT

The peroxyoxalate chemiluminescence (CL) detection of carboxylic acid enantiomers, combined with high-performance liquid chromatography (HPLC), is described. The CL reaction is influenced by various factors (*e.g.*, eluent pH, type of aryl oxalate, relative concentrations of aryl oxalate and hydrogen peroxide and reaction time). Good linearity between CL intensity and injected amounts (5 fmol–5 pmol) of authentic derivatives, DBD-APy-Nap and ABD-APy-Nap, which were synthesized by the reaction with naproxen (Nap) with (+)-4-(N,N-dimethylaminosulphonyl)-7-(3-aminopyrrolidin-1-yl)-2,1,3-benzoxadiazole [(+)-DBD-APy] and (+)-4-(aminosulphonyl)-7-(3-aminopyrrolidin-1-yl)-2,1,3-benzoxadiazole [(+)-ABD-APy], were obtained with the proposed procedures. The reproducibility of the CL intensity during 6 h was also excellent, and no peak decrements were observed. The detection limits (signal-to-noise ratio = 2) of authentic DBD-APy-Nap, ABD-APy-Nap and NBD-APy-Nap {synthesized from naproxen and (+)-4-nitro-7-(3-aminopyrrolidin-1-yl)-2,1,3-benzoxadiazole [(+)-NBD-APyl]} with the bis[4-nitro-2-(3,6,9-trioxadecyloxy)phenyl] oxalate (TDPO)–hydrogen peroxide (H_2O_2) system after separation by HPLC were 0.49, 1.9 and 15 fmol, respectively, whereas those with bis(2,4,6-trichlorophenyl) oxalate (TCPO)–H_2O_2 were 0.74, 2.8 and 29 fmol, respectively. Some carboxylic acid enantiomers were converted on reaction with (+)-DBD-APy into the corresponding fluorescent diastereomers after 2 h at room temperature in the presence of 2,2'-dipyridyl disulphide and triphenylphosphine, activating agents for carboxylic acids. The diastereomers derived from each pair of enantiomers of anti-inflammatory drugs and N-acetylamino acids were efficiently resolved by reversed-phase chromatography with on ODS column and a 0.1 *M* imidazole-NO_3 (pH 7.0)–acetonitrile mixture as the mobile phase. The applicability of the proposed procedure was also evaluated for the detection of racemic ibuprofen (anti-inflammatory drug) added to rat plasma and human urine.

INTRODUCTION

Optical resolution of racemates in high-performance liquid chromatography (HPLC) has been mainly performed by two methods: introduction of an asymmetric environment intramolecularly by conversion into diastereomers and intermolecularly by use of a chiral stationary phase (CSP) [1–4]. Many CSP columns have been successfully applied to the resolution of various kinds of chiral molecules. Compared with the diastereomeric method, however, the CSP method is not advantageous in terms of sensitivity.

In a previous paper [5], we reported the syntheses of the fluorescence chiral reagents [(+)- and (−)-isomers] for the carboxylic acid functional group, 4-(N,N-Dimethylaminosulphonyl)-7-(3-aminopyrrolidin-1-yl)-2,1,3-benzoxadiazole (DBD-APy), 4-(aminosulphonyl)-7-(3-aminopyrrolidin-1-yl)-2,1,3-benzoxadiazole (ABD-APy) and 4-nitro-7-(3-aminopyrrolidin-1-yl)-2,1,3-benzoxadiazole (NBD-APy) (Fig. 1). The reagents were used to resolve carboxylic acid enantiomers by HPLC with fluorescence detection. The diastereomers derived from each pair of enantiomers of drugs and N-acetylami-

Correspondence to: Dr. T. Toyo'oka, Division of Drugs, National Institute of Hygienic Sciences, 1-18-1 Kamiyoga, Setagaya-ku, Tokyo 158, Japan.

0021-9673/92/$05.00

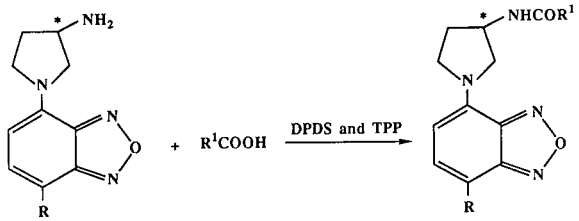

NBD-APy: R=NO_2
ABD-APy: R=SO_2NH_2
DBD-APy: R=$SO_2N(CH_3)_2$

Fig. 1. Labelling reactions of carboxylic acid enantiomers with chiral reagents in the presence of activating agents.

no acids were resolved completely by an ODS column and detected in the 10–30-fmol range (signal-to-noise ratio = 2), The diastereomers produced had the attractive feature of fluorescence at long excitation (460–480 nm) and emission (530–610 nm) wavelengths.

Some fluorescent compounds emit light on chemical reaction without the need for optical excitation with lamps such as the xenon arc. Chemiluminescence (CL) detection is well known to be sensitive and useful for trace analyses for fluorescent compounds [6,7] and hydrogen peroxide (H_2O_2) [8,9]. Among the CL reagents such as luminol and lucigenin, the combination of oxalates and H_2O_2 seems to be suitable as postcolumn CL reagents for the determination of fluorophores, because the reaction conditions at around neutral pH are much milder than those required for other reagents such as luminol.

This paper describes the resolution of carboxylic acid enantiomers (anti-inflammatory drugs and N-acetylamino acids) by HPLC with peroxyoxalate CL detection. Suitable conditions for CL detection were established by investigation of the various factors that affect the CL reaction. Racemic ibuprofen added to rat plasma and human urine was also studied with the recommended procedures.

EXPERIMENTAL

Materials and reagents

The derivatization reagents, (+)-DBD-APy, (+)-ABD-APy and (+)-NBD-APy, were synthesized as described previously [5]. The derivatives of (+)-2-(6-methoxy-2-naphthyl)propionic acid (naproxen) with (+)-DBD-APy, (+)-ABD-APy and (+)-NBD-APy, (designated as DBD-APy-Nap, ABD-APy-Nap and NBD-APy-Nap, respectively), were also synthesized as described [5]. Racemic 2-(6-methoxy-2-naphthyl)propionic acid (*rac*-naproxen), racemic 2-(4-isobutylphenyl)propionic acid (*rac*-ibuprofen) and racemic 2-[*p*-(2-oxocyclopentylmethyl)phenyl]propionic acid (*rac*-loxoprofen) were donated by Tokyo Tanabe Pharmaceutical, Kyowa Hakko Kogyo and Sankyo (all Tokyo, Japan), respectively. N-Acetylamino acid enantiomers were kindly supplied by Ajinomoto (Tokyo, Japan). Bis(2,4,6-trichlorophenyl) oxalate (TCPO) and bis[4-nitro-2-(3,6,9-trioxadecyloxy) phenyl] oxalate (TDPO) (biochemical research grade) were purchased from Wako (Osaka, Japan). Triphenylphosphine (TPP) (Wako), 2,2′-dipyridyl disulphide (DPDS) (Tokyo Kasei, Tokyo, Japan), imidazole (grade for buffer preparation) (Tokyo Kasei) and hydrogen peroxide (H_2O_2) (30% in water) (Wako) were also used as received. Trifluoroacetic acid (TFA), acetonitrile (CH_3CN) and water were of HPLC grade (Wako). All other chemicals were of analytical-reagent grade and were used without further purification.

Stock solutions

A 0.2 *M* buffer solution was prepared by dissolving 13.616 g of imidazole in 950 ml of water, adjusted to pH 6.0–8.0 with 61% HNO_3 and then diluted to 1 l with water. The solution was further diluted with water to prepare buffer solutions of 5 m*M*–0.1 *M*. The reagent solution [10 m*M* (+)-DBD-APy], the authentic derivatives (1 m*M* DBD-APy-Nap, ABD-APy-Nap or NBD-APy-Nap), anti-inflammatory drugs (1 m*M* naproxen, ibuprofen and loxoprofen) and N-acetylamino acids (1 m*M* N-acetylphenylalanine, -tryptophan, -tyrosine, -valine, -methionine, etc.) were also prepared in acetonitrile. The reagent solutions were diluted to appropriate concentrations with acetonitrile. The activation agents (DPDS and TPP) for carboxylic acids were prepared with acetonitrile just prior to use. Fresh solutions of CL reagents (aryl oxalate and H_2O_2) were also prepared every day. All stock solutions except imidazole buffer were stored in a refrigerator at −20°C.

HPLC–CL detection

The high-performance liquid chromatograph consisted of two LC-9A pumps (Shimadzu, Kyoto, Japan) and an SCL-6B system controller (Shimadzu). Sample solutions were injected with a SIL-6B autoinjector (Shimadzu). The analytical column was a 5-μm Inertsil ODS-2 (150 × 4.6 mm I.D.) (GL Sciences, Tokyo, Japan). The column and rotating mixing device (KZS-1) (Kyowa Seimitsu, Tokyo, Japan) were maintained at 30°C with a Model 655A-52 column oven (Hitachi, Tokyo, Japan). A stainless-steel tube (40 cm × 0.1 mm I.D.) was used as a reaction delay coil. A Shodex CL-2 chemiluminescence monitor (single photon counting type) (Showa Denko, Tokyo, Japan) equipped with a 120-μl spiral flow cell was employed for the detection of emitted light. The peak areas corresponding to CL intensity were calculated with a C-R4A Chromatopac (Shimadzu). All mobile phases and chemilumigenic reagents were degassed with an online degasser (DGU-3A; Shimadzu). The flow-rate of the eluent was 0.5 ml/min. The instrumental setup for HPLC–CL analysis is shown in Fig. 2.

The CL intensities of authentic DBD-APy-Nap and ABD-APy-Nap were determined after separation by HPLC under various CL reaction conditions. The signal-to-noise ratios (S/N) were calculated from the difference between the peak height of each diastereomer and the variation of the baseline noise.

The recommended HPLC–CL conditions were as follows: eluent, 0.1 *M* imidazole-NO_3 buffer (pH 6.5)–acetonitrile (2:3) for TDPO–H_2O_2 CL detection system and 0.1 *M* imidazole-NO_3 buffer (pH 7.0)–acetonitrile (2:3) for TCPO–H_2O_2 CL detection system; concentrations of CL reagents, 0.5 m*M* oxalate (TDPO or TCPO) and 15 m*M* H_2O_2 in acetonitrile; and flow-rate of CL reagents, 1.5 ml/min.

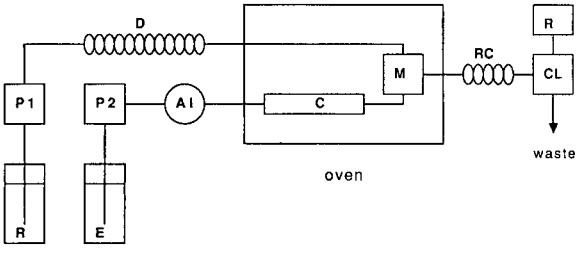

Fig. 2. Schematic flow diagram of the HPLC–CL detection system. P = Pump; D = damper coil; AI = autoinjector; C = column; E = eluent reservoir; R = reagents (oxalate and H_2O_2) reservoir; M = rotating mixing device; RC = reaction delay coil; CL = chemiluminescence monitor; R = recorder

Linearity of the response under the recommended CL detection conditions

Volumes of 5 μl of the mixed solution of DBD-APy-Nap and ABD-APy-Nap (1 n*M*–1 μ*M* concentration) were injected on to the column and detected with the CL monitor under the recommended procedures. The CL intensities of individual peaks were plotted against the injected amount of the diastereomers.

Optical resolution of carboxylic acid enantiomers labelled with (+)-DBD-APy

(+)-DBD-APy (0.25 m*M*) in 0.5 ml of CH_3CN reacts with anti-inflammatory drugs or N-acetylamino acids (*ca.* 1 mg each) at room temperature in the presence of the activation agent consisting of DPDS (4 m*M*) and TPP (4 m*M*). After a 2-h reaction period, an aliquot (5 μl) of the solution was injected into the column, separated with 0.1 *M* imidazole-NO_3 (pH7.0)–CH_3CN (2:3) and detected chemilumigenically with TCPO–H_2O_2. The capacity factor (k'), separation factor (α) and the resolution (R_s) were caluculated from the following equations:

$$k' = (t_R - t_0)/t_0$$

$$\alpha = k'_2/k'_1$$

$$R_s = 2(t_{R_2} - t_{R_1})/(w_1 + w_2)$$

where t_R, t_{R_1} and t_{R_2} are the retention times of the peaks, t_0 is the void volume of the column (2.7 min) and w_1 and w_2 are the bases of triangles derived from the peak.

Determination of carboxylic acid enantiomers in plasma and urine

In general, profens such as naproxen and ibuprofen in biological specimens are separated and extracted well using a solid-phase column such as Sep-Pak C_{18} [10]. Therefore, Bond Elut Certify II columns (developed for acidic pharmaceuticals) were employed for the extraction of *rac*-ibuprofen in rat plasma and human urine.

A 1.0-ml sample of human urine spiked with 8 μl (4 nmol of each enantiomer) of 1 m*M* *rac*-ibuprofen

was adjusted to pH 1–2 with 36% HCl (*ca.* 10 μl), then 3 ml of 10 m*M* sodium acetate buffer (pH 2.0) were added. The acidified urine was applied to a Bond Elut Certify II LRC extraction column (Varian, Harbor City, CA, USA), which was washed with 2 ml of methanol and 2 ml of 10 m*M* sodium acetate buffer (pH 2.0). The column was washed sequentially with 2 ml of 10 m*M* sodium acetate buffer (pH 2.0) and 2 ml of 10% acetic acid. The column was dried under reduced pressure with an aspitator for 5 min. All washings were discarded. *rac*-Ibuprofen was eluted with 2 ml of 0.1% trifluoroacetic acid (TFA)–CH_3CN (1:1). The eluate was evaporated to dryness and the residue was dissolved in 1.0 ml of CH_3CN (urine extraction sample).

A 0.5-ml sample of rat plasma spiked with 2 μl (1 nmol of each enantiomer) of 1 m*M* *rac*-ibuprofen was also adjusted to pH 1–2 with 36% HCl (*ca.* 5 μl), then 3.5 ml of 10 m*M* sodium acetate buffer (pH 2.0) were added. The acidified plasma was applied to the solid-phase column and treated in the same manner as described for the urine sample. The dried eluate containing *rac*-ibuprofen was dissolved in 0.5 ml of CH_3CN (plasma extraction sample).

A 0.25-ml volume of the prepared urine or plasma extract, 0.1 ml of (+)-DBD-APy (2 m*M*) in CH_3CN and 0.15 ml of a mixed solution of DPDS (2 m*M*) and TPP (2 m*M*) in CH_3CN were thoroughly mixed in a 1.5-ml glass vial. The vials were capped and allowed to stand for 2 h at room temperature (20–30°C). An aliquot (5 μl) of the reaction solution, diluted appropriately 100–200-fold with CH_3CN, was injected into the column for HPLC–CL analysis. A blank urine or plasma sample without (+)-DBD-APy was treated in the same manner.

RESULTS AND DISCUSSION

Peroxyoxalate CL detection

Peroxyoxalate chemiluminescence (CL) is based on the reaction of an oxalate and H_2O_2, which was reported by Rauhut *et al.* in 1967 [11]. The CL reaction has been used with HPLC for the determination of fluorophores such as DNS-amines [12,13], OPA-amines [14] and polycyclic aromatic hydrocarbons [15,16]. Detection limits for these compounds in the picomole and sub-femtomole range have been achieved with CL detection. Aryl oxalates and H_2O_2 react with each other to produce unstable and energy-rich intermediates, which cause fluorescent compounds to reach an excited state. The excited fluorescent compounds return to the ground state with the emission of light which has same maximum wavelength as when photochemical excitation is used. Therefore, the compounds excited easily at low-energy show stronger CL intensity. In other words, compounds with long excitation wavelengths provide the most satisfactory results; however, some exceptions have been noted [6]. The CL intensity is also dependent on the fluorescence quantum yield (ϕ_f), the concentration of the fluorophore and the concentration of the energy-rich intermediates produced by CL reaction. When the same fluorescent chromophore is bonded to a variety of compounds, the final detection limits in CL detection depend on the concentration of the excited intermediates that are generated by the CL reaction conditions.

Various aryl oxalates have been reported; TCPO and TDPO were selected for this work. Bis(2,6-dinitrophenyl) oxalate (DNPO) is commonly used, but it and its hydrolysate exhibit strong quenching effects and a high level of background emission in comparison with other oxalates [17,18]. TDPO is more soluble oxalate than TCPO [19] in water-miscible solvents such as CH_3CN. Although ethyl acetate has been employed as a solvent for oxalates, its use should be avoided owing to the biohazard. The highest CL intensity and persistence are obtained with CH_3CN relative to other solvents such as ethyl acetate and acetone [12]. Therefore, the oxalates and H_2O_2 were dissolved in CH_3CN. Imidazole buffer was selected for the separation of the diastereomers, as the catalytic effect of imidazole in the CL reaction is stronger than that of phosphate buffer, which is commonly used as an eluent [20,21]. The purity of imidazole has a great influence on both the level of background emission and the variation of baseline noise. Therefore, high-quality imidazole and water must be used for the preparation of the buffers. The buffer pH was adjusted to 6.0–8.0 with HNO_3 instead of HCl and HBr, as NO_3^- does not quench the CL intensity, where Cl^- and Br^- do [17]. As thorough mixing of the effluent from the column and CL reagents is an important factor in obtaining a stable baseline and reproducible peaks, a rotating mixing device was adopted instead of usual T-type mixer [22]. Stainless-steel

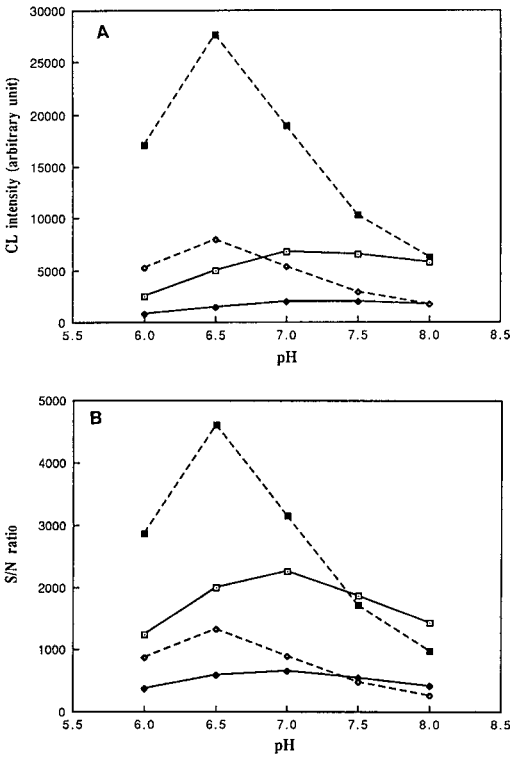

Fig. 3. Effect of eluent pH on CL reaction. (A) Effect on CL intensity; (B): effect on *S/N*. □ = DBD-APy-Nap with TCPO–H_2O_2; ◆ = ABD-APy-Nap with TCPO–H_2O_2; ■ = DBD-APy-Nap with TDPO–H_2O_2; ◇ = ABD-APy-Nap with TDPO–H_2O_2. Conditions: eluent, 0.1 *M* imidazole-NO_3 (pH 6–8)–CH_3CN (2:3); CL reagent flow-rate, 2.0 ml/min; For other conditions, see Experimental.

tubes of 40 cm × 0.1 mm I.D. and 100 cm × 0.1 mm I.D. used as a reaction delay coil and a damper coil for the CL reagent solution, respectively. The CL reaction increases with increasing temperature, but the signal-to-noise ratio was optimum at around room temperature. Therefore, the mixing device was maintained at 30°C in an air oven together with the separation column. The inlet and outlet connections of the detection cell in the CL monitor were made with stainless-steel connectors and tubing to prevent light from entering through the connectors and tubing. Utilizing these conditions, the various factors that influence the CL reaction were investigated with authentic DBD-APy-Nap and ABD-APy-Nap.

Initially, the effect of pH on the CL reaction was examined with TCPO–H_2O_2 and TDPO–H_2O_2 detection systems. As shown in Fig. 3, the optimum pH was different with each oxalate. The CL intensity of the TDPO–H_2O_2 reaction was strongest at pH 6.5, whereas the highest intensity with the TCPO–H_2O_2 reaction was achieved at pH 7.0–7.5 (Fig. 3A). The optimum pH for the TCPO–H_2O_2 reaction was 7.0 as determined by the *S/N* (Fig. 3B). The CL intensities of both diastereomers at the optimum pH with the TDPO–H_2O_2 reaction were approximately three times those of the TCPO–H_2O_2 reaction (Fig. 3A). As both the level of background emission and the variation of the baseline noise were higher in the reaction with TDPO–H_2O_2, the differences in *S/N* obtained from both oxalates were less than threefold (Fig. 3B). The results suggest that the reaction pH is one of the most important factors influencing the CL reaction using oxalate and H_2O_2.

The effect of the concentration of imidazole, which functions as a buffer component for the HPLC eluent and as a base catalyst for the CL reaction, is shown in Fig. 4. When TCPO was used as the oxalate in the CL reaction, the intensity increased with increasing buffer concentration (Fig. 4A). However, 0.1 *M* imidazole was optimum, as determined by studying the *S/N* (Fig. 4B). In the reaction with TDPO and H_2O_2, the highest values of both the intensity and *S/N* were obtained with 0.1 *M* imidazole. Consequently, 0.1 *M* imidazole buffers (pH 6.5 for the TDPO–H_2O_2 system and pH 7.0 for the TCPO–H_2O_2 system) were selected for the CL reactions.

The concentrations of oxalate and H_2O_2 also affect the CL reaction. As depicted in Fig. 5, the CL intensity is greatly dependent on the oxalate concentration in the range tested (2.5 μ*M*–1.0 m*M*) (Fig. 5A), but the variation of the baseline noise also increases. As a result, the optimum TDPO concentration is 0.5 m*M* (Fig. 5B). In contrast, a high TCPO concentration is the predominant factor for the CL reaction judging from the *S/N* data (Fig. 5B). As the solubility in CH_3CN is not great, 0.5 m*M* TCPO was also adopted here. With respect to H_2O_2 concentration, 15 m*M* gave the strongest intensity with TCPO (Fig. 6A). On the other hand, relatively high CL intensities with TDPO were observed at H_2O_2 concentrations between 5 and 15 m*M*. Based on these studies of CL intensity, 0.5

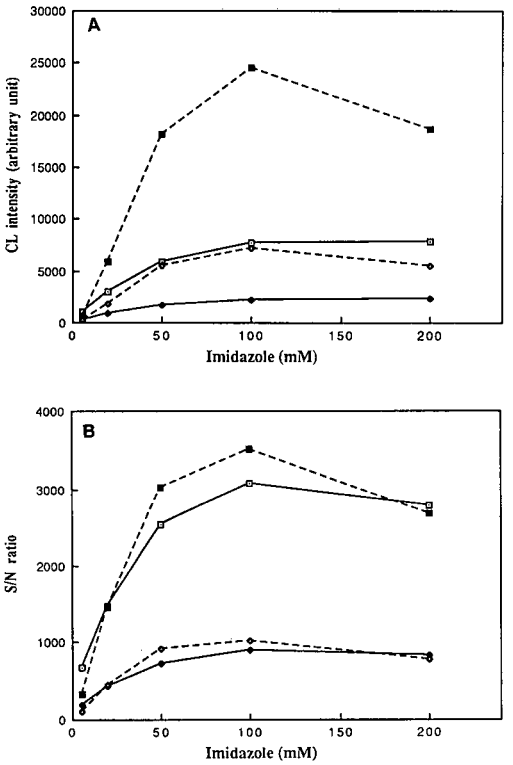

Fig. 4. Effect of imidazole concentration on CL reaction. Symbols as in Fig. 3. Conditions: eluent, 5–200 m*M* imidazole (pH 7.0 for TCPO–H_2O_2, pH 6.5 for TDPO–H_2O_2)–CH_3CN (2:3). For other conditions, see Experimental.

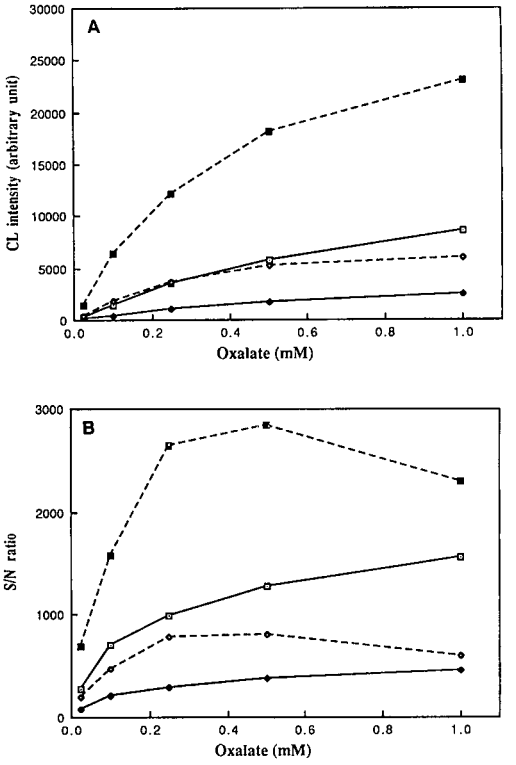

Fig. 5. Effect of aryl oxalate concentration on CL reaction. Symbols as in Fig. 3. Conditions: concentration of TCPO or TDPO, 2.5 μM–1.0 m*M*; eluent, 0.1 *M* imidazole (pH 7.0)–CH_3CN (2:3). For other conditions, see Experimental.

m*M* oxalate and 15 m*M* H_2O_2 in CH_3CN were used as the CL reagent solution.

Finally, the effect of flow-rate of the CL reagent on the CL reaction was tested under the optimum conditions described above. The flow-rates of the eluent and reagent solution affect the CL intensity. When the flow-rate of the eluent was fixed at 0.5 ml/min, the intensity is greatest with a TDPO–

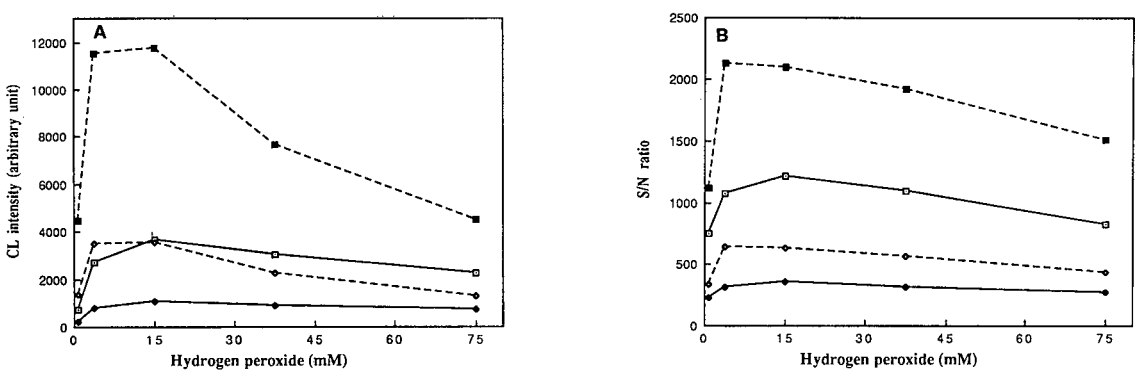

Fig. 6. Effect of H_2O_2 concentration on CL reaction. Symbols as in Fig. 3. Conditions: concentration of H_2O_2, 0.75–75 m*M*; concentration of TCPO or TDPO, 0.25 m*M*. For other conditions, see Experimental.

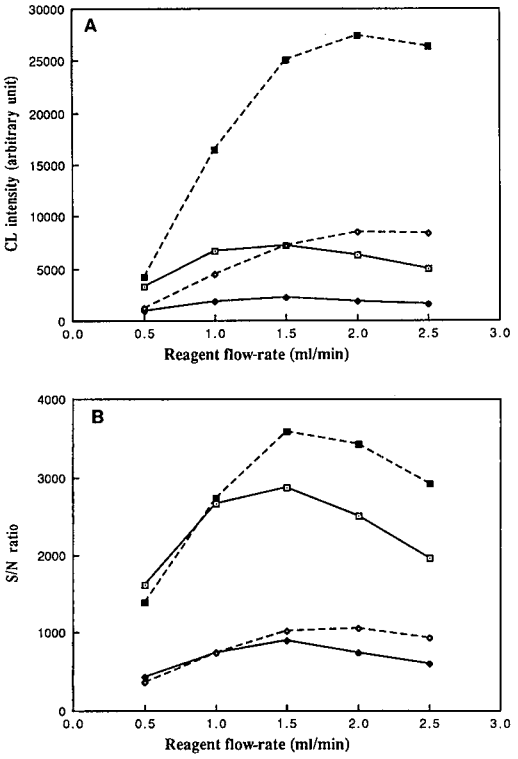

Fig. 7. Effect of flow-rate of CL reagents on CL reaction. Symbols as in Fig. 3. Conditions: flow-rate of CL reagent, 0.5–2.5 ml/min. For other conditions, see Experimental.

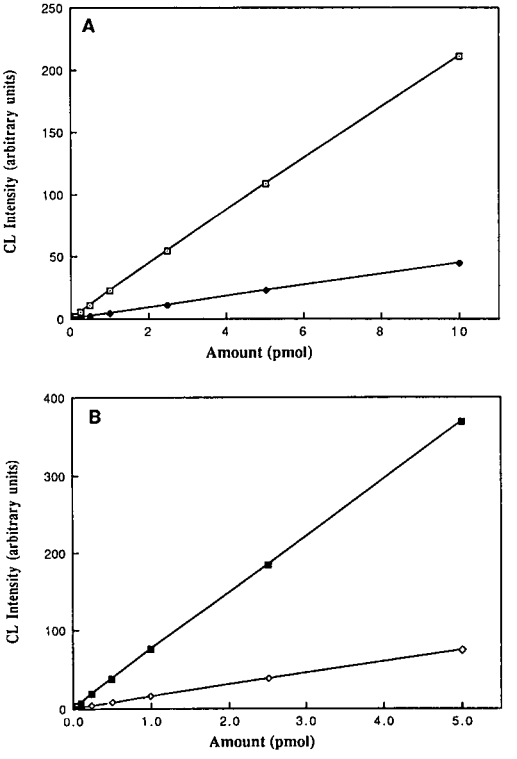

Fig. 8. Linearity of CL intensity under the recommended procedures. Symbols as in Fig. 3. (A) With TCPO–H_2O_2; (B) with TDPO–H_2O_2. For conditions of HPLC separation and CL detection, see Experimental.

H_2O_2 flow-rate of 2.0 ml/min, whereas with TCPO–H_2O_2 it is greatest at 1.5 ml/min (Fig. 7A). However, the optimum *S/N* is realized when the flow-rate of the CL reagent solution is 1.5 ml/min, as shown in Fig. 7B.

Based on the results described above, the CL intensities of the diastereomers, corresponding to the carboxylic acid enantiomers, were measured after separation with an Inertsil ODS-2 column under the following conditions: eluent buffer, 0.1 *M* imidazole-NO_3–CH_3CN (2:3); eluent pH, 6.5 for the TDPO–H_2O_2 and 7.0 for the TCPO–H_2O_2 system; CL reagent concentration, 0.5 m*M* oxalate and 15 m*M* H_2O_2 in CH_3CN; flow-rate, 0.5 ml/min for the eluent and 1.5 ml/min for the CL reagents; mixing temperature, 30°C; and CL reaction time, *ca.* 1 s.

Under the recommended conditions, the relationship between CL intensity and concentration (5 fmol–5 pmol) in the injected solution was linear with a correlation coeffcient (γ) >0.999 (Fig. 8). The slope and the intercept of the linear equations for DBD-APy-Nap were 73.59 and 0.61, respectively, with the TDPO–H_2O_2 system and 21.16 and 0.37, respectively, with the TCPO–H_2O_2 system, whereas those for ABD-APy-Nap were 14.99 and 0.10, respectively, with the TDPO–H_2O_2 system and 4.49 and 0.03, respectively, with the TCPO–H_2O_2 system. With regard to the sensitivity of detection for the diastereomers, DBD-APy-Nap can be measured at roughly one-fifth of the level of ABD-APy-Nap. The proposed postcolumn CL detection is carried out on a one-pump system by using an acetonitrile mixture of oxalate and H_2O_2. Therefore, the peak (corresponding to the CL intensity) may decrease steadily throughout the day owing to the decomposition of oxalates. Imaizumi *et al.* [20] reported that the stability of TCPO depended on the solvent, the temperature of the CL

reagent reservoir and the concentration of H_2O_2. Among the solvents tested, acetonitrile provided the most stable mixture of TCPO and H_2O_2. A lower temperature of the CL reagent mixture and a lower concentration of H_2O_2 also stabilized TCPO in the reservoir. Judging from the data [20], it seems that the decomposition of the oxalates under the proposed conditions is negligible. To confirm this, the variation of the CL peak (1 pmol of DBD-APy-Nap or ABD-APy-Nap) was determined with TCPO and TDPO in the presence of H_2O_2. Although the amount of oxalate decomposition is unknown, the relative CL intensity was independent of the age of the solution for at least 6 h after preparation (less than 3%). Consequently, both oxalates are usable in acetonitrile solution with H_2O_2.

The detection limits (S/N = 2) of DBD-APy-Nap, ABD-APy-Nap and NBD-APy-Nap were determined under the proposed HPLC–CL detection conditions. Fig. 9A and B shows the typical chromatograms of the three mixed diastereomers (corresponding to 10 fmol of DBD-APy-Nap, 30 fmol of ABD-APy-Nap and 200 fmol of NBD-APy-Nap).

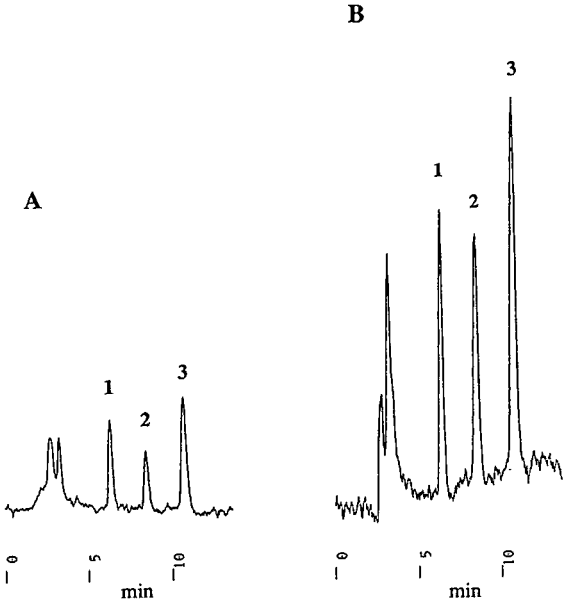

Fig. 9. Chromatograms of authentic diastereomers with CL detection. (A) with TCPO–H_2O_2; (B) with TDPO–H_2O_2. Peaks: 1 = ABD-APy-Nap (30 fmol); 2 = NBD-APy-Nap (200 fmol); 3 = DBD-APy-Nap (10 fmol). Eluent, 0.1 M imidazole-NO_3 (pH 7.0)–CH_3CN (2:3). For other conditions of HPLC separation and CL detection, see Experimental.

The peak heights obtained with the TCPO–H_2O_2 system were 3–4 times lower than those for the TDPO–H_2O_2 system. The corresponding detection limit for the TCPO–H_2O_2 calculated from the S/N was approximately half of that for TDPO–H_2O_2 system, because the variation of the baseline noise also decreased. The detection limits of DBD-APy-Nap, ABD-APy-Nap and NBD-APy-Nap on the chromatograms were 0.49, 1.9 and 15 fmol, respectively, with the TDPO–H_2O_2 system and 0.74, 2.8 and 29 fmol, respectively, with the TCPO–H_2O_2 system. The minimum detectable levels of DBD-APy and ABD-APy-Nap were roughly one order of magnitude lower than those previously reported with fluorescence detection [5]; however, the detection limits for NBD-APy-Nap are in the same range for both detection systems. The results indicate that the DBD-APy moiety is preferable for the highly sensitive detection with peroxyoxalate CL.

HPLC separation and CL detection of diastereomers derived from (+)-DBD-APy

The enantiomeric separation of the racemates of some carboxylic acids, after derivatization with the chiral reagents in the presence of DPDS and TPP, was successfully accomplished with a reversed-phase ODS column, as described previously [5]. Femtomole detection (10–30 fmol) was achieved by HPLC with fluorimetric detection. Among the fluorophores, the DBD-APy structure was chemilumigenically suitable for ultra-trace analysis judging from the chromatograms in Fig. 9. The separations of optical isomers of anti-inflammatory drugs and N-acetylamino acids labelled with (+)-DBD-APy were studied by HPLC under the recommended CL reaction conditions with TCPO–H_2O_2. Fig. 10 shows the chromatograms of the diastereomers derived from carboxylic acid enantiomers and (+)-DBD-APy. The resulting diastereomers of the drugs and the N-acetylamino acids were separated efficiently on the ODS column with 0.1 M imidazole-NO_3 (pH 7.0)–CH_3CN mixture. Differences in peak heights were shown for each pair of some carboxylic acid enantiomers (N-acetyltryptophan and N-acetylvaline), the peaks derived from the (+)-enantiomers being larger than those from the (−)-enantiomers. When (−)-DBD-APy was used instead of (+)-DBD-APy as the tagging reagent for N-acetyltryptophan, the peak of the (−)-

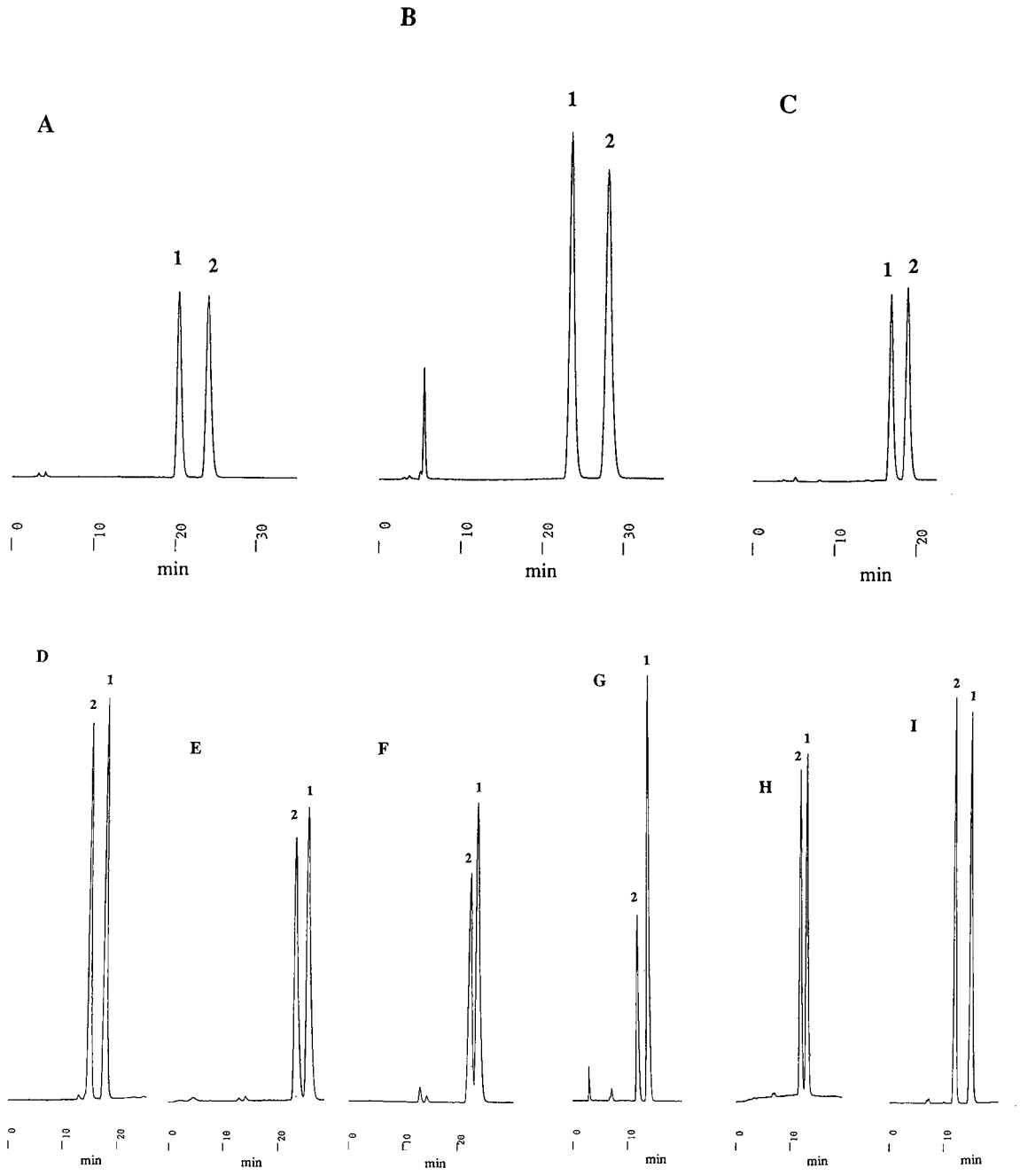

Fig. 10. HPLC separation of carboxylic acid enantiomers labelled with (+)-DBD-APy. (A) ibuprofen; (B) naproxen; (C) loxoprofen; (D) N-acetyltyrosine; (E) N-acetylmethione; (F) N-acetylvaline; (G) N-acetyltryptophan; (H) N-acetylleucine; (I) N-acetylphenylalanine. Peaks: 1 = (+)-enantiomer; 2 = (−)-enantiomer. Eluent: (A) 0.1 *M* imidazole-NO_3 (pH 7.0)–CH_3CN (2:3); (B and C) 0.1*M* imidazole-NO_3 (pH 7.0)–CH_3CN (1:1); (D, E and F) 0.1 *M* imidazole-NO_3 (pH 7.0)–CH_3CN (7:3); (G, H and I) 0.1 *M* imidazole-NO_3 (pH 7.0)–CH_3CN (3:2). For other conditions of HPLC separation and CL detection, see Experimental.

TABLE I

RESOLUTION OF PAIRS OF CARBOXYLIC ACID ENANTIOMERS WITH CL DETECTION

CL reagents, 0.5 m*M* TCPO and 15 m*M* H_2O_2 in CH_3CN; flow-rate, 1.5 ml/min. For other HPLC–CL detection conditions, see Experimental.

Carboxylic acid	(+)-Enantiomer		(−)-Enantiomer		α	R_s	Eluent[a]
	t_R (min)	k'	t_R (min)	k'			
Ibuprofen	20.41	6.56	24.11	7.93	1.21	3.16	A
Naproxen	10.80	3.00	12.02	3.45	1.15	1.73	A
Naproxen	23.62	7.75	28.19	9.44	1.22	3.32	B
Loxoprofen	8.50	2.15	9.08	2.36	1.10	1.00	A
Loxoprofen	16.74	5.20	18.82	5.97	1.15	2.08	B
N-Acetyl-Tyr	17.46	5.47	14.70	4.44	1.23	2.70	C
N-Acetyl-Met	23.22	7.60	25.46	8.43	1.11	1.63	C
N-Acetyl-Val	23.28	7.62	22.10	7.18	1.06	0.94	C
N-Acetyl-Trp	13.76	4.10	11.86	3.39	1.21	2.38	D
N-Acetyl-Leu	13.01	3.82	11.83	3.38	1.13	1.47	D
N-Acetyl-Phe	14.80	4.48	11.85	3.39	1.32	3.47	D

[a] Eluent: (A) 0.1 *M* Imidazole-NO_3 (pH 7.0)–CH_3CN (2:3); (B) 0.1 *M* Imidazole-NO_3 (pH 7.0)–CH_3CN (1:1); (C) 0.1 *M* Imidazole-NO_3 (pH 7.0)–CH_3CN (7:3); (D) 0.1 *M* Imidazole-NO_3 (pH 7.0)–CH_3CN (3:2). Flow-rate, 0.5 ml/min.

enantiomer was larger than that of the (+)-enantiomer. The results with N-acetyltryptophan suggest that the peaks of the (+)-enantiomer with (+)-DBD-APy and the (−)-enantiomer with (−)-DBD-APy are larger than those of the (−)-enantiomer with (+)-DBD-APy and (+)-enantiomer with (−)-DBD-APy. Therefore, the peak difference might be due to the difference in the CL intensity based on the fluorescence quantum yield (ϕ_f) and/or the difference in the derivatization yield. Table I lists the capacity factors (k'), separation factors (α) and resolutions (R_s) for each pair of diastereomers. Complete resolution was achieved with all the carboxylic acids tested. The (+)-enantiomers of the drugs and the (−)-enantiomers of the N-acetylamino acids were eluted faster than the corresponding opposite enantiomers. Their elution orders were the same as those with the 0.1% TFA–CH_3CN eluent described previously [5]. The carboxylic acid enantiomers, having a chiral centre at the α-position to a COOH functional group, were well separated and detected with the proposed HPLC–CL system, as shown in Fig. 10 and Table I. Judging from the results, the separation of carboxylic acid enantiomers when the COOH group is adjacent to a chiral centre may be possible using the proposed system. However, the resolution of racemates containing a COOH group at a β- or γ-position seems to be difficult, because the distances between the chiral centres in the diastereomer, derived from the carboxylic acid and the reagent, increase. The effect of the distance between an asymmetric carbon and a COOH group on separation should be investigated.

Determination of ibuprofen enantiomers after addition of rac-ibuprofen to rat plasma and human urine

The usefulness of the proposed HPLC–CL detection method for the resolution of *rac*-ibuprofen in rat plasma and human urine was examined as a preliminary step in a pharmacokinetic study. Fig. 11A and B shows the chromatograms obtained from rat plasma with the TCPO–H_2O_2 and TDPO–H_2O_2 systems, and Fig. 12A and B those from human urine. Highly sensitive detection of each pair of ibuprofen enantiomers is possible in both biological samples. Further, no interference of endogenous compounds in the samples was observed (data not shown). The proposed HPLC–CL method provides ultra-sensitive detection of carboxylic acid enantiomers.

The proposed methods are the first to be reported

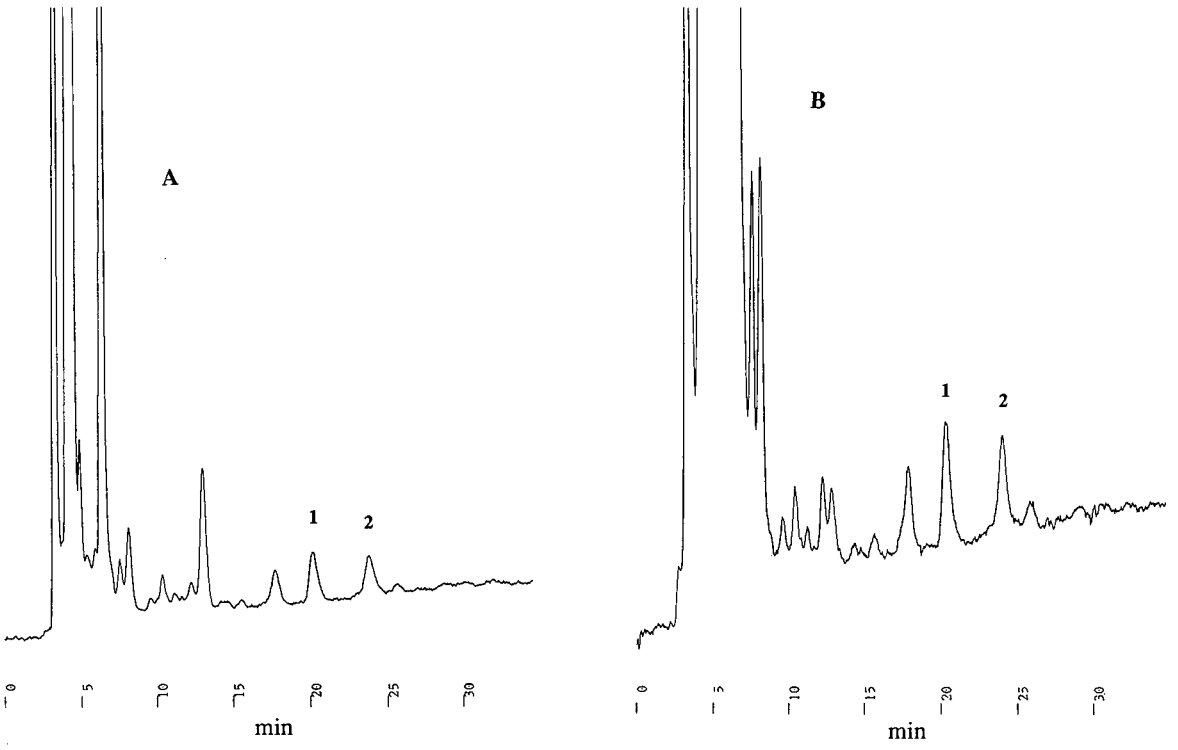

Fig. 11. Chromatograms obtained from rat plasma with CL detection. (A) with TCPO–H_2O_2 (50 fmol each); (B) with TDPO–H_2O_2 (25 fmol each). Peaks: 1 = (+)-ibuprofen; 2 = (−)-ibuprofen. For conditions of HPLC separation and CL detection, see Experimental.

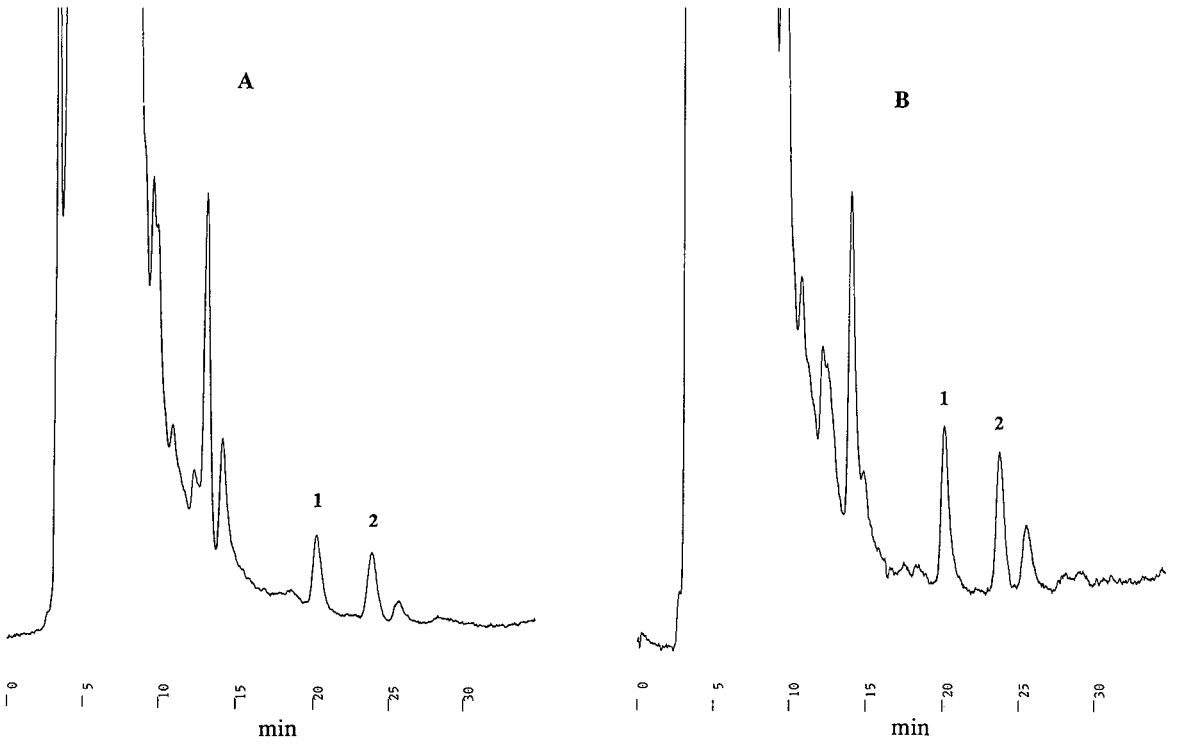

Fig. 12. Chromatograms obtained from human urine with CL detection. (A) with TCPO–H_2O_2 (100 fmol each); (B) with TDPO–H_2O_2 (50 fmol each). Peaks: 1 = (+)-ibuprofen; 2 = (−)-ibuprofen. For conditions of HPLC separation and CL detection, see Experimental.

for the optical resolution of racemates with CL detection. The detection limits of the carboxylic acids after derivatization with (+)-DBD-APy are in the attomole range. The minimum detectable range is lower than that previously reported for the optical resolution of carboxylic acid enantiomers [23-25]. Further, the use of reversed-phase chromatography using an ODS column instead of a normal-phase system is an advantage. Among the fluorophores, the DBD-APy moiety is recommended for the CL detection of carboxylic acid enantiomers because of its high sensitivity. On the other hand, both TDPO and TCPO in the presence of H_2O_2 are applicable in peroxyoxalate CL as described here. The proposed method for the ultra-sensitive and simultaneous determination of enantiomeric drugs in biological fluids may provide more precise information on the pharmacokinetics of drugs such as anti-inflammatories (*e.g.*, ketoprofen and loxoprofen). Further studies are in progress.

ACKNOWLEDGEMENT

The authors thank Dr. C. R. Warner, Food and Drug Administration, Washington, DC, USA, for valuable suggestions on the manuscript.

REFERENCES

1 W. H. Pirkle and T. C. Pochopsky, *Chem. Rev.*, 89 (1989) 347.
2 M. Zief and L. J. Crane (Editors), *Chromatographic Chiral Separation*, Marcel Dekker, New York, 1988.
3 A. M. Krstulovic (Editor), *Chiral Separation by HPLC*, Ellis Horwood, Chichester, 1989.
4 P. Camilleri, *Biomed. Chromatogr.*, 5 (1991) 128.
5 T. Toyo'oka, M. Ishibashi and T. Terao, *Analyst (London)*, 117 (1992) 727.
6 K. Imai, K. Miyaguchi and K. Honda, in K. van Dyke (Editor), *Bioluminescence and Chemiluminescence: Instruments and Application*, Vol. II, CRC Press, New York, 1985, p. 65.
7 K. Imai, *Methods Enzymol.*, 133B (1986) 435.
8 P. V. Zoonen, D. A. Kamminga, C. Gooijer, N. H. Velthorst and R. W. Frei, *Anal. Chim. Acta*, 167 (1985) 249.
9 M. S. Abdel-Latif and G. G. Guilbault, *Anal. Chem.*, 60 (1988) 2671.
10 T. Toyo'oka, M. Ishibashi and T. Terao, *Biomed. Chromatogr.*, 6 (1992) 143.
11 M. M. Rauhut, L. J. Bollyky, B. G. Roberts, M. Loy, R. H. Whitman, A. V. Iannotta, A. M. Semsel and R. A. Clarke, *J. Am. Chem. Soc.*, 89 (1967) 6515.
12 S. Kobayashi and K. Imai, *Anal. Chem.*, 52 (1980) 424.
13 K. Miyaguchi, K. Honda, T. Toyo'oka and K. Imai, *J. Chromatogr.*, 352 (1986) 255.
14 G. Mellbin and B. E. F. Smith, *J. Chromatogr.*, 312 (1984) 203.
15 K. W. Sigvardson and J. W. Birks, *Anal. Chem.*, 55 (1983) 432.
16 M. L. Grayeski and A. J. Weber, *Anal. Lett.*, 17 (1984) 1539.
17 K. Honda, J. Sekino and K. Imai, *Anal. Chem.*, 55 (1983) 940.
18 R. S. Givens, R. L. Schowen, J. Stobaugh, T. Kuwana, F. Alvarez, N. Parekh, B. Matuszewski, T. Kawasaki, O. S. Wong, M. Orlovic, H. P. Chokshi and K. Nakashima, in M. C. Goldberg (Editor), *Peroxyoxalate Chemiluminescence Reaction: Luminescence Application in Biological, Chemical, Environmental and Hydrological Sciences (ACS Symposium Series, Vol. 383)*, American Chemical Society, Washington DC, 1989, p. 127.
19 K. Imai, H. Nawa, M. Tanaka and H. Ogata, *Analyst (London)*, 111 (1989) 209.
20 N. Imaizumi, K. Hayakawa, M. Miyazaki and K. Imai, *Analyst (London)*, 114 (1989) 161.
21 N. Hanaoka, R. S. Givens, R. L. Schowen and T. Kuwana, *Anal. Chem.*, 60 (1988) 2193.
22 S. Kobayashi and K. Imai, *Anal. Chem.*, 52 (1980) 1548.
23 J. Goto, M. Ito, S. Katsuki, N. Saito and T. Nambara, *J. Liq. Chromatogr.*, 9 (1986) 683.
24 J. Goto, N. Goto, A. Hikichi, T. Nishimaki and T. Nambara, *Anal. Chim. Acta*, 120 (1980) 187.
25 J. Goto, N. Goto and T. Nambara, *J. Chromatogr.*, 239 (1982) 559.

Journal of Chromatography, 627 (1992) 87–96
Elsevier Science Publishers B.V., Amsterdam

CHROM. 24 569

Determination of fatty acids in fish oil dietary supplements by capillary liquid chromatography with laser-induced fluorescence detection

Jong Shin Yoo and Victoria L. McGuffin

Department of Chemistry, Michigan State University, East Lansing, MI 48824 (USA)

(First received March 5th, 1992; revised manuscript received August 18th, 1992)

ABSTRACT

The 4-bromomethyl-7-methoxycoumarin derivatives of 14 saturated and unsaturated fatty acids, including the $\omega - 3$ fatty acids, were separated by reversed-phase liquid chromatography and detected by laser-induced fluorescence. Baseline resolution was obtained by using a high-efficiency packed capillary column with 240 000 theoretical plates, together with a systematic optimization of the mobile phase composition. The retention indices of the fatty acid derivatives correlated well with a predictive empirical model, showing accuracy better than 0.46% relative error and reproducibility better than ±0.1% relative standard deviation. The physiologically important fatty acids with 12–22 carbon atoms and 0–6 double bonds were determined at the femtomole level in fish oil dietary supplements by using this methodology.

INTRODUCTION

The polyunsaturated $\omega - 3$ fatty acids such as eicosapentaenoic and docosahexaenoic acids are highly enriched in fish oil extracts from cod, mackerel, sardine, and menhaden [1]. These extracts are commonly ingested as dietary supplements because of their putative therapeutic benefits. Several clinical studies have shown that the administration of fish oils to humans and animals can produce antihypertensive, antihyperlipidemic, and antiaggregatory effects [1,2]. However, these fish oil extracts may contain other saturated and unsaturated fatty acids whose physiological effects are less beneficial or are not fully understood. Consequently, the identification and quantitation of all constituents is an important problem for clinical studies as well as for routine evaluation of commercially available dietary supplements.

Correspondence to: V. L. McGuffin, Department of Chemistry, Michigan State University, East Lansing, MI 48824, USA.

Reversed-phase liquid chromatography (LC) is one of the most important techniques for analytical [3–10] and preparative [11,12] scale separations of fatty acids from animal and plant samples. Most naturally occurring fatty acids possess an even number of carbon atoms (N) with a number of double bonds (n) in the *cis* configuration. The fatty acids, which are represented symbolically as $N{:}n$ (for example, eicosapentaenoic acid is 20:5), exhibit a wide retention range depending on the number of carbon atoms and double bonds. It is commonly believed that the retention order of fatty acids can be expressed in terms of the equivalent chain length (ECL = $N - 2n$) [4]. Separation of fatty acids that have the same ECL has been reported under both isocratic [5–8] and gradient (9,10] mobile phase conditions. However, the resolution of polyunsaturated fatty acids containing three or more double bonds (18:3, 20:3, 20:4, 20:5, and 22:6) is usually incomplete due to co-elution with physiologically important saturated and unsaturated fatty acids with similar retention characteristics [4]. Moreover,

0021-9673/92/$05.00

these polyunsaturated fatty acids do not appear to follow the usual ECL retention rule [4].

The use of fluorescence detection to determine fatty acids at high sensitivity has already been reported for LC. The 4-bromomethyl-7-methoxycoumarin [13], anthryldiazomethane [14,15], 9-aminophenanthrene [16], and 9-chloromethylanthracene [17] derivatives of fatty acids can be analyzed at the picomole level and the 4-bromomethyl-7-acetoxycoumarin [18] derivatives at the femtomole level using conventional fluorescence detection. Using laser-induced fluorescence (LIF) detection, an exceptional sensitivity at the attomole level was achieved for the 4-bromomethyl-7-methoxycoumarin derivatives of fatty acids [19] and related substances such as prostaglandins [20].

In this research, an analytical method has been developed to determine the most important saturated and unsaturated fatty acids in fish oil dietary supplements. The fatty acids were derivatized with 4-bromomethyl-7-methoxycoumarin, separated with high efficiency by using packed capillary LC columns, and detected with high sensitivity by using the LIF method.

EXPERIMENTAL

Reagents

The standard saturated fatty acids such as dodecanoic (lauric, 12:0), tridecanoic (13:0), tetradecanoic (myristic, 14:0), pentadecanoic (15:0), and hexadecanoic (palmitic, 16:0) acids were obtained from Sigma (St. Louis, MO, USA). The standard unsaturated fatty acids such as 9-tetradecenoic (myristoleic, 14:1), 9-hexadecenoic (palmitoleic, 16:1), 9-octadecenoic (oleic, 18:1), 9,12-octadecadienoic (linoleic, 18:2), 6,9,12-octadecatrienoic (gammalinolenic, 18:3), 8,11,14-eicosatrienoic (homogammalinolenic, 20:3), 5,8,11,14-eicosatetraenoic (arachidonic, 20:4), 5,8,11,14,17-eicosapentaenoic (20:5), and 4,7,10,13,16,19-docosahexaenoic (22:6) acids were obtained from Cayman Chemical Company (Ann Arbor, MI, USA) and Nu Chek Prep (Elysian, MN, USA). The commercially available fish oil dietary supplements were Promega Pearls from Parke-Davis (Morris Plains, NJ, USA), Omega-3 and Fish-EPA from North Laboratories (Montague, MI, USA). The fluorescence derivatization reagent 4-bromomethyl-7-methoxycoumarin was purchased from Aldrich (Milwaukee, WI, USA) and was stored at 4°C. The dibenzo-18-crown-6 (Aldrich), sodium sulphate (J. T. Baker, Phillipsburg, NJ, USA), and potassium hydrogencarbonate (Matheson Coleman & Bell, Norwood, OH, USA) were reagent-grade chemicals and were used without further purification. All organic solvents were high-purity, distilled-in-glass grade (Baxter Healthcare, Burdick & Jackson Division, Muskegon, MI, USA); water was deionized and doubly distilled (MP-3A, Corning Glass Works, Corning, NY, USA).

Analytical methods

The fluorescence derivatization procedure was similar to that described previously [19]. A 10^{-3} *M* solution of the fatty acid standards was prepared in dry acetone. To a 500-μl aliquot of this solution were added 5 mg of a powdered, anhydrous mixture (1:1) of sodium sulphate and potassium hydrogencarbonate, and 3.6 mg (10 μmol) of dibenzo-18-crown-6 with stirring. The 4-bromomethyl-7-methoxycoumarin (2.7 mg, 10 μmol) reagent was added, and the derivatization reaction was allowed to proceed in the dark at 37°C. After 6 h, the supernatant liquid was removed from the product mixture, evaporated with dry nitrogen, and kept less than 1 day at 4°C.

Prior to derivatization, a 0.8-g sample of each fish oil dietary supplement was dissolved in 50 ml tetrahydrofuran. The triglyceride or esterified form of the fatty acids was saponified with 10 ml of 1 *M* NaOH solution for 1 h at 45°C. The solution was then acidified with 20 ml of 1 *M* HCl solution and dried with 10 g anhydrous sodium sulphate. The free fatty acids were extracted several times with 50 ml chloroform, and the combined extracts were evaporated with dry nitrogen and stored at 4°C. The resulting fatty acids were derivatized with 4-bromomethyl-7-methoxycoumarin according to the procedure described above. The validation of this analytical methodology, including the accuracy and precision of both qualitative and quantitative measurements, has been described previously [19,20].

Apparatus

A single-piston reciprocating pump (Model 114M, Beckman Instruments, San Ramon, CA, USA) was used to deliver the mobile phase under constant-pressure conditions. Samples were introduced by means of a split injection system using a 1-μl

electrically actuated valve (Model ECI4UW1, Valco Instruments, Houston, TX, USA) at a split ratio from 1:100 to 1:200. The column and splitter were maintained at a constant temperature of 30°C in a thermostated bath (Model 182, Precision Scientific, Chicago, IL, USA). Packed capillary columns were prepared from fused-silica tubing (96 to 178 cm length, 200 μm I.D., Hewlett-Packard, Avondale, PA, USA) according to the slurry-packing procedure described previously [21]. The packing material was a 3-μm spherical silica that was chemically bonded with 3.5 μmol/m^2 octadecylsilane and capped with trimethylsilane (Micro-Pak SP-18, Varian, Walnut Creek, CA, USA). The theoretical plate numbers for these packed capillary columns were 158 000 to 275 000, calculated under standard test conditions [21].

The LIF detector has been described previously [19]. A helium–cadmium laser (Model 3112-10S, Omnichrome, Chino, CA, USA) was used as the excitation source at 325 nm wavelength. The fluorescence emission at 420 nm wavelength was isolated by using a combination of two bandpass interference filters (Corion, Holliston, MA, USA) and a liquid filter (1% aqueous $NaNO_2$), and was detected by using a photomultiplier tube (Model Q4249B, Centronic, Bailey Instruments, Saddle Brook, NJ, USA). The resulting photocurrent was amplified with a picoammeter (Model 480, Keithley Instruments, Cleveland, OH, USA) and displayed on a chart recorder (Model 585, Linear Instruments, Reno, NV, USA).

Computer optimization method

To optimize the separation of the fatty acid derivatives, the window-diagram approach developed by Laub [22,23] was employed. The computer program was revised and rewritten in the BASIC programming language to operate on an IBM personal computer system (Model XT, Boca Raton, FL, USA).

First, the capacity factor (k') for each fatty acid was measured experimentally at different compositions of the mobile phase. A semi-empirical equation, originally developed by Hsu *et al.* [24], was used to relate the inverse of the capacity factor and the volume fraction of organic component in the mobile phase. The fitting parameters for this equation were determined by linear regression analysis. From these regression equations, the resolution (R_s) was calculated for each adjacent pair of solutes:

$$R_s = \frac{\sqrt{N}}{4}\left(\frac{k'_{i+1} - k'_i}{2 + k'_i + k'_{i+1}}\right) \quad (1)$$

where N is the number of theoretical plates.

A window diagram was then prepared to display the resolution as a function of the mobile phase composition. From this diagram, the optimum mobile phase composition and the least-resolved solute pair were visually determined.

RESULTS AND DISCUSSION

Optimization of chromatographic conditions

The retention behavior of physiologically important fatty acids was studied in a reversed-phase LC system using binary aqueous mixtures of methanol and acetonitrile as mobile phases. Four saturated fatty acids (12:0, 13:0, 14:0, and 15:0) and five unsaturated fatty acids (14:1, 18:3, 20:4, 20:5, and 22:6) derivatized with 4-bromomethyl-7-methoxycoumarin were selected as model compounds for initial studies. As shown in Figs. 1 and 2, a non-linear relationship exists between the logarithm of the capacity factor and the mobile phase composi-

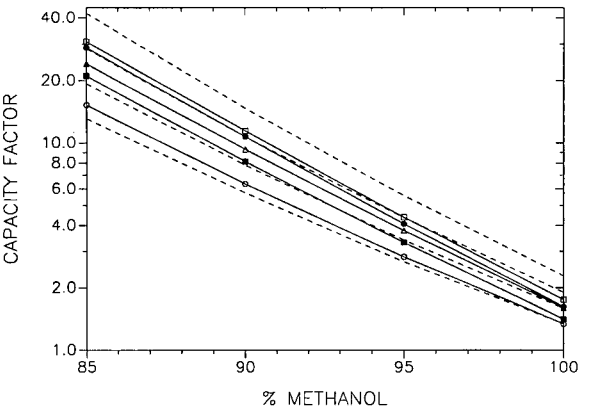

Fig. 1. The relationship between the logarithm of capacity factor (k') for fatty acid derivatives and the mobile phase composition. Column: 96 cm × 200 μm I.D. fused-silica capillary, 3 μm Micro-Pak SP-18 stationary phase. Mobile phase: methanol–water mixtures, 0.75 μl/min, 30°C. Solutes: 14:1 (○), 18:3 (△), 20:4 (□), 20:5 (■) and 22:6 (●); saturated fatty acids from 12:0 (bottom) to 15:0 (top) are represented as dashed lines. Detector: laser-induced fluorescence, 325 nm excitation wavelength, 420 nm emission wavelength.

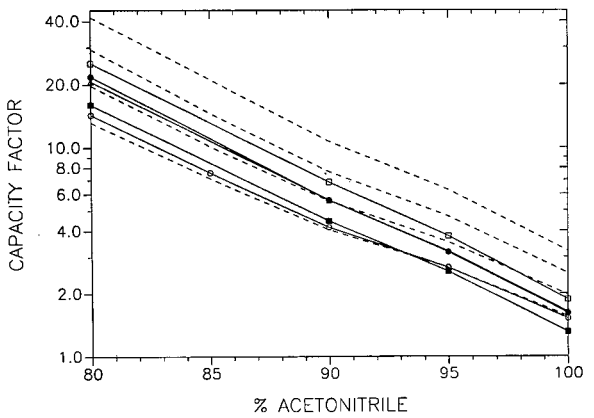

Fig. 2. The relationship between the logarithm of capacity factor (k') for fatty acid derivatives and the mobile phase composition. Mobile phase: acetonitrile–water mixtures, 0.75 μl/min, 30°C. Other experimental conditions and fatty acid symbols as in Fig. 1.

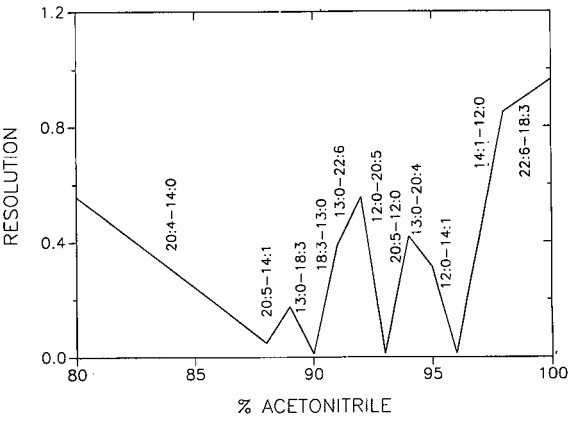

Fig. 4. The relationship between the resolution (R_s) of fatty acid derivatives and the mobile phase composition from Fig. 2.

tion. A significant positive deviation from linearity is observed for all solutes as the fraction of organic component increases from 85 to 100% methanol and from 80 to 100% acetonitrile. It is well known that such non-linear retention behavior can arise from non-ideal solute–solvent and solvent–solvent interactions [25–27].

In general, the logarithm of the capacity factor decreases more rapidly with increasing mobile phase strength for unsaturated than for saturated fatty acid derivatives. In methanol–water mixtures (Fig. 1), the retention order of the unsaturated fatty acids is not changed with mobile phase composition. In acetonitrile–water mixtures (Fig. 2), however, two solute pairs 14:1/20:5 and 18:3/22:6 exhibit an inversion in retention order at 93% and 90% acetonitrile, respectively. For both of these solute pairs, the polyunsaturated fatty acid derivative is less retained at higher acetonitrile composition. It is also apparent, by comparison of the capacity factors for these solute pairs at the same nominal mobile phase composition, that the polyunsaturated fatty acids are less retained in acetonitrile–water than in methanol–water mixtures. These results indicate that acetonitrile has a strong, selective interaction with double bonds, probably arising from dipole induction and orientation forces.

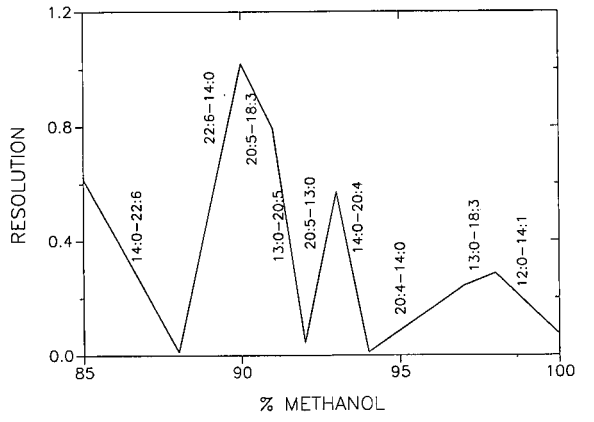

Fig. 3. The relationship between the resolution (R_s) of fatty acid derivatives and the mobile phase composition from Fig. 1.

To optimize the separation of both saturated and unsaturated fatty acid derivatives, a modified window-diagram method was employed [22–24]. The retention data shown in Figs. 1 and 2 were analyzed by linear regression, the resolution between each adjacent pair of solutes was calculated by using eqn. 1, and the resolution of the limiting pair was displayed graphically as a function of the mobile phase composition. Based on the results summarized in Figs. 3 and 4, the optimum composition of the mobile phase was predicted to be 90% methanol and the solute pair 14:0/22:6 was predicted to be the least resolved ($R_s \approx 1.0$). As shown in the experimental study (Fig. 1), however, this solute pair was completely overlapped at the predicted optimum mobile phase composition due to deviation from linear retention behavior. In order to separate 14:0

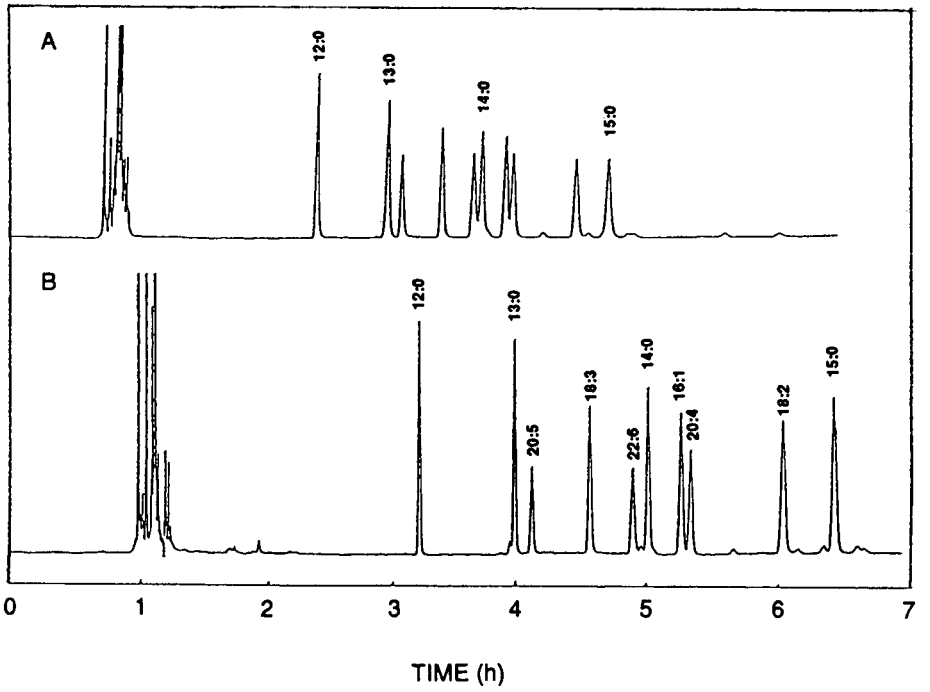

Fig. 5. Separation of standard fatty acid derivatives at the 5–10-femtomole level. Mobile phase: methanol–acetonitrile–water (90:2:8), 0.75 μl/min, 30°C. Column: (A) 96 cm × 200 μm I.D. (158 000 plates), (B) 178 cm × 200 μm I.D. (275 000 plates). Other experimental conditions as in Fig. 1.

and 22:6 without substantially altering the resolution of other fatty acid derivatives, a semi-empirical optimization procedure was employed. Because these solutes differ significantly in the number of double bonds, a small amount of acetonitrile was added to the predicted optimum mobile phase composition in order to reduce the capacity factor of 22:6. Fig. 5A shows the separation obtained for the fatty acid derivatives using a ternary mobile phase mixture of 90% methanol, 2% acetonitrile, and 8% water. Under these conditions, the least-resolved solute pairs were 14:0/22:6 and 16:1/20:4, both of which showed resolution of approximately 1.0. Any further increase in the acetonitrile concentration would be expected to increase the resolution of 14:0/22:6, but would decrease the resolution of 16:1/20:4. Therefore, this mobile phase composition was maintained and a longer chromatographic column was employed to increase the number of theoretical plates. Under these conditions, all fatty acid derivatives showed resolution greater than 1.5 (Fig. 5B).

The optimal separation of 14 fatty acid derivatives using a packed capillary column with 240 000 theoretical plates and the ternary mobile phase mixture of 90% methanol, 2% acetonitrile, and 8% water is represented in Fig. 6. Several additional saturated and unsaturated fatty acids were added to the standard sample for this separation. Nearly baseline resolution was obtained for each component, with no interference from the derivatization reagents or their by-products (Fig. 6, top). It is interesting to note that Halgunset *et al.* [3] also employed a ternary mobile phase mixture of 82% methanol, 9% acetonitrile, and 9% water to separate the *p*-bromophenacyl derivatives of fatty acids. They obtained baseline resolution of 9 fatty acid derivatives, but did not include the polyunsaturated $\omega - 3$ fatty acids.

Determination of fatty acids in fish oil dietary supplements

The fatty acids obtained from fish oil dietary supplements were derivatized with 4-bromomethyl-7-methoxycoumarin and were separated and de-

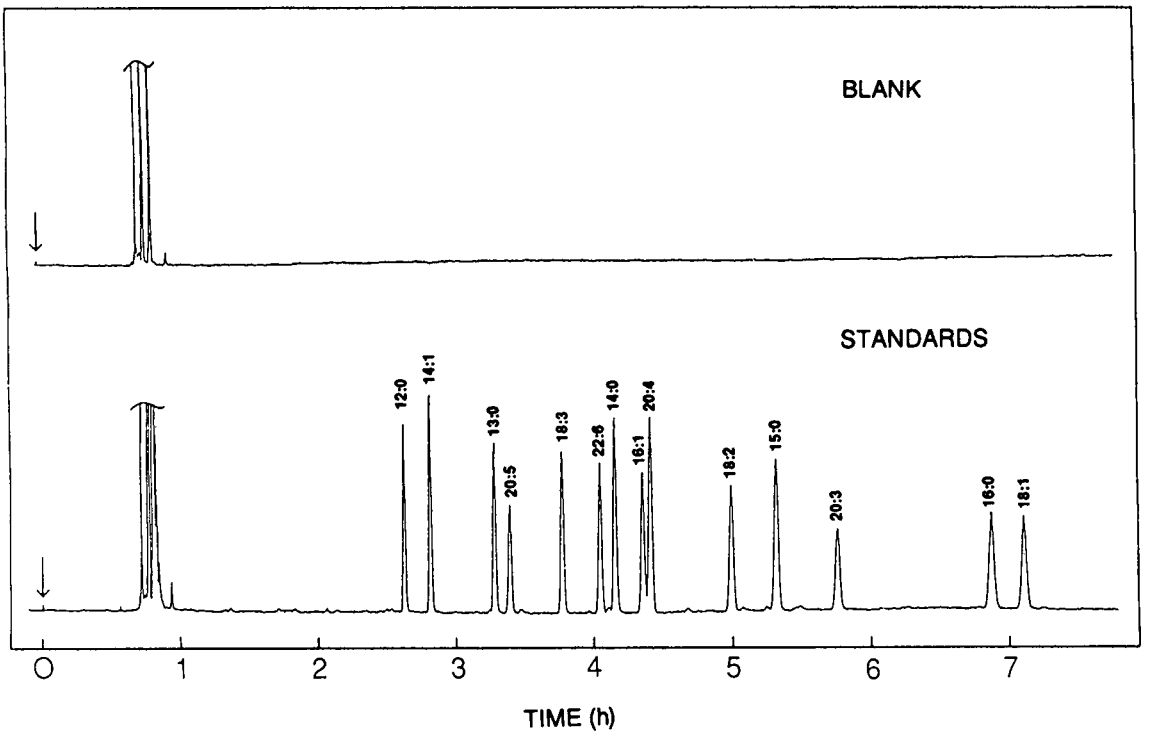

Fig. 6. High-efficiency separation of 14 standard fatty acid derivatives at the 5–10 femtomole level (bottom) and blank (top). Column: 152 cm × 200 μm I.D. (240 000 plates). Other experimental conditions as in Fig. 5.

tected using the analytical methodology described above. The fatty acid composition of Promega Pearls, Omega-3, and Fish-EPA is illustrated in Fig. 7. The major constituents of the fish oil dietary supplements were eicosapentaenoic (20:5) and docosahexaenoic (22:6) acids. Other $\omega - 3$ fatty acids, such as hexadecatetraenoic (16:4) and octadecatetraenoic (18:4) acids, as well as saturated and monounsaturated fatty acids, such as myristic (14:0), palmitic (16:0), palmitoleic (16:1), and oleic (18:1) acids, were the next most abundant components. The minor components were identified as lauric (12:0), hexadecadienoic (16:2), hexadecatrienoic (16:3), linoleic (18:2), linolenic (18:3), arachidonic (20:4), and docosapentaenoic (22:5) acids. The relative amounts of these fatty acids appear to be similar in the Promega Pearls and Omega-3 dietary supplements and are in reasonably good agreement with the manufacturer's specifications (Table I). In contrast, the Fish-EPA supplement contains proportionately greater amounts of saturated and monounsaturated fatty acids, which are of questionable health benefits.

Recently, Beebe and Brown [28] reported a similar analysis of fish oil dietary supplements using reversed-phase LC with a ternary mobile phase of 36% acetonitrile, 20% tetrahydrofuran, and 44% water. They identified the principal components as 20:5, 22:6, 14:0, 16:0, 16:1, 18:1, and 18:2, but were not able to separate and identify the minor components such as 12:0, 16:2, 16:3, 16:4, 18:3, 18:4, 20:4, and 22:5. In addition, the physiologically important $\omega - 3$ fatty acids were not completely resolved from adjacent solutes under their chromatographic conditions. We believe that the results shown in Fig. 7 clearly demonstrate the ability to resolve the physiologically important fatty acids and to detect them at the femtomole level in fish oil dietary supplements. Although the resolution and sensitivity are clearly superior to previous results, these advantages are gained only with a considerable compromise in the analysis time (7.5 h).

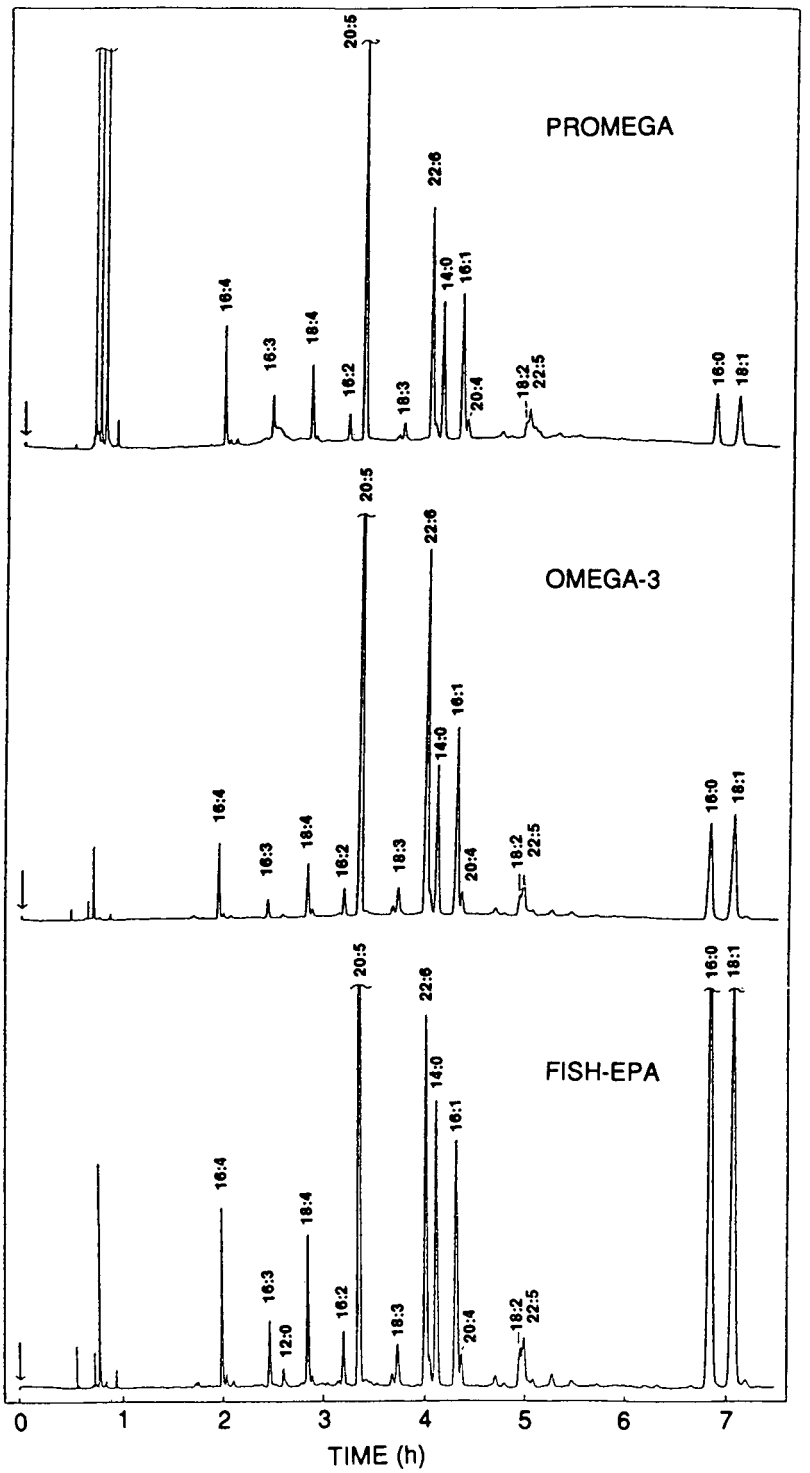

Fig. 7. The chromatograms for the analysis of fatty acid constituents at the femtomole level in fish oil dietary supplements of Promega Pearls, Omega-3, and Fish-EPA. Experimental conditions as in Fig. 6.

TABLE I

COMPOSITION OF POLYUNSATURATED $\omega - 3$ FATTY ACIDS IN COMMERCIALLY AVAILABLE FISH OIL DIETARY SUPPLEMENTS

Data from manufacturer's specifications.

Fatty acid	Promega	Omega-3	Fish-EPA
20:5 (mg/capsule)	168	280	180
22:6 (mg/capsule)	72	120	120
Other $\omega - 3$ (mg/capsule)	60	100	–

Predictive models of fatty acid retention

The retention behavior of the fatty acid derivatives can be described and predicted by means of the retention index system developed by Kovats [29,30]. By using the saturated fatty acids as a standard scale for comparison, the retention index (I) of unsaturated fatty acids can be calculated as follows:

$$I = 100 \left[N + \frac{\log (k'_i/k'_N)}{\log (k'_{N+1}/k'_N)} \right] \quad (2)$$

where k' is the capacity factor for the unsaturated fatty acid (i) that elutes between the saturated fatty acids with carbon numbers N and $N + 1$. Because the unsaturated fatty acids are expressed in terms of the chain length of an equivalent saturated fatty acid, the Kovats retention index system is conceptually equivalent to the ECL model of Özcimder and Hammers [5]. These models are mathematically related in the following manner:

$$I/100 = \text{ECL} = N - yn \quad (3)$$

where N is the number of carbon atoms, n is the number of double bonds, and y is an empirically derived coefficient. When the retention index values for the fatty acids calculated from the experimental data (Figs. 6 and 7) are substituted in eqn. 3, the coefficient y is determined to be 1.419 ± 0.020 by multiple linear regression analysis. The experimentally measured and theoretically predicted values for the retention index of each unsaturated fatty acid are summarized in Table II. Although the average error incurred by using eqn. 3 appears to be rather small (1.83% relative error), it is significantly greater than

TABLE II

RETENTION INDICES (I) OF UNSATURATED FATTY ACID DERIVATIVES

Unsaturated fatty acids	Retention index (I)				
	Experiment	Theory eqn. 3[a]	Relative error[c] (%)	Theory eqn. 4[b]	Relative error[c] (%)
16:4	1064	1032	−3.10	1059	−0.47
16:3	1171	1174	+0.26	1177	+0.51
14:1	1228	1258	+2.44	1229	+0.08
18:4	1238	1232	−0.49	1243	+0.48
16:2	1292	1316	+1.86	1295	+0.23
20:5	1312	1291	−1.60	1309	−0.23
18:3	1358	1374	+1.18	1361	+0.22
22:6	1388	1349	−2.81	1375	−0.94
16:1	1419	1458	+2.75	1414	−0.35
20:4	1424	1432	+0.56	1427	+0.21
18:2	1475	1516	+2.78	1480	+0.34
22:5	1486	1491	+0.34	1493	+0.47
20:3	1532	1574	+2.74	1546	+0.91
18:1	1613	1658	+2.79	1598	−0.93
Average			1.83		0.46

[a] Calculated from the equation $I/100 = N - 1.419n$.

[b] Calculated from the equation $I/100 = 0.922N - 1.184n + 0.570$.

[c] Calculated from the expression $(I_{\text{Experiment}} - I_{\text{Theory}})/I_{\text{Experiment}}$.

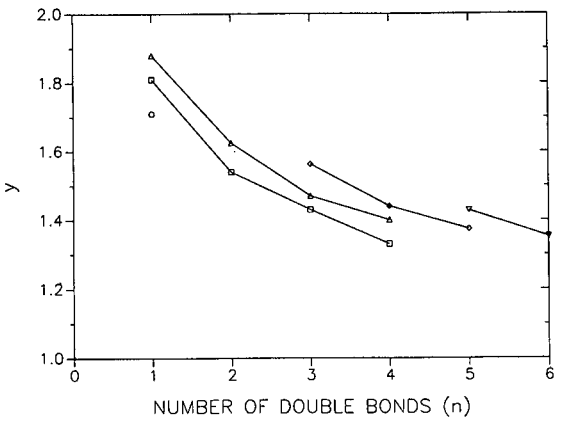

Fig. 8. The relationship between the y coefficient in eqn. 3 and the number of double bonds (n) in fatty acid derivatives with the same number of carbon atoms. Solutes: 14:n (○), 16:n (□), 18:n (△), 20:n (◇) and 22:n (▽). Experimental conditions as in Fig. 6.

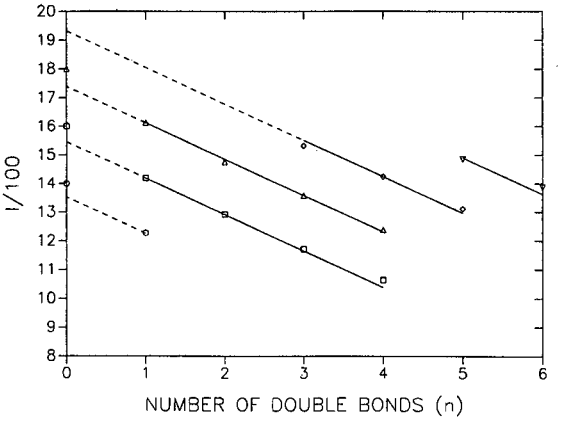

Fig. 10. The relationship between the retention index (I) divided by 100 and the number of double bonds (n) in fatty acid derivatives with the same number of carbon atoms. Solutes: 14:n (○), 16:n (□), 18:n (△), 20:n (◇) and 22:n (▽). Experimental conditions as in Fig. 6.

the precision of replicate measurements (±0.1% relative standard deviation, R.S.D.). More importantly, however, this error results in the incorrect prediction of elution order for all of the polyunsaturated fatty acids with retention characteristics similar to saturated and monounsaturated fatty acids (Table II).

In order to examine this problem in more detail, individual values for the coefficient y were calculated according to eqn. 3 for each unsaturated fatty acid and graphed as a function of the number of double bonds (n). It is apparent from Fig. 8 that the coefficient y decreases as n increases for fatty acids with the same number of carbon atoms, as noted previously by Özcimder and Hammers [5]. In addition, however, the coefficient appears to decrease as N decreases for fatty acids with the same number of double bonds.

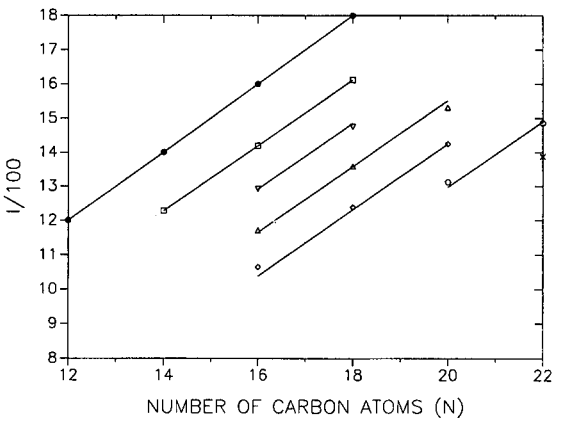

Fig. 9. The relationship between the retention index (I) divided by 100 and the number of carbon atoms (N) in fatty acid derivatives with the same number of double bonds. Solutes: N:0 (●), N:1 (□), N:2 (▽), N:3 (△), N:4 (◇), N:5 (○) and N:6 (×). Experimental conditions as in Fig. 6.

Based on these observations, a more reliable equation to describe and predict the retention behavior of unsaturated fatty acids may be derived. From Fig. 9, a linear relationship is observed between $I/100$ and N for fatty acids with the same number of double bonds. Likewise from Fig. 10, a negative linear relationship is observed between $I/100$ and n for fatty acids with the same number of carbon atoms. Therefore, the retention index can be expressed as a simple linear function of both N and n:

$$I/100 = \text{ECL} = xN - yn + z \quad (4)$$

where x, y and z are empirically derived coefficients. To determine the values of these coefficients, the experimental retention index values for the fatty acids were substituted into eqn. 4 and analyzed by multiple linear regression. The solution of this equation yields $x = 0.922 \pm 0.015$, $y = 1.184 \pm 0.022$, and $z = 0.570 \pm 0.224$ for the unsaturated fatty

acids. As summarized in Table II, the average error in the retention index is 0.46% and all fatty acids are predicted in the correct elution order.

Eqn. 4 represents a simple modification of the classical ECL model for fatty acid retention developed by Özcimder and Hammers [5]. Because this expression is more accurate and precise than eqn. 3, it permits more confident identification of unknown fatty acids in complex mixtures. Although the specific values cited above for the empirical coefficients in eqn. 4 are applicable only under the experimental conditions used in this study, such coefficients can be readily determined under different conditions by using the method described above.

CONCLUSIONS

The retention behavior of 4-bromomethyl-7-methoxycoumarin derivatives of fatty acids with 12–22 carbon atoms and 0–6 double bonds has been studied in reversed-phase LC with aqueous methanol and acetonitrile mobile phases. The baseline resolution for the separation of 14 saturated and unsaturated fatty acids was obtained by using a packed capillary column with 240 000 theoretical plates and a mobile phase composition of 90% methanol, 2% acetonitrile, and 8% water. The fatty acid derivatives were determined at the femtomole level in fish oil dietary supplements with laser-induced fluorescence detection. It was found that the dietary supplements contain predominantly the polyunsaturated eicosapentaenoic (20:5) and docosahexaenoic (22:6) acids as well as lesser amounts of hexadecatetraenoic (16:4) and octadecatetraenoic (18:4) acids. However, they may also contain significant amounts of saturated and monounsaturated fats such as myristic (14:0), palmitic (16:0), palmitoleic (16:1), and oleic (18:1) acids. The retention indices of the unsaturated fatty acid derivatives increased linearly with the number of carbon atoms and decreased linearly with the number of double bonds. The retention indices predicted by using a modified ECL equation showed less than 0.46% relative error and $\pm 0.1\%$ R.S.D.

ACKNOWLEDGEMENTS

This work was supported by the US Department of Energy, Office of Basic Energy Sciences, Division of Chemical Sciences under Contract No. DE-FG02-89ER14056. The authors wish to thank Dr. Kirk Maxey (Cayman Chemical, Ann Arbor, MI, USA) for providing the fatty acid standards and Dr. Thomas V. Atkinson (Michigan State University) for assisting with the multiple linear regression analysis.

REFERENCES

1 W. E. M. Lands, *Fish and Human Health*, Academic Press, New York, 1986.
2 P. M. Herold and J. E. Kinsella, *Am J. Clin. Nutr.*, 43 (1986) 566.
3 J. Halgunset, F. W. Lund and A. Sunde, *J. Chromatogr.*, 237 (1982) 496.
4 P. R. Brown, J. M. Beebe and J. Turcotte, *Crit. Rev. Anal. Chem.*, 21 (1989) 193.
5 M. Özcimder and W. E. Hammers, *J. Chromatogr.*, 187 (1980) 307.
6 J. P. Roggero and S. V. Coen, *J. Liq. Chromatogr.*, 4 (1981) 1817.
7 A. K. Batta, V. Dayal, R. W. Colman, A. K. Sinha, S. Shefer and G. Salen, *J. Chromatogr.*, 284 (1984) 257.
8 C. Osterroht, *Chromatographia*, 23 (1987) 419.
9 H. C. Jordi, *J. Liq. Chromatogr.*, 1 (1978) 215.
10 R. F. Borch, *Anal. Chem.*, 47 (1975) 2437.
11 H. Traitler, H. J. Wielle and A. Studer, *J. Am. Oil Chem. Soc.*, 65 (1988) 755.
12 T. Rezanka and M. Podojil, *J. Chromatogr.*, 346 (1985) 453.
13 W. Dunges, *Anal. Chem.*, 49 (1977) 442.
14 S. N. Barker, J. A. Monti, S. T. Christian, F. Benington and R. D. Morin, *Anal. Biochem.*, 107 (1980) 116.
15 N. Ichinose, K. Nakamura, C. Shimizu, H. Kurokura and K. Okamato, *J. Chromatogr.*, 295 (1984) 463.
16 M. Ikeda, K. Shimada, T. Sakaguchi and U. Matsumoto, *J. Chromatogr.*, 305 (1984) 261.
17 W. D. Korte, *J. Chromatogr.*, 243 (1982) 153.
18 H. Tsuchiya, T. Hayashi, H. Naruse and N. Takagi, *J. Chromatogr.*, 234 (1982) 121.
19 V. L. McGuffin and R. N. Zare, *Appl. Spectrosc.*, 39 (1985) 847.
20 V. L. McGuffin and R. N. Zare, *Proc. Natl. Acad. Sci. U.S.A.*, 82 (1985) 8315.
21 J. C. Gluckman, A. Hirose, V. L. McGuffin and M. Novotny, *Chromatographia*, 17 (1983) 303.
22 R. J. Laub and J. H. Purnell, *J. Chromatogr.*, 112 (1975) 71.
23 R. J. Laub, *J. Liq. Chromatogr.*, 7 (1984) 647.
24 A. J. Hsu, R. J. Laub and S. J. Madden, *J. Liq. Chromatogr.*, 7 (1984) 615.
25 H. B. Patel and T. M. Jefferies, *J. Chromatogr.*, 389 (1987) 21.
26 J. L. Glajch, J. J. Kirkland, K. M. Squire and J. M. Minor, *J. Chromatogr.*, 199 (1980) 57.
27 E. D. Katz, C. H. Lochmuller and R. P. W. Scott, *Anal. Chem.*, 61 (1989) 349.
28 J. M. Beebe and P. R. Brown, *J. Chromatogr.*, 468 (1989) 225.
29 E. Kovats, *Helv. Chim. Acta*, 41 (1958) 1915.
30 L. S. Ettre, *Chromatographia*, 6 (1987) 489.

Journal of Chromatography, 627 (1992) 97–105
Elsevier Science Publishers B.V., Amsterdam

CHROM. 24 595

Use of chiral monohalo-*s*-triazine reagents for the liquid chromatographic resolution of DL-amino acids

Hans Brückner and Bernd Strecker

Institute of Food Technology, University of Hohenheim, W-7000 Stuttgart 70 (Germany)

(First received June 19th, 1992; revised manuscript received August 27th, 1992)

ABSTRACT

Nucleophilic replacement of one halogen atom (chlorine, fluorine) in the trihalo-*s*-triazines (2,4,6-trihalo-1,3,5-triazines), cyanuric chloride or cyanuric fluoride by reaction with either methanol, 2-naphthol, 1-methoxynaphthalene, or 4-aminoazobenzene furnished ultraviolet-absorbing, fluorescent of chromogenic dihalo-*s*-triazines. Substitution of a further halogen atom in these compounds by reaction with L-alanine amide provided chiral monohalo-*s*-triazines. The remaining halogen atom was substituted by reaction with selected D- or L-amino acids to form diastereomeric derivatives which were separated by reverse-phase (C_{18}) high-performance liquid chromatography using mixtures of water, acetonitrile and trifluoroacetic acid as eluents. Because of its possibilities for selection among a large number of detection groups in combination with various chiral moieties, the approach is considered to be a general method for the design and construction of tailor-made reagents suitable for precolumn derivatization and indirect liquid chromatographic separation of amino acid enantiomers.

INTRODUCTION

A number of chiral reagent suitable for precolumn derivatization have been described for the indirect, liquid chromatographic resolution of DL-amino acids (DL-AA) as diastereoisomers. Some examples are naphthylethyl isocyanate [1], 9(+)-fluorenylethyl chloroformate [2], chiral thiols together with *o*-phthaldialdehyde [3], N^2-(5-fluoro-2,4-dinitrophenyl)-L-alanine amide (Marfey's reagent) [4] or structurally related chiral variants of Sanger's reagent [5,6]. The latter reagents deserve attention because of the large differences in the retention times of the diastereomers formed. This observation has been explained in terms of the planar configuration of the dinitrobenzene moiety and the spatial arrangement of the AA units in the diastereomers, which make the formation of an intramolecular hydrogen bond more favourable in the L–L diastereomer than in the L–D diastereomer (the first letter refers to the configuration of the AA in the reagent, *cf.*, Fig. 1).

On the basis of the structural similarity of the diastereomers formed by reactions of DL-AA with chiral fluorodinitrobenzenes and chiral monohalo-*s*-triazines (Fig. 1), it was assumed that the latter derivatives might also be resolvable by high-performance liquid chromatography (HPLC). Owing to the trifunctionality of the starting compound trichloro-*s*-triazine, or the more reactive trifluoro-*s*-triazine, it should be possible to design reagents containing a large selection of detectable groups in addition to chiral moieties.

In principle, the general chemistry used for the syntheses of triazine derivatives used as biocides [7,8] and of reactive dyes with heterocyclic reactive systems [9] is applicable; this also indicates the potential scope of the approach described in this paper. Although triazine derivatives are important fungicides and herbicides [7,8] and triazine reactive dyes are of paramount importance for the dying of wool and cellulose fibres [9–11], a number of

Correspondence to: H. Brückner, Institute of Food Technology, University of Hohenheim, W-7000 Stuttgart 70, Germany.

0021-9673/92/$05.00

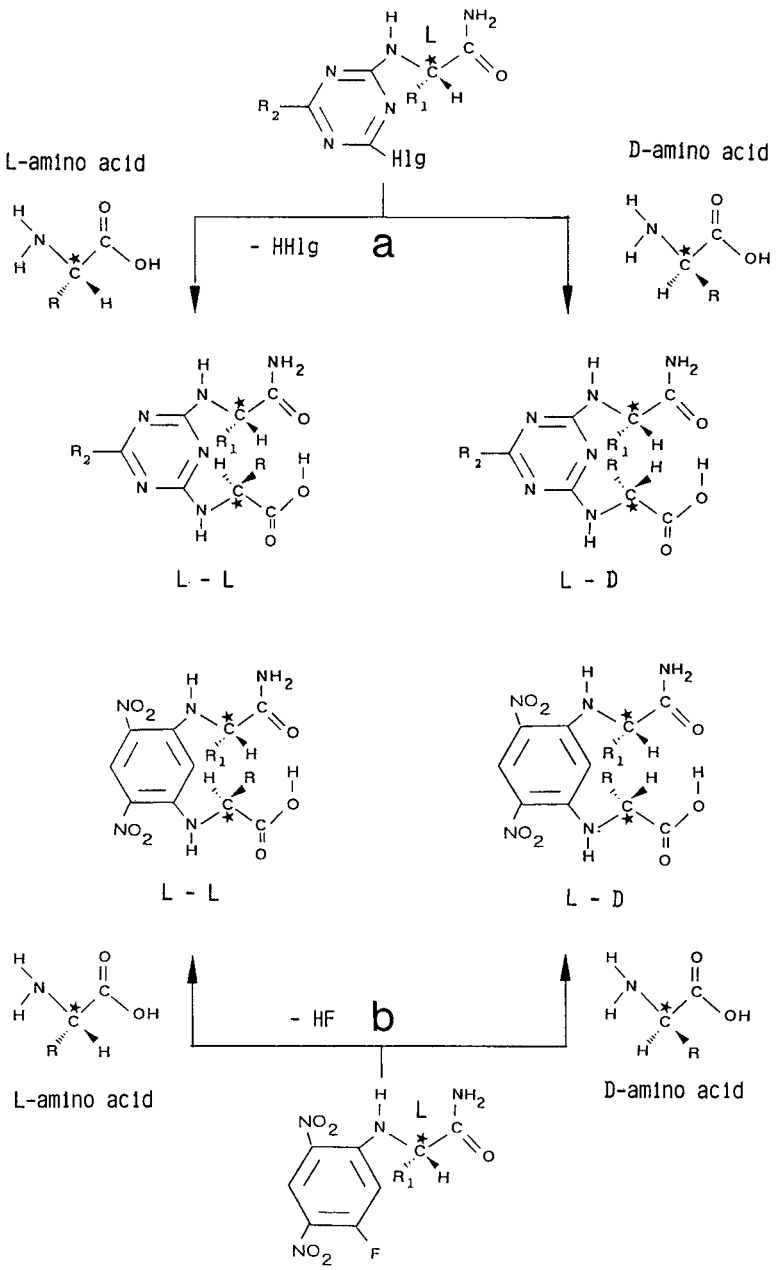

Fig. 1. Structures of diastereomers obtained by derivatization of DL-amino acids with (a) chiral monohalo-*s*-triazines (Hlg = halogen, Cl or F) in comparison with diastereomers formed by reaction with (b) chiral N^2-(5-fluoro-2,4-dinitrophenyl)-L-amino acid amides. R = side-chains of chiral amino acids to be analyzed, R_1 = methyl in alanine amide; R_2 = detectable or otherwise suitable group in (a); asterisks indicate chiral centres.

applications have also been reported in chromatography. Chromogenic reactive dyes are employed in affinity chromatography of proteins [12], dichlorotriazinylaminofluorescein has been used as a fluorescence label for immunoglobulins [13], 1-ethoxy-4-(dichloro-*s*-triazinyl)naphthalene was described as a fluorescent reagent for corticosteroids [14] and chiral *s*-triazines have been used a chiral stationary phases in gas–liquid chromatography [15].

EXPERIMENTAL

Instruments

A JASCO (Kyoto, Japan) instrument consisting of a Model 880 PU reciprocating pump with active damper, a Model 880-02 low-pressure gradient former, a Model 801-SC controller and a Model 875-UV variable-wavelength UV detector or a Model RF-535 fluorescence detector (Shimadzu, Kyoto, Japan) was used for HPLC. A Chromato-Integrator D-2500 (Merck–Hitachi, Darmstadt, Germany) was used for data processing and samples were injected on to the column by means of a Model ISS-100 autosampler (Perkin-Elmer, Überlingen, Germany).

Chromatography

Nucleosil 100 C_{18}, particle size 5 μm (Macherey–Nagel, Düren, Germany), was packed into 250 mm × 4 mm I.D. steel columns equipped with guard cartridges (20 × 4 mm I.D.) packed with the same stationary phase.

Eluents for HPLC are specified in Fig. 3; the water used was deionized by reverse osmosis with a Milli-Q water purification system (Millipore, Bedford, MA, USA); the eluents were filtered through a 0.45-μm filter (HVL P04700; Millipore) and degassed by sonication before used.

Chemicals

Chemicals and solvents used for HPLC were of analytical-reagent or for chromatography grade from Merck (Darmstadt, Germany). Light petroleum was of b.p. 50–70°C. Amino acids were purchased from Sigma (St. Louis, MO, USA) or Fluka (Buchs, Switzerland). L-Alanine amide hydrochloride was obtained from Novabiochem (Läufelfingen, Switzerland), cyanuric chloride and 1-methoxynaphthalene from Aldrich (Steinheim, Germany) and cyanuric fluoride and 4-phenylazoaniline (4-aminoazobenzene) from Fluka.

Derivatization of standard amino acid solutions

Standard solutions of selected DL-amino acids (100 m*M* in 1 *M* HCl) were prepared. To 30 μl (3 μmol) of standard solution, 45 μl of 1.0 *M* $NaHCO_3$ solution and 500 μl (5 μmol) of the reagent solution were added and the mixture was heated for 1 h at 80°C (for FAZT-Ala-NH_2, CNOT-Ala-NH_2 and CMOT-Ala-NH_2) or at 100°C (for CAZT-Ala-NH_2 and CMNT-Ala-NH_2). Then 30 μl of 1.0 *M* HCl and 1.4 ml of dimethyl sulphoxide (DMSO) were added, the mixture was filtered by means of a 0.2-μm disposable filter (Anotop 10, pore size 0.2 μm; Merck) and 1-μl aliquots were injected on to the HPLC column, with the exceptions of CNOT-Ala-NH_2 and CMOT-Ala-NH_2, for which 5 μl were injected.

Syntheses and characterization of dihalo-s-triazines and chiral monohalo-s-triazines

Thin-layer chromatography, mass spectrometry, UV–Vis and fluorescence spectrometry. For thin-layer chromatography (TLC), precoated plates (Kieselgel 60 F_{254}, size 20 × 20 cm; Merck) were used; R_F values were determined at 21°C in glass chambers (Desaga, Heidelberg, Germany) coated with filter-paper; the distance from the start to the front of the TLC plates was 10 cm. The solvent systems were as follows (v/v): (I) light petroleum–acetone (55:45); (II) light petroleum–chloroform–methanol (40:30:30); and (III) ethyl acetate–light petroleum (60:40). Spots were made visible by inspection of the TLC plates under UV light at 254 nm.

Electron impact mass spectrometry was performed at an ionizing energy at 70 eV using a Varian 311 A mass spectrometer. Mass spectra of compounds containing chlorine were calculated for the most abundant isotopes ^{35}Cl and ^{37}Cl; int. refers to intense ions in the mass spectra. Melting points (m.p.) or decomposition temperatures (decomp.) of compounds were determined in open capillaries using a Model 520 melting point apparatus (Büchi, Flawil, Switzerland) and are not corrected.

Spectra in the ultraviolet (UV) and visible (Vis) ranges were taken using a Model DU 64 spectrophotometer (Beckman Instruments); a Model LS 50 luminescence spectrometer with a xenon pulsation lamp (Perkin-Elmer) was used for measurement of the fluorescence spectra. For the measurement of the UV–Vis spectra, 0.1 mmol of the reagents was dissolved in 10 ml of DMSO in volumetric flasks and the solutions were made up to 100 ml by addition of eluent B. The solutions were then further diluted with these eluents until maxima of extinctions in the range 0.5–0.9 were obtained. Spectra were recorded at 20°C. Fluorescence spectra were recorded for 10^{-5} *M* solutions in the eluents used for HPLC.

Molar absorption coefficients (ε) are given in l mol^{-1} cm^{-1}.

*Synthesis of N^2-[2-(4-chloro-6-methoxy-1,3,5-triazinyl)]-L-alanine amide (CMOT-Ala-NH_2) (**a**).* 2,4-Dichloro-6-methoxy-1,3,5-triazine (DCMT) was synthesized according to ref. 7; yield, 3.37 g (30%); m.p., 87°C (lit. [7] m.p., 88–89°C); R_F (I), 0.79; MS, *m/z* 179 and 181 (M^+), 149 and 151 (M − OMe + H), intense.

For the synthesis of **a**, DCMT (0.9 g, 5 mmol) and L-Ala-NH_2 · HCl (623 mg, 5 mmol) were dissolved in a mixture of acetone (15 ml) and water (10 ml) and 1.0 *M* $NaHCO_3$ (15 ml) was added. The mixture was stirred for 2 h at room temperature (r.t.), then neutralized by addition of 0.1 *M* HCl and evaporated to dryness *in vacuo*. The residue was dissolved in ethanol and *n*-hexane was added at 0°C. The precipitate was filtered, the filtrate was evaporated to dryness and the procedure was repeated twice. Total yield, 295 mg (25%), colourless crystals; m.p., 180°C; R_F (I), 0.39; R_F (II), 0.64; MS, *m/z* 187 and 189 (M − $CONH_2$), very intense.

*Synthesis of N^2-[2-(4-chloro-6-(2-naphthoxy)-1,3,5-triazinyl)]-L-alanine amide (CNOT-Ala-NH_2) (**b**).* 2,4-Dichloro-6-(2-naphthoxy)-1,3,5-triazine (DNOT) was synthesized according to ref. 7; yield, 3.9 g (67%), colourless, amorphous powder; m.p., 150°C (lit. [8] m.p., 145–154°C); R_F (I), 0.77; MS, *m/z* 291 and 293 (M^+), 256 and 258 (M − Cl), int., 127 ($C_{10}H_7^+$), intense.

For the synthesis of **b**, 1 *M* $NaHCO_3$ (3 ml) was added to DNOT (292 mg, 1 mmol) and L-Ala-NH_2 · HCl (125 mg, 1 mmol), dissolved in a mixture of acetone (13 ml) and water (2 ml). The mixture was stirred for 12 h, water (20 ml) was added and the white precipitate was filtered, washed with water and dried *in vacuo*. Yield, 293 mg (85%) (amorphous); m.p., 218°C; R_F (I), 0.48; R_F (II), 0.73; R_F (III), 0.11; UV (nm), 232; ε (232 nm), 23 500; MS, *m/z* 343 and 345 (M^+), int., 299 and 301 (M − $CONH_2$), very int., 127 ($C_{10}H_8^+$), intense.

*N^2-[2-(4-Chloro-6-(4-methoxy-1-naphthyl)-1,3,5-triazinyl)]-L-alanine amide (CMNT-Ala-NH_2) (**c**).* 2,4-Dichloro-6-(4-methoxy-1-naphthyl)-1,3,5-triazine (DMNT) was obtained as follows. Solid $AlCl_3$ (2.67 g, 20 mmol) was added to cyanuric chloride (3.69 g, 20 mmol) and 1-methoxynaphthalene (3.16 g, 20 mmol) dissolved in toluene (60 ml) at 5–10°C. The mixture was stirred for 15 h at r.t., the brown precipitate that formed was removed by filtration, washed with toluene and poured into 250 ml of ice-cold 0.1 m*M* HCl. The precipitate was filtered, washed with cold water, dried *in vacuo* and dissolved in boiling toluene. The yellow compound DMNT which precipitated at r.t. was filtered off and dried *in vacuo*. The filtrate was evaporated to dryness and the procedure was repeated twice. Total yield, 3.21 g (52%), amorphous powder that exhibits blue fluorescence in organic solvents; m.p., 128°C; R_F (II), 0.88; MS, *m/z* 305 and 307 (M^+), very intense.

For the synthesis of **c**, DMNT (306 mg, 1 mmol) was dissolved in acetone (200 ml) at 40°C and L-alanine amide · HCl (125 mg, 1 mmol) and 1 *M* $NaHCO_3$ (3 ml) were added. After 90 min at 40°C a precipitate had formed which was filtered off; the filtrate was reduced to about half its volume by evaporation, light petroleum (200 ml) was added and the mixture was stirred for 30 min at 0°C. The colourless precipitate was filtered, washed with light petroleum and water and dried *in vacuo*. Yield, 227 mg (64%), amorphous powder that exhibits blue fluorescence in organic solvents; m.p., 232°C (decomp.); R_F (I), 0.43; R_F (II), 0.75; R_F (III), 0.12; UV (nm), 241, 340; ε (241), 45 000; ε (340), 13 500; MS, *m/z* 358 and 360 (MH^+), int., 314 and 316 (M − $CONH_2$ + H), very intense.

*N^2-[2-(4-Chloro-6-(4-phenylazoanilino)-1,3,5-triazinyl)]-L-alanine amide (CAZT-Ala-NH_2) (**d**).* 2,4-Dichloro-6-(4-phenylazoanilino)-1,3,5-triazine (DAZT) was obtained as follows. 4-Aminoazobenzene (1.97 g, 10 mmol) was dissolved in 120 ml of dioxane and 40 ml of water and a solution of cyanuric chloride (1.88 g, 10 mmol) in 20 ml of dioxane and 5 ml of water was added at 0–5°C. The mixture was maintained at pH 6–7 by addition of 2 *M* Na_2CO_3. The organic solvent was removed *in vacuo*, the precipitate formed was filtered off, dissolved in dioxane (200 ml) and water (250 ml) was added. The orange precipitate was filtered off, washed with water and dried *in vacuo*. Yield, 1.09 g (28%); m.p., 216°C (decomp.) (lit. [8] m.p., 211–213°C), orange, amorphous powder; R_F (I), 0.81; MS, *m/z* 344 and 346 (M^+), int., 239 and 241 (M − $N_2C_6H_5$), very intense.

For the synthesis of **d**, L-Ala-NH_2 · HCl (249 mg, 2 mmol) and 1 *M* $NaHCO_3$ (6 ml) were added to a solution of DATZ (690 mg, 2 mmol) in acetone (60 ml) and water (10 ml). After 1 h at 40°C the

orange precipitate that formed was filtered off, washed with water and dried *in vacuo*. Yield, 656 mg (83%); m.p., 226°C (decomp.); R_F (I), 0.44; R_F (II), 0.75; R_F (III), 0.10; UV (nm), 367; ε (367 nm), 32 700; MS, *m/z* 397 and 399 (MH^+), int., 353 and 355 ($M - CONH_2 + H$), int., 320 ($M - C_6H_5$), int., 292 ($M - N_2C_6H_5$), intense.

N^2-[2-(4-Fluoro-6-(4-phenylazoanilino)-1,3,5-triazinyl)]-L-alanine amide (FAZT-Ala-NH_2) (e). 2,4-Difluoro-6-(4-phenylazoanilino)-1,3,5-triazine (DAZT) was obtained as follows. To 4-phenylazoaniline (789 mg, 4 mmol) in dioxane (40 ml) and water (20 ml), cyanuric fluoride (341 μl, 4 mmol) was added within 20 min at −5 to 0°C, and pH 4–4.5 was maintained by addition of 2 *M* Na_2CO_3. After 20 min at 0°C and 1 h at r.t., the orange precipitate that formed was filtered off, washed with water and dried *in vacuo*. Yield, 966 mg (77%), orange amorphous powder; m.p., 188°C (decomp.); R_F (I), 0.80; MS, *m/z* 312 (M^+), int., 207 ($M - N_2C_6H_5$), very intense.

For the synthesis of **e**, DAZT (312 mg, 1 mmol) and L-Ala-NH_2 · HCl (125 mg, 1 mmol) were dissolved in dioxane (30 ml) and water (10 ml), and the pH was adjusted to 7.5–8 by addition of 1 *M* $NaHCO_3$. After 10 min at r.t. water (20 ml) was added, the precipitate that formed was filtered off, washed with water and dried *in vacuo*. Yield, 241 mg (63%); m.p., 276°C (decomp.); R_F (I), 0.39; R_F (II), 0.70; R_F (III), 0.10; UV (nm), 343; ε (343 nm), 31 300; MS, *m/z* 380 (M^+), int., 336 ($M - CONH_2$), int., 303 ($M - C_6H_5$), 275 ($M - N_2C_6H_5$), intense.

RESULTS AND DISCUSSION

The chiral monohalo-*s*-triazine reagents shown in Fig. 2 were synthesized from cyanuric chloride (2,4,6-chloro-1,3,5-triazine) and in one instance from cyanuric fluoride (2,4,6-fluoro-1,3,5-triazine) via replacement of one halogen atom by reaction with selected nucleophiles. The substituents thus introduced serve either as a blocking group (methoxy in CMOT-Ala-NH_2), a UV-absorbing moiety (2-naphthoxy in CNOT-Ala-NH_2), a fluorophore (1-methoxynaphthyl in CMNT-Ala-NH_2), or a chromogenic group (4-phenylazoanilino in CAZT-Ala-NH_2 or FAZT-Ala-NH_2). In a second derivatization step, one further halogen was substituted by reaction with L-alanine amide, yielding the chiral

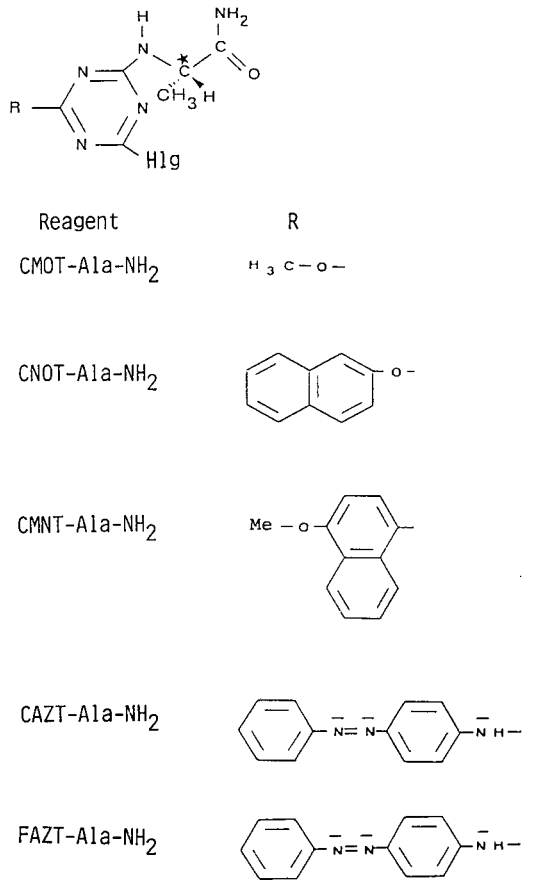

Fig. 2. General structure of chiral monohalo-*s*-triazines and of groups R in reagents abbreviated as follows: (**a**) CMOT-Ala-NH_2; (**b**) CNOT-Ala-NH_2; (**c**) CMNT-Ala-NH_2; (**d**) CAZT-Ala-NH_2; and (**e**) FAZT-Ala-NH_2; the chiral moiety consists of L-alanine amide (Ala-NH_2) and an asterisk indicates the chiral centre; Hlg = Cl in **a**–**d** and F in **e**; Me = methyl; for systematic names of the reagents **a**–**e**, see Experimental.

monohalo-*s*-triazine derivatives shown in Fig. 2. Dihalo- and monohalo-*s*-triazines were isolated and characterized as described under Experimental. In principle, the derivatization reactions may also be carried out in the reverse order. The monohalo-*s*-triazine reagents furnished diastereomeric derivatives on reaction with DL-AA under alkaline conditions with heating at 80–100°C for 1 h. No racemization of the AA to be analysed or of AA in the reagents was observed under these conditions (detection limit *ca.* 0.5% D-AA in an excess of L-AA). Investigation of

TABLE I

NET RETENTION TIMES OF FIRST- ($t'_{R(L-L)}$) AND SECOND- ($t'_{R(D-L)}$) ELUTED DIASTEREOMERS FORMED BY REACTION OF SELECTED DL-AMINO ACIDS WITH CHIRAL MONOHALO-*s*-TRIAZINES, AND DIFFERENCES IN ELUTION TIMES (Δt_R)

The first letter in diastereomers L–L and D–L refers to the configuration of the amino acids to be analysed and the second to that of the amino acid in the chiral reagents.

Reagent[a]	Net retention time (min)[b]														
	Amino acid to be analysed[c]														
	DL-Ala			DL-Val			DL-Phe			DL-Glu			DL-Arg		
	$t'_{R(L-L)}$	$t'_{R(D-L)}$	Δt_R	$t'_{R(L-L)}$	$t'_{R(D-L)}$	Δt_R	$t'_{R(L-L)}$	$t'_{R(D-L)}$	Δt_R	$t'_{R(L-L)}$	$t'_{R(D-L)}$	Δt_R	$t'_{R(L-L)}$	$t'_{R(D-L)}$	Δt_R
CMOT-Ala-NH_2	2.80	3.67	0.87	12.69	19.64	6.95	68.55	99.35	30.80	2.12	2.49	0.37	1.65	1.93	0.28
CNOT-Ala-NH_2	16.31	16.56	0.25	18.32	18.82	0.50	21.25	21.25	0.00	14.80	14.80	0.00	13.35	13.35	0.00
CMNT-Ala-NH_2	15.85	15.85	0.00	16.91	17.41	0.50	19.51	19.79	0.28	14.01	14.01	0.00	12.99	12.99	0.00
FAZT-Ala-NH_2[d]	19.32	19.71	0.39	21.34	22.32	0.98	24.61	25.39	0.78	18.08	18.08	0.00	16.49	16.49	0.00

[a] For abbreviations and structures, see Experimental and Fig. 2.

[b] t_0(DMSO) = 2.16 min.

[c] DL-Ser was not resolved by derivatization with the four reagents.

[d] Diastereomers formed by reaction of DL-amino acids with FAZT-Ala-NH_2 are identical with those formed with CAZT-Ala-NH_2 and therefore show the same retention times.

the derivatization by TLC and spraying with ninhydrin reagent showed >97% completeness of the reactions and no chiral discrimination was detectable under these conditions, as indicated by the equal peak areas of the diastereomers formed from DL-AA. The DL-AA used were selected according to representative side-chain features, Ala (neutral), Val (neutral, sterically hindered), Ser (hydroxymethyl), Phe (aromatic), Glu (acidic) and Arg (basic).

The diastereomers formed were subjected to HPLC using octadecylsilylsilica as the stationary phase and acidic eluents of pH 1.9–2.0. As with diastereomers formed by reaction of DL-AA with chiral variants of Sanger's reagent [5,6], L–L diastereomers eluted before L–D diastereomers (the first letter refers to the configuration of the AA in the reagent). Net retention times and differences in net retention times of the diastereomeric derivatives of DL-AA formed with the reagents are given in Table I and sections of chromatograms of those diastereomers which display resolution are shown in Fig. 3. For the diastereomers formed with CMOT-Ala-NH_2, the ab-

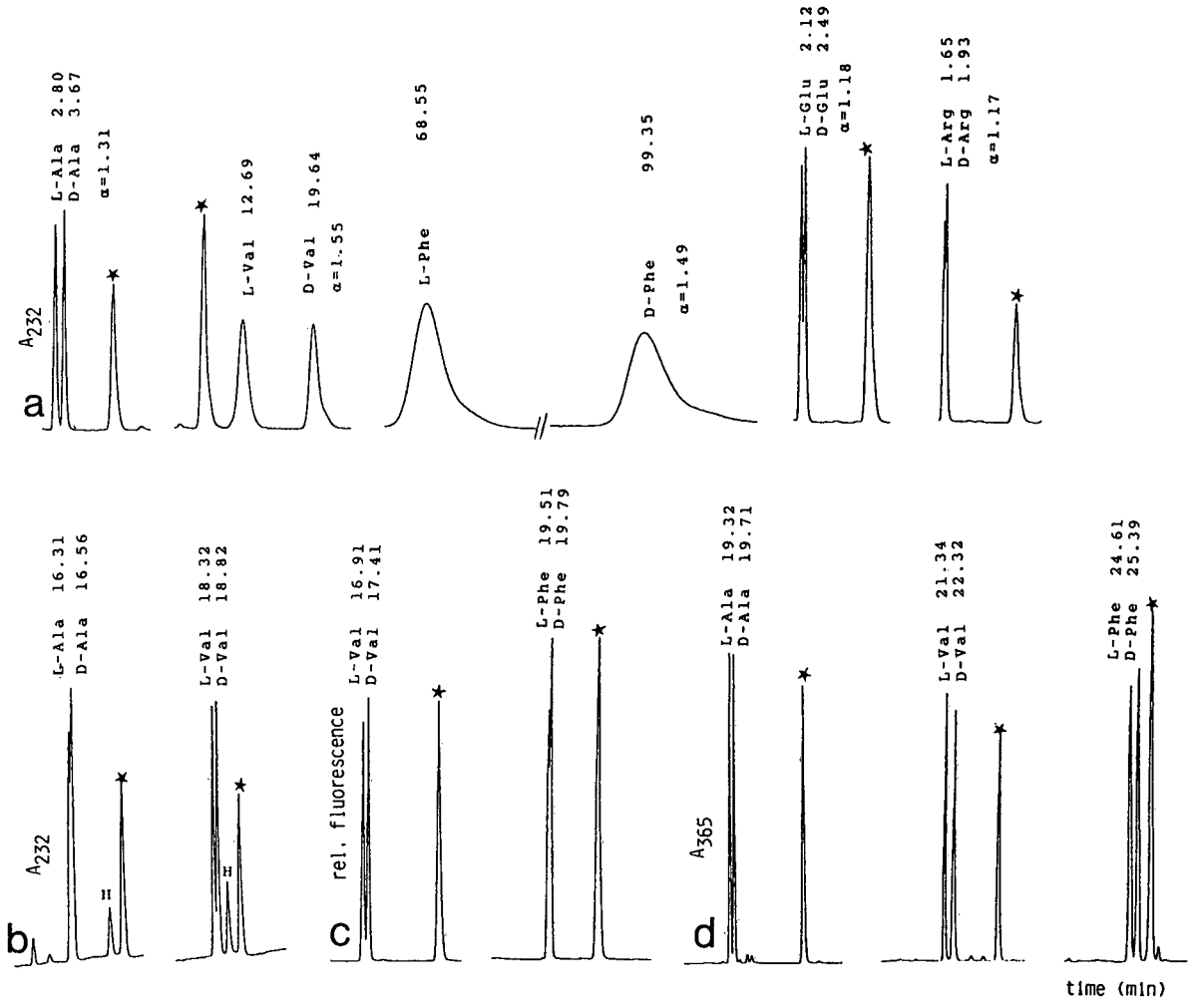

Fig. 3. Sections of chromatograms of diastereomers of selected amino acids (AA) formed by reaction with (a) CMOT-Ala-NH_2, (b) CNOT-Ala-NH_2, (c) CMNT-Ala-NH_2 and (d) FAZT-Ala-NH_2. Designation of the AA to be analysed refers to their configuration in diastereomers; asterisk = reagent peak, H = hydrolysed reagent. Elution conditions: (a) eluent A, isocratic; (b)–(d) 100% A to 100% B in 40 min; eluent A = 100 ml of acetonitrile (MeCN) + 900 ml of water + 1 ml of trifluoroacetic acid (TFA); eluent B = 800 ml of MeCN + 200 ml of water + 1 ml of TFA; flow-rate (a)–(d), 1 ml min^{-1}. A_{232} and A_{365} refers to absorbance at 232 and 365 nm, respectively; the relative fluorescence was measured at 340 nm (excitation) and 415 nm (emission).

sorption of the triazine ring at 232 nm was used for detection. For the detection of diastereomers formed with CNOT-Ala-NH_2, either the absorption maximum of the 2-naphthoxy group at 232 nm or its fluorescence at 352 nm with excitation at 232 nm can be used. The reagent CMNT-Ala-NH_2 and the diastereomers formed therefrom show blue fluorescence in acetone solution when inspected under daylight, and bright blue, intense fluorescence on radiation with a UV lamp at 366 nm. This reagent has favourable fluorescence properties as it has two absorption maxima, at 241 and 340 nm, and shows fluorescence at 415 nm on excitation at the absorption maxima (Fig. 4).

The orange chromogenic reagent CAZT-Ala-NH_2 and its more reactive analogue FAZT-Ala-NH_2 show absorption maxima in the visible range at 367 and 343 nm, respectively. Among the reagents described, CMOT-Ala-NH_2 gave very high resolution for DL-Phe and DL-Val, baseline resolution for DL-Ala and partial resolution for DL-Glu and DL-Arg. None of the other reagents was capable of resolving DL-Glu, DL-Arg and DL-Ser; DL-Ser was also not resolved after reaction with CMOT-Ala-NH_2.

The results demonstrate that the chiral monohalo-*s*-triazines described are capable of resolving certain DL-AA under the conditions used. The resolution of diastereomers is lower in some instances in comparison with those obtained by reaction of the same DL-AA with chiral Sanger-type reagents [5,6]. This suggests a possible contribution of the nitro groups to the resolution of the respective diastereomers (*cf.*, structures shown in Fig. 1). From the inspection of the structure of the reagents (*cf.*, Fig. 1) and the data of Table I, it appears also that increasing bulkiness of the substituents R in the monohalo-*s*-triazine reagents leads to a decrease in resolution.

An important aspect of the use of cyanuric halides as starting materials for the synthesis of chiral reagents is their trifunctionality, which allows the design of tailor-made reagents using the combination of a large number of chiral moieties and of detectable groups. The former can be amino acid derivatives, the latter UV-absorbing, chromogenic or fluorescent groups, or those having favourable

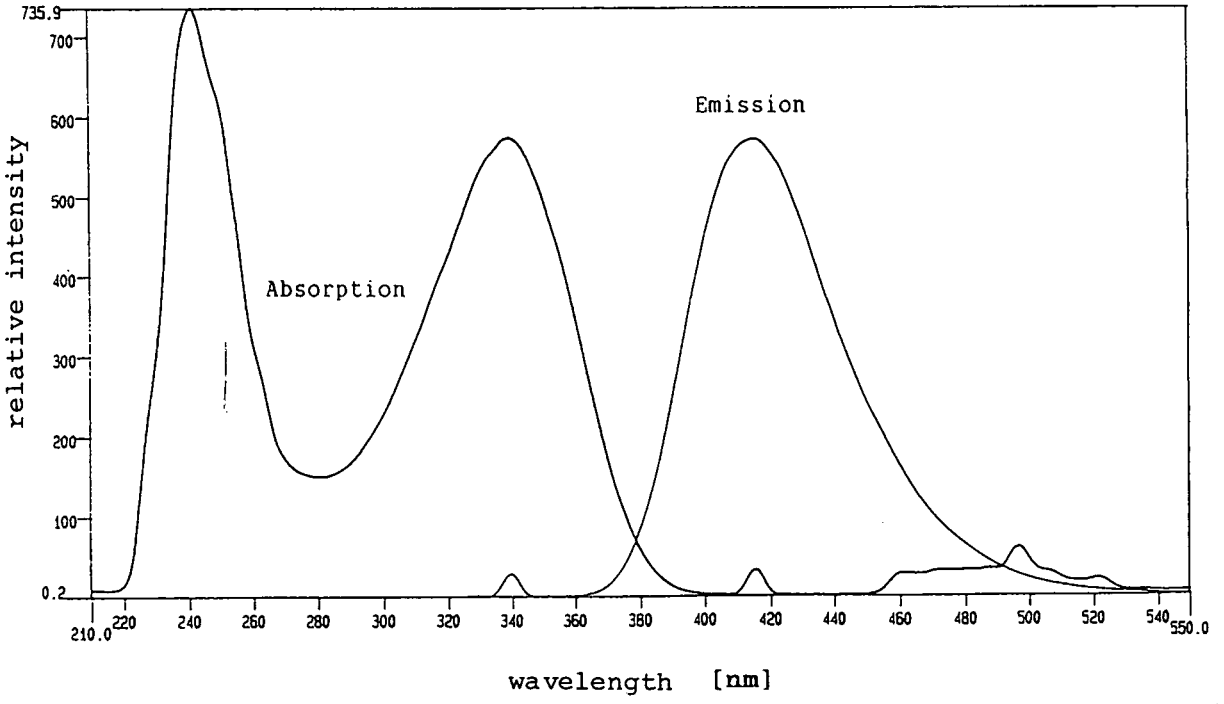

Fig. 4. Fluorescence spectrum of the chiral reagent CMNT-Ala-NH_2. The absorption spectrum was taken with emission at 415 nm and the emission spectrum with excitation at 340 nm.

hydrophobic, hydrophilic, electrochemical or otherwise suitable properties (for potential compounds, see also refs. 7 and 8). From this point of view the approach described is unique among the various methods for the indirect liquid chromatographic resolution of AA enantiomers [17].

REFERENCES

1 D. S. Dunlop and A. Niedle, *Anal. Biochem.*, 165 (1987) 38.
2 S. Einarsson, B. Josefsson, P. Möller and D. Sanchez, *Anal. Chem.*, 59 (1987) 1191.
3 H. Brückner, R. Wittner and H. Godel, *Chromatographia*, 32 (1991) 383, and references cited therein.
4 P. Marfey, *Carlsberg Res. Commun.*, 49 (1984) 591.
5 H. Brückner and C. Keller-Hoehl, *Chromatographia*, 30 (1990) 621.
6 H. Brückner and C. Gah, *J. Chromatogr.*, 555 (1991) 81.
7 H. Koopman, J. H. Uhlenbroek, H. H. Haeck, J. Daams and M. J. Koopmans, *Recl. Trav. Chim. Pays-Bas*, 78 (1959) 967.
8 P. H. Schuldt and C. N. Wolf, *Contrib. Boyce Thompson Inst.*, 18 (1956) 377.
9 F. Lehr, *Dyes Pigments*, 14 (1990) 239.
10 H. Zollinger, *Color Chemistry: Syntheses, Properties and Applications of Organic Dyes and Pigments*, VCH, Weinheim, New York, 1991, pp. 167–179.
11 D. M. Lewis, *J. Soc. Dyers Colour.*, 98 (1982) 165.
12 P. D. G. Dean and D. M. Watson, *J. Chromatogr.*, 165 (1979) 301.
13 D. Blakeslee and M. G. Baines, *J. Immunol. Methods*, 13 (1976) 305.
14 R. Chayen, S. Gould, A. Herrell and C. V. Stead, *Anal. Biochem.*, 39 (1971) 533.
15 N. Ôi, in R. W. Zumwalt, K. C. T. Kuo and C. W. Gehrke (Editors), *Amino Acid Analysis by Gas Chromatography*, Vol. III, CRC Press, Boca Raton, FL, 1987, pp. 47–63.
16 E. Hemingway and G. H. Keats, *Br. Pat.*, 1 028 923 (1966).
17 A. Ahnoff and S. Einarsson, in W. J. Lough (Editor), *Chiral Liquid Chromatography*, Blackie, Glasgow, 1989, pp. 39–80.

Journal of Chromatography, 627 (1992) 107–124
Elsevier Science Publishers B.V., Amsterdam

CHROM. 24 568

Characterization of the influence of displacing salts on retention in gradient elution ion-exchange chromatography of proteins and peptides

Gunnar Malmquist and Niklas Lundell

Institute of Chemistry, Department of Analytical Chemistry, Uppsala University, P.O. Box 531, S-751 21 Uppsala (Sweden)

(First received May 8th, 1992; revised manuscript received July 21st, 1992)

ABSTRACT

It has been shown earlier that the choice of displacing salt has a large effect on the retention in ion-exchange chromatography of proteins and peptides. The influence of different displacing salts cannot be predicted or quantitatively explained, owing to the current lack of an adequate theoretical framework. In this work a general characterization is made by using a considerable number of proteins and peptides and all displacing salts found feasible. Principal component analysis is used to interpret the large amount of data that is generated. The results of the analysis indicate that most of the retention variations are due to non-specific effects and can be explained by changes in the apparent gradient slope, *i.e.*, the increase in elution strength per unit volume, and the elution strength of the starting buffer. This differs from the interpretation given earlier, where the selectivity changes were attributed to specific effects of the salts. However, as it is impossible to test all existing proteins and peptides, specific effects are still possible, but they might be less common than previously considered.

INTRODUCTION

Ion-exchange chromatography (IEC) is a major separation technique for proteins and peptides. Maintaining the biological activity is often crucial for these substances, and ion-exchange chromatography allows the use of mild separation conditions. Further, the load capacity is high and most proteins and peptides can be "trapped" on an ion-exchange column, making it a suitable technique for trace enrichment and preparative separations.

The separation of proteins and peptides by IEC is usually made with a salt gradient, going from a pure buffer solution to a solution of salt and buffer. The concept of *elution strength* is essential in the following discussion and will therefore be presented in some detail. The elution strength of an eluent is the ability to elute solutes from the column. For a given stationary phase, the elution strength is determined by the concentration and type of ionic species in the eluent. The elution strength is therefore lower in the starting buffer than in the eluting buffer. This leads to an increase in elution strength during the gradient. The rate of increase in elution strength per unit volume will in this paper be referred to as the *apparent gradient slope*. The apparent gradient slope can, for a given salt, be altered by changing the salt concentration of the eluting buffer, the flow-rate or the gradient time. It is important to realise, however, that the apparent gradient slope will generally be different if the displacing salt is changed, even if these factors are kept constant. This will be further discussed later in this paper.

The selectivity in IEC can be altered in several ways, but the most obvious parameter to adjust is the pH of the buffer as it directly affects the charge of the solutes. In some instances the available pH range is restricted owing to properties of the sam-

Correspondence to: Gunnar Malmquist, Institute of Chemistry, Department of Analytical Chemistry, Uppsala University, P.O. Box 531, S-751 21 Uppsala, Sweden.

0021-9673/92/$05.00

ple, *e.g.*, solubility or stability. The limited pH range may permit only minor changes in the selectivity, which might not be sufficient for adequate resolution. Previous studies indicate that the choice of displacing salt has a significant impact on the separation [1]. The effect can be non-specific, *i.e.*, just a change in the apparent gradient slope, changing the retention of all solutes in a similar manner. Specific effects, on the other hand, influence individual solutes differently. The conclusions drawn in earlier studies are that both retention and selectivity depend on the type of displacing salt [2]. In addition, it has been observed that in both anion-exchange chromatography (AEC) and cation-exchange chromatography (CEC), the displacing counter-ion and the co-ion are of importance [2–4].

Unfortunately, there is at present no theory that quantitatively explains the effect of changing the displacing salt [2,5]. Studies of various displacing salts therefore tend to be empirical and the results can rarely be generalized.

The aim of this work was to describe and evaluate the effect of various displacing salts. In the absence of a valid theory, an empirical characterization is made by utilizing a multivariate method. This approach is analogous to the method used by Coenegracht *et al.* [6] for the characterization of solvent strength and selectivity in isocratic reversed-phase liquid chromatography. The study presented here includes a considerable number of proteins and peptides and evaluation of all salts found feasible, to make a general characterization. All possible combinations of the selected cations and anions were taken into consideration when establishing the list of suitable salts. The proposed approach should be contrasted with previous studies where only salts having either the cation or the anion in common, *e.g.*, various sodium salts and chlorides, were used [2,3].

Parts of the data presented in this paper have been analysed previously and presented with a different interpretation [7].

METHOD FOR DATA ANALYSIS

The primary outcome of the experiments in this study is a large amount of results, expressed as tables of retention data for proteins and peptides eluted with various salts. There is an obvious need for data reduction and graphical illustration, as the tables are difficult to overview and interpret. Chemometrics provides a tool for this called *principal component analysis (PCA)*, which is an efficient method for analysing and illustrating such data. The results can be presented as plots, illustrating the influence of various displacing salts in a way that enhances and simplifies the interpretation. The fundamental concept of PCA is that the variations observed in a large number of variables essentially is caused by variations in a few underlying properties. The number of underlying sources of variation is usually far less than the number of observed variables.

In this paper, PCA will be explained geometrically and for this distinct application only. The reader is referred to tutorials or chemometrics textbooks for a more complete description [8–10]. For instructive purposes, we shall first assume that only three solutes were used in this study. Elution with one salt will then result in three retention volumes, associated with this particular salt. The salt can be represented as a point in a three-dimensional (three solutes) space. All the other salts can be represented in the same way, resulting in a number of points, as illustrated in Fig. 1. Two salts that give about the same retention volumes will lie close to each other in this space, and a large difference in retention implies a large distance.

Three-dimensional spaces are difficult to illustrate and interpret. The three dimensions are therefore reduced by PCA to a two-dimensional space according to the following procedure. First, a vector, called a *principal component*, is drawn in the direction showing the greatest spread among the points. Second, another principal component, perpendicular to the first, is drawn in the direction were most of the remaining spread is found. This is illustrated in Fig. 2. These two components (designated PC1 and PC2) now define a plane, on which all points can be projected (Fig. 3). This projection expresses as much of the original spread as possible in only two dimensions, making the presentation and interpretation easier. The data reduction described above can be done from any number of dimensions, *i.e.*, any number of *variables*. In this context a variable corresponds to the retention volume for one solute.

There are some important terms in PCA that need to be described in more detail to facilitate the

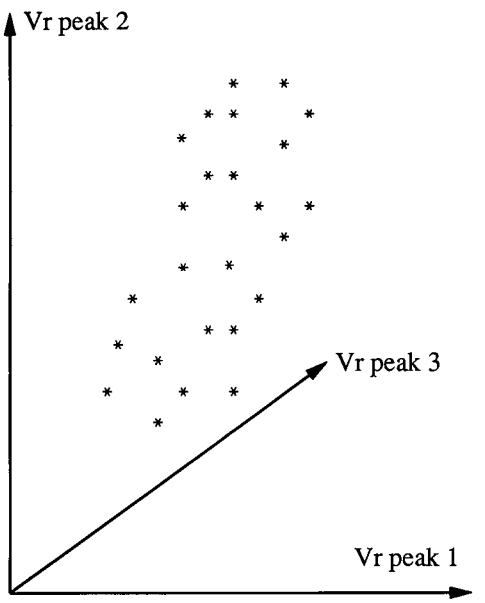

Fig. 1. Retention volumes for three solutes plotted in a three-dimensional coordinate system. The salts (objects) are characterized by the retention volumes (variables).

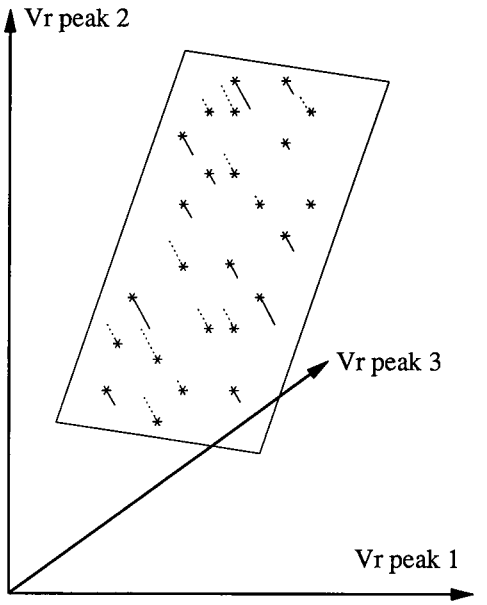

Fig. 3. All objects projected on the plane defined by the two first principal components.

following discussion. Each salt, generally denoted an *object*, is characterized by several retention volumes, *i.e.*, values for the variables. The salts will acquire new values when they are projected on the plane defined by the principal components as illustrated in Fig. 3. These values in the coordinate system constituted of the principal components are referred to as *scores*. The number of principal components that is needed to express the variation, excluding noise or small experimental errors, in the original data is the *rank* of the data. The rank can be determined by several methods, but the most commonly used is cross-validation [8]. In many cases, two or three components are enough to represent the main part of the original spread. Each principal component is a linear combination of the original variables. Depending on the direction of a component in the space it will express a different combination of the original variables. How much of an original variable that goes into a specific component is given by the so-called *loading* of the variable.

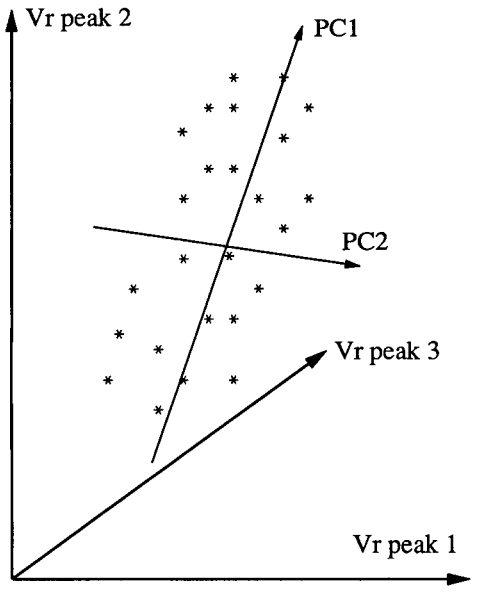

Fig. 2. The two first principal components.

A *score plot* can be produced where the salts are spread out in the plane defined by the principal components showing their general influence on the retention. A *loading plot* shows the mix of the individual solute retentions that is constituting each principal component. When interpreting the plots it is important to realize that although the number of significant principal components is equivalent to

the number of underlying factors, a principal component is not equivalent to an underlying factor. Principal components are always orthogonal, which is not necessarily true for the underlying factors. The underlying factors are combinations of the principal components and vice versa.

Usually, the data are manipulated prior to the determination of the principal components. The variables are often *weighted* to make them more equal in variation. This has not been done in this work as all data have similar experimental errors and are directly comparable.

EXPERIMENTAL

Instrumentation and software

The chromatographic experiments were performed at ambient temperature (22–25°C) using an FPLC system (Pharmacia LKB Biotechnology, Uppsala, Sweden) consisting of two P-500 pumps, MV-7 and MV-8 valves controlled by an LCC-500 liquid chromatography controller. The injections were made with a CMA 200/240 refrigerated (4°C) autosampler (CMA Microdialysis, Stockholm, Sweden) controlled by a Toshiba T-1000 laptop computer. Detection at 214 and 280 nm, for CEC and AEC, respectively, was done with a Linear model 200 (Linear Instruments, Reno, NV, USA) variable-wavelength UV detector coupled to a Spectra-Physics (San Jose, CA, USA) SP4290 integrator. For the proteins a strong anion-exchange column (Mono Q HR 5/5; Pharmacia LKB Biotechnology) was used, while a strong cation-exchange column (Mono S HR 5/5, Pharmacia LKB Biotechnology) was used for the peptides. The pH measurements were carried out with a Metrohm (Herisau, Switzerland) Model 654 pH meter equipped with a combination glass electrode.

The raw data from the integrator were transferred to an IBM PS/2 computer for determination of retention volumes by in-house developed software. The principal component analyses were performed on the IBM PS/2 computer, using the program UNSCRAMBLER (Camo, Trondheim, Norway).

Chemicals and reagents

Horse muscle myoglobin, bovine erythrocyte carbonic anhydrase, human transferrin, bovine serum albumin and soybean trypsin inhibitor were all purchased from Sigma (St. Louis, MO, USA). Calf intestine alkaline phosphatase and *Aspergillus Niger* amyloglucosidase were both purchased from Fluka (Buchs, Switzerland). Human immunoglobulin G and all peptides were provided by Pharmacia LKB Biotechnology.

The buffers were prepared from tris(hydroxymethyl)aminomethane (Tris) (Merck, Darmstadt, Germany), piperazine (Sigma) and phosphoric acid (Merck), all of analytical-reagent grade. Purified water was obtained from a Milli-Q Plus system (Millipore, Bedford, MA, USA) equipped with an Organex-Q cartridge to remove organic contaminants. Acetonitrile was of gradient grade from Merck.

The acids used for pH adjustment of the buffers in AEC were hydrochloric, acetic, hydrobromic, formic, tartaric, citric (May & Baker, Dagenham, UK), phosphoric and sulphuric acid, all of analytical-reagent grade from Merck except for citric acid. For CEC the pH adjustments were done with potassium hydroxide (J.T. Baker, Deventer, Netherlands), sodium hydroxide (Eka Nobel, Surte, Sweden), lithium hydroxide (Riedel-de Haën, Seelze-Hannover, Germany) or ammonia (Merck), all of analytical-reagent grade.

The salts used were all of analytical-reagent grade and the amount of crystal water is indicated in parentheses where appropriate: ammonium acetate, ammonium chloride, ammonium dihydrogenphosphate, ammonium sulphate, calcium chloride(2), lithium chloride, magnesium acetate(4), magnesium chloride(6), magnesium sulphate(7), potassium bromide, potassium chloride, sodium acetate, sodium chloride, sodium formate, sodium dihydrogenphosphate(1), sodium sulphate and sodium tartrate(2) were purchased from Merck, ammonium bromide, ammonium formate, lithium acetate and potassium citrate(1) from BDH (Poole, UK), calcium bromide, lithium citrate(4) and sodium perchlorate from Fluka, lithium bromide, potassium formate and potassium tartrate from Sigma, lithium sulphate(1), potassium sulphate and potassium dihydrogenphosphate from J.T. Baker, calcium acetate (1) and sodium citrate(2) from Fisher (Fair Lawn, NJ, USA), lithium perchlorate from Janssen Chimica (Beerse, Belgium) and sodium bromide from Baker & Adamson (Allied Chemicals, New York, NY, USA).

Chromatographic procedure

For AEC of proteins at pH 8.0, the starting buffer was 10 m*m* Tris and the eluting buffer included 10 m*m* Tris and the displacing salt with a molality corresponding to a displacing ionic strength, defined later in this paper, of 1 *M*. When the AEC experiments were performed at pH 9.6, 10 millimolal piperazine was instead used as the buffer substance. To avoid uptake of carbon dioxide, the pH 9.6 buffers were kept in closed vessels. The pH of the eluents was in both instances adjusted with the acid corresponding to the displacing anion. For the ammonium salts, the pH of the eluting buffer was adjusted using ammonia. All eluents were filtered through 0.22-μm Millipore-GS filters and degassed by sparging with helium for 5 min. The flow-rate was 1 ml/min and the gradients went linearly from 0 to 98% of the eluting buffer in 28 min, corresponding to an increase of 3.5%/ml. Various amounts between 0.3 and 1.3 mg/ml of the protein samples were individually dissolved in the starting buffer at the appropriate pH adjusted with acetic acid. The protein samples were filtered through a 0.45-μm Millex-HV filter (Millipore) before injection of 50 μl of each protein. Prior to the injection, the solubility of each protein in the eluting buffers was tested. The proteins were dissolved in all eluting buffers and incubated at 4°C for 12 h. The presence of an insoluble pellet was examined after centrifugation at 3000 *g* for 5 min.

For CEC of peptides the starting buffer was 12 m*m* phosphoric acid and the eluting buffer consisted of 12 m*m* phosphoric acid and the displacing salt corresponding to a displacing ionic strength of 1 *M*. The pH was adjusted to 2.2 with the base corresponding to the displacing cation. For the magnesium and calcium salts, the pH adjustment was instead performed with lithium hydroxide owing to the limited solubility of $Mg(OH)_2$ and $Ca(OH)_2$. The eluting buffers containing sulphate or phosphate were pH adjusted with sulphuric and phosphoric acid, respectively. After the pH adjustment, 30% (v/v) of acetonitrile was added to both eluents. The eluents were filtered and degassed as described above. The gradients went linearly from 0 to 70% of the eluting buffer in 20 min (increase 3.5%/ml). The peptides were individually dissolved in acetonitrile before injection of 0.5–5 μg of each peptide.

RESULTS AND DISCUSSION

Chromatographic measurements

A careful selection of representative proteins and peptides was used in this study. The eight proteins were systematically chosen with various isoelectric points and molecular masses (see Table I). The nine selected peptides also span a wide range of hydrophobicities (see Table II). However, it is of course impossible to represent all natural variations in solute properties by a small number of proteins and peptides.

IEC can be performed as either a cation- or anion-exchange procedure. AEC was chosen for the protein studies, because it is commonly used and many biological proteins are slightly acidic. For peptides, on the other hand, CEC is usually selected as many biologically active peptides are basic. It will be seen in the following discussion that the choice of ion-exchange mode has an impact on which pH is appropriate, and hence also on buffers and possible salts.

The type of buffer substance that should be used is determined by the ion-exchange mode, pH and detection method. Peptides are preferably detected by UV absorbance at 210–230 nm, which excludes many commonly used buffers. If the cation-exchange mode is used, the only possible buffer substance will be phosphate. To ensure retention one has to operate around the lower pK_a of phosphate and all CEC separations in this work were performed at a pH of 2.2. With proteins, detection is done at

TABLE I

SELECTION OF PROTEINS FOR AEC

Abbreviation[a]	Protein	10^3 M_r[b]	p*I*[b]
Myo	Myoglobin	17.5	6.8, 7.2
CA	Carbonic anhydrase	30	5.9
IgG	Immunoglobulin G	160	7.7
Tra	Transferrin	77	6.0–6.5
APh	Alkaline phosphatase	140	4.4
BSA	Bovine serum albumin	67	5.1
STI	Soybean trypsin inhibitor	21.5	4.5
Amy1, Amy2	Amyloglucosidase	97	3.6

[a] Used for identification of protein peaks in figures and tables.
[b] M_r = relative molecular mass and p*I* = isoelectric point. Data from refs. 11 and 12.

TABLE II

PEPTIDES USED IN CEC

Abbreviation[a]	M_r	p*I*	Hydrophobicity[b]	Sequence
p1	589	3.1	13	Met–Val–Asn–Pro–Glu
p2	561	9.9	10	Ser–Val–Pro–Met–Lys
p3	571	3.1	22	Tyr–Glu–Leu–Phe
p4	626	8.4	24	Pro–Leu–Ile–His–Phe
p5	1071	6.5	26	Thr–Pro–Ile–Pro–Arg–Tyr–Pro–Leu–Asp
p6	1858	3.9	15	His–Thr–Asp–Arg–Glu–His–Thr–Ile–Glu–Thr–Asp–Glu–Met–Glu–Asp
p7	1729	9.5	10	Lys–Tyr–Gly–Asn–Leu–Ser–His–Glu–Lys–Gln–His–Gln–Leu–Phe
p8	1689	3.1	55	Gly–Asn–Gly–Gln–Asp–Val–Met–Ala–Leu–Ala–Thr–Ile–Leu–Ser–Trp–Leu
p9	1722	9.6	45	Gln–Leu–Ser–Leu–Ala–Ile–Phe–His–Ser–Thr–Tyr–Trp–Lys–Ala–Gly

[a] Used for identification of peptides in figures and tables.
[b] Calculated according to ref. 13.

a wavelength in the range 250-280 nm, which extends the range of useful buffers compared with the peptide separations. Tris buffer with a pH of 8.0 was chosen in this study, simply because it is a commonly used buffer for AEC. For comparison some salts were also tested at a pH of 9.6 with piperazine as buffer substance.

Hydrophobic interaction is a common problem in the separation of peptides by ion-exchange columns [14–16]. To minimize this effect, 30% (v/v) of acetonitrile was added to the mobile phases used in the peptide separations.

Since it has been shown that the choice of both the displacing counter-ion and the co-ion can affect the retention, all possible combinations of the cations and anions listed in Table III have been considered. All candidate salts had to fulfil several conditions, listed in Table IV, to qualify for evaluation in this work. These conditions are essentially demands that have to be met for a salt to make it useful in practice. Owing to the different chromatographic conditions and detection wavelengths, different selections of salts were made for the peptide and protein separations. The final selection of the salts found feasible is listed in Table V for protein separations and in Table VI for peptides.

Different salts give different elution strengths. If the same concentration of the displacing salt were used in all eluting buffers, large differences in the apparent gradient slope would appear for salts with different valencies of the displacing ion. In order to minimize the influence of the displacing ion valency, the concentration in the eluting buffer must be adjusted. Intuitively, and according to a proposed theory for ion-exchange chromatography [5], the retention is primarily controlled by the concentration and valency of the displacing ion. The concentrations might thus be adjusted proportionally to the valency of the displacing ion, *i.e.*, making the salt concentration half as high for divalent displacing ions compared with monovalent ions. However, preliminary experiments indicated that large differences in the elution strength still remained. The eluting buffers were therefore instead prepared with constant *displacing ionic strength* (I_D) calculated by the equation $I_D = m_D z_D^2$, where m_D and z_D denotes the molality and valency of the displacing ion, re-

TABLE III

ANIONS AND CATIONS CONSIDERED FOR ION EXCHANGE

Cations	Anions
Potassium	Acetate
Lithium	Hydrogen carbonate
Sodium	Bromide
Ammonium	Chloride
Barium	Formate
Calcium	Iodide
Magnesium	Perchlorate
	Phosphate
	Propionate
	Oxalate
	Sulphate
	Tartrate
	Citrate

TABLE IV

CONDITIONS FULFILLED FOR THE SELECTED SALTS

Condition	Remark
Soluble	The salt should be soluble in the solvent and at the pH used
Non-denaturating	Some salts, *e.g.*, heavy metals, are known to denature several proteins
Stable	The salt has to be stable under normal laboratory conditions; it should not be decomposed by light or be extremely hydroscopic
Transparent	The salt should not interfere with the UV detection at 210–230 nm for peptides or 250–280 nm for proteins
Ionic at relevant pH	Many ions are protolytic and exist as ions only in a specific pH range, *e.g.*, acetate
pH stable	The hydrogencarbonates were discarded owing to the risk of carbon dioxide evolution. When trying the perchlorates at pH 8.0, it was difficult to obtain a stable pH value
Non-hazardous	It should not be dangerous or inconvenient to handle the salt
Available	The salt of analytical-reagent grade should be commercially available

TABLE V

SELECTION OF SALTS FOR AEC OF PROTEINS AT pH 8.0

No.[a]	Salt	Molality		Valency		Ionic strength	
		m_{cation}	m_{anion}	z_{cation}	z_{anion}	I_D[b]	I[c]
1	Lithium acetate	1.0	1.0	1+	1−	1	1.0
2[d]	Sodium acetate	1.0	1.0	1+	1−	1	1.0
3	Ammonium acetate	0.99	1.0	1+	1−	1	1.0
4	Calcium acetate	0.50	1.0	2+	1−	1	1.5
5	Magnesium acetate	0.50	1.0	2+	1−	1	1.5
6	Potassium bromide	1.0	1.0	1+	1−	1	1.0
7[d]	Lithium bromide	1.0	1.0	1+	1−	1	1.0
8	Sodium bromide	1.0	1.0	1+	1−	1	1.0
9	Ammonium bromide	0.99	1.0	1+	1−	1	1.0
10[d]	Calcium bromide	0.50	1.0	2+	1−	1	1.5
11	Potassium chloride	1.0	1.0	1+	1−	1	1.0
12[d]	Lithium chloride	1.0	1.0	1+	1−	1	1.0
13[d]	Sodium chloride	1.0	1.0	1+	1−	1	1.0
14	Ammonium chloride	0.99	1.0	1+	1−	1	1.0
15	Calcium chloride	0.50	1.0	2+	1−	1	1.5
16	Magnesium chloride	0.50	1.0	2+	1−	1	1.5
17[d]	Potassium formate	1.0	1.0	1+	1−	1	1.0
18	Sodium formate	1.0	1.0	1+	1−	1	1.0
19	Ammonium formate	0.99	1.0	1+	1−	1	1.0
20[d]	Potassium sulphate	0.50	0.25	1+	2−	1	0.75
21	Lithium sulphate	0.50	0.25	1+	2−	1	0.75
22	Sodium sulphate	0.50	0.25	1+	2−	1	0.75
23	Ammonium sulphate	0.49	0.25	1+	2−	1	0.75
24	Magnesium sulphate	0.25	0.25	2+	2−	1	1.0
25	Potassium tartrate	0.50	0.25	1+	2−	1	0.75
26[d]	Sodium tartrate	0.50	0.25	1+	2−	1	0.75
27[d]	Potassium citrate	0.33	0.11	1+	3−	1	0.67
28[d]	Lithium citrate	0.33	0.11	1+	3−	1	0.67
29	Sodium citrate	0.33	0.11	1+	3−	1	0.67

[a] Used for identification of salts in figures and tables.

[b] Displacing ionic strength calculated by $I_D = m_{anion} z^2_{anion}$.

[c] Ionic strength in the eluting buffer calculated by $I = 0.5\sum(m_i z_i^2)$. The buffer concentration and protolytic equilibria are taken into account for this calculation only.

[d] Subset of salts selected for AEC at pH 9.6.

TABLE VI

SELECTION OF SALTS FOR CEC OF PEPTIDES AT pH 2.2

No.[a]	Salt	Molality		Valency		Ionic strength	
		m_{cation}	m_{anion}	z_{cation}	z_{anion}	I_D[b]	I[c]
1	Potassium chloride	1.0	1.0	1+	1−	1	1.0
2	Potassium phosphate	1.0	1.0	1+	1−	1	1.0
3	Lithium chloride	1.0	1.0	1+	1−	1	1.0
4	Lithium perchlorate	1.0	1.0	1+	1−	1	1.0
5	Lithium sulphate[d]	1.0	0.24, 0.38	1+	1−, 2−	1	1.4
6	Sodium chloride	1.0	1.0	1+	1−	1	1.0
7	Sodium perchlorate	1.0	1.0	1+	1−	1	1.0
8	Sodium phosphate	1.0	1.0	1+	1−	1	1.0
9	Sodium sulphate[d]	1.0	0.24, 0.38	1+	1−, 2−	1	1.4
10	Ammonium chloride	1.0	1.0	1+	1−	1	1.0
11	Ammonium phosphate	1.0	1.0	1+	1−	1	1.0
12	Ammonium sulphate[d]	1.0	0.24, 0.38	1+	1−, 2−	1	1.4
13	Calcium chloride	0.25	0.50	2+	1−	1	0.76
14	Magnesium chloride	0.25	0.50	2+	1−	1	0.76
15	Magnesium sulphate[d]	0.25	0.12, 0.19	2+	1−, 2−	1	0.94

[a] Used for identification of salts in figures and tables.

[b] Displacing ionic strength calculated by $I_D = m_{cation} z^2_{cation}$.

[c] Ionic strength in the eluting buffer calculated by $I = 0.5\sum(m_i z_i^2)$. The buffer concentration and protolytic equilibria are taken into account for this calculation only.

[d] Molality and valency stated for HSO_4^- and SO_4^{2-}, respectively.

spectively. This corresponds to making the salt concentration for a divalent displacing ion one quarter of the concentration of a monovalent ion (see Tables V and VI). Preparation of the eluting buffers with constant I_D ensures that all gradients have the same rate of increase in displacing ionic strength per unit volume. This should be contrasted with the apparent gradient slope, defined earlier in this paper, as the elution strength depends not only on the ionic strength but also on the identity of the displacing ion. The elution strength of a salt will hereafter refer, except where explicitly stated, to eluents with constant displacing ionic strength.

The ion exchanger will initially be loaded with a certain amount of counter-ions from the pH-adjusting reagent, as the column is equilibrated with the starting buffer. Complications due to mixed ionic forms of the ion exchanger may occur if the pH of the eluents is adjusted with the same acid or base for all salts. The pH of the eluents should therefore be adjusted with the acid or base corresponding to the displacing ion when possible. A certain amount of the displacing ion, determined by the buffer concentration and pH, will inevitably be present in the starting buffer. This leads to differences in the elution strength of the starting buffer, as discussed later in this paper.

The measured retention volumes for anion-exchange chromatography of the eight proteins at pH 8.0 are shown in Table VII. Two peaks were present for the protein amyloglucosidase, leading to a total of nine variables. To give an indication of the elution strength, the average retention volume for each salt is also tabulated. No absolute definition of the elution strength is available in IEC, but a higher elution strength ought to result in a lower average retention volume. As pointed out by Coenegracht *et al.* [6], however, the average retention volume is not an absolute measure of the elution strength only, because specific effects also influence the average retention volume.

In Table VIII the retention volumes for CEC of the nine peptides are shown together with the average retention volumes.

A subset of ten salts, indicated in Table VII, was selected to make a comparison between the effect of

TABLE VII

RETENTION DATA FOR AEC OF PROTEINS AT pH 8.0

Salt[a]	Retention volume (ml)[b]									
	Myo	CA	IgG	Tra	APh	BSA	STI	Amyl	Amy2	Average[c]
1	1.55	2.88	3.94	5.00	12.90	12.87	16.91	14.93	23.32	10.48
2[d]	1.67	2.88	3.86	5.01	13.03	12.98	16.98	14.86	23.22	10.50
3	1.57	3.16	3.70	4.83	12.00	11.91	16.14	13.96	22.47	9.97
4	1.74	2.94	3.25	4.20	8.31	8.35	10.19	10.02	14.70	7.08
5	1.80	2.97	3.37	4.48	9.44	9.37	12.23	11.06	17.49	8.02
6	1.66	3.30	3.90	5.17	8.75	8.73	8.98	8.76	10.95	6.69
7[d]	1.60	3.28	3.95	4.99	8.03	7.95	8.43	8.22	10.10	6.28
8	1.65	3.26	3.92	5.08	8.45	8.45	8.80	8.62	10.72	6.55
9	1.52	3.12	3.74	4.96	8.09	8.00	8.51	8.24	10.45	6.29
10[d]	1.63	3.11	3.24	4.15	5.71	5.75	5.47	5.77	6.75	4.62
11	3.04	3.24	3.97	5.13	10.05	9.95	10.30	10.15	13.39	7.69
12[d]	3.06	3.18	3.88	4.95	8.86	8.96	9.66	9.57	12.11	7.14
13[d]	1.44	2.90	3.73	4.93	9.33	9.26	9.88	9.80	12.70	7.11
14	1.33	3.28	3.62	4.83	8.88	8.82	9.52	9.37	12.28	6.88
15	1.48	2.83	3.08	3.91	5.96	5.93	5.71	6.19	7.44	4.73
16	1.51	2.83	3.17	4.13	6.34	6.34	6.54	6.68	8.30	5.09
17[d]	1.68	3.15	3.96	5.28	12.23	12.23	15.19	13.93	20.93	9.84
18	1.63	3.12	3.93	5.27	13.03	12.97	15.15	14.09	20.93	10.01
19	2.38	2.93	3.66	5.05	11.46	11.40	14.27	13.16	19.66	9.33
20[d]	1.15	1.31	3.24	3.69	10.10	10.05	13.61	13.27	21.56	8.66
21	1.14	1.31	3.20	3.58	9.06	9.04	12.08	11.74	17.69	7.65
22	1.14	1.29	3.17	3.67	9.70	9.62	13.19	12.93	20.47	8.35
23	1.13	1.30	3.20	3.65	9.08	9.09	12.74	12.28	19.49	8.00
24	1.13	1.32	3.01	3.60	7.92	7.83	9.36	9.16	14.17	6.39
25	1.09	1.30	3.25	4.00	10.72	10.74	14.44	13.96	23.15	9.18
26[d]	1.09	1.33	3.29	3.89	10.36	10.39	13.96	13.61	22.19	8.90
27[d]	1.02	1.08	3.38	1.36	6.85	6.74	11.41	11.48	20.02	7.04
28[d]	1.04	1.07	3.30	1.61	6.80	6.53	11.52	11.34	19.21	6.94
29	1.04	1.09	3.22	1.45	6.57	6.96	11.81	11.91	20.82	7.21

[a] For identification of salts, see Table V.
[b] For protein designations, see Table I.
[c] Average retention volume for each salt.
[d] Salts used for comparison with pH effect (see also Table IX).

a change in buffer pH and that of different displacing salts. The retention volumes of the proteins eluted with these salts at pH 9.6 are shown in Table IX.

Analysis of retention data for AEC of proteins at pH 8.0

The retention volumes for the nine protein peaks eluted with 29 salts at pH 8.0 were subjected to principal component analysis. The results of the analysis are summarized in Table X. The main causes of retention variations can be seen from the plot of the scores on the two first principal components (Fig. 4).

The most obvious pattern in the score plot is a clustering of the salts according to the displacing anion. It also can be observed that the scores on the two first principal components are related to the elution strength of the displacing salts. The average retention volume of the salts increases, corresponding to a decrease in elution strength, on going from the lower left to the upper right part of the score plot. The direction of decreasing elution strength correlates more closely with the first than the second component. On the other hand, a separation of the salts with monovalent anions from the multivalent salts can be seen in the scores on the second

TABLE VIII

RETENTION DATA FOR CEC OF PEPTIDES AT pH 2.2

Salt[a]	Retention volume (ml)[b]									
	p1	p2	p3	p4	p5	p6	p7	p8	p9	Average[c]
1	2.66	5.35	3.41	6.06	4.40	12.15	13.47	2.58	6.06	6.24
2	3.33	5.44	3.59	5.96	4.45	10.47	13.17	3.06	6.25	6.19
3	2.92	6.48	3.40	7.85	5.00	14.57	18.45	2.53	7.07	7.59
4	2.78	6.27	3.35	7.16	4.76	13.09	14.78	2.73	6.18	6.79
5	3.15	6.51	3.83	7.84	5.04	10.36	16.18	2.77	7.23	6.99
6	2.70	5.33	3.30	6.17	4.37	11.56	13.52	2.34	5.93	6.14
7	2.68	5.37	3.29	6.01	4.35	11.35	12.33	2.57	5.54	5.94
8	3.30	5.65	3.75	6.52	4.59	10.67	14.27	2.97	6.50	6.47
9	2.83	5.32	3.53	6.13	5.23	8.30	11.67	2.63	5.93	5.73
10	2.74	5.82	3.33	6.65	4.75	13.28	15.57	2.38	6.48	6.78
11	3.28	5.55	3.79	6.83	4.60	10.35	13.66	3.20	6.33	6.40
12	3.01	5.92	3.78	6.85	4.82	9.75	14.19	2.75	6.62	6.41
13	1.21	2.02	1.31	2.08	1.68	4.93	6.20	1.17	2.92	2.61
14	1.26	2.32	1.40	3.15	2.12	6.03	7.51	1.13	3.01	3.10
15	1.26	2.92	1.55	3.28	1.93	5.28	8.20	1.23	3.41	3.23

[a] For identification of salts, see Table VI.
[b] For peptide identification, see Table II.
[c] Average retention volume for each salt.

component. An interpretation of this is given later.

As stated previously, the primary clustering in the score plot involves the displacing anions. The salts with a common anion are subdivided, however, according to the valency of the accompanying cation. This indicates that the use of a constant displacing ionic strength does not compensate sufficiently for the difference in elution strength between salts with varying valencies of the constituent ions. The theory proposed by Ståhlberg *et al.* [17] states that the retention in isocratic IEC is related to the ionic strength in the eluting buffer (*I*), *i.e.*, the ionic

TABLE IX

RETENTION DATA FOR AEC OF PROTEINS AT pH 9.6

Salt[a]	Retention volume (ml)[b]								
	Myo	CA	IgG	Tra	APh	BSA	STI	Amy1	Amy2
2	5.39	5.96	8.25	7.67	16.42	16.32	18.53	16.73	24.73
7	4.11	4.04	5.47	6.08	8.90	8.78	8.72	8.62	10.34
10	3.98	3.64	4.44	4.82	6.27	6.25	5.62	6.18	6.96
12	4.42	4.04	5.75	6.23	10.16	10.08	10.12	10.17	12.64
13	4.26	3.89	5.80	6.32	10.73	10.71	10.57	10.68	13.34
17	4.67	4.32	8.74	7.56	15.56	15.47	16.00	15.04	21.56
20	1.49	2.63	4.61	5.02	13.63	13.69	14.92	15.07	23.37
26	1.75	1.58	4.87	5.12	13.72	13.56	15.46	15.72	24.11
27	1.12	1.09	3.18	3.33	10.35	10.33	12.77	13.38	21.98
28	1.11	1.10	3.12	3.25	9.43	9.33	12.70	12.92	20.78

[a] For identification of salts, see Table V.
[b] For protein designations, see Table I.

TABLE X

SUMMARY OF PCA RESULTS FOR ALL DATA SETS

All data sets are centred around the mean before the analysis.

Data set	Significant PCs[a]	Explained variance (%)[b]		
		PC1	PC2	PC3
AEC, all salts, pH 8.0	2	86.7	98.8	
CEC, all salts, pH 2.2	3	91.7	96.9	99.0
AEC, selected salts, pH 8.0	2	83.8	99.1	
AEC, selected salts, pH 9.6	2	81.7	98.9	
AEC, selected salts, pH 8.0 and 9.6	3	78.4	97.2	98.8

[a] Number of significant principal components according to cross-validation.
[b] Cumulative percentage of the total variance explained after each component.

strength calculated by considering all constituent ions. The displacing ionic strength and the ionic strength in the eluting buffer are given in Table V. On comparing the ionic strengths in the eluting buffers, different values are observed for salts with multivalent cations compared with those with a monovalent cation. The eluting buffers could have been prepared by keeping the ionic strength in the eluting buffer constant, instead of the displacing ionic strength. The resulting elution strength of the eluting buffer would then be lower for the salts consisting of a multivalent cation and a monovalent anion. This would lead to higher average retention volumes, moving them closer to the other salts with the same anion.

The same argument can be made for the salts with multivalent anions, *i.e.*, sulphates, tartrates and citrates. For the divalent anions, the calculated ionic strength in the eluting buffer is less than unity for all salts except magnesium sulphate. A constant ionic strength in the eluting buffer would lead to higher elution strengths for these salts having

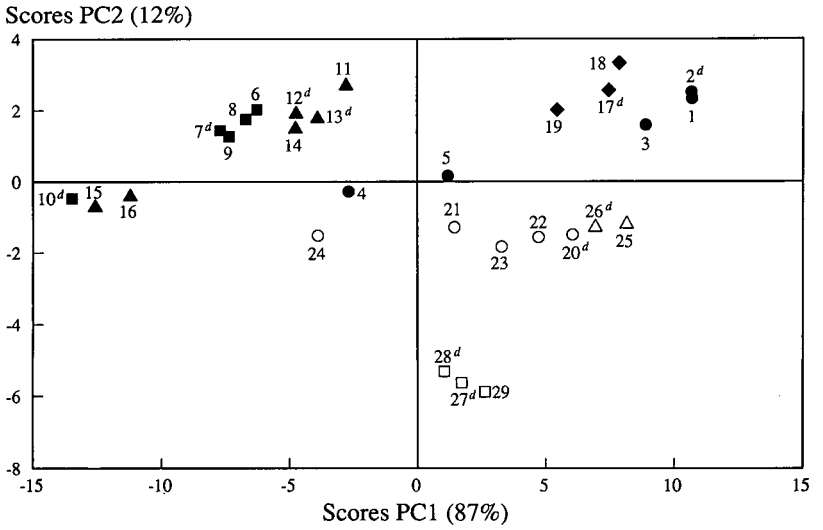

Fig. 4. AEC of proteins at pH 8.0. Score plot of the two first principal components (mean centred data). Unfilled symbols indicate multivalent anions: □ = citrates, △ = tartrates, ○ = sulphates. Filled symbols indicate monovalent anions: ■ = bromides; ▲ = chlorides; ● = acetates; ◆ = formates. For identification of the individual salts, see Table V. [d] Indicates salts selected for comparison with pH 9.6.

monovalent cations, moving them closer to magnesium sulphate. For the trivalent anion citrate, all salts have a lower ionic strength in the eluting buffer than the other salts. By preparing a stronger eluent, keeping the ionic strength in the eluting buffer constant, the citrates would move further to the lower left in the score plot. This agrees with the empirical eluotropic series [18], shown in Table XI, where citrate is listed as the strongest displacer in AEC.

The essence of this discussion is that the eluting buffers should be prepared with the same ionic strength in the eluting buffer for all salts. By instead keeping the displacing ionic strength constant, the resulting elution strength varies between salts with different valencies for the co-ion. This is reflected in the average retention volumes, listed in Table VII, and is also evident in the score plot in Fig. 4.

The second principal component shows a division of the salts mainly according to the valency of the displacing anion. This can be attributed to some extent to differences in the elution strength of the starting buffer. The ionic strength in the starting buffer is higher for salts with multivalent anions compared with salts with monovalent anions. This is an inherent consequence of the pH adjustment of the buffers, as it was done with the acid corresponding to the displacing anion. The approximate ionic strength in the starting buffers used in this part of the study is shown in Table XII for mono-, di- and trivalent anions. These differences in ionic strength exist also during the gradient, but become negligible owing to the increase in the salt concentration. A higher ionic strength at the start of the gradient leads to earlier elution of the moderately retained proteins. The elution strength in the starting buffer is not constant even for salts with the same valency of the anion. The starting eluent is thus stronger for bromides than for acetates. The magnitude of this influence is small, however, compared with the effect of the valency of the anion.

TABLE XI

IONS ARRANGED IN ORDER OF INCREASING ELUTION STRENGTH

Data adapted from ref. 18.

AEC	Acetate < formate < chloride < bromide < sulphate < citrate
CEC	Lithium < sodium < ammonium < potassium < magnesium < calcium

TABLE XII

IONIC STRENGTH IN THE STARTING ELUENT FOR AEC AT pH 8.0

10 millimolal Tris buffer (pK_a = 8.06).

pH adjusted with	Ionic strength
Monovalent acid	0.0053
Divalent acid	0.0080
Trivalent acid	0.0107

The first principal component is dominated by the peaks with high retention volumes, *i.e.*, Amy2, STI and Amy1. This is illustrated in the loading plot for the two first principal components in Fig. 5. The variations in the apparent gradient slope resulting from the different elution strengths of the salts influence the late-eluting peaks to a larger extent than peaks at the beginning of the chromatogram. The peaks with small retention, *i.e.*, CA, Myo, Tra and IgG, have very low loadings on the first component. These peaks are mainly influenced by the elution strength during the beginning of the gradient. Their relatively larger loadings on the second principal component support the interpretation of the second component as primarily a measure of the elution strength in the starting buffer.

The impact of the displacing salts on the retention behaviour of proteins in AEC can be summarized by two principal components, explaining about 99% of the retention variations. Two major contributions to the influence of the displacing salt can be identified, the apparent gradient slope and the elution strength of the starting buffer. These two effects are not independent of each other, as a strong displacer gives both a high apparent gradient slope and a high elution strength in the starting buffer. This is also evident in the score plot as the direction of increasing elution strength of the salts is not orthogonal to the second principal component, associated with the elution strength in the starting buffer. Instead, this direction is tilted downward towards the region of multivalent anions, where the elution strength in the starting buffer is high.

If retention data from duplicate analyses of some salts are included in the PCA, only negligible devia-

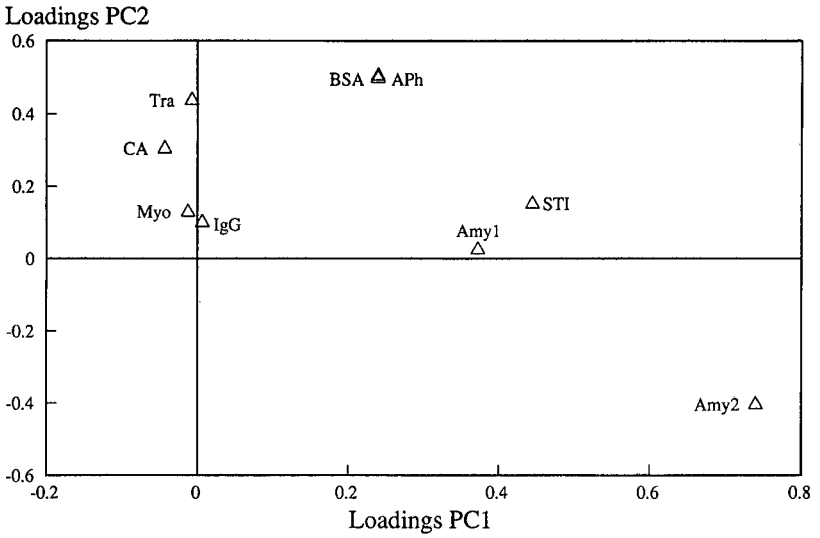

Fig. 5. AEC of proteins at pH 8.0. Loading plot of the two first principal components. For protein designations, see Table I.

tions from the pattern in Fig. 4 are present (data not shown).

Analysis of retention data for CEC of peptides at pH 2.2

The results from the PCA of the cation-exchange data are summarized in Table X. The primary clustering in the score plot of the two first components (Fig. 6) corresponds to the valency of the displacing cation. The salts with divalent cations, *i.e.*, calcium and magnesium, are separated from the other salts that have lower elution strengths. The direction of decreasing elution strength is more or less parallel to the first principal component in this case. By lin-

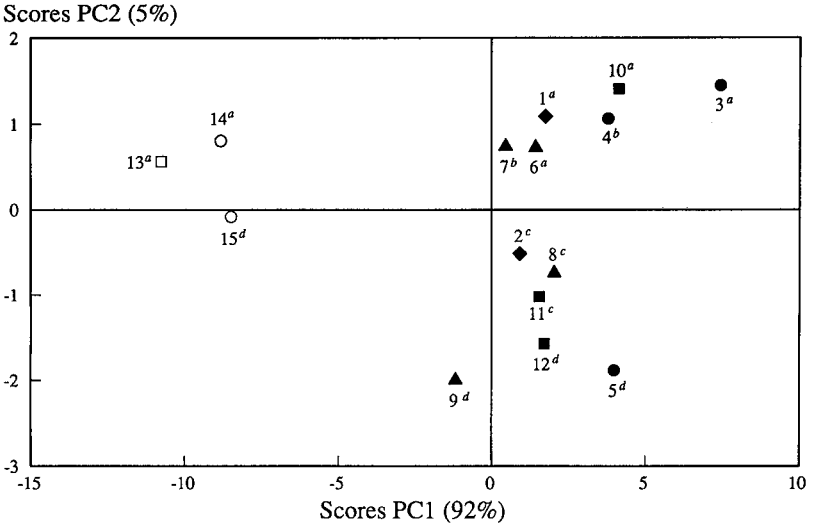

Fig. 6. CEC of peptides at pH 2.2. Score plot of the two first principal components (mean centred data). Unfilled symbols indicate multivalent cations: □ = calcium; ○ = magnesium. Filled symbols indicate monovalent cations: ■ = ammonium; ▲ = sodium; ● = lithium; ◆ = potassium. The anions are indicated by superscript letters: [a] chlorides; [b] perchlorates; [c] phosphates; [d] sulphates. For identification of the individual salts, see Table VI.

ear regression of the average retention volumes as a function of the scores on PC1 a good correlation ($r = 0.994$) can be demonstrated.

In contrast to the AEC experiments, the pH adjustment of the starting buffer was done with a monovalent base, lithium hydroxide, for the salts with divalent cations. This was necessary because of the limited solubility of magnesium hydroxide and calcium hydroxide. As a consequence, only small differences in the elution strength of the starting buffer are present. This explains the absence of a segregation induced by the pH adjustment procedure. The secondary grouping of the salts with monovalent cations is instead related to the accompanying anion, with the sulphates and phosphates separated from the others. Two possible interpretations of this observation will be discussed, although no definitive conclusion can be drawn regarding the actual source of the secondary grouping. It also should be pointed out that the first component explains the main part of the total variations in retention, so the contribution of the second component is relatively small.

In IEC, the pH of the eluate fluctuates during the gradient [19], especially when low buffer concentrations are used as in this study. The pH variations will in this instance affect not only the charge of the solutes but also the charge of the ion exchanger, as a Mono S column exhibits a certain buffer capacity at pH 2.2, in spite of being a strong cation exchanger [20]. The appearance of these pH variations will be different when the gradient is formed with a salt that has an appreciable buffer capacity at the given pH. The secondary grouping may reflect the differences in buffer capacity of the anions, as sulphates and phosphates have the highest buffer capacity at pH 2.2. However, it is not possible to elucidate the precise influence of the pH fluctuations on the individual peptides.

Another possibility for interpretation of the secondary grouping arises from the small hydrophobic interactions that may occur in spite of the presence of 30% of acetonitrile in the mobile phase. The amount of acetonitrile added was chosen to suppress the hydrophobic interactions totally, but at high salt concentrations they still might not be negligible. The chaotropic effect of an ion is the ability to make a solvent less polar. A chaotropic ion has *salting-in* properties, suppressing the hydrophobic interactions even further. An ion with the opposite, *salting-out*, properties is termed kosmotropic and promotes hydrophobic interactions. Kosmotropic ions are known to stabilize protein structure [21], as opposed to the destabilizing properties of chaotropic ions. The chaotropic character of ions has been related to the lyotropic series of Hofmeister that expresses the ion-specific influence on protein solubility [22]. The ions used in this work for CEC are listed according to increasing chaotropic character in Table XIII. By using salts with a kosmotropic anion, *e.g.*, sulphate or phosphate, more hydrophobic interactions are introduced. The grouping of the salts according to the anions may be interpreted in these terms, as the difference in chaotropic character is larger for anions than for cations [4]. The influence of the chaotropic character would be most pronounced for the late-eluting peaks, where the salt concentration is high. Further, the largest effects ought to be seen for hydrophobic peptides as they are more prone to hydrophobic interactions.

The loading plot of the two first principal components is shown in Fig. 7. The first component is dominated by the two late-eluting peptides, p7 and p6. The influence of the individual peaks on PC1 is roughly related to their retention volumes. This is indicative of the correspondence of the first component to the apparent gradient slope. The second component is mainly related to one peptide, p6, with only small contributions from the other peptides. This peptide is indeed eluted at high salt concentrations, but it is not very hydrophobic (see Table II). As a consequence, the loading plot contradicts the interpretation of the secondary grouping as being due to hydrophobic interactions. On the other hand, the loading plot does not make it possible to conclude that the secondary grouping arises from the buffer capacity either. This is prevented by the absence of information regarding the actual effect of pH variations during the gradient.

TABLE XIII

IONS ARRANGED IN ORDER OF INCREASING CHAOTROPIC CHARACTER

Data adapted from refs. 18 and 23.

Anions	Phosphate < sulphate < chloride < perchlorate
Cations	Calcium < magnesium < lithium < sodium < potassium < ammonium

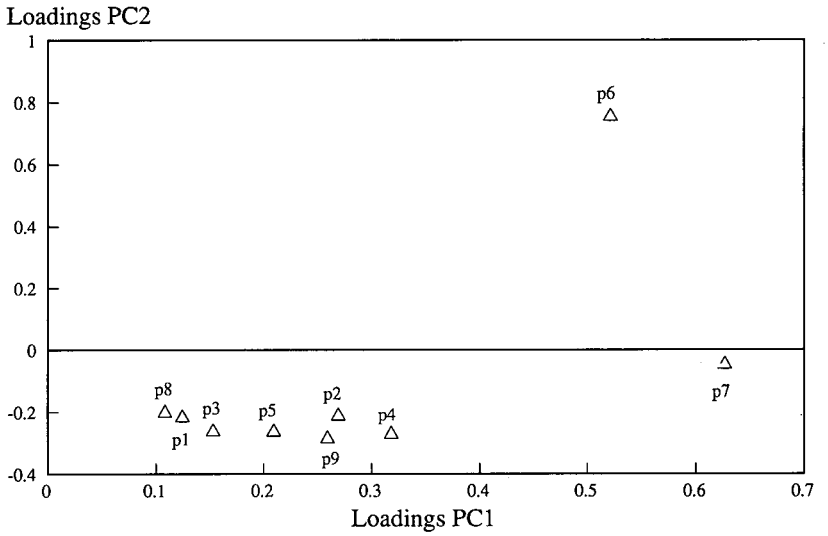

Fig. 7. CEC of peptides at pH 2.2. Loading plot of the two first principal components. For peptide designations, see Table II.

The two first principal components explain about 97% of all variations in the retention volumes. In the absence of substantial differences in the elution strength of the starting buffer, the retention variations depend on the apparent gradient slope to a greater extent compared with the AEC data. The observed secondary grouping according to the anions reflects only a minor contribution to the overall variations, and the cause of it cannot be elucidated.

Practical consequences

The influence of different displacing salts can be divided into non-specific and specific effects. The non-specific effects can be regarded as differences in the apparent gradient slope. On the other hand, the specific effects alter the retention differently for individual peaks. The influence of the elution strength of the starting buffer cannot accurately be regarded as a specific effect, although it affects the retention for the early-eluting peaks only. It can be distinguished from specific effects as all early-eluting peaks will be affected in the same manner. Further, all salts giving the same elution strength at the start of the gradient will have the same influence.

The main effects on retention seen in this work can be explained by differences in the gradient, *i.e.*, the combined effect of the elution strength in the starting buffer and the apparent gradient slope. This disagrees with some of the results of other workers [2,3], where the large selectivity differences demonstrated are attributed to specific, salt-mediated effects. It should be pointed out that the data presented in this paper also include large effects on the selectivity. To illustrate this, the retention ratio between the peaks Amy2 and BSA in AEC at pH 8.0 was calculated for all salts. The values ranged from 1.2 (for calcium bromide) to 3.0 (sodium citrate). The range became narrower (1.3–1.9) when the calculations were restricted to salts having the same ionic strength in the eluting buffer. The differences in selectivity shown by this example are nevertheless to a large extent explained by the elution strength in the starting buffer and the apparent gradient slope.

It must be emphasized that the outcome of the principal component analysis reflects the design of the data set, *i.e.*, the experimental conditions chosen for the compilation of the data set. In this paper, we have presented results from experiments performed by choosing the most intuitive experimental conditions, *e.g.*, regarding the concentration of the eluting buffer and pH adjustment procedure. This makes it possible to relate our results to those in previous work regarding displacing salts. As a consequence, the relatively small specific effects on the

retention that may be present are buried by the large impact on retention due to differences in the elution strength in the starting buffer and the apparent gradient slope. To be able to evaluate the possible specific effects of the displacing salts, another strategy is necessary. By maintaining constant apparent gradient slope and elution strength in the starting buffer for each salt, the influence of the non-specific effects of the salts will be reduced. The score plots, resulting from the principal component analysis of this modified data set, will thus reveal the true specific effects of the displacing salts on the retention. The adjustment of the concentrations can be accomplished by trial and error, or preferably by using the theory of gradient elution in IEC [24,25] allowing the prediction of retention at any gradient from two or more initial gradients.

Comparison of the influence of pH and displacing salts

As pointed out previously, the pH of the buffers is the most obvious property to alter when developing a separation method. This led to an attempt to compare the effect of pH changes, although within a limited range, with the influence of different displacing salts.

Ten salts were selected from diverse parts of the score plot for AEC at pH 8.0 (see Fig. 4). The results from the principal component analysis of this subset of salts are summarized in Table X. The pattern of the salts in the score plot of the two first components is easily recognizable (data not shown), looking very much the same in this subset as in the complete set of salts.

The salts included in the subset were used for elution of the proteins using a piperazine buffer at pH 9.6. The retention data presented in Table IX were subjected to PCA (see Table X). The score plot (data not shown), reveals the same general pattern as at pH 8.0. The close resemblance of the two score plots indicates that the characterization of the retention behaviour made at pH 8.0 may also be valid at other pH values.

The retention data for the selected subset of salts at the two pH values can be joined together and analysed by a joint principal component analysis (see Table X). The score plot of the two first components is shown in Fig. 8. An increase in pH from 8.0 to 9.6 generally results in an increase in the scores on both the first and second component, leading to a movement upwards and slightly to the right in the score plot. It should be pointed out that the two principal components do not reflect the same combination of the original variables as in the PCA of

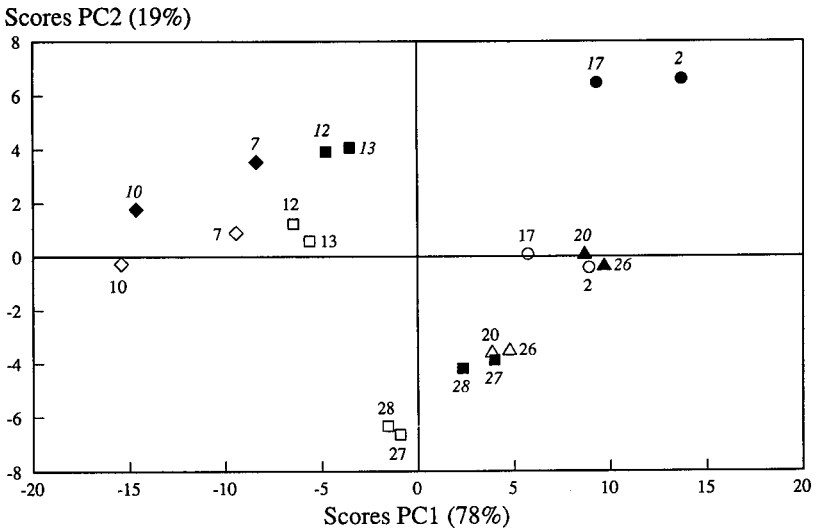

Fig. 8. AEC of proteins at pH 8.0 and 9.6. Score plot of the two first principal components using the selected subset of salts (mean centred data). Unfilled symbols indicate data at pH 8.0: □ = citrate and chloride; △ = sulphate and tartrate; ○ = formate and acetate; ◇ = bromide. Filled symbols and salt designations in italics indicate data at pH 9.6. For identification of individual salts, see Table V.

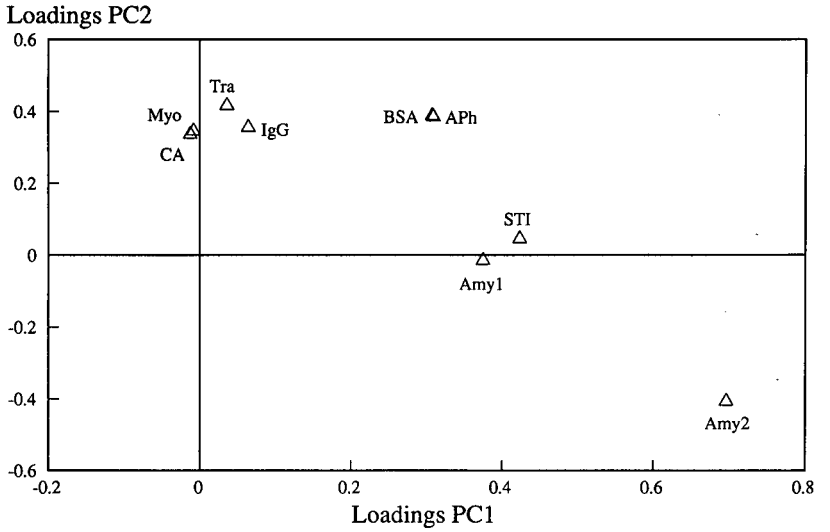

Fig. 9. AEC of proteins at pH 8.0 and 9.6. Loading plot of the two first principal components. For protein designations, see Table I.

the pH 8.0 data only. This implies that the direction of movement when the pH is changed cannot be interpreted in terms of apparent gradient slope or elution strength of the starting buffer. If the joint loading plot (Fig. 9) is compared with the pH 8.0 loading plot (Fig. 5), the most obvious deviation is the increase of the loadings for Myo, CA and IgG on the second component. It is difficult to establish the specificity of the influence of pH changes, but the loading plot supports the self-evident notion that the proteins with isoelectric points closest to 8.0 are relatively more affected by an increase in pH.

It is interesting that the influence of the displacing salts is of the same magnitude as the effect of changing the pH in this limited range, as shown by the score plot. This corroborates the comment of Kopaciewicz and Regnier [2] that the displacing salt is equally important as the pH for controlling retention and selectivity. However, if a broader pH range is considered, greater effects of pH changes will be observed. The retention will be drastically reduced for proteins that are positively charged at the lower pH.

CONCLUSIONS

Principal component analysis has proved to be useful for the characterization of retention behaviour. In applying this method to the ion-exchange chromatography of peptides and proteins, several interesting observations can be made.

A change of the displacing salt has major effects on the retention. If the eluting buffers are prepared with constant ionic strength, which is appropriate, a change of displacing salt will influence the retention in two ways. First the apparent gradient slope, *i.e.*, the increase in elution strength per unit volume, will be affected. Second, the elution strength of the starting buffer will change. With a constant concentration of the buffer substance, the ionic strength in the starting buffer will inevitably vary with the valency of the displacing ion, provided that the pH adjustment is done appropriately. The elution strength in the starting buffer will therefore be higher for multivalent displacing ions at the same buffer concentration. This leads to earlier elution of the moderately retained peaks with multivalent displacing ions, despite a constant ionic strength in the eluting buffer.

An important conclusion is that the main effect of a change of the displacing salt is non-specific. The chromatograms may look very different with different salts, but this is often solely caused by a change in the apparent gradient slope and elution strength of the starting buffer. The observed alterations in retention volumes when changing the displacing salt could often be achieved by modifica-

tions of the gradient with the original salt.

In this work a fairly large number of proteins and peptides were tested. However, all possible variations can never be covered. This study aimed to be more general than previous work, but it must be pointed out that very specific effects are nevertheless possible with individual proteins and peptides. Drastic effects on the selectivity by a change of displacing salt could be caused by alterations in the higher structure of a protein. For many applications this would hardly be a desirable way to adjust the selectivity. Another possibility for specific effects is the promotion or suppression of hydrophobic interactions caused by the chaotropic character of the displacing salt.

Retention control is not the only relevant property of the displacing salt. The displacing salt also affects the solubility and stability of proteins and peptides. In addition, practical considerations, such as whether the salt is corrosive or can be mixed with organic solvents, have to be included. These practical considerations might be more important than selectivity control when selecting the displacing salt.

ACKNOWLEDGEMENTS

We express our gratitude to Pharmacia LKB Biotechnology for providing the chromatographic materials. Lars Hagel, Margareta Tennander, Åke Danielsson and Torvald Andersson, all at Pharmacia, are acknowledged for encouraging and fruitful discussions. Rolf Danielsson in our department is thanked for valuable opinions regarding the chemometric interpretation of the data. We thank Örjan Andersson, also in our department, for providing the data conversion routine.

REFERENCES

1 D. R. Nau, *BioChromatography*, 4, No. 2 (1989) 62.
2 W. Kopaciewicz and F. Regnier, *Anal. Biochem.*, 133 (1983) 251.
3 K. M. Gooding and M. N. Schmuck, *J. Chromatogr.*, 296 (1984) 321.
4 M. T. W. Hearn, A. N. Hodder and M. I. Aguilar, *J. Chromatogr.*, 443 (1988) 97.
5 F. E. Regnier and R. M. Chicz, in K. M. Gooding and F. E. Regnier (Editors), *HPLC of Biological Macromolecules: Methods and Applications*, Marcel Dekker, New York, NY, USA, 1990, Ch. 4, p. 77.
6 P. M. J. Coenegracht, A. K. Smilde, H. Benak, C. H. P. Bruins, H. J. Metting, H. De Vries and D. A. Doornbos, *J. Chromatogr.*, 550 (1991) 397.
7 G. Malmquist and N. Lundell, presented at the *11th International Symposium on HPLC of Proteins, Peptides and Polynucleotides, Washington, DC, October 20–23 1991*, poster 207.
8 S. Wold, K. Esbensen and P. Geladi, *Chemometr. Intell. Lab. Syst.*, 2 (1987) 37.
9 M. A. Sharaf, D. L. Illman and B. R. Kowalski, *Chemometrics*, Wiley, New York, 1986.
10 D. L. Massart, B. G. M. Vandeginste, S. N. Deming, Y. Michotte and L. Kaufman, *Chemometrics: a Textbook*, Elsevier, Amsterdam, 1988.
11 P. G. Righetti and T. Caravaggio, *J. Chromatogr.*, 127 (1976) 1.
12 P. G. Righetti, G. Tudor and K. Ek, *J. Chromatogr.*, 220 (1981) 115.
13 D. Guo, C. T. Mant, A. K. Taneja, J. M. R. Parker and R. S. Hodges, *J. Chromatogr.*, 359 (1986) 499.
14 W. Kopaciewicz, M. A. Rounds and F. E. Regnier, *J. Chromatogr.*, 318 (1985) 157.
15 R. Dawson, Jr., J. P. Steves, J. F. Lorden and S. Oparil, *Peptides*, 6 (1985) 1173.
16 M. P. Henry, in W. S. Hancock (Editor), *High Performance Liquid Chromatography in Biotechnology*, Wiley, Chichester, New York, 1990, Ch. 10, p. 205.
17 J. Ståhlberg, B. Jönsson and Cs. Horváth, *Anal. Chem.*, 63 (1991) 1867.
18 *FPLC Ion Exchange and Chromatofocusing. Principles and Methods.*, Pharmacia LKB Biotechnology, Uppsala, 1985, Ch. 6, p 135.
19 J. Bergström, L. Söderberg, L. Wahlström, R.-M. Müller, A. Domicelj, G. Hagström, R. Stalberg, I. Källman and K.-A. Hansson, *Protides Biol. Fluids, Proc. Colloq.*, 30 (1982) 641.
20 L. Hagel, personal communication, 1991.
21 A. N. Hodder, M. I. Aguilar and M. T. W. Hearn, *J. Chromatogr.*, 476 (1989) 391.
22 W. Melander and C. Horvath, *Arch. of Biochem. Biophys.*, 183 (1977) 200.
23 F. Franks, in F. Franks (Editor), *Characterization of Proteins*, Humana Press, Clifton, NJ, 1988, Ch. 3, p. 53.
24 Y. Baba, *J. Chromatogr.*, 485 (1989) 143.
25 T. Sasagawa, Y. Sakamoto, T. Hirose, T. Yoshida, Y. Kobayashi and Y. Sato, *J. Chromatogr.*, 485 (1989) 533.

Journal of Chromatography, 627 (1992) 125–135
Elsevier Science Publishers B.V., Amsterdam

CHROM. 24 587

Immobilized metal ion affinity chromatography of synthetic peptides

Binding via the α-amino group

Per Hansen and Gunnar Lindeberg

Department of Immunology, Biomedical Center, University of Uppsala, Uppsala (Sweden)

Lennart Andersson

Institute of Biochemistry, Biomedical Center, University of Uppsala, Uppsala (Sweden)

(Received July 3rd, 1992)

ABSTRACT

Peptides synthesized by the solid-phase method can be efficiently purified in a single immobilized metal affinity chromatography step based on interaction with the α-amino group if, after coupling of each amino acid residue, unreacted amino groups are irreversibly blocked by acetylation and if no strongly metal-binding amino acids (His, Trp, Cys) are present in the sequence. A difference in basicity for α- and ε-amino functions of *ca.* 2 pH units is sufficiently large to allow selective binding of peptides to immobilized metal ions via the unprotonated α-amino group. The binding is pH-dependent: on Cu^{2+}- and Ni^{2+}-loaded supports most peptides are maximally retarded at pH values around 7.5 and 8.5, respectively. The decreased binding strength at lower pH values is due to protonation of the α-amino function, whereas the reduced affinity at higher pH is caused by metal ion transfer from the matrix to the peptide. The metal ion is captured in a multidentate chelate where, in addition to the α-amino group, up to three adjacent deprotonated amide nitrogens are coordinated to the metal. If the pH is raised further, additional metal ions may be bound in biuret-like structures. Immobilized Ni^{2+}, owing to its higher selectivity and affinity, is the preferred chromatographic support if slightly basic conditions can be tolerated.

INTRODUCTION

Solid-phase peptide synthesis (SPPS) [1], despite improvements in methodology, suffers from the inherent limitation that side-products resulting from incomplete reaction steps cannot be removed from the desired peptide until the synthesis is finished and the product cleaved from the resin. Whereas small peptides can usually be purified adequately by general separation techniques, particularly reversed-phase high-performance liquid chromatography (RP-HPLC), the similarity between the product and the impurities often makes the isolation of large synthetic peptides a more demanding task.

Attempts have been made to facilitate the purification by attachment of affinity handles onto the side-products [2,3] or the target peptide [4–6] in order to allow the use of more specific separation methods. Selective labelling of the desired peptide is accomplished by irreversible blocking (capping) of remaining amino groups after each coupling step by an efficient acylating agent such as acetic anhydride, followed at the end of the synthesis by attachment of the affinity handle to the α-amino group, which

Correspondence to: G. Lindeberg, Department of Immunology, Box 582, Biomedical Center, University of Uppsala, S-75123 Uppsala, Sweden.

0021-9673/92/$05.00

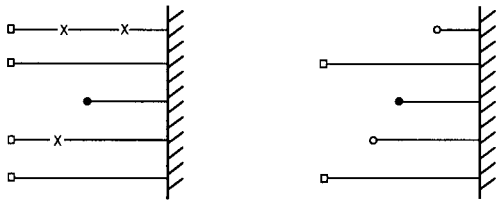

Fig. 1. Schematic composition of (resin-bound) products synthesized (a) without and (b) with the inclusion of a capping protocol. × denotes amino acid deletion, ● truncation and ○ capping, *e.g.* by acetylation. The free α-amino group (□) may be substituted with an affinity handle before removal of the side-chain protecting groups and cleavage of the peptide–resin bond.

will then be present only in the target peptide (Fig. 1). However, in this case the choice of an affinity handle is severely restricted by the requirement that mild conditions must be available for its detachment once the purification is completed. Furthermore, the function of the affinity group may be adversely affected by electrophilic substitution during the cleavage step or by other post-synthetic modifications.

In special cases the presence of certain amino acid residues in the N-terminal part of the peptide may be expoited for affinity purification. Cysteine residues have been used for reversible covalent binding to immobilized mercury derivatives [7] or activated thiols [8], and the use of immobilized metal ion affinity chromatography (IMAC) [9] for the efficient purification of several moderately sized peptides (30–40 amino acid residues) with N-terminal histidine or tryptophan residues was recently described [10]. The simplicity and selectivity of the latter approach prompted the search for more general conditions for its application.

The simplest affinity handle available for metal ion interaction is the α-amino group itself. The participation of unprotonated amino groups in different metal complexes is well established [11], and it has been shown that the α-amino function is of importance in IMAC of peptides [12,13]. Belew and Porath [14] found that peptides lacking His, Trp or Cys were bound to immobilized Cu^{2+} if the α-amino group was free but not if it was blocked and suggested that IMAC could be useful for removing blocked peptides from a crude synthetic mixture. However, this study was limited to pH values below 7. Since pK_a values for α- and ε-amino groups in proteins are higher (*ca.* 8 and 10, respectively) we believed that conditions could be found where this relatively large difference in basicity could be more efficiently exploited for selective binding of a peptide through its α-amino group. This view was further supported by recent findings that α-amino groups in peptides interact strongly with both immobilized Cu^{2+} and Ni^{2+} above pH 7, whereas in proteins they interact only with immobilized Cu^{2+} [15]. We therefore synthesized a number of peptides (Table I) to permit a systematic investigation of the pH dependence and the specificity of the metal binding. Histidine or tryptophan residues were not

TABLE I

STRUCTURE OF PEPTIDES USED IN THIS INVESTIGATION

Peptide	Structure
1	Asp–Ser–Ala–Val–Gly–Tyr–Ala
2	Ac–Asp–Ser–Ala–Val–Gly–Tyr–Ala
3	Gly–Ala–Thr–Lys–Gly–Pro–Gly–Arg–Val–Ile–Tyr–Ala
4	Ac–Gly–Ala–Thr–Lys–Gly–Pro–Gly–Arg–Val–Ile–Tyr–Ala
5	Gly–Ala–Thr–Lys(Ac)–Gly–Pro–Gly–Arg–Val–Ile–Tyr–Ala
6	Ac–Gly–Ala–Thr–Lys(Ac)–Gly–Pro–Gly–Arg–Val–Ile–Tyr–Ala
7	Pro–Ala–Thr–Lys–Gly–Pro–Gly–Arg–Val–Ile–Tyr–Ala
8	Ac–Pro–Ala–Thr–Lys–Gly–Pro–Gly–Arg–Val–Ile–Tyr–Ala
9	β-Ala–Ala–Thr–Lys–Gly–Pro–Gly–Arg–Val–Ile–Tyr–Ala
10	Ac–β-Ala–Ala–Thr–Lys–Gly–Pro–Gly–Arg–Val–Ile–Tyr–Ala
11	Ala–Pro–Ala–Thr–Lys–Gly–Pro–Gly–Arg–Val–Ile–Tyr–Ala
12	Ac–Ala–Pro–Ala–Thr–Lys–Gly–Pro–Gly–Arg–Val–Ile–Tyr–Ala

included in the peptides in order to simplify interpretation of the data.

EXPERIMENTAL

Chemicals

tert.-Butyloxycarbonyl (Boc) amino acids were purchased from Peninsula Laboratories Europe (St. Helens, UK), Bachem Feinchemikalien (Bubendorff, Switzerland) or Novabiochem (Läufelfingen, Switzerland). Boc-amino acyl resins were synthesized according to Horiki *et al.* [16]. Other chemicals were of analytical grade and used as purchased. Chelating Superose and Chelating Sepharose Fast Flow were obtained from Kabi-Pharmacia (Uppsala, Sweden).

Buffers

Buffers were prepared by dissolving all the salts in Milli-Q water and titrating to the appropriate pH with concentrated sodium hydroxide. The volume was then adjusted to yield a final buffer concentration of 50 m*M* if not otherwise stated. Buffer salts used were sodium dihydrogenphosphate, boric acid and sodium hydrogencarbonate. Sodium chloride (1 *M*) was included in all buffers.

Peptide synthesis

The peptides were synthesized by the solid-phase method using an Applied Biosystems 430A instrument with standard procedures and Boc/benzyl protecting groups. However, capping with acetic anhydride was included after each coupling step. Acetylation of the terminal α-amino group in the target peptides was accomplished by the addition of acetic acid (2 mmol) to an empty glycine cartridge and using the standard conditions for this amino acid. Boc-Lys(Ac)-OH was coupled manually with dicyclohexylcarbodiimide (three equivalents each) in 25% dimethylformamide (DMF)-dichloromethane (DCM) for 2 h.

The peptides were deprotected and cleaved from the resin (*ca.* 500 mg) by treatment with anhydrous hydrogen fluoride (5 ml) in the presence of anisole (500 μl) for 1 h at 0°C. The residue obtained after removal of hydrogen fluoride *in vacuo* was washed thoroughly with chloroform and diethyl ether. The peptide was then extracted into trifluoroacetic acid (TFA) (3 × 2 ml), and the resulting solution was concentrated under a stream of dry nitrogen to *ca.* 1 ml. Diethyl ether was added to precipitate the product, which was then collected by centrifugation, washed several times with diethyl ether and dried *in vacuo* over potassium hydroxide.

Mass spectrometry

Synthetic products and chromatographic fractions were analysed by plasma desorption mass spectrometry (PDMS) using a BioIon 20 instrument (Applied Biosystems, Uppsala, Sweden). Samples, usually 5–10 μg dissolved in 5–10 μl of 0.1% TFA containing 20–50% ethanol, were applied on nitrocellulose-coated aluminium foils and dried under a stream of nitrogen. Samples with high salt content, *e.g.* IMAC fractions, were usually rinsed with 10–20 μl of 0.1% TFA or distilled water after drying. Positive-ion spectra were collected, normally for 5–30 min.

Reversed-phase HPLC

Synthetic products and IMAC fractions were also analysed by RP-HPLC using a Pharmacia Pep-RPC 5/5 column. The chromatographic equipment included two Constametric pumps (types I and III), a Gradient Master controller and a Spectromonitor III variable-wavelength detector (LDC, Riviera Beach, FL, USA). The gradient was formed by mixing acetonitrile containing 0.1% TFA with 0.1% aqueous TFA (0–40% acetonitrile in 30 min). The flow-rate was 1 ml/min. Solid samples were dissolved in 0.1% TFA. When necessary, IMAC fractions were neutralized prior to application.

Immobilized metal ion affinity chromatography

The fast protein liquid chromatography (FPLC) system (Kabi-Pharmacia) used for IMAC contained two P-500 pumps, a GP-250 gradient programmer and a UV-1 monitor set at 280 nm. The IMAC supports were Chelating Superose (32 μmol/ml Zn^{2+} capacity) prepacked in a 1.5 × 1 cm I.D. column and Chelating Sepharose Fast Flow packed in a 6.6 × 0.66 cm I.D. column. The columns were charged with Cu^{2+} or Ni^{2+} and loosely bound metal ions were washed off with 4 ml of 0.1 *M* sodium acetate buffer, pH 4.0. The peptides (50–200 μg) were dissolved in 50–200 μl of the appropriate buffer, applied to the column and eluted isocratically at a flow-rate of 1 ml/min. All buffers contained 1 *M*

sodium chloride in order to suppress undesired ion-exchange effects. After each run the column was washed with 4 ml of sodium acetate buffer, pH 4.0. The peptides were characterized by their capacity factors:

$$k = V_e/V_0 - 1$$

where V_e is the elution volume of the peptide and V_0 the elution volume on the metal-free column.

Determination of peptide/Cu^{2+} ratios

Peptide **5** was purified by preparative RP-HPLC and dissolved in water. The peptide concentration (1.27 m*M*) was determined by amino acid analysis. The solution was then diluted with an equal volume of 100 m*M* phosphate–borate–2 *M* sodium chloride at pH 7–11 and 100 μl (63.5 nmol) chromatographed on Cu^{2+}-charged Chelating Superose (1.5 × 1 cm I.D.) as described above. In each case the eluate corresponding to the peptide peak was collected in a preweighed tube and the copper content determined by atomic absorption spectroscopy (Mikro-Kemi, Uppsala, Sweden).

Spectroscopy

Absorption maxima of peptide–Me^{2+} complexes. Peptides **5** and **6** (1 μmol) were each dissolved in 1 ml of 50 m*M* phosphate–borate containing 1 *M* sodium chloride in the pH range 7–11. To each solution was added 100 μl of either 10 m*M* copper sulphate or 10 m*M* nickel nitrate. The resulting mixture was centrifuged and the absorption spectrum in the range 300–700 nm was recorded with the aid of a Pye Unicam SP8-100 spectrophotometer.

Absorption maxima of peptide eluates. Chelating Sepharose (*ca.* 75 μl) was packed in a Pasteur pipette and charged with Cu^{2+} or Ni^{2+}. The peptides **5** and **6** were each dissolved in phosphate–borate–sodium chloride buffers over a pH range of 7–11 at a concentration of 2 m*M*. The column was pre-equilibrated with the appropriate buffer, then 500 μl of the peptide solution were applied and the column was eluted with 1 ml of the same buffer. The absorption maximum of the eluate in the range 300–700 nm was determined.

RESULTS AND DISCUSSION

Influence of buffer concentration

The effect of phosphate and borate concentration on the retention of the peptides **1–4** on Chelating Sepharose–Cu^{2+} at different pH values is shown in Table II. The peptides with blocked α-amino groups (**2** and **4**) are largely unaffected by the buffer concentration and show very low overall retention, whereas those with free α-amino groups (**1** and **3**) are generally more strongly bound although less so at higher buffer concentrations. As 1 *M* sodium chloride is present in all buffers this effect can not be ascribed to ion-exchange properties of the matrix but is most likely due to competition by phosphate and borate ions for the available coordination sites of the immobilized metal ions. However, in borate buffer at pH 8.5 and 9 the effect is reversed and the peptides **1** and **3** are more retarded as the buffer concentration is increased. The negligible influence on the retention of the acetylated peptides rules out the possibility that this might be caused by a general salting-out effect. We favour the interpretation that at this concentration borate ions are so efficiently competing for the coordination sites that, although the peptide may still bind via the α-amino group, chelation by further metal ion coordination to deprotonated amide nitrogens and subsequent release of the peptide as a peptide–metal complex is prevented. This mechanism is discussed in further detail in the following section. At pH 10 the competition by borate may interfere with the binding of the ε-amino group, hence the decreased retention of peptides **3** and **4** in 0.5 *M* buffer.

Influence of pH

The data given in Table II clearly show that the retention of several peptides on immobilized Cu^{2+} is pH-dependent. These effects are also observed in Fig. 2, where mixed phosphate–borate buffers with high buffering capacity over the entire region pH 5–11 were used. Most of the peptides with a free α-amino group (**1**, **3**, **5** and **7**) have a clear retention maximum at pH 7–8, whereas their acetylated counterparts (**2**, **4**, **6** and **8**) are not retained at pH ≤ 9. The peptides **3**, **4**, **7–10** and **12**, which all carry free ε-amino functions, show increased retention at pH > 9. The latter effect is related to binding via the ε-amino group, which gradually becomes de-

TABLE II

CAPACITY FACTORS OF MODEL PEPTIDES CHROMATOGRAPHED ON IMMOBILIZED Cu^{2+} AT DIFFERENT BUFFER CONCENTRATIONS

Sample: 100 μg of peptide dissolved in 100 μl of sodium phosphate–1 *M* sodium chloride or sodium borate–1 *M* sodium chloride. Column: Chelating Sepharose–Cu^{2+} (6.6 × 0.66 cm I.D.). Elution: sample buffer at 1 ml/min. Detection: UV at 280 nm. The α-amino groups of **2** and **4** are acetylated.

Peptide	Buffer concentration (m*M*)	Capacity factor						
		Phosphate			Borate			
		pH 6	pH 7	pH 8	pH 8	pH 8.5	pH 9	pH 10
1	5	0.7	5.4	5.6	6.2	0.1	0.1	0.0
	50	1.0	3.8	3.4	4.6	0.1	0.1	0.0
	500	0.3	3.4	3.0	3.0	0.9	0.5	0.0
2	5	0.0	0.1	0.0	0.1	0.0	0.0	0.0
	50	0.0	0.0	0.0	0.1	0.0	0.0	0.0
	500	0.0	0.0	0.0	0.1	0.0	0.0	0.0
3	5	0.2	2.1	4.0	6.8	0.4	0.5	0.9
	50	0.2	1.4	3.3	5.9	0.4	0.4	0.9
	500	0.1	0.3	2.6	4.8	2.3	1.1	0.6
4	5	0.0	0.1	0.0	0.1	0.2	0.3	0.9
	50	0.0	0.0	0.0	0.1	0.2	0.3	1.0
	500	0.0	0.1	0.0	0.1	0.1	0.2	0.7

protonated in this pH region since peptides without lysine (**1** and **2**) or with a blocked ε-amino function (**5** and **6**) are not retained at pH ≥ 9. Correspondingly, the rise in retention as the pH is increased from 5 to 7–8 reflects deprotonation and binding of the free α-amino group.

At pH values below 7–8 the peptide is bound via the α-amino group or as a bidentate chelate in which the carbonyl oxygen of the N-terminal amino acid is also coordinated to the metal ion in the equatorial plane (Fig. 3a). This is consistent with the formation of ternary complexes in solution, in which case it has been found [17] that the initial step involves coordination of the metal ion to the terminal amino group and the adjacent amide oxygen.

A free amino group is sufficient for anchoring a peptide to immobilized cupric ions, as can be seen for some of the lysine-containing compounds (**4**, **8**, **10** and **12**). Tyramine, which has no amide oxygen or nitrogen that can participate in the metal ion coordination, is also retarded above pH 7.5 (Fig. 4). However, the retention is considerably lower than that for peptide **11**, suggesting that a neighbouring peptide oxygen contributes significantly to the metal binding (see below).

The decrease in retention as the pH is raised further, from 7–8 to 9, is probably not caused by buffer ion competition since the same behaviour is observed in borate, carbonate and mixed phosphate–carbonate buffer (not shown). The coordination of hydroxide ions resulting in a decreased retention seems to be unlikely since these would be expected to also prevent binding of the ε-amino group at pH > 9, at which the hydroxide ion concentration is even higher. Further investigations demonstrated that the lowered retention is caused by metal ion transfer (MIT) from the chelating support to the peptide.

When an excess of peptide with a free α-amino group (**5**) was passed through a column of Cu^{2+}-loaded Chelating Sepharose the process could be observed visually. At pH ≥ 8 the blue colour of the chelated copper at the top of the column faded or disappeared completely while the eluate turned violet. The visible spectra of the eluates in the range 300–700 nm were identical to those obtained by

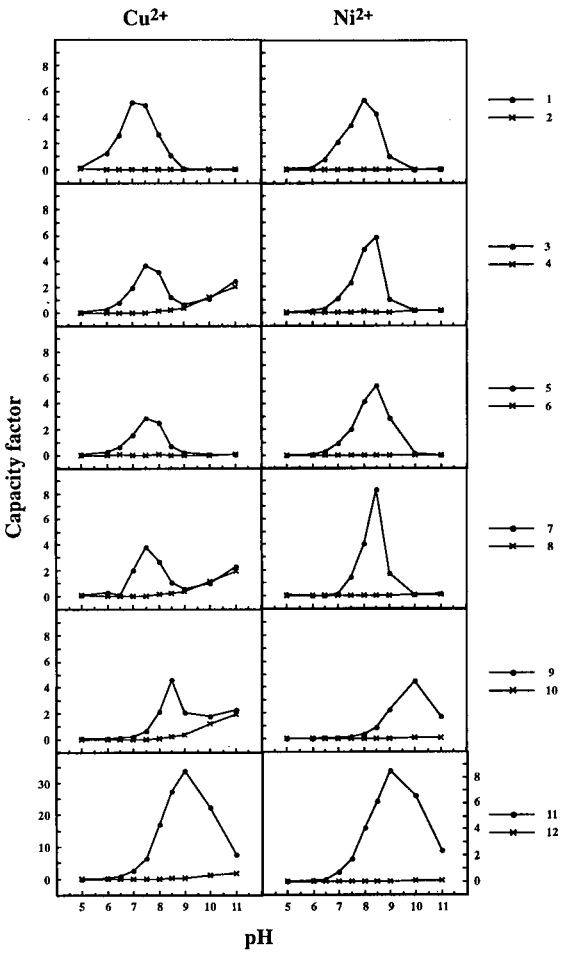

Fig. 2. Retention of peptides **1–12** on immobilized Cu^{2+} and Ni^{2+} at different pH values. Column: Chelating Superose (1.5 × 1 cm I.D.) charged with Cu^{2+} or Ni^{2+}. Sample: 70–130 μg of peptide dissolved in 100 μl of 50 m*M* sodium phosphate–borate–1 *M* sodium chloride. Elution: isocratic with sample buffer at 1 ml/min. Detection: UV at 280 nm. Note change of scale in the lower left-hand corner.

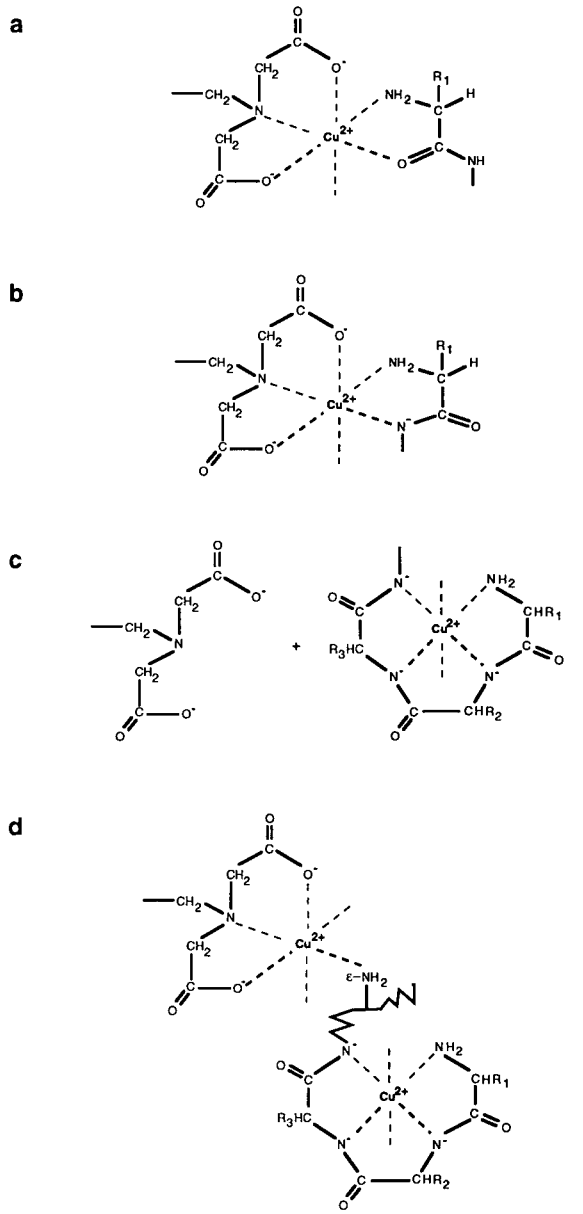

Fig. 3. Proposed mechanism for metal ion transfer from iminodiacetate–Cu^{2+} support to peptide. (a) The peptide is initially bound via the α-amino group or as an N,O complex. (b) At pH > 7 the adjacent amide proton is lost and the peptide reoriented to form an N,N complex. (c) At slightly higher pH values further amide nitrogens are deprotonated and the metal ion captured in a quadridentate chelate. Above pH 10 biuret-like complexes may be formed. (d) At pH > 9 the peptide can bind via the deprotonated ε-amino group.

mixing the peptide and copper sulphate in equimolar amounts in the appropriate buffer. At pH ≥ 9 the absorption maximum occurred at 515 nm, which is characteristic for a quadridentate complex [18]. For the corresponding acetylated peptide (**6**) the loss of copper from the column was observed only at pH ≥ 10 and the absorption maximum was shifted to 560 nm, indicating that three deprotonated amide nitrogens are coordinated to the metal ion.

Metal analysis confirmed that copper was re-

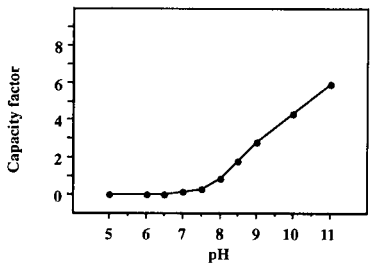

Fig. 4. Retention of tyramine on Cu^{2+}-loaded Chelating Superose at different pH values. Column dimensions: 1.5 × 1 cm I.D. Sample: 35 μg of tyramine dissolved in 100 μl of 50 m*M* sodium phosphate–borate–1 *M* sodium chloride. Elution: isocratic with sample buffer at 1 ml/min. Detection: UV at 280 nm.

moved from the column. When a known amount of peptide **5** was chromatographed on Chelating Superose–Cu^{2+}, the amount of copper transferred to the eluate increased as the pH was raised from 7 to 11 (Table III). The 2:1 Cu^{2+}:peptide ratio at pH 11 is consistent with chelation of a second copper ion in the C-terminal part of the peptide where deprotonated amide nitrogens are coordinated to the metal in a biuret-like fashion.

A possible mechanism of MIT is illustrated in Fig. 3. Amide deprotonation is reinforced by the metalation of the carbonyl oxygen (Fig. 3a). The pK_a value has been shown to drop from about 15 to typically 5–6 for binary and to 6–8 for ternary

TABLE III

AMOUNT OF COPPER TRANSFERRED FROM CHROMATOGRAPHIC SUPPORT TO ELUATE BY PEPTIDE **5** AT DIFFERENT pH VALUES

Sample: 63.5 nmol of **5** dissolved in 100 μl of 50 m*M* sodium phosphate/borate–1 *M* sodium chloride. Column: Chelating Superose–Cu^{2+} (1.5 × 1 cm I.D.). Elution: sample buffer at 1 ml/min. Detection: UV at 280 nm. The copper content in the peptide-containing fraction was determined by atomic absorption spectroscopy.

pH	Cu (nmol)	Cu/peptide ratio
7.0	0	0
8.0	17	0.3
9.0	80	1.2
10.0	69	1.1
11.0	118	1.9

Cu^{2+}-complexes [11]. The change from O- to N-coordination (Fig. 3b) places the deprotonated nitrogen of the neighbouring amide bond in a favourable position for interaction with the adjacent equatorial binding site of the metal ion. Formation of a new bond will displace one of the carboxyls of the iminodiacetate and weaken the interaction between the metal ion and the chromatographic support. As a further consequence of the peptide bond planarity, interaction with the third amide nitrogen will thereby be facilitated, eventually yielding the quadridentate chelate shown in Fig. 3c.

Most of the pH profiles presented in Fig. 2 can be interpreted to be a result of two counteracting effects: binding and metal ion transfer. The profiles of **1–8** might represent the behaviour of many peptides. Peptide **11**, which has a proline as the second amino acid and consequently carries no removable amide proton in this position, is very strongly bound ($k > 30$ at pH 9). The reduced binding at higher pH values for this peptide is again caused by metal ion transfer from the matrix to the peptide, but here the terminal carboxyl rather than the amino group may be involved in the chelate formation. Peptide **9** with an N-terminal β-alanine also behaves anomalously in so far as the retention maximum is shifted *ca.* 1 pH unit upfield. This change may be due to the more basic β-amino group but may also reflect a reduced tendency for amide deprotonation in the less favourable six-membered ring.

Influence of metal ion

When Cu^{2+} is replaced by Ni^{2+} as the immobilized metal ion the general chromatographic behaviour remains the same (Fig. 2). However, maximal adsorption occurs at higher pH values, usually around pH 8.5, which is in agreement with observations on the formation of complexes in solution [11].

Capacity factors are usually at least as high as for immobilized Cu^{2+}. However, for peptide **11**, which has proline as the second residue, the maximal k value is reduced from 30 to 9 upon replacement of Cu^{2+} with Ni^{2+}, which might reflect differences in coordination characteristics for the two metals.

The selectivity for binding via the α- *vs.* the ε-amino group seems to be higher for the Ni^{2+}-loaded support since none of the α-acetylated peptides is

retarded at pH $\leqslant$ 11. For purification of synthetic peptides according to the concepts outlined above, an iminodiacetate–Ni^{2+} support would be the medium of choice, at least in cases where slightly basic conditions can be tolerated.

It can be shown that nickel ions are also transferred from the iminodiacetate to the peptide. At pH 10–11 elution of Chelating Sepharose–Ni^{2+} with peptide **5** produces a yellow colour. The absorption maximum at 420 nm of the eluate is consistent with a square-planar coordination to one amino and three depronated amide nitrogens [11].

Attempts to use other immobilized metal ions (Zn^{2+}, Co^{2+} and Mn^{2+}) were unsuccessful.

*IMAC purification of Gly–Ala–Thr–Lys–Gly–Pro–Gly–Arg–Val–Ile–Tyr–Ala (**3**)*

The usefulness of IMAC based on metal ion interaction with the α-amino group for isolation of synthetic peptides is demonstrated in the purification procedure for peptide **3** which, in addition to the α-amino group, also carries a free ε-amino function.

The crude product was applied on Cu^{2+}- and

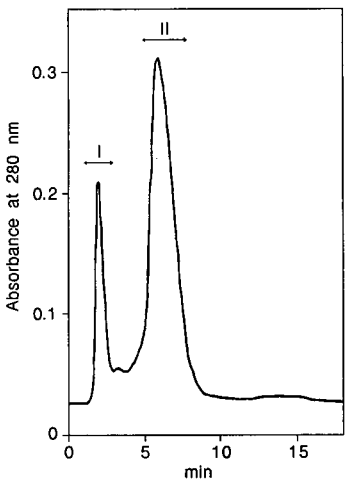

Fig. 5. Chromatography of crude peptide **3** on Chelating Superose–Cu^{2+}. Column dimensions: 1.5 × 1 cm I.D. Sample: 1.25 mg dissolved in 250 μl of 50 m*M* sodium phosphate–borate–1 *M* sodium chloride, pH 7.5. Elution: isocratic with sample buffer at 1 ml/min. For mass spectrometry the fractions indicated were concentrated and desalted on a 5 × 0.5 cm I.D. Pep-RPC column. After adsorption, the column was rinsed with 0.1% TFA and the peptides eluted with a steep acetonitrile gradient (0–60% in 1 min).

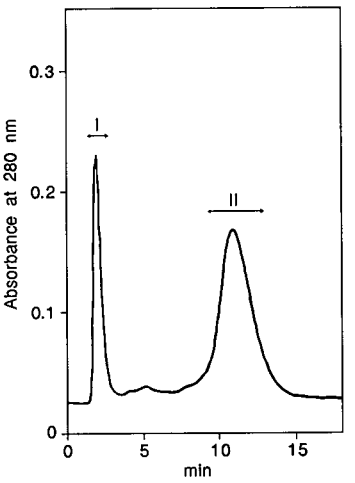

Fig. 6. Chromatography of crude peptide **3** on Chelating Superose–Ni^{2+}. The conditions were as in Fig.5 but the sample and elution buffer was 50 m*M* sodium phosphate–borate–1 *M* sodium chloride at pH 8.5.

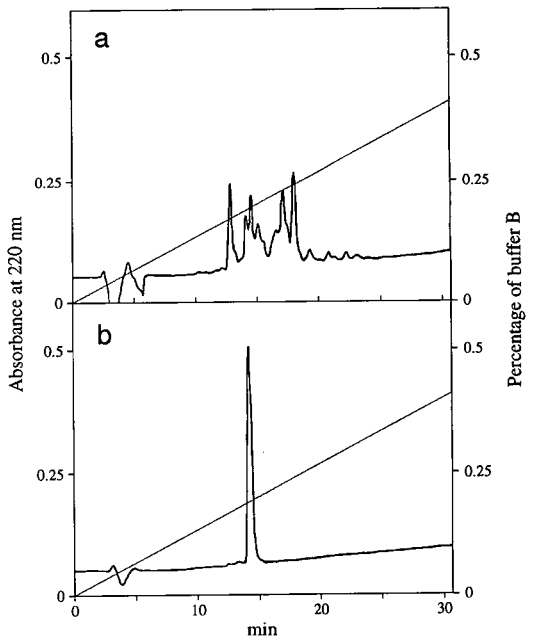

Fig. 7. RP-HPLC of (a) 750 μl (50%) of fraction I and (b) 100 μl (10%) of fraction II from IMAC of peptide **3** on Chelating Superose–Cu^{2+} (Fig. 5). Column: Pep-RPC, 5 × 0.5 cm I.D. Flow-rate: 1 ml/min. Solvent: A: 0.1% aqueous TFA. Solvent B: 0.1% TFA in acetonitrile.

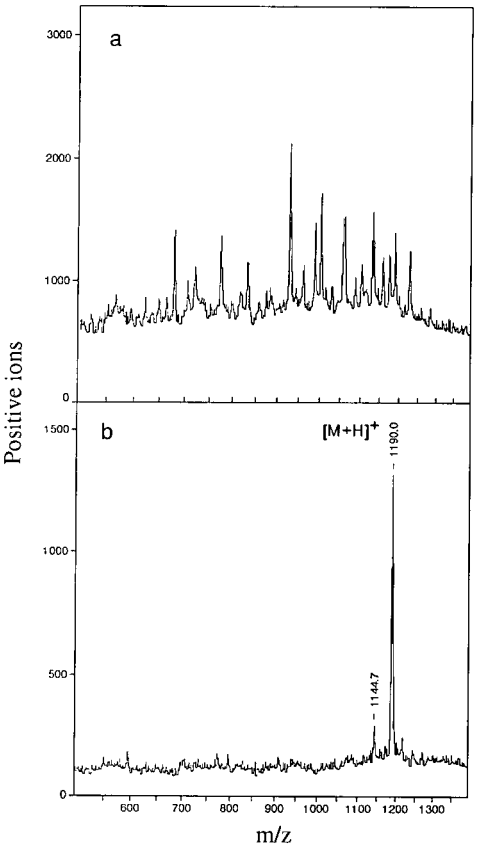

Fig. 8. PDMS of (a) fraction I and (b) fraction II from IMAC of peptide **3** on Cu^{2+}-loaded Chelating Superose (Fig. 5). The desalted samples (5 μl) were mixed with ethanol (2 μl) on nitrocellulose-coated aluminium foils, dried and rinsed with distilled water (20 μl). Most peaks in (a) can be attributed to various acetylated peptides and their fragment ions. The peak at 1144.7 mass units in (b) is due to decarboxylation. The calculated molecular weight for peptide **3** is 1189.4.

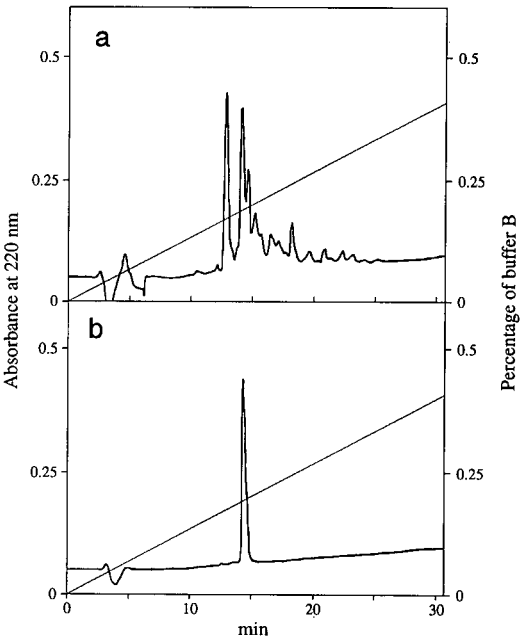

Fig. 9. RP-HPLC of (a) 750 μl (40%) of fraction I and (b) 100 μl (3%) of fraction II from IMAC of peptide **3** on Chelating Superose–Ni^{2+} (Fig. 6). Conditions are as in Fig. 7.

Ni^{2+}-loaded Superose and eluted isocratically at pH 7.5 and 8.5, respectively (Figs. 5 and 6). In both cases two major fractions were obtained, which were further analysed by mass spectrometry and RP-HPLC (Figs. 7–10). As expected, the non-retarded material (I) is a mixture of small amounts of truncated peptides which have been acetylated in the capping steps, whereas in the main fraction (II) only peptide **3** was detected.

*IMAC purification of Ala–Pro–Ala–Thr–Lys–Gly–Pro–Gly–Arg–Val–Ile–Tyr–Ala (**11**)*

Isocratic elution at pH values which yield maximal retardation, *i.e.* pH $\approx$ 7.5 for Cu^{2+}- and pH $\approx$ 8.5 for Ni^{2+}-loaded supports, is adequate for the chromatography of most of the examined peptides. However, for strongly bound compounds such as **11** gradient elution will produce sharper peaks and reduce the time required for the separation (Fig. 11). Since strongly basic conditions should normally be avoided in the handling of peptides, elution by a gradient of decreasing, rather than increasing, pH or by inclusion of a complexing agent such as imidazole or ammonium chloride in the buffer is recommended. As can be seen in the chromatograms the elution profile is largely independent of the type of gradient used, although it seems that imidazole, at least in this case, gives the least satisfactory result. Imidazole, having a high affinity for the Cu^{2+}, displaces the relatively weakly bound peptides which are eluted in a sharp zone ahead of the imidazole. If 1 m*M* imidazole is included in the starting buffer the desired peptide binds weakly to the column and is only partially resolved from the acetylated side-products.

Analysis by RP-HPLC and PDMS (not shown)

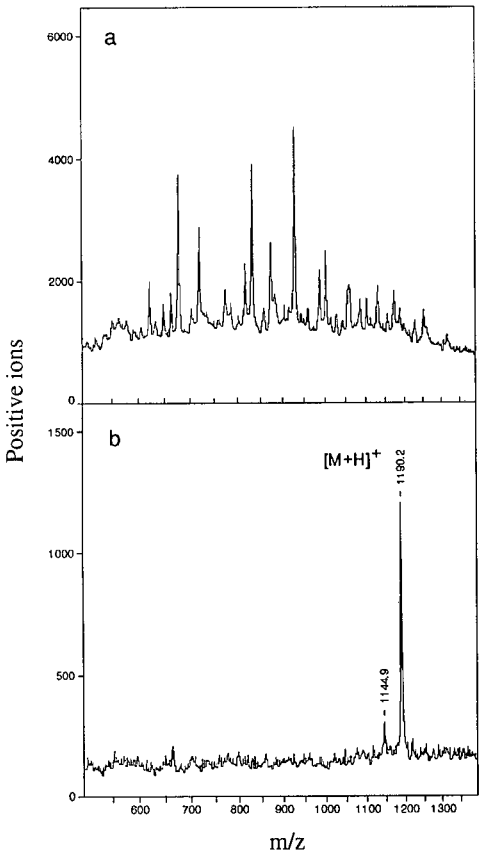

Fig. 10. PDMS analysis of (a) fraction I and (b) fraction II from IMAC of peptide **3** on Ni^{2+}-loaded Chelating Superose (Fig. 6). Conditions are as in Fig. 8.

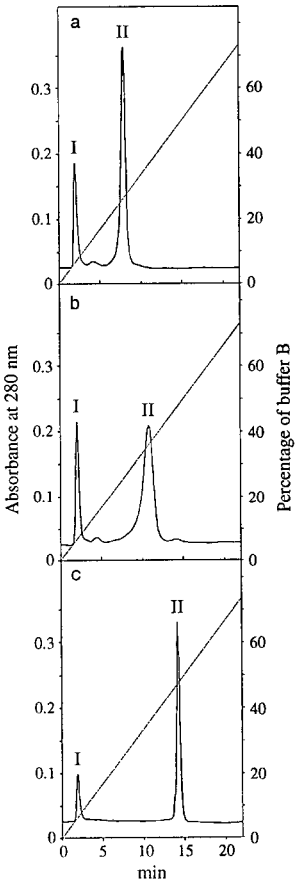

Fig. 11. Chromatography of crude peptide **11** on Chelating Superose–Cu^{2+} (1.5 × 1 cm I.D.). (a) Buffer A: 50 m*M* sodium phosphate–1 *M* sodium chloride, pH 8.0. Buffer B: 50 m*M* sodium phosphate–1 *M* sodium chloride, pH 5.0. Flow-rate: 1 ml/min. Sample: 1.25 mg dissolved in 250 μl of buffer A. (b) Buffer A: 50 m*M* sodium phosphate–1 *M* sodium chloride, pH 8.0. Buffer B: 50 m*M* sodium phosphate–1 *M* sodium chloride–0.1 *M* ammonium chloride, pH 8.0. Flow-rate: 1 ml/min. Sample: 1.25 mg dissolved in 250 μl of buffer A. (c) Buffer A: 50 m*M* sodium phosphate–1 *M* sodium chloride, pH 8.0. Buffer B: 50 m*M* sodium phosphate–1 *M* sodum chloride–20 m*M* imidazole, pH 8.0. Flow-rate: 1 ml/min. Sample: 0.3 mg dissolved in 60 μl of buffer A.

in all cases gives the same general pattern as that observed for peptide **3**: fraction I contains various acetylated peptides, whereas only peptide **11** is detected in fraction II.

CONCLUSIONS

Experimental evidence given in this report suggests that immobilized Cu^{2+} or Ni^{2+} supports can be used for simple and effective separation of side-products from peptides synthesized by the solid-phase method. Future work will clarify whether this mode of affinity purification can be applied to larger peptides and to those containing strongly metal-binding amino acids (His, Trp and Cys) in a suitably protected form.

ACKNOWLEDGEMENTS

This work was supported by The Swedish National Board for Industrial and Technical Development (G. L.) and The Swedisch Natural Science Research Council (L. A.). The pre-packed Chelating Superose column was a generous gift from Dr. L. Kågedal, Kabi-Pharmacia.

REFERENCES

1 R. B. Merrifield, *J. Am. Chem. Soc.*, 85 (1963) 2149–2154.
2 T. Wieland, C. Birr and H. Wissenbach, *Angew. Chem.*, 81 (1969) 782–783.
3 H. Wissman and R. Geiger, *Angew. Chem.*, 82 (1970) 937.
4 R. B. Merrifield and A. E. Bach, *J. Org. Chem.*, 43 (1978) 4808–4816.
5 T. J. Lobl, M. L. Deibel and A. W. Yem, *Anal. Biochem.*, 170 (1988) 502–511.
6 R. A. Houghten and N. Lynam, in G. Jung and E. Bayer (Editors), *Peptides 1988: Proceedings of the 20th European Peptide Symposium, Tübingen, September 1988*, Walter de Gruyter, Berlin, 1989, pp. 214–216.
7 D. E. Krieger, B. W. Erickson and R. B. Merrifield, *Proc. Natl. Acad. Sci. U.S.A.*, 73 (1976) 3160–3164.
8 G. Lindeberg, J. Tengborn, H. Bennich and U. Ragnarsson, *J. Chromatogr.*, 156 (1978) 366–369.
9 J. Porath, J. Carlsson, I. Olsson and G. Belfrage, *Nature (London)*, 258 (1975) 598–599.
10 G. Lindeberg, H. Bennich and Å. Engström, *Int. J. Peptide Protein Res.*, 38 (1991) 253–259.
11 H. Sigel and R. B. Martin, *Chem. Rev.*, 82 (1982) 385–426 and references therein.
12 B. Monjon and J. Solms, *Anal. Biochem.*, 160 (1987) 88–97.
13 T.-T. Yip, Y. Nakagawa and J. Porath, *Anal. Biochem.*, 183 (1989) 159–171.
14 M. Belew and J. Porath, *J. Chromatogr.*, 516 (1990) 333–354.
15 L. Andersson and E. Sulkowski, *J. Chromatogr.*, 604 (1992) 13–17.
16 K. Horiki, K. Igano and K. Inouye, *Chem. Lett.*, (1978) 165–168.
17 H. Sigel, R. Griesser and B. Prijs, *Z. Naturforsch.*, 27b (1972) 353–364.
18 E. J. Billo, *Inorg. Nucl. Chem. Lett.*, 10 (1974) 613–617.

Journal of Chromatography, 627 (1992) 137–143
Elsevier Science Publishers B.V., Amsterdam

CHROM. 24 586

Use of monobromobimane to resolve two recombinant proteins by reversed-phase high-performance liquid chromatography based on their cysteine content

Donald O. O'Keefe

Department of Analytical Research, Merck Research Laboratories, Rahway, NJ 07065 (USA)

Ann L. Lee and Shigeko Yamazaki

Department of Biochemical Process R & D, Merck Research Laboratories, West Point, PA 19486 (USA)

(Received July 2nd, 1992)

ABSTRACT

A rapid reversed-phase HPLC assay useful for fermentation and downstream process development was developed for monitoring transforming growth factor-α-*Pseudomonas aeruginosa* exotoxin A 40 (TGFα-PE40). This protein is a chimeric recombinant protein synthesized in *Escherichia coli*. In the fermentation, full-length TGFα-PE40 is present along with PE40, an $M_r \approx 40\,000$ C-terminal fragment of TGFα-PE40, which co-purifies with TGFα-PE40 in many cases. A highly efficient reversed-phase HPLC assay using ultraviolet absorbance detection provided excellent resolution of the chimeric protein from the host-cell proteins in the crude cell lysate. However, this technique failed to resolve TGFα-PE40 from PE40, thereby limiting its use for in-process quantitation of the product. In order to resolve these two proteins, we have developed a new technique based on the sulfhydryl specificity of the fluorescent probe monobromobimane. Treatment of in-process samples with dithiothreitol followed by monobromobimane produces fluorescently-labeled TGFα-PE40, but does not label PE40 due to the lack of cysteine residues in this fragment. Thus, reversed-phase HPLC analysis using fluorescence detection provides the selectivity necessary to discriminate between TGFα-PE40 and PE40.

INTRODUCTION

Transforming growth factor-α-*Pseudomonas aeruginosa* exotoxin A 40 (TGFα-PE40, $M_r = 44\,960$) is a recombinant fusion protein produced in *Escherichia coli* [1,2]. TGFα-PE40 is a potential anticancer agent that is cytotoxic towards human tumor cells expressing specific growth factor receptors [2]. The N-terminal portion of the protein is composed of transforming growth factor-α (TGFα, 50 amino acids) and is responsible for binding to specific cell surface receptors. The C-terminal portion of the molecule is a fragment of *Pseudomonas aeruginosa* exotoxin A (PE) called PE40 ($M_r \approx 40\,000$) [3]. PE40 contains a domain that translocates the protein's catalytic subunit across cell membranes allowing inactivation of cellular protein synthesis.

To facilitate process development of TGFα-PE40, a rapid assay was needed that could monitor the product at each step of the fermentation and purification process. Process monitoring and quantitation of TGFα-PE40, especially during fermentation, was a challenging endeavor for two main reasons. TGFα-PE40 was an intracellular product which in the early stages of development represented only a small percentage of the total cellular pro-

Correspondence to: D. O. O'Keefe, Department of Analytical Research, Merck Research Laboratories, Merck and Co., Inc., P.O. Box 2000, 80M-112, Rahway, NJ 07065, USA.

0021-9673/92/$05.00

tein. This made monitoring fermentation samples difficult. Nevertheless, despite the crude nature and the low product level of fermentation and early purification samples, a highly efficient reversed-phase HPLC assay was developed that provided excellent resolution from the host-cell proteins. However, it appeared that the synthesis of TGFα-PE40 was accompanied by the production of a related molecule. Electrophoretic and western blot analysis suggested that this molecule was PE40. Although TGFα-PE40 and PE40 differ by approximately 50 amino acids, the reversed-phase HPLC assay with UV absorbance monitoring failed to resolve the two proteins. This led to inaccurate quantitation of fermentation expression levels of the product. Additionally, the assay lost its usefulness in estimating the recovery and yield of TGFα-PE40 at each step in the purification process. Although TGFα-PE40 and PE40 were resolved by western blot analysis, this laborious and low-throughput technique was impractical for process monitoring.

To differentiate PE40 from TGFα-PE40, the 6 cysteine residues exclusively located in the TGFα domain were exploited by labeling them with the sulfhydryl-specific reagent monobromobimane (4-bromomethyl-3,6,7-trimethyl-1,5-diazabicyclo-[3.3.0]octa-3,6-diene-2,8-dione; mBBr) [4]. As a result, TGFα-PE40 was fluorescently labeled and PE40 was not. The fluorescent-labeling did not affect the retention time of TGFα-PE40 so the two products still co-eluted upon reversed-phase analysis. However, by using fluorescence detection and UV absorbance monitoring, the necessary selectivity to discriminate between TGFα-PE40 and PE40 was obtained. This technique provided a more quantitative and accurate method for monitoring TGFα-PE40 during fermentation and downstream processing steps.

EXPERIMENTAL

Materials

Trifluoroacetic acid (TFA) and dithiothreitol (DTT) were obtained from Pierce (Rockford, IL, USA). Tris base was purchased from Boehringer Mannheim (Indianapolis, IN, USA). Acrylamide was acquired from National Diagnostics (Manville, NJ, USA). Other electrophoresis reagents and rabbit anti-goat antibody conjugated to alkaline phosphatase were purchased from Bio-Rad (Richmond, CA, USA). HPLC-grade acetonitrile was acquired from Fisher. Other reagents were obtained from either Fisher or Sigma.

Western blots

Protein samples were electrophoresed through 12% polyacrylamide–sodium dodecyl sulfate (SDS) gels according to the method of Laemmli [5]. The samples did not contain reducing agent and were not heated prior to electrophoresis. After electrophoresis, proteins were transferred to nitrocellulose paper (Schleicher & Schuell, Keene, NH, USA) in a Genie electroblotter (Idea Scientific, Minneapolis, MN, USA) as described by Towbin *et al.* [6] except the transfer buffer was made 0.1% SDS. Proteins bound to the nitrocellulose paper were then probed with either goat anti-TGFα antisera (Biotope, Redmond, WA, USA) or goat anti-PE antisera (List Biologicals, Campbell, CA, USA) as described [7]. Immunoreactive proteins were then detected using rabbit anti-goat antibody conjugated to alkaline phosphatase [8,9]. Control experiments demonstrated that these antisera did not cross react with *E. coli* proteins.

Monobromobimane labeling

To expose cysteine sulfhydryls, purified protein and in-process samples were denatured and reduced in 200 m*M* Tris–HCl, pH 8.0, 1% SDS, 3 m*M* EDTA, 3 m*M* DTT for 20 min at room temperature. mBBr (Molecular Probes, Eugene, OR, USA) was added to a final concentration of 15 m*M* from a 100 m*M* stock solution in acetonitrile. The reaction proceeded for 2 min at room temperature in subdued light before it was terminated by a 10-fold dilution into 4 m*M* cysteine. Cysteine and DTT stock solutions were made fresh.

Chromatography

Proteins were chromatographed on a HY-TACH non-porous C_{18} column (30 × 4.6 mm I.D.) from Glycotech with a linear gradient of 34 to 64% acetonitrile in 0.1% TFA over 6 min at 1.0 ml/min. The column was equipped with a water jacket equilibrated at 80°C by a Lauda RM6 circulating water bath. Control experiments demonstrated that TGFα-PE40 remained intact during the short time it was exposed to elevated temperature. UV absor-

bance was at 280 nm and fluorescence detection was at 470 nm after excitation at 382 nm. The chromatography system consisted of a Waters Model 712 WISP autosampler and a Waters Model 680 automated gradient controller controlling Waters Model 510 and Model M-6000 pumps. A Spectroflow 757 variable-wavelength absorbance detector from Applied Biosystems and a Spectro Vision FD-200 fluorescence detector were in-line to monitor column effluent.

RESULTS AND DISCUSSION

An in-process HPLC assay was developed to monitor TGFα-PE40 levels at each step of the fermentation and purification process. This rapid, reversed-phase HPLC assay employed a short column (30 × 4.6 mm I.D.) packed with a micropellicular, silica-based octadecyl stationary phase operated at elevated temperature and with high mobile phase flow-rate. Under these conditions, which facilitated rapid and highly efficient separations and facile column regeneration [10], the column provided the resolving power required to separate TGFα-PE40 from host-cell proteins in crude cell lysates. For the analysis of crude cell lysates from fermentation broths, samples were mixed with 6 *M* guanidine–HCl, acidified, centrifuged and then injected in the HPLC system. As shown in the upper panel of Fig. 1, TGFα-PE40 was only a minor component in that particular cell lysate. Comparison with the bottom panel indicated that the identified peak is likely to represent the product since its retention time corresponded with the purified reference material. In addition, there was little interference in the 5-min region from *E. coli* proteins determined by analyzing a cell lysate lacking TGFα-PE40. It is also noted that the total time of analysis was only 8 min and column regeneration was completed within 2 min.

During process development, SDS–polyacrylamide gel electrophoresis of TGFα-PE40 samples showed the continual presence of an $M_r \approx 40\,000$ protein. Samples enriched in TGFα-PE40 or the $M_r \approx 40\,000$ protein were prepared and chromatographed on the HY-TACH non-porous C_{18} column using a slightly modified linear gradient of acetonitrile from the conditions described in Fig. 1 (see Experimental). It was found that the two proteins could not be resolved and that they had a retention time of 4.24 min (Fig. 2). Analysis of the samples by

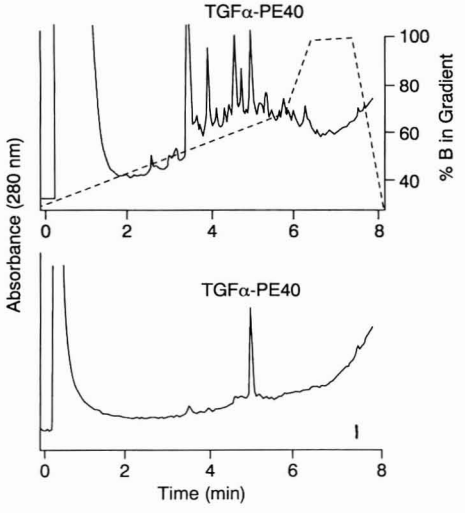

Fig. 1. Rapid reversed-phase HPLC chromatograms of a crude cell lysate and TGFα-PE40. Conditions: Glycotech HY-TACH C_{18} micropellicular (non-porous) silica-based column (30 × 4.6 mm I.D.). Gradient: A: 0.1% TFA in water; B: 0.1% TFA in acetonitrile–water (80:20); temperature, 80°C; flow-rate, 2 ml/min; 0.05 AUFS. Top panel: a crude cell lysate containing TGFα-PE40 was mixed with 6 *M* guanidine HCl, acidified, and centrifuged. Bottom panel: a TGFα-PE40 enriched sample.

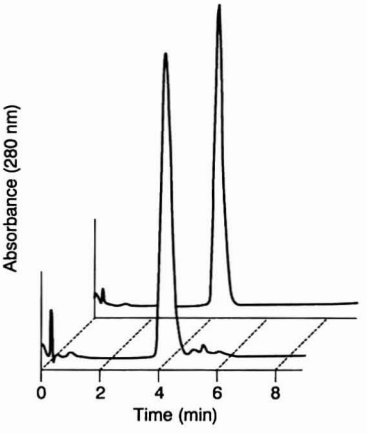

Fig. 2. Reversed-phase chromatograms of samples enriched in TGFα-PE40 or the $M_r \approx 40\,000$ protein. Approximately 7 μg of each protein were injected onto a HY-TACH non-porous C_{18} column and chromatographed as described under Experimental. The top chromatogram respresents TGFα-PE40 and the bottom chromatogram represents the $M_r \approx 40\,000$ protein.

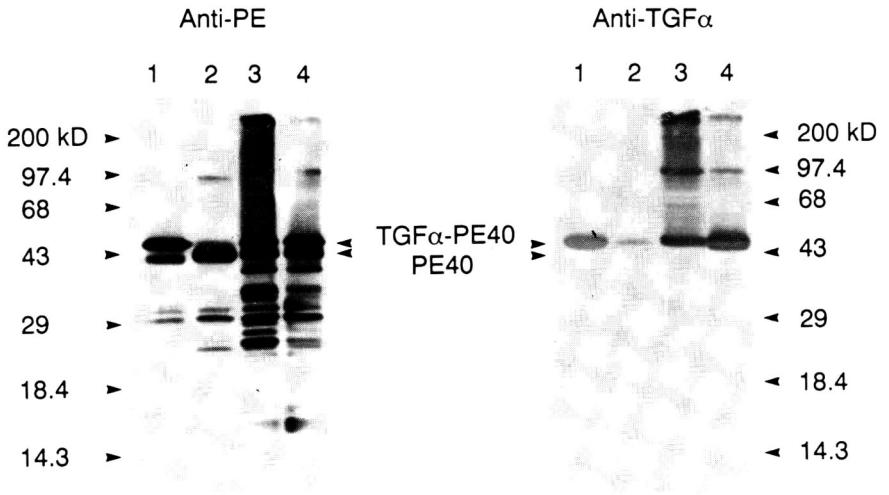

Fig. 3. Western blot analysis of TGFα-PE40 in-process samples. Proteins transferred to nitrocellulose paper were probed with either anti-PE or anti-TGFα antisera. The lanes for each blot correspond to: (1) a TGFα-PE40 enriched sample, (2) a PE40 enriched sample, (3) a cell lysate from *E. coli* that produced TGFα-PE40, and (4) a partially purified TGFα-PE40 sample. Lanes 1, 3, and 4 within each blot contained the same amount of TGFα-PE40 while lane 2 contained an equivalent amount of PE40. The gels were overloaded to highlight TGFα-PE40 aggregates and degradates in the samples. The migration of protein markers is indicated for each blot with masses expressed in kilodaltons (kD).

western blotting using antisera recognizing the PE40 portion of the chimeric protein showed that both proteins reacted with the antisera (Fig. 3). When western blots of these samples used anti-TGFα antisera, the sample enriched with TGFα-PE40 was recognized, but the $M_r \approx 40\,000$ protein was unreactive (Fig. 3). The absence of reactivity to anti-TGFα indicated that the $M_r \approx 40\,000$ protein did not contain TGFα epitopes. This finding, along with the approximate molecular size of the $M_r \approx 40\,000$ protein, prompted us to designate this impurity as PE40, a protein similar to that described by Chaudhary *et al.* [3]. It is not known whether the PE40 found in TGFα-PE40 samples was the result of proteolytic degradation or was synthesized *de novo* from an internal start signal in the messenger RNA.

The identical reversed-phase chromatographic behavior of TGFα-PE40 and PE40 might intially be considered surprising since the two proteins differ by approximately 50 amino acids. This suggests, however, that the 50 amino acid TGFα domain plays a minor role, if any, in the hydrophobic interaction between the protein and the stationary phase. Therefore, the PE40 portion of TGFα-PE40 must contribute significantly to the hydrophobic contact area. Since there are sequences within PE40 that are implicated in the proteins' ability to cross hydrophobic cell membranes [11], it is likely that these hydrophobic membrane-associating sequences are the principal means by which TGFα-PE40 and PE40 interact with the hydrocarbonaceous stationary phase. This interaction is so strong that any contribution from the TGFα domain is negligible.

Numerous attempts were made to resolve TGFα-PE40 from PE40 by reversed-phase HPLC using a number of different columns under a variety of mobile phase conditions. The types of columns tried included different silica-based columns with varying length alkyl side chains as well as wide-pore polystyrene–divinylbenzene polymeric resins. Various mobile phases at pH 2, 4.5, 7, 8.5, and 10 were evaluated, as were a number of organic modifiers. In all cases, TGFα-PE40 could not be fully resolved from PE40. Therefore, an alternative approach was sought to resolve the proteins. A high-resolution reversed-phase-based separation, however, was still desirable due to the need to monitor fermentation and crude samples. Examining the amino acid sequence of TGFα-PE40 revealed that all six of the

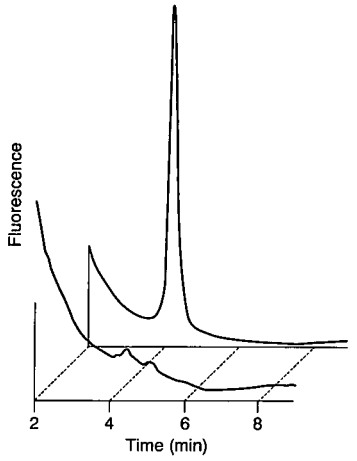

Fig. 4. Reversed-phase chromatograms of TGFα-PE40 and PE40 enriched samples labeled with mBBr. Approximately 7 μg of each protein were injected onto a HY-TACH non-porous C_{18} column and chromatographed as described under Experimental. The top chromatogram represents TGFα-PE40 and the bottom chromatogram represents PE40.

protein's cysteine residues were located in the TGFα domain [12]. This difference in the primary structure of the proteins was exploited by using the sulhydryl-specific fluorescent label mBBr. When samples highly enriched in TGFα-PE40 or PE40 were labeled with mBBr and then chromatographed by reversed-phase HPLC, mBBr-labeled TGFα-PE40 was detected by fluorescence whereas PE40 was not (Fig. 4). The small peak seen in the mBBr-treated PE40 chromatogram at 4.43 min indicates that the sample contained approximately 1% TGFα-PE40, which agrees with the anti-TGFα western blot analysis of that sample in Fig. 3, lane 2. Western blot analysis also revealed other low-molecular-mass fragments besides PE40 in the sample. Nevertheless, even if those fragments co-eluted with TGFα-PE40 by reversed-phase HPLC, the TGFα-PE40 would still be selectively identified since those protein fragments lacked the TGFα domain and therefore would not be labeled with mBBr.

Labeling TGFα-PE40 with mBBr in crude in-process samples, such as *E. coli* cell lysates, proved to be a powerful advantage of this technique. For these samples, labeling was rapid and showed the same dependence on mBBr concentration as it did for purified TGFα-PE40. Reversed-phase chromatograms of mBBr-labeled in-process samples are

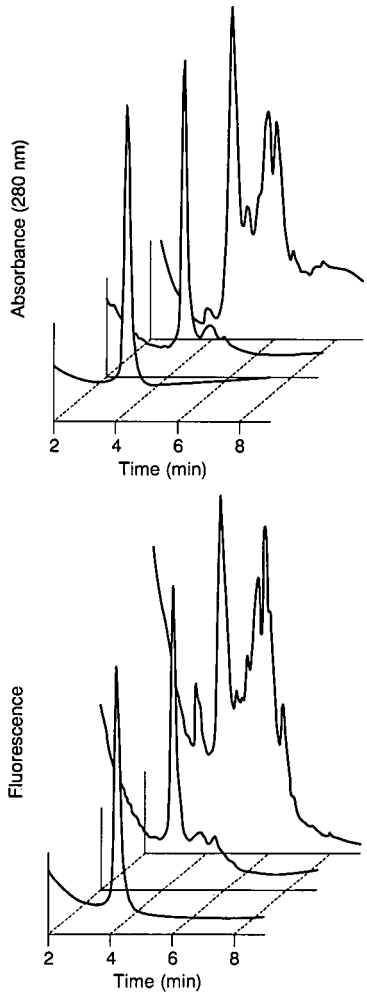

Fig. 5. Reversed-phase chromatograms of mBBr-labeled in-process samples. mBBr-labeled samples were chromatographed as described under Experimental. Column effluents were monitored for absorbance at 280 nm (upper panel) or fluorescence (lower panel). In each set of chromatograms the tracings are ordered from top to bottom as follows: a cell lysate from *E. coli* that produced TGFα-PE40, a partially purified sample of TGFα-PE40, and a TGFα-PE40 enriched sample.

shown in Fig. 5. In general, the profiles were similar whether the column effluent was monitored for absorbance at 280 nm (upper panel) or for fluorescence (lower panel). Control experiments demonstrated that the TGFα-PE40 contained in crude samples was completely labeled. The amount of TGFα-PE40 in each of these in-process samples was

TABLE I

IN-PROCESS QUANTITATION OF TGFα-PE40 BY ABSORBANCE AND FLUORESCENCE OF mBBr-LABELED SAMPLES

mBBr-labeled samples were chromatographed as described under Experimental and monitored simultaneously for absorbance at 280 nm and fluorescence. Standard curves were generated from the peak heights of known amounts of mBBr-labeled TGFα-PE40. The amount of TGFα-PE40 in unknown samples was interpolated from the two standard curves.

TGFα-PE40 Sample	Absorbance at 280 nm (mg/ml)	Fluorescence detection (mg/ml)
E. coli cell lysate	1.9	1.2
Partially purified sample	1.3	1.0
TGFα-PE40 enriched sample	1.6	1.6

interpolated from standard curves generated by chromatographing purified mBBr-labeled TGFα-PE40 and monitoring fluorescence and absorbance at 280 nm simultaneously. The TGFα-PE40 content in the cell lysate and the partially purified sample was lower by fluorescence detection than by absorbance at 280 nm (Table I). This was ture for many additional in-process samples. This suggested that proteins other than TGFα-PE40 were present in the TGFα-PE40 peak. A large component of this additional protein was PE40 (see Fig. 3). Therefore, quantitation without fluorescence detection would yield erroneous results leading to an overestimation of product levels. In the case of a highly enriched sample of TGFα-PE40, the assay showed that the TGFα-PE40 content was identical regardless of whether absorbance at 280 nm or fluorescence detection was used as the standard curve (Table I). Analysis of this same sample by Coomassie Blue staining of SDS-polyacrylamide gels verified the absence of PE40. These results demonstrate that mBBr-labeled samples provided the selectivity necessary to discriminate between TGFα-PE40 and PE40 allowing more accurate in-process quantitation of TGFα-PE40.

Although the reversed-phase separation originally provided the necessary efficiency to resolve TGFα-PE40 from host-cell proteins, it was possible that upon labeling the samples with mBBr the chromatographic behavior of other proteins could be affected and as a consequence, interfere with the TGFα-PE40 and PE40 peak. These labeled impurities would contribute to the TGFα-PE40 peak height for both UV absorbance and fluorescence detection leading to an overestimation of TGFα-PE40 levels by either detection method. Control experiments demonstrated that the UV absorbance chromatograms of mBBr-labeled in-process samples and unlabeled samples were not significantly different suggesting that the fluorescent tag did not alter the retention of labeled host-cell proteins.

The approach for selectively labeling TGFα-PE40 with mBBr for in-process monitoring and quantitation may be extended to other proteins that are difficult to resolve from impurities. Although the impurity described here may be unique, *i.e.* PE40 lacked sulfhydryls that were found in TGFα-PE40, there are a variety of other fluorescent compounds that are reactive with amine and carboxylic acid side chains in proteins [13,14]. A higher content of any one of these amino acid side chains in a protein compared to an impurity may provide enough discrimination to differentiate the two proteins. Fluorescent reagents that react with carbohydrates also exist [13]. This provides an additional avenue of analysis for recombinant proteins derived from mammalian cells. Whether any of these other fluorescent reagents are able to react quickly with their target protein under mild conditions in crude in-process samples remains to be determined. Finally, the absence of appropriate amino acid residues in recombinant proteins does not preclude the method described here. Specific amino acids can be engineered into proteins so that a fluorescent label may be attached to facilitate in-process monitoring and quantitation.

ACKNOWLEDGEMENTS

We gratefully acknowledge the support and en-

couragement of Drs. Hillel Cohen, Robert Sitrin and David Wonnacott. We are also grateful to C. Meacham Harrell and Anthony Paiva for assistance with polyacrylamide gel electrophoresis analysis and to Dr. Edgar Scattergood for his assistance throughout the course of this work.

REFERENCES

1 G. M. Edwards, D. Defeo-Jones, J. Y. Tai, G. A. Vuocolo, D. R. Patrick, D. C. Heimbrook and A. Oliff, *Mol. Cell. Biol.*, 9 (1989) 2860.
2 D. C. Heimbrook, S. M. Stirdivant, J. D. Ahern, N. L. Balishin, D. R. Patrick, G. M. Edwards, D. Defeo-Jones, D. J. FitzGerald, I. Pastan and A. Oliff, *Proc. Natl. Acad. Sci. U.S.A.*, 87 (1990) 4697.
3 V. K. Chaudhary, Y-H. Xu, D. FitzGerald and I. Pastan, *Proc. Natl. Acad. Sci. U.S.A.*, 85 (1988) 2939.
4 N. S. Kosower and E. M. Kosower, *Methods. Enzymol.*, 143 (1987) 76.
5 U. K. Laemmli, *Nature (London)*, 227 (1970) 680.
6 H. Towbin, T. Staehelin and J. Gordon, *Proc. Natl. Acad. Sci. U.S.A.*, 76 (1979) 4350.
7 R. K. Tweten and R. J. Collier, *J. Bateriol.*, 156 (1983) 680.
8 M. S. Blake, K. H. Johnston, G. J. Russell-Jones and E. C. Gotschlich, *Anal. Biochem.*, 136 (1984) 175.
9 K-J. Pluzek and J. Ramlau, in O. J. Bjerrum and N. H. H. Heegaard (Editors), *CRC Handbook of Immunoblotting of Proteins*, Vol. 1, CRC Press, Boca Raton, FL, 1988, p. 177.
10 J. Frenz, W. S. Hancock, W. J. Henzel and Cs. Horváth, in K. Gooding and F. Regnier (Editors), *HPLC of Biological Macromolecules, Methods and Applications*, Vol. 51, Marcel Dekker, New York, 1990, p. 145.
11 J. Hwang, D. J. FitzGerald, S. Adhya and I. Pastan, *Cell*, 48 (1987) 129.
12 D. Defeo-Jones, J. Y. Tai, R. J. Wegrzyn, G. A. Vuocolo, A. E. Baker, L. S. Payne, V. M. Garsky, A. Oliff and M. W. Riemen, *Mol. Cell. Biol.*, 8 (1988) 2999.
13 Y. Ohkura and H. Notha, *Adv. Chromatogr. (NY)*, 29 (1989) 221.
14 R. F. Chen and C. H. Scott, *Anal. Lett.*, 18 (A4) (1985) 393.

Journal of Chromatography, 627 (1992) 145–151
Elsevier Science Publishers B.V., Amsterdam

CHROM. 24 616

Heterogeneous binding of aldolase to phosphocellulose

Interpretation in terms of a "concerted cluster" model of multivalent affinity

V. Dowd and R. J. Yon

School of Biological and Chemical Sciences, University of Greenwich, Woolwich Campus, Wellington Street, London SE18 6PF (UK)

(First received April 23rd, 1992; revised manuscript received September 8th, 1992)

ABSTRACT

It has been suggested that when multi-site protein molecules bind to immobilised ligands on an inflexible matrix, they should encounter discrete sets of single and clustered ligands, binding to clusters being concerted and very tight [R. J. Yon, *J. Chromatogr.*, 457 (1988) 13–23]. To test this model, the aldolase–phosphocellulose interaction was re-examined at low protein concentrations, with and without the presence of soluble ligands. In all cases the data plotted as non-linear (concave upwards) Scatchard plots, indicating at least two populations of adsorption sites, while soluble ligands produced competitive effects as expected. When fitted to a 2-population Langmuir model based on the concerted cluster concept, the data suggested that (a) a very small proportion (about 0.3%) of the total immobilised phosphate was accessible as matrix ligand; (b) of this, about 8% comprises accessible pairs; (c) the matrix ligand was non-randomly distributed within the actual matrix volume; (d) affinity constants for soluble ligands were close to their published values, and (e) the effective matrix ligand is a bisphosphate structure in phosphocellulose. It is suggested that the concerted-cluster model may be valid for an affinity system based on a "hard" matrix such as cellulose.

INTRODUCTION

Analysis of the interactions of multisite proteins (*i.e.*, proteins having several identical ligand binding sites) with immobilized ligands (*e.g.*, in affinity chromatography) have given rise to a number of theoretical models [1–5]. The problem of the expected co-operativity due to proximity that should arise when a multi-site protein molecule encounters a static cluster of ligands was first addressed by Kyprianou and Yon [4] and later extended by Yon [1]. This last paper proposed a "concerted cluster" theory which predicted that, at sufficiently high densities of immobilized ligands on a matrix that prevented translatory motion of these ligands, the protein should encounter a heterogeneous collection of distinct adsorption sites which respectively bound the protein monovalently, bivalently etc. Bivalent and higher-order clusters of immobilized ligands should have very large stoichiometric association constants, but are likely to be present at very low concentrations. As a first approximation the distribution of the immobilized ligand was assumed to be uniformly random, *i.e.*, determined by a Poisson distribution.

Experimental data on the partitioning of rabbit muscle aldolase between free solution and the adsorbent phosphocellulose, in the presence and absence of the soluble ligand phosphate, were used to support a theory of multivalent affinity partitioning based on reacted-site probability theory [3]. Inspection of some of these data when plotted in a

Correspondence to: R. J. Yon, School of Biological and Chemical Sciences, University of Greenwich, Woolwich Campus, Wellington Street, London SE18 6PF, UK.

0021-9673/92/$05.00

Scatchard format, showed suggestions of adsorption-site heterogeneity, which was taken by one of us to be evidence of ligand clustering, and accordingly was interpreted in terms of the concerted cluster theory [1,6]. However, it was recognised that the experimental evidence needed re-examining for two reasons: (a) more data at lower protein concentrations were needed (when the clusters might be expected to significantly influence the binding isotherm), and (b) the effect of a multi-phosphate ligand such as hexitol bisphosphate should also be examined for competition, since the heterogeneity might simply reflect two (different) binding sites on aldolase. For reasons of simplicity a bisphosphate ligand (hexitol bisphosphate) was chosen in preference to more complex multi-phosphate ligands of aldolase such as inositol triphosphate. In the present paper we report an extended set of binding data and interpret them in terms of the concerted cluster model. The opportunity is also taken to extend and improve analysis by using a binding equation of the Langmuir type, and to introduce a factor allowing for high local concentrations of the immobilized ligand.

EXPERIMENTAL

Materials

Fructose-1,6-bisphosphate aldolase from rabbit muscle (13 units/mg), fructose-1,6-phosphate, β-NADH, α-glycerophosphate dehydrogenase (165 units/mg), triosephosphate isomerase (1700 units/mg) and phosphocellulose (medium mesh grade) were obtained from Sigma, Poole, UK. Sephadex G-25 was supplied by Pharmacia-LKB, Milton-Keynes, UK. Buffer components and other materials were from Sigma or BDH, Poole, UK. Hexitol bisphosphate was synthesised from fructose-1,6-bisphosphate according to Bragg and Hough [7]. The product was obtained in 72% yield and was essentially pure by paper chromatography [8].

Buffers [3] have a nominal ionic strength of 0.15 *M* and consist of imidazole (0.01 mol/l; pH 7.4 adjusted with hydrochloric acid) with remaining ionic strength provided by sodium chloride with allowances being made, as necessary, for the presence of soluble ligand.

Enzyme assay

Aldolase was assayed by enzyme activity, essentially using the method of Rajkumar *et al.* [9] which couples aldolase to triosephosphate isomerase and α-glycerophosphate dehydrogenase. Linearity of the assay and stability of enzyme activity was confirmed at low enzyme concentration (down to 1 n*M*).

Partitioning experiments

Prior to affinity binding studies, aldolase, as an ammonium sulphate resuspension, was desalted into the relevant buffer by passage through a Sephadex G-25 column. Adsorption of aldolase by phosphocellulose was determined using the mix-centrifuge method of Harris and Winzor [10]. Phosphocellulose was washed [3,8] and a sample resuspended in the appropriate buffer (0.30 g wet cake weight, equivalent to 0.028 g dry weight, in 3.0 ml total volume). An aliquot (20 μl) of aldolase solution was added. This suspension was mixed by gentle rotation for 5 min, followed by centrifugation at 250 *g* for a further 5 min. The concentration of the non-bound aldolase was determined by enzymic assay using an aliquot (20 μl) of supernatant. An isochoric affinity system was maintained by addition of relevant stock enzyme solution. This procedure was repeated to give 15–20 additions of aldolase, with corresponding increases in unbound aldolase. At the end of each experiment the phosphocellulose was washed and dried [3] before being weighed. The phosphate content of the dry matrix was determined after ashing [11].

THEORY AND DATA TREATMENT

Our discussion will use the following symbols for experimental variables: $[P_s]$ and $[P_b]$ denote concentrations of non-adsorbed (including soluble complexes) and adsorbed protein, respectively; [S] denotes the concentration of soluble ligand when this is included. The other terms are model parameters; in the present interpretation they are as follows: [M] = total concentration of accessible matrix ligand, $[X_1]$ = concentration of accessible isolated, single matrix ligands, $[X_2]$ = concentration of accessible immobilized ligand pairs, K_M = microscopic (site) association constant for binding matrix ligand, K_1 = stoichiometric association constant for binding to isolated, single matrix ligand, K_2 = stoichio-

metric association constant for concerted binding to paired matrix ligands, K_S = microscopic constant for binding the soluble competing ligand. Concentrations are in mol/l and association constants are in M^{-1}. Triplet and higher order clusters were neglected. These and other aspects of the concerted cluster theory are discussed in ref. 1.

We choose in the present paper to discuss binding phenomena in terms of a Langmuir-type equation, which is generally more familiar than the R (partitionig ratio) *vs.* $[P_t]$ (total concentration of protein) function used previously [1] and is well suited to batchwise binding experiments (the R *vs.* $[P_t]$ format is better suited to frontal chromatography experiments). Derivation of the appropriate equation (eqn. 1 below) is presented in an Appendix to this paper.

Protein adsorption to two independent sets of adsorption sites, in the presence of soluble ligand, is governed by the equation:

$$[P_b] = \frac{K_1[X_1][P_s]}{K_1[P_s] + 1 + K_S[S]} + \frac{K_2[X_2][P_s]}{K_2[P_s] + (1 + K_S[S])^2} \quad (1)$$

The concerted-cluster model [1] provides expressions for the constants $[X_1]$, $[X_2]$, K_1 and K_2 as follows:

$$[X_2] = \frac{6504([M]F)^3}{F(e^{161.3[M]F} - 1)} \quad (2)$$

$$[X_1] = [M] - 2[X_2]$$

$$K_1 = 4K_M$$

$$K_2 = 0.00134 \cdot \frac{K_M^2}{([M]F)^2} \quad (3)$$

Thus in applying the cluster model to eqn. 1, [M], K_M, K_S and F are treated as independent parameters (to be obtained by the data-fitting procedure), after which K_1, K_2, $[X_1]$ and $[X_2]$ are derived according to the above equations. Eqns. 2 and 3 relate to bivalent adsorption, and are derived from eqns. 5 and 9, respectively, in the previous paper [1]. The numerical factors include the radius of aldolase taken as 4 nm (the mean of the crystallographic unit cell dimensions [12]), and the assumption of four binding sites on aldolase. The factor F requires special comment, since it was not discussed in the original model. The concentration of ligand pairs is calculated on the assumption of a uniformly random (Poisson) distribution of matrix ligands. With $F = 1$ this distribution is calculated relative to the entire reaction volume; use of this factor led to a rather poor fit to the experimental data, especially at the lowest protein concentrations, indicating a substantial underestimation of $[X_2]$. Since the distribution must in practice be non-uniform (partly because the suspended matrix occupies only about 0.4% of the reaction volume, and partly because of unknown non-uniformity within the matrix itself) there will be local concentrations of ligand that are much higher than the concentration averaged over the whole reaction space, increasing the probability of pairs and higher clusters. Implicit in our use of the factor F are the assumptions that (i) the local concentration is F times greater than the average concentration over the whole reaction volume, and (ii) that the Poisson distribution can be applied to this local concentration, *i.e.*, within the local environment the distribution is uniformly random.

The parameters [M], K_M, K_S and F were estimated by non-linear regression using the simplex method [13]. To achieve a more even weighting of residual errors, proportional rather than absolute errors in $[P_b]$ were used (proportional error is defined as the difference between theoretical and experimental values divided by the theoretical value). Four separate fits were made, to assess the internal consistency of the results: (1) [M], K_M and F were fitted to 19 data points in the absence of soluble ligands; (2) [M], K_M, $K_{S(\text{phosphate})}$ and F were fitted to 34 data points in the presence of two concentrations of phosphate; (3) [M], K_M, $K_{S(\text{hexitol biphosphate})}$ and F were fitted to 30 data points in the presence of two concentrations of hexitol bisphosphate; (4) a global fit of [M], K_M, $K_{S(\text{phosphate})}$, $K_{S(\text{hexitol bisphosphate})}$ and F was made to all the previous 83 data points. Since the simplex method does not provide estimates of standard errors directly, standard errors were obtained by a Monte Carlo method [13], in which 10 sets of simulated data were generated, each with random errors distributed about the theoretical best-fit with the same mean and standard deviation as the experimental data. These provided 10 values of each of the parameters; the standard errors reported in Table I are for these parameter-sets.

TABLE I

P_i = Phosphate; HBP = hexitol bisphosphate.

Parameter	Fit to data in absence of ligands	Fit to data in presence of phosphate	Fit to data in presence of HBP	Global fit (all data)
(a) Fitted parameters, with S.E.M.				
$10^7 \cdot [M]$	6.97 ± 0.24	7.67 ± 0.44	6.79 ± 0.38	7.09 ± 0.23
$10^{-6} \cdot K_M$	1.11 ± 0.10	0.94 ± 0.14	1.34 ± 0.20	1.13 ± 0.09
$10^{-3} \cdot F$	3.16 ± 0.26	3.91 ± 0.43	2.66 ± 0.38	3.20 ± 0.21
$10^{-2} \cdot K_{S(P_i)}$	–	9.19 ± 1.62	–	7.80 ± 0.43
$10^{-6} \cdot K_{S(HBP)}$	–	–	1.25 ± 0.29	1.24 ± 0.05
(b) Calculated parameters				
$[X_1]$	$0.601\ \mu M$			
$[X_2]$	$0.054\ \mu M$			
K_1	$4.52 \cdot 10^6\ M^{-1}$			
K_2	$1.77 \cdot 10^{18}\ M^{-1}$			

RESULTS

Examination of the binding of aldolase to phosphocellulose at low protein concentrations reveal a pronounced heterogeneity of matrix binding sites, as indicated by severely non-linear, concave-upwards Scatchard plots (Fig. 1). Although non-linearity in each plot is due to relatively few points at the lowest protein concentrations, the effect is highly reproducible; in addition to results reported here, a similar effect has been shown using data from an independent laboratory (data from ref. 3, reinterpreted in refs. 1 and 6). Moreover the effect is detected by two assay methods, spectroscopy [3,6] and enzyme assay (present paper).

We examined the fit of the present experimental data to a model postulating that heterogeneous adsorption arises from binding of the multisite protein to accessible singlets and clusters (predominately pairs) of immobilized ligands. In this interpretation, the near-horizontal right-hand limb of each curve (see Fig. 1A) is asymptotic to a straight line denoting a population of sites assumed to be isolated matrix-ligands that bind the protein monovalently. The steeper left-hand limb is asymptotic to an essentially vertical straight line denoting a second population, assumed to be paired immobilized ligands to which the protein binds bivalently, concertedly and extremely tightly (asymptotes indicated in dotted lines in Fig. 1A). Concentrations of triplet and higher-order sites were assumed to be negligible [1].

The fitted parameters are presented in Table I. Independent fits of data in the absence of ligands, and in the presence of phosphate and hexitol bisphosphate, were generally consistent with each other and with a global fit to all the data, by the criterion that their S.E.M. ranges overlap. The only exception is the estimated value of F, which in one subset of data (in the presence of phosphate) is estimated to be significantly different, by the above criterion, from other estimates of F. We shall use the values from the global fit (Table I) is subsequent discussion.

The estimate of [M] suggests a very low value ($0.7\ \mu M$) of total accessible matrix ligand, or $7\ \mu M$ relative to the packed wet matrix. This is a small fraction of the 2.3 mM phosphate in the packed adsorbent, *i.e.*, only 0.3% of the phosphate comprise accessible matrix ligand. The microscopic (site) association constant for binding matrix ligand is $1.13 \cdot 10^6\ M^{-1}$. Initially, attempts to fit the experimental data to eqn. 1 with $F = 1$, led to a rather poor fit which did not model well the steep upwards curvature towards the left, *i.e.*, the fit underestimated $[X_2]$. To improve the fit, F was treated as an additional independent parameter, leading to a much improved fit (continuous line in Fig. 1A). The best fit was obtained with $F = 3200$, *i.e.*, a local concentration of matrix ligand 3200 times greater than the concentration averaged over the whole

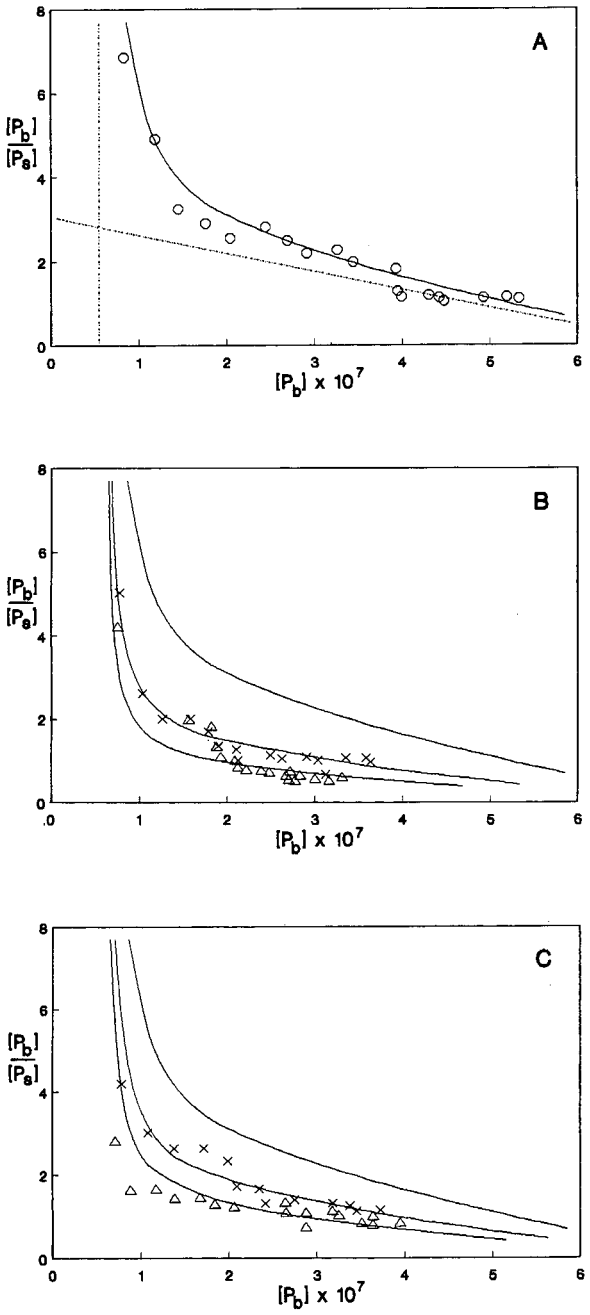

Fig. 1. Scatchard representation of the adsorption of aldolase to phosphocellulose. (A) Data collected in the absence of soluble ligands. (B) Data collected in the presence of 1.43 mM (×) and 2.86 mM (△) phosphate. (C) Data collected in the presence of 0.59 (×) and 1.18 μM (△) hexitol bisphosphate. The curves are theoretical, based on the concerted-cluster model [1] and the parameters from the global fit (Table I). The dotted straight lines in A are asymptotes to the theoretical curve. The theoretical curve from A is overlayed on B and C for comparison.

reaction volume. Volume-displacement experiments with dry phosphocellulose showed that the water-free matrix occupied approximately 4% (v/v) of a packed wet cake, and hence 0.4% (or 1/250) of the reaction volume in our experiments. Purely on comparison of relative volumes, therefore, one may expect a minimum value of 250 for F, not counting further apparent concentration due to non-uniformity within the matrix. The fact that F is well in excess of this minimum value suggests further non-uniformity within the matrix space, *i.e.*, the matrix ligand appears to occupy about 1/12 of the local matrix volume (itself 0.4% of the total reaction volume).

Both phosphate and hexitol bisphosphate are known to be competitive inhibitors of the natural substrate, fructose-1,6-bisphosphate [8,14]. In both cases the expected competition was seen in the displacement of the curves (Fig. 1B, C) at increasing concentrations of soluble ligand, supporting the suggestion that phosphocellulose is an affinity matrix for aldolase. The association constant K_S was found to be 780 M^{-1} for phosphate and $1.24 \cdot 10^6$ M^{-1} for hexitol bisphosphate. These values are somewhat higher, but of the same order as published values of 350 M^{-1} (phosphate) and $8.3 \cdot 10^5$ M^{-1} (hexitol bisphosphate) found in free solution binding studies [8], 350 M^{-1} (phosphate) by competitive inhibition [3] and 400 M^{-1} (phosphate) by batch-wise adsorption of aldolase to myofibrils [15]. The differences may be due a batch-to-batch variations in commercial aldolase.

DISCUSSION

The present experiments, as in previous work [3], support a specific interaction between aldolase and phosphocellulose, since (a) the enzyme is known to bind a number of phosphate-containing ligands in competition with the substrate, fructose bisphosphate; (b) there is clear evidence of competition between the matrix and these ligands; (c) these and earlier experiments [3] were performed in relatively high salt concentration (ionic strength 0.15 M) to suppress non-specific cation-exchange effects; (d) the concentration of accessible immobilized ligand is a small fraction (0.3%) of the total phosphate immobilized. The aldolase–phosphocellulose system may therefore reasonably be used as a model for multivalent affinity interactions.

The pronounced heterogeneity in matrix adsorption sites shown in the present study does not itself provide proof that the high-affinity sites are due to ligand clusters in phosphocellulose. Nevertheless the cluster idea does provide a simple rational explanation for the observed binding heterogeneity, and the quantitative treatment above shows that it is not inconsistent with the observed binding behaviour at low protein concentrations. A necessary consequence of using the concerted cluster theory is the very large difference in affinities between adsorption to monovalent sites and clusters which it predicts. The reasons for this have been discussed in detail [1]. Effectively, for a monovalent binding constant (K_1) of the order $10^6\ M^{-1}$, binding to a cluster is predicted to be irreversible (hence the K_2 value of the order $10^{18}\ M^{-1}$, see Table I, depicted by the essentially vertical left-hand asymptote in Fig. 1A). Practical limits to the sensitivity of the assay have prevented us obtaining more data points along this upwards curve of the Scatchard plot, hence the approach to irreversibility remains to be demonstrated conclusively.

The magnitude of its binding constant suggests that the immobilized ligand group may not simply be a phosphate group. The estimate of $1.13 \cdot 10^6\ M^{-1}$ for the microscopic association constant for binding to the immobilized ligand is nearly 3000-fold greater than the constant for phosphate measured in free solution. Since both free ligands (phosphate and hexitol bisphosphate) compete with the immobilized ligand on these experiments, the immobilized ligand could resemble either. The microscopic binding constant for the immobilized ligand is similar to that of hexitol bisphosphate ($1.24 \cdot 10^6\ M^{-1}$). Moreover, immobilized ligands occur infrequently in the matrix, since they comprise about 0.3% of the total phosphate immobilized. For these reasons, we speculate that the effective immobilized ligand is a bisphosphate group in phosphocellulose.

The cluster theory treats aldolase as a sphere of radius 4 nm, and assumes that whenever two or more ligands are clustered within the bounds of an equivalent sphere, and are encountered by an enzyme molecule, all the bounded ligands will bind concertedly, up to a maximum of four. The model postulates an immovable, rigid, matrix to fix the clusters in space; however we also envisage considerable local movement of a non-translatory nature (rotations about single bonds, for example) to assist matrix ligands to meet the spatial requirement for specific binding. It is possible that the microcrystalline structure of cellulose approximates to the rigid, inflexible matrix required to hold the component ligands of a cluster permanently in juxtaposition. Interestingly, Yon and Easton [16] were unable to show strong evidence of clusters in Blue Sepharose binding to lactate dehydrogenase. Sepharose is a much "softer" matrix, with much more flexibility and local movement in its polymer chains; ligand-clusters would have only a fleeting existence, if any, in such a structure. It will be necessary to examine other affinity matrices of both types to confirm whether, as we suspect, the clustering phenomenon will be observed only when a "hard" matrix such as cellulose is used.

ACKNOWLEDGEMENT

This work is supported by a grant from the Biotechnology/Chemical Engineering Directorate of the Science and Engineering Research Council, UK.

APPENDIX

Derivation of a Langmuir-type equation for concerted protein adsorption that blocks i sites on a N-site protein

We consider a protein molecule P with N identical sites for binding soluble ligand S. This protein is adsorbed reversibly at a matrix site X, such that i of the S-binding sites are blocked to S. The remaining $N - i$ sites are able to bind S with the same intrinsic affinity as sites in the unadsorbed protein. Adsorption is concerted, *i.e.*, the i sites are blocked in an all-or-none manner.

Let $[P_s]$ denote the concentration of all soluble protein forms, *i.e.*, the unadsorbed protein measured by experiment. Then, following Klotz [17],

$$[P_s] = [P] + [PS] + [PS_2] + \ldots + [PS_N]$$
$$= [P](1 + K_S[S])^N \quad \text{(A1)}$$

where [P] denotes the concentration of free (unbound) protein, $[PS_j]$ denotes concentrations of soluble complexes and K_S is the microscopic (site) association constant for binding S.

Similarly, the total concentration of adsorbed protein is given by

$$[P_b] = [PX] + [PXS] + [PXS_2] \ldots + [PXS_{N-i}]$$
$$= [PX](1 + K_S[S])^{N-i}$$
$$= K_i[P][X](1 + K_S[S])^{N-i} \quad \text{(A2)}$$

where $[PXS_j]$ are the concentrations of adsorbed complexes, K_i is the (stoichiometric) association constant for adsorption of P to X, and [X] is the concentration of unoccupied X. Note that $[P_b]$ is the adsorbed protein obtained by experiment.

The total concentration of adsorption sites $[X_t]$ is $[X_t] = [X] + [P_b]$. Substituting from eqn. A2, this becomes

$$[X_t] = [X]\{1 + K_i[P](1 + K_S[S])^{N-i}\} \quad \text{(A3)}$$

Substituting from eqns. A1 and A3 into eqn. A2 to eliminate [P] and [X], we obtain

$$[P_b] = \frac{K_i[X_t][P_s]}{K_i[P_s] + (1 + K_S[S])^i} \quad \text{(A4)}$$

which is in the required Langmuir format.

For several independent populations of adsorption sites, the total adsorbed protein is the sum of several terms of the type in eqn. A4. Thus for two X-populations which block 1 and 2 S-sites respectively, the adsorbed protein will be

$$[P_b] = \frac{K_1[X_1][P_s]}{K_1[P_s] + (1 + K_S[S])} + \frac{K_2[X_2][P_s]}{K_2[P_s] + (1 + K_S[S])^2}$$

which is eqn. 1 in the main text.

REFERENCES

1 R. J. Yon, *J. Chromatogr.*, 457 (1988) 13–23.
2 I. M. Chaiken, *Anal. Biochem.*, 97 (1979) 1–10.
3 L. W. Nichol, L. D. Ward and D. J. Winzor, *Biochemistry*, 20 (1981) 4856–4860.
4 P. Kyprianou and R. J. Yon, *Biochem. J.*, 207 (1982) 549–556.
5 H. W. Hethcote and C. DeLisi, in I. M. Chaiken, M. Wilcheck and I. Parikh (Editors), *Affinity Chromatography and Biological Recognition*, Academic Press, London, 1983, pp. 119–134.
6 R. J. Yon, *Biochem. Soc. Trans.*, 16 (1988) 543–544.
7 P. D. Bragg and L. Hough, *J. Chem. Soc.*, (1957) 4347–4352.
8 A. Ginsbergh and A. H. Mehler, *Biochemistry*, 5 (1966) 2623–2634.
9 T. V. Rajkumar, B. M. Woodfin and W. J. Rutter, *Methods Enzymol.*, 9 (1966) 479–498.
10 S. J. Harris and D. J. Winzor, *Biochem. Biophys. Acta*, 999 (1989) 95–99.
11 B. N. Ames and D. T. Dubin, *J. Biol. Chem.*, 235 (1960) 769–775.
12 J. Sygusch, H. Boulet and D. Beaudry, *J. Biol. Chem.*, 260 (1985) 15286–15290.
13 M. S. Caceci and W. P. Cacheris, *Byte*, May (1984) 340–362.
14 A. H. Mehler, *J. Biol. Chem.*, 238 (1963) 100–104.
15 M. R. Kuter, C. J. Masters and D. J. Winzor, *Arch. Biochem. Biophys.*, 225 (1983) 384.
16 R. J. Yon and M. J. Easton, in M. A. Vijayalakshmi and O. Bertrand (Editors), *Protein–Dye Interactions*, Elsevier Applied Science, London, New York, 1988, pp. 72–79.
17 I. M. Klotz, *Arch. Biochem.*, 9 (1946) 109–117.

Journal of Chromatography, 627 (1992) 153–162
Elsevier Science Publishers B.V., Amsterdam

CHROM. 24 548

Purification, subunit structure and inhibitor profile of cathepsin A

James J. Miller[☆,☆☆]

Department of Biochemistry, University of Louisville School of Medicine, Louisville, KY 40292 (USA)

David G. Changaris

Department of Neurology, University of Louisville School of Medicine, Louisville, KY 40292 (USA)

Robert S. Levy

Department of Biochemistry and Laboratory of Biological Psychiatry, University of Louisville School of Medicine, Louisville, KY 40292 (USA)

(First received May 25th, 1992; revised manuscript received August 10th, 1992)

ABSTRACT

Cathepsin A (EC 3.4.16.1), a lysosomal carboxypeptidase, has been purified 1374-fold from pig kidney. Purification steps included concanavalin A-Sepharose and phenyl-Sepharose chromatography and chromatofocusing. The specific activity (16.9 U/mg) of the purified enzyme was significantly higher than previously reported values. The enzyme preparation appeared homogeneous when analyzed by non-denaturing polyacrylamide gel electrophoresis and was free of detectable protease contamination. The molecular mass (M_r = 97 000), isoelectric point (5.0), and sensitivity to inhibitors were consistent with reported properties of cathepsin A. However, the previously reported three-peptide chain structure was not observed. Sodium dodecyl sulfate–polyacrylamide gel electrophoresis in the presence or absence of 2-mercaptoethanol demonstrated that the enzyme is composed of two M_r 47 000 subunits, each of which dissociate in the presence of 2-mercaptoethanol into two polypeptide chains of 19 000 and 31 000.

INTRODUCTION

We previously have reported the presence of angiotensin carboxypeptidase (ACP) activity in a partially-purified preparation of renin from the human kidney [1]. This ACP sequentially removes the C-terminal leucine and histidine from angiotensin I (AI) to form the potent vasopressor hormone, angiotensin II (AII). The amino acid sequences of these and other peptides mentioned below are shown in Fig. 1.

Preliminary characterization [1] of the ACP re-

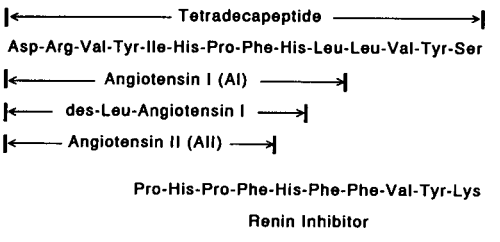

Fig. 1. Amino acid sequences and abbreviations of angiotensin-related peptides.

Correspondence to: Dr. Robert S. Levy, Department of Biochemistry and Laboratory of Biological Psychiatry, University of Louisville School of Medicine, Louisville, KY 40292, USA.

☆ Glenmore Foundation Fellow.

☆☆ In partial fulfillment of the requirements for the degree of Doctor of Philosophy in Biochemistry at the University of Louisville School of Medicine, Louisville, KY 40292, USA.

0021-9673/92/$05.00

vealed that it had a number of similarities to the lysosomal carboxypeptidase, cathepsin A (EC 3.4.16.1), including: (1) stimulation and stabilization by chloride ions and sucrose, (2) lack of requirement for sulfhydryl reagents for activity, (3) presence of an essential sulfhydryl group and (4) a similar molecular mass [2–4]. However, the ACP seemed to have higher activity on peptides with angiotensin-like amino acid sequences than on peptides with unrelated sequences. Besides its activity on AI and des-Leu-AI, the effect of ACP on AI was strongly inhibited by the synthetic tetradecapeptide renin substrate and by a decapeptide renin inhibitor, but it was only weakly inhibited or unaffected by unrelated peptides such as leucine enkephalin, substance P, bradykinin, Pro–Leu–Gly–amide and β-endorphin. AII, however, was neither a substrate nor an inhibitor [1].

These results did not substantiate the reported broad specificity for cathepsin A action on both N-blocked dipeptides [5–7] and natural peptides [7]. Matsuda [7] reported on the hydrolysis of adrenocorticotropin, AI, AII, bradykinin, oxytocin and substance P by cathepsin A. In particular, the hydrolysis of AII occurring nearly as rapidly as AI by cathepsin A is different from the hydrolytic properties of ACP. In addition, Longunov and Orekhovich [8] reported that bovine spleen cathepsin A cleaved Asn^1-Val^5-AII at the Tyr–Val bond, an endopeptidase cleavage. The work of Iodice and coworkers [9,10] demonstrated the carboxypeptidase nature of cathepsin A which suggests that the observation of endopeptidase activity in cathepsin A preparations is probably due to contamination by cathepsin D or other proteinases.

In a subsequent report [11], pig kidney ACP (AI as substrate) was shown by us to co-purify with cathepsin A (benzyloxycarbonyl-glutamyl-tyrosine (Z–Glu–Tyr) as substrate), and it was concluded that most, if not all, of the ACP activity of pig kidney is due to the action of cathepsin A. In light of these results, it was of interest to re-evaluate the substrate specificity of cathepsin A. The purpose of the present work was to prepare highly purified cathepsin A to be used to determine whether or not cathepsin A displays greater activity on peptides with angiotensin-like sequences compared to a variety of peptides with dissimilar sequences. We report here on the purification of cathepsin A from porcine kidney, its subunit structure, and its sensitivity to a variety of inhibitors.

MATERIALS AND METHODS

Materials

Benzyloxycarbonyl-glutamyl-tyrosine (Z–Glu–Tyr), benzyloxy-carbonylglutamic acid (Z-Glu), concanavalin A (Con A)-Sepharose, α-methylmannoside, fluorescein isothiocyanate (FITC)-casein, trypsin, cathepsin D, mersalyl acid 2-(N-morpholino)ethanesulfonic acid (MES), and 3-(N-morpholino)propanesulfonic acid (MOPS) were obtained from Sigma (St. Louis, MO, USA). DEAE-Sephadex, Sephadex G-200, phenyl-Sepharose, Polybuffer Exchanger 94 and Polybuffer 74 were supplied by Pharmacia (Piscataway, NJ, USA). Silver stain kits were from Bio-Rad (Richmond, CA, USA). Fresh pig kidneys were obtained locally from Fischer Packing (Louisville, KY, USA). Des-Leu-AI was custom synthesized by Bachem (Torrance, CA, USA) and all other peptides were purchased from Sigma.

Standard cathepsin A assay

Cathepsin A was assayed with Z–Glu–Tyr as the substrate, and the progress of the reaction was monitored by measurement of the Z–Glu formed by the HPLC method described previously [11]. The assay used 0.25 ml of 3 m*M* Z–Glu–Tyr in 0.1 *M* sodium acetate, 0.1 *M* NaCl, 0.1 *M* sucrose, 1 m*M* EDTA, pH 5.2, pre-warmed to 37°C. Enzyme was added, and the reaction was allowed to proceed for 5–15 min. The reaction was stopped by the addition of 0.75 ml of 250 m*M* phosphoric acid, and the Z–Glu was measured by HPLC. After addition of the phosphoric acid, the Z–Glu concentration was stable. A unit (U) of activity is defined as 1 μmol of product formed per minute. Specific activity is expressed as units per mg protein. Protein was measured by the method of Lowry *et al.* [12] with bovine serum albumin as the standard.

Purification

All of the purification procedures were carried out at 0–4°C. The buffer used for most steps in the purification procedure consisted of 0.1 *M* sodium acetate, 0.1 *M* NaCl, 0.1 *M* sucrose, 1 m*M* EDTA, pH 5.2, and will be referred to as buffer 1. Batches

of six to eight kidneys at a time were processed through the end of step 2. After 18–22 kidneys had been processed during one week, the preparations were pooled and further purified by Con A-Sepharose in step 3. These steps were repeated for two more weeks and then the three post-Con A-Sepharose preparations from a total of 66 kidneys were combined for further purification.

Step 1: tissue extraction

Sixty-six fresh pig kidneys weighing a total of 9.03 kg were obtained locally and processed either the same day or the following day. Whole kidneys were trimmed of most of the tubules and cut into small pieces. The pieces were homogenized in a blender at high speed for 30 s in two volumes of buffer 1. This crude extract was centrifuged at 1 000 *g* for 10 min. The supernatant was saved, and the pellet was re-homogenized in 1 volume of buffer 1. This second homogenate was centrifuged, and the supernatant was combined with the first supernate. The combined supernatants were filtered through five layers of cheesecloth.

Step 2: differential centrifugation

The filtrate was centrifuged at 16 000 *g* for 20 min. The pellet which comprises the mitochondrial/lysosomal fraction was suspended in two volumes of 10 m*M* sodium acetate, 20 m*M* NaCl, 1 m*M* EDTA, pH 5.2, frozen and thawed twice, and then centrifuged at 100 000 *g* for 60 min.

Step 3: ammonium sulfate fractionation

The protein in the 100 000 *g* supernatant was further purified and concentrated by collecting by centrifugation the protein precipitating between 25 and 60% saturation with ammonium sulfate. This pellet was dissolved in a small volume of buffer 1 and frozen until further processing was undertaken.

Step 4: Con A-Sepharose affinity chromatography

A column of Con A-Sepharose (18.6 × 2 cm; 58 ml) was equilibrated with buffer 1 (without EDTA). The enzyme from step 3 (approximately 300 U; 2.7 g) was applied to the column, and 16-ml fractions were collected. The column was washed with the same buffer supplemented with 0.5 *M* NaCl. The enzyme was eluted with 0.1 *M* sodium acetate, 0.5 *M* NaCl, 0.1 *M* sucrose, 1 m*M* EDTA, 0.5 *M* α-methylmannoside, pH 5.2. Fractions containing cathepsin A activity were pooled and concentrated by the addition of ammonium sulfate to 80% saturation. The pellet was resuspended in buffer 1 and frozen until further processed. This step was repeated two more times with the remainder of the enzyme from step 3.

Step 5: phenyl-Sepharose chromatography

A column (11.1 × 2.4 cm; 50 ml) of phenyl-Sepharose was equilibrated with buffer 1. The enzyme from step 4 (463 U, 800 mg) was applied to the column and 16-ml fractions were collected. After application of the sample, the column was washed with a low-ionic-strength buffer (buffer 2) consisting of 0.01 *M* sodium acetate, 0.02 *M* NaCl, 0.1 *M* sucrose, 1 m*M* EDTA, pH 5.2 until the A_{280} of the effluent was below 0.03. The enzyme was eluted with a linear gradient consisting of 250 ml of buffer 2 and 250 ml of 80% ethylene glycol in buffer 1. The active fractions were pooled, dialyzed briefly against buffer 1 to lower the ethylene glycol concentration, concentrated by ultrafiltration using an Amicon PM-30 membrane, and then dialyzed three times against five volumes of buffer 2.

Step 6: DEAE-Sephadex chromatography

A column (20 × 2.4 cm; 90.5 ml) of DEAE-Sephadex A-50 was equilibrated with buffer 2. The enzyme from step 5 (178 U, 46 mg) was applied to the column, and 200-ml fractions were collected. After application of the sample, the column was rinsed with three column volumes of buffer 2, and then a linear gradient was begun which consisted of 250 ml each of buffer 2 and buffer 2 with an additional 0.2 *M* NaCl added. Fractions 20–27 were pooled, and the protein was precipitated with 80% ammonium sulfate. The precipitated protein was collected by centrifugation and resuspended in a small volume of buffer 1.

Step 7: Sephadex G-200 chromatography

A column of Sephadex G-200 (63 × 2.6 cm; 334 ml) was equilibrated with buffer 1. One-half of the enzyme from step 6 (15 ml, 62 U, 5 mg) was applied, and 5-ml fractions were collected. This step was repeated using the remainder of the enzyme from step 6. Fractions containing cathepsin A activity (fractions 34–43) were pooled and concentrated by ultra-

filtration. This pooled and concentrated preparation was re-applied to the same Sephadex G-200 column to ensure complete removal of high-molecular-mass, inactive protein. Again, fractions 34–43 were pooled and concentrated by ultracentrifugation.

Step 8: Chromatofocusing

A column (19 × 1 cm; 14.9 ml) of Pharmacia Polybuffer Exchanger 94 was equilibrated with 0.025 *M* imidazole hydrochloride, 0.1 *M* sucrose and 1 m*M* EDTA, pH 6.8. The enzyme from step 7 was dialyzed briefly (about 4 h) against this starting buffer and applied to the column. The column was eluted with a 1:8 dilution of Pharmacia Polybuffer 74 containing 0.1 *M* sucrose and 1 m*M* EDTA, adjusted to pH 4.0 with HCl. Fractions of 1.8 ml were collected.

Electrophoresis

Non-denaturing polyacrylamide gel electrophoresis (PAGE) was carried out at 4–6°C in 7% polyacrylamide tube gels in the presence of 14 m*M* sodium acetate, 0.1 *M* sucrose and 20 m*M* NaCl at pH 4.0. Electrophoresis was performed in the direction of the cathode at 3 mA per gel tube for 1 and 3.5 h. Gels were stained with Coomassie Blue R250.

Discontinuous sodium dodecyl sulfate (SDS)-PAGE was performed by the method of Laemmli [13] using 0.7 mm 12% gels and the Bio-Rad Mini-Protean II Dual Slab Cell. In addition, the continuous SDS-PAGE system of Weber and Osborn [14] was performed using 7.5% polyacrylamide. Samples were prepared both with and without 2-mercaptoethanol (2-ME), heated at 95°C for 4 min, and run at 200 V (125 V for the Weber and Osborn method) until the bromphenol blue tracking dye reached the bottom of the slabs. Gels were stained either with Coomassie Blue or with silver.

Proteinase assays

The FITC–casein procedure described by Twining [15] was used. FITC–casein (Sigma Type III; 72 μg FITC/mg casein) was dissolved in 50 m*M* sodium phosphate, pH 7.0, at a concentration of 5 mg/ml. The reaction mixture contained 40 μl of enzyme, 80 μl FITC–casein, and 80 μl of the appropriate buffer. The assay buffer for trypsin was 100 m*M* sodium phosphate, 150 m*M* NaCl, pH 7.8. The buffer for cathepsin D was 250 m*M* sodium acetate, pH 4.5. The purified cathepsin A was assayed in the cathepsin D buffer and also in 250 m*M* sodium acetate, pH 5.2, containing 0.1 *M* NaCl and 0.1 *M* sucrose. The reaction was carried out in closed microfuge vials at 37°C for 1 h in the dark. The reaction was stopped by the addition of 480 μl of 5% trichloroacetic acid. The vials were allowed to stand at room temperature for 1 h in the dark and then centrifuged for 5 min in a Beckman microfuge. A 400-μl aliquot of the supernatant was added to 1.6 ml of 0.5 M Tris–HCl, pH 8.5. Fluorescence was determined with an excitation wavelength of 490 nm and an emission wavelength of 535 nm.

RESULTS

Cathepsin A was purified from pig kidney lysosomes by the sequential use of Con A-Sepharose chromatography, phenyl-Sepharose chromatography, DEAE-Sephadex chromatography, gel filtration Sephadex G-200 chromatography, and chromatofocusing.

The enzyme was bound tightly to Con A-Sepharose (Fig. 2) and required relatively high levels of

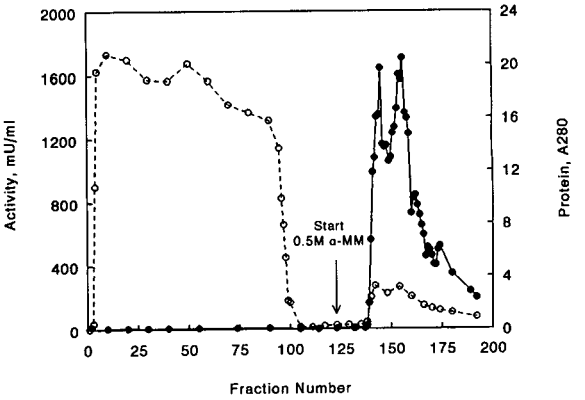

Fig. 2. Con A-Sepharose chromatography of cathepsin A. The 25–60% ammonium sulfate fraction of the lysosomal lysate was applied to a column (18.6 × 2 cm) of Con A-Sepharose equilibrated with buffer 1 (without EDTA). After application of the sample and rinsing with one column volume of buffer 1 (without EDTA) supplemented with 0.5 *M* NaCl, the enzyme was eluted with buffer 1 (with EDTA) containing 0.5 *M* NaCl and 0.5 *M* α-methylmannoside (α-MM). Fractions of 16 ml were collected. All fractions with cathepsin A activity were pooled. This is a representative pattern of the chromatography, which was performed three times. ● = Activity; ○ = A_{280}.

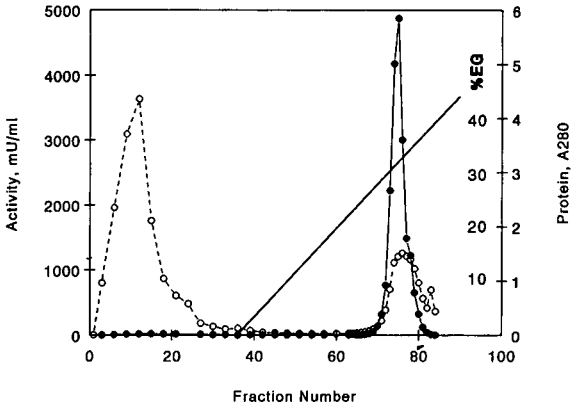

Fig. 3. Phenyl-Sepharose chromatography. The cathepsin A from Con A-Sepharose chromatography was applied to a column (11.1 × 2.4 cm) of phenyl-Sepharose equilibrated with buffer 1. After application of the sample, the column was rinsed with a low-ionic-strength buffer (0.01 *M* sodium acetate, 0.02 *M* NaCl, 0.1 *M* sucrose, 1 m*M* EDTA). The bound enzyme was eluted with a linear gradient from 0–80% ethylene glycol (EG). No additional activity and little additional protein eluted between 40 and 80% EG. Fractions of 16 ml were collected. ● = Activity; ○ = A_{280}.

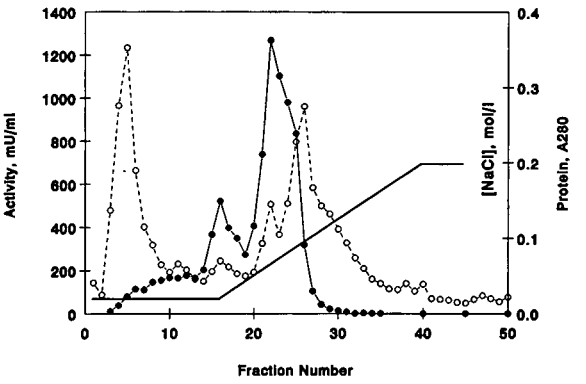

Fig. 4. DEAE-Sephadex chromatography. The cathepsin A recovered from the phenyl-Sepharose step, after concentration and dialysis against 0.01 *M* sodium acetate, 0.02 *M* NaCl, 0.1 *M* sucrose, 1 m*M* EDTA, pH 5.2, was applied to a column (20 × 2.4 cm) of DEAE-Sephadex equilibrated with the same buffer. The column was washed with three volumes of the same buffer and then a linear gradient from 0.02 to 0.2 *M* NaCl was begun. The major peak of activity eluted in fractions 20–27 and was pooled for further purification. Fractions of 20 ml were collected. ● = Activity; ○ = A_{280}.

α-methylmannoside to be eluted from the column. The multiple peaks of activity that are seen in Fig. 2 are partly due to the heterogeneity of the enzyme and partly due to stopping the flow during elution to allow the α-methylmannoside to displace the enzyme more completely. It is of interest to note that 0.1 *M* sucrose, which stabilized cathepsin A, did not interfere with its binding to Con A-Sepharose. This step effected a 5-fold purification with a 50% recovery.

Cathepsin A was further purified by hydrophobic interaction chromatography using phenyl-Sepharose (Fig. 3). The enzyme was bound tightly to phenyl-Sepharose and required about 30% ethylene glycol for elution. The specific activity was increased by a factor of 6.7 by this procedure, and the recovery was 38%.

Approximately 30% of the cathepsin A activity applied to the DEAE-Sephadex column did not bind under the conditions used (Fig. 4). High-molecular-mass forms of cathepsin A which do not bind to DEAE-Sephadex under these conditions had been reported previously [2,11,16–18]. Fractions 5–13 and fractions 14–19 were pooled separately, concentrated and applied to gel filtration chromatography (data not shown). The activity of both of these pools eluted with an apparent molecular mass of 97 000. These unbound forms of cath-

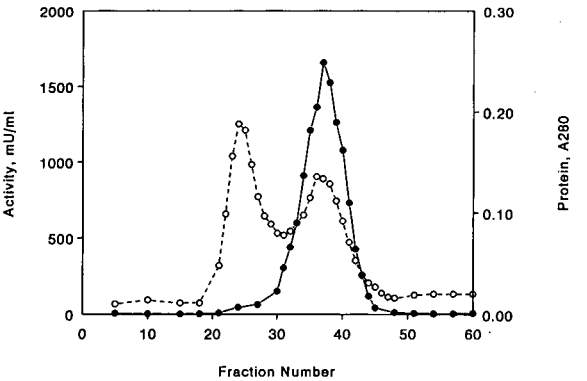

Fig. 5. First Sephadex G-200 chromatography. One-half of the enzyme recovered from the previous DEAE-Sephadex step was applied to a column (63 × 2.6 cm) of Sephadex G-200 equilibrated with buffer 1. The sample volume was 15 ml which was less than 5% of the column volume. Fractions of 5 ml each were collected. The major peak of activity, which eluted in fractions 34–43, was pooled. The peak of enzymatic activity in fraction 37 corresponds to a molecular mass of 97 000. This chromatography was repeated on the other half of the enzyme preparation. ● = Activity; ○ = A_{280}.

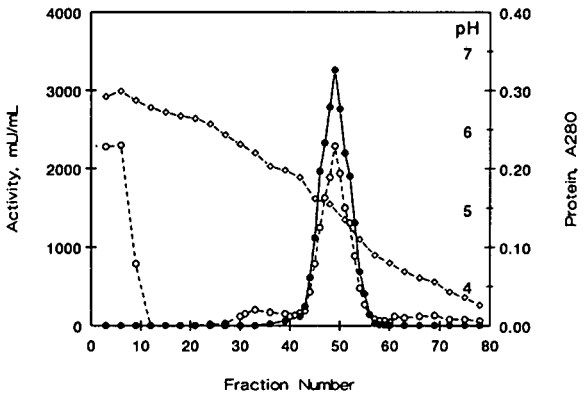

Fig. 6. Chromatofocusing of cathepsin A. A column (19 × 1 cm) of Polybuffer Exchanger 94 was equilibrated with 0.025 *M* imidiazole–HCl, 0.1 *M* sucrose, 1 m*M* EDTA, pH 6.8. The cathepsin A from the second Sephadex G-200 step was dialyzed briefly against the buffer and applied to the column. The pH gradient was generated by eluting the column with Polybuffer 74 (1:8 dilution) adjusted to pH 4.0. The fraction size was 1.8 ml. ● = Activity; ○ = A_{280}; ◇ = pH.

epsin A were not included in subsequent purification steps. The major enzyme form (60%) was bound to the DEAE-Sephadex column and subsequently eluted from it by the salt gradient. This step increased the specific activity by a factor of 3.2 and the recovery in this step was 73%.

After DEAE-Sephadex chromatography, the enzyme was further purified by Sephadex G-200 gel filtration chromatography (Fig. 5). A large amount of high-molecular-mass inactive protein was separated from the enzyme. The elution volume of this cathepsin A activity corresponded to a molecular mass of 97 000. The Sephadex G-200 chromatography was repeated (data not shown) to insure complete removal of the high-molecular-mass contaminant seen in Fig. 5. The combined purification of this step was 1.4-fold with a yield of 36%.

Only trace amounts of inactive protein were removed by chromatofocusing (Fig. 6), and the specific activity did not increase as a result of this step —the yield for this step was 82%. The isoelectric point (p*I*) of cathepsin A determined by this procedure was 5.0.

Using this purification procedure, summarized in Table I, the enzyme was purified nearly 1400-fold over the crude extract. The final specific activity was 16.9 U/mg, and the overall yield was 0.31%. This specific activity was 74% higher than the 9.7 U/mg measured for the cathepsin A purified by Kawamura *et al.* [4]. The composition of the buffer in our standard cathepsin A assay differed slightly from the assay buffer used in that study. Their buffer consisted of 50 m*M* acetate buffer (instead of 0.1 *M*), pH 5.2, 1.0 *M* sucrose (instead of 0.1 *M*) and 0.1 *M*

TABLE I

PURIFICATION SUMMARY

Step	Total activity (U)	Total protein (mg)	Yield (%)		Specific activity (U/mg)	Purification	
			Overall	Per step		Overall	Per step
Crude extract	11 800	959 000	(100)	–	0.0123	(1.0)	–
1000 *g* supernatant	10 200	580 000	86.4	86.4	0.0176	1.4	1.4
16 000 *g* pellet	4 500	170 000	38.1	44.1	0.0265	2.2	1.6
100 000 *g* supernatant	1 290	15 900	10.9	28.6	0.0811	6.6	3.0
$(NH_4)_2SO_4$ (25–60%)	916	8 035	7.8	71.6	0.114	9.3	1.4
Con A-Sepharose	463	800	3.9	50.0	0.579	47	5.1
Phenyl-Sepharose	178	46	1.5	38.5	3.87	315	6.7
DEAE-Sephadex	124	9.95	1.1	73.3	12.5	1016	3.2
Sephadex G-200	44.3	2.62	0.38	35.7	16.9	1374	1.4
Chromatofocusing	36.5	2.16	0.31	81.6	16.9	1374	1.0

KCl (instead of 0.1 *M* NaCl). In addition, their buffer did not include 1 m*M* EDTA. The Z–Glu–Tyr concentration was the same. In order to determine whether the increased specific activity was due to increased activity in our standard assay, the activity of the purified cathepsin A was compared using both conditions. Activity was 8% higher with our standard assay, therefore the increased specific activity is primarily due to increased purity compared to the preparation of Kawamura *et al.* [4]. Product formation was linear for at least one hour under both conditions.

As shown in Fig. 7, non-denaturing polyacrylamide tube gel electrophoresis (pH 4.0) of the purified enzyme showed a single protein band. Tubes 1 and 2 (Fig. 7) contained 10 μg of purified cathepsin A electrophoresed for 1 h and 3.5 h, respectively. There was no detectable fast moving contaminant in tube 1 and no detectable slow moving contaminant in tube 2. Tube 3 contained a mixture of bovine serum albumin (BSA), myoglobin and cytochrome *c* (0.5 μg each). There was good resolution of the proteins, and 0.5 μg were easily detected with the Coomassie Blue stain. If an acidic contaminant with an isoelectric point less than 4 were present, it would have a negative charge, migrate toward the anode, and therefore not enter the gel under these conditions. To check for such a contaminant, in a separate experiment, 10 μg of cathepsin A (tube 4) was electrophoresed under the same conditions except toward the anode for 3.5 h. No contamination by more acidic proteins was observed.

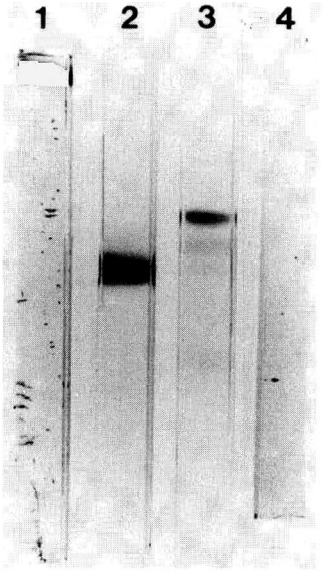

Fig. 7. Non-denaturing PAGE of purified cathepsin A. Electrophoresis was carried out at 4–6°C in 7% polyacrylamide tube gels in the presence of 14 m*M* sodium acetate, 20 m*M* NaCl, 0.1 *M* sucrose, pH 4.0. After application of the samples, electrophoresis was performed in the direction of the cathode at 3 mA per gel tube. Gels were stained with Coomassie Blue R250. Tubes: 1 = 10 μg cathepsin A run for 1 h; 2 = 10 μg cathepsin A run for 3.5 h; 3 = 0.5 μg each of BSA, cytochrome *c* and myoglobin run for 3.5 h; 4 = 10 μg cathepsin A run for 3.5 h in the direction of the anode.

To test for the possible presence of thiol-dependent carboxypeptidases, the effect on activity of the addition of 3 m*M* cysteine was determined. Cysteine had no effect on activity at pH 3.5 or 5.2, with Z–Glu–Tyr or AI as substrates. To test for the possible presence of proteinases, the activity of the purified cathepsin A on FITC–casein was compared with the activity of trypsin and cathepsin D (Fig. 8). Expressed as relative fluorescence units per h per μg of protein, the activities of trypsin at pH 7.8 and cathepsin D at pH 4.5 were 900 and 94, respectively. The activity of cathepsin A at pH 4.5 was 0.38, and its activity at pH 5.2 was 1.25. The maximum level of contamination with cathepsin D is estimated to be less than 0.4%, and it is probable that the low level of apparent endopeptidase activity by cathep-

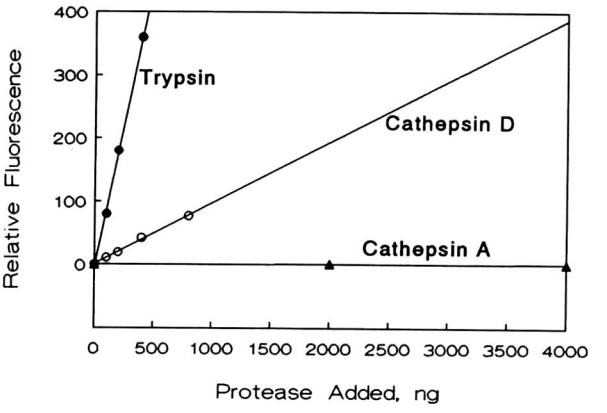

Fig. 8. FITC–Casein proteinase assay. The indicated amounts of trypsin, cathepsin D or the purified cathepsin A were incubated with FITC–casein at 37°C for 1 h. Trichloroacetic acid-soluble fluorescein was measured with an excitation wavelength of 490 nm and an emission wavelength of 525 nm. The small amount of activity by cathepsin A is equivalent to less than 0.4% contamination with cathepsin D.

sin A is actually due to its carboxypeptidase action releasing C-terminal FITC-labelled amino acids.

The effects of several inhibitors and potential activators were tested, and these results are summarized in Table II. This cathepsin A preparation was markedly inhibited by DFP (see Table II for abbreviations) which suggests that the enzyme has an activated serine in its active site. The chymotrypsin inhibitor, TPCK, had a moderate inhibitory effect, but the trypsin inhibitor, TLCK, did not. The inhibition by PCMBS, mersalyl acid (and possibly zinc) indicates the presence of an essential sulfhydryl moiety. The lack of inhibition by EDTA indicates that metal ions are not required for activity. These results are all consistent with previously reported properties of cathepsin A [4]. In addition, the lack of activation by divalent metal ions is evidence for the absence of metal ion-dependent carboxypeptidases in the preparation.

Discontinuous SDS-PAGE by the method of Laemmli [13] in the presence or absence of 2-ME (Fig. 9) demonstrated that the M_r 97 000 protein is composed of two apparently identical subunits of M_r 47 000 in size. Each of these subunits is composed of two disulfide-bonded peptide chains of M_r 31 000 and 19 000. Because these results did not agree (see Discussion) with those of Kawamura *et al.* [19] who used the continuous SDS-PAGE method of Weber and Osborn [14], a sample of cathepsin A was electrophoresed by this method with and without 2-ME. The results (not shown) were essentially the same as with the discontinuous method, although the apparent molecular masses were higher. The non-reduced subunit had an apparent M_r of 61 000, and the separated peptide chains were 35 000 and 24 000 in size.

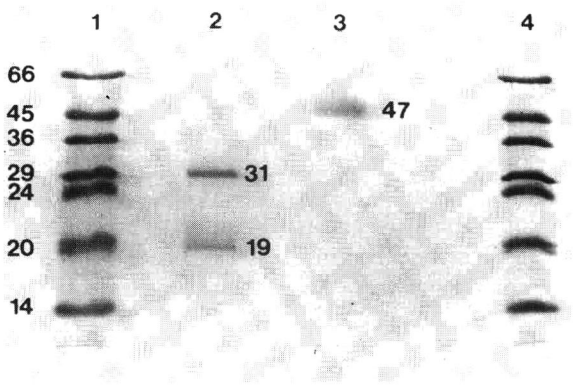

Fig. 9. Discontinuous SDS-PAGE of cathepsin A. SDS-PAGE was performed in 12% gels according to Laemmli [13] in the presence (lane 2) or absence (lane 3) of 2-mercaptoethanol. Cathepsin A samples were 2 μg. Lanes 1 and 4 molecular-mass ($\times 10^{-3}$) markers (BSA, 66 000; ovalbumin, 45 000; glyceraldehyde dehydrogenase, 36 000; carbonic anhydrase, 29 000; trypsinogen, 24 000; soybean trypsin inhibitor, 20 000; α-lactalbumin, 14 200). The gel was stained with Coomassie Blue R250.

TABLE II

EFFECTS OF INHIBITORS AND ACTIVATORS ON CATHEPSIN A ACTIVITY

Inhibition was tested with 68 μ*M* AI as substrate at pH 5.8. Abbreviations: DFP = diisopropylfluorophosphate; TPCK = *p*-tosylphenylalanyl-chloromethylketone; TLCK = *p*-tosyl-lysyl-chloromethyl-ketone; PCMBS = *p*-chloromercuribenzene sulfonate.

Addition	Concentration (mol/l)	% of Control
None (Control)	–	(100)
DFP	$1 \cdot 10^{-4}$	22
TPCK	$1 \cdot 10^{-4}$	71
TLCK	$1 \cdot 10^{-4}$	96
PCMBS	$1 \cdot 10^{-4}$	36
Mersalyl acid	$1 \cdot 10^{-4}$	15
EDTA	$5 \cdot 10^{-3}$	98
$CaCl_2$	$5 \cdot 10^{-3}$	101
$MnCl_2$	$5 \cdot 10^{-3}$	100
$Zn(OAc)_2$	$5 \cdot 10^{-3}$	91

DISCUSSION

Cathepsin A purified from pig kidney lysosomes by the methods described above has a molecular mass of 97 000. This agrees well with the 100 000 value reported [4] for pig kidney cathepsin A,S (S for small). The enzyme also was found to have the same isoelectric point, 5.0, and similar sensitivity to inhibitors. However, this enzyme, which was homogenous by non-denaturing PAGE, had a specific activity of 16.9 U/mg. The preparation by Kawamura *et al.* [4] had a specific activity of 9.7 U/mg. As mentioned in the results section, the assay conditions we used resulted in an 8% higher measured rate compared with the conditions used by Kawamura *et al.* [4] and accounts for only a small percentage of the increased specific activity of our preparation. Ap-

parently, our preparation is significantly more pure, although it is possible that the preparation of Kawamura *et al.* [4] was pure, but partially inactive.

Purification steps not previously used for cathepsin A include Con A-Sepharose chromatography, phenyl-Sepharose chromatography, and chromatofocusing. The strong binding to Con A-Sepharose and elution by α-methylmannoside provides evidence that the enzyme is a glycoprotein. This result was anticipated, since cathepsin A is a lysosomal enzyme [20–22]. This step provided a 7-fold purification. Preliminary experiments suggested that various gradients of α-methylglucoside and α-methylmannoside may be useful to separate various forms of cathepsin A. However, since some microheterogeneity may well exist in the carbohydrate portion of the enzyme, it was decided to avoid separation of enzyme forms at this point in the purification.

The enzyme was found to bind tightly to phenyl-Sepharose and required about 30% ethylene glycol for elution. After the subsequent ion-exchange and gel filtration chromatography steps, it was found that all three of the enzyme forms separated by the ion-exchange step had molecular masses of 97 000. None of the previously reported high-molecular-mass forms were observed [2,11,16–18]. Matsuda and Misaka [2] presented evidence that the high-molecular-mass forms of cathepsin A present in rat liver were aggregates of the low-molecular-mass (approximately 100 000) form and that hydrophobic bonds held the aggregates together. The most likely reason for the absence of the aggregates in the present preparation is their elimination in the phenyl-Sepharose step. It is not known whether this elimination was due to irreversible binding to the phenyl-Sepharose or to dissociation of the aggregates by the ethylene glycol.

The chomatofocusing step only removed a small amount of inactive protein and did not measurably increase the specific activity. The isoelectric point of 5.0 determined in this step is identical to that reported by Kawamura *et al.* [4] by isoelectric focusing.

During discontinuous SDS-PAGE (Fig. 9) in the absence of 2-ME, a sample of the enzyme migrated as a single protein with an M_r of 47 000. This result suggests that the 97 000 native enzyme is a homodimer. The 47 000 subunit completely dissociated into peptides of 31 000 and 19 000 in the presence of 2-ME. These results do not corroborate the subunit structure reported by Kawamura *et al.* [19]. Their SDS-PAGE gels, run only in the presence of 2-ME, show peptide chains of 55 000, 25 000 and 20 000, all having about the same staining intensity. These authors used the continuous SDS-PAGE method of Weber and Osborn [14]. Electrophoresis of our preparation with this method confirmed the subunit structure observed with discontinuous system (Fig. 9).

It is unlikely that the presence of their 55 000 peptide is due to incomplete reduction of disulfide bonds in their samples, since they showed that [^{32}P]-diisopropylfluorophosphate only labelled their 25 000 peptide. If their 55 000 peptide was composed of the two disulfide bonded chains (25 000 and 20 000 chains), it too should have been labelled. It is possible that their 55 000 peptide is a contaminant. As indicated above, the specific activity of our preparation was nearly twice that of theirs [4].

In summary, the purified preparation of pig kidney lysosomal cathepsin A described here had a higher specific activity than preparations previously described and was shown to be free of contaminating endopeptidases and other carboxypeptidases. The molecular mass, isoelectric point and sensitivity to inhibitors were consistent with the previously reported properties of cathepsin A. Although the subunit composition of our preparation of cathepsin A differed from that reported previously, our preparation was considerably more pure based on specific activity. The substrate specificity of this preparation of cathepsin A is currently under investigation.

ACKNOWLEDGEMENTS

The authors wish to thank the Glenmore Foundation, the Glenmore Distilleries Co., and the Humana Center for Excellence —Humana Heart Institute International, all of Louisville, KY, USA for their support of this work.

REFERENCES

1 D. G. Changaris, J. J. Miller and R. S. Levy, *Biochem. Biophys. Res. Commun.*, 138 (1986) 573–579.
2 K. Matsuda and E. Misaka, *J. Biochem.*, 78 (1975) 31–39.

3 E. Doi, *J. Biochem.*, 75 (1974) 881–887.
4 Y. Kawamura, T. Matoba, T. Hata and E. Doi, *J. Biochem.*, 77 (1975) 729–737.
5 S. L. Taylor and A. L. Tappel, *Biochim. Biophys. Acta*, 341 (1974) 112–119.
6 Y. Kawamura, T. Matoba, T. Hata and E. Doi, *J. Biochem.*, 81 (1977) 435–441.
7 K. Matsuda, *J. Biochem.*, 80 (1976) 659–669.
8 A. I. Logunov and V. N. Orekhovich, *Biochem. Biophys. Res. Commun.*, 46 (1972) 1161–1168.
9 A. A. Iodice, V. Leong and I. M. Weinstock, *Arch. Biochem. Biophys.*, 117 (1966) 477–486.
10 A. A. Iodice, *Arch. Biochem. Biophys.*, 121 (1967) 241–242.
11 J. J. Miller, D. G. Changaris and R. S. Levy, *Biochem. Biophys. Res. Commun.*, 154 (1988) 1122–1129.
12 O. H. Lowry, N. J. Rosebrough, A. L. Farr and R. J. Randall, *J. Biol. Chem.*, 193 (1951) 265–275.
13 U. K. Laemmli, *Nature (London)*, 227 (1970) 680–685.
14 K. Weber and M. Osborn, *J. Biol. Chem.*, 244 (1969) 4406–4412.
15 S. S. Twining, *Anal. Biochem.*, 143 (1984) 30–34.
16 E. Doi, Y. Kawamura, T. Matoba and T. Hata, *J. Biochem.*, 75 (1974) 889–894.
17 Y. Kawamura, T. Matoba, T. Hata and E. Doi, *J. Biochem.*, 76 (1974) 915–924.
18 K. Matsuda and E. Misaka, *J. Biochem.*, 76 (1974) 639–649.
19 Y. Kawamura, T. Matoba and E. Doi, *J. Biochem.*, 88 (1980) 1559–1561.
20 S. Shibko and A. L. Tappel, *Biochem. J.*, 95 (1965) 731–741.
21 J. W. Coffey and C. de Duve, *J. Biol. Chem.*, 243 (1968) 3255–3263.
22 P. Jablonsky and M. T. McQuillan, *Biochim. Biophys. Acta*, 132 (1967) 454–471.

Journal of Chromatography, 627 (1992) 163–172
Elsevier Science Publishers B.V., Amsterdam

CHROM. 24 610

Purification and determination of the binding site of lactate dehydrogenase from chicken breast muscle on immobilized ferric ions

Grigory Chaga*, Lennart Andersson and Jerker Porath

Biochemical Separation Centre, Uppsala University, Box 577, S-751 23 Uppsala (Sweden)

(First received May 14th, 1992; revised manuscript received August 31st, 1992)

ABSTRACT

Lactate dehydrogenase from chicken breast muscle was purified to homogeneity in one step by immobilized metal ion affinity chromatography. The purified enzyme was used to localize the binding site to immobilized Fe(III) ions. After cyanogen bromide degradation and digestion with trypsin, small enzyme fragments capable of binding to immobilized Fe(III) ions were obtained. It is proposed that several histidyl groups are involved in the binding.

INTRODUCTION

Several years of investigation of the mechanism of adsorption on immobilized transition metals, such as Cu(II), Ni(II) and Zn(II), indicate that histidyl groups are the dominant electron donors. The number and sometimes the distribution of histidyl groups dictate almost exclusively their retention behaviour on these metals when immobilized on iminodiacetate-agarose (IDA-agarose) [1].

Protein binding to immobilized hard metals such as Fe(III), Al(III) or Ca(II) clearly involves oxygen atoms as electron donors. Therefore, phosphate [2,3] or carboxylate groups [4] are proposed to be primarily responsible for the adsorption on these metals.

Recently, we showed that lactate dehydrogenase (LDH) from chicken muscle, which lacks phosphate, binds very strongly to Fe(III) [5]. With respect to immobilized metal ion affinity chromatography (IMAC), the M form of this enzyme has an intriguing amino acid sequence: residues Nos. 5, 8, 11, 15, 17 and 19 are histidyl residues [6]. These observations stimulated us to examine the possibility to purify the enzyme on Cu(II)–, Ni(II)– or Zn(II)–IDA-agarose and to localize the binding site for immobilized Fe(III) ions.

EXPERIMENTAL

Materials

Frozen chicken breast muscle was purchased from food stores. Iron(III) chloride was obtained from Merck–Schuchardt (No. 803945; Munich, Germany), nickel nitrate hexahydrate from J. T. Baker (Lot No. 12944; Phillipsburg, NJ, USA), cyanogen bromide and 2,4,6-trinitrobenzenesulphonic acid (TNBS) from Fluka (Buchs, Switzerland), N-tosyl-L-phenylalanine chloromethyl ketone (TPCK)-treated trypsin (Type XIII) from Sigma (St. Louis, MO, USA), chelating Sepharose FF and Pep RPC HR 5/5 from Pharmacia–LKB (Uppsala, Sweden) and trifluoroacetic acid (TFA) and acetonitrile from Merck (Darmstadt, Germany).

Synthetic peptides were generously supplied by

Correspondence to: L. Andersson, Biochemical Separation Centre, Uppsala University, Box 577, S-751 23 Uppsala, Sweden.

* Permanent address: Institute for Bioproducts, 10 Mizia str., 4003 Plovdiv, Bulgaria.

0021-9673/92/$05.00

Dr. G. Lindeberg, Institute of Medical Immunology, Biomedical Centre, Uppsala, Sweden. The peptide preparations were not subjected to a final purification.

Chromatography

Chelating Sepharose FF packed into a column (5.4 × 2 cm I.D.) was charged with Ni(II) ions by applying four column volumes of 20 m*M* $Ni(NO_3)_2 \cdot 6H_2O$, followed by washing with four column volumes of deionized water and equilibration with 50 m*M* sodium phosphate–60 m*M* imidazole (1.0 *M* NaCl) (pH 7.1).

Columns of Fe(III)–IDA-agarose (2 ml) were prepared by applying sterile-filtered 20 m*M* iron (III) chloride. Excess of metal ions were washed out with deionized water. The columns were then washed with 5 ml of 0.1 *M* sodium phosphate (pH 7.1), followed by the equilibrating buffer. Reversed-phase chromatography was performed using the fast protein liquid chromatography system of Pharmacia–LKB on a Pep RPC HR 5/5 column with a linear gradient of acetonitrile.

Analysis of chromatographic fractions

Protein concentrations were calculated from absorbance measurements at 280 nm. Peptide peaks in eluates from reversed-phase chromatography were detected at 214 nm. Peptide concentrations were determined after reaction with TNBS [7]: 0.5 ml of 0.1 *M* borax, 0.5 ml of sample and 0.5 ml of 0.1% TNBS were mixed in glass tubes (75 × 12 mm I.D.), the tubes were left for 1 h at 40°C and the absorbance was measured at 420 nm against a blank. A calibration graph was prepared with glycine. Muscle extracts, purified enzyme and large peptides were analysed by sodium dodecyl sulphate (SDS) gel electrophoresis on Pharmacia Phast System using Pharmacia Phast Gel Gradient slabs 8–25 and SDS buffer strips. For peptide fractions, Pharmacia High Density Phast Gel was used. Peptide components in gel slabs were revealed by silver staining. Peptides were identified by determination of amino acid compositions after hydrolysis for 24 h with 6 *M* hydrochloric acid.

Protein and peptide cleavage procedures

Cyanogen bromide (CNBr) cleavage was carried out by a standard procedure [8] in 70% formic acid using a 50-fold excess of CNBr. The reaction mixture was freeze-dried twice after dilution with deionized water. Tryptic hydrolysis of peptides was done by addition of 30 μg of TPCK-treated trypsin to 1 μmol of peptide dissolved in 2 ml of 25 m*M* piperazine-N,N′-bis(2-ethanesulphonic acid) disodium salt (PIPES)–20 m*M* $CaCl_2$ (pH 7.1). The reaction was allowed to proceed for 3 h at 37°C.

Sample preparation

Chicken muscle extract was prepared according to Petell *et al.* [9]. Proteins and peptides were desalted or transferred into equilibration buffers by gel filtration on Sephadex columns. Small peptide sample (0.75 ml) were applied on a Sephadex G-10 column (5 × 1.8 cm I.D.), equilibrated with 20 m*M* acetic acid and the fraction between effluent volumes of 2.75 and 3.75 ml was recovered.

Enzyme assay

LDH was determined according to the method described by Kubowitz and Ott [10].

RESULTS

Purification of lactate dehydrogenase

A 100-ml volume of muscle extract was chromatographed on a Sephadex G-25 (medium) col-

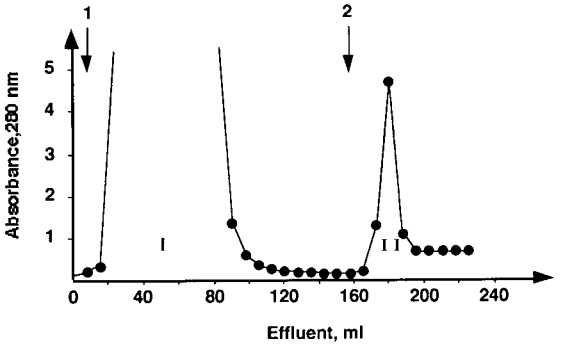

Fig. 1. Preparative purification of LDH on Ni(II)–chelating Sepharose FF. A 150-ml volume of chicken muscle extract in 50 m*M* sodium phosphate–1.0 *M* sodium chloride–60 m*M* imidazole (pH 7.1) was loaded on to an Ni(II)–Chelating Sepharose FF column (5.4 × 2 cm I.D.) equilibrated with the same buffer. The non-adsorbed material was washed out with the equilibrium buffer (arrow 1). The adsorbed material was eluted with 50 m*M* sodium phosphate–1.0 *M* sodium chloride–0.3 *M* imidazole (pH 7.1) (arrow 2). The flow-rate was 2.5 ml/min throughout.

umn (19 × 5 cm I.D.) in 50 m*M* sodium phosphate–1.0 *M* NaCl–60 m*M* imidazole (pH 7.1). Pooled fractions containing the enzyme (150 ml) were then applied, at a flow-rate of 2.5 ml/min, to a column of Ni(II)–IDA-agarose (5.4 × 2 cm I.D.) equilibrated in the same buffer. Fig. 1 illustrates the purification of the enzyme. Non-bound proteins were washed out with additional buffer. On increasing the imidazole concentration to 300 m*M* a second protein peak appeared. Gel electrophoresis showed that the breakthrough peak contained most of the applied proteins, whereas the second peak contained a single protein with a relative molecular mass of 40 000 (Fig. 2, lanes 2 and 3, respectively). This component represented 95% of the applied LDH activity. Fractions containing the purified LDH were pooled, desalted by dialysis and freeze-dried.

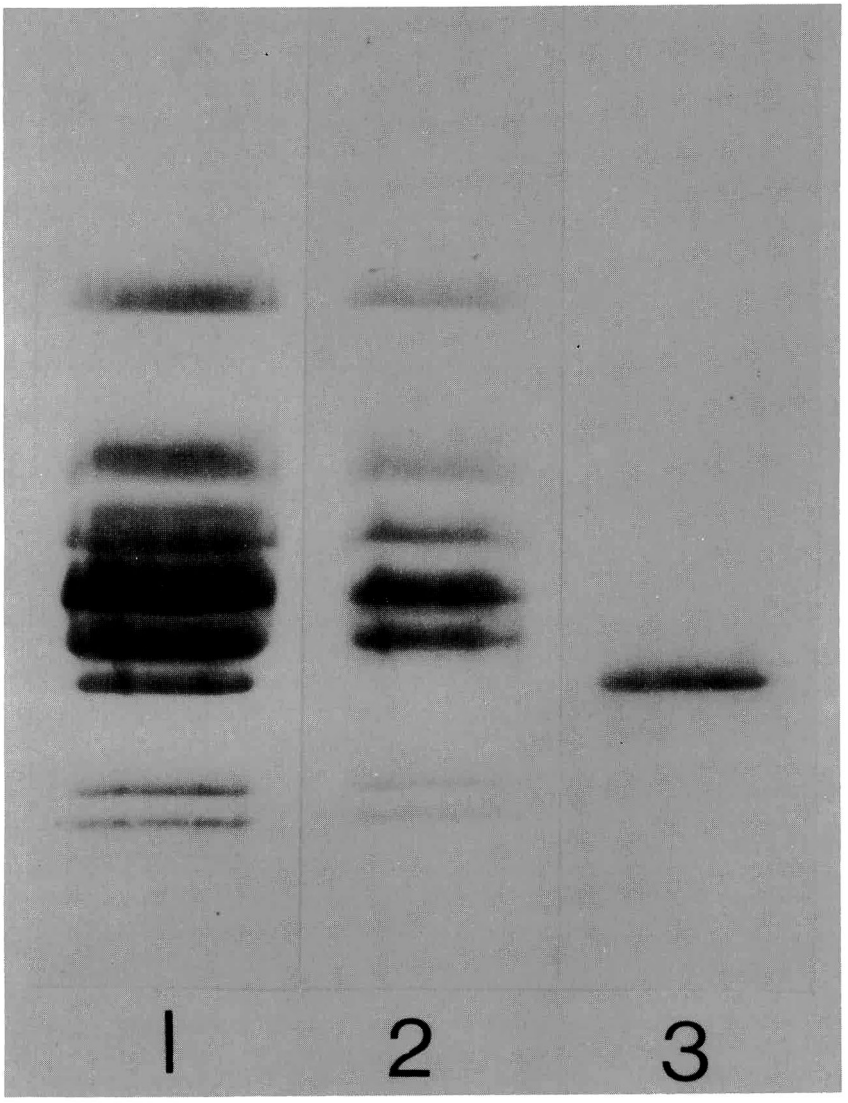

Fig. 2. SDS electrophoresis of the fractions obtained after the purification of LDH. Lanes: 1 = chicken muscle extract; 2 = peak I (Fig. 1), non-adsorbed material; 3 = peak II (Fig. 1), eluted with 0.3 *M* imidazole.

Chromatography of CNBr fragments on immobilized Fe(III) ions

The buffer systems used were (a) 25 m*M* acetate (pH 5.6) and (B) 25 m*M* PIPES (pH 7.1).

In the first experiment, 10 mg of CNBr fragments were dissolved in system A (4 ml). The sample was applied to Fe(III)–IDA-agarose equilibrated with the same buffer. Non-adsorbed material was washed out as peak I (Fig. 3a). Elution of the adsorbed peptides was accomplished by introducing 25 m*M* sodium phosphate (pH 7.0) (peaks II_1 and II_2) and further elution (peak III) by applying 25 m*M* sodium phosphate (1.0 *M* NaCl) (pH 7.0). Amino acid analyses (Table I) revealed that peak II_2 had a composition similar to the enzyme fragment 1 (residues 1–32) and peak III corresponded in composition to the enzyme fragment 8 (residues 264–279). Peak II_1 did not correspond to any of the expected nine CNBr fragments and was discarded.

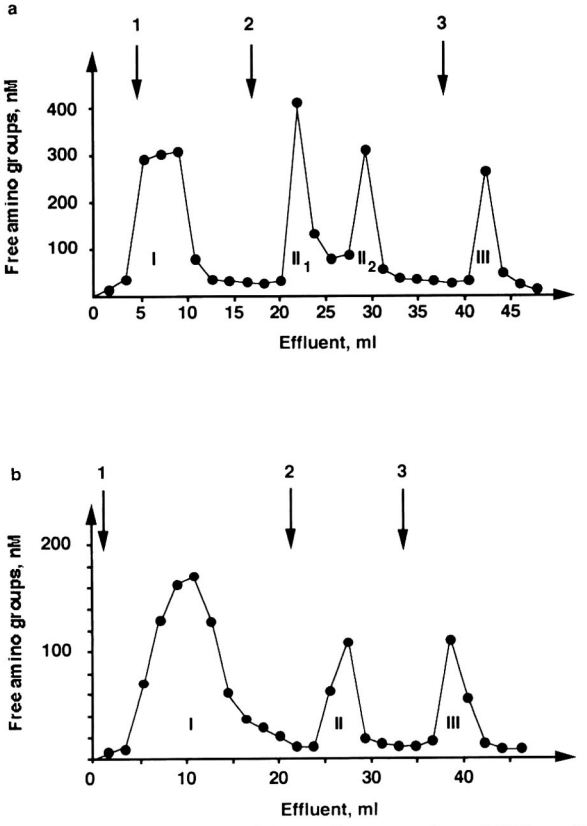

Fig. 3. Chromatography of CNBr fragments from LDH on Fe (III)–Chelating Sepharose FF. (a) 10 mg of CNBr fragments in 4 ml of 25 m*M* sodium acetate (pH 5.6) were loaded on to an Fe(III)–Chelating Sepharose FF column (2.55 × 1 cm I.D.) equilibrated with the same buffer. The non-adsorbed material was washed out by the equilibrium buffer (arrow 1). The adsorbed material was eluted by 25 m*M* sodium phosphate (pH 7.0) (arrow 2), followed by 25 m*M* sodium phosphate–1.0 m*M* chloride (pH 7.0) (arrow 3). The flow-rate was 30 ml/h throughout. (b) 10 mg of CNBr fragments in 4 ml of 25 m*M* PIPES (pH 7.1) was loaded on to an Fe(III)–Chelating Sepharose FF column (2.55 × 1 cm I.D.) equilibrated with the same buffer. The non-adsorbed material was washed out by the equilibrium buffer (arrow 1). The adsorbed material was eluted by 25 m*M* sodium phosphate (pH 7.0) (arrow 2), followed by 25 m*M* sodium phosphate–1.0 *M* sodium chloride (pH 7.0) (arrow 3). The flow-rate was 30 ml/h throughout.

When a similar run was performed using system B (Fig. 3b), the amount of adsorbed material became lower and only a single peak was obtained when 25 m*M* phosphate was applied. This peak (II) contained the N-terminal CNBr fragment (residues 1–32) as evidenced by amino acid analysis (Table I). Peak III again corresponded to CNBr fragment 8 (residues 264–279). Control experiments showed that the material present in peak II was unretarded on a metal-free column under the conditions described in the latter experiment (not shown), whereas the peak III material was bound. This confirms that the binding of the material in peak II was due to the presence of Fe(III) on the adsorbent.

Preparation of purified binding fragment 1

Material from peak II (Fig. 3b) was applied to a Pep RPC HR 5/5 column equilibrated with 0.1% TFA. A linear gradient of acetonitrile was used to elute the adsorbed material shown in Fig. 4a. The desired fragment appeared at 28% acetonitrile. This experiment was used as a guide for obtaining the desired material from crude CNBr peptides as illustrated in Fig. 4b. Several runs were made to recover sufficient material for subsequent experiments. The purity of the collected material was ascertained from SDS gel electrophoresis (Fig. 5). Its relative molecular mass was estimated to be 3300 (Fig. 5, lane 3). The material could be identified as the predicted CNBr fragment (residues 1–32).

Preparation of subfragments with binding properties

The purified and freeze-dried fragment (residues 1–32) was dissolved and subjected to trypsinolysis. The peptide mixture obtained was immediately chromatographed on Fe(III)–IDA-agarose equilibrated in 25 m*M* PIPES (pH 7.1). The result is

TABLE I

AMINO ACID COMPOSITION OF THE PEPTIDE FRACTIONS NUMBERED IN FIGS. 3a AND 3b

Amino acid residue	Fig. 3a, peak II_2		Fig. 3a, peak III		Fig. 3b, peak II	
	Detected (nmol per nmol peptide)	Expected (nmol per nmol peptide)	Detected (nmol per nmol peptide)	Expected (nmol per nmol peptide)	Detected (nmol per nmol peptide)	Expected (nmol per nmol peptide)
Aspartic acid	2.9	3	1.0	1	3.2	3
Threonine	0.2	0	1.0	1	0.2	0
Serine	2.2	2	1.0	1	2.3	2
Proline	0	0	1.0	1	0.2	0
Glutamic acid	2.4	2	0	0	2.1	2
Glycine	3.3	3	1.0	1	3.4	3
Alanine	2.9	3	1.0	1	3.1	3
Valine	4.5	5	2.0	2	4.5	5
Isoleucine	1.9	2	1.0	1	2.0	2
Leucine	2.1	2	1.0	1	2.1	2
Histidine	5.1	6	0.9	1	5.1	6
Lysine	2.7	3	2.0	2	3.2	3
Arginine	0.1	0	1.8	2	0.1	0
Homoserine	0.8	1	0.5	1	0.9	1

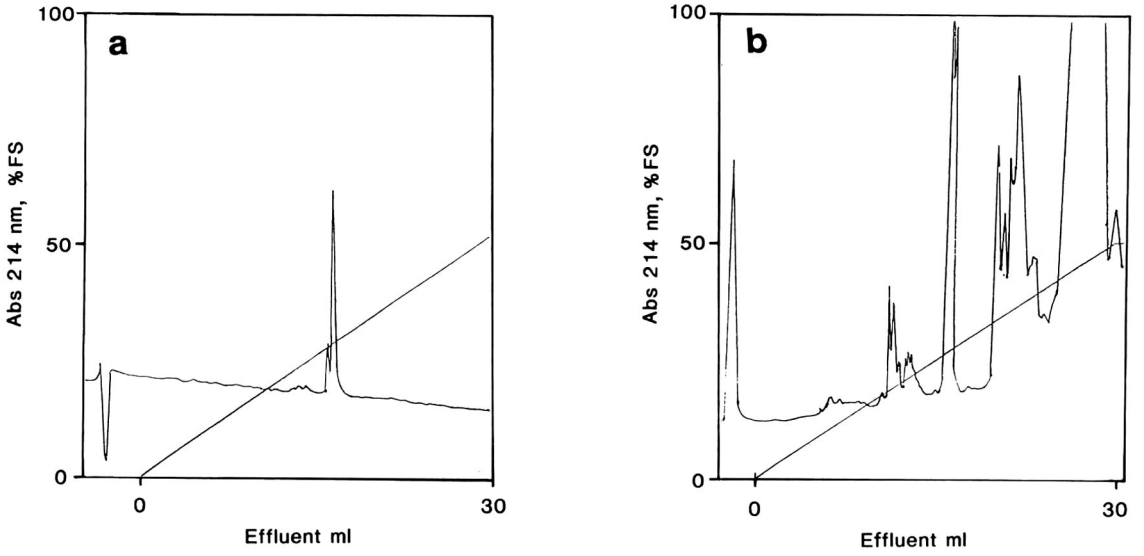

Fig. 4. RPC of CNBr fragments from LDH on Pep RPC HR 5/5. The samples dissolved in 0.1% TFA were loaded on to the reversed-phase chromatography column and eluted by a linear acetonitrile gradient from 0 to 50% in 0.1% TFA. The flow-rate was 0.7 ml/min throughout. The absorbance was monitored at 214 nm at a chart speed of 0.5 cm/ml. (a) 200 ml of peak II (Fig. 3b) were loaded on to the reversed-phase chromatography column. (b) 4.44 mg of CNBr fragments in 0.5 ml of 0.1% TFA were loaded on to the reversed-phase chromatography column. The same chromatography was performed nine times.

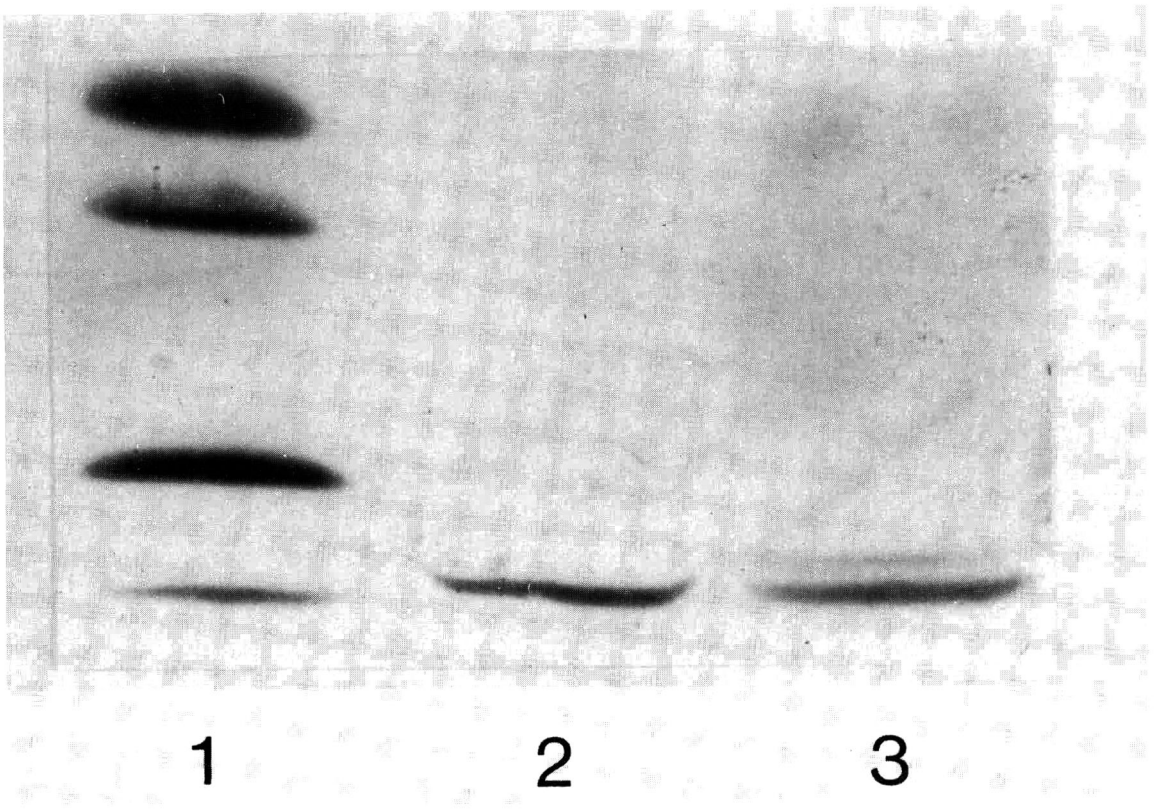

Fig. 5. SDS electrophoresis on High Density Phast Gel with Phast System. Lanes: 1 = Polypeptide molecular mass calibration kit (Pharmacia–LKB), M_r 10 804, 8266, 6413 and 2555 CNBr fragments from myoglobin; 2 = peak II (Fig. 3b); 3 = material containing CNBr fragments 1–32 obtained after reversed-phase chromatography represented in Fig. 4b.

shown in Fig. 6. Peak II, the material eluted with 25 m*M* phosphate, was analysed by SDS gel electrophoresis (Fig. 7). The relative molecular mass of the material in peak II was estimated to be 1000–1500.

The material was further chromatographed on a Superose 12 column equilibrated with 20 m*M* acetic acid. Essentially one peak was obtained (Fig. 8). Amino acid analysis of this material (Table II) showed the absence of the fragments 1–3 (SLK) and 22–32 (ISVVGVGAVGM), which obviously are trypsin degradation products that do not bind. The material corresponds to the peptide segment 4–21 (DHLIHNVHKEEHAHAHNK). Considering its low relative molecular mass it seemed that this material contained a roughly equimolar mixture of the two tryptic fragments (4–12) and (13–21). Apparently both subfragments, if present, became bound to Fe(III)–IDA-agarose.

The chromatographic behaviour of the synthesized peptides DHLIHNVHK (synthetic peptide 1) and EEHAHAHNK (synthetic peptide 2) was investigated. These peptides correspond to the two tryptic subfragments found to be bound to immobilized Fe(III). The peptides were run according to the same protocol in 25 m*M* PIPES (pH 7.1) on Fe(III)–IDA-agarose and separately on metal-free IDA agarose. On the former gel the peptides were retained in the starting buffer and eluted with 25 m*M* phosphate (Fig. 9a and b), but appeared in the breakthrough fraction from the metal-free gel (not shown). Amino acid analyses of the peaks eluted with phosphate were in agreement with the expected results. The material from unretained peak I (Fig. 9b) had a composition lacking one histidine compared with that of peptide (13–21) (Table III). Analysis by mass spectrometry confirmed that the

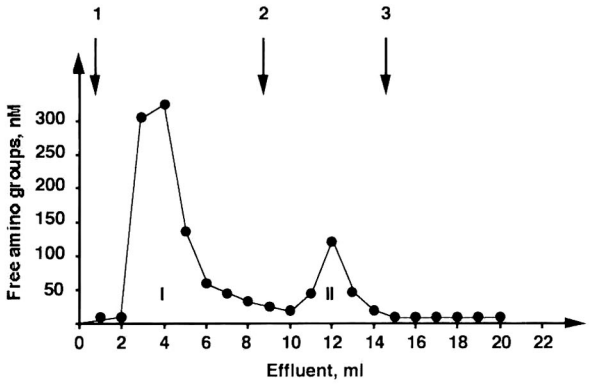

Fig. 6. Chromatography of the tryptic digest of fragment 1 on Fe(III)–Chelating Sepharose FF. A 2-ml volume of 25 m*M* PIPES (pH 7.1) containing the tryptic digest of fragment 1 was applied to an Fe(III)–Chelating Sepharose FF column (2.55 × 1 cm I.D.) equilibrated with the same buffer. The non-bound material was washed out with the equilibrium buffer (arrow 1). The adsorbed material was eluted by 25 m*M* sodium phosphate (pH 7.0) (arrow 2), followed by 25 m*M* sodium phosphate–1.0 *M* sodium chloride (pH 7.0) (arrow 3). A flow-rate of 30 ml/h was kept constant during the chromatography.

second synthetic preparation contained a substantial amount of a substance with a relative molecular mass lower than that of synthetic peptide 2 by one histidyl residue.

DISCUSSION

Work in this and other laboratories has shown that two exposed histidyl groups are a minimum requirement for adsorption of a protein molecule to immobilized Ni(II) ions [1]. Unusually tight binding of the M form of LDH subunit to immobilized Cu (II), Ni(II) and Zn(II) ions can be expected in view of the chemical structure of its N-terminal part, where six histidyl residues occur in a stretch of 20 residues [6]. In contrast, the H subunit does not contain a single residue in the same region. The isolation procedure thus selects the M subunit of the enzyme. Control experiments with the different forms of isoenzymes confirm this (not shown).

Several attempts have been made in this labora-

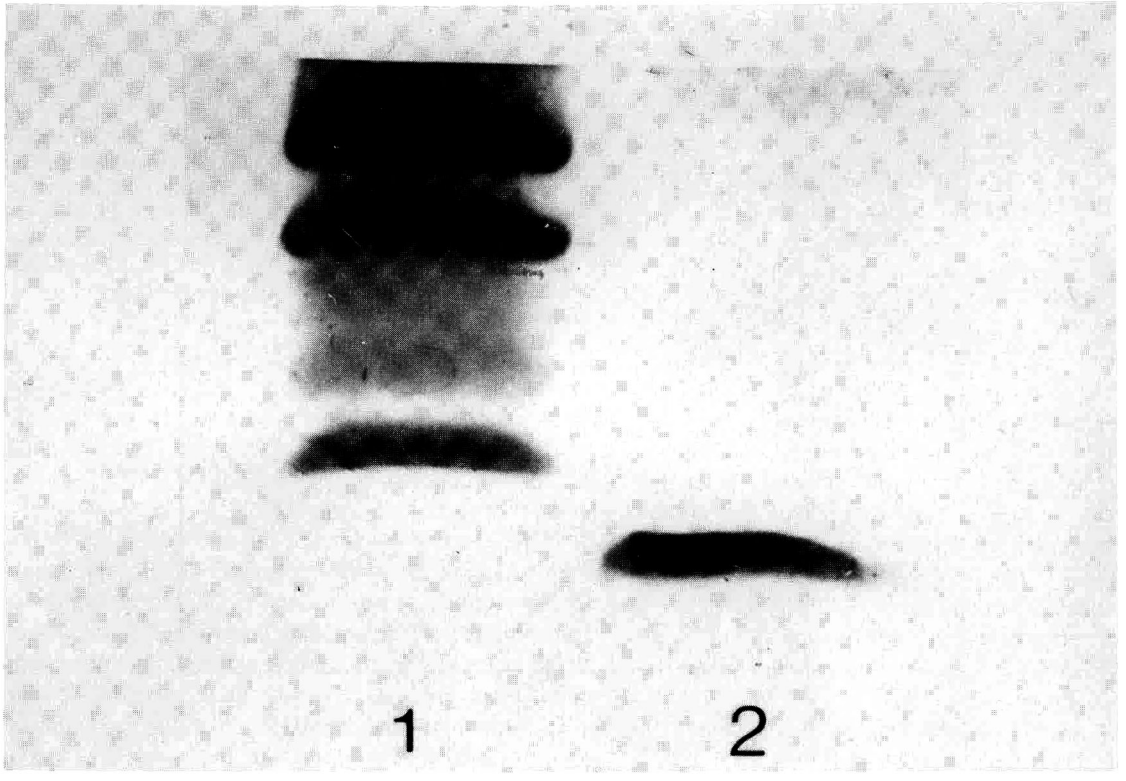

Fig. 7. SDS electrophoresis on High Density Phast Gel with Phast System. Lanes: 1 = Polypeptide molecular mass calibration kit (Pharmacia–LKB), M_r, 10 804, 8266, 6413 and 2555 CNBr fragments from myoglobin; 2 = peak II (Fig. 6).

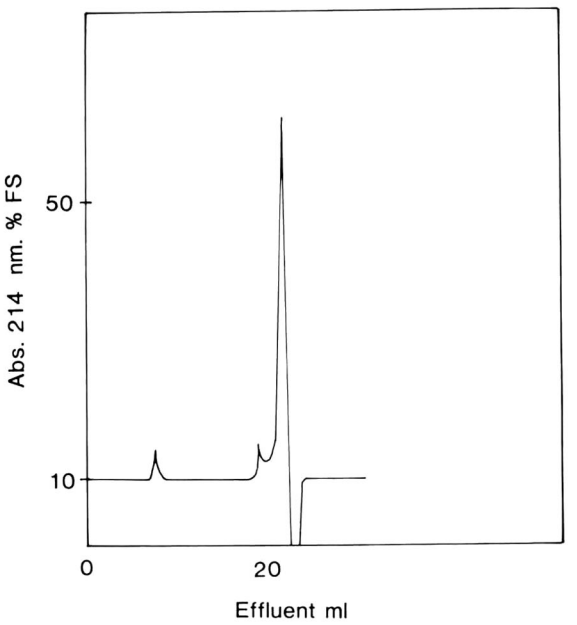

Fig. 8. Size exclusion chromatography of peak II, Fig. 6, on Superose 12. A 200-μl volume of peak II (Fig. 6) was applied to a Superose 12 HR 10/30 column equilibrated with 20 mM acetic acid at a flow-rate of 0.4 ml/min. The absorbance was followed at 214 nm at a monitor sensitivity of 0.1 a.u.f.s. and recorded at a chart speed of 0.25 cm/ml.

TABLE II

AMINO ACID COMPOSITION OF THE PEPTIDE FRACTION NUMBERED IN FIG. 6

Amino acid residue	Fig. 6, peak II	
	Detected (nmol per nmol peptide)	Expected (nmol per nmol peptide)
Aspartic acid	2.7	3
Threonine	0.2	0
Serine	0.2	0
Glutamic acid	2.0	2
Proline	0.3	0
Glycine	0.3	0
Alanine	2.0	2
Valine	1.3	1
Isoleucine	1.2	1
Leucine	1.2	1
Tyrosine	0.1	0
Phenylalanine	0.2	0
Histidine	5.1	6
Lysine	2.4	2
Arginine	0.4	0

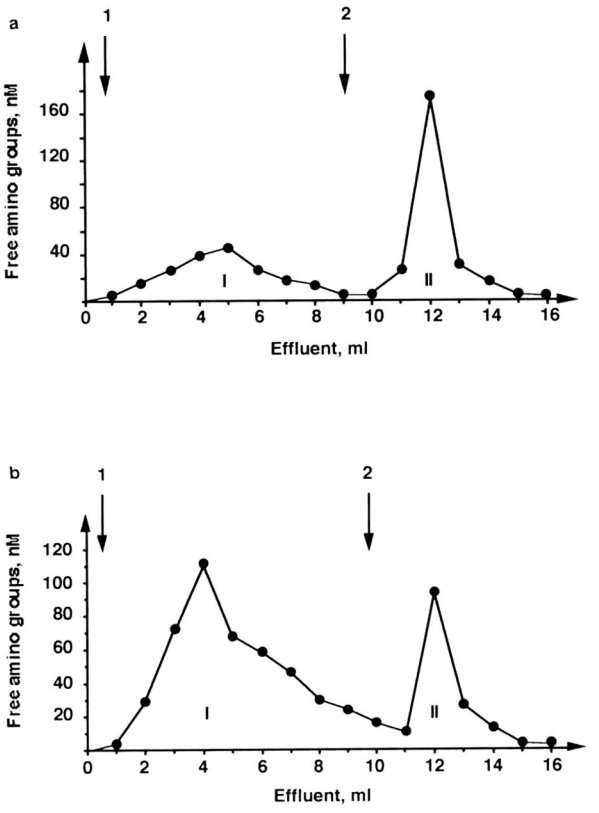

Fig. 9. Chromatography of synthetic peptides 1 and 2 on Fe(III)–Chelating Sepharose FF. (a) 0.42 mg of synthetic peptide 1 in 1 ml of 25 mM sodium acetate (pH 5.6) was loaded on to an Fe(III)–Chelating Sepharose FF column (2.5 × 1 cm I.D.) equilibrated with the same buffer. The non-adsorbed material was washed out by the equilibrium buffer (arrow 1). The adsorbed material was eluted by 25 mM sodium phosphate (pH 7.0) (arrow 2). The flow-rate was 30 ml/h throughout. (b) 0.5 mg of synthetic peptide 2 in 1 ml of 25 mM PIPES (pH 7.1) was loaded on to an Fe(III)–Chelating Sepharose FF column (2.5 × 1 cm I.D.) equilibrated with the same buffer. The non-adsorbed material was washed out by the equilibrium buffer (arrow 1). The adsorbed material was eluted by 25 mM sodium phosphate (pH 7.0) (arrow 2). The flow-rate was 30 ml/h throughout.

tory to account for the binding of non-phosphorylated proteins to immobilized Fe(III) ions. Affinities for the natural free amino acids were found to be small as judged from retention data [2,4]. Individual carboxylic groups [3] and clusters of carboxylic side-chains or combinations of tyrosyl phenol groups and carboxylate side-chain groups have been suggested as binding sites [11]. These models for binding are clearly not applicable to explain the

TABLE III

AMINO ACID COMPOSITION OF THE PEPTIDE FRACTIONS NUMBERED IN FIGS. 9 AND 9b

Amino acid residue	Fig. 9a, peak II		Fig. 9b, peak I		Fig. 9b, peak II	
	Detected (nmol per nmol peptide)	Expected (nmol per nmol peptide)	Detected (nmol per nmol peptide)	Expected (nmol per nmol peptide)	Detected (nmol per nmol peptide)	Expected (nmol per nmol peptide)
Aspartic acid	2.0	2	1.1	1	1.1	1
Glutamic acid	0	0	2.1	2	1.8	2
Alanine	0	0	2.0	2	1.8	2
Valine	1.0	1	0	0	0	0
Isoleucine	1.0	1	0	0	0	0
Leucine	1.0	1	0	0	0	0
Histidine	2.9	3	2.0	3	3.2	3
Lysine	1.1	1	1.1	1	1.1	1

properties of LDH. Our data rather suggest that the binding is confined to a restricted area of the protein molecule, namely segment (4–21), or rather to several side-chains within this segment. It seems safe to conclude that at least one and probably several histidyl side-chains participate in the binding. Possibly one or two carboxylate groups also interact with the metal, but this is less certain. One is tempted to propose that very likely at least three histidyl side-chains are necessary for sufficiently strong binding to immobilized Fe(III) ions. This proposal is supported by the behaviour of the synthetic peptides: the material from peak I, Fig. 9b, which contains only two histidyl groups is not retained on immobilized Fe(III) ions, whereas the material containing three histidyl groups (peak II, Fig. 9a and b) is adsorbed on the column in the starting buffer. Conclusive proof for this suggestion can only be obtained after more extensive studies with synthetic peptides of appropriate structures.

It should be noted that the putative binding peptide segment in the LDH molecule protrudes from the body of the protein molecule, forming a loosely structured part of the peptide chain. All side-chains are well exposed and accessible for binding [12]. LDH is built up of four identical subunits arranged in a symmetrical manner; this might be a feature that significantly enhances the binding to immobilized Fe(III) through multiple site interaction.

The enzyme fragment (residues 264–273) was adsorbed both on metal-loaded and metal-free gel. It contains five cationic side-chains, one of which is histidine. It is therefore likely that the adsorption is not due to the metal but to anionic groups on the agarose gel. Immobilized Fe(III) ions behave much as a cation exchanger under the conditions used in the experiments [13]. The interactive gel-immobilized ionic species may have a structure with a negative charge (*i.e.*, with $n = 2$ or 3):

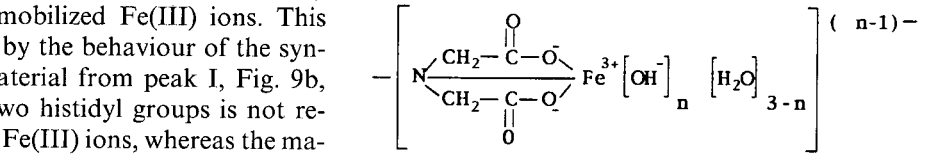

In summary, the present results seem to indicate that the Fe(III)-binding site of each LDH subunit resides in a short segment at the N-terminus of the polypeptide chain. The binding peptide segment is coordinated to the metal by at least two side-groups, one of which must be a histidyl side-chain. This is a minimum requirement; probably there are more histidyl groups involved. That histidyl groups can participate in Fe(III) binding is well documented for several iron(III) metalloproteins [14–16]. More detailed information on the molecular interactions must await more sophisticated techniques than those available today.

ACKNOWLEDGEMENTS

We are grateful to Dr. David Eaker at the Institute of Biochemistry, Uppsala University, for linguistic revision of the manuscript and to Mrs. Inga Johansson for secretarial help.

REFERENCES

1 E. S. Hemdan, Y.-j. Zhao, E. Sulkowski and J. Porath, *Proc. Natl. Acad. Sci. U.S.A.*, 86 (1989) 1811.
2 L. Andersson and J. Porath, *Anal. Biochem.*, 154 (1986) 250.
3 G. Muszynska, L. Andersson and J. Porath, *Biochemistry*, 25 (1986) 6850.
4 N. Ramadan and J. Porath, *J. Chromatogr.*, 321 (1985) 105.
5 G. Chaga, L. Andersson, B. Ersson and J. Porath, *Biotechnol. Appl. Biochem.*, 11 (1989) 424.
6 H. G. Torff, D. Becker and J. Schwarzwalder, in H. Sund (Editor), *Pyridine Nucleotide Dependent Dehydrogenases*, Walter de Gruyter, Berlin, 1977, p. 31.
7 A. F. S. A. Habeeb, *Anal. Biochem.*, 14 (1966) 328.
8 E. Gross and B. Witkop, *J. Am. Chem. Soc.*, 83 (1961) 1510.
9 J. K. Petell, M. S. Sardo and H. G. Lebherz, *Prep. Biochem.*, 11 (1981) 69.
10 F. Kubowitz and P. Ott, *Biochem. Z.*, 314 (1943) 94.
11 G. Muszynska, G. Dobrowolska, A. Medin, P. Ekman and J. Porath, *J. Chromatogr.*, 604 (1992) 19.
12 J. J. Holbrook, A. Liljas, S. J. Staindel and M. G. Rossman, in P. D. Boyer (Editor), *The Enzymes*, Vol. XI, Academic Press, New York, 1975, p. 191.
13 E. Sulkowski, *Makromol. Chem., Macromol. Symp.*, 17 (1988) 335.
14 M. R. Mauk and A. W. Girotti, *Biochemistry*, 13 (1974) 1757.
15 M. F. Perutz; P. D. Pulsinelli and H. M. Ranney, *Nature (London)*, 237 (1972) 259.
16 H. C. Watson and B. Chance, in B. Chance, R. W. Estabrook and T. Yonetani (Editors), *Hemes and Hemoproteins*, Academic Press, New York, 1966, p. 149.

Journal of Chromatography, 627 (1992) 173–186
Elsevier Science Publishers B.V., Amsterdam

CHROM. 24 547

Thermospray, particle beam and electrospray liquid chromatography–mass spectrometry of azo dyes

Rolf Straub, Robert D. Voyksner and Jeffrey T. Keever

Analytical and Chemical Sciences, Research Triangle Institute, P.O. Box 12194, Research Triangle Park, NC 27709 (USA)

(First received June 16th, 1992; revised manuscript received August 10th, 1992)

ABSTRACT

A high-performance liquid chromatographic–mass spectrometric (HPLC–MS) method was used for the analysis and characterization of fourteen commercial azo and diazo dyes. Thermospray analysis of these dyes using the "filament-on" chemical ionization operation mode produced mass spectra consisting primarily of $[M + H]^+$ ions with very few fragments. Particle beam electron impact ionization mass spectrometric analysis resulted in molecular ion information and various fragment ions. Characterization of the azo dyes could be achieved by observing typical fragment ions formed by cleavage of the C–N bonds on either side of the azo linkage, and cleavage of the N = N double bond with transfer of one or two hydrogen atoms to form an imine or amine. Many commercial azo dyes contain precursors, by-products of the synthesis, degradation products or other impurities. Some of these components were tentatively identified by their mass spectra and by review of the chemistry of dye manufacture. Electrospray negative ion operation was suitable for the characterization of a disulfonated azo dye and showed singly and doubly charged molecular ions and fragment ions at higher capillary–skimmer potential differences. The base peak was attributed to a doubly charged naphthol cleavage product.

INTRODUCTION

Azo dyes have been manufactured in the USA since the early 1900s and are still a very important class of synthetic chemicals. They are widely used as colorants in a variety of products, such as textiles, paper, leather, gasoline and foodstuffs [1]. These widely distributed chemicals represent a potential human health risk, as some have been shown to be carcinogenic [2–7]. It has also been shown that synthetic precursors, intermediates, by-products and degradation products of these dyes could be potential health hazards owing to both their toxicity and their carcinogenicity.

Commercial dyes are not single chemical compounds but instead are mixtures of compounds including dyes and impurities that have been standardized for their end use. Some azo dyes are of high purity (except for colorless diluents or dispersing agents) or can be readily purified further by appropriate isolation procedures and crystallization. However, other dyes, especially those prepared by several coupling reactions and those containing several sulfonic groups, are difficult to isolate in the pure state [8–10]. Sometimes manufacturers have refused to divulge structural details of their dyes [11]; also, some organic dyes have occasionally been sold under false labeling [12]. These are extreme examples, but they illustrate the need for comprehensive analysis of commercial dyes by methods designed for specific purposes. Analytical methods such as thin-layer (TLC), paper, high-performance liquid (HPLC) and gas-liquid chromatography, infrared and nuclear magnetic resonance spectroscopy, X-ray powder diffraction, chemical degradation and mass spectrometry (MS) are mainly used to detect and identify dyestuffs in various matrices [13]. However, these techniques have several disadvantages stemming from non-specific detection [14], lack of sensitivity or incompatibility with non-vola-

Correspondence to: R. D. Voyksner, Analytical and Chemical Sciences, Research Triangle Institute, P.O. Box 12194, Research Triangle Park, NC 27709, USA.

0021-9673/92/$05.00

tile, thermally unstable organic compounds. On-line HPLC–MS using thermospray (TSP) has been used to overcome some of these disadvantages for the analysis of environmental hazardous compounds [15,16] and has proved to be a suitable technique for many azo dyes [17–28]. Further HPLC–particle beam (PB) MS [29–31] has been demonstrated to generate electron impact ionization (EI) mass spectra from a series of commercial dyes [32]. A technique termed "ion spray" [33] was shown to generate ions of mono- and disulfonated azo dyes amenable to mass spectrometry [34,35].

This paper describes the analysis of fourteen commercial dyes, some of which are on the US Environmental Protection Agency list of toxic substances (Fig. 1), by HPLC–TSP-MS and HPLC–PB-MS. Both methods were compared and used to identify the parent azo dyes and their synthetic intermediates, by-products, additives or degradation products in these particular samples of interest. In addition, electrospray (ESP)-MS [36,37] was investigated for the mass spectrometric characterization of the acid dye.

EXPERIMENTAL

Materials

The following fourteen dyestuffs, listed in Fig. 1 and identified by their Color Index (C.I.), name and number, were obtained from the sources indicated: Nos. **1–7** and **14** (Aldrich, Milwaukee, WI, USA); **8** (Ciba-Geigy, Dyestuffs and Chemicals Division, Greensboro, NC, USA); **9** (BASF, Charlotte, NC, USA); **10** (Eastman Chemicals, Kingsport, TN, USA); **11** (Sandoz Colors and Chemicals, Charlotte, NC, USA); and **12** and **13** (Cromton & Knowles, Charlotte, NC, USA). All other chemicals were purchased from Aldrich. Some products with low dye contents were used after further extraction; the other commercial dyes were used without further purification. The solvents used for extraction, reaction or liquid chromatography were of HPLC/GC grade (Baxter Healthcare, Muskegon, MI, USA), and the water was doubly distilled and filtered through a Milli-Q water purification system (Millipore, Bedford, MA, USA) prior to use.

TLC was performed on normal-phase Macherey–Nagel SIL G/UV_{254} plates (Alltech, Avondale, PA, USA) with the mobile phase toluene–ethyl acetate (EtOAc) (4:1) for solvent dyes. For all other dyes, the TLC analysis was conducted using toluene–EtOAc (1:4). The use of a more polar eluent to study the product of the disperse dyes was essential to resolving components that would otherwise have remained at the origin. The acid dye was eluted with the mobile phase 96–99% ethanol–EtOAc (4:1).

Purification

HPLC–MS analysis was usually performed on the commercial dyes without purification. Because some of the commercial dyes had a diluent content of over 50% (**5**, **6**, **7**, **8**, and **13** in Fig. 1), they were first extracted with pure dichloromethane to separate them from material such as salts and surfactants. These extracts were then evaporated to dryness and dissolved in acetonitrile or methanol for analysis by HPLC–MS. To obtain highly pure azo dye standards, the pure (96–99%) or previously purified commercial dyes were additionally recrystallized from toluene–light petroleum (1:1) and dried. These standards were normally used at a concentration of 500 ng/μl for comparison purposes and further diluted to estimate detection limits.

Analysis

Prior to the HPLC–MS analysis, the melting points (m.p.) of all azo dyes were determined and TLC analysis was performed to screen for major visible organic impurities. The m.p. in °C (retardation factor, R_F) were as follows: **1**, 111, decomp. (0.97); **2**, 101–102 (0.87); **3**, 132–135 (0.98); **4**, 156–157 (0.98); **5**, 159–160 (0.65); **6**, 153–154 (0.90); **7**, 172–173 (0.89); **8**, 194–195 (0.80); **9**, 121–124 (0.54); **10**, 149–152 (0.1); **11**, 138–140 (0.35); **12**, 141–143 (0.65); **13**, 154–156 (0.31); **14**, 319–321 (0.0).

Equipment for HPLC–TSP-MS

The HPLC mobile phases were delivered by two Waters Series 6000A solvent-delivery systems (Waters, Milford, MA, USA) controlled by a Chem-Research chromatographic data management/system controller, Version 2.4.5 (ISCO, Lincoln, NE, USA). The samples were injected with a Waters U6K injector and separated on a Spherisorb ODS II, 5-μm particle size, 25 cm × 4.6 mm I.D. column (Regis Chemical, Morton Grove, IL, USA). A Waters Model 440 absorbance detector set at 254 nm was connected in-line before the TSP interface.

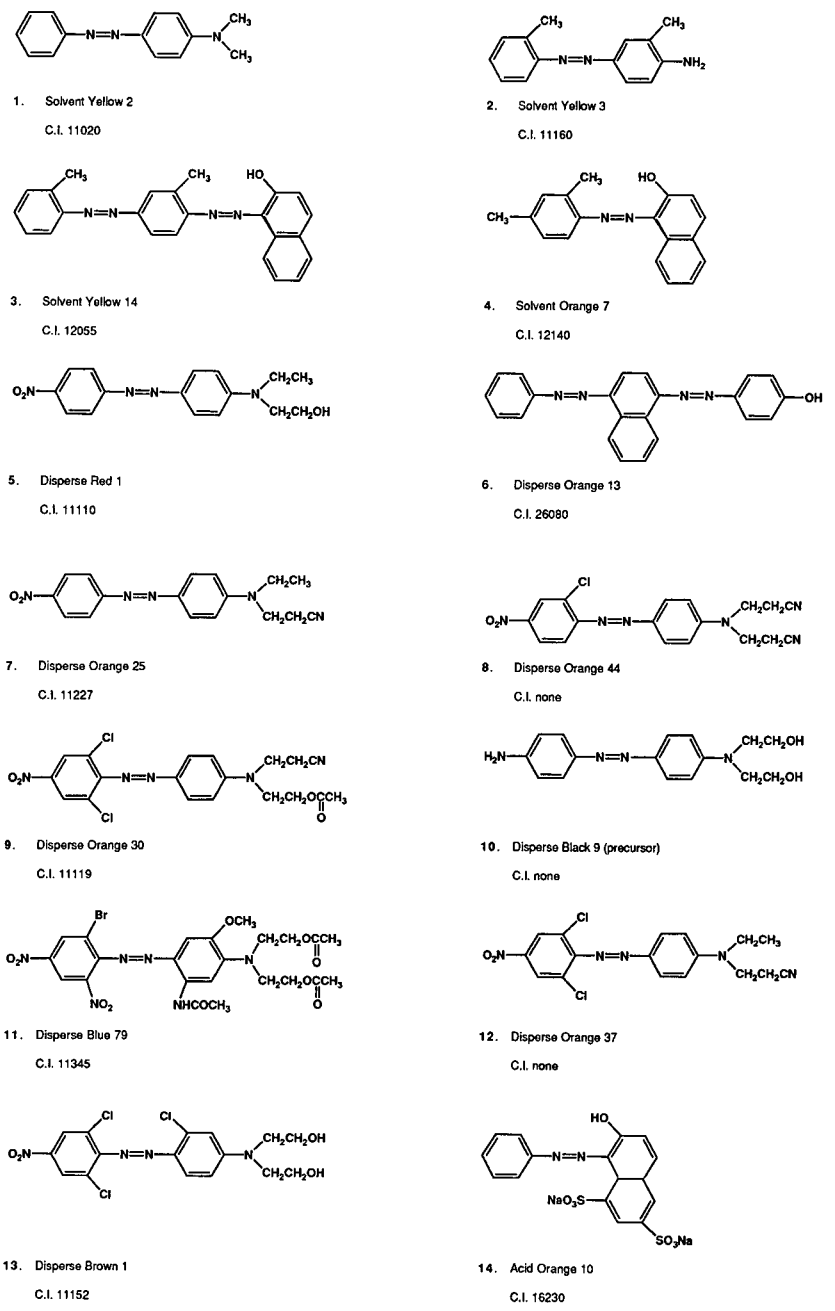

Fig. 1. Structures, names and Colour Index (C.I.) numbers of the azo dye samples used.

Postcolumn buffer addition was performed using a Waters Model 6000 pump to deliver an ammonium acetate solution to a coaxial mixing tee [38].

A Vestec HPLC–TSP-MS Interface Model 701C [39] (Vestec, Houston, TX, USA) was installed on a Finnigan MAT (San Jose, CA, USA) Model 4500

quadrupole mass spectrometer. The solvent was pumped out of the source through a liquid nitrogen cryogenic trap prior to a mechanical rough pump.

HPLC–TSP-MS conditions

The injection volume was 75 μl and the measurements were performed with a methanol–water gradient (from 40% to 100% methanol in 15 min) at a flow-rate of 0.5 ml/min. Ammonium acetate buffer (0.2 *M*) was added postcolumn at 0.5 ml/min to improve sensitivity [40]. The vaporizer temperature was 210–220°C, the tip heater was 290°C, the source block temperature was 260°C and the instrument was operated in the "filament-on" chemical ionization (CI) mode with the repeller set to 0 V. The mass spectrometer instrument scanned from *m/z* 150 to 650 at a rate of 1 s per scan in the pulsed positive/negative-ion detection mode.

Equipment for HPLC–PB-MS

HPLC was performed using a Waters Series 600 multi-solvent delivery system controlled by a Waters 600-MS system controller. The samples were injected with a Waters U6K injector and separated on a Spherisorb ODS II column. A Waters 484 MS tunable absorbance detector set at 254 nm was placed in-line before the Model 59980A PB interface (Hewlett-Packard, Palo Alto, CA, USA). The PB interface was connected to a Hewlett-Packard Model 5988A single quadrupole mass spectrometer.

HPLC-PB-MS conditions

The injection volume was 75 μl and the measurements were performed with a methanol–water gradient (from 40% to 100% methanol in 15 min) at a flow-rate of 0.5 ml/min. The PB desolvation chamber temperature was set to 60°C and a helium inlet pressure of 2.75 bar was maintained. The ion source was operated at 200°C. The filament emission current was 0.3 mA, the electron energy was set at 70 eV and the electron multiplier voltage at 2230 V. The manifold temperatures were set to 90°C (front) and 45°C (rear). The sensitivity of the system was checked by analyzing caffeine.

Equipment for ESP-MS

A Sage Model 341B (Orion Research, Boston, MA, USA) microsyringe pump was used for the flow-injection (FI) analysis of the acid dye **14**. A 50-μl PS C-160 FN syringe for a Waters U6K injector (Dynatech, Baton Rouge, LA, USA) was used for the infusion into the Analytica HPLC–ESP-MS Model 100547-3 interface (Analytica of Branford, Branford, CT, USA). The ESP interface was connected to a Hewlett-Packard Engine Model HP 5989A quadrupole mass spectrometer. The solvent was pumped out of the source in two different pumping stages by two auxiliary mechanical rough pumps.

ESP-MS conditions

The dye was dissolved at a concentration of 100 ng/μl in 2-propanol–water (1:1) and infused at a flow-rate of about 1.2–3.6 μl/min into the ESP interface. The adjustable ESP needle used a 50 μm I.D. stainless-steel tube to deliver solvent and an additional outer concentric tube to add dry oxygen gas to prevent coronal discharges in the negative-ion operation mode (oxygen acts as an electron scavenger). In this ESP interface, the needle is grounded and charging occurs by keeping the cylindrical electrode (V_1) at about 2.8 kV, the end plate (V_2) at 2.6 kV and the capillary (V_3) at 3 kV (positive-ion operation required reverse polarity, and V_{1-3} operated about 1 kV higher than in negative-ion operation). The best results for negative ions were obtained with skimmer (S) and lens (L) voltage of $S_1 = -40$ V, $S_2 = -16$ V, $L_1 = 38$ V, $L_2 = 83$ V and $L_3 = 36$ V. The potential difference between the skimmer and the end of the capillary controlled the extent of fragmentation through collisional-activated dissociation (CAD). The potential difference was varied between −40 and −400 V. The mass spectrometer scanned from *m/z* 40 to 500 at a step size of 0.1 unit and a rate of 0.5 scan per second. The threshold value was set to 100. The system was checked by analyzing adenosine-5′-monophosphate in 2-propanol–water (1:1) for negative-ion and arginine–gramicidin S in methanol–water (1:1) for positive-ion operation.

Equipment and conditions for high-resolution measurements

The VG ZAB-E high-resolution mass spectrometer (Fisons Instruments, Manchester, UK) scanned from *m/z* 50 to 500 at a rate of 10 s per scan with a reset time of 2 s and a response time of 0.01 ms. The ion source was operated at 200°C. The trap

current was 100 μA and electron energy was set to 70 eV.

RESULTS AND DISCUSSION

The TLC analysis of the fourteen azo dyes indicated no significant visible impurities, and the melting point determination indicated no major difference between the tested samples and additionally purified standards or reported values [41]. Both methods are simple and fast but are not suitable for the detection and characterization of trace components. Therefore, a more sensitive and specific procedure such as HPLC–MS was needed for the separation, detection and characterization of non-volatile azo dyes and their by-products. Table I lists the retention times, the major fragments observed under TSP and PB conditions and the percentage of UV absorption[a] of the corresponding component peak for the fourteen commercial dyes and their detectable impurities; Figs. 2–8 show mass spectra of seven selected solvent and disperse azo dyes.

HPLC–TSP-MS

In TSP chemical ionization (CI) mass spectrometry, most of the ion current is concentrated in a single ion, usually the protonated molecule $[M+H]^+$ of the parent azo dye. All solvent and disperse dyes tested remained very stable, and lower molecular mass fragment ions with a relative intensity of over 25% were not detected. Fig. 2A and 3A show the TSP mass spectra of the isomeric azo dyes Solvent Yellow 2 and 3 (**1** and **2**). Both mass spectra are very similar and provide only an $[M+H]^+$ ion peak without any structural information. As shown in Figs. 4A and 5A, Solvent Yellow 14 (**3**) and Disperse Orange 13 (**6**) show an intense $[M+H]^+$ ion and little or no fragmentation in the CI process. Only Disperse Orange 44 (**8**) shows an additional $[M+NH_4]^+$ adduct ion at *m/z* 400, but with a low relative intensity of only 1%. The most difficult dyes to study by mass spectrometry are the acid dyes. The salts of sulfonic acid dyes cannot be volatilized without thermal degradation. Even the free acids are extremely non-volatile and their $[M+H]^+$ ions are usually not very intense. Only an $[MH-2Na+2H]^+$ ion at *m/z* 409 of Acid Orange 10 (**14**) has been tentatively identified. A similar fragment ion has been identified in the TSP mass spectrum of Acid Blue 113 as base peak [22]. The base peak in the mass spectrum of dye **14** is at *m/z* 326 and is probably due to a partially desulfonated $[M-Na-NaSO_3]^+$ ion.

In some of the commercial azo dyes, by-products were separated and characterized by mass spectrometry. Solvent Yellow 2 (**1**) contained a dye residue with a partially demethylated amino group (*m/z* 211) and Solvent Yellow 3 (**2**) contained a small amount of isomer with the methyl group in the 2′-position (instead of the more favorable 3′-position) on the phenyl ring. Neither of these by-products was detected by HPLC–PB-MS (possibly owing to the non-volatility or low concentration of these products) and are therefore not fully confirmed. In addition, Disperse Orange 30 (**9**) showed the protonated parent dye at *m/z* 450 and an ion at *m/z* 416 that was attributed to a substitution of one chlorine ($[M+H-Cl+H]^+$). Fig. 6 shows the total ion current (TIC) chromatogram, the corresponding TSP mass spectrum of the parent azo dye (mass peak number 2) and the TSP spectrum of its hydrolyzed by-product (mass peak number 1). Disperse Blue 79 (**11**) contained at least three degradation products (*m/z* 582, 325 and 310), but only in small amounts and not fully resolved by the chromatographic system. The peak at *m/z* 582 can probably be attributed to the hydrolysis product $[M-COCH_3+H]^+$; the peak at *m/z* 325 resulted from the amine formed after a reductive cleavage of the azo linkage; *m/z* 310 is consistent with the partially hydrolyzed compound produced under heterolytic azo bond cleavage conditions seen as R^3 in the footnote of Table I. Disperse Orange 37 (**12**) possessed a structurally unknown impurity with the base peak at *m/z* 105; it was not detectable by HPLC–PB-MS.

HPLC–PB-MS

From most parent azo dyes it was possible to obtain molecular ion information and characteristic fragmentation patterns for structural elucidation. Figs. 2B–4B list EI mass spectra of solvent dyes, and Figs. 5B, 7 and 8 list mass spectra of more com-

[a] The UV absorption chromatograms of the azo dyes are not reported, and only the percentage of UV absorption is listed to estimate the relative content of the detected components under the assumption of similar molar absorptivities.

TABLE I

THERMOSPRAY AND PARTICLE BEAM MASS SPECTRA OF AZO DYES

t_R = Mean retention time in TIC chromatograms (min); M_r = calculated molecular mass; UV (%) = UV peak area based on chromatogram obtained with UV detection at 254 nm used for independent detection of the components and to estimate their approximate content; Unknown = structure unknown; N.D. = not detected by this method. Amount injected on HPLC column, 37 μg; solvent, methanol–water gradient.

No.	Dye	By-product or contamination[a]	M_r	t_R (min)	*m/z* (relative intensity, %)		UV (%)
					Thermospray	Particle beam	
1	Solvent Yellow 2		225	25.1	226(100); 227(15)	225(58); 148(11); 120(67); 77(100); 51(37)	95
		$C_6H_5N_2C_6H_4NHCH_3$	211	20.5	229(1); 212(100)	N.D.	4
2	Solvent Yellow 3		225	24.8	234(1); 226(100)	225(59); 134(14); 106(100); 91(21); 77(22); 75(14); 51(3)	90
		$C_6H_5N_2C_6H_4N(CH_3)_2$	225	20.4	234(1); 226(100)	N.D.	8
3	Solvent Yellow 14		248	29.8	252(1); 251(5); 250(32); 249(100)	248(90); 220(4); 219(8); 171(19); 143(100); 115(97); 105(2); 89(14); 77(40); 51(17)	97
4	Solvent Orange 7		276	41.6	279(11); 278(37); 277(100)	276(100); 248(12); 247(36); 171(10); 143(94); 115(83); 105(86); 77(43); 65(12)	90
		Unknown	281	25.0	282(100); 281(16)	N.D.	10
5	Disperse Red 1		314	30.4	315(100); 285(6)	314(15); 283(100); 255(4); 237(6); 133(30); 105(8); 76(6)	85
6	Disperse Orange 13		352	39.0	353(100); 264(5); 248(4)	352(98); 326(2); 263(9); 247(54); 231(32); 142(31); 121(54); 105(20); 93(100); 77(95); 65(44)	70[b]
7	Disperse Orange 25		323	30.4	324(100); 294(13); 181(4)	323(34); 308(4); 283(100); 253(10); 173(17); 133(38); 105(12); 104(18); 76(14)	84[b]
		Unknown	338	28.3	N.D.	338(5); 310(59); 243(8); 180(1); 158(100); 120(29)	2
8	Disperse Orange 44		382	26.2	400(1); 383(100); 353(17); 300(6)	382(14); 352(7); 342(29); 329(31); 299(33); 198(32); 158(29); 145(100); 105(62); 92(30); 65(28)	90[b]
9	Disperse Orange 30		449	29.9	452(63); 450(100); 416(19); 118(10); 90(11)	220(11); 218(22); 192(28); 190(36); 158(100); 144(64); 118(69); 109(95); 87(68); 77(90); 54(48)	60
		$RN(C_2H_4CN)(C_2H_4OH)$	407	26.4	412(18); 410(74); 408(100); 374(15); 227(18)	220(13); 218(26); 192(18); 190(26); 158(100); 144(96); 118(44); 109(65); 74(55); 54(44)	36

10	Disperse Black 9		300	19.8	301(100)	300(35); 282(1); 269(100); 225(13); 194(3); 192(17); 190(26); 149(12); 120(10); 92(24); 77(9); 65(12)	97
11	Disperse Blue 79		624	30.2	625(50); 547(24); 368(100); 353(36)	188(1); 87(15); 71(7); 57(100)	95
		R^1-$N(C_2H_4OCOCH_3)(C_2H_4OH)$ or R^2-NH_2	582	28.1[c]	600(1); 583(100)	N.D.	4
		R^3-NH_2	325		343(<1); 326(100)	N.D.	
		R^3-H	310		328(5); 311(100)	N.D.	
12	Disperse Orange 37		391	33.6	394(71); 392(100)	391(24); 351(56); 194(<1); 192(1); 190(2); 173(77); 133(100); 104(32); 77(20)	94
		Unknown		21.0	122(2); 105(100)	N.D.	5
13	Disperse Brown 1		432	29.3[c]	435(99); 433(100); 321(7)	434(15); 432(15); 403(100); 401(99); 357(20); 194(1); 192(7); 190(9); 183(81); 139(76); 138(27); 104(31)	87[b]
		Unknown		30.3[c]	N.D.	390(4); 367(19); 323(4); 239(6); 198(20); 170(55); 139(100); 104(31); 75(22)	N.D
		Unknown		34.3	N.D.	239(4); 189(5); 176(14); 149(34); 140(18); 124(100); 98(54); 84(34); 74(34); 57(20)	2[b]
		Unknown		36.3		327(1); 267(8); 134(45); 112(31); 98(100); 84(68); 74(53); 57(42)	4[b]
		Unknown	186	19.2	188(29); 187(100)		4[b]
14	Acid Orange 10		452	5.0	409(8); 326(100); 239(15)	246(1); 245(2); 218(1); 167(14); 142(10); 124(16); 94(100); 93(50); 66(55)	95

[a] R = $(O_2N)Cl_2C_6H_2N_2C_6H_4$; R^1 = $(O_2N)_2BrC_6H_2N_2C_6H_2(NHCOCH_3)OCH_3$; R^2 = $(O_2N)_2BrC_6H_2N_2C_6H_2[(NHCOCH_3)_2]OCH_3$; R^3 = $C_6H_2[N(C_2H_4OCOCH_3)C_2H_5OH]OCH_3$.

[b] Dye content in commercial product below 50% (sample extracted to separate dye, and organic by-products from loading material).

[c] Not fully resolved peak in HPLC separation.

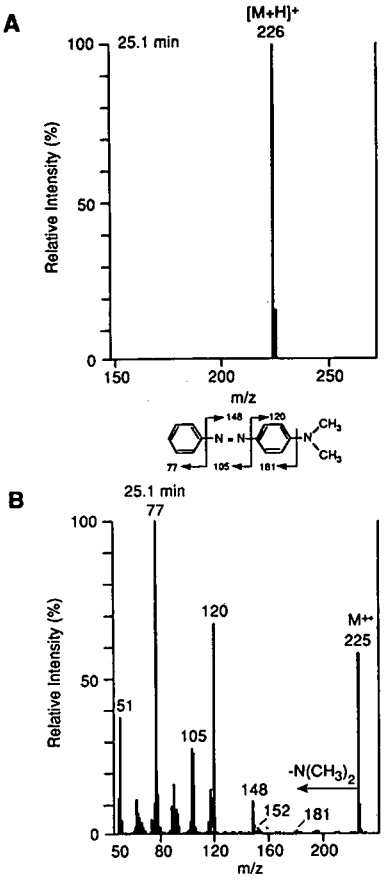

Fig. 2. (A) HPLC–TSP and (B) HPLC–PB mass spectra of Solvent Yellow 2 (**1**; M_r 225). Amount injected, 37 μg; solvent, methanol–water gradient.

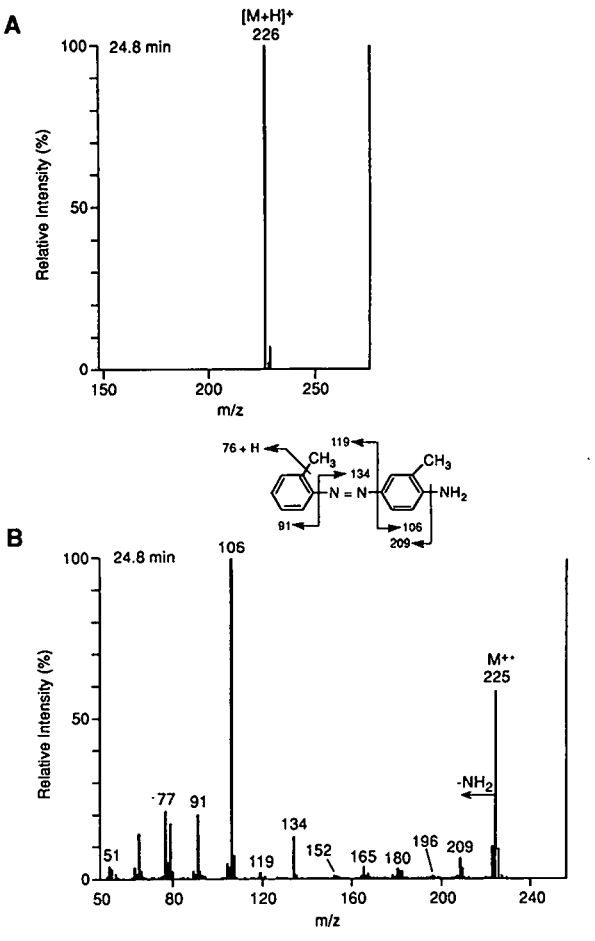

Fig. 3. (A) HPLC–TSP and (B) HPLC–PB mass spectra of Solvent Yellow 3 (**2**; M_r 225). Amount injected, 37 μg; solvent methanol–water gradient.

plex disperse dyes. The EI mass spectra of Disperse Orange 30 (**9**) and its degradation product provide no molecular ion information. Fig. 7 shows the TIC chromatogram and the fragment-rich EI mass spectra of the resolved components. Molecular mass information was only obtained by TSP-MS, as seen in Fig. 6. Disperse Blue 79 (**11**), which had the highest number of substituents of all the tested dyes, shows an easily detectable $[M+H]^+$ ion in the TSP spectrum, but the corresponding EI spectrum indicates strong fragmentation with no sign of the $M^{+\bullet}$ ion or nitro- and bromine-containing aromatic fragment ions. Only a cleaved tertiary amine fragment $[N(C_2H_4OCOCH_3)_2]^+$ with *m/z* 188 could be tentatively identified (*cf.*, Table I). A similar result was obtained on a triple-stage quadrupole instrument using a ThermaBeam EI interface [32]. The EI mass spectrum of Acid Orange 10 (**14**) indicated complete desulfonation (*m/z* 246) accomplished thermally in the mass spectrometer, as well as characteristic fragment ions of naphthol-containing azo dyes.

Particle beam EI spectral fragmentation of these azo dyes centers around cleavage of the azo linkage. Cleavage of the azo linkage under mass spectrometric conditions can occur in three ways: at the N–C bond on the coupler side of the azo linkage (the positive charge often remains with the coupler component) [13,17], at the C–N of the remaining aromatic fragment or at the double bond between

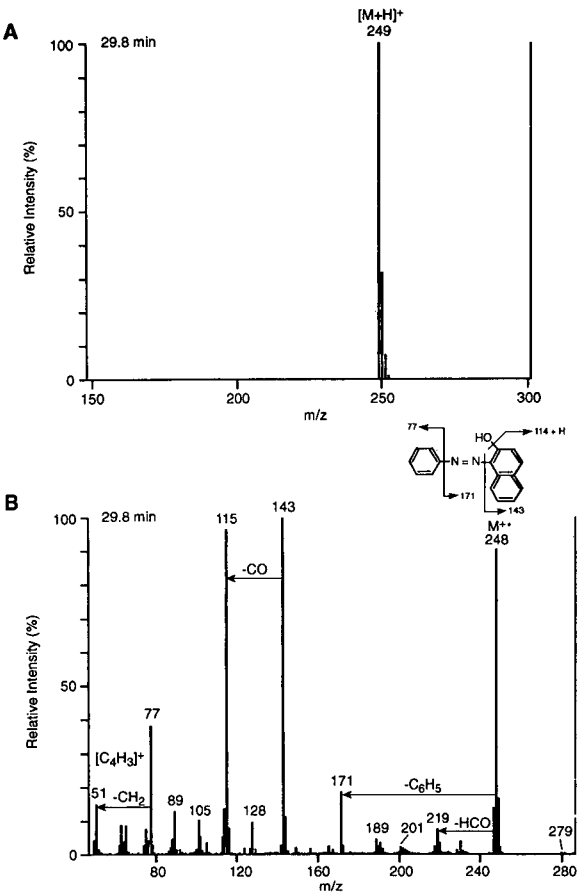

Fig. 4. (A) HPLC–TSP and (B) HPLC–PB mass spectra of Solvent Yellow 14 (3; M_r 248). Amount injected, 37 μg; solvent, methanol–water gradient.

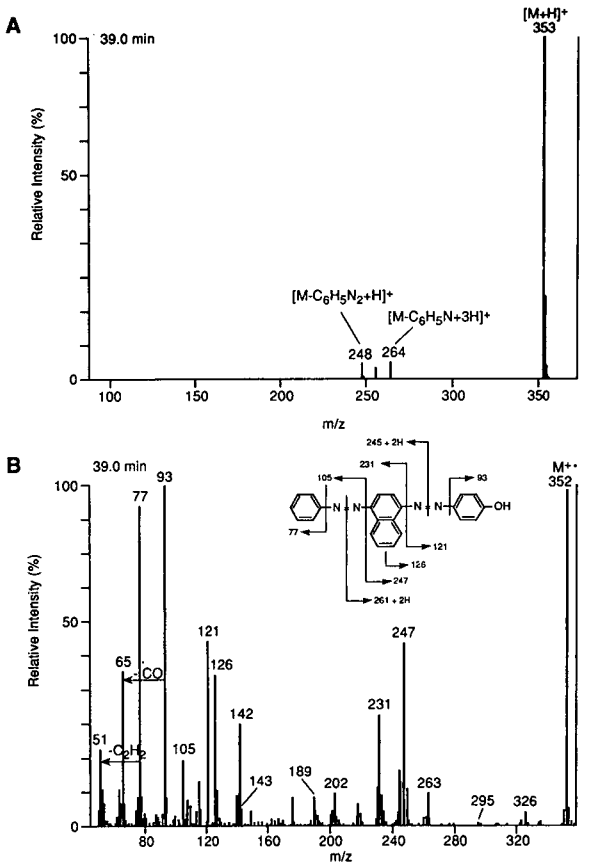

Fig. 5. (A) HPLC–TSP and (B) HPLC–PB mass spectra of Disperse Orange 13 (6; M_r 352). Amount injected, 37 μg; solvent, methanol–water gradient.

the two N atoms of the azo linkage. Cleavage of the C–N and N–C bonds on either side of the azo linkage has been observed previously in azo dyes [13,32] and in substituted azobenzene [13,42].

The EI mass spectrum of Solvent Yellow 2 (Fig. 2B) shows an $M^{+\bullet}$ ion at *m/z* 225, an N–C cleavage product at *m/z* 148 and a C–N product at *m/z* 120. The base peak at *m/z* 77 has been attributed to $[C_6H_5]^+$ and *m/z* 51 to the following fragment $[C_4H_3]^+$. The isomeric dye Solvent Yellow 3 shows an EI spectrum (Fig. 3B) with an $M^{+\bullet}$ ion at *m/z* 225, a $[CH_3H_2NC_6H_3N_2]^+$ ion at *m/z* 134 and a $[CH_3C_6H_4]^+$ ion at *m/z* 91. The base peak at *m/z* 106 has been tentatively proposed as $[CH_3C_6H_4NH]^+$. Such transfer of one hydrogen atom was previously reported in the secondary ion mass spectra of azo dyes [43]. The ions $[C_6H_5]^+$ and $[C_4H_3]^+$ at *m/z* 77 and 51 again indicate the presence of a phenyl group. The naphthol-containing azo dye Solvent Yellow 14 gives a very intense $M^{+\bullet}$ ion peak at *m/z* 248 in the EI spectrum (Fig. 4B). The spectrum illustrates a number of fragmentations characteristic of a hydroxyl group on an aromatic ring. The odd-electron $[M-CO]^+$ peak at *m/z* 220, which is accompanied by $[M-CHO]^+$ at *m/z* 219, is especially useful in recognizing this functional group. The peaks of N–C cleavage products $[HOC_{10}H_6N_2]^+$ and $[C_6H_5N_2]^+$ at *m/z* 171 and 105, respectively, are not very intense. The base peak at *m/z* 143 has been tentatively attributed to the C–N cleavage product $[HOC_{10}H_6]^+$. Again,

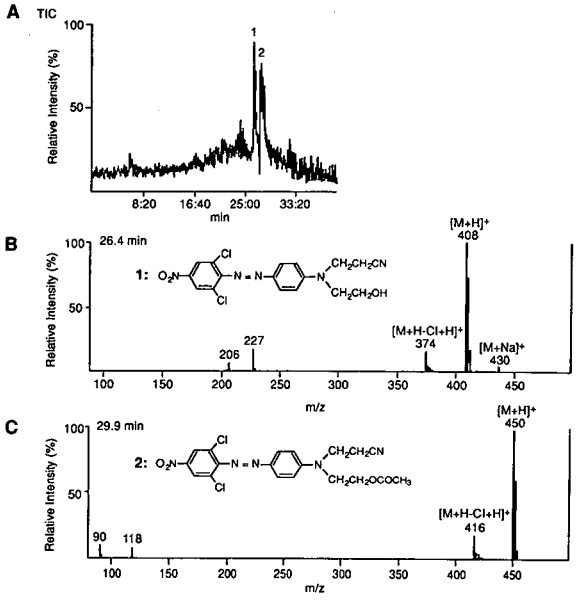

Fig. 6. (A) HPLC–TSP-MS TIC chromatogram of Disperse Orange 30 (**9**; M_r 449) and (B and C) corresponding TSP CI mass spectra. (B) Peak 1 = hydrolyzed decomposition product and (C) peak 2 = parent dye. Amount injected, 37 μg; solvent, methanol–water gradient.

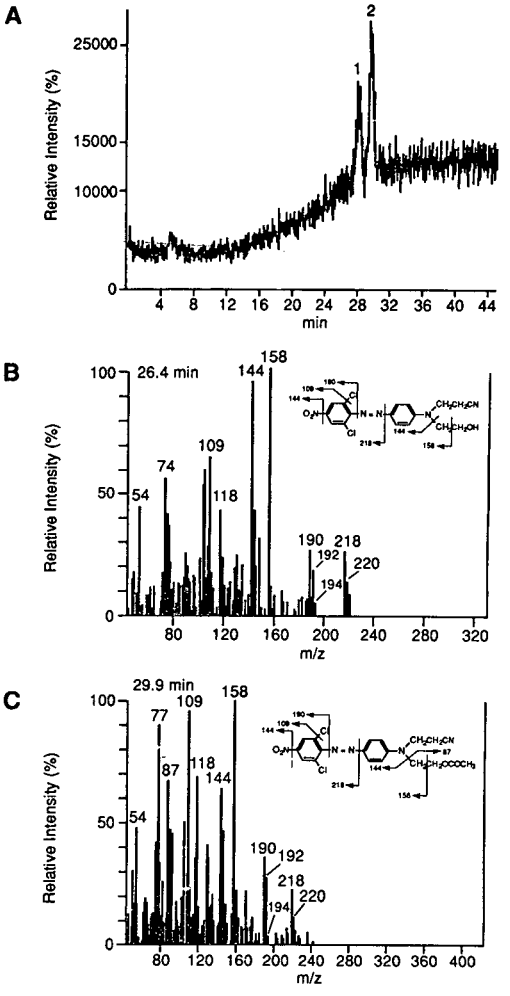

Fig. 7. (A) HPLC–PB-MS TIC chromatogram of Disperse Orange 30 (**9**; M_r 449) and (B and C) corresponding PB EI mass spectra. (B) Peak 1 = hydrolyzed decomposition product and (C) peak 2 = parent dye (no molecular ion information obtained). Amount injected, 37 μg; solvent, methanol–water gradient.

ions at *m/z* 77 and 51 indicate a phenyl fragment.

The $M^{+\bullet}$ ion at *m/z* 276 is the prominent ion of the naphthol-containing azo dye Solvent Orange 7 (**4**), followed by the characteristic C–N cleavage products $[HOC_{10}H_6]^+$ at *m/z* 143 and $[(CH_3)_2C_6H_3]^+$ at *m/z* 105. The charged N–C cleaved fragment $[HOC_{10}H_6N_2]^+$ with low intensity can be seen at *m/z* 171. Also, the characteristic loss of CO and HCO can be registered at *m/z* 348 and 347.

The EI mass spectrum (Fig. 5B) of the more complex diazo dye Disperse Orange 13 (**6**) presents fragment ions that occurred from cleavage of both azo linkages. Besides the C–N and N–C cleavage products ions at *m/z* 77, 93, 105, 121, 126 and 231, an ion at *m/z* 263 appears to come from cleavage between the two azo nitrogen atoms, with transfer of two hydrogen atoms to form the amine. This is an example of the fourth possibility to cleave a dye's azo bond under mass spectrometric conditions. Such a cleavage, with transfer of two hydrogen atoms, was previously reported in the EI mass spectra of 2-methoxyazobenzene [44] and diverse azo dyes [13,32]. The low-resolution measurements did not allow a clear distinction of isomeric fragment ions. The ion at *m/z* 247 could be formed either by a C–N cleavage reaction or by cleavage of the azo linkage with transfer of two hydrogen atoms. Additional high-resolution measurements confirmed the C–N cleavage product $[C_{10}H_6N_2C_6H_4OH]^+$ (deflection 1.1 ppm) seen in Fig. 5B.

Fragmentation β to the amine nitrogen usually leaves the charge with the amine moiety. If the amine substituent is $-CH_2CH_2X$, where X is OH, OR, OCOR or CN, β fragmentation is very common [13]. The mass spectra of dyes **5**, **10** and **13** show intense $[M-CH_2OH]^+$ ions. A similar β fragmentation mechanism forming $[M-CH_2CN]^+$ ions can be observed with dyes **7**, **8** and **12** (Table I). Charged fragments with strong electron-withdrawing substituents are not very stable and appear only with weak intensity in the mass spectrum. Usually, these peaks are not very characteristic of identification. In the PB mass spectrum of Disperse Orange 30 (**9**), the peak at *m/z* 190 implies the presence of the C–N cleavage product $[O_2N(Cl_2)C_6H_2]^+$. The fragmentation pattern *m/z* 190, 192 and 194 in the two mass spectra of Fig. 7 is consistent with the isotopic abundances for combinations of two chlorine atoms. Disperse Orange 37 (**12**) and Disperse Brown 1 (**13**), with the same phenyl substituent in the molecule, show a similar fragmentation pattern for this C–N cleavage product but with weaker intensity. In Disperse Orange 25 (**7**), a small amount of a structurally unknown impurity with $M^{+\bullet}$ at *m/z* 338 has been separated and detected. Disperse Orange 30 (**9**) contained a considerable amount (about one third of the content) of hydrolyzed by-product (mass peak number 1 in Fig. 7) with $M^{+\bullet}$ at *m/z* 582.

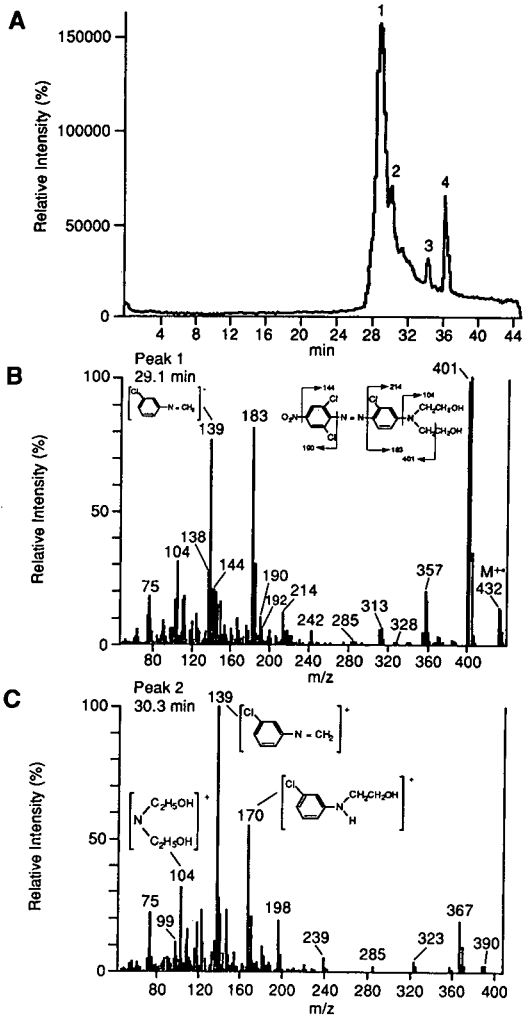

Fig. 8. (A) HPLC–PB-MS TIC chromatogram of Disperse Brown 1 (**13**; M_r 432) and (B and C) corresponding PB EI mass spectra. (B) Peak 1 = parent dye ($M^{+\bullet}$ = 432) and (C) peak 2 = decomposition product. Amount injected, 37 μg; solvent, methanol–water gradient.

Fig. 8 shows the TIC chromatogram of Disperse Brown 1 (**13**) and the corresponding PB mass spectra of two resolved components. The major peak number 1 at a retention time (t_R) of 29.1 min shows a mass spectrum with a relatively weak $M^{+\bullet}$ ion at *m/z* 432 and an intense β cleavage fragment $[M-CH_2OH]^+$ at *m/z* 401, as well as an intense C–N cleavage product at *m/z* 183. Additional high-resolution measurements confirm the molecular ion (deflection 4.0 ppm) and the structure of the *m/z* 139 ion (deflection 5.5 ppm). The mass spectrum of the shoulder peak at t_R 30.3 min could only be partially characterized. The structure of the *m/z* 139 ion was again confirmed by high-resolution measurements. The two smaller peaks, numbers 3 and 4 (mass spectra not shown), may come from plasticizer impurities. However, no accurate structural characterization was possible from the data obtained. Other dye samples analyzed in other investigations [45] showed similar structurally unidentifiable mass spectra in the same retention time range when they were stored in plastic containers for a long period.

Detection limits

The detection limits[a] of the dye standards were in

[a] The detection limits were calculated by multiplying the analyte concentration by the applied flow-rate and the total acquisition time used for the particular mass spectrum.

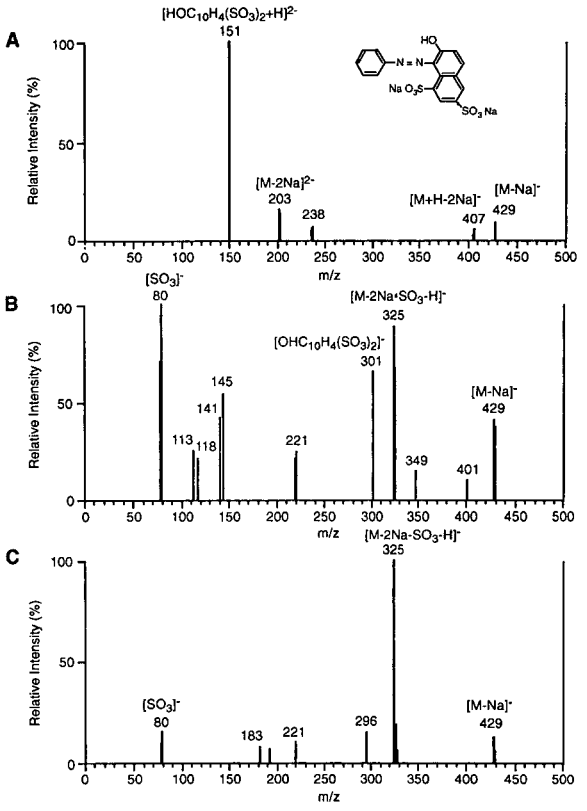

Fig. 9. Flow-injection–ESP mass spectra of 100 ng/μl Acid Orange 10 (**14**; M_r 452) in 2-propanol–water (1:1) at CAD voltages of (A) −100, (B) − 200 and (C) −300 V.

the range of 500 ng to 5 μg for HPLC–PB-MS recording the mass chromatogram of characteristic intense ions of the dyes under full mass scan and with a signal-to-noise ratio of at least 3:1. Measurements with HPLC-TSP-MS under full-scan MS conditions were at least two to three orders of magnitude more sensitive. Selected ion monitoring was not evaluated as a method of improving detection limits at this early experimental stage. More measurements will be needed to obtain more accurate information about detection limits of specific azo dyes.

ESP-MS

The disulfonated azo dye Acid Orange 10 (**14**) showed a weak $[MH-2Na+2H]^+$ ion in TSP ionization and underwent considerable thermal degradation in EI ionization (Table I). A promising alternative for the analysis of acid dyes is the relatively "soft" ESP ionization process [33–35]. Owing to the strong acid characteristics of this azo dye, ESP in the negative-ion operation mode was able to detect characteristic anions formed in the solution. The negative-ion ESP spectra in Fig. 9 were recorded under three representative capillary–skimmer potential differences of −100 V (A), −220 V (B) and −300 V (C). Lower potential differences minimized CAD energies resulting in the formation of singly charged ions $[M-Na]^-$ at *m/z* 429, $[M+H-2Na]^-$ ion at *m/z* 407 and a doubly charged $[M-2Na]^{2-}$ ion at *m/z* 203. The base peak at *m/z* 151 has been tentatively attributed to the C–N naphthol cleavage product $[HOC_{10}H_4(SO_3)_2+H]^{2-}$. Higher CAD energies (larger capillary-skimmer potential differences) resulted in more fragmentation with some losses in sensitivity. The peak at *m/z* 151 disappeared, and $[M-2Na-SO_3-H]^-$ ions at *m/z* 325 and SO_3^- ions at *m/z* 80 appeared from cleavage of the sulfonic group. At a capillary–skimmer potential difference of −300 V and higher, only the *m/z* 325 peak was present in the mass spectrum. Increasing the pH of the solution from 3.5 to 10 by adding 1% ammonia solution decreased the intensity of the base peak in the spectrum in Fig. 9A approximately fourfold. Also, a minor decrease of the *m/z* 407 peak was observed. The alkaline conditions did not affect the abundances of the other peaks in the mass spectrum. The ESP-MS detection limit[a] in negative ion operation under full-scan MS conditions was 10 ng.

CONCLUSIONS

It has been demonstrated that molecular mass information on azo dyes can be obtained by recording their CI mass spectra by using a TSP interface on a single quadrupole mass spectrometer. To gain useful structural information on these dyes, it is neces-

[a] In contrast to this, positive ESP ionization of the acid dye showed an almost 50-fold lower sensitivity. Only a weak sodium adduct $[M+Na]^+$ ion at *m/z* 475 has been tentatively identified at the corresponding positive potentials of 100, 240 and 300 V (mass spectra not shown).

sary to record their EI mass spectra with an HPLC–MS system using a PB interface. Only through the complementary application of both techniques could the azo dyes be satisfactorily characterized. In some instances, additional organic impurities could be identified by one or both of the techniques. These components were derived from decomposition of the parent dye, from the coupling reaction process or from external sources during the handling of the commercial products. Characteristic fragmentation in azo dyes included cleavage of the C–N and N–C bonds on either side of the azo linkage, and cleavage of the N=N double bond with transfer of one or two hydrogen atoms, to form an imine or amine, respectively. Most azo dyes showed a molecular ion, and fragmentation from ring cleavage was observed. Naphthol-containing azo dyes presented $[M-CO]^+$ and $[M-HCO]^+$ fragment ions, which are not very intense but characteristic of a hydroxyl group on an aromatic ring.

ESP ionization was successful in generating characteristic singly and doubly charged negative ions of the strongly acidic azo dye, Acid Orange 10 (**14**). A weak adduct between the molecule and a sodium ion $[M+Na]^+$ was the only positive ion identified for this azo dye.

ACKNOWLEDGEMENTS

We thank Dr. L. Don Betowski of EPA, Las Vegas, NV, USA, for the helpful discussions concerning the project, dye manufacturers for the azo dye standards and Professor Harold Freeman and W. N. Hsu of the College of Textile Chemistry, North Carolina State University, Raleigh, NC, USA, for the TLC screening and desalting of the dyes.

Although the research described in this paper has been funded in part by the US Environmental Protection Agency through contract Number 68-02-4544 to Research Triangle Institute, it has not been subjected to agency review. Therefore, it does not necessarily reflect the views of the agency. Mention of trade names of commercial products does not constitute endorsement or recommendation for use.

REFERENCES

1 M. S. Reisch, *Chem. Eng. News*, 66 (1988) 7.
2 W. C. Hueper, *Occupational and Environmental Cancers of the Urinary System*, Yale University Press, New Haven, CT, 1969.
3 *IARC Monographs on the Evaluation of the Carcinogenic Risk of Chemicals to Man*, Vol. 8, IARC, Lyon, 1975.
4 C. E. Searly (Editor), *Chemical Carcinogenesis (ACS Monograph No. 173)*, American Chemical Society, Washington, DC, 1976.
5 J. F. Robens, G. S. Diu, J. M. Ward, J. R. Joiner, R. A. Griesemer and J. F. Douglas, *Toxicol. Appl. Pharmacol.*, 54 (1980) 431.
6 M. Boeninger, *The Carcinogenicity and Metabolism of Azo Dyes, Especially Those Derived from Benzidine*, Publication No. 80-119, U.S. Department of Health and Human Services, National Institute for Occupational Safety and Health, 1980.
7 H. S. Freeman, J. F. Esancy, K. P. Mills and W. M. Whaley, *Dyes Pigments*, 8 (1987) 417.
8 P. Rabin, *Nature (London)*, 199 (1963) 596.
9 R. L. Reeves, R. S. Kaiser and K. T. Finley, *J. Chromatogr.*, 47 (1970) 217.
10 R. L. Reeves, *J. Am. Chem. Soc.*, 97 (1975) 6019.
11 J. E. Scott, *Histochemie*, 29 (1972) 129.
12 K. H. Drexhage, in F. P. Schäfer (Editor), *Topics in Applied Physics*, Vol. 1, Springer, Berlin, 1971, p. 178.
13 K. Venkataraman (Editor), *The Analytical Chemistry of Synthetic Dyes*, Wiley, New York, 1977.
14 A. Shan, D. Harbin and C. W. Jameson, *J. Chromatogr. Sci.*, 26 (1988) 439.
15 A. L. Yergey, C. G. Edmonds, I. A. S. Lewis and M. L. Vestal, *Liquid Chromatography/Mass Spectrometry, Techniques and Applications*, Plenum Press, New York, 1990.
16 M. A. Brown (Editor), *Liquid Chromatography/Mass Spectrometry, Application in Agricultural, Pharmaceutical, and Environmental Chemistry (ACS Symposium Series*, No. 420), American Chemical Society, Washington, DC, 1990.
17 J. M. Bellard and L. D. Betowski, *Org. Mass Spectrom.*, 21 (1986) 575, and references cited therein.
18 T. Covey and J. Henion, *Anal. Chem.*, 55 (1983) 2275.
19 L. D. Betowski and J. M. Ballard, *Anal. Chem.*, 56 (1984) 2604.
20 R. D. Voyksner, *Anal. Chem.*, 57 (1985) 2600.
21 L. D. Betowski, S. M. Pyle, J. M. Ballard and G. M. Shaul, *Biomed. Environ. Mass Spectrom.*, 14 (1987) 343.
22 J. Yinon, T. L. Jones and L. D. Betowski, *Biomed. Environ. Mass Spectrom.*, 18 (1989) 445.
23 R. D. Voyksner, T. W. Pack, C. A. Haney, H. S. Freeman and W.-N. Hsu, *Biomed. Environ. Mass Spectrom.*, 18 (1989) 1079.
24 J. Yinon, T. L. Jones and L. D. Betowski, *Rapid Commun. Mass Spectrom.*, 4 (1990) 245.
25 A. Groepplin, M. W. Linder, K. Schellenberg and H. Moser, *Rapid Commun. Mass Spectrom.*, 5 (1991) 203.
26 C. Lindberg and J. Paulsen, *J. Chromatogr.*, 394 (1987) 117.
27 W. H. McFadden and S. A. Lammert, *J. Chromatogr.*, 385 (1987) 201.
28 W. H. McFadden, D. A. Garteiz and E. G. Siegmund, *J. Chromatogr.*, 394 (1987) 101.
29 R. C. Willoughby and R. F. Browner, *Anal. Chem.*, 56 (1984) 2626.
30 R. C. Willoughby and F. Poeppel, presented at the *35th Annual Conference on Mass Spectrometry and Allied Topics*, Denver, CO, USA, May 24–29, 1987, p. 289.

31 K. Vekey, D. Edwards and L. F. Zerelli, *J. Chromatogr.*, 488 (1989) 73.
32 J. Yinon, T. L. Jones and L. D. Betowski, *J. Chromatogr.*, 489 (1989) 75.
33 A. P. Bruins, T. R. Covey and J. D. Henion, *Anal. Chem.*, 59 (1987) 2642.
34 A. P. Bruins, L. O. G. Weidolf, J. D. Henion and W. L. Budde, *Anal. Chem.*, 59 (1987) 2647.
35 E. D. Lee, W. Mück, J. D. Henion and T. R. Covey, *Biomed. Environ. Mass Spectrom.*, 18 (1989) 844.
36 C. M. Whitehouse, R. N. Dreyer and J. B. Fenn, *Anal. Chem.*, 57 (1985) 675.
37 J. B. Fenn, M. Mann, C. K. Meng, S. F. Wong and C. M. Whitehouse, *Mass Spectrom. Rev.*, 9 (1990) 37.
38 R. D. Voyksner, J. T. Bursey and E. D. Pellizzari, *Anal. Chem.*, 56 (1984) 1507.
39 *Thermospray LC–MS Instruction Manual for Model 701C Edition Finnigan 4500*, Vestec, Houston, TX, 1988.
40 R. D. Voyksner and C. A. Haney, *Anal. Chem.*, 57 (1985) 991.
41 *Beilstein's Handbuch der Organischen Chemie*, Springer Verlag, Berlin, Vol. 16, 1993, pp. 168, 300, 312, 344; Vol. 16 (2), 1951, p. 53; Vol. 16 (4), 1986, p. 460. Chem. Abstr. Registry Nos. 3118-97-6; 1936-15-8; 60-11-7; 97-56-3; 6253-10-7; 2872-52-8; 3148-56-1; 842-07-9.
42 J. C. Gilland, Jr., and J. S. Lewis, *Org. Mass Spectrom.*, 9 (1974) 1148.
43 S. M. Scheifers, S. Verma and R. G. Cooks, *Anal. Chem.*, 55 (1983) 2260.
44 J. H. Bowie, G. E. Lewis and R. G. Cooks, *J. Chem. Soc.*, B, 621 (1961).
45 R. D. Voyksner, R. Straub and J. T. Keever, Research Triangle Institute, unpublished results.

Journal of Chromatography, 627 (1992) 187–191
Elsevier Science Publishers B.V., Amsterdam

CHROM. 24 598

Lithium isotope effects in water–dimethyl sulphoxide mixed-solvent ion-exchange chromatography

Takao Oi, Takuji Imai and Hidetake Kakihana

Department of Chemistry, Sophia University, 7-1 Kioicho, Chiyodaku, Tokyo 102 (Japan)

(First received June 22nd, 1992; revised manuscript received September 1st, 1992)

ABSTRACT

Cation-exchange chromatography of lithium was successfully carried out to investigate the lithium isotope effects in water–dimethyl sulphoxide (DMSO) mixed-solvent ion-exchange systems at 25°C. The value of the separation factor minus 1 (ε) was $1.4 \cdot 10^{-3}$ to $2.2 \cdot 10^{-3}$; ε had a maximum value of $2.2 \cdot 10^{-3}$ when the molar fraction of water in the solution phase, x_{water}, was about 0.57, and decreased as x_{water} deviated from this value. A consideration based on a theory of isotope distribution between two phases indicated that DMSO was slightly preferentially fractionated into the ion-exchanger phase rather than into the solution phase.

INTRODUCTION

Studies on lithium isotope separation by ion exchange are old; the first use of an ion exchanger for this purpose is found in a publication by Taylor and Urey [1] in 1937. The topic, however, still draws continuing interest, in part because of the importance of the individual stable isotopes of lithium, ^{6}Li and ^{7}Li, in nuclear science and technology. The magnitudes of lithium isotope effects observed in aqueous ion-exchange systems, especially systems with commercially available organic ion exchangers, are in general small, of the order of 10^{-3} [2], and attempts to seek systems with larger isotope effects have been made. The use of inorganic lithium-specific adsorbents [3] and a cryptand resin [4,5] is one such attempt.

A second way to realize greater lithium isotope effects may be to use mixed solvents instead of water. The lithium isotope effects observed in ion-exchange systems mostly come from the difference in solvation state of lithium ions in the solution and the ion-exchange phases [6], and hence mixed solvents may increase (or, contrary to our intention, decrease) the effects if the mixing ratios of solvent differ between the two phases.

Nandan and Gupta [7] measured the magnitude of the lithium isotope effect in the ion-exchange system with a 50:50 (v/v) solvent mixture of water and dimethyl sulphoxide (DMSO) and reported that the effect is similar to that observed in the aqueous medium. They attributed this to the lack of the solvent fractionation in water–DMSO mixtures between the solution and the ion-exchange phases [8]. In spite of their non-affirmative conclusion, we carried out ion-exchange chromatographic separation of lithium isotopes in water–DMSO mixed solvents with the expectation of obtaining large lithium isotope effects compared with that in the aqueous medium. Our expectation was based on the experimental fact that the magnitude of the Gibbs free energy change upon lithium ion transfer from water to a water–DMSO mixture is very large [9], and consequently even a slight solvent fractionation between the solution and the ion-exchange phases may result in a large change in lithium isotope effect. In this paper, we report the results of chromatographic experiments on lithium isotope separation employing

Correspondence to: T. Oi, Department of Chemistry, Sophia University, 7-1 Kioicho, Chiyodaku, Tokyo 102, Japan.

0021-9673/92/$05.00

TABLE I

EXPERIMENTAL CONDITIONS

Ion exchanger = strongly acidic Toray TIN-100 ion-exchange fibre in the H^+ form; temperature = 25.0 ± 0.2°C; Ac = acetate ion.

Parameter	Run no.				
	LiAc1	LiAc2	LiAc3	LiAc4	LiAc5
Water/DMSO mixing ratio (v/v)	100:0	50:50	25:75	5:95	5:95
Ion-exchanger bed height (cm)	203.0	195.2	206.0	203.2	184.1
Operating manner	Band	Band	Band	Band	Breakthrough
Band length (cm)	48.0	50.1	37.2	40.2	–
Lithium acetate concentration in feed (mol/dm^3)	0.100	0.100	0.097	0.096	0.098
Potassium acetate concentration in eluent (mol/dm^3)	0.108	0.110	0.099	0.097	–
Flow-rate (cm^3/cm^{2}h)	12.61	6.02	6.18	1.85	12.64
Band velocity (cm/h)	2.75	1.06	1.30	0.34	1.85

lithium acetate (LiAc) as lithium salt and performed in water–DMSO mixed solvent media at 25°C.

EXPERIMENTAL

Reagents

The ion exchanger used was a highly efficient, cylindrical strongly acidic cation exchange fibre, Toray TIN-100, reinforced with polyethylene and manufactured by Toray. Its average size is 0.5 mm × 50 μm I.D. and its exchange group is the sulpho group. All the reagents used were of analytical-reagent grade and were used without further purification. Distilled water was used in every experiment.

Chromatographic process

Five chromatographic experiments were carried out; four operated in a band displacement manner and one in a breakthrough manner. Their experimental conditions are summarized in Table I. The mixing ratio of water and DMSO was varied from 100:0 to 5:95 (v/v). A Pyrex glass column of 210 cm × 1 cm I.D. with a water jacket was used as the separation column in each experiment, so that the exchanger bed height was *ca.* 200 cm.

In a band displacement chromatographic experiment, the ion exchanger packed in the column was first conditioned to the H^+ form in the usual manner by using a water–DMSO solution as solvent. A lithium feed solution (lithium acetate solution) was then fed to the column at a constant flow-rate to form a lithium adsorption band with an appropriate length. This band was eluted by an eluent containing potassium as the displacement ion for lithium ion. The effluent from the bottom of the column was collected and divided into small fractions (10 cm^3). The temperature of the column was kept constant at 25.0 ± 0.2°C throughout the experiment by passing temperature-controlled water through the water jacket.

The breakthrough experiment designed to examine the reproducibility of the lithium isotope effect in our experiments was performed in the usual way.

Analysis

The lithium and potassium concentrations in each fraction of the effluents were determined flame photometrically with a Daini Seikosha Model SAS-727 atomic absorption spectrometer.

For the feed solution and selected fractions of the effluent of each experiment, the $^7Li/^6Li$ isotopic ratio was measured, the procedure for which was the same as that in the previous paper [2] except for one point: when necessary, DMSO was separated from lithium by heating at about 150°C after the chemical form of lithium was converted from lithium acetate to lithium hydroxide. The lithium isotopic ratio measurements were performed with a double-filament thermal ionization technique on a Varian MAT CH-5 mass spectrometer. The relative standard deviation of a measurement was typically 0.1%.

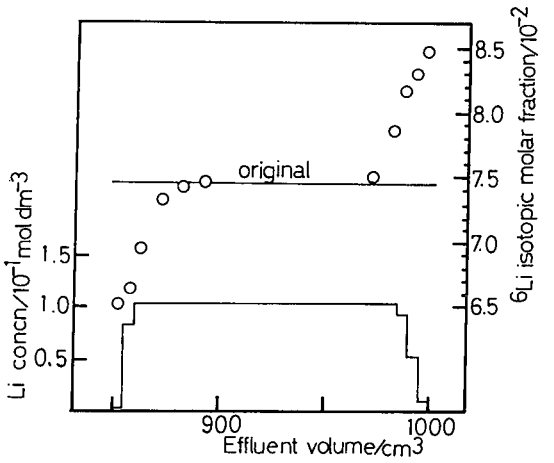

Fig. 1. Chromatogram and ^{6}Li isotopic molar fractions in run LiAc2. Experimental conditions are summarized in Table I. The solid step-like line denotes the total lithium concentration, the open circles the ^{6}Li isotopic molar fractions and the "original" line that in the feed solution. The ^{6}Li isotopic molar fraction in the feed was 0.07451.

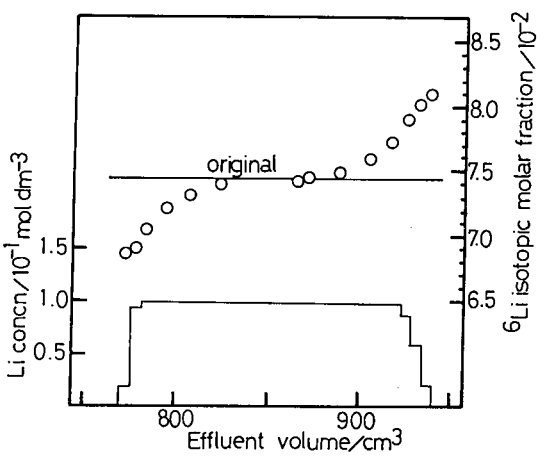

Fig. 2. Chromatogram and ^{6}Li isotopic molar fractions in run LiAc3. Experimental conditions are summarized in Table I. The solid step-like line denotes the total lithium concentration, the open circles the ^{6}Li isotopic molar fractions and the "original" line that in the feed solution. The ^{6}Li isotopic molar fraction in the feed was 0.07441.

RESULTS AND DISCUSSION

Examples of chromatograms and ^{6}Li isotopic molar fractions obtained are shown in Figs. 1 and 2. Fig. 1 presents the analytical results of run LiAc2 and Fig. 2 those of run LiAc3. In each figure, the solid step-like line represents the lithium concentration profile, the open circles the ^{6}Li isotopic molar fractions and the "original" line that of the feed solution. The chromatograms have satisfactorily sharp boundaries at both their ends, as is seen in the figures, and the band widths were virtually unchanged during the chromatographic operation. Thus, band displacement chromatography was realized in runs LiAc2 and LiAc3. Like the chromatogram of LiAc1 with the aqueous solvent, even that of LiAc4 with the 5:95 (v/v) water–DMSO mixed solvent had fairly sharp boundaries at both its ends, showing the realization of band displacement chromatography.

In order to compare the magnitudes of the lithium isotope effect observed in the present experiments, the single-stage separation factor, S ($= 1 + \varepsilon$), for the $^{7}Li/^{6}Li$ isotopic pair was calculated. S is defined as:

$$S = ([^{7}Li]/[^{6}Li])/(\overline{[^{7}Li]}/\overline{[^{6}Li]})$$

where [A] and $\overline{[A]}$ denote the concentrations of isotope A in the external solution phase and in the ion-exchange phase, respectively. The ε value is calculable with experimentally determinable quantities by using the equation [10]

$$\varepsilon = \sum [\,|\,R_i - R_0\,|\,f_i]/[R_0(1 - R_0)Q]$$

The meanings of the symbols in the above equation are the same as those in the previous paper [2]. The ε values thus calculated are listed in Table II, together with the previous data [2,7]. All the values are of the order of 10^{-3}. The ε values of runs LiAc1, LiAc2 and LiAc3 are the averages of the ε values calculated by using the data in the front and rear parts of the chromatograms, while those of runs LiAc4 and LiAc5 are obtained only from the data in the front parts. The ε values of runs LiAc4 and LiAc5 are the same within experimental errors, and so are those of LiAc1 and Li09 in the previous paper [2], both suggesting satisfactorily high reproducibility of our chromatographic experiments.

In Fig. 3, ε is plotted against the molar fraction of water, x_{water}, in the water–DMSO mixed solvent in the solution phase. As can be seen, ε has a maximum at around $x_{water} = 0.57$ (volume ratio of water to DMSO = 25:75) and decreases as x_{water} deviates from this value in either direction.

TABLE II

PREVIOUS AND NEW ε VALUES IN LITHIUM ACETATE SYSTEMS WITH WATER–DMSO MIXED SOLVENTS AT 25°C

Run no.	Water/DMSO ratio (v/v)	Ion exchanger	Lithium acetate concentration (mol/dm^3)	ε ($\times 10^{-3}$)	Ref.
LiAc1	100:0	Toray TIN-100	0.1	1.7	This work
Li05	100:0	Toray TIN-100	0.1	1.6	2
Li09	100:0	Asahi LS-6	0.1	1.0	2
	100:0	Dowex 50W-X8	0.2 (?)	1.3	7
LiAc2	50:50	Toray TIN-100	0.1	2.0	This work
	50:50	Dowex 50W-X8	0.2	1.5	7
LiAc3	25:75	Toray TIN-100	0.1	2.2	This work
LiAc4	5:95	Toray TIN-100	0.1	1.4	This work
LiAc5	5:95	Toray TIN-100	0.1	1.5	This work

In ion-exchange systems of the alkali metals, the overall isotope effect, which is the one experimentally obtained, is in general composed of four fundamental isotope effects, *i.e.* the one arising from phase change, a second originating from solvation state change, and the third and fourth effects accompanying complex formations (including ion associations) in the solution phase and in the ion-exchanger phase, respectively [11]. Since (1) no complex formation is expected to occur in the ion-exchanger phase in the present systems, (2) no appreciable lithium isotope effect accompanying complex formation between lithium ion and acetate ion in the solution phase was observed in an aqueous medium [2] and a similar situation is expected to hold in water–DMSO mixture media, and (3) the fundamental lithium isotope effect owing to phase change is generally considered to be small, the change in ε value observed in Fig. 3 must mostly come from the change in the solvation state of the lithium ion between the two phases. Based on a theory of isotope distribution between two phases [12], ln S can then be approximated as:

$$\ln S \simeq \ln f_{Li} - \ln g_{Li}$$

where f_{Li} and g_{Li} are the isotopic reduced partition function ratios [13] of the solvated lithium ion in the solution phase and in the ion-exchange phase, respectively. $f_{Li} > g_{Li}$ because $S > 1$, that is lithium ions are more strongly solvated in the solution phase than in the ion-exchange phase. Cations are more strongly solvated in DMSO than in water,

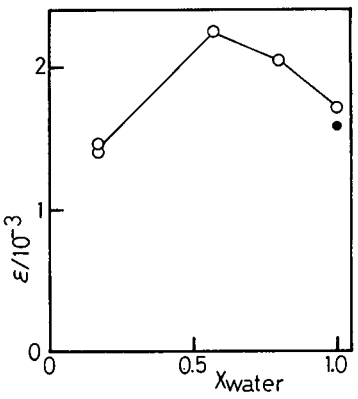

Fig. 3. The plot of ε (= S − 1) against molar fraction of water in the solution phase (x_{water}). (○) Present work; (●) from ref. 2.

and consequently the present results of the change in ε value indicate that DMSO is slightly more preferentially fractionated into the solution phase than water and that the degree of solvent fractionation is largest at around $x_{water} = 0.57$.

Although Van Wart and Janauer [8] reported that in the ion-exchange systems of the Bio-Rad 50W-X8 resin in the Li^+ form with water–DMSO mixed solvent media, water is very slightly more preferentially distributed into the solution phase than into the ion-exchanger phase at 25°C, their results do not necessarily contradict ours. Firstly, we are dealing with different ion exchangers; they showed that even a change in the degree of cross-linking of the resin affects the solvent fractionation.

Secondly, in our chromatographic experiments, the ion exchanger in the lithium adsorption bands was not entirely in the Li^+ form but more or less in the mixed form of Li^+ and H^+, while their experiments were carried out with the resin in the complete Li^+ form, and with the Bio-Rad 50W-X12 resin in the H^+ form DMSO is slightly preferentially distributed into the solution phase for $x_{water} > 0.5$ [8]. Experimental errors involved in the determinations of DMSO and water [14] should also be pointed out. In any case, very accurate determination of DSMO and water in the two phases will be needed to clarify the correlation of the magnitude of the lithium isotope effect with the degree of solvent fractionation in the ion-exchange systems with water–DMSO mixed solvents.

The water–DMSO mixed solvent increased the ε value for the lithium isotopes, as is seen above. However, even the enhanced ε value is still much smaller than those obtained in the systems with a cryptand [4,5] and with lithium-specific adsorbents [3], and a continuing effort has to be made to search for mixed solvent systems with much larger lithium isotope effects.

CONCLUSION

The major findings of the present study are as follows.

(1) The ε values obtained were between $1.4 \cdot 10^{-3}$ and $2.2 \cdot 10^{-3}$ at 25°C.

(2) ε has its maximum value when the molar fraction of water in the solution phase, x_{water}, is about 0.57 and decreases as x_{water} deviates from this value.

(3) It was inferred that there is a slight solvent fractionation between the solution and the ion-exchange phases, and DMSO slightly prefers the latter to the former.

ACKNOWLEDGEMENTS

We would like to acknowledge Professor M. Okamoto of the Tokyo Institute of Technology (TIT) for offering the use of the mass spectrometer and Dr. M. Nomura of TIT for his assistance in lithium isotopic ratio measurements.

REFERENCES

1 T. I. Taylor and H. C. Urey, *J. Chem. Phys.*, 5 (1937) 597.
2 See, for instance, T. Oi, K. Kawada, M. Hosoe, and H. Kakihana, *Sep. Sci. Technol.*, 26 (1991) 1353.
3 T. Oi, H. Ogino, N. Izawa, H. Kakihana, K. Ooi, Y. Miyai and S. Katoh, in M. Abe, T. Kataoka and T. Suzuki (Editors), *New Development in Ion Exchange*, Kodansha, Tokyo, 1991, pp. 613–618.
4 S. Fujine, K. Saito, and K. Shiba, *J. Nucl. Sci. Technol.*, 20 (1983) 439.
5 K. Nishizawa and H. Watanabe, *J. Nucl. Sci. Technol.*, 23 (1986) 843.
6 D. A. Lee and G. M. Begun, *J. Am. Chem. Soc.*, 81 (1959) 2332.
7 D. Nandan and A. R. Gupta, *Ind. J. Chem.*, 16A (1978) 256.
8 H. E. Van Wart and G. E. Janauer, *J. Phys. Chem.*, 78 (1974) 411.
9 A. K. Das and K. K. Kundu, *J. Chem. Soc., Faraday Trans. 1*, 70 (1974) 1452.
10 H. Kakihana and T. Kanzaki, *Bull. Tokyo Inst. Technol.*, 90 (1969) 77.
11 K. Kawada, T. Oi, M. Hosoe and H. Kakihana, *J. Chromatogr.*, 538 (1991) 355.
12 H. Kakihana and M. Aida, *Bull. Tokyo Inst. Technol.*, 116 (1973) 39.
13 J. Bigeleisen and M. G. Mayer, *J. Chem. Phys.*, 15 (1947) 261.
14 G. E. Janauer, H. E. van Wart and J. T. Carrano, *Anal. Chem.*, 42 (1970) 215.

Journal of Chromatography, 627 (1992) 193–201
Elsevier Science Publishers B.V., Amsterdam

CHROM. 24 578

Quantitative comparisons of reaction products using gas chromatography–mass spectrometry and dual-isotope techniques

Lawrence C. Thomas, John A. Edwards and Kathleen M. Fiehrer

Department of Chemistry, Seattle University, Seattle, WA 98122 (USA)

(First received May 14th, 1992; revised manuscript received August 21st, 1992)

ABSTRACT

Special dual-isotope methods for GC–MS measurements show response relations necessary for quantitative comparisons of reaction product abundances, even for multiple-pathway reaction systems. The quantitative comparisons are compatible with the use of isotopically labeled reference substances generated by reference reactions, for which suites of reaction products may be compared via compounds common to both reference and sample reaction systems. The results of comparisons studied are fairly insensitive to large variations in relative concentrations and to high uncertainties in individual analyte measurements. Moreover, the approach may, for some circumstances, be used for analytes of unknown identities or with reference compounds of unknown concentrations. The dual-isotope GC–MS methods described are suitable for photolysis reactions and should be especially helpful in toxicologic metabolism comparisons, environmental degradation studies or other kinetic systems.

INTRODUCTION

GS–MS measurements are especially helpful in experiments involving many analytes, partly because GC–MS can provide excellent selectivity and high sensitivity. Resulting low limits of detection and freedom from many interferences can thus make GC–MS procedures powerful quantitative methods. The use of GC–MS for complicated analyses is well established, and a variety of versatile commercial instruments are available. However, several factors plague GC–MS procedures for analyte measurements from complex sample matrices, predominantly in pretreatment steps [1]. Variations in extraction efficiencies and variable losses during solvent volume reductions can be partially compensated by traditional recovery standard and internal standard techniques [2], sometimes using added compounds which are isotopically labeled but otherwise identical to target analytes [3,4]. Consequently, those techniques require both availability and careful characterization of appropriate reference materials for *every* measured component. However, for complex systems such as studies of metabolisms or environmental exposures several reaction product analytes may be measured for each sample, which exacerbates difficulties associated with use of traditional methods, especially if pure reference materials are not available for every analyte. Moreover, identities of the reaction product analytes are not always known, which precludes use of conventional internal or external standard methods.

Analyses using added isotopically labeled substances can be very powerful for quantitative measurements and comparisons [3–9]. Use of two or more radioactive isotopes is not uncommon and exploits the great selectivities and sensitivities of ra-

Correspondence to: L. C. Thomas, Department of Chemistry, Seattle University, Seattle, WA 98122, USA.

0021-9673/92/$05.00

dioactivity measurements. However, potential health hazards and regulations make alternatives to use of radiolabeled materials attractive. Consequently, isotope selective methods which use non-radioactive substances, *e.g.* MS or atomic emission, are attractive options to radiometric procedures if appropriate isotope selectivities with sufficient corresponding sensitivities can be attained.

Dual-isotope methods with MS of equilibrated mixtures of target analytes with appropriate isotopically labeled compounds have been used for many years for accurate analyses [4]. Approaches which mimic isotope dilution and use GC–MS have gained general acceptance for use in important environmental analyses [3]. For those procedures an isotopically labeled form of each target analyte is added to samples before pretreatment and the two forms of each analyte thereby undergo essentially identical effects during sample preparation. Subsamples are then analyzed by GC–MS using accepted procedures, with each analyte and its isotopically labeled form being measured via their respective characteristic m/z values. However, the good selectivity and sensitivity of GC–MS is sometimes not sufficient to allow for reliable measurements via those approaches, partly due to variations in ionization efficiencies in the MS source, perhaps from variable source pressures or coeluting interfering compounds. Ensuring coelution of both forms of each analyte can partially remedy effects of varying ionization efficiencies [10], even those caused by interfering compounds or variable source pressures.

We have developed dual-label radiometric methods for measurements via chromatography, exploiting the good selectivity and high sensitivity fo radioactivity measurements [4–9]. In previous work, compounds labeled with two different radioactive isotopes were used with HPLC for special dual-label procedures which mimic multiple internal standard methods. In those studies biologically generated radiolabeled reference solutions were used and their components separated along with differently labeled respective coeluting reaction products from samples from reaction experiments. One method employs a homogeneous reference solution of multiple radiolabeled reaction products, generated by a reference reaction system, as a mixed internal standard reference solution [5,6,8]. A known amount of the reference solution is added to each experimental sample containing corresponding differently labeled reaction products before sample preparation, but after investigated reactions have taken place. This procedure may be used to quantitatively compare reaction product profiles and to test for differences between control *versus* test groups in reaction efficacy, *e.g.*, in metabolism or environmental degradation experiments.

The dual-label approach described above allows for compensation for variations in extraction efficiencies, variable losses during volume reduction of extracts, imprecisions of volume measurements and uncertainties in specific activities of reactant compounds and reaction products. The procedures may greatly obviate difficulties caused by unavailability of pure reference compounds. Also, the method yields great improvements in data quality for quantitative measurements [8]. Moreover, theoretically valid comparisons which may be tested statistically are allowed via these methods and show dramatic increases in quality of results *versus* conventional procedures [8,9]. The dual-label techniques are powerful for comparing reaction efficiencies for multiple-pathway reactions [6,8] and for assessing complications caused by impurities or isotope effects [7,9].

Dual-isotope GC–MS procedures reported in this study show advantages of the dual-label radiometric method described above, but avoid use of radioactive materials.

THEORY

A main advantage of the dual-isotope procedures for GC–MS measurements described below is that several special ratios may yield well defined, theoretically predictable results which could be tested statistically [6–9]. Herein we call normal-isotope-composition compounds "Y-labeled compounds".

Dual-isotope reaction product determination

In the absence of pure standards, a fixed known volume, V_a, of a homogeneous internal standard solution generated by a reference reaction system which contains several isotopically labeled reference compounds could be used in place of a conventional standard solution made by mixing known quantities of pure labeled substances [5,6,8]. One may add these X-labeled reference compounds to

subsamples of mixtures of normal isotopic composition, *i.e.* Y-labeled compounds, of unknown concentrations which have been generated from reactions being investigated. By judicious selection, some of the X-labeled components would be chemically identical to the Y-labeled components, except for their respective molecular weights. Hence, pretreatments of the mixtures should yield equivalent extraction/concentration/dilution efficiencies, E_i, for the two extractable forms of each common component; thus, if V_t is the volume of the prepared subsample, and V_{ss} is the reproducible volume of the prepared subsample used for chromatographic separation, then $E_{Y,i} = A_{X,i}V_t(A_{s,X,i}V_{ss})^{-1} = E_{X,i}$, where $A_{X,i}$ and $A_{s,X,i}$ are measured GC–MS areas for the X-labeled component i for samples from the volumes V_{ss} and V_a, respectively. This equivalence is a reasonable assumption when isotope exchange is negligible, and the two forms are chemically alike and are not entrapped or bound in tissue or precipitates.

This method is similar to use of several isotopically labeled internal standards using conventional internal standard calculations. Consequently, the amount of each normal-isotopic-composition component from the sample could be determined by using that subsample component's integrated MS ion current data from the dual-isotope chromatograms, $A_{X,i}$ and $A_{Y,i}$, and the X-label areas for a sample from volume V_a for the reference solution, $A_{s,X,i}$. These quantitative determinations may be useful but are subject to several uncertainties and restrictions which could be avoided by use of the powerful *R* and *U* ratio methods discussed below.

Single-component comparisons between experiments using the R-ratio

In many experminents the absolute amounts of analytes are often less important than their relative concentrations between experiments, *e.g.* in comparisons of metabolism in control *versus* test organisms [5,6]. Such comparisons may be suitable for use of multiple internal standards generated by a reference reaction system and the dual-isotope procedures described herein.

One can expose two sets of reactions, 1 *versus* 2, to the same homogeneous dosage of normal isotopic composition Y-labeled compound, add volume V_a of *X*-labeled reference solution to each resulting sample, and then pretreat and separate each, with GC–MS measurements of eluates. If $V_{a,1} = V_{a,2}$, then $A_{s,X,1} = A_{s,X,2}$. Moreover, if $V_{t,1} = V_{t,2}$ and $V_{ss,1} = V_{ss,2}$ by design, and M is the mass of selected analyte in the indicated subsample, then

$$R_{12} = (M_1/M_2) = (A_{Y,1}A_{X,2})\,(A_{Y,2}A_{X,1})^{-1} \quad (1)$$

for the component of interest, and this R ratio may be calculated from GC–MS area data only.

If reaction efficacy were hypothesized to be not different between two groups, *e.g.* control *versus* test groups, then $R_{12} = 1$ if this null hypothesis is valid and replicated R_{12} values could be tested statistically to ascertain if R_{12} were different from unity for the specified component of interest, *e.g.* if the compound reacts differently in the compared systems.

Multiple-component comparisons using the U ratio

If the procedure used for the R ratio above is extended to several reaction products, then the resulting multi-parametric method could be used to characterize several reaction pathways. Thus, relative magnitudes of several intra-sample parameters may be tested and yield results which are more important than their absolute magnitudes or individual single-component comparisons between groups. For those comparisons, an extension of the R ratio method can be formulated for groups 1 *versus* 2 and components i *versus* j such that

$$U_{12} = (R_{12,i}/R_{12,j}) = (A_{Y,i,1}A_{X,j,1}A_{Y,j,2}A_{X,i,2})\,(A_{Y,j,1}A_{X,i,1}A_{Y,i,2}A_{X,j,2})^{-1} \quad (2)$$

where X and Y represent the measured forms, subscripts i and j indicate the two components of interest, the subscripts 1 and 2 indicate samples from which the components were isolated and A indicates measured GC–MS areas. If the reaction product profile for both groups were the same, then $U_{12} = 1$. This U ratio may be tested statistically, and the null hypothesis of identical relative reaction rates for those components could be assumed unless U_{12} is shown to be significantly different from unity.

Of course, by comparing several components, i, j, k, l..., one might evaluate reaction product profiles representing several modes, *e.g.* several metabolism pathways.

EXPERIMENTAL

Reagents

All organic solvents used were Mallinkrodt ChomAR grade. Anthracene and decadeuteroanthracene were purchased from Aldrich, both at > 99% purity. Helium carrier gas was > 99.9999% pure.

Apparatus

A Hewlett-Packard Model 5971A mass-selective detector interfaced to a Hewlett-Packard Model 5890 Series II gas chromatograph was used, controlled and monitored by a Hewlett-Packard Model QS-20 Vectra computer. Helium carrier gas was used with a pressure of 15 kPa in the split–splitless inlet, yielding a carrier gas flow-rate of 1.0 ml/min at 25°C. Splitless mode was used for all injections and elutions. Injections of 1.0 μl were used unless otherwise stated.

The GC column used was a 12 m × 0.2 mm I.D.

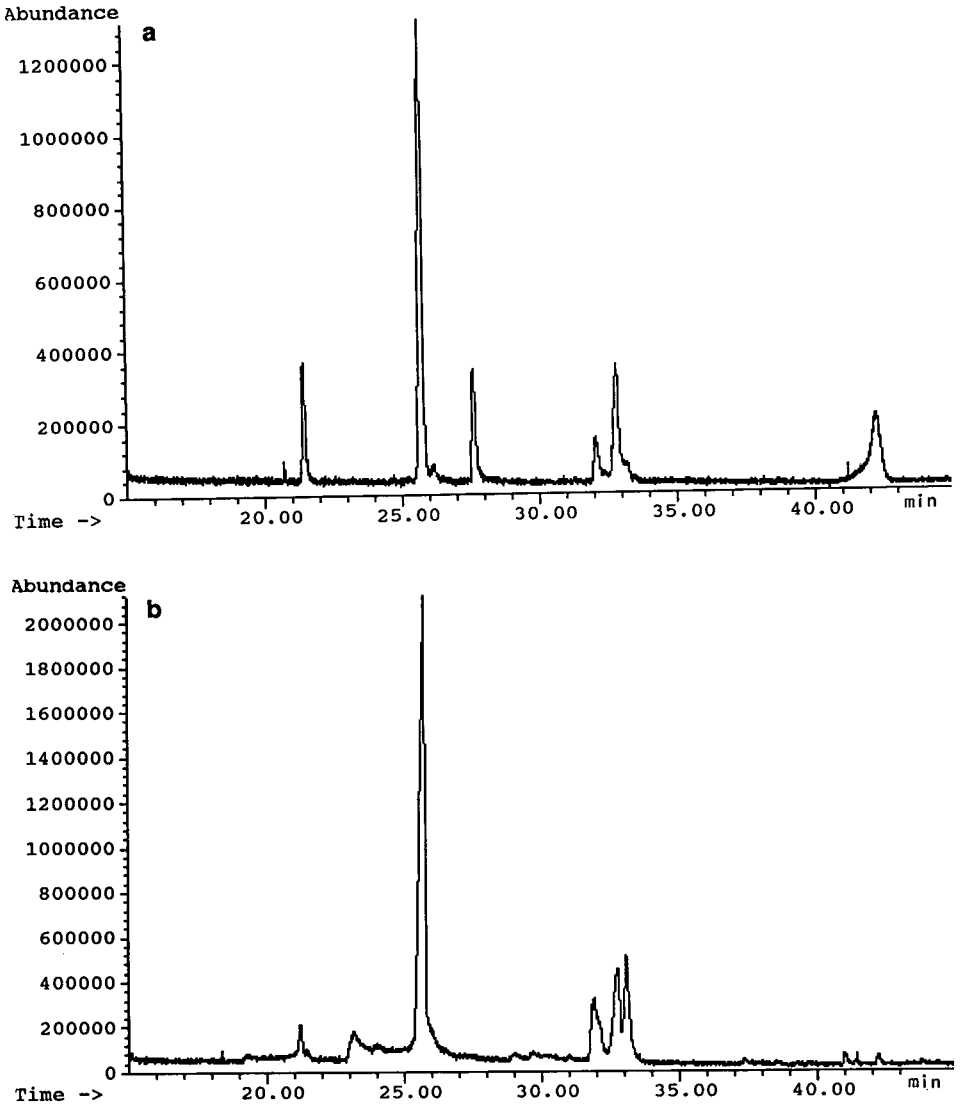

Fig. 1. Total ion chromatograms for 1-μl subsamples of (a) photolyzed methanolic anthracene and (b) photolyzed methanolic [$^2H_{10}$]anthracene.

fused-silica capillary column with a 0.33-μm-thick cross-linked methyl silicone stationary phase.

Procedure

Separate saturated mixtures, with excess solid substance, were made by mixing 10.0 ml of methanol and 10^{-4} mol of either anthracene or [$^2H_{10}$]anthracene. Both of these mixtures were exposed to sunlight, through window glass, for 35 days and then maintained at 4°C in darkness until use. The methanolic solutions above the remaining crystals were mixed, 100 μl of [$^2H_{10}$]anthracenic solution

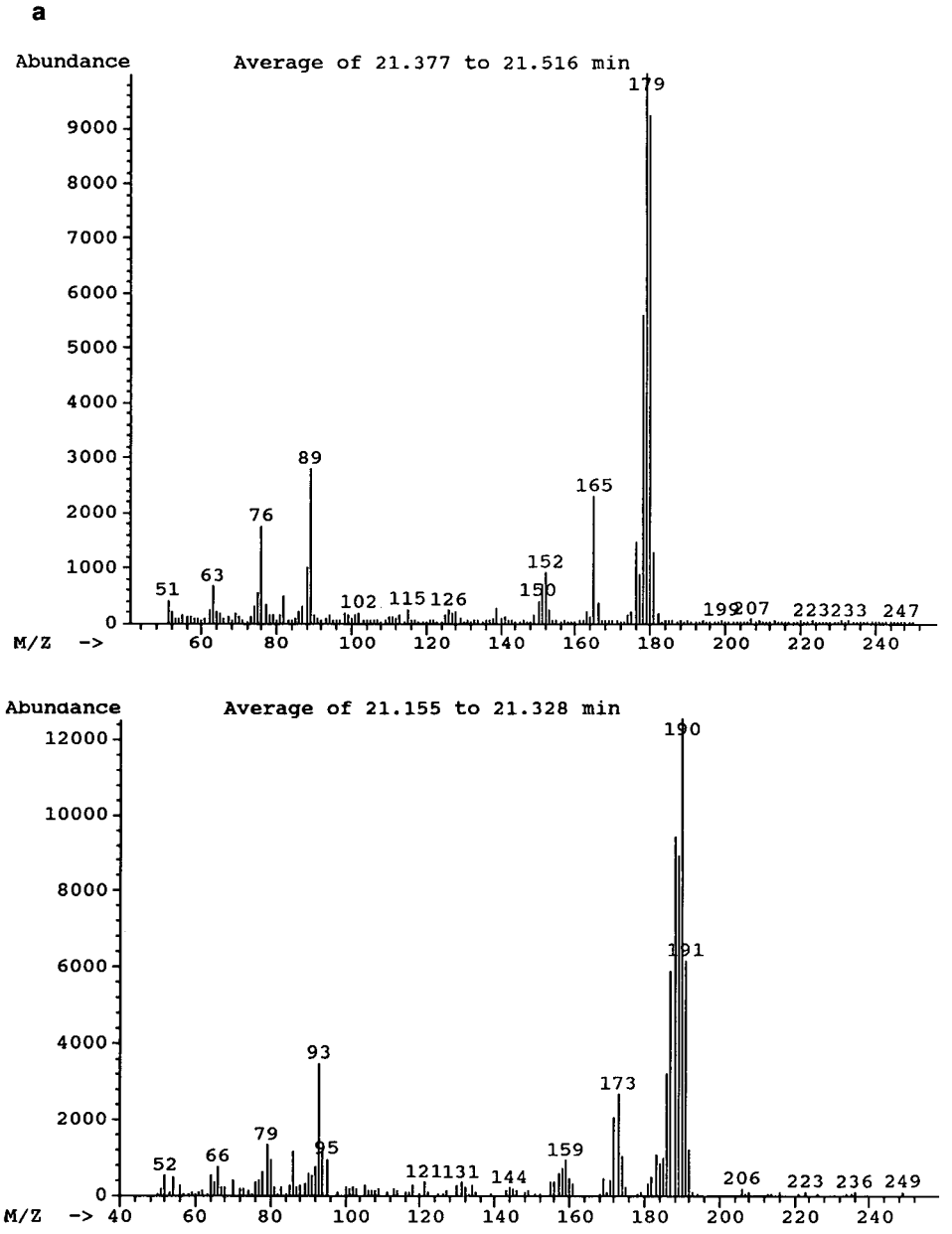

Fig. 2.

(Continued on p. 198)

plus 5–1000 μl of anthracenic solution and diluted to 1.50 ml with methanol. Actual concentrations of constituents were thus unknown, other than the saturation of the anthracenes. Triplicate dilutions were made for all relative concentrations.

Triplicate subsamples for all dilutions of the methanolic reactants and their photolysis products were analyzed by GC–MS. Subsamples of 1 μl were injected into the 325°C injector, in the splitless mode, with the oven temperature at 60°C. The 60°C initial temperature was maintained for 5 min, then raised to 120°C at 10°C/min, held at 120°C for 2 min, raised to 160°C at 2°C/min, held at 160°C for 2 min, raised to 250°C at 5°C/min and maintained at

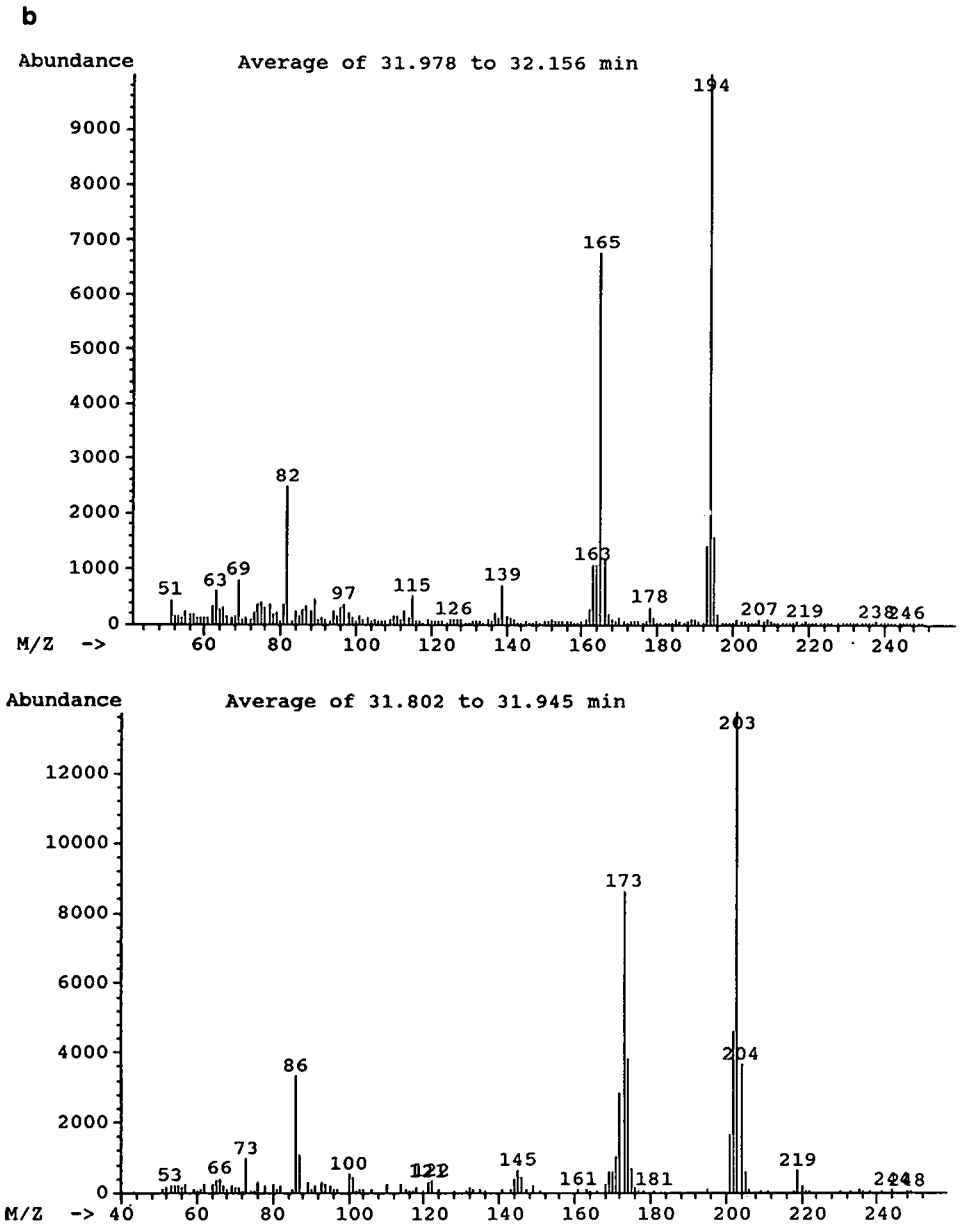

250°C for 2 min. The GC–MS transfer line was isothermal at 285°C.

Eluates were measured by selected ion detection (SID) unless stated otherwise. Between retention times of 15 and 30 min, ions at *m/z* 178, 180, 188, 190, 208 and 216 were monitored every 0.81 s with 100-ms measurement times for each. Between retention times of 30 min and 45 min, ions at *m/z* 194, 202, 203, 208, 216 and 217 were monitored every 0.69 s with 100-ms measurement times for each. For

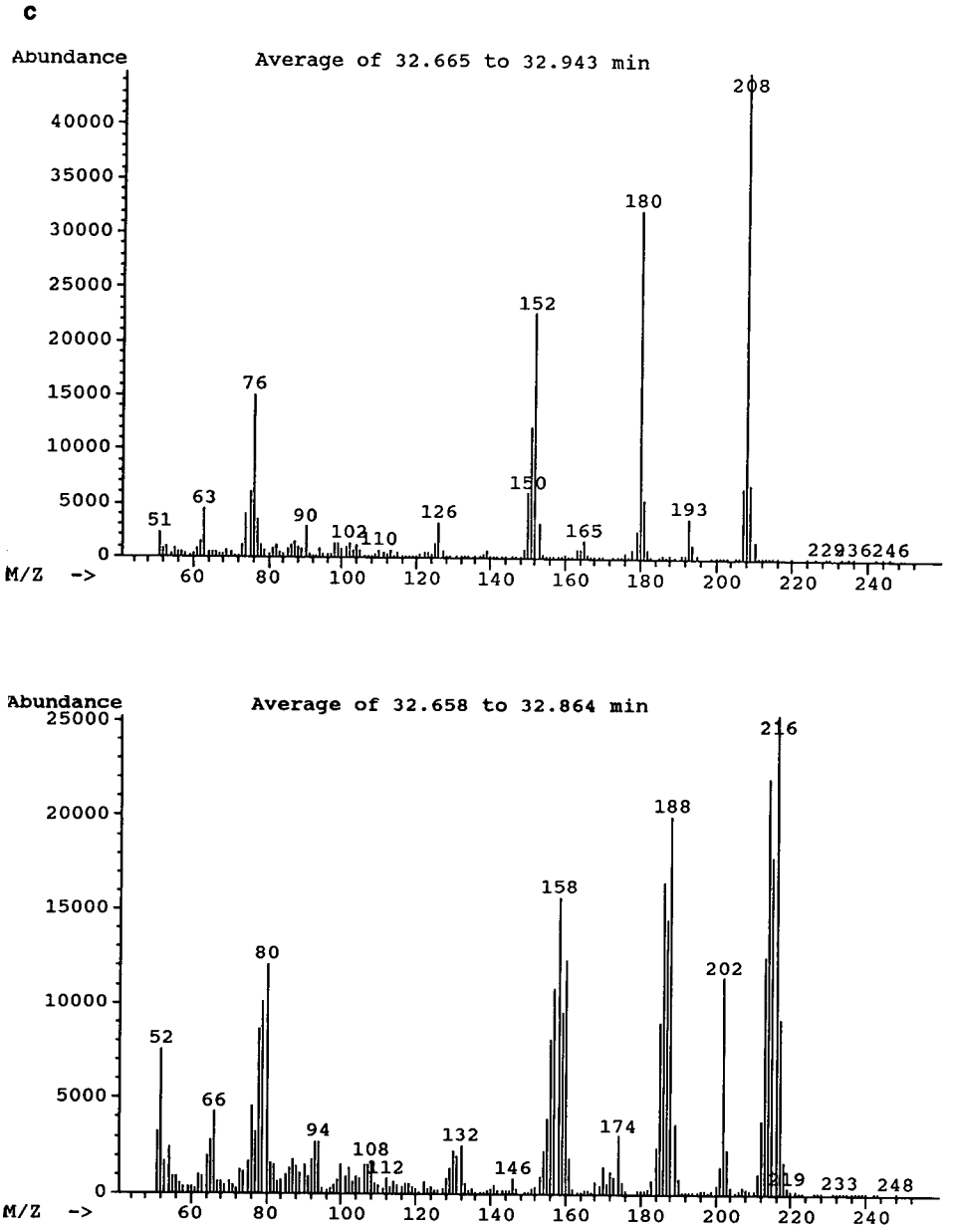

Fig. 2. Mass spectra for tentatively identified anthracene products and corresponding [$^2H_{10}$]anthracene products, derived from GC–MS measurement of mixed solutions of anthracene, decadeuteroanthracene and their photolysis products in methanolic mixtures: (a) likely 9,10-dihydroanthracenes, (b) possibly 9-anthracenones, and (c) likely anthraquinones.

eluate measurements using m/z scanning, detector currents for m/z values between 50 and 250 were measured at a rate of 2.4 scans/s between retention times of 15 and 45 min. Total ion chromatograms (TIC) and selected ion chromatograms were produced and integrated via provided algorithms, and statistical calculations were made by conventional techniques.

RESULTS AND DISCUSSION

Subsamples of the separate methanolic anthracene or [$^2H_{10}$]anthracene mixtures and their respective photolysis products were separated via GC–MS with m/z scanning (Fig. 1) The anthracene and its photolysis products showed several TIC peaks similar to peaks corresponding to [$^2H_{10}$]anthracene and its products. Mass spectra for anthracene (M.W. = 178 u) eluting at 25.7 min and for decadeuteroanthracene (M.W. = 188 u) eluting at 25.7 min were adequate to identify those eluates.

Mass spectra (Fig. 2) for the anthracene product eluting at 21.4 min were like reference spectra for 9,10-dihydroanthracene (M.W. = 180 u), and the [$^2H_{10}$]anthracene product eluting at 21.3 min showed mass spectra like that for 9,10-dihydroanthracene but displaced 10 m/z units, consistent with its being 9H,9^{2}H,10H,10^{2}H-dihydrodecadeute-

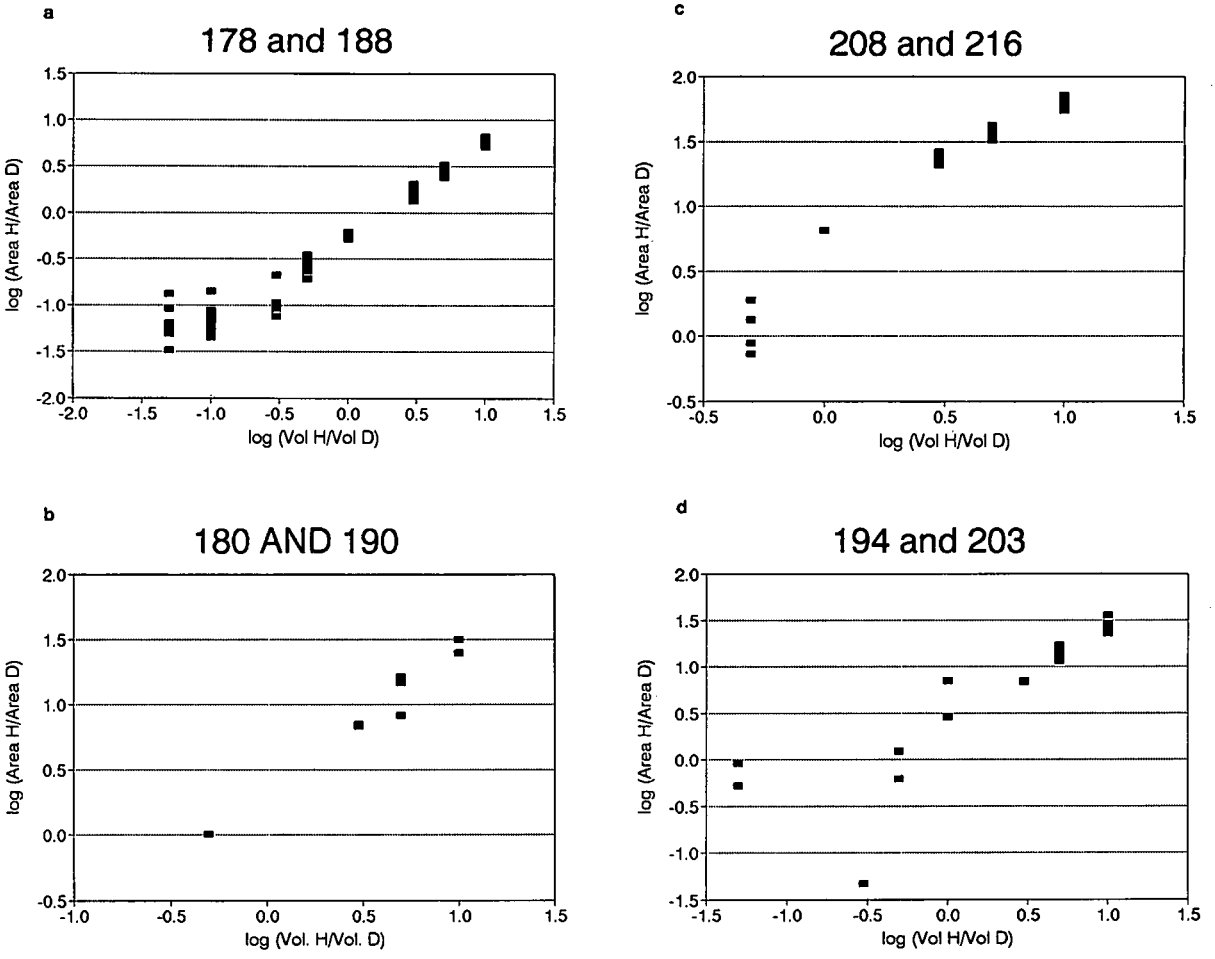

Fig. 3. Relative GC–MS response relations, log(area H/area D) *versus* log(volume H/volume D), with concentration of deuterated species constant for selected eluates including (a) anthracenes, (b) likely 9,10-dihydroanthracenes, (c) likely anthraquinones and (d) possibly 9-anthracenones.

roanthracene (M.W. = 190 u). Similarly, an eluate at 32.8 min showed mass spectra like 9,10-anthracenedione (M.W. = 208 u) (anthraquinone) with the corresponding octadeuteroanthraquinone (M.W. = 216 u) eluting at 32.6 min. Another eluate, at 31.9 min, was tentatively identified as 9-anthracenone (M.W. = 194 u) with its corresponding 9-[$^2H_9$]anthracenone (M.W. = 203 u) eluting at 31.8 min. Derivations could be done for improved identifications but may not be required for dual-isotope comparisons discussed herein. Other photolysis product eluates were present, but significant peak overlaps and low ion currents precluded confident accumulations of mass spectra for them, and corresponding SID measurements for them were inconclusive.

All four selected eluate pairs showed constant relative sensitivities, *i.e.* linear relative response *versus* relative concentration relations: linear log/log relations with slope = 1, over nearly three orders of magnitude of relative concentrations (see Fig. 3). All were calculated relative to responses from eluates from the reproduced 100 μl of [$^2H_{10}$]anthracenic photolysis product solution diluted to 1.50 ml with methanol and anthracene product solution, with none of the concentrations known. Consequently, the respective measured deuterated eluates derived from the [$^2H_{10}$]anthracene reference reaction system may serve as appropriate internal standards for calculations of relative concentrations, as described above for R and U ratios.

Uncertainties in easily measured relative responses for specified relative concentrations typically varied between 6% (R.S.D.) and 12% (R.S.D.), but became greater at low concentrations of anthracenic substances near the limits of reliable measurement, as expected. Corresponding expected uncertainties for R ratios would approximate 10–15% (R.S.D.) and for U ratios approximately 15–25% (R.S.D.). Consequently, for relative responses which can be measured with typical reasonable precisions, *e.g.* ± 5–10% R.S.D., products formed in reactions may be compared with good reliability without determining their actual concentrations, sometimes without their identifications, via use of appropriate isotopically labeled substances generated by a reference reaction.

Use of the dual-isotope GC–MS procedures discussed above have potential for dramatically improving statistical comparisons between reaction product profiles in experiments. This is mainly due to the theoretically valid predictability for the R and U ratios, *i.e.* $R = 1$ or $U = 1$ for the null hypothesis. Also, because the reproducibly added reference substances may be used as internal standards, contributions due to uncertainties in recoveries, volume measurements, etc. can be compensated, resulting in the small standard deviations for corresponding R and U ratios, as indicated above.

ACKNOWLEDGEMENT

We thank the Petroleum Research Foundation for support of this work via Grant PRF 25307-B5.

REFERENCES

1 W. D. MacLeod, Jr., A. J. Friedman and D. W. Brown, *Mar. Environ. Res.*, 26 (1988) 209.
2 W. D. MacLeod, Jr., P. G. Prohaska, D. D. Genero and D. W. Brown, *Anal. Chem.*, 54 (1982) 386.
3 *Method 1624 and Method 1625*, US Environmental Protection Agency, Washington, DC, 1988.
4 A. V. Grosse, S. G. Hindin and A. D. Kirshenbaum, *Anal. Chem.*, 21 (1949) 386.
5 L. C. Thomas, W. D. MacLeod and D. C. Malins, *Publication No. 519*, National Bureau of Standards, Gaithersburg, MD, 1979, p. 79.
6 L. C. Thomas and T. L. Ramus, *Anal. Chim. Acta*, 154 (1983) 143.
7 L. C. Thomas and T. L. Ramus, *Anal. Lett.*, 17 (1984) 2001.
8 L. C. Thomas and C. L. Wood, *J. Chromatogr.*, 522 (1990) 117.
9 L. C. Thomas, *Talanta*, 39 (1992) 599.
10 L. C. Thomas and W. Weichman, *J. Chromatogr.*, 587 (1991) 255.

Journal of Chromatography, 627 (1992) 203–217
Elsevier Science Publishers B.V., Amsterdam

CHROM. 24 507

Programmed-temperature gas chromatography

Comparative study of retention temperatures on four unequally polar stationary phases

J. A. García Domínguez and J. M. Santiuste

Instituto de Química Física "Rocasolano", CSIC, C/Serrano 119, 28006 Madrid (Spain)

(Received April 27th, 1992)

ABSTRACT

Retention temperatures (T_R) of a series of solutes on four packed columns coated with OV-105, PS-255, di-*n*-decyl phthalate and OV-275 were measured at different programming rates and compared with other T_R values calculated by some current equations, confirming that the equations of Curvers *et al.*, Krupčík *et al.* and Akporhonor *et al.* predict the retention temperatures closest to the observed T_R values. Programmed-temperature retention indices (PTRIs) calculated by cubic splines interpolation of both the experimental and some other calculated T_R values were also compared, taking the former as standard, the resulting PTRI values differing by only 2% for at least 90% of the solutes on the low-polarity stationary phases.

INTRODUCTION

Retention times and temperatures are the most important retention data in programmed-temperature gas chromatography (GC). This technique is advantageously used when dealing with analyses of complex mixtures. As in isothermal GC, the retention index of a given compound has to be calculated in order to identify it among the other peaks in a mixture.

The retention data available to a chromatographer have been chiefly obtained under isothermal conditions, and therefore it has always been an aim to utilize such data in order to interpret programmed-temperature information. Habgood and Harris [1], Grant and Hollis [2] and Curvers *et al.* [3] have shown the feasibility of predicting programmed-temperature retention data from data obtained at various isothermal temperatures. With a very similar formulation, Akporhonor *et al.* [4] calculated retention times at programmed temperatures from retention data obtained from isothermal chromatograms.

Early, empirical equations relating linearly retention temperatures (T_R) with an equivalent temperature were reported, for example, the equations of Giddings [5] and Guiochon [6] in the 1960s. In the 1980s, Lee and Taylor [7], Krupčík *et al.* [8] and Said [9] published other equations with which approaches to calculating programmed-temperature retention indices (PTRIs) could be made.

The objective of this work was to carry out a survey study of all of these retention temperatures for eleven *n*-alkane and fifteen non-*n*-alkane solutes using seventeen temperature programmes developed on four packed columns coated with both low- and high-polarity stationary phases. An empirical equation to calculate T_{eq} in terms of the logarithm of the

Correspondence to: Dr. J. M. Santiuste, Instituto de Química Física "Rocasolano", C/Serrano 119, 28006 Madrid, Spain.

0021-9673/92/$05.00

measured retention time from chromatograms was also tested.

Comparisons were made both graphically, observing the ΔT_R differences between the observed and the equivalent/calculated T_R values of the distinct solutes *versus* their corresponding observed retention times, and also by calculating the variance of these differences.

The final aim of obtaining retention times (t_R) and T_R values at programmed temperatures for the above-mentioned solutes by applying directly the equations examined in this study was to be able to calculate at once their PTRIs, which cannot be determined by direct application of the Kováts [10] equation. The purpose of all of this is to reduce the need to obtain many programmed-temperature chromatograms.

Expressions such as those of Van den Dool and Kratz [11] and several others [12–17] have recently been reviewed and as a result of this study [18,19] it is noted that the cubic splines [20] interpolation offers the best results for the calculation of PTRIs and it is now preferred by many workers because it can be applied over broader retention temperature intervals.

PTRIs were obtained by interpolating the T_R values of fifteen non-*n*-alkane solutes for the seventeen afore-mentioned programmes and the differences between experimental PTRIs (using experimental T_R values) and calculated PTRIs (making use of T_R calculated by three equations) were calculated with the purpose of checking which equation yields T_R values closest to those measured from the chromatograms.

THEORY

It has been said that retention temperature is to programmed-temperature GC as retention time is to isothermal GC. Like the latter, retention temperature is in fact the peak fingerprint that enables the chromatographer to carry out its unequivocal identification in a mixture using temperature programming. Put more properly, the retention index is the parameter that finally leads to the achievement of the identification of a given peak and it is the main intention when programmed-temperature GC is undertaken.

If PTRI data are available, a solute in a mixture can be identified with temperature programming as easily as by using an isothermal temperature. On the other hand, it is more convenient to apply temperature programming because the peak separation is improved and peaks are eluted in a shorter time, are narrower and so can be measured better. If the temperature programme is simple, T_R values can be obtained directly from the chromatograms. Today, most chromatograms are measured with temperature programming.

If T_R values are unavailable, the use of equivalent or calculated temperatures may be of help in determining approximate PTRIs.

Equivalent temperatures (T_{eq})

The equivalent temperature is the retention temperature of a peak that would have the same retention time in a programmed-temperature run as it would in an isothermal run. Akporhonor *et al.* [21] distinguished between this temperature and another that they defined as that which would yield the same retention index in a programmed-temperature run as in an isothermal run. The two differ very little.

Calculated retention temperatures

There are three equations for determining T_R values from isothermal data: the equation of Curvers *et al.* [3], which calculates T_R values directly, the equation of Akporhonor *et al.* [4], which computes retention times, and the equation of Krupčík *et al.* [8], which involves retention temperatures of a standard *n*-alkane series.

The first two equations permit advantage to be taken of the enormous number of isothermal data that are available, although it is argued that the thermodynamic parameters of chromatographic peaks obtained from the isothermal capacity factors or retention times show some inaccuracies in their measurements owing to the very nature of the approach used in these treatments. This gives support to the argument that they are not as fine calculation methods as was at first thought [22]. Moreover, it is questioned whether *n*-alkanes may be used as reference solutes when one uses very polar phases [23].

On the other hand, the entropic term $\exp[(\Delta S/R)/\beta]$ (see eqn. 4 below) depends on the phase ratio, in the measurement of which some uncertainty exists, especially when packed columns are involved [24]. In

addition, the enthalpic term also depends slightly on the phase ratio [21].

Krupčík *et al.*'s equation calculates T_R values of non-*n*-alkane solutes from isothermal retention data for *n*-alkanes, that is, the isothermal retention index at a given temperature, thermal gradient of the retention index of the peak and the retention temperatures of the *n*-alkanes eluted before and after the solute under study.

Current equations

The seven expressions used in the calculations in this paper (Table I) are as follows:

(1) Equation of Giddings [5]:

$$T_{eq} = 0.92T_R \quad (1)$$

(2) Equation of Guiochon [6]:

$$T_{eq} = T_R - 20 \quad (2)$$

(3) Equation of Lee and Taylor [7]:

$$T_{eq} = 2\ T_R T_0/(T_R + T_0) \quad (3)$$

where
T_{eq} = equivalent temperature (K);
T_0 = initial temperature (K);
T_R = measured retention temperature (K).

(4) Equation of Curvers *et al.* [3]:

$$r = \int_{T_0}^{T_R} dT/t_m(T)[1 + (a/\beta)\ \exp(\Delta H/RT)] \quad (4)$$

where
$a = \exp(\Delta S/R)$ and $\Delta H/R$ are the entropic and enthalpic parameters;
r = programming rate;
$t_m(T)$ = hold-up time function.

TABLE I

RETENTION TEMPERATURE EQUATIONS

Workers	Eqn. No.	Year	Ref.
Giddings	1	1962	5
Guiochon	2	1964	6
Lee and Taylor	3	1982	7
Curvers *et al.*	4	1985	3
Krupčík *et al.*	5	1986	8
Said	6	1988	9
Akporhonor *et al.*	7	1989	4

(5) Equation of Krupčík *et al.* [8]:

$$T_{R,i} = \frac{[I(T_1) - 100\ Z - T_1(dI/dT)](T_{R,Z+1} - T_{R,Z}) + 100}{100 - (dI/dT)(T_{R,Z+1} - T_{R,Z})} \quad (5)$$

where
$T_{R,i}$ = retention temperature of compound i;
$I(T_1)$ = isothermal retention index at temperature T_1;
dI/dT = isothermal retention index gradient;
$T_{R,Z+1}$, $T_{R,Z}$ = retention temperatures of the $Z + 1$ and Z reference *n*-alkanes.

(6) Equation of Said [9]:

$$T_{eq} = (T_{Ri} - T_0)[\exp(-1.55\ \Delta t_p/t_{Ri})] + T_0 \quad (6)$$

where
$\Delta t_p = t_{R,Z+1} - t_{R,Z}$;
$T_{R,i}$ = retention temperature of a solute i;
Δt_p = retention time differences of reference *n*-alkanes;
t_R = retention time of a solute i;
T_0 = initial temperature.

(6) Equation of Akporhonor *et al.* [4]:

$$1 = \int_0^{t_R} dt/t_m(T)\ \{1 + k_1\exp[k_2/(T_0 + k_3 t)]\} \quad (7)$$

where
$t_m(T)$ = hold-up time function;
$k_1 = \beta\exp(\Delta S/R)$ = entropic term;
$k_2 = -\Delta H/R$ = enthalpic term;
k_3 = programming heating rate;
$\beta = V_L/V_M$ = phase volume ratio.

(7) In addition to the above equations, the following empirical equation has been tried:

$$t_{eq} = 0.805\log\ (T_R - T_0) \quad (8)$$

where
T_R = retention temperature;
T_0 = temperature at which the programme starts;
t_{eq} = temperature expressed in °C.

EXPERIMENTAL

The columns used were 2 m × $\frac{1}{8}$ in. O.D. and 4 m × $\frac{1}{8}$ in. O.D. stainless-steel, packed with PS-255, OV-105, di-*n*-decyl phthalate and OV-275 stationary phases on Chromosorb W AW.

The solutes were C_5–C_{17} *n*-alkanes, the ten McReynolds' probes and acetone, cyclopentanone,

toluene, *o*-xylene, ethyl acetate, *n*-octanol and dimethylaniline.

Isothermal temperatures used were 68, 79, 80, 90, 100, 110, 113, 120, 130, 140, 150 and 179°C. With temperature programming the initial temperatures were 50, 60, 70 and 80°C and the heating rates were 1, 1.5, 2, 3, 4, 6 and 10°C/min.

The chromatograph was a Perkin-Elmer Sigma 2 with a flame ionization detector. The oven temperature was monitored to within ±0.2°C. Minigrator and Varian 4270 electronic integrators were used. The carrier gas was nitrogen at a flow-rate of 10 ml/min.

RESULTS AND DISCUSSION

Experimental T_R values obtained directly from retention times obtained from programmed-temperature chromatograms via a linear programming temperature relationship have recently been reported [19]. The equivalent or calculated T_R values under the same conditions were obtained using eqns. 1–8.

Comparison of the two sets of T_R values was carried out in two manners, graphically, plotting the ΔT_R(exp. − eq.)/ΔT_R(exp. − calc.) *versus* the corresponding experimental retention times, and in terms of the variances of the same differences, $[\sum_{i=1}^{N} (\Delta T_R)^2]^{\frac{1}{2}}/(N-1)$, where N is the number of solutes. To compare all the different equations only retention temperatures of the non-*n*-alkanes were included in the plots, as same equations do not calculate *n*-alkane T_R values. For the calculation of the variances, data for all the solutes were taken.

ΔT_R *difference curves*

Fig. 1 shows the shapes of the difference curves, that is, the differences between the observed T_R values and the equivalent or calculated temperatures for solutes other than *n*-alkanes using all the equations. Five programmes were featured.

Obviously, the errors given by the Giddings, Guiochon and Lee and Taylor straight lines are large, of the order of 20°C (as a reference, the Guiochon parallel straight line at 20°C has been drawn in the plots). The difference between the Giddings and Lee and Taylor lines is the greater slope of the latter.

Considering the other equations, the ΔT_R differences are clearly curves and it is observed that only minor errors result when the equations of Curvers *et al.* and Krupčík *et al.* are applied.

When the equations of Akporhonor *et al.* and Said are used, errors lying between the above and those deduced from the reference Guiochon equation line are obtained.

With regard to OV-275, it can be said that the Lee and Taylor straight line represents smaller errors than for less polar phases. Moreover, all the errors are smaller for the polar OV-275. The same tendency was observed with other programme run.

With respect to the *n*-alkanes the same results are obtained, *i.e.*, the least errors are produced by the retention temperatures calculated with the equations of Curvers *et al.* and Akporhonor *et al.* and large errors are observed for the equivalent temperature empirical straight lines.

Therefore, it seems hat the equivalent temperatures are grosser approximations than the calculated temperatures.

Curvers et al. and Akporhonor et al. ΔT_R *curves*

An example of the differences between the T_R values calculated using eqns. 7 and 4 and the experimental temperatures is shown in Fig. 2A and B. Fig. 2A shows that in every case the points that represent the errors which result on applying Akporhonor *et al.*'s equation in the calculation of the T_R values of solutes other than *n*-alkanes fall more or less on the curve that contains these errors (the terms "error" and "difference" are used indistinctly) computed for the T_R values of the standard *n*-alkane homologues. With OV-275 all the lines occur at smaller differences values than for the other stationary phases. The only major disagreement is observed with the more polar solutes such as *n*-octanol and cyclopentanone using the more polar stationary phase, OV-275.

Fig. 2B depicts the error curves provided by the Curvers *et al.* equation. The situation is very similar. The *n*-alkane error points fall on curves and around them are located the corresponding error points deduced for the other solutes.

Again, it becomes evident that both the nearly non-polar OV-105 and PS-255 and the low-polarity di-*n*-decyl phthalate stationary phases behave in a different way to the polar OV-275 phase with respect to the way in which the differences between the

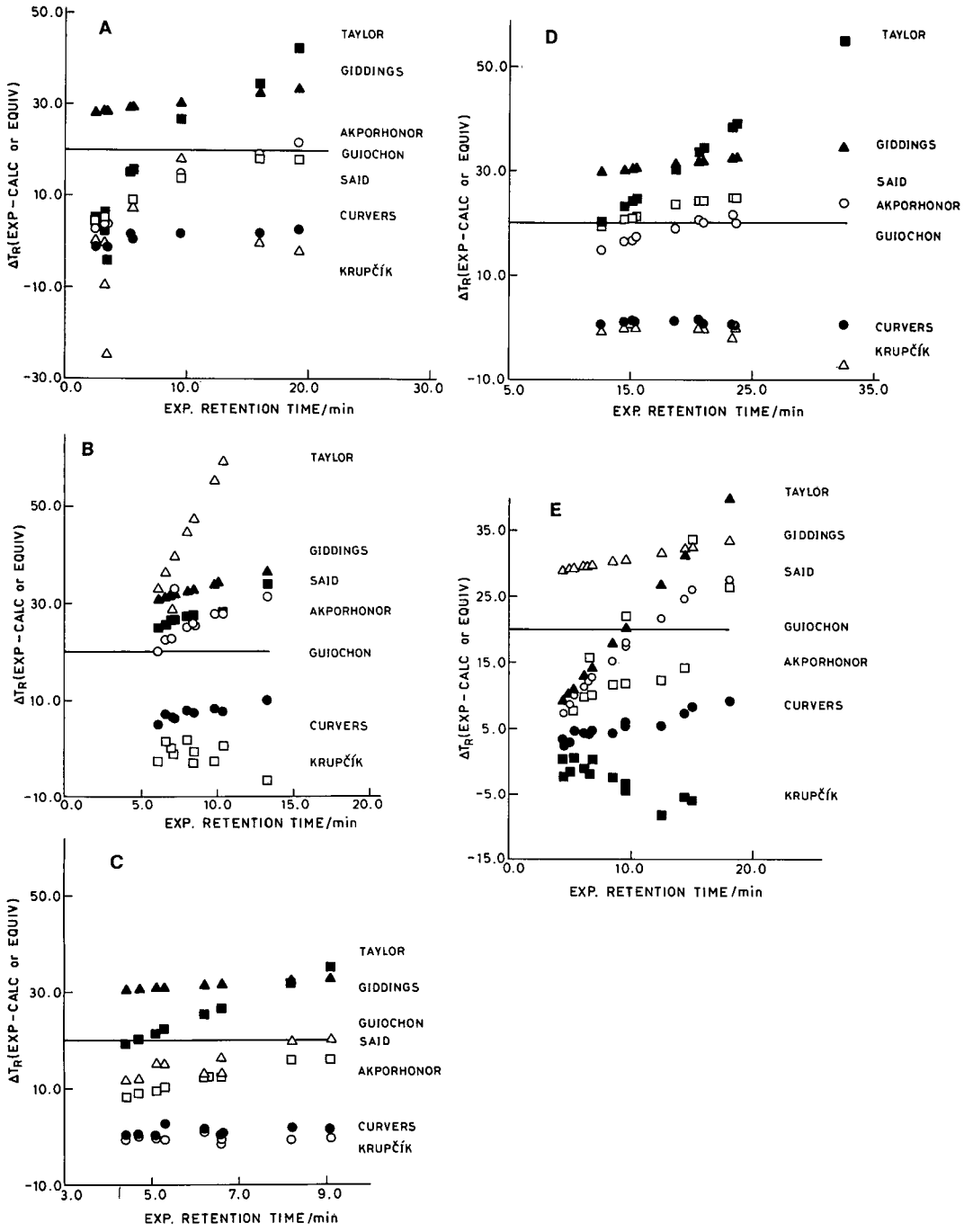

Fig. 1. Plots of ΔT_R(exp. − eq.) or ΔT_R(exp. − calc.) *vs.* the experimental retention times for solutes other than *n*-alkanes. Eqns. 1–8 were used in the calculations. Stationary phases and programmes: (A) PS-255, $T_0 = 70°C$, $r = 4°C/min$; (B) OV-105, $T_0 = 50°C$, $r = 10°C/min$; (C) OV-105, $T_0 = 80°C$, $r = 6°C/min$; (D) di-*n*-decyl phthalate, $T_0 = 60°C$, $r = 3°C/min$; (E) OV-275, $T_0 = 70°C$, $r = 4°C/min$.

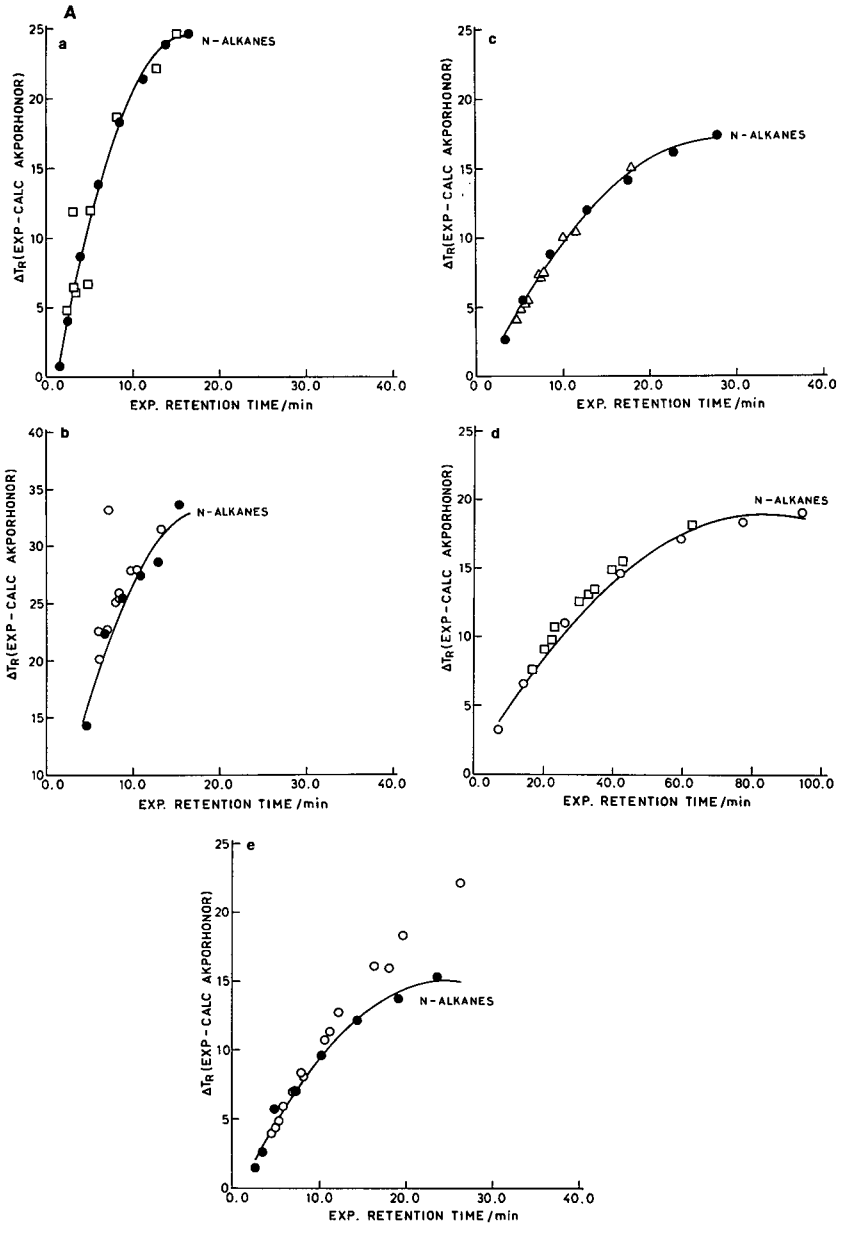
A
a
N-ALKANES
ΔTR(EXP-CALC AKPORHONOR)
EXP. RETENTION TIME/min
b
N-ALKANES
ΔTR(EXP-CALC AKPORHONOR)
EXP. RETENTION TIME/min
c
N-ALKANES
ΔTR(EXP-CALC AKPORHONOR)
EXP. RETENTION TIME/min
d
N-ALKANES
ΔTR(EXP-CALC AKPORHONOR)
EXP. RETENTION TIME/min
e
N-ALKANES
ΔTR(EXP-CALC AKPORHONOR)
EXP. RETENTION TIME/min

Fig. 2.

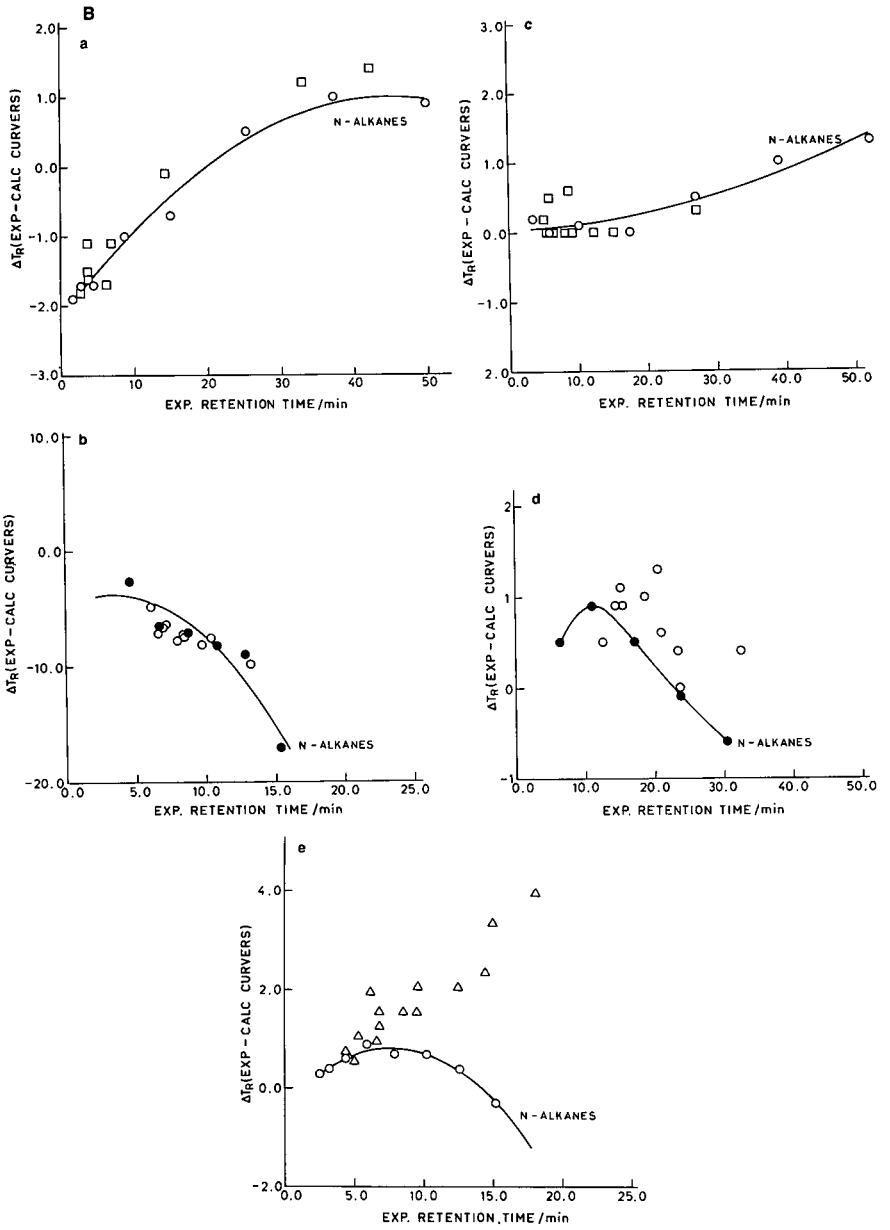

Fig. 2. (A) Plots of the errors of ΔT_R(exp. − calc. by eqn. 7) *vs.* experimental t_R values. All the solutes combined. Stationary phases and programmes: (a) PS-255, $T_0 = 70°C$, $r = 6°C/min$; (b) OV-105, $T_0 = 50°C$, $r = 10°C/min$; (c) OV-105, $T_0 = 80°C$, $r = 3°C/min$; (d) di-*n*-decyl phthalate, $T_0 = 60°C$, $r = 1°C/min$; (e) OV-275, $T_0 = 70°C$, $r = 2°C/min$. (B) Plots of the errors ΔT_R(exp. − calc. by eqn. 4) *vs.* experimental t_R values. All the solutes combined. Stationary phases and programmes: (a) PS-255, $T_0 = 70°C$, $r = 2°C/min$; (b) OV-105, $T_0 = 50°C$, $r = 10°C/min$; (c) OV-105, $T_0 = 80°C$, $r = 1°C/min$; (d) di-*n*-decyl phthalate, $T_0 = 60°C$, $r = 3°C/min$; (e) OV-275, $T_0 = 70°C$, $r = 4°C/min$.

measured and equivalent/calculated T_R values for both non-*n*-alkanes and *n*-alkanes lie close together for the former three phases; conversely, some dispersion of the T_R values for the non-*n*-alkane solutes with respect to the way in which the *n*-alkanes differences accumulate is observed with the strongly polar OV-275 stationary phase.

TABLE II

RETENTION TEMPERATURE DIFFERENCES FOR SEVERAL PROGRAMMES

Calculated variances for ΔT_R(exp. – eq.) or ΔT_R(exp. – calc.) according to eqns. 1–8. Solutes: *n*-alkanes, non-*n*-alkanes and all of the solutes combined.

Stationary phase	Eqn. No.	*n*-Alkanes	Non-*n*-alkanes	All solutes
PS-255 (T_0 = 70°C, r = 6°C/min)	1	12.7	11.4	7.9
	2	8.1	7.5	5.1
	3	12.6	10.1	7.5
	4	1.2	0.9	0.7
	5		5.2	5.2
	6		4.7	4.7
	7	6.8	5.4	1.3
	8	4.3	4.4	2.9
Di-*n*-decyl phthalate (T_0 = 60°C, r = 1.5°C/min)	1	11.9	10.5	8.0
	2	8.8	7.1	5.1
	3	7.5	8.4	7.0
	4	0.6	0.5	0.3
	5		0.4	0.4
	6		6.6	6.6
	7	4.5	5.5	2.1
	8	7.4	4.3	6.3
OV-105 (T_0 = 50°C, r = 2°C/min)	1	13.3	10.6	7.9
	2	8.8	7.1	5.1
	3	15.0	7.0	6.9
	4	0.8	0.9	0.6
	5		0.3	0.3
	6		5.7	5.7
	7	6.1	4.5	1.2
	8	13.2	11.9	8.3
OV-105 (T_0 = 80°C, r = 3°C/min)	1	14.0	10.6	7.9
	2	8.8	7.1	5.1
	3	11.8	4.8	5.2
	4	0.2	0.1	0.1
	5		1.8	1.8
	6		4.3	4.3
	7	5.3	3.0	1.8
	8	3.0	2.1	1.6
OV-275 (T_0 = 70°C, r = 4°C/min)	1	11.4	8.4	6.5
	2	7.5	5.5	4.2
	3	8.2	5.8	4.5
	4	0.8	1.5	1.0
	5		1.4	1.4
	6		2.8	2.8
	7	4.5	4.7	0.9
	8	4.3	2.9	2.3

Variance of retention temperature errors

To know which equations yield retention temperatures closest to the experimental values, the error ΔT_R(exp. − eq.) or ΔT_R(exp. − calc.) variances for all the solutes over all the seventeen programmes run were calculated according to eqns. 1–8.

Variances for *n*-alkanes and the other solutes for five programmes can be compared in Table II. The first column gives the equation used and the other three columns give the variance values for the *n*-alkanes, the non-*n*-alkanes and all of the solutes combined.

In all instances the *n*-alkane variances show the highest values. Also, it is apparent that the lowest variance values result from applying eqns. 4, 7 and 5 when all the solutes are considered. Clearly larger values are associated with eqns. 1 and 3, in agreement with Fig. 1.

A more general review of the variance behaviour for all the solutes with the seventeen programmes executed is shown in Table III. Eqn. 2 is the standard straight line in the plots in Fig. 1 and logically yields the same value irrespective of the rate being considered. It is observed that the variance increases with increase in the rate of heating and that eqns. 4, 7 and 5 yield low values of the variance. According to Akporhonor *et al.* [21], their equation works well for capillary columns but does not seem to perform as well for packed columns, maybe because it is difficult and erratic to measure β [24] and this parameter takes part in the formulation (see eqn. 7) affecting the entropic term which, on the other hand, depends on the phase ratio, two aspects that must be accounted for. Said's equation (eqn. 6), the empirical equation proposed on this paper and the equations of Guiochon, Lee and Taylor and Giddings give increasingly larger variances.

Table IV is intended to give an overall view of the performance of these equations and the extent to which they can be used to obtain approximate retention temperatures without having to measure any programmed-temperature chromatograms. The values given represent the averages of the variances in Table III for all the heating rates for each stationary phase and for each equation, all of them referred to the value of the variance corresponding to eqn. 2. For instance, considering PS-255, $1.49 = (1/4)[7.3 + 7.5 + 7.7 + 7.9]/5.1$, and so on. Table IV indicates that for every stationary phase the smallest values result when the equations of Curvers *et al.*, Akporhonor *et al.* and Krupčík *et al.* are used to calculate the T_R values. The three least suitable equations are those of Giddings, Guiochon and Lee and Taylor, and eqns. 6 (Said) and 8 are located in the middle of the eight. The bottom row in Table IV gives the results of adding the figures for the four stationary phases for each equation, and corroborates the above conclusion for the four stationary phases separately. It should be remembered that eqns. 5 and 6 do not calculate retention temperatures for *n*-alkanes.

Retention indices error

It seems widely accepted that the retention indices closest to the true values are the PTRIs calculated by cubic splines interpolation of experimental retention temperatures of the *n*-alkanes in ref. 20, as becomes evident on observing the T_R *vs.* Z curves for these solutes where excellent cubic splines fits are obtained [18,19].

In this work, a comparison was made between the cubic splines PTRIs computed for the above T_R values and for those calculated via eqns. 4, 7 and 8. Table V shows these values for some programmes.

The relative errors of the retention indices were calculated for all the non-*n*-alkane solutes and mean values for each equation all over the programmes were also evaluated, as shown in Table VI. Again it can be seen how much better the Curvers *et al.* equation performs compared with the other two.

The number of solutes with errors up to 2%, the value usually accepted, is included in Table VII, expressed as a percentage of solutes with respect to the total of all the programmes run. It is seen that the three approaches behave in the same way when the low-polarity stationary phases are considered, but less successfully for the high-polarity OV-275. PTRI determinations giving errors >2%, say about 2–5%, were as follows: six cases with PS-255 (ethyl acetate and pyridine were the solutes involved), three determinations with OV-105 (solute 2-pentanone) and no cases with di-*n*-decyl phthalate. With OV-275 the situation is worse, about ten solutes giving errors >2% when eqns. 4 and 8 are used and almost twice this number when eqn. 7 is used to obtain the retention temperatures. 1-Iodobutane, cyclopentanone, *n*-octanol, pyridine, 2-pentanone, 1-nitropropane and *n*-butanol are, among others,

TABLE III

VARIANCES OF THE ΔT_R(exp. – eq.) OR ΔT_R(exp. – calc.) DIFFERENCES FOR ALL OF THE SOLUTES OVER THE 17 PROGRAMMES

Stationary phase	Eqn. No.	r (°C/min)			
		1	2	4	6
PS-255 (T_0 = 70°C)	1	7.3	7.5	7.7	7.9
	2[a]	5.1	5.1	5.1	5.1
	3	3.0	4.4	6.1	7.5
	4	0.3	0.3	0.4	0.7
	5	1.8	2.9	4.3	5.2
	6	2.4	3.2	4.2	4.7
	7	0.9	1.1	1.3	1.3
	8	6.7	3.9	2.7	2.9
		r (°C/min)			
		1.0	1.5	2.0	3.0
Di-*n*-decyl phthalate (T_0 = 60°C)	1	7.7	8.0	8.2	8.6
	2[a]	5.1	5.1	5.1	5.1
	3	6.2	7.0	7.9	9.2
	4	0.1	0.3	0.3	0.3
	5	1.3	0.4	0.5	0.9
	6	5.8	6.6	7.3	7.6
	7	2.1	2.1	2.4	2.8
	8	6.1	6.3	6.4	6.2
		r (°C/min)			
		2	6	10	
OV-105 (T_0 = 50°C)	1	7.5	7.5	8.2	
	2[a]	5.1	5.1	5.1	
	3	6.9	11.5	13.5	
	4	0.6	1.0	2.2	
	5	0.3	0.5	0.9	
	6	5.7	8.2	9.1	
	7	1.2	1.6	1.2	
	8	8.3	7.0	5.4	
		r (°C/min)			
		1	3	6	
OV-105 (T_0 = 80°C)	1	7.6	7.9	8.3	
	2[a]	5.1	5.1	5.1	
	3	2.7	5.2	8.5	
	4	0.1	0.1	0.4	
	5	0.1	1.8	0.3	
	6	2.3	4.3	5.9	
	7	1.2	1.8	2.2	
	8	4.5	1.6	2.7	

TABLE III *(continued)*

Stationary phase	Eqn. No.	r (°C/min)		
		1	2	4
OV-275 (T_0 = 70°C)	1	6.1	6.2	6.5
	2[a]	4.2	4.2	4.2
	3	2.0	3.1	4.5
	4	0.4	0.6	1.0
	5	0.3	1.0	1.4
	6	1.8	2.7	2.8
	7	0.6	0.7	0.9
	8	4.0	2.4	2.3

[a] Eqn. 2 is taken as a reference.

TABLE IV

RETENTION TEMPERATURE VARIANCES OF ΔT_R(exp. – eq.) OR ΔT_R(exp. – calc.) DIFFERENCES (OVERALL VIEW)

Stationary phase	T_R calculated by eqn.							
	1	2	3	4[a]	5[a]	6	7[a]	8
PS-255 (4 programmes)	1.49	1.0	1.02	0.08	0.69	0.71	0.23	0.80
OV-105 (6 programmes)	1.53	1.0	1.58	0.14	0.12	1.16	0.29	0.96
Di-*n*-decyl phthalate (4 programmes)	1.59	1.0	1.49	0.05	0.16	1.33	0.45	1.23
OV-275 (3 programmes)	1.49	1.0	0.76	0.16	0.21	0.58	0.17	0.69
All four stationary phases (17 programmes)	6.11	4.0	4.86	0.43	1.18	3.78	1.16	3.67

[a] The lowest values of the variance correspond to the eqns. 4, 5 and 7.

TABLE V

CUBIC SPLINES PROGRAMMED-TEMPERATURE RETENTION INDICES USING EXPERIMENTAL AND CALCULATED T_R VALUES FOR SEVERAL PROGRAMMES IN ACCORDANCE WITH EQNS. 4, 7 AND 8

Stationary phase	Solute	T_R (exp.)	T_R calculated from eqn.		
			4	7	8
OV-105 (T_0 = 50°C, r = 6°C/min)	Benzene	677	675	674	676
	n-Butanol	701	696	696	696
	2-Pentanone	716	717	720	716
	1-Nitropropane	780	782	783	777
	Pyridine	775	779	779	777
	2-Methyl-2-pentanol	765	761	764	760
	1-Iodobutane	839	835	832	836
	2-Octyne	875	875	875	876
	1,4-Dioxane	726	727	728	725
	cis-Hydrindane	1014	1011	1004	1011

(Continued on p. 214)

TABLE V *(continued)*

Stationary phase	Solute	T_R (exp.)	T_R calculated from eqn.		
			4	7	8
OV-105 (T_0 = 80°C, r = 6°C/min)	Benzene	679	681	681	683
	n-Butanol	694	694	695	695
	2-Pentanone	714	718	721	717
	1-Nitropropane	782	784	786	783
	Pyridine	780	784	783	783
	2-Methyl-2-pentanol	766	761	764	759
	1-Iodobutane	844	840	837	841
	2-Octyne	875	875	875	875
	1,4-Dioxane	727	729	731	727
	cis-Hydrindane	1017	1015	1007	1014
PS-255 (T_0 = 70°C, r = 4°C/min)	Ethyl acetate	602	605	563	605
	Benzene	659	661	657	655
	n-Butanol	658	658	661	655
	2-Pentanone	668	679	681	678
	Pyridine	749	738	739	740
	Toluene	757	759	757	760
	o-Xylene	886	882	882	885
	n-Octanol	1058	1062	1065	1061
	Dimethylaniline	1143	1146	1142	1146
Di-*n*-decyl phthalate (T_R = 60°C, r = 3°C/min)	Benzene	728	730	729	729
	n-Butanol	769	768	770	767
	2-Pentanone	759	759	759	759
	1-Nitropropane	858	856	854	856
	Pyridine	853	847	844	847
	2-Methyl-2-pentanol	823	820	820	820
	1-Iodobutane	894	892	886	891
	2-Octyne	898	897	899	897
	1,4-Dioxane	775	774	774	774
	cis-Hydrindane	1032	1032	1023	1032
OV-275 (T_0 = 70°C, r = 2°C/min)	Benzene	1125	1131	1128	1133
	n-Butanol	1307	1296	1287	1295
	2-Pentanone	1227	1213	1209	1212
	1-Nitropropane	1479	1482	1452	1483
	Pyridine	1442	1424	1400	1425
	2-Methyl-2-pentanol	1228	1218	1220	1218
	1-Iodobutane	1192	1182	1176	1183
	2-Octyne	1087	1085	1089	1084
OV-275 (T_0 = 70°C, r = 2°C/min)	1,4-Dioxane	1325	1314	1300	1314
	cis-Hydrindane	1145	1123	1117	1124
	Acetone	1103	1106	1100	1106
	Toluene	1204	1208	1209	1208
	o-Xylene	1349	1323	1309	1324
	Cyclopentanone	1511	1492	1459	1492
	n-Octanol	1661	1612	1575	1611

TABLE VI

MEAN VALUES OF THE PTRI ERRORS CALCULATED BY CUBIC SPLINES USING T_R VALUES CALCULATED BY EQNS. 4, 7 AND 8 OVER ALL THE PROGRAMMES

$$\text{Error} = \frac{\text{PTRI (exp.)} - \text{PTRI (calc.)}}{\text{PTRI (exp.)}} \times 100.$$

Stationary phase	Eqn. No.	r (°C/min)			
		1	2	4	6
PS-255 (T_0 = 60°C)	4	0.85	1.10	0.53	0.55
	7	1.27	1.79	1.27	1.29
	8	0.83	0.90	0.61	0.39
		r (°C/min)			
		2	6	10	
OV-105 (T_0 = 50°C)	4	0.32	0.33	0.31	
	7	0.32	0.45	0.45	
	8	0.54	0.29	0.27	
		r (°C/min)			
		1	3	6	
OV-105 (T_0 = 80°C)	4	0.56	0.62	0.32	
	7	0.68	0.85	0.50	
	8	0.80	0.58	0.32	
		r (°C/min)			
		1	1.5	2.0	3.0
Di-*n*-decyl phthalate (T_0 = 60°C)	4	0.37	0.34	0.45	0.21
	7	0.48	0.50	0.42	0.39
	8	0.56	0.36	0.45	0.21
		r (°C/min)			
		1	2	4	
OV-275 (T_0 = 70°C)	4	1.41	1.02	2.07	
	7	1.79	1.79	3.25	
	8	1.47	1.02	1.98	

the solutes with poorer PTRI predictions. The high-polarity of the OV-275 phase may be the cause of such unfavourable results. As has been pointed out, it is a poorly behaving phase because it uses the unsuitable *n*-alkanes with very low retention times, which may be a source of errors [23].

Of the three equations compared, eqn. 7 is the least reliable, with errors on various solutes being

TABLE VII

STATISTICS OF CUBIC SPLINES PTRI DETERMINATIONS FOR THE 15 NON-*n*-ALKANE SOLUTES ON THE FOUR COLUMNS OVER ALL THE 17 PROGRAMMES RUN

Stationary phase	% of solutes with error in PTRI $\leqslant 2\%$		
	T_R calculated by eqn.		
	4	7	8
PS-255	97	89	97
OV-105[a]	100	100	100
OV-105[b]	97	97	97
Di-*n*-decyl phthalate	100	100	100
OV-275	78	56	73

[a] $T_0 = 50°C$.
[b] $T_0 = 80°C$.

larger than the permitted 2%. A common factor here seems to be the solutes for which the retention index predictions are more erratic, that is, most of them are polar solutes chromatographed on a very polar stationary phase.

The result for ethyl acetate on PS-255, a nearly non-polar stationary phase, may be due to the fact that this peak has a low retention temperature approaching the abrupt zone of the cubic splines where errors become important. The same effect might occur with 2-pentanone. For pyridine, the error may be due to the fact that it is a tailed, broad and peculiar peak with a t_R that is difficult to measure.

Final hints

On comparing retention temperatures deduced from the published equations for both *n*-alkanes and other solutes and the retention indices of non-*n*-alkane solutes, some differences seem to arise depending on how polar the stationary phase under consideration is. The retention temperatures are better predicted with the low-polarity stationary phases than with OV-275, although for the latter the differences between the T_R values compared in this paper tend to smooth with respect to the other three much lesser polar stationary phases. On the other hand, retention indices (up to a 2% error) are reproduced with almost 100% accuracy for OV-105, PS-255 and di-*n*-decyl phthalate, whereas the prediction is much worse for OV-275. Hence the polarity of the stationary phase seems to be important for this kind of prediction, and the polarity of the solutes involved might also play an important role.

The least errors in the prediction of the retention temperatures are produced with the Curvers *et al.* and the Krupčík *et al.* equations; the Akporhonor *et al.* and Said equations follow with larger errors, but by far the largest errors result when using the early empirical equations of Giddings, Guiochon and Lee and Taylor.

When cubic splines retention indices are compared it is found that the equation of Curvers *et al.* again has a better performance than the other two compared.

Except for OV-275, the percentage of solutes for which the prediction is made with an error up to the tolerated 2% is 89–100% for T_R obtained with eqn. 7 and 97–100% for T_R obtained with eqns. 4 and 8.

It is apparent that the Akporhonor *et al.* equation works less well than the Curvers *et al.* equation, perhaps owing to the uncertainty in the measurement of the phase ratio, β, on packed columns.

For the polar stationary phase OV-275, there are various solutes for which predictions are made with errors >2%, *e.g.*, the mean value of the error for a heating rate $r = 4°C/min$ is 3.25% (see Table VI). Consequently, none of the equations can be recommended for calculating retention indices on this type of phase.

For non-polar and low-polarity stationary phases it has been shown that one can calculate PTRIs by cubic splines interpolation of T_R values calculated by the treatments of Curvers *et al.* or Akporhonor *et al.* with fair agreement with the experimental values. This is very important as it permits one to operate with isothermal retention data, saving a lot of experimental work in many instances, which facilitates the identification of difficult peaks for complicated multi-component mixtures.

ACKNOWLEDGEMENT

We thank Professor D. R. Taylor for providing his calculation programme which was widely applied in this work.

REFERENCES

1 H. W. Habgood and W. E. Harris, *Anal. Chem.*, 32 (1960) 450.
2 D. W. Grant and M. G. Hollis, *J. Chromatogr.*, 158 (1978) 3.
3 J. Curvers, J. Rijks, C. Cramers, K. Knauss and P. Larson, *J. High Resolut. Chromatogr. Chromatogr. Commun.*, 8 (1985) 607.
4 E. E. Akporhonor, S. Le Vent and D. R. Taylor, *J. Chromatogr.*, 463 (1989) 271.
5 J. C. Giddings, in N. Brenner, J. E. Callen and M. D. Weiss (Editors), *Gas Chromatography*, Academic Press, New York, 1962, p. 57.
6 G. Guiochon, *Anal. Chem.*, 36 (1964) 661.
7 J. Lee and D. R. Taylor, *Chromatographia*, 16 (1982) 286.
8 J. Krupčík, P. Cellar, D. Repka, J. Garaj and G. Guiochon, *J. Chromatogr.*, 351 (1986) 111.
9 A. S. Said, *J. High Resolut. Chromatogr. Chromatogr. Commun.*, 11 (1988) 678.
10 E. Kováts, *Helv. Chim. Acta*, 41 (1958) 1915.
11 H. van den Dool and P. D. Kratz, *J. Chromatogr.*, 11 (1963) 463.
12 R. V. Golovnya and V. P. Uraletz, *J. Chromatogr.*, 36 (1968) 276.
13 L. Erdey, J. Takács and C. Szalànczy, *J. Chromatogr.*, 46 (1970) 29.
14 I. G. Zenkevich and B. V. Ioffe, *J. Chromatogr.*, 439 (1988) 185.
15 T. Wang and Y. Sun, *J. Chromatogr.*, 390 (1987) 261.
16 L. Podmanicky, L. Szepesy, K. Lakszner and G. Schomburg, *Chromatographia*, 21 (1986) 387.
17 B. Chen, X. Guo and S. Peng, *Chromatographia*, 23 (1987) 888.
18 E. Fernández Sánchez, J. A. García Domínguez, V. Menéndez and J. M. Santiuste, *J. Chromatogr.*, 498 (1990) 1.
19 J. A. García Domínguez and J. M. Santiuste, *Chromatographia*, 32 (1991) 115.
20 W. A. Halang, R. Langlais and E. Kugler, *Anal. Chem.*, 50 (1978) 1829.
21 E. E. Akporhonor, S. Le Vent and D. R. Taylor, *J. Chromatogr.*, 504 (1990) 269.
22 G. Tarján, S. Nyiredy, M. Györ, E. R. Lombosy, T. S. Lombosy, M. V. Budahegyi, S. Y. Mészàros and J. M. Takács, *J. Chromatogr.*, 472 (1989) 1.
23 M. B. Evans and J. K. Haken, *J. Chromatogr.*, 472 (1989) 93.
24 Y. Guan, J. Kiraly and J. Rijks, *J. Chromatogr.*, 472 (1989) 129.

Journal of Chromatography, 627 (1992) 219–226
Elsevier Science Publishers B.V., Amsterdam

CHROM. 24 551

Trapping efficiencies of capillary cold traps for C_2–C_{10} hydrocarbons

Xu-Liang Cao and C. Nicholas Hewitt

Institute of Environmental and Biological Sciences, Lancaster University, Lancaster LA1 4YQ (UK)

(First received May 12th, 1992; revised manuscript received August 4th, 1992)

ABSTRACT

The trapping performance of four different capillary cold traps (deactivated, coated, Tenax-TA and Chromosorb 101 packed traps) for C_2–C_5 *n*-alkenes, isoprene, benzene, toluene, *p*-xylene, *o*-xylene, mesitylene, α-pinene, β-pinene, 1,2,4-trimethylbenzene and 1,2,3-trimethylbenzene were determined over the temperature range −20 to −180°C. All the hydrocarbons except ethylene were found to be retained by all the traps at different temperatures, but only the Chromosorb 101 capillary trap retained ethylene, and then not completely. The coatings were found to increase the trapping efficiency for the higher hydrocarbons ($\geq C_6$), whereas the packings increased the trapping efficiency for all compounds (C_2–C_{10}). A linear relationship was found between the boiling point of the compound and its maximum trapping temperature. The flow-rate of the carrier gas (10–60 ml/min) was found to affect the trapping efficiency of the C_2–C_4 hydrocarbons.

INTRODUCTION

Sampling by adsorption, with subsequent thermal desorption, is widely used for the sampling and analysis of very low concentration volatile organic compounds (VOCs) in ambient air. The whole sample can be analysed in this way, and the best sensitivity of analysis can be obtained. During the process of thermal desorption, the desorbed analytes invariably require reconcentration in a cold trap before being injected on to the GC capillary column for analysis. This is necessary for two main reasons: preconcentration of the sample and solute band concentration. Two types of cold trap are used with different dimensions: packed and capillary cold traps. Capillary cold traps are more compatible with a capillary column in the gas chromatograph than the packed traps. The latter may result in incomplete sample transfer from the trap to the capillary column because of the differences in the flow-rate required for complete and rapid desorption from a packed trap and the flow-rate through a capillary column in the gas chromatograph [1,2]. Many different capillary traps are available, coated, uncoated, packed and unpacked, etc., and these are all becoming more widely used with the rapidly increasing use of capillary analytical columns [3–14].

Trapping efficiency is one of the most important properties of cold traps. It may vary with the trapping temperature, flow-rate of the carrier gas, coating and packings inside the capillary and the length of the trap etc. Although the commonly used cooling medium, liquid nitrogen, is inexpensive, some capillary traps may not trap some hydrocarbons at all, especially the lighter ones, or cannot trap completely, even at the lowest temperature achievable with liquid nitrogen (−196°C). This may lead to errors in the sampling and analysis of VOCs in ambient air, or reduce the sensitivity of analysis. Hence trapping efficiency should be studied as a function of trapping temperature and flow-rate for different

Correspondence to: X.-L. Cao, Institute of Environmental and Biological Sciences, Lancaster University, Lancaster LA1 4YQ, UK.

0021-9673/92/$05.00

capillary traps in order to select suitable capillary traps for particular applications. To date little work has been done in this area.

In this work, trapping efficiencies for the C_2–C_{10} hydrocarbons were investigated as a function of both trapping temperature and flow-rate for four different commercially available capillary traps. The relationships between the maximum trapping temperature and the boiling point for each compound are also discussed.

EXPERIMENTAL

Gas chromatographic measurements were made using a Hewlett-Packard 5890 Series II gas chromatograph with flame ionization detection (FID). The carrier gas was helium and the make-up gas was nitrogen. The GC capillary column used was an Ultra 2 (cross-linked 5% phenyl–methylsilicone) of 25 m × 0.2 mm I.D. with a film thickness of 0.33 μm (Hewlett-Packard). The injector temperature was 220°C and the detector temperature 300°C. The sample vapours were injected into the carrier gas stream by means of a 1-ml gas-tight syringe via a Chrompack thermal desorption cold trap (TCT) injector, which was interfaced with the gas chromatograph. The injected vapours were then carried by helium through a heated (230°C) empty Perkin-Elmer stainless-steel tube to the capillary trap, which was cooled by liquid nitrogen. The range of trapping temperatures which can be controlled by the TCT injector unit is from 0 to −180°C. However, a trapping temperature as low as −190°C could sometimes be reached when the temperature on the control unit was a minimum. The trap was then flash-heated to 220°C at 15°C/s for 1 min, and the trapped vapours injected on to the GC capillary column in the splitless mode.

The following hydrocarbons were selected for study, based on their contributions to the formation of ozone in the troposphere [15–17]: C_2–C_5 *n*-alkenes, isoprene, benzene, toluene, *p*-xylene, *o*-xylene, mesitylene, 1,2,4-trimethylbenzene, 1,2,3-trimethylbenzene, α-pinene and β-pinene. Mixtures of hydrocarbons were prepared by diluting 1000 ppmv Scotty standard calibration mixtures of *n*-alkenes or injecting known volumes of liquid hydrocarbon into a 1-l flask which had been purged with nitrogen for 3 min. The flask and syringes were kept warm at 55 ± 5°C in order to prevent vapour condensation and adsorption on surfaces. The amount of hydrocarbons injected on to the column for analysis was 10–20 ng.

Four different capillary cold traps (obtained from Chrompack) were investigated: (i) a deactivated uncoated fused-silica capillary (40 cm × 0.53 mm I.D.), catalogue number 4076 [18]; (ii) a fused-silica capillary (40 cm × 0.53 mm I.D.) coated with CP-Sil 8 CB (film thickness 5 μm), catalogue number 16274 [19]; (iii) a fused-silica capillary (40 cm × 0.53 mm I.D.) coated with CP-Sil 8 CB (film thickness 5 μm) and packed with Tenax-TA (length 15 mm), catalogue number 16425 [19]; and (iv) a fused-silica capillary (40 cm × 0.53 mm I.D.) coated with CP-Sil 8 CB (film thickness 5 μm) and packed with Chromosorb 101 (length 15 mm) catalogue number 16426 [19].

RESULTS AND DISCUSSION

Effect of trapping temperature on trapping efficiency

The trapping efficiencies of the four different cap-

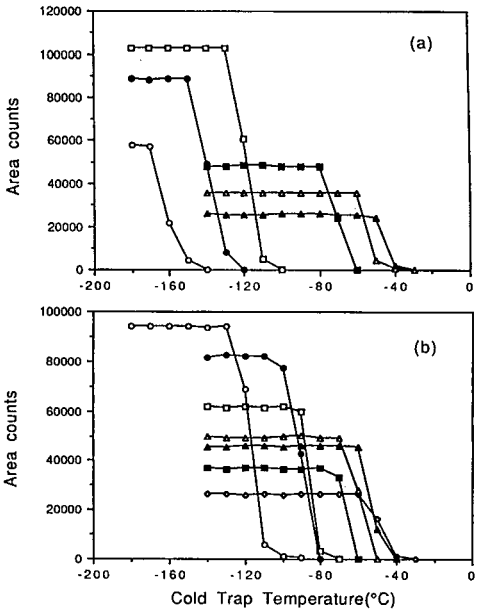

Fig. 1. Trapping curves of the deactivated capillary cold trap for different hydrocarbons. (a) ○ = Propylene; ● = 1-butene; □ = 1-pentene; ■ = *p*-xylene; △ = β-pinene; ▲ = 1,2,3-trimethylbenzene. (b) ○ = Isoprene; ● = benzene; □ = toluene; ■ = *o*-xylene; △ = α-pinene; ▲ = mesitylene; ◇ = 1,2,4-trimethylbenzene.

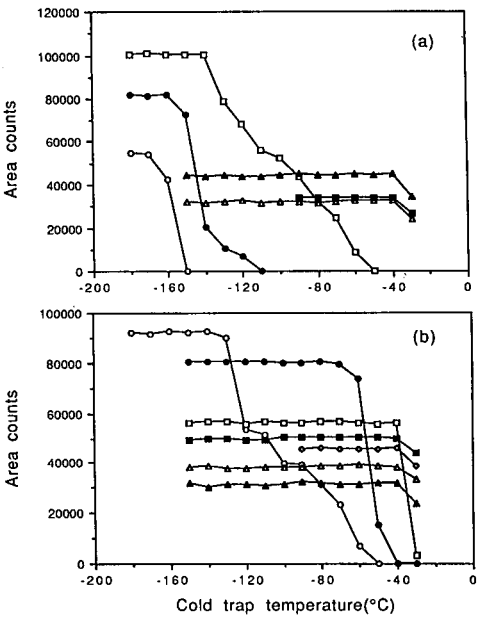

Fig. 2. Trapping curves of the coated capillary cold trap for different hydrocarbons. (a) ○ = Propylene; ● = 1-butene; □ = 1-pentene; ▲ = mesitylene; △ = 1,2,3-trimethylbenzene; ■ = β-pinene. (b) ○ = Isoprene; ● = benzene; □ = toluene; ■ = *p*-xylene; △ = *o*-xylene; ▲ = 1,2,4-trimethylbenzene; ◇ = α-pinene.

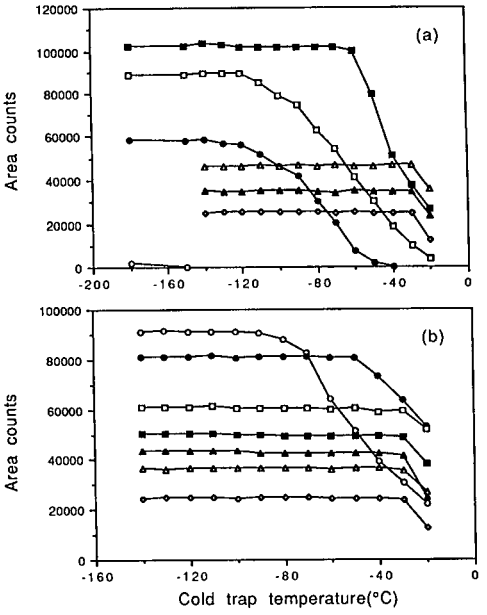

Fig. 3. Trapping curves of the Tenax-TA capillary cold trap for different hydrocarbons. (a) ○ = Ethylene; ● = propylene; □ = 1-butene; ■ = 1-pentene; ◇ = 1,2,3-trimethylbenzene; △ = α-pinene; ▲ = β-pinene. (b) ○ = Isoprene; ● = benzene; □ = toluene; ■ = *p*-xylene; △ = *o*-xylene; ▲ = mesitylene; ◇ = 1,2,4-trimethylbenzene.

illary cold traps for the C_2–C_{10} hydrocarbons were determined over the temperature range −20 to −180°C by injecting the same amount of organic mixtures each time. The results obtained are shown in Figs. 1–4. The plateau of each trapping curve indicates the complete trapping of each compound. The maximum trapping temperatures at which compounds can be trapped completely were derived from Figs. 1–4 and are listed in Table I for each trap and each compound.

It can be seen from Table I that the maximum trapping temperatures for the C_6–C_{10} hydrocarbons of the different capillary traps generally have the following order: deactivated capillary trap < coated capillary trap < Tenax-TA capillary trap ≈ Chromosorb 101 capillary trap; and for the C_2–C_5 hydrocarbons, deactivated capillary trap ≈ coated capillary trap < Tenax-TA capillary trap < Chromosorb 101 capillary trap. This indicates that coating a capillary with a liquid film which can increase its trapping capacity may lead to higher trapping efficiencies for the heavier hydrocarbons ($\geq C_6$). However, the trapping efficiencies for the lighter hydrocarbons (C_2–C_5) cannot be improved by a liquid film coating. In fact, ethylene cannot be trapped at all in these two traps. This may be because the coatings behave as solids at low temperatures [20,21]. The capillary traps with packings (Tenax-TA or Chromosorb 101) showed higher trapping efficiency than the non-packed traps (both coated and uncoated), especially for the lighter hydrocarbons.

Although the trapping efficiencies of the Chromosorb 101 capillary trap for the C_5–C_{10} hydrocarbons are generally similar to those of the Tenax-TA capillary trap, the trapping efficiencies of the former trap for the lighter hydrocarbons (C_2–C_4) are higher than those of the Tenax trap on which ethylene is very inefficiently trapped. This is due to the higher adsorption capacity of Chromosorb 101 (BET specific surface area < 50 m^2/g) than that of Tenax-TA (BET specific surface area 20 m^2/g). The Chromosorb 101 capillary trap is the only one of the four

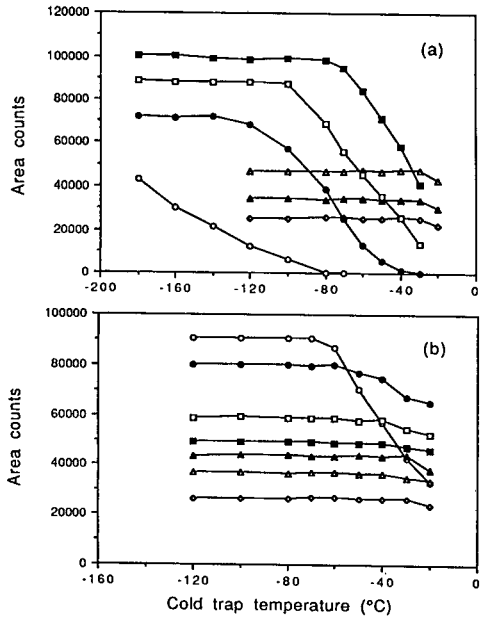

Fig. 4. Trapping curves of the Chromosorb 101 capillary cold trap for different hydrocarbons. (a) ○ = Ethylene; ● = propylene; □ = 1-butene; ■ = 1-pentene; ◇ = 1,2,4-trimethylbenzene; △ = α-pinene; ▲ = β-pinene. (b) ○ = Isoprene; ● = benzene; □ = toluene; ■ = *p*-xylene; △ = *o*-xylene; ▲ = mesitylene; ◇ = 1,2,3-trimethylbenzene.

traps investigated which can trap ethylene with a significant efficiency. However, as can be seen from Fig. 4b, the trapping curve for ethylene did not reach a plateau, even at the lowest temperature, which indicates incomplete trapping of ethylene on the Chromosorb 101 trap. Hence stronger adsorbents, such as Carbotrap (100 m^2/g) or Chromosorb 106 (800 m^2/g), are needed for packing capillary traps in order to trap the most volatile hydrocarbons completely.

It is interesting to note from Table I that although the trapping efficiency of the deactivated capillary trap for the C_9–C_{10} hydrocarbons is improved by using a coated capillary trap, there is a very slight improvement by using Tenax-TA packing, and no further improvement at all by using Chromosorb 101 packing. This may indicate that there may be an upper limit for the maximum trapping temperature of −30°C, *i.e.*, the maximum trapping temperature for the C_2–C_{10} hydrocarbons cannot be greater than the upper limit (−30°C) even when the capillary cold trap with the highest trapping efficiency is used.

It can also be seen from the trapping curves in Figs. 1–4 that the trapping efficiency of the uncoated deactivated capillary trap for the C_2–C_{10} hydrocarbons dropped sharply once the maximum trapping temperature for each compound was exceeded.

TABLE I

MAXIMUM TRAPPING TEMPERATURES (°C) OF DIFFERENT CAPILLARY TRAPS FOR C_2–C_{10} HYDROCARBONS

Hydrocarbon	B.p./m.p. (°C)	Capillary cold trap			
		Deactivated	Coated	Tenax-TA	Chromosorb 101
Ethylene	−104/−169	–	–	–	-180
Propylene	−47.7/−185.2	−180	−180	−140	-120
1-Butene	−6.3/−185.3	−150	−160	−120	-100
1-Pentene	30/−138	−130	−140	−70	−80
Isoprene	34/−146	−130	−140	−90	−70
Benzene	80.1/5.5	−110	−70	−50	−60
Toluene	110.6/−95	−100	−40	−30	−40
p-Xylene	138.3/13.3	−80	−40	−30	−40
o-Xylene	144.4/−25.2	−80	−40	−30	−40
α-Pinene	155.5/−62	−70	−40	−30	−30
Mesitylene	164.7/−44.7	−60	−40	−30	−30
β-Pinene	166/−61	−60	−40	−30	−30
1,2,4-Trimethylbenzene	168/−44	−60	−40	−30	−30
1,2,3-Trimethylbenzene	175.5/−25	−60	−40	−30	−30

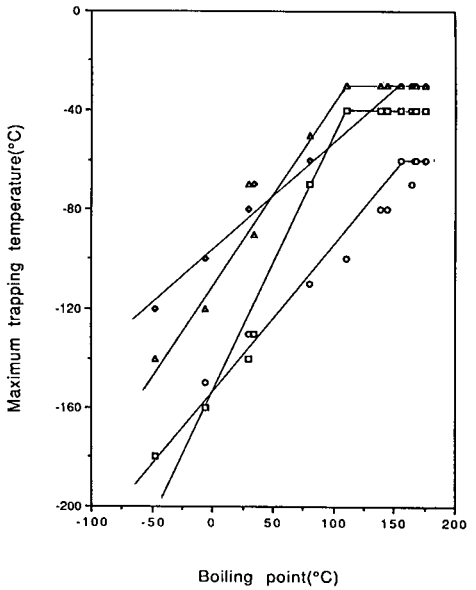

Fig. 5. Variation of the maximum trapping temperature with boiling point for different traps. ◇ = Chromosorb 101; △ = Tenax-TA; □ = coated; ○ = deactivated trap.

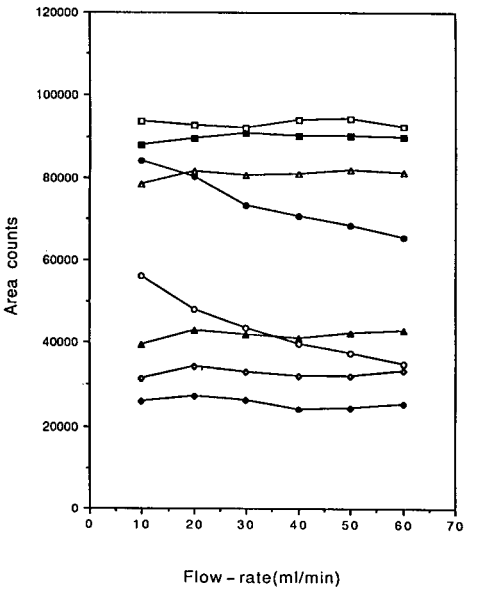

Fig. 6. Variation of trapping efficiency of the deactivated capillary trap with flow-rate for different hydrocarbons. ○ = propylene; ● = 1-butene; □ = 1-pentene; ■ = isoprene; △ = benzene; ▲ = mesitylene; ◆ = 1,2,4-trimethylbenzene; ◇ = β-pinene.

For the coated and packed capillary traps, the trapping efficiencies decreased gradually as the maximum trapping temperature was exceeded. This shows the important roles in improving the trapping efficiency played by the coatings, especially the packings inside the capillary traps which absorb or adsorb compounds.

As the volatility of the hydrocarbon increases, so the maximum trapping temperature was found to decrease. This is shown in Table I and Fig. 5, where the boiling point of each compound is plotted against the maximum trapping temperature for each capillary cold trap. It can be seen from Fig. 5 that as the boiling point increases, *i.e.*, the hydrocarbon becomes less volatile, the maximum trapping temperature generally increases linearly for all of these four capillary traps until a plateau is reached, which is due to the upper limit of the maximum trapping temperature.

Effect of flow-rate on trapping efficiency

The effect of the flow-rate of the helium carrier gas through the cold trap on the trapping efficiency was investigated for the deactivated, Tenax-TA and

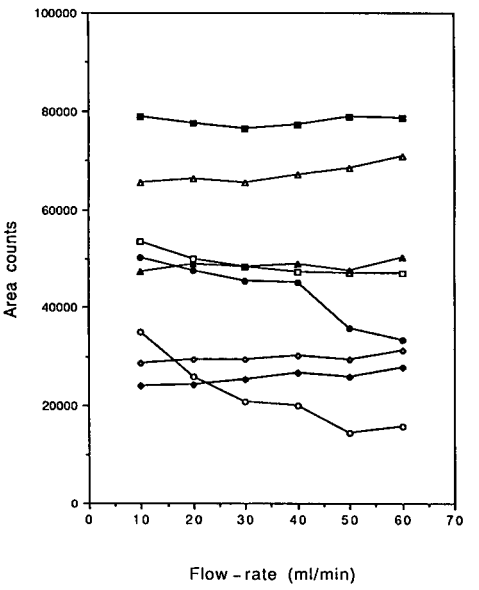

Fig. 7. Variation of trapping efficiency of the Tenax-TA capillary trap with flow-rate for different hydrocarbons. ○ = propylene; ● = 1-butene; □ = 1-pentene; ■ = isoprene; △ = benzene; ▲ = toluene; ◇ = *o*-xylene; ◆ = α-pinene.

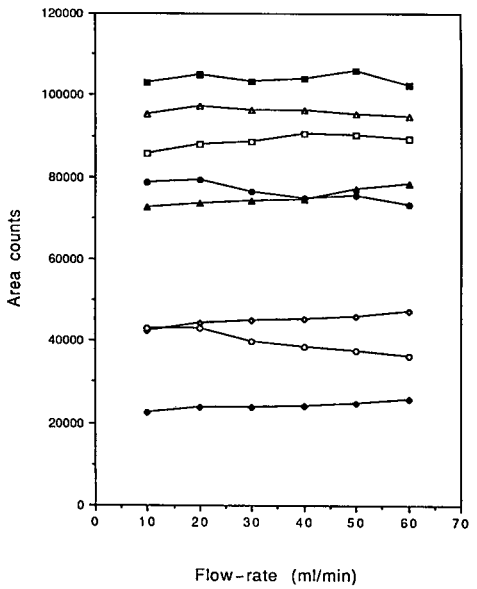

Fig. 8. Variation of trapping efficiency of the Chromosorb 101 capillary trap with flow-rate for different hydrocarbons. ○ = Ethylene; ● = propylene; □ = 1-butene; ■ = 1-pentene; △ = isoprene; ▲ = benzene; ◇ = *p*-xylene; ◆ = 1,2,3-trimethylbenzene.

Chromosorb 101 capillary cold traps, by injecting the same amount of hydrocarbon mixtures into each trap at −180°C and varying the flow-rate from 10 to 60 ml/min.

Representative plots of area counts against flow-rate for the deactivated trap, the Tenax-TA trap and the Chromosorb 101 trap are shown in Figs. 6, 7 and 8, respectively. It can be seen that the trapping efficiencies of all these traps for the heavier hydrocarbons ($\geqslant C_5$) are generally insensitive to the flow-rate. However, breakthrough did occur for the C_2–C_4 hydrocarbons at higher flow-rates, especially for the deactivated and Tenax-TA traps, which have less affinity for these very volatile hydrocarbons. The trapping efficiencies of the Chromosorb 101 trap dropped only slightly for ethylene and propylene at higher flow-rates, owing to the relatively higher adsorption capacity of Chromosorb 101. Hence care should be taken when using capillary traps to keep the flow-rate of the carrier gas constant, especially for the analysis of these very volatile hydrocarbons.

Blanks of capillary cold traps

One of the primary areas of concern when sampling and analysing very low concentrations of vol-

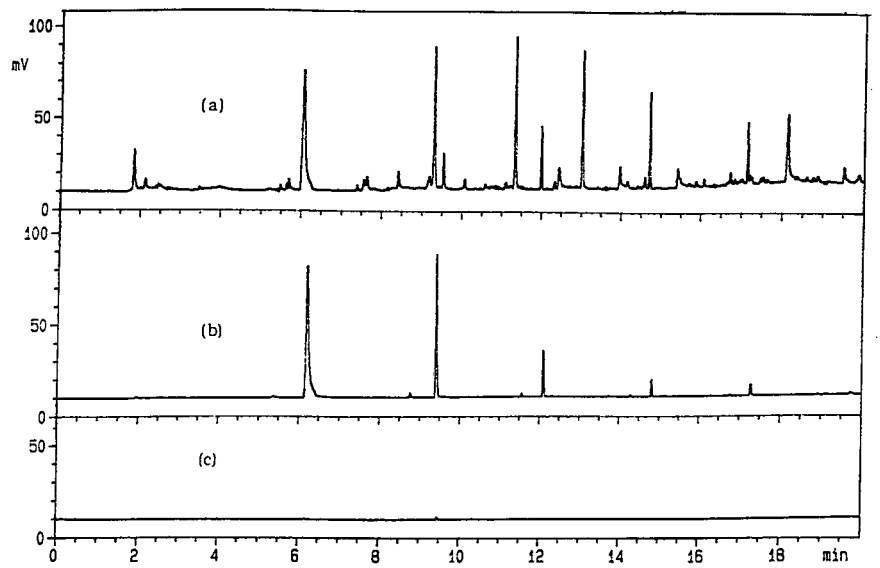

Fig. 9. Blank chromatograms of different capillary cold traps. GC oven temperature programme: 40°C (2 min) to 200°C (2 min) at 10°C/min. TCT: desorption temperature, 230°C; desorption time, 4 min; injection temperature, 220°C; injection time, 1 min. (a) Chromosorb 101 capillary trap; (b) coated and Tenax-TA capillary traps; (c) deactivated capillary trap.

atile organic compounds in ambient air is the analytical detection limit. This is affected not only by the blank levels of the adsorbents used, but also by the blank levels of the capillary cold traps. It is therefore much better wherever possible to use those adsorbents with the lowest blank levels for sampling VOCs in ambient air. Similarly, the capillary cold trap packings with the lowest blank values will give the lowest analytical detection limits.

The blank levels of all these four capillary cold traps, conditioned overnight at 240°C, were determined under the same conditions. Typical chromatograms are shown in Fig. 9. The blank chromatogram of the coated capillary cold trap is similar to that of the Tenax-TA capillary trap, and is not shown in Fig. 9. It can be seen that the deactivated capillary cold trap is very clean, whereas the coated, Tenax-TA and Chromosorb 101 capillary traps are very "dirty". The blank peaks from the coated and Tenax-TA capillary traps, shown in Fig. 9b, are from the leakage of the coated liquid film of the capillary. The blank peaks from the Chromosorb 101 capillary, shown in Fig. 9a, are from both leakage of the coated film and bleeding from the Chromosorb 101 packing. Hence, although the trapping efficiency of the capillary cold trap may be improved by using coated film or packing, the detection limit may be sacrificed to some extent. For the analysis of $\geqslant C_3$ hydrocarbons in ambient air, therefore, the deactivated capillary cold trap should be used. However, in order to analyse the very volatile hydrocarbons, *e.g.*, ethylene, it is suggested that capillary cold traps be prepared by packing uncoated capillary with "clean" and stronger adsorbents, such as Tenax and Carbotrap, and that rigorous cleaning procedures be used to condition the trap.

It should be mentioned that better blank levels of the capillary traps may be obtained if a lower capillary trap desorption temperature is used, but the oven desorption temperature and desorption time will also affect the blank levels of capillary traps because the upper end of the capillary traps interfaced with the desorption oven is heated by the heat wave from the oven. In environmental analysis, the oven desorption temperature is usually above 240°C for more than 5 min in order to desorb the analytes from the adsorbents with the highest efficiency.

CONCLUSIONS

For the application of capillary cold traps to atmospheric samples, it is very important to select suitable cold traps, because some capillary cold traps may not trap the compounds of interest. The results of this work show that deactivated and coated capillary traps cannot trap ethylene at all, even at the lowest trapping temperature (−180°C), and similarly the Tenax-TA capillary trap is also unable to trap ethylene. The Chromosorb 101 capillary trap can retain ethylene at −180°C, but not completely. Although coatings inside the capillary can increase its trapping capacity, this has almost no effect on the trapping efficiency compared with the uncoated capillary trap, especially for the C_2–C_5 hydrocarbons. Packings inside the capillary can increase not only the trapping capacity but also the trapping efficiency of the capillary trap. It is noted that there is a linear relationship between the boiling point of the compound and its maximum trapping temperature.

Although the flow-rate of the carrier gas (10–60 ml/min) has no effect on the trapping efficiency of the capillary traps for the $\geqslant C_5$ hydrocarbons, breakthrough does occur for the C_2–C_4 hydrocarbons at higher flow-rates. Therefore, care should be taken to keep the flow-rate constant in the application of capillary cold traps.

Although the coated and packed capillary cold traps may have improved trapping capacity and trapping efficiency compared with the uncoated, their blank levels are usually very high owing to leakage from the coating or bleeding from the adsorbents. This will adversely affect sensitivity of the method. Therefore, for the analysis of $\geqslant C_3$ hydrocarbons in ambient air, a deactivated capillary cold trap should be used. In order to trap the very volatile hydrocarbons, *e.g.*, ethylene, it is suggested that uncoated capillary cold traps with a packing of preconditioned "clean" and stronger adsorbent, such as Tenax and Carbotrap, be used.

ACKNOWLEDGEMENTS

We thank Mr. Keith Waterhouse for excellent technical assistance and the Government of China, The British Council and the Natural Environment Research Council for funding.

REFERENCES

1 K. Grob and A. Habich, *J. Chromatogr.*, 321 (1985) 45–58.
2 B. V. Burger and Z. Munro, *J. Chromatogr.*, 370 (1986) 449–464.
3 B. V. Burger, M. Leroux and W. J. G. Burger, *J. High Resolut. Chromatogr.*, 13 (1990) 777–779.
4 B. V. Burger, A. E. Nell and W. G. B. Petersen, *J. High Resolut. Chromatogr.*, 14 (1991) 718–723.
5 B. V. Burger, M. Leroux, Z. M. Munro and M. E. Wilken, *J. Chromatogr.*, 552 (1991) 137–151.
6 M. Klemp and R. Sacks, *J. High Resolut. Chromatogr.*, 14 (1991) 235–240.
7 S. Muller and M. Oehme, *J. High Resolut. Chromatogr.*, 13 (1990) 34–39.
8 R. F. Mouradian, S. P. Levine and R. D. Sacks, *J. Chromatogr. Sci.*, 28 (1990) 643–648.
9 A. Hagman and S. Jacobsson, *J. Chromatogr.*, 395 (1987) 271–279.
10 P. Werkhoff and W. Bretschneider, *J. Chromatogr.*, 405 (1987) 87–98.
11 P. Werkhoff and W. Bretschneider, *J. Chromatogr.*, 405 (1987) 99–106.
12 A. Hagman and S. Jacobsson, *J. High Resolut. Chromatogr. Chromatogr. Commun.*, 8 (1985) 332–336.
13 S. Berg and A. Jonsson, *J. High Resolut. Chromatogr. Chromatogr. Commun.*, 7 (1984) 687–695.
14 H. T. Badlings, C. de Jong and R. P. M. Dooper, *J. High Resolut. Chromatogr. Chromatogr. Commun.*, 8 (1985) 755–763.
15 R. G. Derwent and M. E. Jenkin, *Atmos. Environ.*, 25A (1991) 1661–1678.
16 R. G. Derwent and M. E. Jenkin, *AERE Report R 13736*, H. M. Stationery Office, London, 1990.
17 R. G. Derwent and M. E. Jenkin, *AERE Report R 13816*, H. M. Stationery Office, London, 1990.
18 *The Chrompack Guide to Chromatography, General Catalog*, Chrompack, Middelburg, 1991.
19 *Chrompack Thermal Desorption Cold Trap Injector Installation Manual*, Chrompack, Middelburg, 1988.
20 J. W. Graydon and K. Grob, *J. Chromatogr.*, 254 (1983) 265–269.
21 A. Hagman and S. Jacobsson, *J. Chromatogr.*, 448 (1988) 117–126.

Journal of Chromatography, 627 (1992) 227–239
Elsevier Science Publishers B.V., Amsterdam

CHROM. 24 531

Gas chromatographic retention behaviour of alkylated phenanthrenes on a smectic liquid crystalline phase

Application to organic geochemistry

H. Budzinski

URA 348 CNRS, Université de Bordeaux I, F-33405 Talence Cedex (France)

M. Radke

Institute of Petroleum and Organic Geochemistry, Research Centre Jülich (KFA), W-5170 Jülich (Germany)

P. Garrigues

URA 348 CNRS, Université de Bordeaux I, F-33405 Talence Cedex (France)

S. A. Wise

Organic Analytical Chemistry Division, National Institute of Standards and Technology, Gaithersburg, MD 20899 (USA)

J. Bellocq

URA 348 CNRS, Université de Bordeaux I, F-33405 Talence Cedex (France)

H. Willsch

Institute of Petroleum and Organic Geochemistry, Research Centre Jülich (KFA), W-5170 Jülich (Germany)

(First received May 25th, 1992; revised manuscript received July 28th, 1992)

ABSTRACT

The retention indices for the 30 C_2 phenanthrenes and 33 trimethylphenanthrenes were determined by gas chromatography on a smectic liquid crystalline phase. The retention behaviour of these alkylated phenanthrenes was related to molecular shape considerations: length-to-breadth ratio, dihedral angle and substitution pattern. In addition, the influence on the retention behaviour of the arc-like shape of the phenanthrene molecule was investigated. Based on these results, 12 C_2 phenanthrenes and 25 trimethylphenanthrenes were identified in natural samples, such as crude oils and rock extracts.

Correspondence to: P. Garrigues, URA 348 CNRS, Université de Bordeaux I, F-33405 Talence Cedex, France.

0021-9673/92/$05.00

INTRODUCTION

Aromatic compounds are major components of crude oils and rock extracts. They represent 20–45% by weight of the fraction boiling above 210°C of crude oils [1] and contain numerous isomeric structures. The relative distribution of the alkylated aromatic isomers provides information about the maturity levels of the samples [2–9] and about the origin of the organic matter [2,8,10,11]. In order to make valid assessments of maturity and origin, precise identifications of the isomers are required. Identification by gas chromatography (GC) on non-polar phases (DB-5 or similar) often suffers from coelution problems and, thus, must be complemented by measurements such as using phases of different polarity [12,13]. High-performance liquid chromatographic (HPLC) fractionation and high-resolution spectrofluorimetry (Shpol'skii effect; see refs. 14 and 15) were successfully applied in an alternative approach to individual isomer identification. Because those latter techniques were off-line-coupled, they were rather time-consuming and laborious. Development of a capillary GC technique allowing isomer identification in a single step was thus desirable.

Liquid crystalline phases were most promising since they have proved to be very selective in the GC analysis of aromatic compounds [16–18]. In contrast to the non-polar phases, elution is not only controlled by the boiling temperature but also by the geometry of the solutes [19]. In the present study, the retention indices, as determined for 30 C_2 phenanthrenes (C_2-Ps) on a smectic liquid crystalline phase, have been related on one hand to length-to-breadth (L/B) ratio and on the other hand to molecular shape. In subsequent tests, the identification of dimethylphenanthrenes (DMPs) in natural samples was examined.

With a view to exploring further the geochemical utility of alkylphenanthrenes, the smectic liquid crystalline phase was also used to investigate trimethylphenanthrenes (TMPs) in natural samples. They are ubiquitous in petroleum and in organic extracts of sedimentary rocks, but owing to the isomeric complexity of the mixtures and to the low concentrations of TMPs, only 1,2,8-TMP has been previously isolated and identified precisely in a Kuwait oil [20]. Some preliminary studies by liquid and gas chromatography have been performed [21], but owing to numerous coelutions on capillary GC non-polar phases, precise identifications were difficult to obtain. In this study, the retention indices of 33 TMP isomers on the smectic phase are reported, and relationships between the retention behaviour and the molecular shape are discussed.

In addition, we report the identification of DMP and TMP isomers in crude oils and rock extracts using the liquid crystalline phase for capillary GC–mass spectrometry (MS) analyses.

EXPERIMENTAL

Materials

All the C_2-Ps [25 DMPs and five ethylphenanthrenes (EtPs)] and 33 TMPs (of 56 possible ones) isomers were available in this study (Tables I and II). Five TMPs were purchased from Chiron Labs. (Trondheim, Norway) and 28 TMPs were synthesized at the Institute of Petroleum and Organic Geochemistry (Germany), in the same way as the C_2-Ps [7,22] through oxidative photocyclization of alkylated stilbenes. Identification of DMP, EtP and TMP standards was based on ^{1}H NMR data. The numbering of the position of substitution on the aromatic rings is given in Fig. 1. In the following discussion, the term molecular shape will refer to the arc-like shape of the phenanthrene molecule, *i.e.*, the three aromatic rings are annulated in an arc arrangement (Fig. 1).

Three geological samples were investigated: a rock extract 20 from the Handil field, Kalimantan (Indonesia), a condensate 102 from the Aquitaine basin (France) and a crude oil 27 from the Handil field, Kalimantan (Indonesia). The diesel particulate sample was a methylene chloride extract of Standard Reference Material 1650, Diesel Particulate Matter (SRM 1650), which was obtained from the Standard Reference Material Program at the National Institute of Standards and Technology (NIST) [23]. Triaromatic fractions were collected after HPLC on an aminosilane stationary phase, as described elsewhere [14].

Chromatographic and detection conditions

The alkylated phenanthrene standards and the triaromatic HPLC fractions were analysed by GC–MS using an HP 5890 series II gas chromatograph

TABLE I

RETENTION INDICES, SHAPE PARAMETERS AND ENTHALPIES OF FORMATION FOR DMP AND EtP ISOMERS

I values were determined by experiment and I_C values were calculated using eqn. 2 (see text) (D = dihedral angle; n.d. = not determined).

Compound	I	L/B	I_C	Deviation (%)	D (°)	ΔH_f^0 (kcal/mol)
1,2-DMP	335.01	1.58	330.63	−1.3	0.10	37.1
1,3-DMP	316.51	1.28	318.51	+0.6	0.05	35.7
1,4-DMP	318.92	1.32	320.12	+0.4	6.95	43.7
1,5-DMP	320.81	1.31	319.72	−0.3	6.40	43.5
1,6-DMP	321.68	1.37	322.14	+0.1	0.05	35.6
1,7-DMP	333.69	1.59	331.03	−0.8	0.05	35.6
1,8-DMP	327.76	1.55	329.41	+0.5	0.00	37.5
1,9-DMP	317.01	1.28	318.51	+0.5	0.05	37.6
1,10-DMP	326.12	1.29	318.91	−2.2	0.45	42.8
2,3-DMP	322.51	1.38	322.55	0.0	0.00	34.8
2,4-DMP	321.24	1.38	322.55	+0.4	3.35	41.2
2,5-DMP	323.01	1.38	322.55	−0.1	3.10	41.1
2,6-DMP	322.84	1.40	323.35	+0.2	0.00	33.6
2,7-DMP	335.95	1.70	335.47	−0.1	0.00	33.6
2,9-DMP	323.67	1.37	322.14	−0.5	0.00	35.6
2,10-DMP	320.83	1.37	322.14	+0.4	0.00	35.6
3,4-DMP	321.94	1.31	319.72	−0.7	11.90	43.6
3,5-DMP	312.63	1.29	318.91	+2.0	3.90	41.3
3,6-DMP	308.63	1.33	320.53	+3.9	3.73	33.7
3,9-DMP	315.94	1.12	312.04	−1.2	0.00	35.7
3,10-DMP	313.36	1.12	312.04	−0.4	0.00	35.6
4,5-DMP	296.39	1.29	318.91	+7.4	27.20	52.3
4,9-DMP	315.21	1.29	318.91	+1.2	5.70	43.4
4,10-DMP	314.53	1.13	312.45	−0.7	6.50	43.7
9,10-DMP	323.11	1.28	318.51	−1.4	1.28	41.6
1-EtP	316.06	1.59	n.d.	n.d.	n.d.	n.d.
2-EtP	323.63	1.77	n.d.	n.d.	n.d.	n.d.
3-EtP	306.33	1.09	n.d.	n.d.	n.d.	n.d.
4-EtP	301.09	1.09	n.d.	n.d.	n.d.	n.d.
9-EtP	306.67	1.09	n.d.	n.d.	n.d.	n.d.

equipped with a splitless injector (purge delay, 30 s; purge flow-rate, 60 ml/min). The column was 50 m × 0.22 mm I.D. SB-Smectic phase (Dionex, Lee Scientific Division, Salt Lake City, UT, USA), film thickness 0.1 μm. Helium was used as the carrier gas with 2.5 bar as the inlet pressure. The detector was an HP 5970 mass selective detector (electron impact 70 eV; selected ion monitoring (SIM) mode: m/z 206 for C_2-Ps and m/z 220 for TMPs at 2 scans/s; voltage, 2200 V). The temperature programme included an initial isothermal period of 2 min at 50°C, then programming at 10°C/min to 140°C, followed by an isothermal period of 2 min at 140°C, then programming at 2°C/min to 250°C with an isothermal period of 30 min at 250°C. The injector and the transfer line were kept at 250°C.

Retention indices

Retention data are expressed as retention indices (I). I values are based on a comparison of the retention times of the compounds of interest with those of reference standards included with the solutes. Kovats [24], in his original I scale, used isothermal conditions and homologous n-alkanes for calibration [24]. In contrast, for the analysis of polycyclic aromatic hydrocarbons (PAHs), which is

TABLE II

RETENTION INDICES, SHAPE PARAMETERS AND ENTHALPIES OF FORMATION FOR THE 33 TMP ISOMERS STUDIED

I values were determined by experiment and I_C values were calculated from eqn. 3 (see text) (D = dihedral angle; n.d. = not determined).

Compound	I	L/B	I_C	Deviation (%)	D (°)	ΔH_f^0 (kcal/mol)
1,2,5-TMP	353.23	1.40	336.99	−4.6	22.96	35.9
1,2,6-TMP	340.61	1.46	340.45	0.0	0.42	28.9
1,2,7-TMP	353.23	1.67	352.55	−0.2	0.23	28.9
1,2,8-TMP	348.70	1.40	336.99	−3.4	0.46	30.8
1,2,9-TMP	335.72	1.36	334.68	−0.3	0.43	30.9
1,3,5-TMP	322.43	1.16	323.16	+0.2	22.23	34.5
1,3,6-TMP	320.69	1.20	325.46	+1.5	0.25	27.4
1,3,7-TMP	334.96	1.38	335.84	+0.3	0.02	27.4
1,3,8-TMP	330.94	1.19	324.89	−1.8	0.18	29.4
1,3,9-TMP	321.46	1.01	314.51	−2.2	0.07	29.4
1,3,10-TMP	318.53	1.12	320.85	+0.7	2.78	34.5
1,4,6-TMP	327.13	1.31	331.80	+1.4	22.17	34.5
1,4,7-TMP	335.49	1.37	335.26	−0.1	22.38	34.5
1,4,8-TMP	329.89	1.27	329.50	−0.1	22.85	36.4
1,5,6-TMP	336.96	1.33	332.96	−1.2	24.79	36.3
1,5,9-TMP	322.75	1.20	325.46	+0.8	24.29	36.6
1,6,7-TMP	338.86	1.45	339.87	+0.3	0.19	28.0
1,6,9-TMP	324.69	1.22	326.62	+0.6	0.19	29.3
1,7,9-TMP	330.78	1.30	331.23	+0.1	0.00	29.3
2,3,5-TMP	329.25	1.39	336.41	+2.2	18.52	33.0
2,3,6-TMP	325.25	1.30	331.23	+1.8	0.16	26.0
2,3,7-TMP	340.08	1.46	340.45	+0.1	0.24	26.0
2,3,10-TMP	325.95	1.20	325.46	−0.1	0.15	28.0
2,5,6-TMP	338.24	1.48	341.60	+1.0	23.65	33.1
2,5,9-TMP	326.94	1.23	327.19	+0.1	21.76	34.5
2,5,10-TMP	327.86	1.24	327.77	0.0	21.22	34.4
2,6,9-TMP	327.62	1.29	330.65	+0.9	0.21	27.3
2,6,10-TMP	328.75	1.34	333.53	+1.5	0.26	27.3
2,7,9-TMP	337.82	1.45	339.87	+0.6	0.03	27.3
3,4,6-TMP	324.59	1.21	326.04	+0.4	23.44	34.0
3,4,10-TMP	319.72	1.22	326.62	0.0	25.10	32.3
3,5,9-TMP	322.46	1.11	320.28	−0.7	22.18	34.6
3,5,10-TMP	319.72	1.14	322.00	+0.7	21.74	34.4

commonly performed by linear programmed temperature GC, Lee *et al.* [25] have introduced a calibration scale based on the following aromatic standards: benzene, naphthalene, phenanthrene, chrysene and picene. These compounds were assigned I values of 100, 200, 300, 400 and 500, respectively, and I was calculated according to eqn. 1 [25]:

$$I = 100 \cdot \frac{t_{r(X)} - t_{r(z)}}{t_{r(z+1)} - t_{r(z)}} + 100z \quad (1)$$

where t_r is retention time, X is the compound of interest (in this study the phenanthrene derivatives) and z and $z + 1$ are the number of aromatic rings in the standard aromatics eluting prior to (phenanthrene) and after (chrysene) the compounds studied (here $z = 3$).

Molecular mechanics and L/B ratio calculations

The calculations for the L/B values were carried out for the C_2-Ps [26] with a VAX computer using

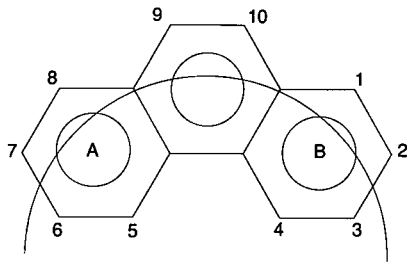

Fig. 1. Numbering of the phenanthrene molecule.

the MM2MMP2 empirical force field method (version 1982, Molecular Design, San Leandro, CA, USA [27,28]). For the TMP isomers, they were performed on a desk-top microcomputer (Tandy 3000 NL), using the MMIIPC software (QCPE, Indiana University, Bloomington, IN, USA), derived from the original MM2MP2 empirical force field method [27,28]. The calculations provided an estimate of the steric energy and the heat of formation of the compounds (ΔH_f^0) at 298 K in the gas phase. They also yielded the geometry of the molecule [bond lengths, angles and particularly the dihedral angle between ring A and ring B (see Fig. 1)]. In-house software was used to provide the length (L) and the breadth (B) of the molecule: these values correspond to the dimensions of a minimized rectangle for each molecule studied, calculated according to the approach of Radecki *et al.* [29] and Wise *et al.* [30]. Both calculation softwares give comparable results for geometry and enthalpy values.

RESULTS AND DISCUSSION

C_2-P analysis

An SIM chromatogram of some C_2-P standards used in the determination of retention indices is shown in Fig. 2. These particular isomers were chosen because they are those generally present in crude oils and rock extracts [7] and are also representative of the retention behaviour of C_2-Ps. The I values determined on the smectic liquid crystalline stationary phase for all the C_2-P isomers are given in Table I. One unit of I corresponds to a difference in retention times of 40 s. Compounds differing by 0.50 I unit are baseline-resolved, those differing by 0.25 I unit are 50% resolved, and those differing by 0.15 I unit are 30% resolved. From the data presented in Table I, it follows that severe coelution

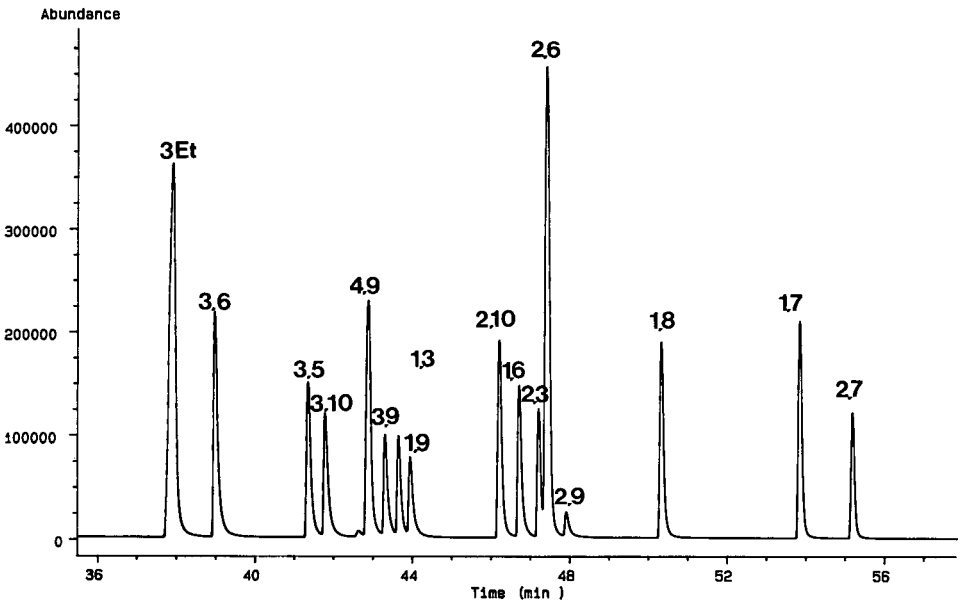

Fig. 2. Partial gas chromatogram of reference C_2-P standards used in the determination of GC retention indices (see text for experimental conditions). Peaks: 3Et = 3-ethylphenanthrene; 1,3 = 1,3-dimethylphenanthrene.

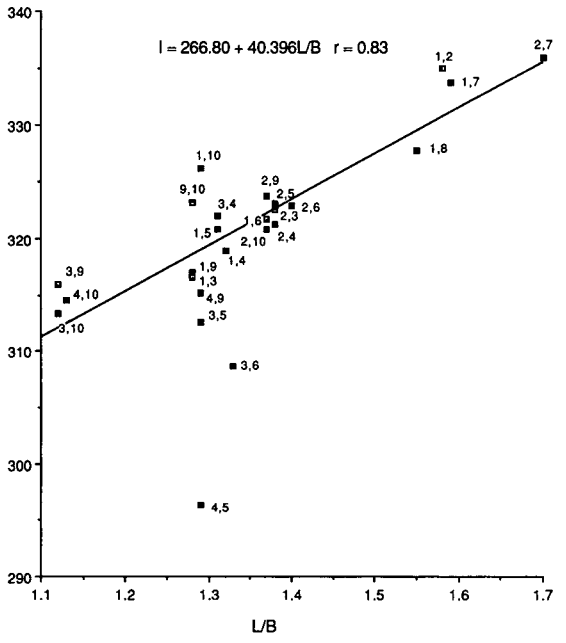

Fig. 3. Plot of GC retention indices *versus* L/B values for all 25 DMP isomers.

occurs only in one case, *i.e.*, between 2,10- and 1,5-DMP. Otherwise, the partial resolution (I difference in parentheses) between 2,10- and 2,4-DMP (0.41 I), between 2,4- and 1,6-DMP (0.44 I), between 1,6- and 3,4-DMP (0.27 I), between 2,3- and 2,6-DMP (0.33 I), between 2,6- and 2,5-DMP (0.17 I), and between 2,5- and 9,10-DMP (0.1 I) is sufficient for the identification of these isomers in natural samples. Furthermore, some of these partially resolved isomers (2,4-, 3,4-, 2,5- and 9,10-DMP), which exhibit strained molecular structures with rather large dihedral angles (see Table I), are quite unstable (they have the largest ΔH_f^0 values, see Table I) and seem to be not present in natural samples [7]. Only one of the partially resolved pairs (2,3-DMP and 2,6-DMP) has been reported to be present in natural samples [7]. The 50% resolution obtained in this case is sufficient for identification and even for quantification.

The DMP isomers differ significantly in L/B values and also in dihedral angle values (see Table I). The elution order of DMP isomers roughly follows increasing L/B values (see Fig. 3). Unstrained long or narrow DMP molecules are generally more retained than those having a square-like shape. For instance, 2,7- and 1,7-DMP, which exhibit high L/B values of 1.7 and 1.6, respectively, are eluted later, whereas 3,9- and 3,10-DMP with low values of L/B (1.1) are eluted more rapidly. On the other hand, compounds with large dihedral angles generally elute before the unstrained DMP with a low L/B. For example, 4,5-DMP exhibits a dihedral angle of 27.20° and, despite a rather high L/B value of 1.3, elutes much earlier ($I = 296.39$) than the other isomers.

Fig. 3 shows the correlation between I and L/B for the 25 DMP isomers. The correlation equation obtained for DMP, is

$$I = 266.80 + 40.396\ L/B \qquad (2)$$

with a correlation coefficient $r = 0.83$ (4,5-DMP has been omitted from the calculation because it obviously has very different retention behaviour from the other DMP isomers). Predicted retention indices (I_C) are calculated from eqn. 2 and compared with measured I values. The average deviation between I_C and I is *ca.* 0.83 when 4,5-DMP is not considered. The highest deviation is 7.4% for 4,5-DMP. Two other DMP, 3,6- and 1,10-DMP, exhibit rather significant deviations when compared with the average deviation, *i.e.*, 3.9% and −2.2%, respectively. The other DMP isomers show deviations of less than 2%, with the majority less than 1%. Although the linear model represented by eqn. 2 generally has a reasonable predictive ability, parameters other than L/B values must be considered in order to understand the strong deviations observed in some cases. Thus, the molecular shapes, which have already been shown to have an influence on the retention of PAHs on liquid crystalline phases [31,32], and the dihedral angles, which have already been mentioned as an important factor affecting retention in HPLC on polymeric C_{18} phases [26,33], were investigated.

4,5-DMP, which deviates in retention behaviour the most significantly from the global set of DMP (deviation of 7.4%), is eluted much earlier than predicted. This isomer has a very strained molecular structure (dihedral angle greater than 27°), and its retention behaviour is compatible with the previous "slot" model proposed by Wise and Sander [34] in reversed-phase liquid chromatography. Strained molecules such as 4,5-DMP, which interact weakly with the stationary phase, will be retained less. The

distortion of the molecules hinders penetration of the solutes into the slots. The effect is less pronounced with 4,9-DMP, despite the large dihedral angle (5.7°). However, steric exclusion is indicated also in this case by the earlier than expected elution (deviation 1.2%).

The other DMP isomers showing "anomalous" behaviour are 3,6- and 3,5-DMP, which elute earlier than predicted with deviations of 3.9% and 2.0%, respectively, and 9,10-, 3,9-, 1,10- and 1,2-DMP, which elute later than predicted with deviations of −1.4%, −1.2%, −2.2% and −1.3%, respectively. For these isomers the dihedral angle does not account for these deviations and the molecular shape has to be considered.

Other authors have introduced the concept of the arc-like arrangement to explain certain retention behaviour on liquid crystalline phases [32]. Phenanthrene is a molecule with aromatic rings annelated in a curved arrangement (see Fig. 1). Methyl groups in positions 3, 4, 5 and 6 are "inside the arc". Methyl groups in positions 3 and 6 retain the arc arrangement and even continue the arc, whereas methyl groups in positions 1, 8, 9 and 10 are attached to the outer curved side of the arc. The elution of 3,6-DMP earlier than expected from its L/B value (I deviation 3.9%) is attributed to the fact that the two methyl groups are in line with the arched arrangement of the aromatic rings, hence continuing and even emphasizing the arc-like topography of the phenanthrene molecule. Likewise, the relative early elution of 3,5-DMP (I deviation 2.0%) is believed to result from an extension of the molecular arc by the methyl group in position 3. Because the methyl group inside the arc (position 5) does not contribute to the effect, the deviation is less pronounced in this case.

1,2-, 9,10- and 1,10-DMP, which have their methyl substituents attached to the outer curved side of the arc, are eluted later than predicted from their L/B values. 3,9-DMP has one methyl group outside the arc (position 9) and is also retained longer than predicted. In the cases of 1,2- and 9,10-DMP, the two adjacent methyl groups may also explain retention times that are longer than predicted. This *ortho*-effect is already known for alkylated benzenes [35], alkylated naphthalenes [36] and alkylated benzothiophenes [37], and it is explained as a function of the lower vapour pressure exhibited by *ortho*-isomers [35]. Furthermore, this *ortho*-effect has been already mentioned for liquid crystalline phases [38].

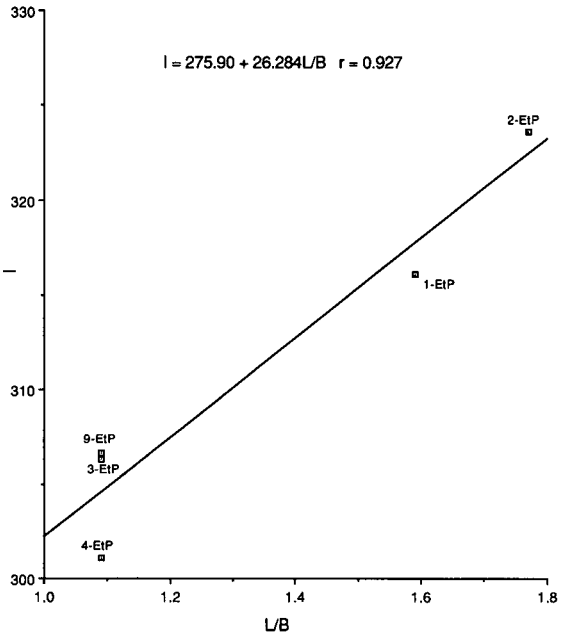

Fig. 4. Plot of GC retention indices *versus* L/B values for all EtP isomers.

The same considerations apply to EtPs, which are eluted according to their L/B values (see Fig. 4), *i.e.*, 2-EtP, which has the largest L/B value, is eluted after 1-, 3- and 9-EtP. 4-EtP, as a very strained molecule, should have a significant dihedral angle. This would explain its elution before 3- and 9-EtP despite coincident L/B values.

Among the different factors governing the retention behaviour of EtP and DMP isomers, the L/B ratio is still the major factor. However, other parameters, such as the dihedral angle, the molecular shape and the *ortho*-effect, also influence the elution order. For the majority of the C_2-P isomers, the second and third parameters seem to compensate one another and the retention behaviour is determined mainly by the L/B ratio. In those cases when one of these parameters is stronger than the others, deviations are observed: a large dihedral angle is responsible for early elution; the *ortho*-effect results in late elution of the isomers; finally arc-like molecules with substituents that maintain the arc arrangement (3,6- and 3,5-DMP) seem to elute earlier than expected, whereas molecules with substituents

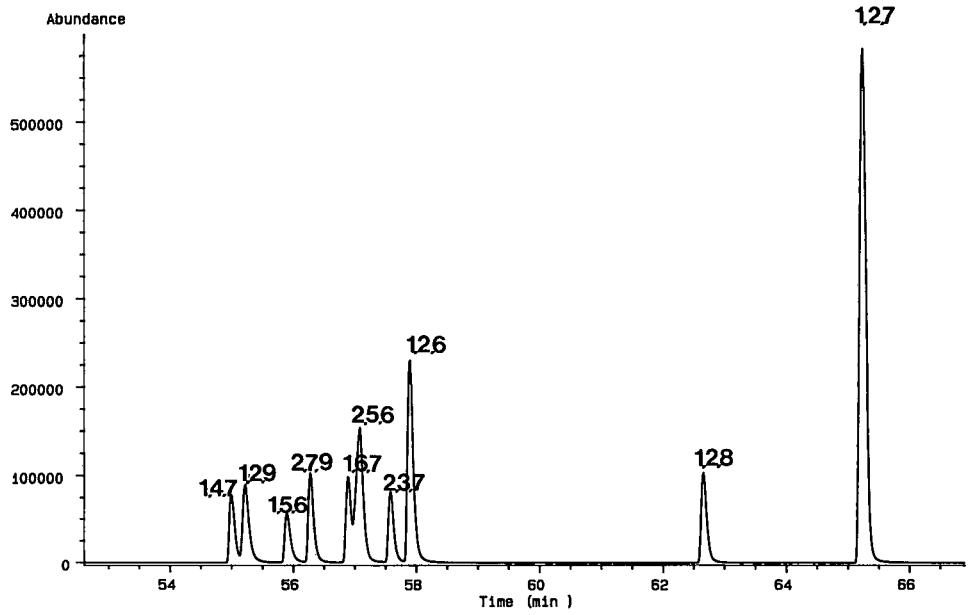

Fig. 5. Partial gas chromatogram of reference TMP standards used in the determination of GC retention indices (see text for experimental conditions). 1,2,8 = 1,2,8-Trimethylphenanthrene.

attached to the outer curved side of the arc are retained longer. This behaviour is compatible with previous studies [29,30] and perhaps could be attributed to specific interaction of arc-like molecules with the liquid crystalline stationary phase.

TMP analysis

An SIM chromatogram of TMP standards used in the determination of retention indices is shown in Fig. 5. The *I* values determined on the smectic liquid crystalline phase for the 33 available TMP isomers are given in Table II. As in the case of C_2-P isomers, one unit of *I* corresponds to a difference in retention times of 40 s. Compounds differing by 0.50 *I* unit are baseline-resolved, those differing by 0.25 *I* unit are 50% resolved, and those differing by 0.15 *I* unit are 30% resolved. From the data presented in Table II, it follows that severe coelution occurs in five cases, *i.e.*, 1,6,9-/3,4,6-TMP, 1,7,9-/1,3,8-TMP, 3,5,9-/1,3,5-TMP, 1,2,7-/1,2,5-TMP and 3,4,10-/3,5,10-TMP. Otherwise the partial resolution (*I* difference in parentheses) between 3,5,9-/1,3,5- and 1,5,9-TMP (0.32 *I*), between 2,5,9- and 1,4,6-TMP (0.19 *I*), between 2,6,9- and 2,5,10-TMP (0.24 *I*), between 1,4,7- and 1,2,9-TMP (0.23 *I*) and between 2,7,9-

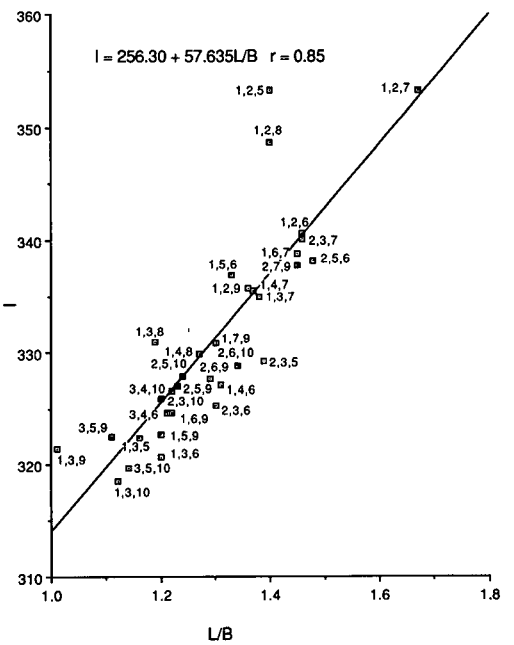

Fig. 6. Plot of GC retention indices *versus* *L/B* values for 33 TMP isomers.

and 2,5,6-TMP (0.42 *I*) is sufficient for the identification of these isomers in natural samples.

As in the case of DMPs, TMP isomers differ significantly in *L/B* values (see Table II). The elution order of TMPs generally follows increasing *L/B* values. For instance, 1,2,7- and 1,2,6-TMP, which exhibit the highest *L/B* values (1.7 and 1.5, respectively) elute later, and 3,5,9- and 1,3,9-TMP, with low *L/B* values (1.1 and 1.0, respectively) elute very early.

Fig. 6 shows the correlation obtained for the 33 TMPs when *I* is plotted *versus L/B*, where linear regression gives

$$I = 256.30 + 57.635\ L/B \quad (3)$$

and a correlation coefficient $r = 0.85$. Predicted I_C values were calculated from eqn. 3 and compared with the measured *I* values. The average deviation is *ca.* 1%. The highest deviations are −4.6% and −3.4% for 1,2,5- and 1,2,8-TMP. The remaining TMP isomers have deviations of *ca.* 2% or less, the majority being less than 1%. TMP isomers showing deviations greater than 1% are the following: 1,3,9-TMP (−2.2%), 1,5,6-TMP (−1.2%), 1,3,8-TMP (−1.8%), 2,6,10-TMP (1.5%), 1,4,6-TMP (1.4%), 2,3,5-TMP (2.2%), 2,3,6-TMP (1.8%) and 1,3,6-TMP (1.5%). The retention behaviour is predicted quite well by eqn. 3; however, as was the case with the DMP isomers, the molecular shape, dihedral angle and *ortho*-substitution pattern must also be taken into account to explain the deviations.

Like 1,2-DMP, the two TMP isomers (1,2,8- and 1,2,5-TMP) with the most significant deviations elute much later than predicted, as was also observed for 1,2-DMP, for these isomers also possess the 1/2 substitution sequence, *i.e.*, the *ortho*-effect could explain the deviation. Moreover, they have two (1,2,5-TMP) or three (1,2,8-TMP) methyl substituents attached to the outer curved side of the arc. Two other TMPs that are retained longer than predicted (1,3,9- and 1,3,8-TMP) are also in this category, with two substituents outside the arc. Their retention behaviour should be compared with that of 3,9-DMP. 1,5,6-TMP has two substituents inside the arc and, one outside, and shows an *ortho*-effect. These last two characteristics seem to control the retention behaviour of this compound, *i.e.*, elution is delayed.

In the case of 1,3,6- and 2,3,6-TMP, the methyl substituents maintain the arc shape. These isomers are retained less than predicted from the *L/B* values, and can be compared with 3,6-DMP, which is also retained less than expected. 2,6,10- and 1,4,6-TMP have two substituents maintaining the arc shape and are eluted earlier than predicted. 2,3,5-TMP has its substituents inside the arc and also shows the *ortho*-effect. Since it is eluted earlier than predicted, the *ortho*-effect must be of minor importance compared with the molecular shape. Its retention behaviour should be compared with that of 3,5-DMP, which is also eluted earlier than expected.

It seems that, as in the case of DMP isomers, the TMP isomers with substituents outside the arc elute later than expected and those with substituents that maintain the arc are retained less than predicted from *L/B* values. The contribution of the dihedral angle to the retention behaviour of TMP isomers is difficult to estimate because of the lack of very strained reference compounds (*i.e.*, with 4/5 substitution pattern).

In conclusion it can be stated that, as was the case for the DMP, the *L/B* ratio is the major TMP retention behaviour parameter. It appears that secondary factors are the molecular shape (arc arrangement) and the *ortho*-effect. The molecular shape appears to have a stronger influence on retention behaviour than the *ortho*-effect (see the case of 2,3,5-TMP). Finally, the dihedral angle appears to have an influence only for very strained isomers, but this last point needs to be confirmed with additional reference compounds.

Identification of C_2-Ps and TMPs in natural samples

Figs. 7 and 8 show identifications performed for C_2-Ps and TMPs in a sample of a crude oil. True identifications were achieved by capillary GC–MS and co-injection with pure standards.

Tables III and IV give the relative abundances of C_2-Ps and TMPs in natural samples (crude oil, rock extract, condensate and diesel exhaust). It is evident that the relative amounts of the isomers vary from sample to sample. The origin of these individual variations would be of great interest in geochemical studies, as discussed elsewhere [39].

Nevertheless, it is interesting to note that 1,2-DMP, which has not been identified previously in natural samples, was observed in all the investigated samples. We can also note the presence of 2-EtP,

TABLE III

RELATIVE DISTRIBUTION OF C_2-Ps IN NATURAL SAMPLES

Values are percentages of the total C_2-P content.

Sample	Relative abundance of C_2-phenanthrenes (%)																
	9Et	3Et	3,6	3,10	3,9	1,3	1,9	2,10	1,6	2,3	2,6	2,9	1,8	1,7	2,7	1,2	2Et
Crude oil 27	0.0	2.9	5.3	8.1	7.3	4.8	4.7	7.8	6.0	3.8	13.9	7.3	2.3	12.8	7.0	2.1	3.7
Rock 20	0.0	3.3	2.9	5.9	6.2	4.6	4.5	5.5	6.4	3.7	11.8	7.9	5.0	17.7	4.7	4.2	5.5
Condensate 102	0.0	0.0	12.5	8.6	7.3	6.1	2.2	6.1	5.7	6.9	21.9	6.3	1.4	5.3	8.4	1.3	0.0
Diesel	0.6	1.6	6.5	7.0	6.1	6.7	3.0	8.1	6.3	7.5	15.2	7.4	2.0	8.1	9.0	2.4	2.5

TABLE IV

RELATIVE DISRIBUTION OF TMPs IN NATURAL SAMPLES

Values were calculated using the chromatographic peaks corresponding to the TMP isomers identified in natural samples.

Sample	Relative abundance of trimethylphenanthrenes (%)																			
	1,3,10	3,5,10	1,3,6	1,3,9	1,3,5 + 3,5,9	1,5,9	1,6,9 + 3,4,6	2,3,6	2,3,10	2,6,9	2,6,10	1,7,9 + 1,3,8	1,3,7	1,2,9	2,7,9	1,6,7	2,3,7	1,2,6	1,2,8	1,2,7 + 1,2,5
Crude oil 27	7.6	1.0	5.3	3.6	2.5	1.4	4.7	5.1	6.8	10.6	7.2	10.9	6.3	1.5	7.3	3.4	5.9	3.4	4.3	3.2
Rock 20	4.7	0.0	2.9	3.9	2.9	2.8	5.6	3.8	2.9	11.8	4.3	10.2	5.3	n.d.	6.1	3.0	8.7	4.9	9.1	4.1
Condensate 102	11.1	0.0	8.7	3.1	0.2	0.6	2.9	9.3	4.8	10.9	9.1	7.9	8.0	0.4	7.5	2.8	9.0	1.3	1.4	1.2
Diesel	6.2	0.0	6.2	3.0	1.1	2.3	3.7	7.1	4.0	8.5	6.6	10.1	8.1	1.1	8.8	4.3	11.0	2.3	3.0	2.7

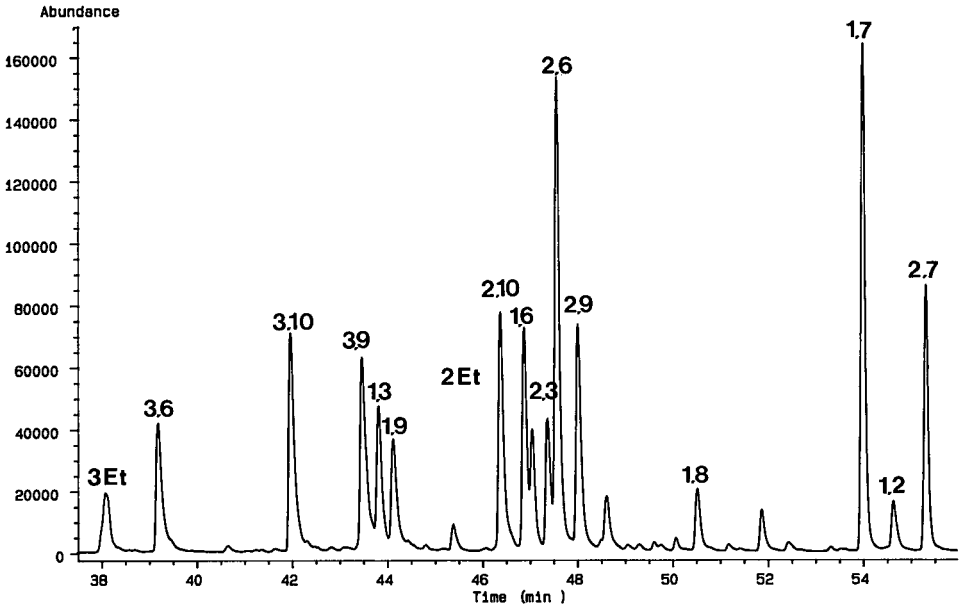

Fig. 7. Partial SIM (*m/z* 206) chromatogram of a triaromatic fraction of crude oil #27; identification of C_2-P isomers by co-injection with standard compounds. Peaks: 2Et = 2-ethylphenanthrene; 2,6 = 2,6-dimethylphenanthrene.

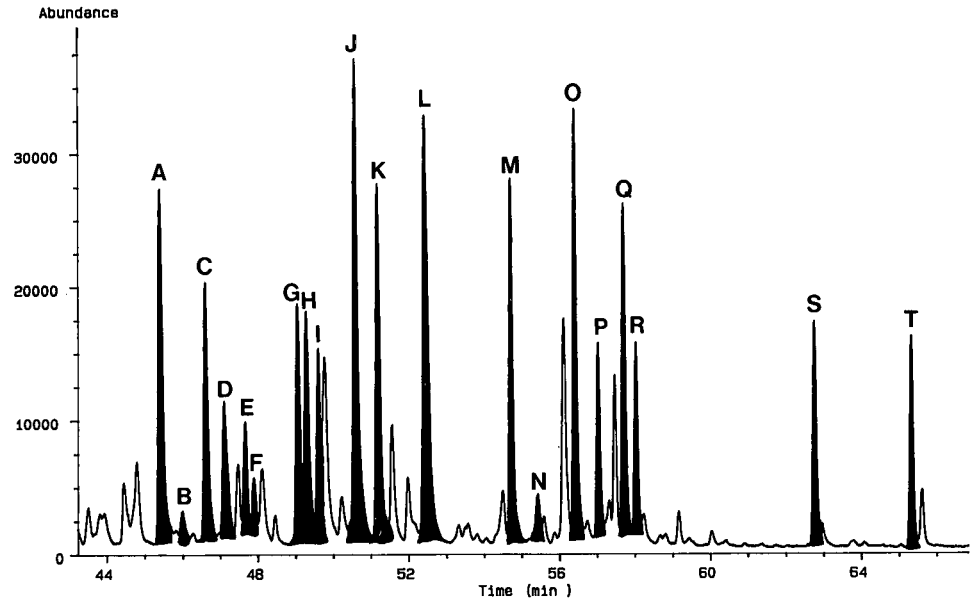

Fig. 8. Partial SIM (*m/z* 220) chromatogram of a triaromatic fraction of crude oil 27; identification of TMP isomers by co-injection with standard compounds. Peaks: A = 1,3,10-TMP; B = 3,5,10-TMP; C = 1,3,6-TMP; D = 1,3,9-TMP; E = 1,3,5-TMP + 3,5,9-TMP; F = 1,5,9-TMP; G = 1,6,9-TMP + 3,4,6-TMP; H = 2,3,6-TMP; I = 2,3,10-TMP; J = 2,6,9-TMP; K = 2,6,10-TMP; L = 1,7.9-TMP + 1,3,8-TMP; M = 1,3,7-TMP; N = 1,2,9-TMP; O = 2,7,9-TMP; P = 1,6,7-TMP; Q = 2,3,7-TMP; R = 1,2,6-TMP; S = 1,2,8-TMP; T = 1,2,7-TMP + 1,2,5-TMP.

which was difficult to confirm otherwise. The strained C_2-P isomers (wih methyl or ethyl groups in positions 4 and 5), which are unstable, were absent in these samples, as reported previously in other studies [7].

Among the 33 available TMP standards, the most stable ones (*i.e.*, the 18 showing the lowest ΔH_f^0 values, see Table II) were all found in the natural samples investigated. In highly thermally stressed samples, such as diesel exhaust and oil condensate, an increase in the abundance of the most stable TMP isomers (*i.e.*, 2,3,6-, 2,3,7-, 1,3,6- and 1,3,7-TMP), compared with the TMP distribution in the crude oil and in the rock extract, can be noted. Conversely, the abundance of a less stable TMP, such as 1,2,8-TMP, decreases with increasing thermal maturity (from the rock extract to the oil condensate). The least stable isomers (*i.e.*, with $\Delta H_f^0 > 32$ kcal/mol) were not present.

The case of 1,3,10-TMP is ambiguous because, based on its retention time, it is present in natural samples; however, owing to its rather high ΔH_f^0 (34.5 kcal/mol) it should not be present in the amount found in the investigated samples. Possible coelution with another TMP not yet available but more stable could explain these results. Theoretical calculations suggest 2,3,9-TMP as a possible candidate. Indeed, it has a L/B value of 1.20 and a ΔH_f^0 value of 27.96 kcal/mol. From this value of the enthalpy of formation compared with the others (see Table II, *e.g.*, it is as stable as 2,3,10-TMP and more stable than 1,6,9- or 1,3,10-TMP, which are present in natural samples), it is reasonable to suspect its presence in natural samples. Its calculated I value from eqn. 3 (with $L/B = 1.20$) is 325.46. This is consistent with possible coelution between 1,3,10- and 2,3,9-TMP. In such a case, the deviation, for 2,3,9-TMP, of 1.4% between $I_C = 325.46$ and $I = 318.53$ (the value obtained for 1,3,10-TMP) could be explained by the influence of the molecular shape as in the case of 1,3,5-TMP (see above). These assumptions need to be proved, and the synthesis of the 2,3,9-TMP is now under progress.

The quantitative results (percentage relative abundance) for the TMP isomers corroborate quite well the thermodynamic calculations performed on them.

CONCLUSIONS

The smectic liquid crystalline phase used in this study has provided an alternative tool for individual identification of C_2-Ps, and it has allowed the determination of C_2-Ps not yet identified in natural samples. In the case of TMP analysis, the smectic liquid crystalline phase provides useful GC patterns that allow identification of some of the most abundant isomers.

Furthermore, this study illustrates the potential of theoretical methods to generate molecular parameters, such as L/B ratios and dihedral angles, which can then be used to predict or at the least to explain the elution order of C_2-P and TMP isomers on liquid crystalline phases, even if, up to now, the contribution to the final elution order of parameters such as the dihedral angle or the molecular shape cannot be quantitated. The natural occurrence of TMP isomers could also be predicted according to their calculated ΔH_f^0 values.

ACKNOWLEDGEMENTS

We are indebted to J. Connan [SNEA (P)] and to J. L. Oudin (TOTAL-CFP) for providing sample sets for this study and for permission to publish. TOTAL-CFP and SNEA (P) are acknowledged for financial support. NATO (No. 870486) and PROCOPE programme are also acknowledged for financial support.

REFERENCES

1 B. P. Tissot and D. H. Welte, *Petroleum Formation and Occurrence*, Springer, Berlin, 2nd ed., 1984, 699 pp.
2 M. Radke, *Adv. Petroleum Geochem.*, 2 (1987) 141.
3 M. Radke, *Marine Petroleum. Geol.*, 5 (1988) 224.
4 M. Radke, H. Willsch, D. Leythaeuser and M. Teichmüller, *Geochim. Cosmochim. Acta*, 46 (1982) 1831.
5 P. Garrigues, R. de Sury, M. L. Angelin, J. Bellocq, J. L. Oudin and M. Ewald, *Geochim. Cosmochim. Acta*, 52 (1988) 375.
6 P. Garrigues, R. de Vazelhes de Sury, M. L. Angelin, M. Ewald, J. L. Oudin and J. Connan, *Org. Geochem.*, 6 (1984) 829.
7 M. Radke, P. Garrigues and H. Willsch, *Org. Geochem.*, 15 (1990) 17.
8 M. G. Strachan, R. Alexander and R. I. Kagi, *Geochim. Cosmochim. Acta*, 52 (1988) 1255.
9 R. Alexander, R. I. Kagi, S. J. Rowland, P. N. Sheppard and T. V. Chirila, *Geochim. Cosmochim. Acta*, 49 (1985) 385.

10 W. Püttman and H. Villar, *Geochim. Cosmochim. Acta*, 51 (1987) 3023.
11 P. Garrigues, A. Saptorahardjo, C. Gonzalez, P. Wehrung, P. Albrecht, A. Saliot and M. Ewald, *Org. Geochem.*, 10 (1986) 959.
12 S. J. Rowland, R. Alexander and R. I. Kagi, *J. Chromatogr.*, 294 (1984) 407.
13 R. Alexander, R. I. Kagi and P. N. Sheppard, *J. Chromatogr.*, 267 (1983) 367.
14 P. Garrigues and M. Ewald, *Anal. Chem.*, 55 (1983) 2155.
15 M. Radke, H. Willsch, P. Garrigues, R. de Sury and M. Ewald, *Chromatographia*, 19 (1984) 355.
16 G. M. Janini, K. Johnston and W. L. Zielinski, Jr., *Anal. Chem.*, 47 (1975) 670.
17 G. M. Janini, G. M. Muschik and W. L. Zielinski, Jr., *Anal. Chem.*, 48 (1976) 809.
18 F. Janssen, *Int. J. Environ. Anal. Chem.*, 13 (1982) 37.
19 Z. Witkiewicz, *J. Chromatogr.*, 251 (1982) 311.
20 W. Carruthers and A. G. Douglas, *J. Chem. Soc.*, (1957) 278.
21 M. Radke, H. Budzinski, C. Pierard, H. Willsch and P. Garrigues, *J. Pol. Arom.*, (1992) in press.
22 P. Garrigues, E. Parlanti, M. Radke, J. Bellocq, H. Willsch and M. Ewald, *J. Chromatogr.*, 395 (1987) 217.
23 *Certificate of Analysis, Standard Reference Material 1650, Diesel Particulate Matter*, National Institute of Standards and Technology, Gaithersburg, MD, Feb. 1985.
24 E. Kovats, *Helv. Chim. Acta*, 41 (1958) 1915.
25 M. L. Lee, D. L. Vassilaros, C. M. White and M. Novotny, *Anal. Chem.*, 51 (1979) 768.
26 P. Garrigues, M. Radke, O. Druez, H. Willsch and J. Bellocq, *J. Chromatogr.*, 473 (1989) 207.
27 N. L. Allinger, J. T. Sprague and T. J. Liljefors, *J. Am. Chem. Soc.*, 96 (1974) 5100.
28 J. Kao and N. L. Allinger, *J. Am. Chem. Soc.*, 99 (1977) 975.
29 A. Radecki, H. Lamparczyk and R. Kaliszan, *Chromatographia*, 12 (1979) 595.
30 S. A. Wise, W. J. Bonnett, F. R. Guenther and W. E. May, *J. Chromatogr. Sci.*, 19 (1981) 457.
31 H. Budzinski, P. Garrigues and J. Bellocq, *J. Chromatogr.*, 590 (1992) 297.
32 M. Nishioka, B. A. Jones, B. J. Tarbet, J. S. Bradshaw and M. L. Lee, *J. Chromatogr.*, 357 (1986) 79.
33 S. A. Wise, L. C. Sander, R. Lapouyade and P. Garrigues, *J. Chromatogr.*, 514 (1990) 111.
34 S. A. Wise and L. C. Sander, *J. High Resolut. Chromatogr. Chromatogr. Commun.*, 8 (1985) 248.
35 J. Macak, V. Nabivach, P. Buryan and S. Sindler, *J. Chromatogr.*, 234 (1982) 285.
36 I. M. Mutton, *J. Chromatogr.*, 172 (1979) 438.
37 F. A. Beland and R. D. Geer, *J. Chromatogr.*, 84 (1973) 59.
38 B. B. Ghatge and N. V. Bhalerao, *J. Chromatogr.*, 549 (1991) 423.
39 H. Budzinski, M. Radke, P. Garrigues, J. Bellocq and H. Willsch, *Geochim. Cosmochim. Acta*, submitted for publication.

Journal of Chromatography, 627 (1992) 241–245
Elsevier Science Publishers B.V., Amsterdam

CHROM. 24 576

Identification of very-long-chain acids from peat and coals by capillary gas chromatography–mass spectrometry

T. Řezanka

Institute of Microbiology, Vídeňská 1083, 14220 Prague (Czechoslovakia)

(First received May 28th, 1992; revised manuscript received July 29th, 1992)

ABSTRACT

Long-chain monocarboxylic (fatty) and dicarboxylic acids, up to 36 and 33 carbon atoms, respectively, were identified in peat, lignite, brown coal, bituminous coal, anthracite and graphite using capillary gas chromatography–mass spectrometry (60-m polar capillary column with Supelcowax in the quadrupole mass spectrometer, *i.e.* QP-1000 from Shimadzu). The concentrations of acids decreased as coal rank increased. Branched and unsaturated acids disappeared sooner than alkanoic acids.

INTRODUCTION

The occurrence of very-long-chain fatty acids (VLCFAs) in nature has recently been reviewed [1]. In the animal kingdom VLCFAs are found in tissues ranging from the most primitive life forms (sponges) to the most advanced ones (mammalian skin or brain). In plants they appear mostly in waxes on the plant surface [2]. Several studies have dealt with the presence of VLCFAs in peat [3–5] or, exceptionally, in coal [6,7]. Studies by Ekman and Fagernäs [3] succeeded in determining a variety of acyclic acids, including dicarboxylic ones, with chains longer than 22 carbon atoms; all the acids were unbranched and saturated.

Our experience with analysis of VLCFAs in biological materials and the results of analyses of VLCFAs from unusual sources [8–11] formed the basis of our attempts at identifying VLCFAs in samples ranging from peat to coal to graphite.

Correspondence to: T. Řezanka, Institute of Microbiology, Vídeňská 1083, 14220 Prague, Czechoslovakia.

EXPERIMENTAL

Chemicals

Dicyclohexylcarbodiimide and 2-amino-2-methylpropanol were obtained from Sigma (St. Louis, MO, USA); other chemicals and solvents were from Lachema (Brno, Czechoslovakia).

Lipid extraction and derivatization

The samples, peat, lignite, brown coal, bituminous coal, anthracite and graphite (see Table I), were dried and ground to less than 0.1-mm-diameter particles. In free form fatty acids occur in concentrations from approximately 1.3% (peat) to 3.8% (anthracite); in graphite free fatty acids were not identified because their concentration is very low. In this paper only total fatty acids after hydrolysis are analysed. We do not examine TLC of some esters. Alkaline extraction was carried out by suspending 10 g of ground sample in 100 ml of ethanolic (90%) 0.5 *M* potassium hydroxide. The suspension was kept at 70°C for 4 h with continuous stirring. The suspension was diluted with water (1:1, v/v) and extracted three times with 10 ml of diethyl ether to remove non-acidic compounds. The suspension was acidified (pH 2) with 0.5 *M* sulphuric

0021-9673/92/$05.00

acid and extracted three times with 100 ml of diethyl ether. The combined ether extracts were washed and evaporated. One half of the extracted acids was treated with a solution of diazomethane in diethyl ether, and the resulting methyl esters were separated by solid-phase extraction (SPE). Free acids (*i.e.* fatty acids and dicarboxylic acids) are very poorly resolved by TLC (see ref. 12); their methyl esters give better resolution, but this TLC is useless.

Oxazolines were prepared from the second half of the extracted acids using a modified method of Yu *et al.* [13]: 5 mg of dicyclohexylcarbodiimide were added to a solution of 5 mg of fatty acids in 1 ml of dichloromethane. After stirring for 10 min, 2-amino-2-methylpropanol (5 mg) was added at 20°C and stirred for 4 h. The evaporated mixture was dissolved in 1 ml of diethyl ether and treated with 0.5 ml of $SOCl_2$ (20°C, 1 h), then washed with ice-cold water and dried by anhydrous sodium sulphate.

Solid-phase extraction

The silica-cart plastic cartridge system, Separon SGX C_{18} (1-ml tubes) (Tessek, Prague, Czechoslovakia), was used. A total amount of 1–2 mg of methyl esters was applied to the column in a small volume of dichloromethane. A methanol–isopropanol (98:2) mixture was allowed to flow under slight syringe pressure, at a rate of approximately 0.5 ml/min; 0.1-ml fractions were collected manually. The solvent was then evaporated in a vacuum and each fraction was analyzed by GC–MS. The retention volume for fatty acid methyl ester (FAME) 22:0 was 2.1 ml. For scanning infrared spectroscopy of the methyl esters after SPE (in carbon tetrachloride) a Perkin-Elmer Model 1310 (Perkin-Elmer, Norwalk, CT, USA) infrared spectrophotometer was used. The methyl esters and oxazolines were silylated before GC–MS according to the literature [5].

Gas chromatography–mass spectrometry

For identification of FAMEs, a Shimadzu QP-1000 (Shimadzu, Kyoto, Japan) GC–MS system with a 60 m × 0.32 mm I.D. (0.25 μm particle size) SPB-1 fused-silica capillary column (Supelco, Gland, Switzerland), split/splitless injector and helium as a carrier gas was used. Oven temperature was programmed from 100 to 320°C at a rate of 4°C/min. Ionization energy was 70 eV; the electron multiplier voltage was 2.5 kV.

Oxazolines were identified under conditions similar to the methyl esters, with the only difference being in the column temperature. In this case the oven was progammed from 150 to 330°C at a rate of 5°C/min. Separate peaks were identified by total mass spectra (from *m/z* 50 to 500) according previous papers [11,13].

RESULTS AND DISCUSSION

Peatification of plant tissues involves physico-chemical and microbial processes that cause loss of carbon dioxide, water and ammonia and the formation of peat. Further coalification produces different types of coals. Coals are products of solely physico-chemical processes acting on plant remnants. The biochemical and microbial phase ends with the formation of peat; it is followed by the geochemical phase, which involves a rise in temperature and pressure in the deposit.

Table I shows that increasing age (coalification) of the deposit is accompanied by a sharp drop in the content of total extractable carboxylic acids. In peat their content is of the order of one part per hundred, whereas in graphite it amounts to one part per million. It should be noted here that Bouška [14] graphite is composed solely of carbon without any organic compounds, although other elements or inorganic compounds can naturally be present. The presence of trace amounts of carboxylic acids in

TABLE I

COMPOSITION OF LIPIDS AND FATTY ACIDS FROM VARIOUS COALS

Sample	Source	Amount of acid (μg/g of coal)
Peat	Volary	65480[a]
Lignite	Mydlovary	9740[b]
Brown coal	Sokolov	2130
Bituminous coal	Nýřany	863
Anthracite	Úsilné	19
Graphite	Černá	0.9

[a] Ekman and Fagernäs [3,4] described amounts in the range of tens of milligrams (60.1 mg per g of dry peat and/or 85–170 mg/g, depending on the type of extraction procedure.

[b] Kiya *et al.* [6] described yields of 0.98–1.20% from original coals.

BLE II

TTY ACID COMPOSITION (μg/g) FROM DIFFERENT SAMPLES

ity d[a]	Peak No.	Peat	Lignite	Brown coal	Bituminous coal	Anthracite	Graphite
22:0	1	104.76[b,c]	39.93	0	0	0	0
22:1	2	65.48	0	0	0	0	0
22:0	3	497.64	117.85	37.70	12.60	0.07	0
19:0	4	19.64	34.09	1.06	0.08	0	0
23:0	5	72.02	15.58	1.06	0	0	0
23:1	6	91.67	0	0	0	0	0
23:0	7	39.28	28.24	1.06	0	0	0
23:0	8	150.60	38.96	4.68	0	0	0
20:0	9	78.57	6.81	4.68	3.02	0.06	0
24:0	10	52.38	11.68	1.06	0	0	0
24:1	11	72.02	0	0	0	0	0
24:1	12	150.60	18.50	0	0	0	0
24:0	13	1080.42	192.85	57.08	25.80	0.71	0.06
21:0	14	6.54	1.94	1.27	0.25	0	0
25:0	15	32.74	11.68	2.55	0	0	0
25:0	16	52.38	15.58	0	0	0	0
25:1	17	26.19	0	0	0	0	0
25:0	18	98.22	32.14	5.75	0	0	0
22:0	19	183.34	27.27	6.39	4	0.13	0
26:0	20	85.12	11.68	1.06	0	0	0
26:1	21	104.76	0	0	0	0	0
26:0	22	772.66	128.56	41.53	18.38	0.57	0.02
23:0	23	137.50	22.40	1.70	0.08	0	0
27:0	24	32.74	6.81	0	0	0	0
27:0	25	52.38	7.79	0	0	0	0
27:0	26	65.48	15.58	2.55	0	0	0
24:0	27	294.66	45.77	5.96	5.35	0.21	0.01
28:0	28	72.02	3.89	0	0	0	0
28:1	29	52.38	0	0	0	0	0
28:0	30	366.68	7.79	10.22	12.08	0.08	0
25:0	31	19.64	4.87	1.91	0.08	0	0
29:0	32	32.74	3.89	0	0	0	0
29:0	33	72.02	11.68	2.76	0	0	0
26:0	34	242.27	30.19	5.75	3.10	0.07	0
30:0	35	78.57	3.89	0	0	0	0
30:0	36	189.89	15.58	4.68	0	0	0
27:0	37	85.12	4.87	1.70	0	0	0
31:0	38	32.74	7.79	0	0	0	0
31:0	39	39.28	0	0	0	0	0
31:0	40	65.48	11.68	0	0	0	0
28:0	41	170.24	6.81	3.62	1.03	0	0
32:0	42	124.41	11.68	2.55	0	0	0
29:0	43	39.28	2.92	0.21	0	0	0
30:0	44	117.86	1.94	1.49	0.08	0	0
34:0	45	13.09	0	0	0	0	0
34:0	46	72.02	3.89	0	0	0	0
31:0	47	52.38	0.97	0.21	0	0	0
32:0	48	85.12	2.92	0.42	0	0	0
36:0	49	13.09	0	0	0	0	0
36:0	50	85.12	3.89	0	0	0	0
33:0	51	6.54	0.97	0.21	0	0	0

ercentage of total acids longer than C_{18}, see Experimental section. i = *iso*; ai = *anteiso*; di = dicarboxylic acid.
.D. was in the range 0.005–0.01.
ach value represents the mean ± S.D. from five analyses.

graphite can be the result of contamination. This possibility has been described by Polzer and Bächmann [15], who found VLCFAs in rain water, into which they were carried by wind from plant surfaces.

A variety of carboxylic acids have been described to be present in peat. As seen from earlier studies [3,4] they consist mostly of saturated acids, whether mono- or dicarboxylic, with an even number of carbon atoms, with chain length of up to C_{30}. Coals were found to contain straight-chain fatty acids of up to 32 carbon atoms [6]. A small amount of hydroxy fatty acids, especially in peat, was present, but they were not identified. Unfortunately, the authors were unable to separate and fully identify all methyl esters by GC; they succeeded merely in identifying methyl esters of even-numbered straight-chain fatty acids. Niwa *et al.* [7] used the method of field desorption MS to analyse complex lipids (waxes). They also identified fatty acids and alcohols in the range C_{24}–C_{34}, with a maximum at C_{26}. Our results extend these carboxylic acid compositions.

Table II shows the presence of branched acids (*iso* and *anteiso*), arising probably by microbial biosynthesis during peatification, and monoenoic acids. The presence of unsaturated acids in samples of different geological ages has been shown repeatedly [16]. With increasing age of the peat and coals both the total amount of the acids and the proportion of their different groups are seen to decrease, as expected. Lignite contains practically all the acids identified in peat, while progressive coalification, beginning with brown coal, is seen to be reflected in a marked change in both the quantity and type of acid components. Graphite was found to contain only trace amounts of acids (see the above note on possible contamination).

Identification of FAMEs was performed based on our previous report (11). Double bonds were located in monoenoic acids by splitting the carbon chain of oxazoline in a mass spectrum [11,13]. A common method of determining the configuration of double bond(s) includes infrared spectroscopy. Some peaks at 967 cm^{-1}, *i.e.* the characteristic absorbance for *trans* isomer(s), were not identified. From the above argument it is to be expected that double bond(s) are *cis*. The use of single-ion monitoring (SIM) for base peaks of methyl esters (*e.g.* *m/z* 74 for methyl ester monocarboxylic acids and

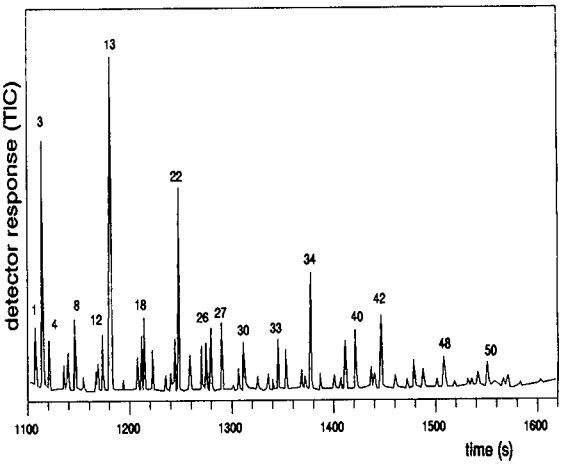

Fig. 1. Capillary gas chromatogram of long-chain fatty acid methyl esters and dicarboxylic acid methyl esters from lignite. For analytical conditions, see the Experimental section. Peaks 1–50 are methyl esters (see Table II).

m/z 98 for methyl ester dicarboxylic acids) enabled us to identify many individual acids in the very complex mixture represented by coal extract. Fig. 1 shows the profile of methyl esters of mono- and dicarboxylic acids. All peaks representing individual methyl esters are satisfactorily separated; their sequence (equivalent chain length or relative retention time) corresponds to previously published data

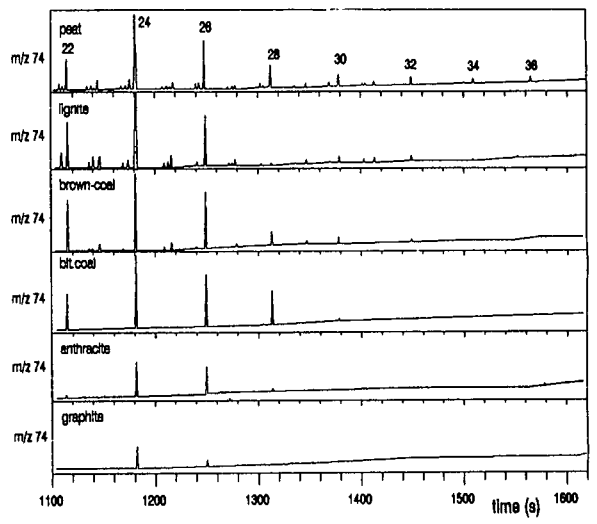

Fig. 2. GC–MS of fatty acid methyl esters from different samples by means of single-ion monitoring of ion *m/z* 74 (base peak for methyl esters).

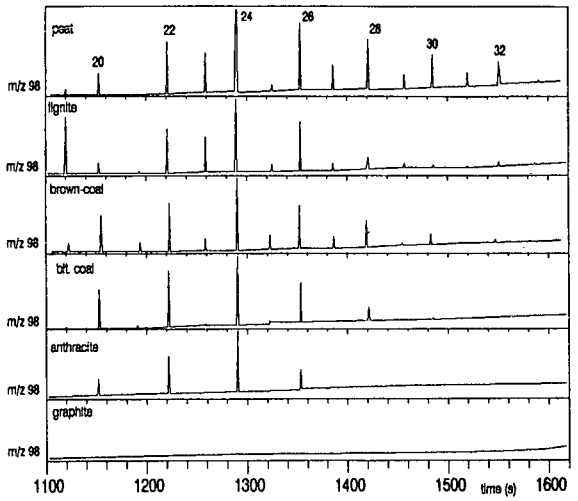

Fig. 3. GC–MS of dicarboxylic acid methyl esters from different samples by means of single-ion monitoring of ion m/z 98 (base peak for dimethyl esters).

[9,12]. With the aid of mass spectra, these results allowed us to identify unequivocally individual components.

Figs. 2 and 3 give the SIM of m/z 74 and m/z 98 ions in different types of coals. Application of capillary GC–MS enabled us to identify even trace amounts of acids. The method is augmented by using SPE as a prior purification and separation step.

In conlusion, it can be stated that the theory [14] (that carboxyl groups are usually present in brown coal and absent from bituminous coal, anthracite and graphite; with 85% carbon in coal, *i.e.* all coals, with exception of peat and lignite, the carboxyl groups are usually lacking) has not been fully substantiated because marked amounts of acids were found even in bituminous coal and anthracite. However, several rules can be used to generalize the overall occurrence. Monoenoic acids are found only in peat and in lignite and are probably thermally degraded at later stages. On the other hand, dicarboxylic acids have a general occurrence. VLCFAs are likely to undergo thermal degradation and their amount decreases with progressive coalification.

REFERENCES

1 T. Řezanka, *Prog. Lipid Res.*, 28 (1989) 147.
2 G. Riley, R. J. Collier, D. M. Jones and G. Eglinton, *Org. Geochem.*, 17 (1991) 901.
3 R. Ekman and L. Fagernäs, *Finn. Chem. Lett.*, (1983) 129.
4 L. Fagernäs and R. Ekman, *Tech. Res. Cent. Finl.*, 23 (1985) 1.
5 P. Karunen and R. Ekman, *Physiol. Plant.*, 54 (1982) 162.
6 K. Kiya, K. Mashimo and T. Wainai, *Fuel*, 66 (1987) 1447.
7 Y. Niwa, M. Yumura, K. Ishikawa, Y. Kuriki and M. Kawamura, *Fuel*, 67 (1988) 98.
8 T. Řezanka and M. Podojil, *Lipids*, 19 (1984) 472.
9 T. Řezanka, T. Koza, R. Kysilka, I. Viden and M. Wurst, *J. Chromatogr.*, 472 (1989) 290.
10 T. Řezanka, M. Yu. Sokolov and I. Víden, *FEMS Microbiol. Ecol.*, 73 (1990) 231.
11 T. Řezanka, I. V. Zlatkin, I. Viden, O. I. Slabova and D. I. Nikitin, *J. Chromatogr.*, 558 (1991) 215.
12 I. Víden and T. Řezanka, *J. Chromatogr.*, 465 (1989) 390.
13 Q. T. Yu, B. N. Liu, J. Y. Zhang and Z. H. Huang, *Lipids*, 23 (1988) 804.
14 V. Bouška, *Geochemistry of Coal; Coal Science and Technology*, Vol. 1, Elsevier, Amsterdam, 1981.
15 J. Polzer and K. Bächmann, *Fresenius Z. Anal. Chem.*, 340 (1991) 555.
16 K. Kawamura and R. Ishiwatari, *Geochem. Cosmochim. Acta*, 45 (1981) 149.

Journal of Chromatography, 627 (1992) 247–254
Elsevier Science Publishers B.V., Amsterdam

CHROM. 24 627

Supercritical fluid chromatography of *Fusarium* mycotoxins

J. Christopher Young

Plant Research Centre, Agriculture Canada, Ottawa, Ontario K1A 0C6 (Canada)

David E. Games

Mass Spectrometry Research Unit, Department of Chemistry, University College of Swansea, Singleton Park, Swansea SA2 8PP, Wales (UK)

(First received May 22nd, 1992; revised manuscript received September 16th, 1992)

ABSTRACT

Capillary- and packed-column supercritical fluid chromatography has been used for the separation of *Fusarium* mycotoxins of various structure types such as the trichothecenes including deoxynivalenol and its acetylated derivatives and T-2 toxin, as well as butenolide, culmorin, sambucinol and zearalenone. The effect of modifier concentration and column temperature and pressure was also studied. Retention indices based on alkylphenones were determined for these mycotoxins on two of the capillary columns employed.

INTRODUCTION

The fungi of the genus *Fusarium* are capable of producing an impressive diversity of secondary metabolites that cause a variety of toxic effects on humans, animals and plants [1,2]. These metabolites (mycotoxins) include (see Fig. 1): simple monocyclic compounds such as butenolide, sesquiterpenes such as the trichothecenes 4-deoxynivalenol and T-2, the modified trichothecenes such as sambucinol and longifolene-like culmorin, and aromatic lactones such as zearalenone.

The analysis of these compounds typically involves extraction from the sample matrix, some preliminary cleanup, chromatographic separation [thin-layer (TLC), gas (GC) or high-performance liquid (HPLC)], and detection [3]. GC requires that the compounds be volatile and relatively non-polar. Many of the above compounds are sufficiently non-volatile to require reaction, such as silylation or polyfluoroacylation, to afford a volatile derivative. Such steps add to the complexity of the analysis. Typical universal GC detection methods include flame ionization (FID) and mass spectrometry (MS), while electron-capture detection (ECD) require an element such as fluorine to be present in the molecule. Liquid chromatography generally does not require derivatization to aid in the chromatography, however the commonly used ultraviolet (UV) or fluorescence detectors require the presence of UV or fluorescence chromophores in the molecule. HPLC–MS is more universally applicable although the type of interface employed may place limits on the chromatographic solvents that can be used.

Supercritical fluid chromatography (SFC) adds a new dimension to the analysis of mycotoxins. SFC can be conducted with heavily cross-linked bonded fused silica columns of 50 μm or 100 μm I.D. or with columns packed with conventional HPLC

Correspondence to: J. C. Young, Plant Research Centre, Agriculture Canada, Ottawa, Ontario K1A 0C6, Canada.

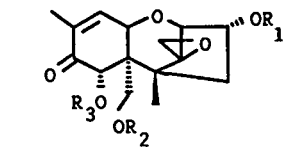

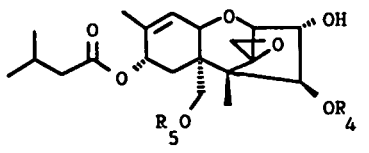

	R_1	R_2	R_3	R_4	R_5
3-Acetyldeoxynivalenol	Ac	H	H	-	-
15-Acetyldeoxynivalenol	H	Ac	H	-	-
3,7,15-Triacetyldeoxynivalenol	Ac	Ac	Ac	-	-
Deoxynivalenol	H	H	H	-	-
HT-2 Toxin	-	-	-	H	Ac
T-2 Toxin	-	-	-	Ac	Ac
T-2 Triol	-	-	-	H	H

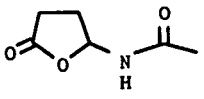

Butenolide

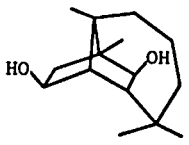

Culmorin

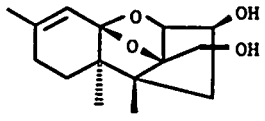

Sambucinol

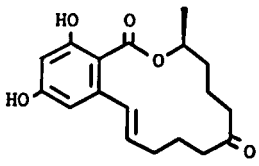

Zearalenone

Fig. 1. Structures of some *Fusarium* mycotoxins.

packings or those designed for SFC. In addition to temperature as a variable to aid in eluting compounds from a capillary column, SFC also permits pressure/density programming and addition of modifying solvents. This enables temperatures to be kept low for thermally unstable substances. Detection requirements are the same for both SFC and conventional GC/HPLC. However, SFC is more amenable to interfacing with a mass spectrometer than HPLC because of the lower mobile phase gas volumes generated.

Retention indices (*I*), such as the Kováts scale [4], have been used for many years for standardization of GC data [5]. Such indices have only recently been used for HPLC data [6]. Homologous series employed for generation of HPLC *I* values include alkan-2-ones [7,8], aryl ketones [9] and 1-nitroalkanes [8,10,11]. The alkylphenones [8,12–15] and the related 1-[*p*-(2,3-dihydroxypropoxy)phenyl]-1-alkanones [16] have been investigated the most extensively. HPLC *I* values for some *Fusarium* and other mycotoxins have been determined [13,14,16]. The alkylphenones have also been used to determine *I* under packed-column SFC conditions [17].

This study was initiated to determine the efficacy of SFC for the resolution and possible analysis of some *Fusarium* mycotoxins that exhibit a wide variety of structure types. The SFC–MS analysis of only a few trichothecene mycotoxins on capillary columns has been previously published [18–20],

however to our knowledge, SFC analyses of *Fusarium* mycotoxins on packed columns have not been reported. In this study, the SFC of selected *Fusarium* mycotoxins on three capillary and six packed columns is reported along with a comparison of retention indices.

EXPERIMENTAL

Mycotoxin standards

HT-2 toxin and T-2 triol were from Sigma, St. Louis, MO, USA. The remainder were obtained from liquid cultures of various *Fusarium* spp. (prepared in the Plant Research Centre laboratories, Ottawa, Canada). Standard solutions were prepared with dichloromethane as solvent. A solution of zearalenone in a clear glass vial was allowed to stand at room temperature exposed to light for several weeks to give a mixture of starting material and a photo isomer.

Reagents

All reagents and solvents were of analytical-reagent grade. The series of C_8–C_{24} alkylphenone standards was obtained in kit form (catalogue No. 29 858-1) from Aldrich, Milwaukee, WI, USA. Approximately 15 mg/ml solutions of the alkylphenones in methanol and dichloromethane were prepared for analysis on the capillary and packed columns, respectively. Instrument-grade carbon dioxide supplied in cylinders with a dip tube (BOC, London, UK) and glass-distilled methanol were used as eluents.

Chromatographic columns

The SB-Methyl-100, SB-Biphenyl-30 and Carbowax capillary columns (each 10 m × 50 μm I.D. with adsorbent in a 0.25 μm film) were obtained from Lee Scientific (Division of Dionex, Salt Lake City, UT, USA). The packed columns (each 250 × 4.6 mm I.D.) were filled with one of Apex II Diol, Apex Phenyl S5B, Partisil 10 ODS3, Spherisorb Amino 5 μm, Spherisorb Cyano 3 μm or Spherisorb Silica 5 μm.

Chromatographic equipment

A Carlo Erba Model SFC 3000 series SFC LC fitted with a flame ionization detector (Carlo Erba, Milan, Italy) was used for the capillary column analyses. Injections were made into a pneumatic-activated VICI valve containing a 200-nl injection loop with a 150 to 200 ms injection time. Pure carbon dioxide was used as eluent.

Packed column SFC analyses were conducted on either (1) a Hewlett-Packard 1084B liquid chromatograph (Hewlett-Packard, Avondale, PA, USA) modified for SFC [21] with a Hewlett-Packard VWD-79875 variable-wavelength detector set at 224 nm or (2) a system consisting of a Gilson 302-303 pump system (Gilson, Villiers-Le-Bel, France), a Carlo Erba oven and an ABI Analytical Kratos Division Spectroflow 757 UV detector set at 224 nm.

The liquid carbon dioxide and the pump heads of the various chromatographs were cooled to −25°C using a Neslab RTE-4Z refrigerated bath (Neslab Instruments, Newington, NH, USA).

LC analyses

Capillary column analyses were typically made at 100°C using a 0.2 to 0.7 g/ml density program with a 0.01 g/ml per min linear gradient. Packed column analyses were made at an eluent flow-rate of 4 ml/min.

Retention indices

A mixture of the alkylphenones was coinjected with the mycotoxins. Retention indices were determined by a comparison of capacity factors (k').

RESULTS AND DISCUSSION

Retention indices

The relationship between carbon number and k' for the alkylphenones and capillary columns employed in this study is shown in Fig. 2. The plots were curvilinear and the data could be fitted by linear regression analyses to the equation

$$k' = A(1 - e^{-bN}) + c$$

where A, b and c are constants and N is the equivalent carbon number.

The calculated I values ($N \times 100$) for selected *Fusarium* mycotoxins on two of the capillary columns are listed in Table I. The alkylphenones were readily resolved on Carbowax, however they eluted before any of the mycotoxins, so I values could not be determined for this column. These data show

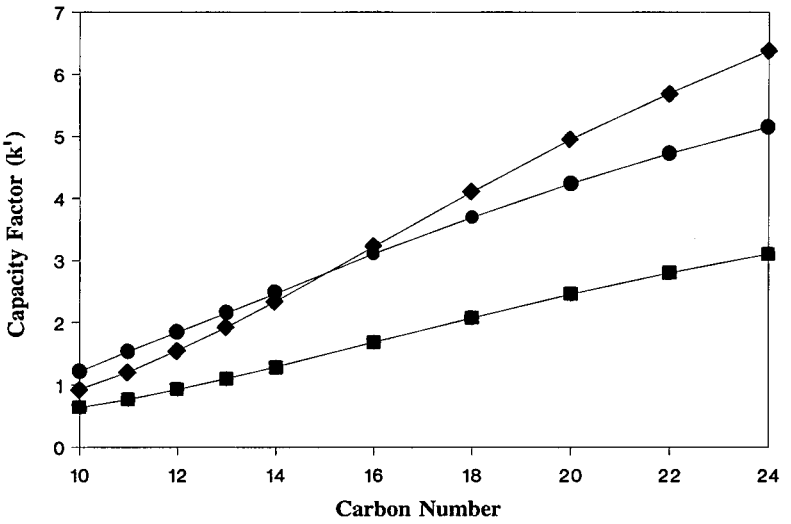

Fig. 2. Plot of capacity factors *vs.* alkylphenone carbon number for SFC at 100°C on 10 m × 50 μm I.D. capillary columns with 0.25 μm film of (◆) SB-Methyl-100, (●) SB-Biphenyl-30 and (■) Carbowax. Eluent, supercritical CO_2, density programmed from 0.2 to 0.7 g/ml at 0.01 g/ml per min.

TABLE I

RETENTION INDICES OF SELECTED *FUSARIUM* MYCOTOXINS ON CAPILLARY COLUMNS UNDER SUPERCRITICAL FLUID CHROMATOGRAPHIC CONDITIONS

Columns 10 m × 50 μm I.D. with 0.25 μm adsorbent coating. Eluted with supercritical CO_2 with a linear density program from 0.2 to 0.7 g/ml at 0.01 g/ml per min at 100°C. Indices based on homologous *n*-alkylphenones.

Compounds	SFC capillary columns		Literature for conventional reversed-phase HPLC
	Methyl	Biphenyl	
3-Acetyldeoxynivalenol	2046	2414	–
15-Acetyldeoxynivalenol	1990	2341	–
Triacetyldeoxynivalenol	1984	2107	–
Butenolide	1170	1657	–
Culmorin	1575	1701	–
Diacetoxyscirpenol	1956	2264	866, 1326[b]
Deoxynivalenol	2060	2646[c]	689, 1037[b]
HT-2 toxin	2249	2555[c]	1434[b]
Sambucinol	1837	2212	–
T-2 toxin	2198	2300	1016, 1513[b]
T-2 triol	2339	2797[c]	–
Zearalenone	2589[c]	3765[c]	1069[a], 1024[d]
Zearalenone isomer	2482[c]	2420[c]	–

[a] Ref. 14. Indices based on homologous *n*-alkylphenones.
[b] Ref. 16. Indices based on homologous 1-[*p*-(2,3-dihydroxypropoxy)phenyl]-1-alkanols.
[c] Estimated by extrapolation.
[d] Ref. 13.

that *I* values are column dependent. It is not surprising that Frisvad and Thrane [14] noted some differences between their results and those of Hill *et al.* [13] under conventional HPLC conditions.

The alkylphenones were not retained on any of the six packed HPLC columns investigated under SFC conditions. They eluted as one broad unresolved band immediately after the solvent peak and well before any of the mycotoxins. Thus if *I* values for *Fusarium* mycotoxins on packed SFC columns are to be developed, either a homologous series other than simple alkylphenones, perhaps such as that

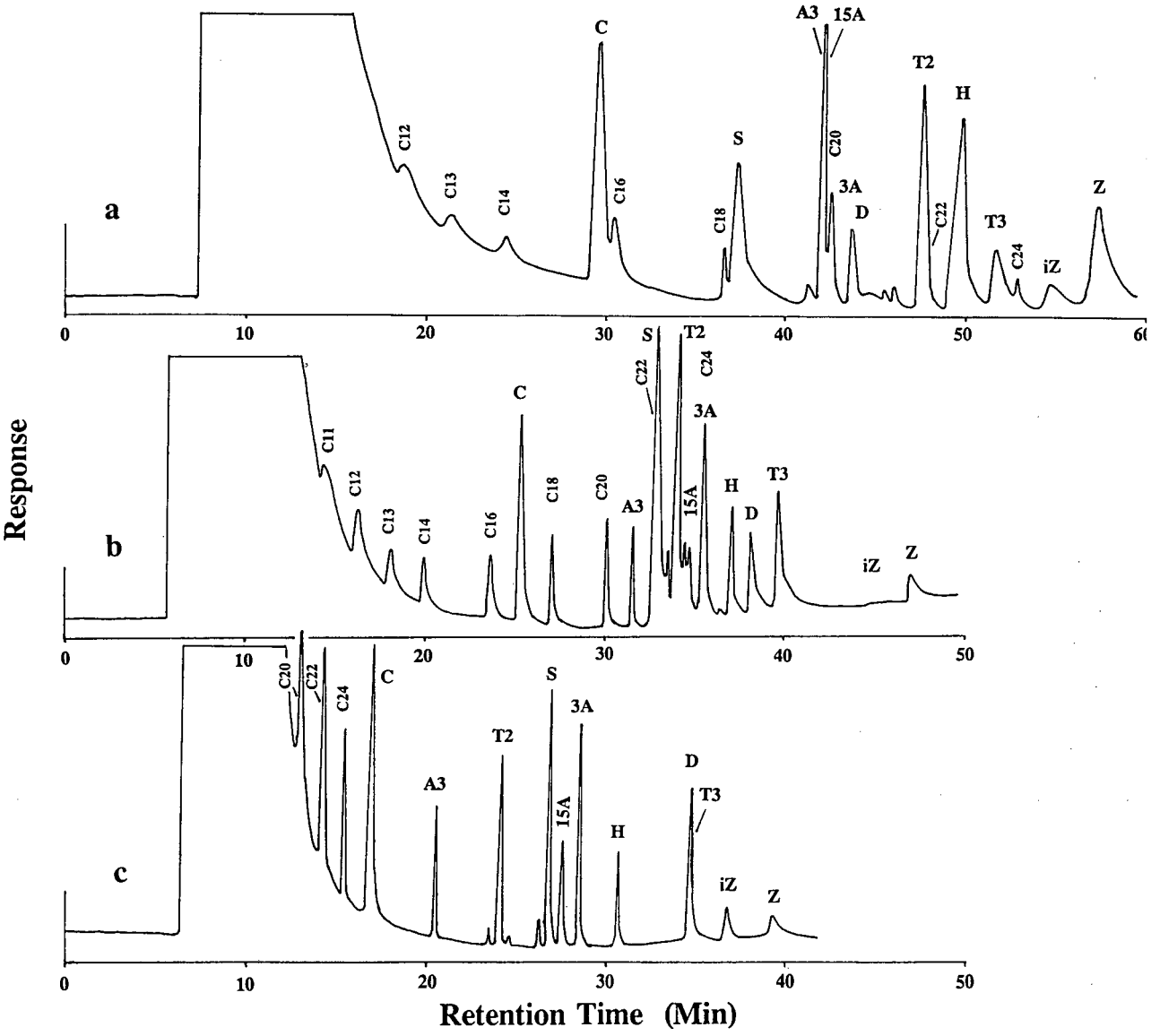

Fig. 3. Chromatograms of a mixture of *Fusarium* mycotoxins (A3) triacetyldeoxynivalenol, (3A) 3-acetyldeoxynivalenol, (15A) 15-acetyldeoxynivalenol, (C) culmorin, (D) deoxynivalenol, (H) HT-2 toxin, (S) sambucinol, (T2) T-2 toxin, (T3) T-2 triol, (Z) zearalenone and (iZ) zearalenone isomer separated by SFC with eluent supercritical CO_2 at 100°C on 10 m × 50 μm I.D. capillary columns with 0.25 μm film and detected by FID. (a) SB-Methyl-100, density programmed from 0.2 to 0.7 g/ml at 0.01 g/ml per min. (b) SB-Biphenyl-30, density programmed from 0.2 to 0.7 g/ml at 0.01 g/ml per min. (c) Carbowax, density programmed from 0.2 to 0.7 g/ml at 0.015 g/ml per min.

investigated by Kostiainen and Kuronen [16], or another HPLC column, such as polystyrene–divinylbenzene employed by Smith and Sanagi [17], will have to be used.

Capillary column separation of Fusarium mycotoxins

Separations of selected *Fusarium* mycotoxins on capillary columns under SFC conditions were investigated. The variables included eluent density and column polarity.

The mycotoxins investigated eluted faster at higher eluent density, due to the increased solvating power of the supercritical CO_2. Because of the substantial differences in compound polarities, density programming was employed to achieve elutions in the least possible times while retaining sufficient resolution. The retention times for capillary column SFC were much longer than those observed for packed-column SFC (see below).

There were no apparent trends upon going from low- (methyl) through mid- (biphenyl) to high-polarity (Carbowax) columns. The best chromatography (resolution and peak shape) was achieved on Carbowax (Fig. 3). Relative and absolute k' values were highly variable and column dependent (Fig. 4). The order of elution on all the columns investigated tended to follow increased solute polarity (*e.g.* triacetyldeoxynivalenol < 15-acetyldeoxynivalenol < 3-acetyldeoxynivalenol < deoxynivalenol and T-2 toxin < HT-2 toxin < T-2 triol) although a few compounds (*e.g.* butenolide and T-2 toxin) showed highly variable relative elution orders from column to column (Fig. 4).

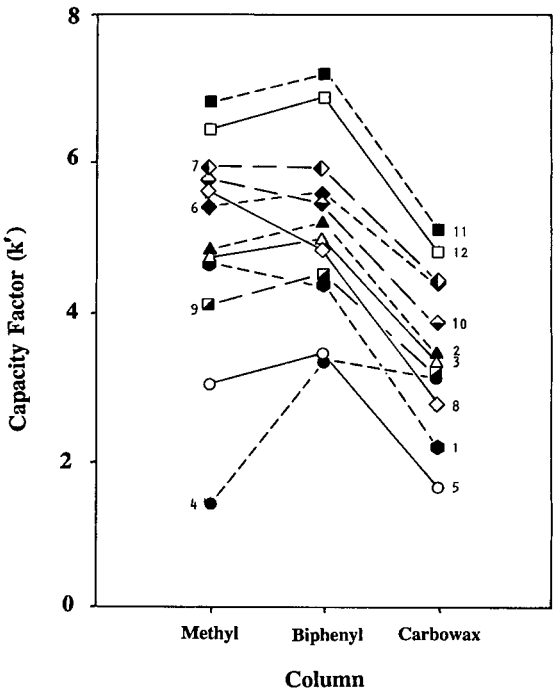

Fig. 4. Capacity factors for mixture of *Fusarium* mycotoxins (1) triacetyl-deoxynivalenol, (2) 3-acetyldeoxynivalenol, (3) 15-acetyldeoxynivalenol, (4) butenolide, (5) culmorin, (6) deoxynivalenol, (7) T-2 triol, (8) T-2 toxin, (9) sambucinol, (10) HT-2 toxin, (11) zearalenone and (12) zearalenone isomer separated by SFC with eluent supercritical CO_2 at 100°C on 10 m × 50 μm I.D. capillary columns with 0.25 μm film of SB-Methyl-100 and SB-Biphenyl-30 density programmed from 0.2 to 0.7 g/ml at 0.01 g/ml/min and Carbowax density programmed from 0.2 to 0.7 g/ml at 0.015 g/ml/min. Detection by flame ionization.

Packed-column separation of Fusarium mycotoxins

In addition to the conventional HPLC variables (adsorbent, eluent and temperature), packed-column SFC also has eluent density available. Each of these parameters was investigated for those UV absorbing mycotoxins that were available.

Differences in resolving power under identical operating conditions for the six packings are illustrated in Fig. 5. The phenyl, amino and diol columns, which gave higher k' values, showed the best resolution. The best chromatography was achieved on the amino column (Fig. 6), the only column to give baseline resolution of the zearalenone isomers, whereas silica appeared to be the least efficient. The diol and phenyl columns also gave relatively sharp peaks with only slight tailing. Under SFC conditions, all packings behave as normal phases and k' values increase with increased solute polarity. As noted for the capillary columns, butenolide showed variable relative elution order on the packed columns.

Capacity factors became smaller as pressure increased (Fig. 7) due to increased solvating power of supercritical CO_2. The rate of change of k' values for butenolide was different from the other compounds. Resolution, with respect to deoxynivalenol, decreased with increased pressure on the phenyl, cyano and ODS columns.

Addition of increasing amounts of methanol as a modifier to the CO_2 also resulted in reduced capacity factors (Fig. 8) due to increased solvating power.

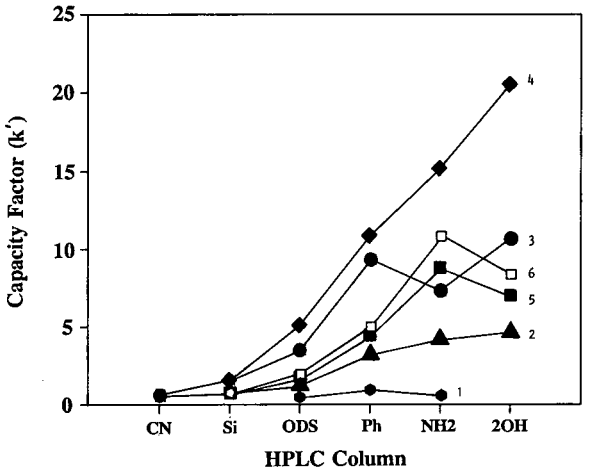

Fig. 5. Capacity factors for mixture of *Fusarium* mycotoxins (1) triacetyldeoxy-nivalenol, (2) 3-acetyldeoxynivalenol, (3) butenolide, (4) deoxynivalenol, (5) zearalenone and (6) zearalenone isomer separated by SFC with eluent supercritical CO_2 containing 5% methanol at 60°C and a pressure of 265 bar on 250 × 4.6 mm I.D. stainless steel columns containing (CN) Spherisorb Cyano 3 μm, (Si) Spherisorb Silica 5 μm, (ODS) Partisil 10 ODS3, (Ph) Apex Phenyl S5B, (NH_2) Spherisorb Amino 5 μm and (2OH) Apex II Diol. Detection by UV at 224 nm.

The influence on resolution appears to be solute dependent; higher concentrations of methanol resulted in reduced resolution between butenolide and deoxynivalenol but increased resolution between the zearalenone isomers.

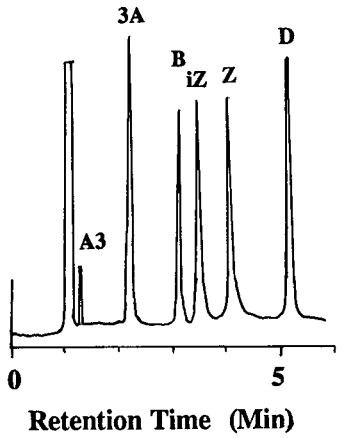

Fig. 6. Chromatogram of mixture of *Fusarium* mycotoxins (A3) triacetyldeoxynivalenol, (3A) 3-acetyldeoxynivalenol, (B) butenolide, (D) deoxynivalenol, (Z) zearalenone and (iZ) zearalenone isomer separated by SFC with eluent supercritical CO_2 containing 10% methanol at 70°C and a pressure of 293 bar on 250 × 4.6 mm I.D. stainless-steel column of Spherisorb Amino 5 μm. Detection by UV at 224 nm.

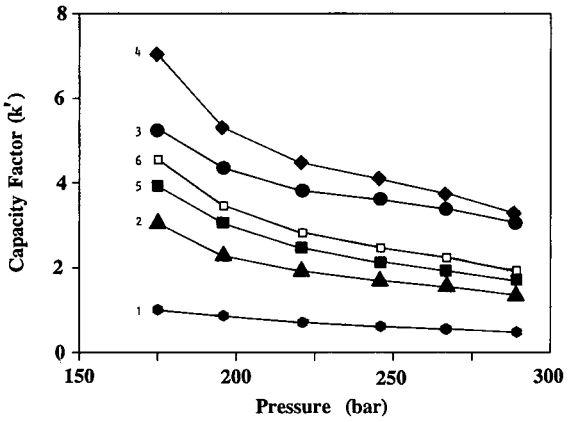

Fig. 7. Effect of pressure on capacity factors for mixture of *Fusarium* mycotoxins (1) triacetyldeoxynivalenol, (2) 3-acetyldeoxynivalenol, (3) butenolide, (4) deoxynivalenol, (5) zearalenone and (6) zearalenone isomer separated by SFC with eluent supercritical CO_2 containing 10% methanol and at a temperature of 60°C on 250 × 4.6 mm I.D. stainless-steel column of Apex Phenyl S5B. Detection by UV at 224 nm.

The effect of temperature is opposite to that typically observed in conventional GC and HPLC; both k' and resolution increased with temperature (Fig. 9). The reason is that at constant pressure, as the temperature increases, the density of CO_2 de-

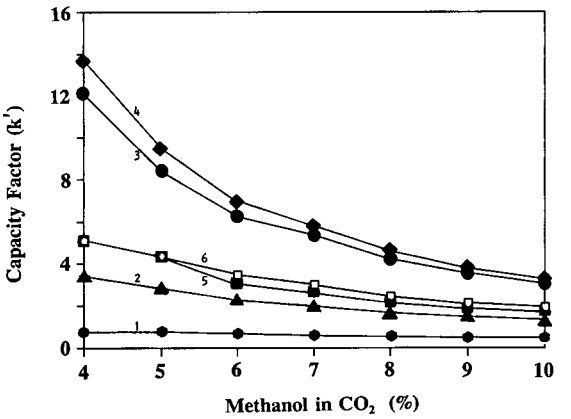

Fig. 8. Effect of modifier concentration on capacity factors for mixture of *Fusarium* mycotoxins (1) triacetyldeoxynivalenol, (2) 3-acetyldeoxynivalenol, (3) butenolide, (4) deoxynivalenol, (5) zearalenone and (6) zearalenone isomer separated by SFC with eluent supercritical CO_2 containing methanol at a temperature of 60°C and pressure of 289 bar on 250 × 4.6 mm I.D. stainless-steel column of Apex Phenyl S5B. Detection by UV at 224 nm.

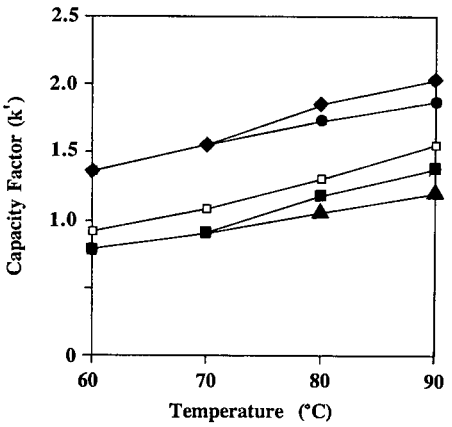

Fig. 9. Effect of temperature on capacity factors for mixture of *Fusarium* mycotoxins (▲) 3-acetyldeoxynivalenol, (●) butenolide, (◆) deoxynivalenol, (■) zearalenone and (□) zearalenone isomer separated by SFC with eluent supercritical CO_2 containing 3% methanol and a pressure of 276 bar on 250 × 4.6 mm I.D. stainless-steel column of Spherisorb Cyano 3 μm. Detection by UV at 224 nm.

creases with a concomittent loss of solvation power.

Compared with conventional HPLC, packed-column SFC results in an order of magnitude greater resolution per unit time (*i.e.* shorter retention times) and narrower peaks (only several seconds as compared with 0.5 to 1 min reported by Kostiainen *et al.* [22]).

CONCLUSIONS

A wide variety of *Fusarium* mycotoxin structure types can be readily separated by SFC on both capillary and packed columns. The best resolution and sharpest peaks were obtained on the Carbowax capillary and Spherisorb Amino packed columns. Resolution was influenced by column temperature, pressure/density of the liquid carbon dioxide eluent and by concentration of modifier (in this case, methanol) added to the eluent; the specific effect was dependent upon the solute and column packing material.

SFC retention times on packed columns are up to 8 times shorter than those on capillary columns. Compared with conventional HPLC, packed-column SFC offers faster analysis times and gives narrow peak widths usually associated with capillary column GC.

Homologous *n*-alkylphenones could be used to generate retention index values on two of the capillary columns investigated. However they were not sufficiently retained on any of the packed columns. A more polar homologous series is required for SFC packed column indices.

ACKNOWLEDGEMENTS

J.C.Y. wishes to thank D.E.G. for being able to spend a year on sabbatical leave in the latter's laboratory.

This paper is PRC Contribution No. 1426.

REFERENCES

1 M. E. Savard, R. Greenhalgh and J. W. ApSimon, in Atta-ur-Rahman (Editor), *Studies in Natural Products Chemistry*, Vol. 6, Part D, Elsevier, Amsterdam, New York, 1990, p. 213.
2 J. F. Grove, *Nat. Prod. Rep.*, 5, (1988) 187.
3 R. J. Cole (Editor), *Modern Methods in the Analysis and Structural Elucidation of Mycotoxins*, Academic Press, Orlando, FL, 1986.
4 E. Kováts, *Helv. Chim. Acta*, 41 (1958) 1915.
5 L. S. Ettre, *Anal. Chem.*, 36 (1964) 31A.
6 R. M. Smith, *Adv. Chromatogr.*, 26 (1987) 277.
7 J. K. Baker and C.-Y. Ma, *J. Chromatogr.*, 169 (1979) 107.
8 R. M. Smith and N. Finn, *J. Chromatogr.*, 537 (1991) 51.
9 C. F. Culberson, W. L. Culberson and A. Johnson, *Mycologia*, 78 (1986) 888.
10 M. Bogusz and R. Anderjan, *J. Chromatogr.*, 435 (1988) 43.
11 M. Bogusz, *LC · GC*, 9 (1991) 290.
12 R. M. Smith, *J. Chromatogr.*, 236 (1982) 313.
13 D. W. Hill, T. R. Kelley, K. J. Langner and K. W. Miller, *Anal. Chem.*, 56 (1984) 2576.
14 J. C. Frisvad and U. Thrane, *J. Chromatogr.*, 404 (1987) 195.
15 C. R. Yonker and R. D. Smith, *Anal. Chem.*, 59 (1987) 727.
16 R. Kostiainen and P. Kuronen, *J. Chromatogr.*, 543 (1991) 39.
17 R. M. Smith and M. M. Sanagi, *Chromatographia*, 26 (1988) 77.
18 R. D. Smith, H. R. Udseth and B. W. Wright, *J. Chromatogr. Sci.*, 23 (1985) 192.
19 H. T. Kalinowski, H. R. Udseth, B. W. Wright and R. D. Smith, *Anal. Chem.*, 58 (1986) 2421.
20 J. A. Roach, J. A. Sphon, J. A. Easterling and E. M. Calvey, *Biomed. Environ. Mass Spectrom.*, 18 (1989) 64.
21 D. R. Gere, R. D. Board and D. McManigill, *Anal. Chem.*, 54 (1982) 736.
22 R. Kostiainen, K. Matsuura and K. Nojima, *J. Chromatogr.*, 538 (1991) 323.

Journal of Chromatography, 627 (1992) 255–261
Elsevier Science Publishers B.V., Amsterdam

CHROM. 24 560

Supercritical fluid extraction and gas chromatographic determination of the sesquiterpene lactone parthenolide in the medicinal herb feverfew (*Tanacetum parthenium*)

Roger M. Smith and Mark D. Burford*

Department of Chemistry, Loughborough University of Technology, Loughborough, Leics. LE11 3TU (UK)

(First received May 5th, 1992; revised manuscript received August 11th, 1992)

ABSTRACT

Supercritical carbon dioxide was used to extract the sesquiterpene lactone parthenolide, which is reported to be the active component of the medicinal herb feverfew (*Tanacetum parthenium*), from dried plant material for gas–liquid chromatographic analysis. The extracts also contained significant amounts of camphor and chrysanthenol acetate. The pressure and densities required for quantitative extraction and the methods of sample collection were studied. The addition of methanol or acetonitrile as modifiers in the carbon dioxide gave higher yields of parthenolide but the extractions were less selective and considerable amounts of co-extractives were obtained. By employing a trapping column made of cellulose or silica the purity of the extracts could be improved and a practical method for the rapid isolation of parthenolide is described.

INTRODUCTION

Supercritical fluid extraction (SFE) has been used for many years for the preparative-scale isolation of compounds from plant matrices, such as hops, spices and coffee beans [1,2]. In recent years there has also been considerable interest in the application of SFE as an analytical extraction method for sample preparation prior to chromatographic analysis either as an off-line extraction step or on-line with gas chromatography (GC) or other chromatographic systems [3,4]. A major advantage of this technique compared with solvent extraction is that if carbon dioxide is used as the extraction solvent, it can be readily removed from the product by depressurization. As supercritical fluid extractions can be achieved under mild conditions this technique should also reduce the thermal degradation and the poor collection efficiencies of volatile analytes that can sometimes occur during the steam distillation or solvent extraction of essential oils and fragrance components [5]. This advantage has been demonstrated by Stahl and Keller [6] in the isolation of the thermally unstable sesquiterpene β-asarone from *Acorus calamus*.

Previous workers have applied analytical SFE to a wide range of plant materials, including lemon peel [7] and many household spices, such as basil, thyme, rosemary, cloves and oregano [8–11]. A number of these studies included direct coupling of the extraction to a gas chromatograph or a GC–MS system. The quantitative trapping or collection of the volatile extractives was often a problem and has been studied in detail [9,10]. However, many of the reported extractions were qualitative rather than quantitative although comparisons were sometimes made with the chromatograms obtained by alterna-

Correspondence to: Dr. Roger M. Smith, Department of Chemistry, Loughborough University of Technology, Loughborough, Leics. LE11 3TU, UK.

* Present address: Energy and Environmental Research Center, University of North Dakota, Grand Forks, ND, USA.

0021-9673/92/$05.00

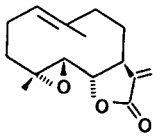

Fig. 1. Structure of parthenolide.

tive extraction techniques, such as solvent extraction [8,10].

Little previous work has been reported on the application of SFE to the examination or isolation of components from medicinal herbs. The herb feverfew [*Tanacetum parthenium* (L.) Schultz Bip.] has recently attracted considerable interest for the treatment of migraine and arthritis [12–14] and contains the sesquiterpene lactone parthenolide (Fig. 1) [15], which is reported to be the active principle [16]. In order to monitor the concentration of the active component in any samples being prepared for medicinal use, assay methods are required. Previous methods for the determination of parthenolide in feverfew have been reported by a number of groups and were usually based on selective solvent extraction followed by infrared spectrometry [17] or extraction and high-performance liquid chromatography (HPLC) [18]. More recently, two further methods based on HPLC determinations have been reported [19, 20]. The isolation of larger amounts of parthenolide has also been carried out using droplet counter-current chromatography [21], but this method is slow.

However, as parthenolide is relatively unstable and degrades on storage [15], there was concern that losses might occur on solvent extraction. In this study we therefore examined the application of SFE followed by capillary GC for the determination of parthenolide from feverfew. We also examined methods for the rapid preparative-scale extraction of feverfew. The extraction conditions and sample collection technique were based the optimum conditions obtained from an initial study of the extraction of a range of terpenoids, including the sesquiterpene lactone santonin, from an α-cellulose model plant matrix [22]. In a subsequent study [23] SFE was also used to obtain the essential oils of feverfew and the related species, tansy and German chamomile, which have been reported as substitutes for commercial feverfew samples.

EXPERIMENTAL

Chemicals

Air-dried powdered feverfew was supplied by British Analytical Control (Burton, UK) (Batch no. A3783). Feverfew plants were grown locally from seed. Feverfew varieties came from the medicinal herb collection at the Chelsea Physic Garden, London, UK. The carbon dioxide was of industry grade (99.98%) supplied by BOC (Middlesex, UK). Acetonitrile was of HPLC grade from FSA Scientific Apparatus (Loughborough, UK). Water was scrubbed and deionized. Parthenolide standard was donated by Dr P. J. Hylands of Chelsea College, London, UK.

SFE equipment

Supercritical extractions and separations were carried out using a system consisting of a Jasco Model 880 pump (Japan Spectroscopic, Tokyo, Japan) for the delivery of carbon dioxide, which was fitted with a cooling jacket around the pump head attached to a Haake KT2 cooling system. A second Jasco Model 880 pump for the addition of modifier was linked through a Gilson Model 811b dynamic mixer. A Jasco 1-ml extraction vessel was mounted in the sample loop position of a Rheodyne (Cotati, CA, USA) Model 7125 valve housed in a Jasco Model 815 oven. The eluent was monitored at 220 nm using a Jasco Model 870 absorbance detector fitted with a high-pressure flow cell. The pressure in the system was maintained using a Jasco Model 880-81 back-pressure regulator and the extracts were collected in a trap made from a 100-ml round-bottomed flask fitted with a side-arm and cooled in liquid nitrogen.

The carbon dioxide flow-rate was measured using a rotameter to give a volume flow-rate. The modifier concentration was calculated as percentage by mass of the mobile phase.

For the trapping studies, either a short column (50 × 4.6 mm I.D.) dry packed with Spherisorb S5W (12 μm, Phase Separations) or a 10-ml Jasco extraction vessel packed with α-cellulose (Sigma) was placed in the oven between the Rheodyne valve and the detector.

Analytical scale extraction

The extraction vessel (1 ml) was packed with

plant material (*ca.* 0.5 g) and was extracted with supercritical carbon dioxide at 250 bar and 45°C at 0.85 ml min^{-1}. The eluent from the extraction was trapped in a flask cooled in liquid nitrogen at −170°C. The solidified carbon dioxide was allowed to evaporate at −10°C in a refrigerator and the residue was dissolved in dichloromethane. The composition of the extraction was determined by GC.

GC analysis of extract

The GC analyses were performed using a Carlo Erba Vega 6000 gas chromatograph. Samples (0.5 μl were injected using a 10-μl syringe in the split injection mode (splitting ratio 20:1) on to a BP1 polydimethylsiloxane fused-silica column (5-μm film thickness, 12 m x 0.33 mm I.D.) (Scientific Glass Engineering). The injection port was maintained at 180°C and the column oven was programmed from 60 to 300°C at 8°C min^{-1}, then held isothermal at 300°C for 8 min. The analytes were detected using a flame ionization detector and the results were recorded using a Perkin-Elmer Nelson 2600 data system on an Opus III computer. The concentration of the parthenolide was calculated from calibration graphs by comparison with safrole (1 mg ml^{-1}), which was added to the extracts as an internal standard.

Solvent extraction methods

French Pharmacopoeia method [18]. Dried powdered feverfew (10 g) was extracted with methanol (100 ml) at 45°C for 30 min and then with fresh methanol (40 ml) for 40 min. The methanol extracts were combined and evaporated to dryness and the residue was dissolved in methanol for analysis.

Marchand et al. [24] method. Dried feverfew (10 g) was extracted with chloroform (100 ml) at room temperature for 30 min. The solution was filtered and the filtrate evaporated to dryness. The residue was dissolved in methanol (10 ml), filtered, the solvent evaporated and the residue dissolved in methanol for analysis.

Bloszyk et al. [17] method. Dried feverfew (10 g) was extracted with three 200-ml portions of methanol at 40°C. The extracts were combined and evaporated to 10 ml. Water (50 ml) was added and the remaining methanol evaporated under vacuum. Saturated lead acetate solution was added until precipitation ceased and the mixture was left for 1 h then centrifuged. The supernatant was extracted with chloroform (3 × 100 ml) and the extracts were combined, filtered and evaporated. The residue was dissolved in chloroform for analysis.

Govindachari et al. [15] method. Dried feverfew (10 g) was extracted with hexane (2 × 100 ml) and the extracts were combined, filtered and evaporated to 3 ml. The solution was passed through a column of neutral alumina with toluene, the eluate was evaporated to dryness and the residue was dissolved in 2 ml of hexane–dichloromethane (1:1) for analysis.

DISCUSSION AND RESULTS

Initial studies

To evaluate the efficiency of SFE as a method for the determination of parthenolide in feverfew, a trial extraction of a commercial sample of powdered dried feverfew, using carbon dioxide at 250 bar and 40°C, was compared by capillary GC with extracts of the same material obtained using three published methods for the determination of parthenolide [15,17,18] and a general extraction method for sesquiterpene lactones [24].

The French Pharmacopoeia method of extraction with methanol (which is normally assayed by HPLC) [18] gave a dark green extract and a yield of 0.04% of parthenolide. The method of Bloszyk *et al.* [17], in which methanol extraction was followed by treatment with lead acetate and re-extraction into chloroform, gave a cleaner yellow extract and a 0.02% yield of parthenolide. A general method for the extraction of sesquiterpene lactones devised by Marchand *et al.* [24], in which the sample is extracted with chloroform, yielded only a small amount of parthenolide (0.006%) but a larger amount of a closely related material. However, extraction of feverfew with hexane followed by chromatography on alumina as reported by Govindachari *et al.* [15], as a source of parthenolide yielded only monoterpenes. The SFE and collection of the extract at room temperature gave a yellow orange oil and a yield of 0.03% of parthenolide. This method could be completed in only 20 min, rather than the several hours for the other methods, and required no solvent evaporation stages.

SFE extraction of feverfew

A detailed study was therefore undertaken to improve the yield and selectivity of the SFE method. Because of the complexity of the feverfew extract and problems with the instability of parthenolide, initially a model plant matrix prepared from α-cellulose, spiked with mono- and sesquiterpenes and the sesquiterpene lactone santonin, was examined [22]. The optimum extraction conditions for this system were determined to be carbon dioxide at 250 bar and 40°C for 15–20 min at 0.8 ml min^{-1}. To avoid losses of volatile components, the extract was collected as solid carbon dioxide using a trap cooled in liquid nitrogen at −170°C followed by slow evaporation of the carbon dioxide in a refrigerator.

In comparative extractions there were significant differences in the overall parthenolide content between older commercial samples (used in the trial studies), freshly dried plant material and stored dried plant material (which might be up to 2 years old). These differences could result both from differences in the original parthenolide content of the plants and from the degradation of parthenolide with time. Consequently, when this method was evaluated for the extraction of dried feverfew samples care had to be taken in comparing the results of experiments carried out at different times. However, comparisons on a single source of plant material could be made within a short series of experiments such as changing the conditions used for extraction.

Extraction of a new sample of recently dried feverfew leaves with carbon dioxide at 250 bar and 45°C at 0.85 ml min^{-1} and trapping in liquid nitrogen gave 0.07% of parthenolide in a pale yellow extract. Milder extraction conditions using a pressure of only 120 bar gave a very similar yield (0.08%). The chromatogram (Fig. 2) of the extract at 250 bar showed that more monoterpenes had been collected than in the trial study, confirming the improvement in the trapping efficiency. The other major peaks were subsequently identified, by GC–MS [23] and a comparison with standards, as chrysanthenol acetate (0.10%) and camphor (0.08%), both of which have been reported previously from feverfew [25]. A minor peak with a similar retention to parthenolide was identified as dihydroparthenolide.

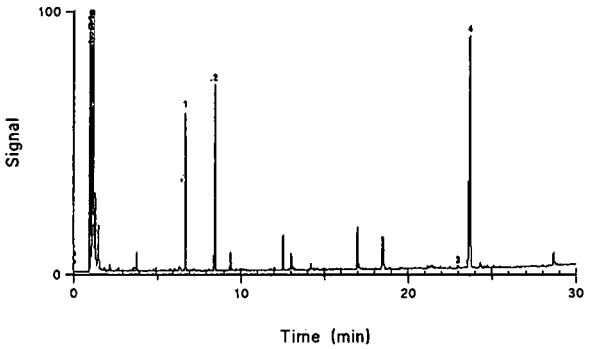

Fig. 2. Gas chromatogram of an extract of freshly dried feverfew obtained with carbon dioxide at 250 bar and 45°C at 0.85 ml min^{-1}. Conditions: column, BP1 (25 m × 0.25 mm I.D.); temperature, increased from 60 to 300°C at 8°C min^{-1}, then isothermal at 300°C for 8 min. Peaks: 1 = camphor; 2 = chrysanthenol acetate; 3 = dihydroparthenolide; 4 = parthenolide.

Extraction using modified carbon dioxide

Because the yields of parthenolide were lower than the average content of 0.42% reported by Jessup [26] for freshly dried material, the effect of modifiers in the extraction fluid was examined. These often increase the recoveries of relative polar analytes from complex matrices [27, 28]. The addition of either 4% of methanol or 4% of acetonitrile at 250 bar and 45°C gave a waxy green extract from dried feverfew and the yield of parthenolide virtually doubled from 0.07% to 0.16% or 0.14%, respectively. In each instance the yields of the more volatile and less polar monoterpenes were virtually unchanged, which suggested that they had been fully extracted with carbon dioxide alone. Water saturated carbon dioxide (produced by bubbling the liquid carbon dioxide through a water trap at room temperature) was also examined but although it gave a yield of 0.14% of parthenolide, it gave a slightly reduced yield of the less polar essential oils (chrysanthenol acetate was reduced from 0.10% to 0.06% and camphor from 0.08% to 0.04%).

All the modifiers had the disadvantage that they were less selective than carbon dioxide and increased the amount of extraneous material that was extracted. For example, methanol or acetonitrile modifiers gave a dark green waxy material with a spectrum corresponding to chlorophyll (characteristic peaks at 214, 322, 436 and 665 nm). In contrast, carbon dioxide alone gave a yellow–orange extract, the colour of which could be attributed to carotenoids (the UV spectrum contained three

characteristic bands around 446 nm). The presence of carotenoids was expected, as Favati *et al.* [29] have reported that at 300 bar and 40°C, 96% of the carotene and 30% of lutein could be extracted from plant samples by SFE with carbon dioxide.

The solubility of the parthenolide in carbon dioxide was not thought to be the cause of its low extraction with the unmodified fluid, as oxygenated sesquiterpenes have been reported to have good solubility in supercritical carbon dioxide [30]. It was also possible to extract readily the related sesquiterpene lactone santonin from the cellulose model sample matrix with carbon dioxide alone [22]. It therefore appeared that parthenolide may be present at different sites on the plant matrix, from some of which it can be readily extracted, but it is more tightly held to others and would require the addition of a polar modifier to be released. This idea of an analyte being present as a "free" and "bound" form has also been put forward by King *et al.* [31], who investigated the extraction of rape seed with liquid carbon dioxide.

An alternative idea was that parthenolide may be microencapsulated physically within the plant by means of the glandular trichomes, which are present on the leaves of feverfew [32]. The effect of extraction on these trichomes was investigated by using scanning electron microscopy (SEM) to examine air-dried feverfew leaves exposed to various conditions. Before extraction the glandular trichomes were intact but after extraction the trichomes were ruptured and empty. Sugiyama and Saito [7] have reported that supercritical carbon dioxide could rupture similar oil-containing structures present on lemon peel. However, physical entrapment is unlikely to be the cause of the limited recovery as the trichomes were ruptured with carbon dioxide alone.

The feverfew samples were also exposed to supercritical carbon dioxide plus 10% of methanol but the glandular trichomes underwent a different physical change, "collapsing" on exposure to the solvent. Blakeman and Atkinson [32] discovered a similar phenomenon with the feverfew glandular trichomes when using conventional liquid extraction with chloroform.

Timed extractions from plant material

To determine if parthenolide was being only slowly released from the plant material, extraction with carbon dioxide at 250 bar and 45°C was monitored by collecting extracts at 1-min intervals. Almost all of the "free" parthenolide was collected in the second min and the extraction was apparently complete within 4 min. This contrasted with the extraction of santonin from the α-cellulose model matrix, which took 20 min using similar extraction conditions [22]. This rapid but incomplete extraction from the feverfew plant material suggested that only surface or "unbound" oils were being extracted under these conditions.

Use of an in-line cellulose or silica trap

Because of the colour and extraneous material in the extract, the use of on-line traps was investigated to try to obtain a cleaner extract. A second extraction vessel (10 ml) packed with powdered α-cellulose was placed in the column oven between the sample extraction vessel and the detector. On extraction of feverfew with carbon dioxide, at 250 bar and 45°C most of the plant pigments were retained on the cellulose to give a pale yellow extract. The gas chromatogram showed that virtually none (<5%) of the volatile components had been retained and this was confirmed by subsequently washing the cellulose with methanol-modified carbon dioxide (5:95). With carbon dioxide extractions this trap would retain the pigments for about 2 h of extraction before a significant colour started to appear in the extracts.

To obtain greater discrimination, the cellulose trap was replaced by a short chromatographic column packed with Spherisorb S5W silica. This combination had been successfully tried during the studies with the model plant system and enabled a discrimination to be obtained between the terpene hydrocarbons and the sesquiterpene lactone santonin [22]. On extraction of feverfew with carbon dioxide at 250 bar and 45°C a series of six bands were detected by the UV monitor and collected separately. On analysis by GC these showed only poor discrimination between the volatile terpenes. Both chrysanthenol acetate and camphor were present in fractions C, D and E (Fig. 3). When no more components were being eluted from the column, the extraction vessel was switched out of the eluent stream. The silica column was then eluted with methanol–carbon dioxide (10:90) to give a final

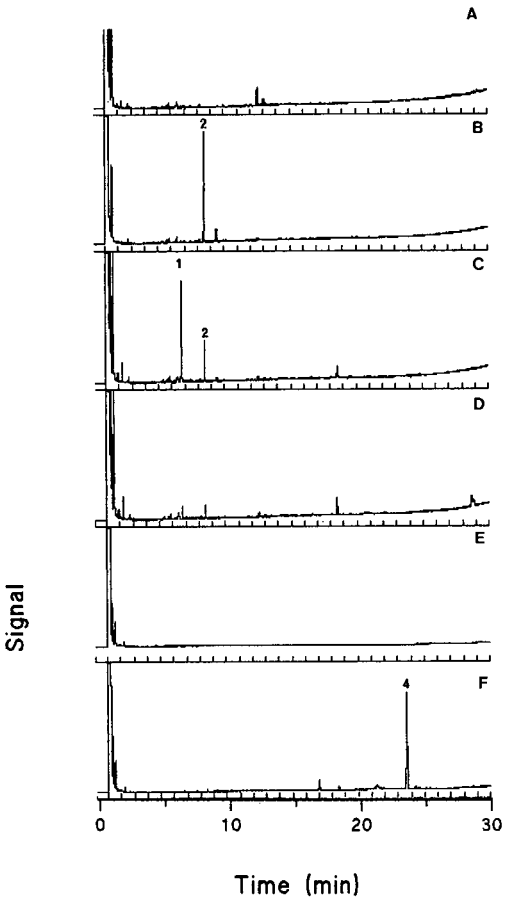

Fig. 3. Selective extraction of feverfew using an on-line silica trap. Chromatograms of successive fractions from freshly dried feverfew with a silica trap in-line. Eluent: carbon dioxide at 250 bar and 45°C at 0.85 ml min^{-1} to give fractions A–E then 10% methanol in carbon dioxide with the extraction vessel switched out of the eluent flow to give fraction F. GC conditions and peaks as in Fig. 2.

fraction which contained about 80% pure parthenolide in a yield of 0.18% (Fig. 3F). Because the modified eluent was only used after the extraction vessel had been switched out of the system, no extraction of the more polar materials or pigments occurred from the plant material.

Preparative-scale SFE

In order to prepare a larger amount of parthenolide, a new sample of dried feverfew (10 g) was extracted with carbon dioxide at 250 bar, 45°C and 0.85 ml min^{-1} to give an orange-yellow extract. This was separated on a silica gel TLC plate using chloroform–acetone (95:5) to give parthenolide (14.3 mg, 98% pure by GC), whose structure was confirmed by comparison using IR, ^{1}H and ^{13}C NMR spectroscopy and mass spectrometry with literature values and with an authentic sample.

Effect of sample preparation

Because many of the components of feverfew were volatile or unstable and might be lost on drying or storage, extracts of freshly dried leaves and stored dried samples were compared. With carbon dioxide a sample of freshly dried leaves (4 h at 50°C) gave a yield of parthenolide of 0.38%, which decreased on storage at room temperature for 1 year to 0.31% and after 2 years to 0.18%. A number of additional peaks were present in the extracts of the older samples and can be attributed to degradation products (Fig. 4). Commercial feverfew samples which were 4 years old yielded only 0.002% of parthenolide. The monoterpenes had also decreased markedly and were virtually absent after 4 years.

Differences of more than 20% in the initial parthenolide levels were observed between freshly dried materials from individual plants, whether collected in the wild or cultivated. Triplicate samples were therefore taken from a single plant and examined by SFE and GC. The variation in the parthenolide content was about 14% R.S.D., similar to that obtained by Hawthorne *et al.* [10] in a study of basil (R.S.D. 6–17%).

As it has been reported that the trichomes on the

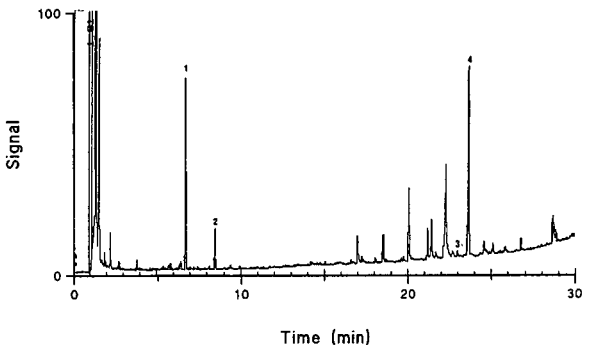

Fig. 4. Gas chromatogram of an extract of a 1-year-old sample of dried feverfew from the same plant as Fig. 2. Extraction, analysis and peaks as in Fig. 2.

leaves were the source of parthenolide [32], parts of two plants grown from seeds obtained from different suppliers were compared but the levels of parthenolide in the leaves and in the flowering heads were 0.26% and 0.21%, respectively for the first plant, and 0.18% and 0.16% for the second. In each instance the monoterpenes patterns were very similar.

Varieties

A number of samples of leaves were taken from different varieties of feverfew grown in the Chelsea Physic Garden. Two-year-old dried plant material was examined and the most common variety Schultz Bip. contained 0.13% of parthenolide. Similar levels were present in Balkan Peninsula (0.13%) and Schneeball varieties (0.12%) but lower levels were found in Golden Veis (0.05%), Boule de Neige (0.05%), and Flore Pleno (0.01%) varieties. The Boule de Neige and Schneeball plants were thought to be the same variety from different original locations. These differences may not be very significant, as Hylands [33] found a similar variation in parthenolide content during a season and between seasons.

These differences emphasize a probable need to assay and control the level of parthenolide present in commercial herbal products as plant mass alone is not a good indication of the amount of the lactone. A brief survey of a range of tablets and capsules marketed as containing feverfew, which had been stored for 2 years, suggested that many contained little or no parthenolide, with many of the tablets having less than 10% of the expected level from the stated content of plant material. This result agrees with a study of the biological activity of commercial samples which found levels much lower than claimed [34]. These results emphasize a need for levels of parthenolide in herbal medicines to be controlled and for the probable necessity to indicate an effective shelf life and storage conditions.

ACKNOWLEDGEMENTS

The authors thank the Science and Engineering Research Council for a studentship to M.D.B., Ciba-Corning for the loan of a JASCO SFE/SFC system, British Analytical Control and the Chelsea Physic Garden for gifts of feverfew and Phase Separations for Spherisorb. M. Kingswood and I. Ekcan are thanked for preliminary experiments.

REFERENCES

1 D. F. Williams, *Chem. Eng. Sci*, 36 (1981) 1769.
2 A. B. Caragay, *Perfum. Flavor.*, 6 (1981) 43.
3 S. B. Hawthorne, *Anal. Chem.*, 62 (1990) 633A.
4 R. W. Vannoort, J.-P. Chervet, H. Lingeman, G. J. De Jong and U. A. Th. Brinkman, *J. Chromatogr.*, 505 (1990) 45.
5 J. Garnero and R. Tabacchi, in P. Sandra and C. Bicchi (editors), *Capillary Gas Chromatography in Essential Oil Analysis*, Hüthig, Heidelberg, 1987, p. 359.
6 E. Stahl and K. Keller, *Planta Med.*, 47 (1983) 75.
7 K. Sugiyama and M. Saito, *J. Chromatogr.*, 442 (1988) 121.
8 S. B. Hawthorne, M. S. Kreiger and D. J. Miller, *Anal. Chem.*, 60 (1988) 472.
9 S. B. Hawthorne, D. J. Miller and M. S. Kreiger, *Fresenius Z. Anal. Chem.*, 330 (1988) 211.
10 S. B. Hawthorne, D. J. Miller and M. S. Kreiger, *J. Chromatogr. Sci.*, 27 (1989) 347.
11 S. B. Hawthorne, D. J. Miller and M. S. Kreiger, *J. High Resolut. Chromatogr.*, 12 (1989) 714.
12 M. I. Berry, *Pharm. J.*, (1984) 611.
13 E. S. Johnson , N. P. Kadam, D. M. Hylands and P. J. Hylands, *Br. Med. J.*, 291 (1985) 569.
14 A. Groenewegen and S. Heptinstall, *J. Pharm. Pharmacol.*, 42 (1990) 553.
15 T. R. Govindachari, B. S. Joshi and V. N. Kamat, *Tetrahedron*, 21 (1965) 1509.
16 W. A. Groenewegen, D. W. Knight and S. Heptinstall, *J. Pharm. Pharmacol.*, 38 (1986) 709.
17 E. Bloszyk, B. Geppert, and B. Drozdz, *Planta Med.*, 34 (1978) 79.
18 Commission Française de Pharmacopée, *French Pharmacopoeia*, Maisonneuve, Paris, 1987, Grand Camomille 87/1, .
19 D. Fontanel, S. Bizot and P. Beaufils, *Plant Med. Phytother.*, 24 (1990) 231.
20 D. V. C. Awang, B. A. Dawson, D. G. Kindack, C. W. Crompton and S. Heptinstall, *J. Nat. Prod.*, 54 (1991) 1516.
21 A. Kéry, Gy. Turiák and P. Tétényi, *J. Chromatogr.*, 466 (1988) 157.
22 R. M. Smith and M. D. Burford, *J. Chromatogr.*, 600 (1992) 175.
23 R. M. Smith and M. D. Burford, *J. High Resolut. Chromatogr.*, submitted for publication.
24 B. Marchand, H. M. Behl and E. Rodriguez, *J. Chromatogr.*, 265 (1983) 97.
25 F. Bohlmann and C. Zdero, *Phytochemistry*, 21 (1982) 2543.
26 D. M. Jessup, *PhD Thesis*, University of London, 1982.
27 J. R. Wheeler and M. E. McNally, *J. Chromatogr. Sci.*, 27 (1989) 534.
28 S. B. Hawthorne and D. J. Miller, *J. Chromatogr. Sci.*, 24 (1986) 258.
29 F. Favati, J. W. King, J. P. Friedrich and K. Eskins, *J. Food Sci.*, 53 (1988) 1532.
30 E. Stahl and G. Gerard, *Perfum. Flavor.*, 10 (1985) 29.
31 M. B. King, T. R. Bott, M. R. Barr and R. S. Mahmud, *Sep. Sci. Technol.*, 22 (1987) 1103.
32 J. P. Blakeman and P. Atkinson, *Physiol. Plant Pathol.*, 15 (1979) 183.
33 P. J. Hylands, personal communication.
34 W. A. Groenewegen and S. Heptinstall, *Lancet*, No. 8471 (1986) 44.

Journal of Chromatography, 627 (1992) 263–271
Elsevier Science Publishers B.V., Amsterdam

CHROM. 24 592

Capillary isotachophoretic analyte focusing for capillary electrophoresis with mass spectrometric detection using electrospray ionization*

N. J. Reinhoud, A. P. Tinke, U. R. Tjaden, W. M. A. Niessen and J. van der Greef

Division of Analytical Chemistry, Center for Bio-Pharmaceutical Sciences, Leiden University, P.O. Box 9502, 2300 RA Leiden (Netherlands)

(Received July 15th, 1992)

ABSTRACT

An improvement in detectability in capillary electrophoresis–mass spectrometry (CE–MS) was realized using isotachophoretic analyte focusing. The practical approach is described for the on-line coupling of capillary isotachophoresis–capillary electrophoresis–mass spectrometry (ITP–CE–MS) using an electrospray interface. An equation was derived for the calculation of the splitting ratio of ITP zones into the CE system. The applicability of analyte focusing is demonstrated for the analysis of a mixture of anthracyclines. Initial experiments showed a 200-fold improvement in concentration detection limit for ITP–CE–MS compared with CE–MS.

INTRODUCTION

Capillary electrophoresis (CE) in combination with mass spectrometry (MS) can be a potentially powerful tool in the analysis of various compounds [1–9]. Especially in the area of protein and peptide analysis there is growing interest in a highly efficient separation technique such as CE in combination with the high selectivity of MS detection. CE–MS interfaces described in the literature are continuous-flow fast atom bombardment (CF-FAB), electrospray (ESP) and ionspray (ISP) types.

The application of CF-FAB has been realized by either a liquid-junction interface (LJI) or a coaxial approach for addition of the necessary make-up fluid for this type of ionization. In the coaxial approach [10] the separation capillary is inserted in the CF-FAB capillary and ends only a few millimetres before the tip of the CF-FAB probe. This minimizes the dead volume and facilitates highly efficient separations.

In the other approach of CE–CF-FAB-MS, an LJI for the electric decoupling and for addition of make-up fluid is used [2,11,12]. This type of interface utilizes a transport capillary between the CE capillary and the mass spectrometer. Transport of ions in this capillary is facilitated by means of a hydrodynamic flow generated by the vacuum in the ion source of the mass spectrometer. It is evident that this type of CE–MS coupling results in considerable more peak broadening than the coaxial approach.

On the other hand, the coaxial approach requires the use of 10 μm I.D. capillaries in order to prevent a hydrodynamic flow in the CE capillary because of the vacuum of the ion source at the CE capillary outlet. This means a considerable drawback with respect to the loadability and the corresponding sample concentration detection limits in CE–MS [9].

Correspondence to: U. R. Tjaden, Division of Analytical Chemistry, Center for Bio-Pharmaceutical Sciences, Leiden University, P.O. Box 9502, 2300 RA Leiden, Netherlands.

* Presented at the *4th International Symposium on High Performance Capillary Electrophoresis, Amsterdam, February 1992*. The majority of the papers presented at this symposium were published in *J. Chromatogr.*, Vol. 608 (1992).

0021-9673/92/$05.00

Although the use of an LJI results in band broadening, the mass flow to the mass spectrometer will be superior for the LJI type of interfaces where 75 μm I.D. capillaries are used with a *ca.* 50-fold higher loadability than the 10 μm I.D. capillaries. Nevertheless, the loadability is limited to the nanolitre range, resulting in relatively high minimum detectable concentrations. An important improvement in detectability was realized by using a PATRIC (position- and time-resolved ion counting) array detector for CE–CF-FAB-MS [3].

The ESP interface for CE–MS described by Smith and co-workers [13,14] has several advantages over the CF-FAB interface. First, the CE capillary is inserted in the ion source and the migrating ions are electrosprayed from the capillary outlet directly into the mass spectrometer, implying that no additional peak broadening after the CE separation is introduced. Second, the use of a sheath flow with an approximately tenfold higher flow-rate allows the use of CE buffers with minor consideration of the ionization compatibility. In peptide analysis CE can be performed in buffers with high pH, while positive ions are detected in the mass spectrometer because of addition of acetic acid to the sheath flow. Third, the ion source is at atmospheric pressure, resulting in the absence of a hydrodynamic flow and 75 μm I.D. CE capillaries can be used. Finally, the ESP interface permits the analysis of high-molecular-mass compounds such as proteins. Because of multiple charges on the large molecules, the corresponding mass-to-charge ratios are within the detectable range of the mass spectrometer.

The coupling of CE–MS using electrospray with pneumatically assisted nebulization (ionspray) has been described utilizing either an LJI [15] or a coaxial approach [16]. In a recent investigation both approaches have been compared [17].

Isotachophoresis (ITP) is a capillary separation technique which is capable of concentrating trace components and diluting of major constituents of the sample. The combination of these features makes ITP in principle an ideal technique for sample treatment. The use of ITP for sample pretreatment in CE has been described [18–21].

The degree of the concentration effect of ITP can be derived from the Kohlrausch equation:

$$C_A = C_L \cdot \frac{\mu_A}{\mu_A + \mu_R} \cdot \frac{\mu_L + \mu_R}{\mu_L} \quad (1)$$

where C_L is the molarity of the leading buffer, C_A the analyte concentration and μ the electrophoretic mobility (the subscript R refers to the counter ion). From this equation it can be seen that the final concentration of the analyte is proportional to the molarity of the leading buffer. This equation can be written as

$$C_A = C_L K \quad (1a)$$

where K is a proportionality factor. In the case of similar mobilities, K will have a value of about 1. Eqn. 1a clearly demonstrates the tremendous concentration potential of ITP. In this paper we describe the preliminary results of the on-line coupling of ITP–CE–MS with an ESP interface. For the coupling of ITP with CE we used the same set-up as described previously [18,19], where we demonstrated a decrease in the concentration detection limits by a factor of 100–1000. The CE–MS coupling was similar to that described by Smith *et al.* [13]. The potential of the ITP–CE–MS coupling is demonstrated with the analysis of a mixture of anthracyclines.

EXPERIMENTAL

Isotachophoresis

ITP was effected in a laboratory-made apparatus consisting of Plexiglas electrode vials and a PTFE capillary (150 × 0.32 mm I.D.). The terminating buffer consisted of 10 mmol/l histidine (HIS) (pH 7.2) in 60% (v/v) methanol (MeOH). Sodium phosphate (10 mmol/l, pH 7.2) in 60% MeOH was used as the leading buffer. Injection of 5 μl of analyte into the ITP system was done with a 100-μl injection syringe. No detector was used as the ITP zones of anthracyclines could be seen. For the determination of low concentrations one of the anthracyclines was used as a marker and added in a high concentration. The voltage was supplied by a Model RR100-1.5R power supply (Gamma High Voltage Research, Mt. Vernon, NY, USA) operating in the constant-current mode at 60 μA. For injection of ITP zones into the CE system by means of electrical splitting an additional power supply (Model RR40-1.5P; Gamma High Voltage Research) was used. The current was measured over a 350-Ω resistance placed in series with the capillary using a microamperometer (Model 134312; Goerz, Vienna, Austria).

Capillary electrophoresis

CE was carried out in a 700 × 0.075 mm I.D. (for CE–MS) or 700 × 0.040 mm I.D. (for CE–MS and ITP–CE–MS) fused-silica capillary (SGE, Ringwood, Australia) using an electrophoresis buffer composed of 10 mmol/l sodium acetate (pH 7.5)–60% MeOH (for CE–MS) or 10 mmol/l sodium phosphate (pH 7.2)–60% MeOH (for ITP–CE–MS).

The power supply was operated in the constant-voltage mode at 20 kV for CE. Samples were electrokinetically injected, applying 6 kV for 6 s.

On-capillary absorbance detection in CE took place at 350 mm from the anodic end, using a Spectra 100 UV–Vis absorbance detector (Spectra-Physics, Mt. View, CA, USA) at a wavelength of 210 nm.

Isotachophoresis–capillary electrophoresis

Coupling of ITP and CE was done as described previously [19] by inserting the CE capillary in the ITP capillary through a septum in the cathode compartment of the ITP system (Fig. 1). As the ITP zones approached the CE inlet, injection took place by means of electrical splitting proportional to the current distribution over the CE and ITP capillary. After injection the ITP capillary was carefully flushed with leading buffer and the CE run was started. The CE buffer was the same as the leading buffer.

Capillary electrophoresis–mass spectrometry

A Finnigan (San Jose, CA, USA) MAT TSQ 70 triple-quadrupole mass spectrometer equipped with an ESP system (Finnigan MAT) was used in the positive-ion mode. A sheath flow-rate of 1 μl/min was applied by means of a syringe pump (Model 2400; Harvard Apparatus, Edinbridge, UK). For the on-line coupling of the CE and MS systems it is essential to make electrical contact between the ESP needle and the CE capillary outlet. The sheath liquid consisted of 1% glacial acetic acid in ethanol–water (3:2, v/v). The current in the CE capillary was monitored as described under the CE conditions. The counter electrode of the electrospray was set at −4 kV and the ESP needle was grounded. The distance from the outlet of the CE capillary to the counter electrode was *ca.* 20 mm. Height differences between electrode vials and electrospray were avoided to prevent any hydrodynamic flow. All experiments were performed in the multiple ion detection (MID) mode.

Chemicals

Doxorubicin (DOX), carminomicin (CAR) and epirubicin (EPI) were available as 1 mg/ml chlorohydrate solutions containing 5 mg/ml of lactose and were purchased from Carlo Erba (Nivelles, Belgium). Daunorubicin (DAU) was purchased from Rhone-Poulenc (Paris, France). Histidine, methanol, sodium hydrogenphosphate and sodium dihydrogenphosphate were purchased from Merck (Darmstadt, Germany). All other chemicals were of analytical-reagent grade. Demineralized water was used in all experiments.

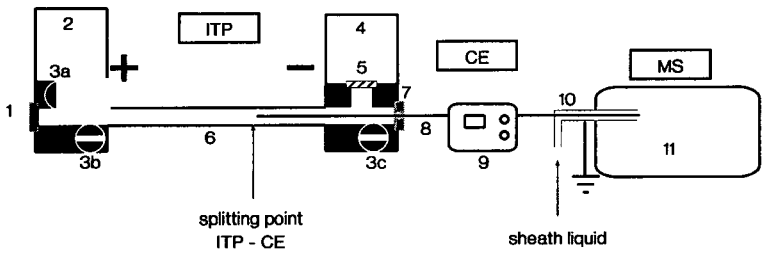

Fig. 1. Representation of on-line ITP–CE–MS coupling. Injection takes place through a silicone-rubber septum (1) by means of a syringe inserted up to valve 3b. The valves (3a–c) are used for flushing the ITP capillary with buffer. The terminating buffer vial (2) is connected to a positive voltage and the leading buffer (4) vial to earth during ITP and is raised to +2 kV at the time of injection. ITP takes place in a 150 × 0.320 mm I.D. capillary (6). The capillary is closed by a membrane (5) to prevent hydrodynamic flow. For the CE run the electrode in vial 2 is disconnected and the electrode in vial 4 is set at a positive voltage. CE takes place in either a 700 × 0.075 mm I.D. or 700 × 0.04 mm I.D. capillary (8) and was inserted into the ITP system through a septum (7). The UV absorbance detector (9) was placed 350 mm from the CE capillary end. The sheath needle (10) for electrospray MS (11) was always grounded.

RESULTS AND DISCUSSION

CE and ITP of anthracyclines

Several preliminary experiments were carried out for the optimization of the CE separation. Anthracyclines adsorb on the capillary wall, glassware and other laboratory materials, introducing a source of irreproducibility especially at low concentrations [22]. One way to overcome this problem is to use an organic modifier in the stock solutions and the electrophoresis buffers [23]. Therefore, either acetonitrile (ACN) or MeOH was added to the electrophoresis buffer.

Although the use of volatile buffers is often preferred in MS to prevent contamination of the ion source by salt formation, it was possible to work for several days with a 10 m*M* sodium phosphate or sodium acetate buffer before crystallization was notable and the ion source had to be cleaned. The low flow-rate in CE and the use of a volatile sheath liquid allowed the optimization of the CE buffer almost regardless of its MS compatibility.

The ITP separations of anthracyclines were performed in the cation mode because of their positive charge below pH 7.5. The ITP buffer system is a modification of the system described by Akedo and Shinkai [24], who used a leading buffer of sodium acetate at pH 6.0 and a terminating buffer of β-alanine in 60% MeOH for the determination of doxorubicin and doxorubicinol in plasma. Under these conditions, however, the mobility of some anthracyclines appeared to be higher than that of sodium. Therefore, the pH was increased to 7.2, thus lowering the mobility of the anthracyclines. Histidine was chosen as the terminating buffer because its p*I* of 7.5 is close to the working pH, resulting in the lowest mobility.

CE–MS of anthracyclines

In the coupling of CE with MS, the electrical contact between the electrospray needle and the capillary outlet appeared to be very important. Disruption of this contact could lead to electroperforation of the capillary because of the grounded stainless-steel electrospray needle surrounding the CE capillary over a length of 15 cm. By addition of 1% of glacial acetic acid to the sheath liquid this problem could be overcome, possibly owing to improved wetting of the fused silica and the stainless-steel ESP needle and to the higher conductivity of the sheath flow solvent.

Tuning of the mass spectrometer was done using a continuous flow of leading buffer containing 184 μmol/l of DOX at a flow-rate of 10 nl/min using the syringe pump. During the tuning of the mass spectrometer it appeared that the signal was not only determined by the concentration but also by the hydrodynamic flow-rate.

Fig. 2 shows the UV signal and the mass electropherogram of a mixture of DAU, EPI and DOX at concentrations of 66, 83 and 83 μg/ml, respectively. The UV trace shows no resolution between the stereoisomers DOX and EPI. In the mass electropherogram a shoulder is formed on the peak at $m/z = 544$, indicating a small difference in electrophoretic mobility. Also, the resolution between the peak of DAU and the peak of DOX and EPI has improved with respect to the UV signal. The mass electropherogram was monitored at 35 cm from the UV detector, resulting in a larger difference in migration time. The efficiency calculated as the plate number from the UV absorbance and the mass spectrometric peak of DAU was in both instances *ca.* 120 000, indicating that the electrospray does not significantly contribute to peak broadening.

In Fig. 3 the separation of the stereoisomers EPI and DOX is more pronounced. By changing the pH of the electrophoresis buffer from 4.6 to 7.2, the pH is closer to the pK_a values of EPI and DOX which are 7.7 and 8.2, respectively. This permitted an almost baseline separation of both compounds.

ITP–CE—MS of anthracyclines

The diameter of the CE capillary in ITP–CE–MS experiments was smaller than that in CE–MS experiments. It was necessary to use a 40 μm I.D. CE capillary in the ITP–CE mode in order to reduce the hydrodynamic flow in the CE capillary when the ITP capillary was flushed with leading buffer. Flushing of the ITP capillary was done after injection of ITP zones into the CE capillary. A syringe filled with leading buffer was connected to valve 3c (Fig. 1), valves 3c and 3b were opened and valve 3a was closed. Pressure was applied to the syringe and the ITP tube was flushed to establish a continuous buffer system during the CE run. The pressure applied to the ITP system through valve 3c is distributed over the ITP capillary and the CE

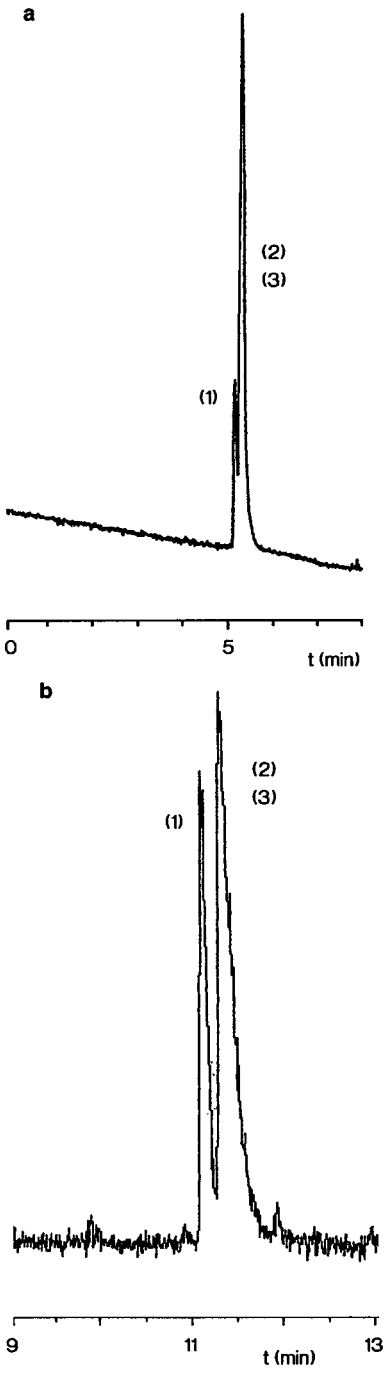

Fig. 2. Electropherograms of the UV absorbance (a) and mass spectrometric (b) detection of DAU (1), EPI (2) and DOX (3) (66, 83 and 83 μg/ml, respectively). CE took place in a 700 × 0.075 mm I.D. capillary using a 10 mmol/l sodium acetate buffer (pH 4.6) in 70% ACN, and a voltage of 20 kV.

Fig. 3. CE–MS of the stereoisomers EPI (1) and DOX (2) (250 μg/ml each) in 10 mmol/l sodium acetate buffer (pH 7.5) and 60% methanol using a 700 × 0.040 mm I.D. capillary and a voltage of 20 kV at the anodic end.

capillary. This resulted in a hydrodynamic flow that is proportional to the capillary radius to the power 4 and to the reciprocal of the capillary length. This hydrodynamic flow was a major source of peak broadening of the CE zones after ITP focusing when 75 μm I.D. CE capillaries were used. By using 40 μm I.D. capillaries this peak broadening could be considerably reduced.

Injection of the ITP zones into the CE capillary was done by electrical splitting [25]. The CE inlet is positioned between the anode and cathode vial of the ITP, at *ca.* 3 cm from the cathode. The CE capillary outlet is always grounded by means of the ESP interface. This means that during the ITP run a potential drop exists over the CE capillary. By raising the cathode voltage of the ITP from 0 to +2 kV the splitting ratio was increased in favour of the CE.

The ITP–CE coupling can be represented as an electrical circuit. When the influence of the electro-

osmotic flow is negligible, the splitting ratio between the CE and the ITP capillary can be calculated by the current ratios I_2/I_3 (see Fig. 4) [25]. In order to manipulate the splitting ratio, it is convenient to know the parameters that are influencing I_2 and I_3. Therefore, an equation is derived giving the splitting ratio I_2/I_3 as a function of the dimensions of the capillaries using the resistance ratio R_3/R_2, and of the voltages applied at the time of injection. The currents I_2 and I_3 can be written as

$$I_2 = (V_1 - I_1R_1 - V_2)/R_2 \quad (2)$$

and

$$I_3 = (V_1 - I_1R_1)/R_3 \quad (3)$$

and the ratio as

$$\frac{I_2}{I_3} = \frac{R_3}{R_2} \cdot \frac{V_1 - I_1R_1 - V_2}{V_1 - I_1R_1} \quad (4)$$

where V_1 and V_2 are the potentials of the anode and cathode vial of the ITP, respectively, at the time of

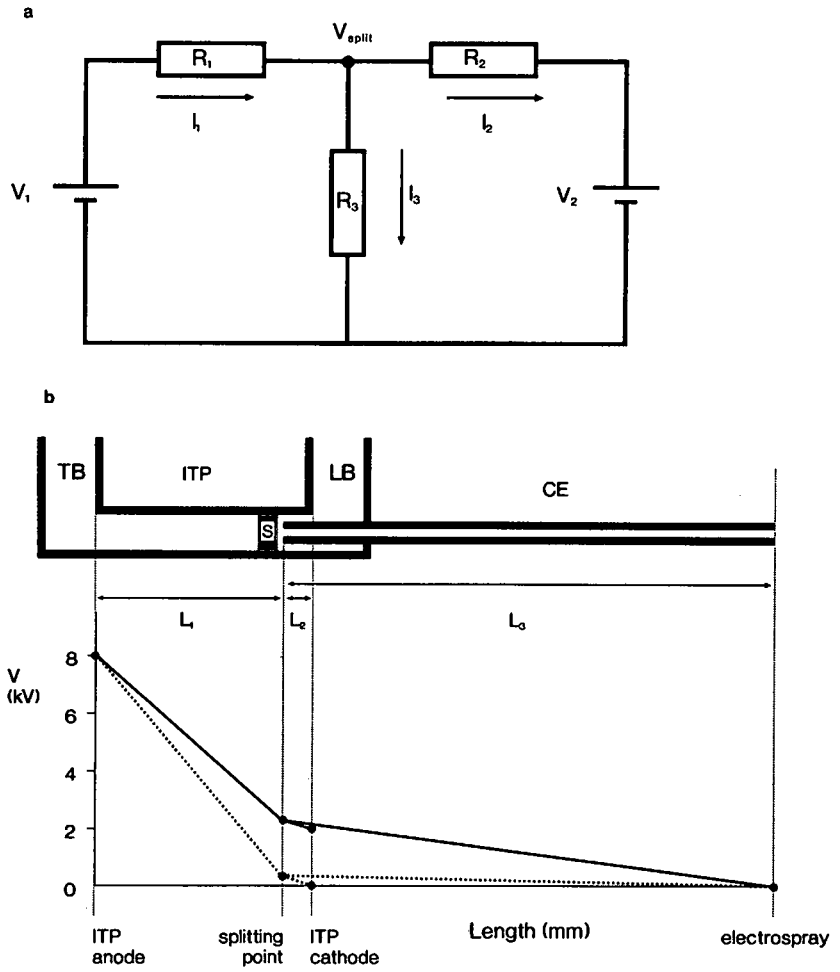

Fig. 4. (a) Schematic representation of the electrical circuit in ITP–CE–MS at the time of injection. R_1, R_2 and R_3 are the electrical resistances of the ITP capillary up to the point of injection (V_{split}), the ITP capillary from V_{split} to the cathode vial with correction for the inserted CE capillary outer diameter and the CE capillary, respectively. I_1, I_2 and I_3 are the corresponding currents through the capillaries. V_1 is the ITP anode voltage and V_2 is the ITP cathode voltage at the time of injection. (b) The voltage distribution over the capillaries at the time of injection is given for $V_2 = 0$ kV (dashed line) and for $V_2 = 2$ kV (solid line) at a constant voltage V_1 of 8 kV. L_1, L_2 and L_3 represents the lengths of the corresponding capillaries as used in eqns. 8, 12 and 13. S is the sample zone and TB and LB are the terminating and leading buffer, respectively.

injection and R_1, R_2 and R_3 are the electrical resistance of the ITP capillary from the anode to the splitting point and of the ITP capillary from the splitting point to the cathode and of the CE capillary, respectively.

As $V_1 - I_1R_1$ represents the voltage at the splitting point at the time of injection (V_{split}), eqn. 4 becomes

$$\frac{I_2}{I_3} = \frac{R_3}{R_2}\left(1 - \frac{V_2}{V_{split}}\right) \quad (5)$$

When the cathode of the ITP is grounded at the time of injection ($V_2 = 0$), the equation is simplified and the splitting ratio is

$$I_2/I_3 = R_3/R_2 \quad (6)$$

In this instance the splitting ratio is independent of V_{split}, which means that the filling of the ITP capillary with terminating buffer does not influence the splitting ratio. It should be noted that the current I_2 (Fig. 4a) can become negative. When V_2 approaches V_1 and $V_2 > V_{split}$ then the direction of the current is reversed, the ions will migrate in the opposite direction and the ITP conditions no longer exist. Just before that, when $V_2 = V_{split}$, the current ratio $I_2/I_3 = 0$, which means that theoretically 100% of the analyte will migrate into the CE system. However, in this instance small changes in the voltage will cause large differences in the splitting ratio. In our experiments the splitting ratio was considerably lower in order to prevent overloading of the CE system and to have a reproducible splitting ratio. The capillary resistance R can be calculated from

$$R = L/\pi r^2 K \quad (7)$$

where L is the capillary length, r is the capillary radius and K is the conductivity of the buffer. As both the CE capillary and the ITP capillary from the splitting point to the cathode are filled with the same leading buffer, the resistance ratio R_3/R_2 can be written as

$$\frac{R_3}{R_2} = \frac{L_3}{L_2} \cdot \frac{r_{ITP}^2 - r_{CE,o}^2}{r_{CE,i}^2} \quad (8)$$

where L_3/L_2 is the ratio of the total CE capillary length to the ITP capillary length from splitting point to the cathode. The ITP capillary radius r_{ITP} is corrected for the inserted CE capillary outer radius $r_{CE,o}$; $r_{CE,i}$ is the inner radius of the CE capillary. The voltage at the splitting point at the time of injection is calculated from

$$I_3 = I_1 - I_2 \quad (9)$$

$$\frac{V_{split}}{R_3} = \frac{V_1 - V_{split}}{R_1} - \frac{V_{split} - V_2}{R_2} \quad (10)$$

$$V_{split} = \frac{V_1 + \frac{R_1}{R_2} \cdot V_2}{1 + \frac{R_1}{R_3} + \frac{R_1}{R_2}} \quad (11)$$

The resistance ratios are

$$\frac{R_1}{R_2} = \frac{L_1}{L_2} \cdot \frac{K_L}{K_T} \cdot \frac{r_{ITP}^2 - r_{CE,o}^2}{r_{ITP}^2} \quad (12)$$

and

$$\frac{R_1}{R_3} = \frac{L_1}{L_3} \cdot \frac{K_L}{K_T} \cdot \frac{r_{CE,i}^2}{r_{ITP}^2} \quad (13)$$

The resistance ratios are corrected for differences in conductivities using the conductivity ratio K_L/K_T because at the time of injection the ITP capillary is filled to the splitting point with terminating buffer. The conductivity ratio can easily be measured by the ratio of the voltage drop over the ITP capillary before the ITP run when the capillary is filled with leading buffer and at the end of the ITP run when the capillary is filled with terminating buffer at a constant current. The measured difference in voltage drop is caused by a proportional difference in conductivity of the leading buffer with respect to the terminating buffer.

When in the described system the ITP cathode is grounded ($V_2 = 0$), the current ratio can be calculated from eqns. 6 and 8, using the capillary lengths L_3, L_2 and radius r_{ITP}, $r_{CE,o}$ and $r_{CE,i}$ which are 70 cm, 3 cm, 160 μm, 100 μm and 20 μm, respectively (Fig. 4b). This results in a current ratio of 910, which means that 0.1% of the total current is split to the CE.

Raising the voltage in the ITP cathode compartment appeared to be a convenient way to manipulate the splitting ratio. At a cathode voltage, V_2, of 2 kV, the splitting ratio was calculated to be 128, implying that 0.8% was split into the CE system (L_1 = 12 cm,

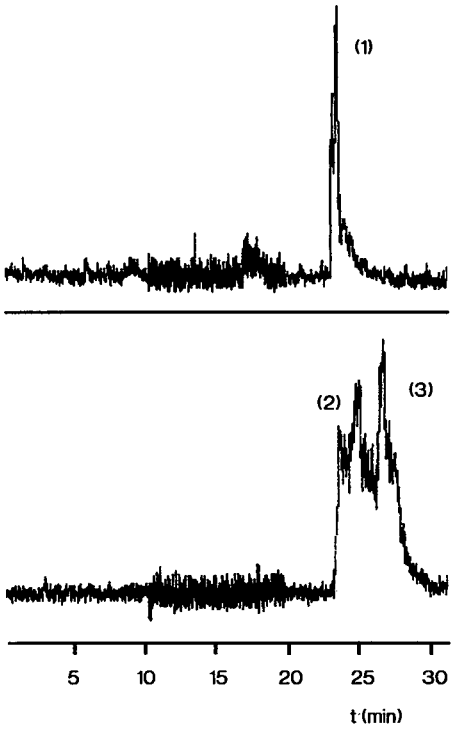

Fig. 5. Mass spectrometric electropherogram obtained in ITP–CE–MS of DAU (1), EPI (2) and DOX (3) (3, 8 and 8 μg/ml, respectively).

$K_L/K_T = 7$, $V_1 = 8$ kV). This splitting ratio was used in further experiments. Although this splitting ratio is low, V_2 was not increased further because this would lead to overloading and unwanted effects caused by the electroosmotic flow in the CE capillary. An increase in V_2 with a constant V_1 reduces the total current in the ITP system and slows the ITP process at the time of injection. At the same time, however, the voltage drop over the CE capillary will cause an increased migration rate in the direction of the CE cathode and will result in peak broadening during injection. This phenomenon and the effect of electrical splitting using a constant current in ITP are still under investigation.

To study the potential of isotachophoretic analyte focusing in CE–MS, several ITP–CE–MS experiments were performed. The standard mixture of anthracyclines was diluted to 5, 20, 50 and 200 times lower concentrations than in the CE–MS experiments. A 5-μl volume of a mixture of DAU, EPI and DOX at concentrations of 3, 8 and 8 μg/ml, respectively, was injected into the ITP system. CAR was added as a marker at a concentration of 10 μg/ml. The mass electropherogram after ITP–CE separation (Fig. 5) shows considerable peak broadening due to overload of the CE capillary after the ITP step.

Lowering the concentration by a factor of 10 improved the peak shape considerably (Fig. 6). In this instance the concentration of the marker CAR was 30 μg/ml.

The improvement in detectability is clearly illustrated in Fig. 7, which shows the CE–MS results for 66 μg/ml DAU (a) in comparison with ITP–CE–MS results for 0.3 μg/ml DAU (b). The improvement in detectability is at least a factor of 200.

CONCLUSIONS

This work has demonstrated the possibility of analyte focusing using on-line ITP–CE–MS. An improvement in detectability of at least a factor 200 has been demonstrated for the analysis of DAU. Although in the ITP–CE–MS mode the concentra-

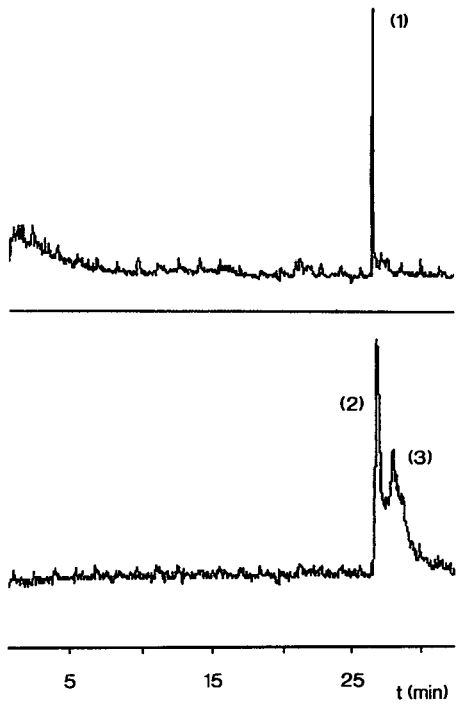

Fig. 6. Mass spectrometric electropherogram obtained in ITP–CE–MS of DAU (1), EPI (2) and DOX (3) (0.3, 0.8 and 0.8 μg/ml, respectively).

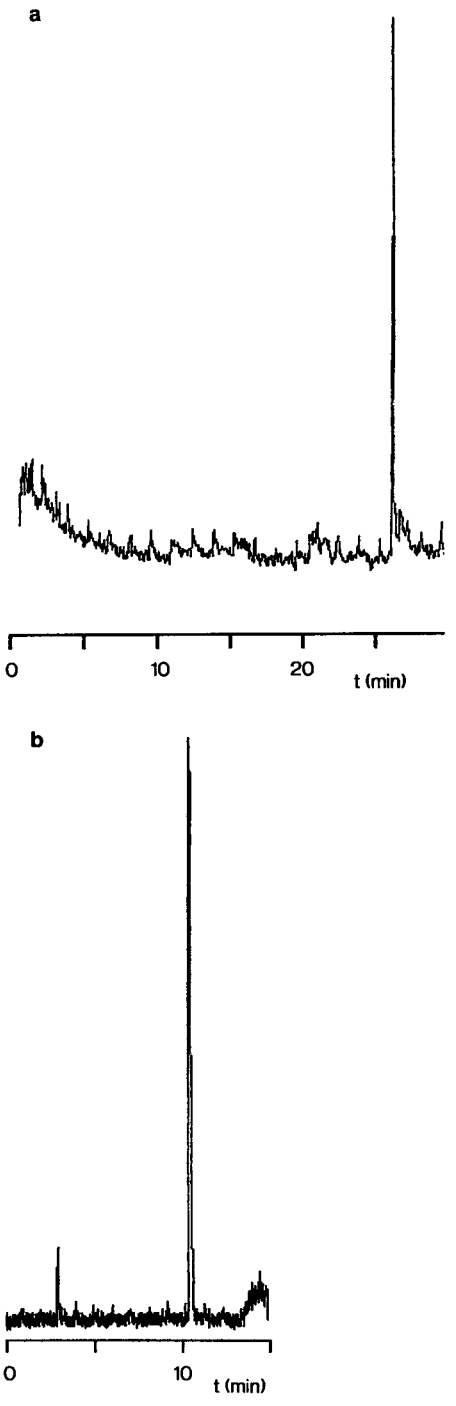

Fig. 7. Mass spectrometric detection of (a) 0.3 μg/ml of DAU by ITP–CE–MS and (b) 66 μg/ml of DAU by CE–MS.

tion of the anthracyclines was lowered by a factor of 5–200, some overloading of the CE system could still be seen.

REFERENCES

1 R. D. Smith, J. A. Loo, C. J. Barinaga, C. G. Edmonds and H. R. Udseth, *J. Chromatogr.*, 480 (1989) 211.
2 R. M. Caprioli, W. T. Moore, M. Martin, B. DaGue, K. Wilson and S. Moring, *J. Chromatogr.*, 480 (1989) 247.
3 N. J. Reinhoud, E. Schröder, U. R. Tjaden, W. M. A. Niessen, M. C. ten Noever de Brauw and J. van der Greef, *J. Chromatogr.*, 516 (1990) 147.
4 M. A. Moseley, L. J. Deterding, K. B. Tomer and J. W. Jorgenson, *Anal. Chem.*, 63 (1991) 109.
5 I. M. Johansson, R. Pavelka and J. D. Henion, *J. Chromatogr.*, 559 (1991) 515.
6 P. Ferranti, A. Malorni, P. Pucci, S. Fanali, A. Nardi and L. Ossicini, *Anal. Biochem.*, 194 (1991) 1.
7 M. J. F. Suter, B. B. Dague, W. T. Moore, S. N. Lin and R. M. Caprioli, *J. Chromatogr.*, 553 (1991) 101.
8 I. M. Johansson, E. C. Huang, J. D. Henion and J. Zweigenbaum, *J. Chromatogr.*, 554 (1991) 311.
9 L. J. Deterding, C. E. Parker, J. R. Perkins, M. A. Moseley, J. W. Jorgenson and K. B. Tomer, *J. Chromatogr.*, 554 (1991) 329.
10 M. A. Moseley, L. J. Deterding, K. B. Tomer and J. W. Jorgenson, *Rapid Commun. Mass Spectrom.*, 3 (1989) 87.
11 N. J. Reinhoud, W. M. A. Niessen, U. R. Tjaden, L. G. Gramberg, E. R. Verheij and J. van der Greef, *Rapid Commun. Mass Spectrom.*, 3 (1989) 348.
12 R. D. Minard, D. Chin-Fatt, P. Curry and A. Ewing, in *Proceedings of the 36th Conference on Mass Spectrometry and Related Topics, June 5–10, 1988, San Francisco, CA*, American Society for Mass Spectrometry, East Lansing, MI, 1988, p. 950.
13 R. D. Smith, C. J. Barinaga and H. R. Udseth, *Anal. Chem.*, 60 (1988) 1948.
14 R. D. Smith, J. A. Loo, C. G. Edmonds, C. J. Barinaga and H. R. Udseth, *J. Chromatogr.*, 516 (1990) 157.
15 E. D. Lee, W. Muck, J. D. Henion and T. R. Covey, *Biomed. Environ. Mass Spectrom.*, 18 (1989) 844.
16 P. Thibault, C. Paris and S. Pleasance, *Rapid Commun. Mass Spectrom.*, 5 (1991) 484.
17 S. Pleasance, S. W. Ayer, M. V. Laycock and P. Thibault, *Rapid Commun. Mass Spectrom.*, 6 (1992) 14.
18 D. S. Stegehuis, H. Irth, U. R. Tjaden and J. van der Greef, *J. Chromatogr.*, 538 (1991) 393.
19 D. S. Stegehuis, U. R. Tjaden and J. van der Greef, *J. Chromatogr.*, 591 (1992) 341.
20 D. Kaniansky and J. Marak, *J. Chromatogr.*, 498 (1990) 191.
21 F. Foret, V. Sustacek and P. Bocek, *J. Microcol. Sep.*, 2 (1990) 229.
22 U. R. Tjaden and E. A. de Bruijn, *J. Chromatogr.*, 531 (1990) 235.
23 N. J. Reinhoud, U. R. Tjaden, H. Irth and J. van der Greef, *J. Chromatogr.*, 574 (1992) 327.
24 H. Akedo and K. Shinkai, *J. Chromatogr.*, 227 (1982) 262.
25 M. Deml, F. Foret and P. Bocek, *J. Chromatogr.*, 320 (1985) 159.

Journal of Chromatography, 627 (1992) 273–279
Elsevier Science Publishers B.V., Amsterdam

CHROM. 24 600

Determination of propionate in bread using capillary zone electrophoresis

M. T. Ackermans, J. C. J. M. Ackermans-Loonen and J. L. Beckers

Laboratory of Instrumental Analysis, Eindhoven University of Technology, P.O. Box 513, 5600 MB Eindhoven (Netherlands)

(Received July 20th, 1992)

ABSTRACT

A method for the determination of propionate in bread is described. The propionate was extracted from the bread with a repeated extraction procedure and measured using capillary zone electrophoresis in the indirect UV mode applying a background electrolyte of 0.005 *M* Tris adjusted at pH 4.6 by adding benzoic acid. Using laboratory-baked bread containing known amounts of sodium propionate, recoveries of *ca.* 95% could be established, validating the method.

INTRODUCTION

In the preparation of bread, propionate is often applied because of its anti-bacterial properties. According to the Dutch Food and Drugs Act, maximum values are prescribed with respect to the presence of propionate in bread, hence there is a need for its determination. Gas chromatography (GC), high-performance liquid chromatography (HPLC) and ion chromatography (IC) can be applied for this purpose. A disadvantage of GC is that derivatization is necessary and in HPLC and IC matrix effects can be troublesome. As capillary zone electrophoresis (CZE) is suitable for the determination of ionic species in a complex matrix [1–3], we studied the ability of CZE for the determination of propionate in bread. Special attention was paid to the identification of propionate and a simple extraction procedure for isolating propionate from a bread matrix. As the preparation of calibration graphs is time consuming, we further studied the possibility of repeated injections of several standard sample solutions within one electrophoretic run. The determination of propionate in bread and the recoveries with the extraction procedures were evaluated using laboratory-baked bread containing different known amounts of propionate.

Correspondence to: J. L. Beckers, Laboratory of Instrumental Analysis, Eindhoven University of Technology, P. O. Box 513, 5600 MB Eindhoven, Netherlands.

EXPERIMENTAL

Instrumentation

For all experiments a P/ACE System 2000 HPCE instrument (Beckman, Palo Alto, CA, USA) was used. All experiments were carried out with Beckman eCAP capillary tubing (75 μm I.D.) with total length 46.7 cm and a distance between injection and detection of 40.0 cm. The wavelength of the UV detector was set at 214 nm. All experiments were carried out applying a constant voltage of 10 kV, unless stated otherwise, with anode at the inlet and cathode at the outlet side (cationic mode). Sample introduction was achieved by pressure injection with injection volumes of about 6.0 nl/s. Data analysis was performed using the laboratory-written data analysis program CAESAR.

Chemicals

All chemicals were of analytical-reagent grade. Sodium propionate was obtained from Sigma (St. Louis, MO, USA). Before making the stock solu-

0021-9673/92/$05.00

tions the sodium propionate was dried at 100°C for 30 min. Yeast, wheat flour and the all-purpose flour were obtained at a local bakery and brown sugar, margarine and salt were obtained at a local supermarket.

Bread preparation

For the preparation of a bread, 75 g of wheat flour, 50 g of all-purpose flour, 6.5 g of yeast, 2.5 g of salt, 5 g of brown sugar, 5 g of margarine and 70 g of water were mixed manually in a large bowl, until the dough was stiff enough to leave the side of the bowl. The dough was placed in a warm location for 1 h to rise, then kneaded thoroughly and was left for 30 min in the warm location to rise. The dough was then kneaded once again, shaped into the final form of the bread and allowed to rise once again for 45 min. Finally, the bread was baked in an oven at 120°C for 45 min or 225°C for 25 min. If the bread was spiked with sodium propionate, the sodium propionate was dissolved in the water, before preparing the dough.

RESULTS AND DISCUSSION

Identification of propionate

Important questions with regard to the determination of propionate in bread are whether propionate can be separated from the bread matrix and how it can be recognized. Migration times often cannot be used to identify components owing to varying velocities of the electroosmotic flow (EOF). Effective mobilities, however, can be used for peak recognition because after the calculation of the effective mobilities the effect of the EOF is eliminated. Further, effective mobilities give information on how to separate the components from the matrix if needed [4]. If no specific interactions occur, such as complex formation, the effective mobility in a specific background electrolyte can be calculated from the ionic mobility at infinite dilution and the pK value of the component. For propionate we calculated and measured the effective mobilities for several background electrolytes at different pH values. In Table I the compositions of all background electrolytes are given. For the determination of the non-UV-absorbing propionate the indirect UV mode must be applied. For this reason, all background electrolytes contain the UV-absorbing negative ionic species benzoic acid. In Fig. 1 the calculated relationship (solid line) between effective mobility and pH and several measured values of the effective mobilities are given. The ionic strength was not identical for all background electrolytes. The measured values cover the calculated values, showing the usefulness of this principle. As can be seen in Fig. 1, relatively small variations in pH, especially near the pK value of the component (the pK value of propionate is 4.87), result in large changes in effective mobilities. This explains the differences in

TABLE I

COMPOSITIONS OF BACKGROUND ELECTROLYTES AT DIFFERENT pH VALUES

All buffers were prepared by adding benzoic acid to the cations until the desired pH was reached.

Cation	pH	Cation	pH
0.005 *M* Tris	4.18	0.01 *M* Histidine	6.24
0.005 *M* Tris	4.58	0.01 *M* Histidine	6.67
0.005 *M* Tris	4.99	0.01 *M* Tris	7.05
0.005 *M* Tris	5.39	0.01 *M* Tris	7.90
0.01 *M* Histidine	5.84	0.01 *M* Tris	8.01

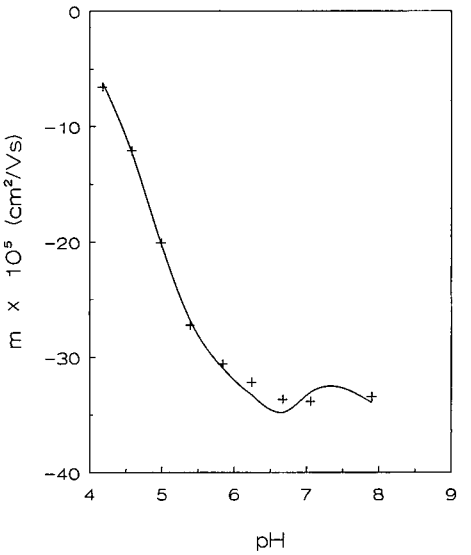

Fig. 1. Calculated relationship (solid line) between the effective mobility of propionate and pH and (+) measured values determined for several different background electrolytes.

effective mobilities obtained with different batches of background electrolytes. The effective mobility of propionate measured in the matrix was always checked by measuring the effective mobility of propionate in the standard solution for each background electrolyte.

Calibration graphs in CZE

Although for the determination of propionate in the indirect UV mode an internal standard can be applied, so that calibration graphs are superfluous [5], we studied the construction of calibration graphs. In principle a calibration graph can be set up in two ways, either by injecting equal injection volumes (or a constant pressure-injection time) of different sample concentrations or by injecting a specific sample concentration with several different injection volumes. For the construction of such a calibration graph, about six analyses have to be carried out, which is time consuming. Because CZE is an elution technique, it is possible to repeat injections during one electrophoretic run. In this way it is possible to construct a calibration graph by injecting different standard solutions (or pressure-injection times) of propionate within one electrophoretic run. Of course, this principle is only valid at a constant velocity of the EOF during the whole electrophoretic run.

To check this principle, the calibration graphs obtained in the different ways were compared. In Fig. 2 the calibration graphs of propionate are shown for (+) several different sample concentrations (in the range $5 \cdot 10^{-5}$– $5 \cdot 10^{-4}$ *M*) with a 3-s pressure-injection time, (△) injection of $5 \cdot 10^{-5}$ *M* propionate with different pressure-injection times in the range 3–30 s and (○) repeated injections (time between two injections 1 min) within one electrophoretic run of different sample concentrations with a 3-s pressure-injection time, for a background electrolyte of 0.02 *M* Tris adjusted to pH 8.0 and 0.005 *M* Tris adjusted to pH 4.6 by adding benzoic acid. The amount injected is given in m*M*s, *i.e.*, the product of concentration (m*M*) and injection time (s).

It can be seen that in both background electrolytes nearly identical calibration graphs are obtained for the three methods. In Table II the regression coefficient, slope, intercept and limit of detection [6] are given for all calibration graphs. In Fig. 3

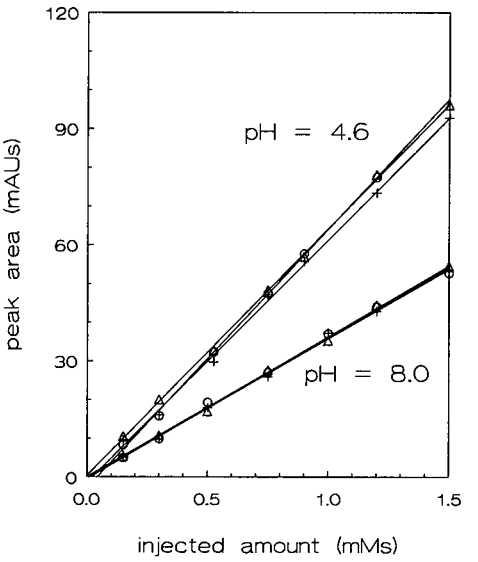

Fig. 2. Calibration graphs of propionate for (+) different sample concentrations with equal (3 s) pressure-injection time, (△) injection of $5 \cdot 10^{-5}$ *M* propionate with different pressure-injection times and (○) repeated injections (time between two injections 1 min) within one electrophoretic run of different sample concentrations with a 3-s pressure-injection time, for a background electrolyte of 0.02 *M* Tris adjusted to pH 8.0 and 0.005 *M* Tris adjusted to pH 4.6 by adding benzoic acid. The amount injected is indicated in m*M*s (molarity multiplied by pressure-injection time).

an electropherogram with a seven-times repeated injection applying a background electrolyte at pH 8.0 is given. The seven EOF dips and seven propionate dips with linearly increasing peak area can be clearly seen. It is notable that the non-UV-absorbing sodium ions in the sodium propionate solutions show a positive UV peak. According to the Kohlrausch regulation function, the total ionic concentration in a sample zone of an ion with a higher effective mobility than that of the co-ion of the background electrolyte is higher than that of the background electrolyte. According to the electroneutrality condition, the concentration of the UV-absorbing buffering counter ions is also higher, which explains the UV peaks for non-UV-absorbing sample ions. Although this background electrolyte is far from ideal for the determination of sodium ions, a regression coefficient of 0.9985 for the calibration graphs using the peak area is fairly good.

TABLE II

REGRESSION COEFFICIENT, r, SLOPE, INTERCEPT AND LIMIT OF DETECTION (LOD) FOR CALIBRATION GRAPHS OF PROPIONATE SHOWN IN FIG. 2

Background pH	Method[a]	r	Slope (AU/M)	Intercept (mAUs)	LOD (mMs)
8.0	1	0.9989	35.96	−0.284	0.0813
8.0	2	0.9992	36.71	−0.518	0.0792
8.0	3	0.9984	35.97	0.067	0.0899
4.6	1	0.9992	62.76	−1.463	0.0882
4.6	2	0.9998	63.57	0.810	0.0316
4.6	3	0.9995	66.95	−2.867	0.0848

[a] Method by which the calibration graph was obtained: 1 = using different concentrations; 2 = using one concentration and different injection times; 3 = using repeated injection method.

Matrix effects in CZE

As shown before, propionate can be recognized through its effective mobility and quantified in the indirect UV mode. In order to choose a suitable background electrolyte for the determination of propionate in bread, matrix effects have to be known. For this reason, laboratory-baked bread was prepared with and without the addition of sodium propionate before the baking process. For the extraction of the propionate from the bread matrix, in the first instance a slice of bread was taken, a specific volume of water was added, the mixture was sonicated for 10 min and analysed, after filtration, with several background electrolytes at different pH values. In fact, all background electrolytes (see Table I) can be applied for the determination of propionate in bread, although at some pH values matrix components interfere with the propionate peak. In Fig. 4, typical electropherograms of (a) a standard solution of propionate and of bread (b) without and (c) with propionate added are shown measured with background electrolytes at pH 4.6 and 8.0. It can be clearly seen that at pH 8.0 a component X of the bread matrix coincides with propionate, which is not visible (at the position of propionate) in the electropherogram measured at pH 4.6. Also, some cations (although UV peaks are visible, it may be non-UV-absorbing cations) and several anions in the indirect UV mode are present. Although owing to variation in the velocity of the EOF the migration times sometimes differ, the effective mobilities are almost constant (see also Tables III–V).

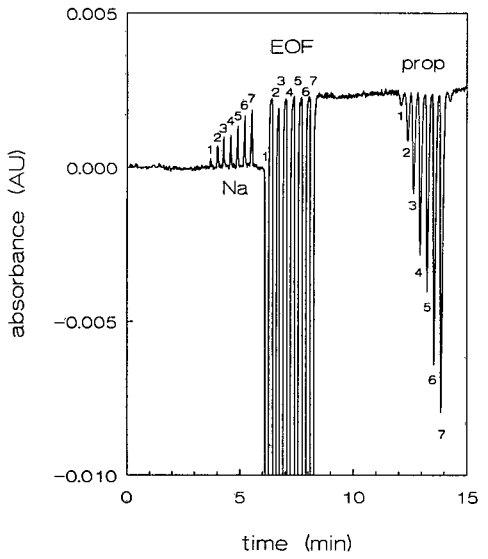

Fig. 3. Electropherogram showing the principle of repeated injections. A sample injection was made seven times (time between injections 0.3 min) with different sample concentrations with a pressure-injection time of 3 s. The seven sodium peaks (for explanation, see text), seven EOF dips and seven propionate peaks can clearly be distinguished.

Preliminary experiments showed also that the determination of propionate in a bread matrix resulted in varying velocities of the EOF, possibly owing to protein adsorption on the capillary wall. In all further quantitative experiments we therefore applied calibration graphs measured with identical pressure-injection times of 3 s and different concentrations, whereby temporal peak areas were recalculated to spatial peak areas [7]. Before all experiments rinsing steps for 2 min with 1 M KOH, for 2

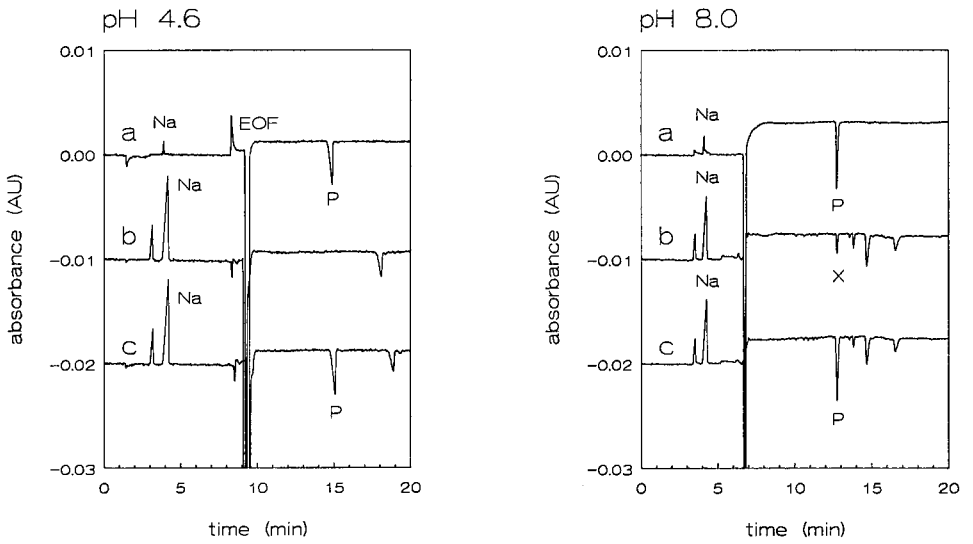

Fig. 4. Typical electropherograms of (a) a standard solution of propionate and of bread (b) without and (c) with propionate added, measured with background electrolytes at pH 4.6 and 8.0. P = propionate; Na = sodium; X = unknown component.

min with water and for 3 min with background electrolyte were carried out.

Extraction procedure and recovery

To extract the propionate from the bread, a slice of bread (containing a proportional part of crust and inside) was weighed accurately and a volume of water that was ten times the mass of the bread was added. After sonication and filtration, the sample solution was diluted in order to obtain a concentration near the centroid of the calibration graphs. The determined values for propionate were recalculated to milligrams of propionate per gram of bread (the mass of a bread was measured after the baking process). In order to study the effect of extraction time, recoveries were measured after several sonication times. In Table III the measured values applying a background electrolyte at pH 4.6 are given, showing an average recovery of about 80% with a sonication time of more than 20 min.

TABLE III

DETERMINED AMOUNT, RECOVERY OF THE EXTRACTION OF SODIUM PROPIONATE IN BREAD (ADDED AMOUNT 2.211 mg/g BREAD) AND CALCULATED EFFECTIVE MOBILITY AS A FUNCTION OF TIME OF SONICATION

Applied background electrolyte, 0.005 *M* Tris–benzoate (pH 4.6).

Time (min)	Determined (mg/g bread)	Recovery (%)	m_{eff} (10^{-5} cm^2/V · s)
10	1.634	73.9	−12.41
20	1.763	79.7	−12.38
30	1.779	80.5	−12.37
40	1.805	81.6	−11.99
50	1.809	81.8	−12.33

To study whether the recovery of *ca.* 80% is connected with a distribution equilibrium of propionate over bread and water phase or whether part of the propionate disappeared during the baking process, recoveries were measured for bread baked at 120°C and 225°C applying both a single extraction step and a five-times repeated extraction step. In the single extraction step 100 g of water were added to 10 g of bread, followed by sonication for 30 min and filtration. In the repeated extraction step, 100 g of water were added to 10 g of bread, followed by sonication for 10 min. After filtration of the bread this step was repeated four times and all fractions of filtered water were collected and analysed.

All the results are given in Table IV. From the

TABLE IV

ADDED AMOUNT OF SODIUM PROPIONATE, DETERMINED AMOUNT OF SODIUM PROPIONATE, RECOVERY FOR THE FIVE BREADS, BAKED AT 225 AND 120°C, AND EFFECTIVE MOBILITY

Applied background electrolyte, 0.005 *M* Tris–benzoate (pH 4.6).

Baking temperature (°C)	Bread No.	Added (mg/g bread)	Single extraction			Repeated extraction		
			Determined (mg/g bread)	Recovery (%)	m_{eff} (10^{-5} cm^2/V · s)	Determined (mg/g bread)	Recovery (%)	m_{eff} (10^{-5} cm^2/V · s)
225	1	0	0	–	–	0	–	–
	2	0.744	0.604	81.3	−12.42	0.702	94.4	−12.26
	3	1.452	1.180	81.2	−12.42	1.427	98.3	−12.69
	4	2.211	1.772	80.2	−12.27	2.017	95.6	−12.21
	5	6.947	5.847	84.2	−12.27	6.589	94.8	−12.21
120	1	0	0	–	–	0	–	–
	2	0.721	0.619	85.8	−12.45	0.709	98.3	−12.16
	3	1.413	1.249	88.4	−12.51	1.413	94.3	−12.23
	4	2.122	1.847	87.0	−12.40	2.122	98.5	−12.12
	5	6.837	6.723	83.6	−12.45	6.190	90.5	−12.79

recoveries of *ca.* 95% for the repeated extraction for the breads baked at both 120 and 225°C it can be concluded that during the baking process no loss of propionate occurs and recoveries of *ca.* 80% for a single extraction or *ca.* 95% for repeated extraction could be established.

Determination of propionate in commercially available bread

To test the applicability of the method we determined propionate in five breads from a local bakery and four kinds of pumpernickel, applying the five-times repeated extraction procedure using the background electrolyte at pH 4.6 in order to avoid interfering components possibly present in the bread matrix. The results are given in Table V. As can be seen, propionate was found only in the pumpernickel and not in the breads from the local bakery.

CONCLUSIONS

CZE is a suitable separation technique for the determination of propionate in bread. With a repeated extraction procedure propionate can be ex-

TABLE V

DETERMINED AMOUNT OF SODIUM PROPIONATE AND EFFECTIVE MOBILITY FOR COMMERCIAL BREADS

Applied background electrolyte, 0.005 *M* Tris–benzoate (pH 4.6).

Bread	Determined amount (mg/g bread)	m_{eff} (10^{-5} cm^2/V · s)
White bread 1	–	–
White bread 2	–	–
Whole-meal bread	–	–
White bread roll	–	–
Whole-meal bread roll	–	–
Pumpernickel 1	1.71	−12.03
Pumpernickel 2	0.72	−12.14
Pumpernickel 3	1.69	−12.05
Rheinisches Schwarzbrot	0.64	−12.06

tracted from the bread matrix with an average recovery of *ca.* 95%. For peak recognition the effective mobility can be used. The procedure has been tested with laboratory-baked bread containing known amounts of propionate.

One of the problems encountered in the propionate determination is the possible presence of interfering components in the bread matrix. At pH 4.6 no matrix components interfering with propionate were measured in the laboratory-baked bread. To show the applicability of the method, propionate was determined in five different commercial breads from the local bakery and four different kinds of pumpernickel. Only in the prepacked pumpernickels propionate was found, with amounts below the allowed limit of 0.3%.

REFERENCES

1 J. W. Jorgenson and K. D. Lukacs, *Anal. Chem.*, 53 (1981) 1298.
2 F. E. P. Mikkers, F. M. Everaerts and Th. P. E. M. Verheggen, *J. Chromatogr.*, 169 (1979) 11.
3 J. W. Jorgenson, *Trends Anal. Chem.*, 3 (1984) 51.
4 J. L. Beckers, F. M. Everaerts and M. T. Ackermans, *J. Chromatogr.*, 537 (1991) 407.
5 M. T. Ackermans, F. M. Everaerts and J. L. Beckers, *J. Chromatogr.*, 549 (1991) 345.
6 M. T. Ackermans, J. L. Beckers, F. M. Everaerts and I. G. J. A. Seelen, *J. Chromatogr.*, 590 (1992) 341.
7 X. Huang, W. F. Coleman and R. N. Zare, *J. Chromatogr.*, 452 (1988) 615.

Journal of Chromatography, 627 (1992) 281–286
Elsevier Science Publishers B.V., Amsterdam

CHROM. 24 483

Separation of tetracycline and its degradation products by capillary zone electrophoresis

Chao-Xuan Zhang, Zeng-Pei Sun, Da-Kui Ling and Ya-Jun Zhang

National Institute for the Control of Pharmaceutical and Biological Products, Temple of Heaven, Beijing 100050 (China)

(First received November 21st, 1991; revised manuscript received June 16th, 1992)

ABSTRACT

The capillary zone electrophoresis of tetracycline and its degradation products is described. Various substances, including surfactants and metal ions, were employed as additives in the running electrolyte to improve the resolution. Using disodium ethylenediaminetetraacetate as an additive in phosphate buffer solution, tetracycline and its degradation products were completely separated from each other. The baseline separation obtained completely meets the needs for determining the contents of tetracycline, 4-epitetracycline, anhydrotetracycline (ATC) and 4-epianhydrotetracycline (EATC) in tetracycline samples. Further, two unknown substances co-existing with ATC and EATC were separated that had not been mentioned or separated before. Further investigations using other techniques are needed to determine the structures of these two unknown substances. The pH dependence of the migration behaviour of tetracycline and its degradation products was also explored. The migration behaviour of zwitterionic substances is so dependent on the pH of the buffer than the elution order may be changed with change in pH. The pH dependence of electroosmotic flow over the pH range 4–11 was also determined.

INTRODUCTION

Capillary zone electrophoresis (CZE) has been used in a variety of modes to separate diverse molecules as a complementary technique to HPLC. Small metal ions [1] and large nucleic acids [2], in addition to electrically neutral species such as chlorinated benzenes [3], have been successfully separated by CZE.

The migration of a solute in CZE is influenced by both the electroosmotic and electrophoretic mobilities. The electroosmotic flow allows solutes of opposite charges to migrate toward the detector end. The electrophoretic mobility may vary from one solute to another, which leads to different net velocities for the various analytes and brings about their separation. To induce different electrophoretic velocities for the solutes to be separated, reagents that may associate with the analytes either strongly or weakly are added to the buffer. These interactions between additives and solutes cause the solutes to migrate at different velocities owing to the difference in the magnitude of solute–additive association. The reagents that have been employed as buffer additives in CZE include surfactants [4–7], organic solvents [8–10], inorganic salts [11,12] and tetraalkylammonium salts [13]. In this work disodium ethylenediaminetetraacetate (EDTA) was used as the additive, by means of which tetracycline and its degradation products were successfully separated.

Tetracycline (TC) is one of the most important broad-spectrum antibiotics, and in acidic media (pH < 2) may be degraded to form anhydrotetracycline (ATC). In acidic solutions (pH 2–6), TC and ATC also epimerize to form 4-epitetracycline (ETC) and 4-epianhydrotetracycline (EATC), respectively [14]. The structures of these substances are shown in Table I.

Commercial tetracycline samples usually contain

Correspondence to: C.-X. Zhang, National Institute for the Control of Pharmaceutical and Biological Products, Temple of Heaven, Beijing 100050, China.

0021-9673/92/$05.00

TABLE I

STRUCTURES OF THE FOUR TETRACYCLINES

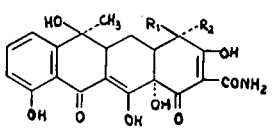

I

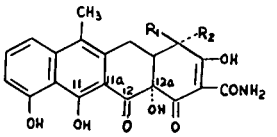

II

Compound	Abbreviation	No. on Figs.	Structure	R_1	R_2
Tetracycline	TC	1	I	$N(CH_3)_2$	H
4-Epitetracycline	ETC	2	I	H	$N(CH_3)_2$
Anhydrotetracycline	ATC	3	II	$N(CH_3)_2$	H
4-Epianhydrotetracycline	EATC	4	II	H	$N(CH_3)_2$

ETC, ATC and EATC, and differ widely in biological potency. Many papers concerning the determination and separation of tetracyclines by HPLC have been published, but the use of CZE has not previously been reported. This paper describes the separation of tetracycline and its degradation products, ETC, ATC and EATC, by CZE. The dependence of the migration behaviour of tetracyclines on the pH of the buffer medium was examined. The effect of disodium EDTA on the separation of tetracyclines was also studied. As will be shown, the selectivity of tetracyclines could be improved by the addition of EDTA. The mechanism by which EDTA improved the separation of tetracyclines is discussed.

EXPERIMENTAL

Apparatus

CZE was performed on an HPE 100 high-performance capillary electrophoresis system from Bio-Rad Labs. (Richmond, CA, USA), in the positive polarity mode, using an uncoated fused-silica capillary cartridge of 20 cm × 25 μm I.D. The applied voltage was 10 kV. Sample solutions were injected into the capillary by electromigration for 5 s at 1 kV. All analyses were carried out at ambient temperature (295–300 K). Detection was performed by monitoring the absorbance at 265 nm. The signal from the detector was processed with a C-R3A Chromatopac (Shimadzu, Kyoto, Japan).

Chemicals and reagents

Phosphoric acid, sodium dihydrogenphosphate, disodium hydrogenphosphate and disodium EDTA were of analytical-reagent grade from Beijing Chemical Reagent Co. (Beijing, China). TC was a National Reference Standard (China) for potency assay and ETC, ATC and EATC were reference substances for purity testing by TLC inspection according to the Chinese Pharmacopoeia.

Procedures

Phosphate buffers in the pH range 2–9 were prepared by mixing solutions of phosphoric acid, sodium dihydrogenphosphate and disodium hydrogenphosphate, all of concentration 0.02 *M*, in appropriate proportions. TC, ETC, ATC and EATC were freshly dissolved in 0.02 *M* phosphate buffer (pH 2.2) to give a series of test solutions of concentration 0.05–0.2 mg/ml. Solutions of neutral solutes (20 mg/ml methanol, 0.001 mg/ml phenol and 0.01 mg/ml benzene) for monitoring electroosmotic flow were prepared in the same way as for tetracyclines. Each value of the migration time in the figures was the average of three repeated runs, the R.S.D. being from 0.3% to 3%.

RESULTS AND DISCUSSION

pH dependence of the separation of tetracyclines

Electroosmotic flow in fused-silica capillaries is influenced by the pH of the medium because the

dissociation of the silanol groups on the fused-silica capillary surface is pH dependent. The electrophoretic flow of a solute is related to its charge, size, etc. Tetracyclines are amphoteric in aqueous solution, the charge and sign being dependent on the pH of the solution. Therefore, the pH of the running electrolyte is important for the separation of tetracyclines. Electroosmotic flow transports all the solutes at the velocity of the medium solution, which shortens the migration time. To determine the electroosmotic velocity, a neutral substance such as methanol [15] or phenol [16] was added to the sample solutions. In our experiments a mixed sample solution of methanol, phenol and benzene was injected into the capillary and detection was performed at 190 nm. These three different components wih different structures and hydrophilic characters always coeluted in the pH range 2–9, which shows that neither of the neutral components undergoes interaction with the capillary wall and their migrations were cuased solely by the electroosmosis, thus providing a means for the determination of the electroosmotic flow.

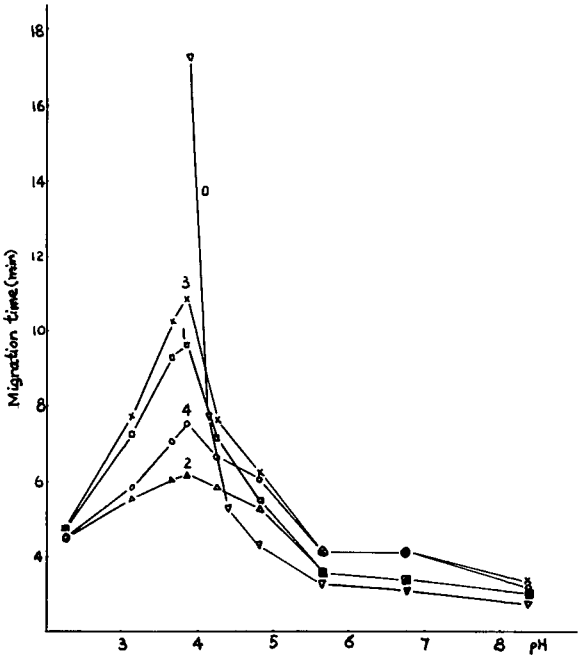

Fig. 1. Dependence of migration time of tetracyclines and neutral solutes on the pH of the buffer in CZE. The numbers on the plots corespond to the solutes in Table I; in addition, 0 is used to designate the mixture of neutral solutes. Conditions: capillary, 20 cm × 50 μm I.D., uncoated; buffers, 0.02 *M* phosphate solutions of various pH; applied voltage, 10 kV; current, 17–20 μA; electroinjection, 1 kV for 5 s; temperature, ambient (295–300 K); detection wavelength, 265 nm for tetracyclines and 190 nm for the neutral solutes.

The pH dependence of the migration time of tetracyclines and the neutral solutes is shown in Fig. 1. The electroosmotic flow velocity indicated by the neutral solutes increases with increase of pH, which can be ascribed to the increasing dissociation of silanol groups on the capillary wall. The migration times of the neutral solutes changed sharply near pH 4.

Tetracyclines have three functional groups relevant to acid–base equilibrium in aqueous solution, namely a dimethylamino group (D, pK_a = 9.5), a phenolic diketone group (P, pK_a = 7.7) and a tricarbonylmethane group (T, pK_a = 3.3) [17]. When the pH of the buffer was below the isoelectric point, tetracyclines were positively charged and migrated towards the negative electrode in the same direction with electroosmotic flow due to the protonated D group, and consequently eluted before the neutral solutes, as shown in Fig. 1. In contrast, at pH above the isoelectric point, owing to the dissociation of the T and P groups, the negatively charged tetracyclines eluted after the neutral solutes. According to our experimental CZE results, the isoelectric points of tetracyclines are in range pH 4.0–4.5, which are below the calculated value of pH 5.5.

The dependence of the migration time of a solute is the sum of the dependences of its electrophoretic movement and electroosmotic movement. At pH < 4, the migration time of tetracyclines increased with increase in pH, which shows that a decrease in the electrophoretic movement of tetracyclines had occurred as positive ions had overcome the increase in electroosmotic flow. However, at pH > 4.5, the increase in the electroosmotic flow became dominant and consequently the migration times decreased with increase in pH.

It can be seen from Fig. 1 that the pH of the running buffer could dramatically affect the separation of tetracyclines and the optimum pH value was in range 3.5–4.5, near their isoelectric points. A typical electropherogram of tetracyclines at pH 3.9 is shown in Fig. 2.

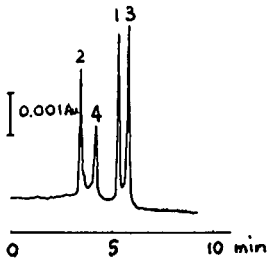

Fig. 2. Electropherogram of tetracycline and its degradation products at the best pH value 3.9. Other conditions as in Fig. 1 and solute numbers as in Table I.

Effect of EDTA on the separation of tetracyclines

To improve the resolution of tetracyclines, metal ion additives that may chelate with them were tested. When $CuSO_4$, $ZnSO_4$ and $MgSO_4$ were added to the buffer, no improvement in resolution was achieved. When EDTA was added to the phosphate buffer, a dramatic improvement in the resolution was observed. Complete separation of TC, ETC, ATC and EATC was achieved with relatively sharp peaks by addition of 0.005 *M* EDTA to 0.02 *M* phosphate buffer (pH 3.9), as shown in Fig. 3. Their resolution is sufficient to be able to determine unequivocally the contents of TC, ETC, ATC and EATC in samples. In comparison with the HPLC trace obtained by US Pharmacopeia method [18], the results shown in Fig. 3 have the advantages of better resolution and shorter analysis time, in addition to the simplicity of CZE.

EDTA is a well known complexing reagent,

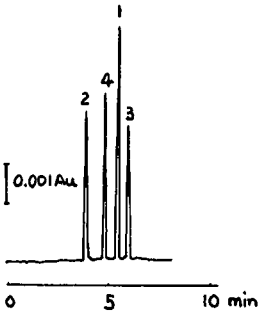

Fig. 3. Separation of tetracycline and its degradation products by CZE with 0.005 *M* EDTA as additive in 0.02 *M* phosphate buffer (pH 3.9). Other conditions as in Fig. 1 and solute numbers as in Table I.

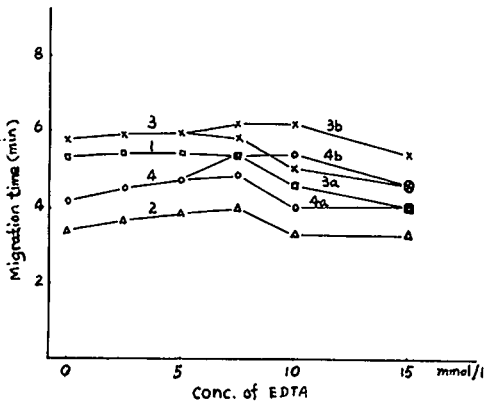

Fig. 4. Effect of EDTA concentration on the separation of tetracycline and its degradation products by CZE. Other conditions as in Fig. 3. Solute numbers as in Table I; in addition, 3a, 3b, 4a and 4b correspond to ATC-a, ATC-b, EATC-a and EATC-b, respectively.

which acquires a negative charge in aqueous solution near pH 4 and may interact with the positively charged tetracyclines to form ion pairs. These interactions lead to a decrease in the electrophoretic mobility of tetracyclines as positive ions, and as a result the migration times gradually increase with increasing EDTA concentration below 0.0075 *M*, as shown in Fig. 4. However, at EDTA concentrations > 0.0075 *M*, the variation of the migration time became equivocal owing to the splitting of the ATC and EATC peaks.

TC, ETC, ATC and EATC could be completely separated using EDTA concentrations from 0.002 to 0.005 *M*. However, at higher EDTA concentrations each peak corresponding to ATC and EATC split into two with nearly the same peak areas as shown in Figs. 4 and 5. The ATC samples employed here contained a small amount of its opposite epimer EATC, and the EATC samples contained some ATC. As Fig. 5A shows for ATC samples, the second peak relating to ATC, is larger and the smaller peak (the first peak) relates to EATC, whereas for EATC samples as shown in Fig. 5B, the first peak, relating to EATC, is larger and the smaller peak (the second peak) relates to ATC. However, at 0.0075 *M* EDTA, each of the ATC and EATC peaks divided into two, as shown in Fig. 5C and D. These phenomena cannot yet be interpreted, but they may tentatively explained as follows.

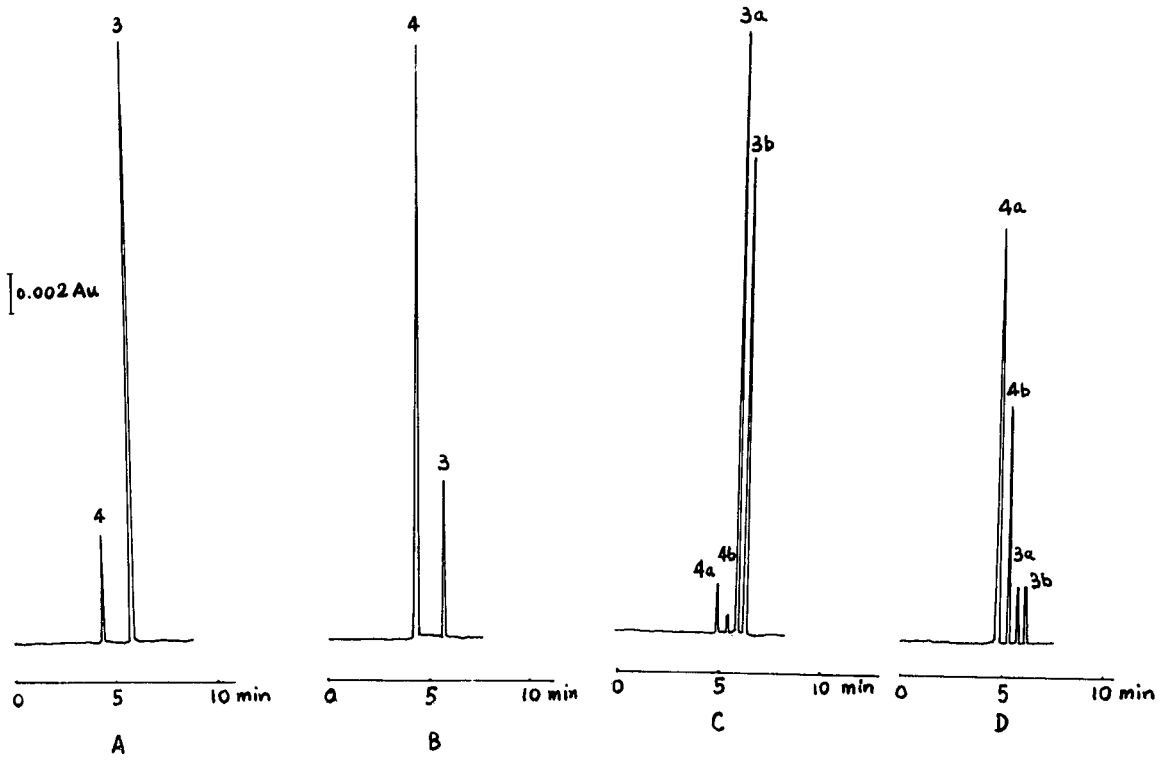

Fig. 5. CZE of ATC and EATC samples with EDTA as additive in 0.02 *M* phosphate solution (pH 3.9). (A) ATC samples, EDTA concentration 0.0025 *M*; (B) EATC samples, EDTA concentration 0.0025 *M*; (C) ATC samples, EDTA concentration 0.0075 *M*; (D) EATC samples, EDTA concentration 0.0075 *M*. Other conditions and solute number are as in Fig. 4.

The splitting of ATC and EATC peaks cannot be generated either with the injection technique or by a mismatch in the pH of the sample and running buffer, because the same phenomenon did not occur for the TC and ETC peaks simultaneously. The experimental results therefore suggest that there are two major components with about the same concentration in each of the ATC or EATC samples. For ATC samples (Fig. 5C), the responses of the last two peaks are greater than those of the first two, whereas for EATC samples (Fig. 5D), the result is exactly the reverse. Hence the last two peaks correspond to the two components relating to ATC samples, which we name ATC-a and ATC-b. The first two peaks correspond to the two components relating to EATC samples, named EATC-a and EATC-b. These four unknown degradation products of TC have not been mentioned or separated by any technique previously. It can be seen from Fig. 4 that ATC-a co-eluted with ATC-b and EATC-a co-eluted with EATC-b when the EDTA concentrations were below 0.005 *M*. At 0.015 *M* EDTA, EATC-a co-eluted with TC and EATC-b

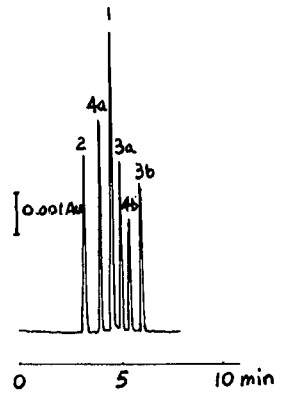

Fig. 6. Separation of tetracycline and its five degradation products by CZE with 0.01 *M* EDTA as additive in 0.02 *M* phosphate buffer (pH 3.9). Other conditions and solute numbers as in Fig. 4.

co-eluted with ATC-a. TC and its five degradation products, ETC, ATC-a, ATC-b, EATC-a and EATC-b, could be successfully separated from one another using 0.01 *M* EDTA, as shown in Fig. 6.

The determination of the structures of the four unknown substances requires further study by other techniques. We consider that ATC-a and ATC-b or EATC-a and EATC-b may be pairs of isomers. The difference in structure between such pairs of isomers perhaps lies in the exchange of positions of hydroxy and carbonyl groups at C-11 and C-12, or the stereo direction of the hydroxy group at C-12a.

CONCLUSIONS

The pH of the buffer is a critical factor for the separation of zwitterionic substances, the charge and sign of which are considerably affected by the pH. The migration behaviour and selectivity of these substances are so dependent on pH that the elution order may be changed. The optimum pH for the separation of TC and its degradation products was in range 3.5–4.5, slightly below the isoelectric point of TC of pH 5.5. However, even at the optimum pH complete separation was not achieved in phosphate buffer without any additive. The addition of EDTA to the buffer yielded a baseline separation of TC and its degradation products. The EDTA buffer system is suitable for the determination of the contents of TC, ETC, ATC and EATC in one analysis. Further, each of the ATC and EATC samples was separated into two large peaks and two small peaks at higher EDTA concentration, which had not been reported previously. The structures of the compounds represented by these four peaks need further study by other techniques.

REFERENCES

1 D. F. Swaile and M. J. Sepaniak, *Anal. Chem.*, 63 (1991) 179.
2 O. Row, W. H. Griest and M. P. Maskarinec, *J. Chromatogr.*, 409 (1987) 193.
3 S. Terabe, Y. Miyashita, O. Shibata, E. R. Barnhart, L. R. Alexander, D. G. Patterson, B. L. Karger, K. Hosoya and N. Tanaka, *J. Chromatogr.*, 516 (1990) 23.
4 S. Terabe, K. Otsuka, K. Ichikawa, A. Tsuchiya and T. Ando, *Anal. Chem.*, 56 (1984) 113.
5 D. E. Burton, M. J. Sepaniak and M. P. Maskarinec, *J. Chromatogr. Sci.*, 25 (1987) 514.
6 H. Nishi, N. Tsumagari, T. Kakimoto and S. Terabe, *J. Chromatogr.*, 465 (1989) 331.
7 S. Terabe, M. Shibata and Y. Miyashita, *J. Chromatogr.*, 480 (1989) 403.
8 Y. Walbroehl and J. W. Jorgenson, *Anal. Chem.*, 58 (1986) 479.
9 A. T. Balchunas and M. J. Sepaniak, *Anal. Chem.*, 59 (1987) 1470.
10 R. Weinberger, E. Sapp and S. Moring, *J. Chromatogr.*, 516 (1990) 271.
11 P. Gozel, E. Gassmann, H. Michelsen and R. N. Zare, *Anal. Chem.*, 59 (1987) 44.
12 A. S. Cohen, S. Terabe, J. A. Smith and B. L. Karger, *Anal. Chem.*, 59 (1987) 1021.
13 H. Nishi and N. Tsumagari, *Anal. Chem.*, 61 (1989) 2434.
14 N. H. Khan, P. Wera, E. Roets and J. Hoogmartens, *J. Liq. Chromatogr.*, 13 (1990) 1351.
15 S. Terabe, K. Otsuka and T. Ando, *Anal. Chem.*, 57 (1985) 834.
16 H. T. Rasmussen and H. M. McNair, *J. Chromatogr.*, 516 (1990) 223.
17 K. Kovas and J. H. Burchhalter, *Essentials of Medicinal Chemistry*, Wiley, New York, 1976, p. 513.
18 *United States Pharmacopeia XXII Revision*, United States Pharmacopeial Convention, Rockville, MD, 1989, p. 1355.

Journal of Chromatography, 627 (1992) 287–293
Elsevier Science Publishers B.V., Amsterdam

CHROM. 24 667

Short Communication

Determination of oxytetracycline in marine shellfish (*Crassostrea gigas, Ruditapes philippinarum* and *Scrobicularia plana*) by high-performance liquid chromatography using solid-phase extraction

Hervé Pouliquen, Djénéba Keita and Louis Pinault

Service de Pharmacie et Toxicologie, École Nationale Vétérinaire de Nantes, C.P. 3013, 44087 Nantes Cedex 03 (France)

(First received July 14th, 1992; revised manuscript received September 29th, 1992)

ABSTRACT

A reversed-phase high-performance liquid chromatographic method was developed to detect oxytetracycline (OTC) in three species of marine shellfish (*Crassostrea gigas, Ruditapes philippinarum* and *Scrobicularia plana*). Shellfish tissues were analysed after solid-phase extraction by using a mobile phase containing acetonitrile and 0.02 *M* orthophosphoric acid solution. The linearity and precision of the method were checked over the concentration range 0.100–1.500 μg/g. The limits of detection and determination of OTC were 0.040 and 0.100 μg/g, respectively. The recovery of OTC from spiked shellfish tissues was 79.8%. The OTC concentration in oyster (*Crassostrea gigas*) spiked at 0.500 μg/g and stored at −20°C was stable for 6 weeks. The method was applied to a 21-day experimental study performed with oysters.

INTRODUCTION

Because of its wide antibacterial spectrum and high potency, oxytetracycline (OTC) is a common antibiotic used against bacterial infections in fish farming. The drug is administered to fish mixed with feed at a dosage rate of 50–100 mg per kg of biomass per day for 8–10 days. The first sign of an infectious and systemic disease in fish is usually a reduced feed intake. Further, OTC is very poorly absorbed through the intestinal tract of fish [1]. Therefore, a large part of the medicated feed presumably reaches the environment of the fish farms.

The environmental effects of OTC used in marine aquaculture are largely unknown. The development of fish farming in salt marshes along the French Atlantic coastline has been shown to be responsible for the pollution of sea water and sediment by OTC [2,3]. There is no published information on residues of OTC in marine shellfish. Hence an adequate method for the determination of OTC in marine shellfish is needed.

The commonly used bacterial bioassay methods for determining OTC are less sensitive and less specific than high-performance liquid chromatographic (HPLC) methods [4,5]. Several methods using HPLC with C_{18} and C_8 columns for the determination of OTC in fish plasma and tissues have been

Correspondence to: H. Pouliquen, Service de Pharmacie et Toxicologie, École Nationale Vétérinaire de Nantes, C.P. 3013, 44087 Nantes Cedex 03, France.

0021-9673/92/$05.00

described [4–15]. No analyses have been undertaken for marine shellfish.

The aim of this study was to develop a simple, rapid and accurate HPLC method for the determination of OTC in three species of marine shellfish (*Crassostrea gigas, Ruditapes philippinarum* and *Scrobicularia plana*) and to apply this method to an experimental study performed with *Crassostrea gigas*.

EXPERIMENTAL

Chemicals and reagents

Citric acid monohydrate, oxalic acid dihydrate, phosphoric acid and disodium ethylenediaminetetraacetate dihydrate ($Na_2EDTA \cdot 2H_2O$) were supplied by Merck (Darmstadt, Germany), perchloric acid and disodium hydrogenphosphate dodecahydrate by Prolabo (Paris, France), HPLC-grade acetonitrile by BDH Chemicals (Toronto, Canada), HPLC-grade methanol by Carlo Erba (Milan, Italy) and oxytetracycline hydrochloride (91% purity) by Pfizer (Amboise, France). All other reagents were of analytical-reagent grade.

McIlvaine buffer (pH 3.0) consisted of 0.1 *M* citric acid–0.2 *M* disodium hydrogenphosphate (79.45:20.55, v/v); 0.1 *M* Na_2EDTA McIlvaine buffer (pH 4.0) [16] was prepared by dissolving 37.224 g of $Na_2EDTA \cdot 2H_2O$ in water, adjusting the pH to 4.0 with McIlvaine buffer (pH 3.0) and diluting to 1 l with water.

HPLC apparatus

The analyses were performed on a Varian (Palo Alto, CA, USA) Model 5000 chromatograph equipped with a Valco injection valve. The analytical column was 5-μm LiChrospher 100 RP-18E (125 × 4.6 mm I.D.) (Merck) equipped with a 5-μm LiChrospher 100 RP-18E guard column (4 × 4.6 mm I.D.). The detector was a Vari-Chrom UV 50 (Varian). Peak heights were calculated on a D-2500 integrator (Merck). The data were handled with a Deskpro 386/s Model 40 3.5 computer (Compaq, Houston, TX, USA) equipped with the HPLC Manager Software System (Merck).

Operating conditions

The mobile phase was acetonitrile–0.02 *M* orthophosphoric acid solution, pH 2.3 (24:76, v/v) [17]. The mixture was filtered with a Millipore (Bedford, MA, USA) HPLC solvent filtration system and Nalgene 47-mm, 0.20-μm nylon filters (Nalge, Rochester, NY, USA) and then sonicated for 15 min. The chromatographic experiments were performed at room temperature (24–25°C). The flow-rate was 1.2 ml/min and the UV detector was set at 355 nm and 0.01 a.u.f.s. The sample volume injected on to the column was 50 μl. The guard column was changed at intervals of 150–200 sample injections. The new columns were conditioned prior to use by flushing with acetonitrile–water [75:25 (v/v) for 2 h, 50:50 (v/v) for 2 h, 40:60 (v/v) for 2 h, 30:70 (v/v) for 2 h] and mobile phase (for 5 h) at a flow-rate of 0.2 ml/min. The columns were reconditioned for 2 h after each day of operation with acetonitrile–water (50:50, v/v) at a flow-rate of 0.2 ml/min.

Preparation of standard solutions

A stock standard solution of OTC in methanol (1 mg/ml) was prepared and was stable for 1 month when stored at −20°C. A stock standard solution (100 μg/ml) in methanol was also prepared immediately before use. Working standard solutions were prepared by diluting aliquots of the latter stock standard solution with 0.1 *M* perchloric acid. All these solutions were protected from light throughout the analyses because of the instability of OTC to light. A 50-μl aliquot of the standard solutions (0.500 and 1.000 μg/ml) was injected on to the HPLC column at the beginning of each day of operation. The calibration graph was based on peak-height measurements.

Sample preparation

The sample preparation was adapted from that used by Oka *et al.* [16] for the determination of tetracycline residues in animal liver. Shellfish tissues (*Crassostrea gigas, Ruditapes philippinarum* or *Scrobicularia plana*) were homogenized using a high-speed blender (Ultra-Turrax; Bioblock, Illkirch, France). A 1-g amount of the homogenate was transferred into a polypropylene tube (8 ml) and extracted three times with 4, 4 and 2 ml of 0.1 *M* Na_2EDTA McIlvaine buffer (pH 4.0). After centrifugation at 3500 *g* for 10 min at 4°C in a Jouan (Saint Herblain, France) Model MR 1822 centrifuge, the combined supernatants were filtered through 90-mm Whatman No. 541 filter-paper

(Whatman, Maidstone, UK) and then concentrated by passing through 3-ml Bond-Elut solid-phase extraction cartridges (Analytichem International, Harbor City, CA, USA). Before use, the cartridges were activated with methanol (4 ml) and water (4 ml). After the samples had been passed, OTC was eluted with 2 ml of 0.01 *M* methanolic oxalic acid solution and collected in a 3-ml flask. The eluate was evaporated to dryness under nitrogen in a water-bath at 30°C and reconstituted to 1.0 ml in 0.1 *M* perchloric acid. The sample was then centrifuged at 13 000 *g* for 10 min at 4°C in a Jouan Model MR 1822 centrifuge. The supernatant was filtered through an Analypore MC 25-mm, 0.45-μm filter (OSI, Paris, France). A 50-μl aliquot was injected on to the HPLC column. All the aforementioned steps were conducted in subdued light.

Method of validation

Overall validation of the method was performed using oyster (*Crassostrea gigas*). A calibration graph was obtained daily by spiking oysters at four concentrations of OTC (0.100, 0.250, 0.500 and 1.500 μg/g) and analysing two replicates on three consecutive days. The precision of the method was tested by spiking oysters at a concentration of 0.500 μg/g with OTC and analysing six replicates on two consecutive days. The extraction recoveries of OTC were determined for three consecutive days by comparing the peak heights from the analyses of oysters spiked at 0.100, 0.250, 0.5000 and 1.500 μg/g with those resulting from direct injection of standard solutions in 0.1 *M* perchloric acid. A study of stability was peformed by storing at −20°C oyster samples spiked at a concentration of 0.500 μg/g with OTC and analysing them during a 6-week period.

A simplified validation of the method was performed using *Ruditapes philippinarum* and *Scrobicularia plana*. The calibration curve, precision and extraction recoveries of OTC were determined as previously, except the analyses only lasted one day.

Experimental conditions and device

An experimental study was performed in order to estimate the contamination of simulated oyster farms polluted by a seawater effluent; this effluent contained OTC and was released by a fish farm model.

A raceway, consisting of a long, rectangular tank (10 × 1 × 1 m) used in intensive fish breeding (seabass and sea-bream), simulated a fish farm located in a salt marsh. The shellfish farms were simulated in four tanks (2 × 2 × 0.6 m), A, B, C and T. All the tanks were run through by the water of the raceway, except tank T, which was the control tank. All the tanks were supplied with an 8-cm sediment layer and 42 oysters (*Crassostrea gigas*). The seawater flows were 6.7 l/min in the raceway and 2.2 l/min in the four tanks. The daily changes of sea water in the raceway and in the tanks were 128% and 182%, respectively. All the tanks were exposed to natural sunlight so that the nights were about 10 h long. The average temperature, pH and salt content of the sea water were 14.5°C, 8.64 and 33.1‰, respectively.

OTC was added in the raceway at a dosage rate of 45 g per day for 7 days. The medicated feed containing OTC was prepared each morning and was distributed in the raceway at 9 a.m. and 5 p.m. The experiment continued for 21 days and was divided into two periods: a 7-day "treatment" period during which OTC was distributed in the raceway and a 14-day "post-treatment" period.

During the 21 days of the experiment, three oysters were removed from each tank on each sampling day and then stored at −20°C until such time as the analysis was carried out. The method described previously was used for determining the OTC residues in oyster from the four tanks. A mixture of the three oysters picked from each tank on each sampling day was used for determining each OTC concentration.

RESULTS AND DISCUSSION

Reversed-phase HPLC has often been used for determining tetracycline antibiotics in fish plasma and tissues. In our experiment, a LiChrospher 100-RP 18E prepacked column was also used as a reversed-phase column in order to determine OTC in shellfish tissues. When using acetonitrile–0.02 *M* orthophosphoric acid solution, pH 2.3 (24:76, v/v) as the mobile phase, the chromatograms were free from intefering peaks. However, baseline drift and severe peak tailing were consistently noted. These effects are due to the presence of either residual free silanol groups or metal ion contamination in the base silica of the reversed phase [18]. Chelating

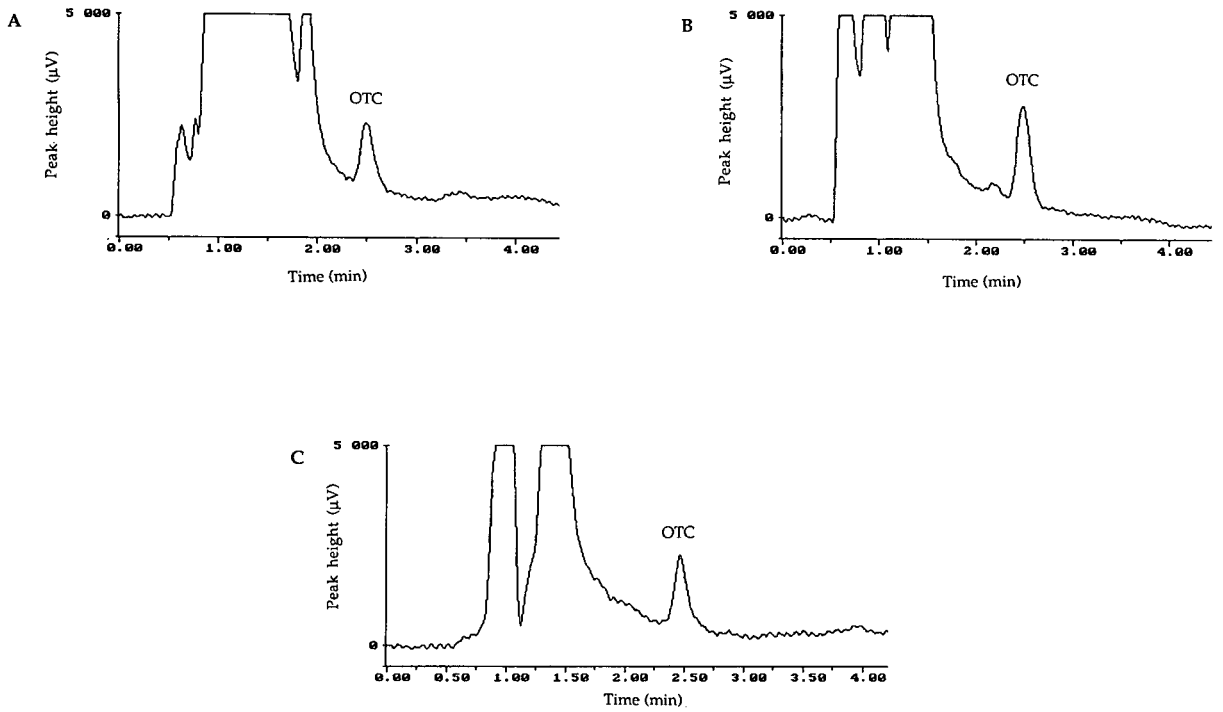

Fig. 1. HPLC of shellfish tissues. (A) *Crassostrea gigas* sample containing OTC at a concentration of 0.475 μg/g; (B) *Ruditapes philippinarum* sample containing OTC at a concentration of 0.660 μg/g; (C) *Scrobicularia plana* sample containing OTC at a concentration of 0.455 μg/g. Conditions: mobile phase, acetonitrile–0.02 *M* orthophosphoric acid solution, pH 2.3 (24:76, v/v); column, 125 × 4 mm I.D., C_{18} (5 μm); flow-rate, 1.2 ml/min; wavelength, 355 nm; recorder sensitivity, 0.01 a.u.f.s.; injection volume, 50 μl.

agents, such as EDTA, were added to the mobile phase in order to block the reactive sites of the silica. Their presence did not completely eliminate peak tailing. It was found that, by recycling after each day of operation acetonitrile–water (50:50, v/v) through the HPLC column for 2 h, the peak response was consistently high and neither tailing nor baseline drift were evident.

The tetracycline antibiotics have a tendency to combine with proteins and to form chelate com-

TABLE I

LINEARITY AND REGRESSION DATA FOR THE CALIBRAITON GRAPHS OBTAINED FROM *CRASSOSTREA GIGAS, RUDITAPES PHILIPPINARUM* AND *SCROBICULARIA PLANA* TISSUES SPIKED WITH OXYTETRACYCLINE FROM 0.100 TO 1.500 μg/g

$y = ax + b$; y = peak height (μV); x = oxytetracycline concentration (μg/g); a = slope; b = intercept.

Species	Slope	Intercept	Correlation coefficient	Variance	$F_{2,4}$ linearity
Crassostrea gigas					
Day A	2769.76	98.01	0.997	7676.04	0.241
Day B	2624.74	134.59	0.999	2208.74	0.829
Day C	2648.10	124.37	1.000	600.40	0.489
Ruditapes philippinarum	2799.73	109.66	1.000	774.30	0.349
Scrobicularia plana	2654.09	146.98	1.000	925.77	0.948

TABLE II

CALCULATION OF THE LIMIT OF DETERMINATION OF OTC IN OYSTER (*CRASSOSTREA GIGAS*) (0.100 μg/g)

Day	Peak height (μV)
A	383.00
B	366.00
C	375.00
D	400.00
E	302.00
Mean	365.20
Standard deviation (S.D.)	37.47
$T = 362.00/(37.47/\sqrt{5}) = 21.60$ ($t_4 = 2.77$ at $P = 0.10$)[a]	
3 × S.D. = 112.41 μV	

[a] Student's *t*-test with 4 degrees of freedom.

plexes with metal ions [16,18]. Therefore, it is difficult to extract these antibiotics from animal tissues. In our experiments, the efficiency of the extraction of OTC from shellfish tissues with 1 *M* hydrochloric acid, 50% trichloracetic acid and 0.1 *M* Na_2EDTA McIlvaine buffer (pH 4.0) was examined. The extracting solvent giving the highest recovery of OTC from shellfish tissues was 0.1 *M* Na_2EDTA McIlvaine buffer (pH 4.0) [16].

No endogenous material interfered with the separation and determination of the OTC. No changes in retention times were noted with continuous column use. OTC was eluted in 2.50 min. Typical chromatograms of shellfish tissues are shown in Fig. 1.

A statistical test of linearity was performed for each calibration graph separately, using a weighted analysis of variance (ANOVA) [19,20]. All the calibration graphs showed linearity in the range examined (0.100–1.500 μg/g) at the 0.05 level (Table I). A good correlation was obtained between concentrations and peak heights: all the correlation coefficients were between 0.997 and 1.000 (Table I).

The limits of detection and determination of OTC in shellfish tissues were 0.040 and 0.100 μg/g (precision ± 10%), respectively. This concentration of 0.100 μg/g was accepted as the limit of determination because a *t*-test with four degrees of freedom showed that this is significantly different from zero and the mean repsonse was greater than three standard deviations. An example of the calculation of the limit of determination in oysters is shown in Table II.

The relative standard deviations (R.S.D.s) of within-day precision for shellfish tissues spiked with OTC at 0.500 μg/g were 2.5%, 3.7% and 1.8% (n = 6) for *Crassostrea gigas, Ruditapes philippinarum* and *Scrobicularia plana*, respectively. The R.S.D. of between-day precision for oyster tissues spiked with OTC at 0.500 μg/g was 2.2% (n = 6 per day). In oysters, an ANOVA showed that there was no significant difference between the within- and between-day precisions at the 0.05 level.

OTC was recovered from shellfish tissues using the solid-phase extraction procedure described. The mean recoveries (n = 12) of OTC were 79.4% (R.S.D. = 2.6%) from *Crassostrea gigas*, 79.7% (R.S.D. = 3.5%) from *Ruditapes philippinarum* and 80.4% (R.S.D. = 2.1%) from *Scrobicularia plana* over the concentration range 0.100–1.500 μg/g. No significant difference was apparent between the three species of shellfish at the 0.05 level.

A study of the stability of OTC in oyster samples spiked at a concentration of 0.500 μg/g and stored at −20°C was performed. An average chart was constructed using the recovery results from the validation; its limits were determined using the principles based on control charts for individuals [19,20]. With this chart, there was a basis for monitoring the degradation of OTC in oysters stored at −20°C. The results are shown in Fig. 2. All the recoveries of

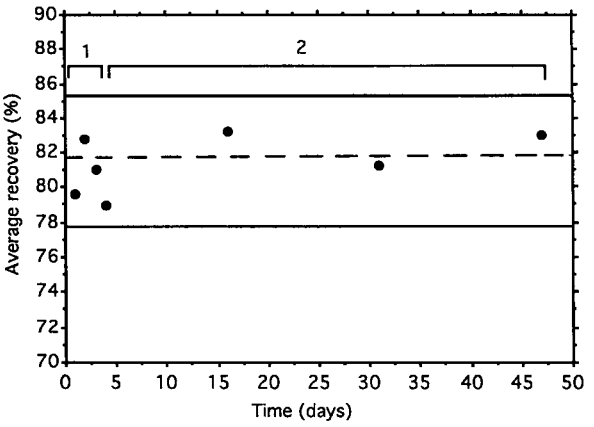

Fig. 2. Average chart of the recovery of OTC from oyster (*Crassostrea gigas*) spiked at 0.500 μg/g and stored at −20°C for 6 weeks. 1 = Validation; 2 = stability study.

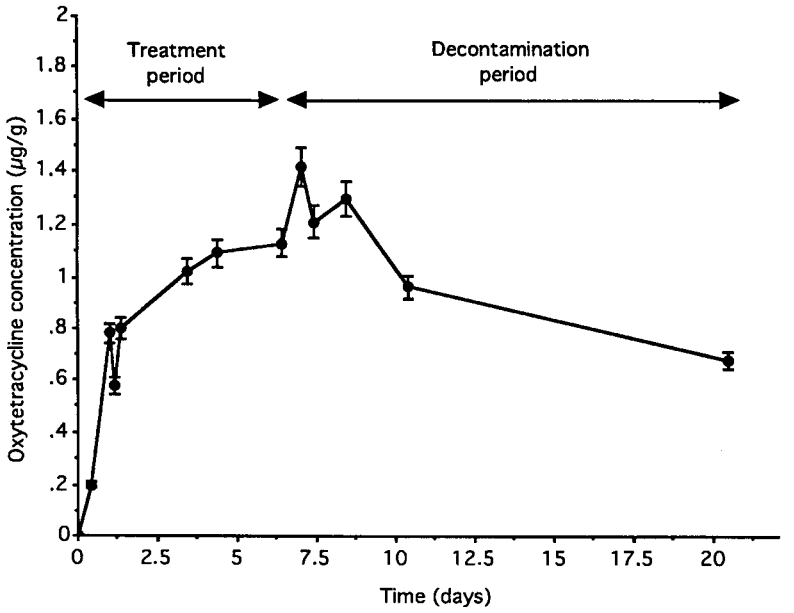

Fig. 3. Uptake and decline of OTC in oyster tissues (*Crassostrea gigas*) from tanks A, B and C after administration of medicated feed in the raceway. Each data point represents the average concentration of the samples assayed from oysters from the three tanks on the sampling day ± standard deviation. For further details, see text.

OTC from the oyster samples stored at −20°C fall within the average limits. Moreover, there was no significant decrease in the OTC recovery from oysters maintained at −20°C for 6 weeks.

The results of the experimental study are shown in Fig. 3. The OTC concentrations in oysters increased to reach a peak 7 days after the beginning of the antibiotic treatment and then decreased slowly. Fourteen days after the end of the antibiotic treatment, the OTC concentration in oysters was still high (average 0.680 μg/g). The OTC concentrations in oysters from tank T were always below the limit of detection of the method.

The main results of the procedure that allowed the efficacy of the analytical protocol to be ascertained showed the method to have good specificity, sensitivity, precision and accuracy. Because the clean-up procedure only involved filtration, centrifugation and solid-phase extraction, the method is simple, rapid and not too expensive. An analyst familiar with the method could easily process fifteen samples a day. In conclusion, the proposed HPLC method is an efficient and reliable means for pharmacokinetic and residue studies on OTC in marine shellfish.

ACKNOWLEDGEMENTS

We thank Ms. Michaëlle Larhantec for technical assistance. This research was supported by a grant from the Regional Council of Pays-de-la-Loire and the General Councils of Loire-Atlantique and Vendée and conducted with the experimental facilities of the Ifremer Aqualive Laboratory (Noirmoutier, France) in collaboration with the Department of Aquaculture of the National Veterinary School of Nantes (France).

REFERENCES

1 J. P. Cravedi, G. Choubert and G. Delous, *Aquaculture*, 60 (1987) 133–141.
2 H. Pouliquen, H. Le Bris and L. Pinault, *Aquaculture*, in press.
3 H. Pouliquen, H. Le Bris and L. Pinault, *Mar. Ecol. Prog. Ser.*, in press.
4 Y. Onji, M. Uno and K. Tanigawa, *J. Assoc. Off. Anal. Chem.*, 64 (1984) 1135–1137.
5 I. Nordlander, H. Johnsson and B. Osterdahl, *Food Addit. Contam.*, 4 (1987) 291–296.
6 H. Bjorklund, *J. Chromatogr.*, 432 (1988) 381–387.
7 J. Murray, A. MacGill and R. Hardy, *Food Addit. Contam.*, 5 (1988) 77–83.

8 A. Rogstad, V. Hormazabal and M. Yndestad, *J. Chromatogr.*, 11 (1988) 2337–2347.
9 K. Einvindvik and K. E. Rasmussen, *J. Liq. Chromatogr.*, 12 (1989) 3061–3071.
10 B. Iversen, A. Aanesrud and A. K. Kolstad, *J. Chromatogr.*, 493 (1989) 217–221.
11 R. Ueno, K. Uno, S. S. Kubota and Y. Horiguchi, *Nippon Suisan Gakkaishi*, 55 (1989) 1273–1276.
12 A. R. Long, L. S. Hsieh, M. S. Malbrough, C. R. Short and S. A. Barker, *J. Assoc. Off. Anal. Chem.*, 73 (1990) 864–867.
13 T. Agasoster and K. E. Rasmussen, *J. Chromatogr.*, 570 (1991) 99–107.
14 R. G. Aoyama, K. M. McErlane and H. Erber, *J. Chromatogr.*, 588 (1991) 181–186.
15 W. H. H. Farrington, J. Tarbin, J. Bygrave and G. Shearer, *Food Addit. Contam.*, 8 (1991) 55–64.
16 H. Oka, H. Matsumoto, K. Uno, K. Harada, S. Kadowaki and M. Suzuki, *J. Chromatogr.*, 325 (1985) 265–274.
17 D. J. Fletouris, J. E. Psomas and N. A. Botsoglou, *J. Agric. Food Chem.*, 38 (1990) 1913–1917.
18 J. H. Knox and J. Jurand, *J. Chromatogr.*, 186 (1979) 763–782.
19 J. R. Lang and S. Bolton, *J. Pharm. Biomed. Anal.*, 9 (1991) 357–361.
20 J. R. Lang and S. Bolton, *J. Pharm. Biomed. Anal.*, 9 (1991) 435–442.

Journal of Chromatography, 627 (1992) 294–299
Elsevier Science Publishers B.V., Amsterdam

CHROM. 24 701

Short Communication

Hydrogen bonding

XXIII. Application of the new solvation equation to log V_g values for solutes on carbonaceous adsorbents

Michael H. Abraham and David P. Walsh

Department of Chemistry, University College London, 20 Gordon Street, London WC1H 0AJ (UK)

(First received June 30th, 1992; revised manuscript received October 20th, 1992)

ABSTRACT

Truncated versions of our new solvation equation can be used to correlate and to predict log V_g values for solutes on adsorbents such as Carbotrap, Carbosieve and charcoal cloths. The two truncated equations are log $V_g = c + rR_2 + l \log L^{16}$ and log $V_g = c + l \log L^{16}$, where V_g is the retention volume for a series of solutes on a given carbon, R_2 is the solute excess molar refraction, L^{16} is the solute gas–liquid partition coefficient on hexadecane at 298 K and c, r and l are constants. The equation in R_2 and log L^{16} is shown to be very much better in the correlation of log V_g values than previous equations in log (vapour pressure) or in normal boiling point and can reproduce log V_g to within 0.4 to 0.9 log units when V_g covers a range of up to 15 orders of magnitude. The above two equations can be used to select the adsorbent giving rise to the largest V_g values for any particular adsorbate for which R_2 and log L^{16} are known.

INTRODUCTION

We have recently shown how phases such as common gas–liquid chromatographic stationary phases [1,2], ionic salts [1], candidate phases for piezo-electric chemical sensors [3] and polymers [4] can be characterised through our new solvation equation (eqn. 1). In this equation, *SP* represents a set of retention data for a series of solutes on a given phase: *SP* can be *L* (the gas–liquid partition coefficient), or V_g (the specific retention volume) or τ (the adjusted relative retention time). All these quantities as *SP* will yield the same constants in eqn. 1, except for the *c* constant.

$$\log SP = c + rR_2 + s\pi_2^H + a\alpha_2^H + b\beta_2^H + l \log L^{16} \quad (1)$$

The solute parameters used as descriptors or explanatory variables in eqn. 1 are R_2 (an excess molar refraction [5]), π_2^H (our new solute dipolarity/polarisability parameter [6]), α_2^H and β_2^H (the effective hydrogen-bond acidity and basicity [6]) and log L^{16}, where L^{16} is the solute gas–liquid partition coefficient on hexadecane at 298 K [7]). The various constants (c, r, s, a, b and l) in eqn. 1 that serve to characterise the particular phase are found by the method of multiple linear regression analysis.

In a recent paper, Pankow [8] attempted to corre-

Correspondence to: M. H. Abraham, Department of Chemistry, University College London, 20 Gordon Street, London WC1H 0AJ, UK.

0021-9673/92/$05.00

late log V_g values for 38 solutes on the graphitised material Carbotrap, with vapour pressure (as log P in Torr at 293 K; 1 Torr = 133.322 Pa) and with normal boiling point (T_b, in K). Although Pankow obtained some correlations of log V_g by rather arbitrarily selecting four different regression lines in each case, there was but little overall correlation of log V_g with either log P or with T_b Since adsorption of gaseous solutes by materials such as Carbotrap is of considerable practical importance, we have investigated the applicability of eqn. 1 to the Carbotrap results, in the hope that we might be able to generate better equations for the prediction of log V_g values.

TABLE I

SPECIFIC RETENTION VOLUME (V_g) FOR ORGANIC COMPOUNDS ON CARBOTRAP AT 293 K, AND COMPOUND PARAMETERS

Compound	log P (293 K) (Torr)	log V_g (293 K) (l/g)[a]	T_b (°C)	R_2	log L^{16}
Ethane	4.47	−1.76	−88	0.000	0.492
Propane	3.81	−1.26	−42	0.000	1.050
n-Butane	3.18	−0.39	0	0.000	1.615
n-Pentane	2.63	0.77	36	0.000	2.162
n-Hexane	2.08	1.90	69	0.000	2.668
n-Octane	1.04	4.21	126	0.000	3.677
n-Decane	0.43	6.68	174	0.000	4.686
n-Dodecane	−0.52	11.21	216	0.000	5.696
n-Tetradecane	−1.57	13.92	252	0.000	6.705
1,2-Dichloroethane	1.78	0.29	84	0.416	2.573
1,1,1-Trichloroethane	1.78	1.10	87	0.369	2.733
1,1,2-Trichloroethane	1.28	1.39	114	0.499	3.290
Butanone	1.88	0.58	80	0.166	2.287
Heptan-4-one	−0.08	3.39	149	0.113	3.705
Cyclohexanone	0.60	3.31	157	0.403	3.792
n-Butylamine	1.86	3.32	78	0.224	2.618
Acetic acid	1.07	−0.15	118	0.265	1.750
Propanoic acid	0.46	0.22	141	0.233	2.290
Pentanoic acid	−0.82	2.63	187	0.205	3.380
Ethanol	1.64	−0.31	78	0.246	1.485
Butan-1-ol	0.64	1.28	118	0.224	2.601
2-Methylpropan-2-ol	1.49	0.81	83	0.180	1.963
Benzene	1.88	1.07	80	0.610	2.786
Toluene	1.34	2.81	111	0.601	3.325
Ethylbenzene	0.85	4.31	136	0.613	3.778
p-Xylene	0.81	4.63	138	0.613	3.839
n-Propylbenzene	0.40	6.24	159	0.604	4.230
Isopropylbenzene	0.51	5.23	153	0.602	4.084
n-Butylbenzene	−0.05	6.77	183	0.600	4.730
n-Hexylbenzene	−1.16	9.85	226	0.591	5.720
n-Octylbenzene	−2.15	12.12	262	0.579	6.714
Biphenyl	−1.41	9.57	258	1.360	6.063
Chlorobenzene	0.94	3.20	132	0.718	3.640
1,4-Dichlorobenzene	−0.22	4.13	173	0.825	4.446
Acetophenone	−0.46	4.81	202	0.818	4.483
Benzylamine	−0.24	4.35	184	0.829	4.319
Phenol	−0.70	2.79	182	0.805	3.897
p-Cresol	−1.40	4.31	202	0.820	4.307

[a] Data from Pankow [8].

RESULTS AND DISCUSSION

The log V_g values at 293 K, together with vapour pressures as log P with P in Torr at 293 K, and normal boiling points were all taken from Pankow [8] except that we include two extra log P values for hexylbenzene and octylbenzene to complete the set. These are all given in Table I, together with values of R_2 and log L^{16} to which we shall refer below. Units of R_2 are $(cm^3/mol)/10$, whilst L^{16} is dimensionless [5,7]. Application of the full eqn. 1 to the 38 log V_g values showed that most of the explanatory variables were not statistically significant, as judged by Student's t-test, and we were left with eqn. 2, or the abbreviated eqn. 3.

$$\log V_g = -4.73 - 2.27R_2 + 2.65 \log L^{16} \quad (2)$$
$$n = 38,\ \rho = 0.9737,\ \text{S.D.} = 0.88,\ F = 318$$

$$\log V_g = -4.82 + 2.41 \log L^{16} \quad (3)$$
$$n = 38,\ \rho = 0.9570,\ \text{S.D.} = 1.10,\ F = 392$$

These may be compared with the corresponding equations in T_b/K or in log P, again for all 38 solutes,

$$\log V_g = -12.64 + 0.040\ T_b/K \quad (4)$$
$$n = 38,\ \rho = 0.8262,\ \text{S.D.} = 2.14,\ F = 77$$

$$\log V_g = 5.14 - 2.00 \log P \quad (5)$$
$$n = 38,\ \rho = 0.7869,\ \text{S.D.} = 2.34,\ F = 59$$

In eqns. 2–5, n is the number of solutes, ρ is the overall correlation coefficient, S.D. is the standard deviation in log V_g and F is the Fisher F-statistic. It is clear that log L^{16} is a very much better descriptor than either T_b/K or log P; this is shown rather well in Figs. 1–3.

Pankow [8] pointed out that some of the V_g values at 293 K had been obtained by extrapolation from higher temperatures, and this probably accounts for the rather large S.D. values in eqns. 2–5. Nevertheless, either eqn. 2 or eqn. 3 could be used to estimate log V_g values for any solute from R_2 and log L^{16}. The former can be calculated from the liquid refractive index at 293 K as described before [5], or can be estimated quite reliably, whilst the latter can be obtained experimentally relatively easily [7], and in any case is known for a large number of compounds, already [6,7].

Although the S.D. value in eqn. 2 is 0.88 log units, it should be remembered that the spread in the experimental log V_g values covers over 15 log units. The rather large S.D. value is unlikely to originate from errors in our R_2 and log L^{16} parameters, at least to any extent, because even for the n-alkanes (for which we have very reliable parameters) application of eqn. 3 leads to an S.D. of 0.94 log units.

As mentioned in the Introduction, Pankow used different regression lines, against both T_b/K and log P, when discussing the log V_g values. Lines were obtained by arbitrarily dividing up the data into

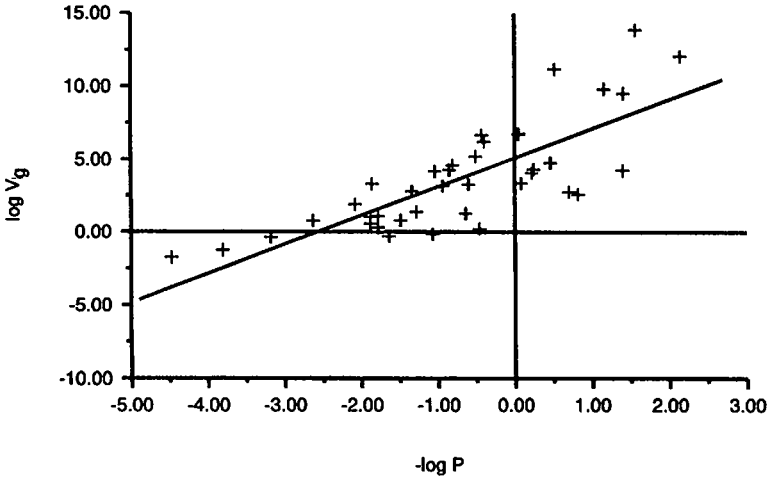

Fig. 1. Log V_g *vs.* $-\log P$ for compounds on Carbotrap at 293 K.

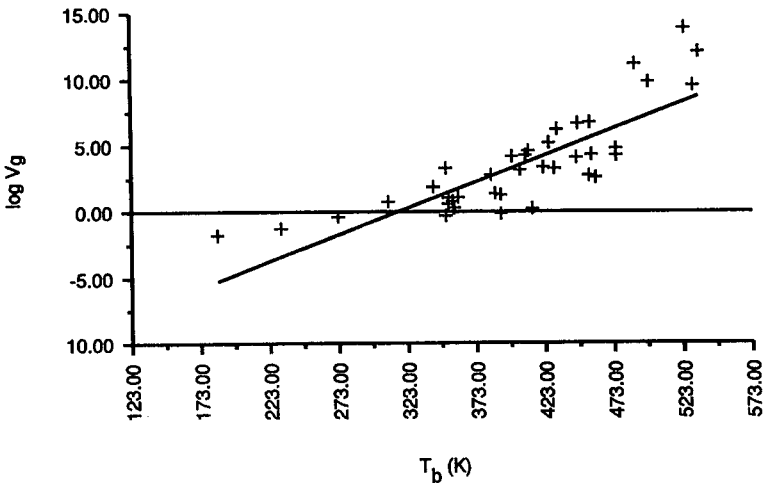

Fig. 2. Log V_g *vs.* T_b (K) for compounds on Carbotrap at 293 K.

sets for which log $P < 1.6$ and $T_b/K > 373$ and log $P > 1.6$ and $T_b/K < 373$, and by taking acids and phenols separately, alcohols being excluded. The only compound-specific linear equations listed by Pankow were for the five acids and phenols in Table I, for which he obtained eqns. 6 and 7,

$$\log V_g = -20.9 + 0.0522\ T_b/K \quad (6)$$
$$n = 5,\ \rho = 0.9732,\ \text{S.D.} = 0.50,\ F = 54$$

$$\log V_g = 1.45 - 1.83 \log P \quad (7)$$
$$n = 5,\ \rho = 0.9831,\ \text{S.D.} = 0.40,\ F = 87$$

However, judging by the *F*-statistic, there is not much to choose between eqns. 6 and 7 and eqns. 4 and 5, whilst eqns. 6 and 7 are definitely inferior to the "all-solute" eqns. 2 and 3. Our conclusion is that the "all-solute" equations are to be preferred, especially since these are likely to be the most useful in predictions of log V_g values.

We can also test our general equation using the data of Cao [9] who obtained V_g values for a variety of hydrocarbons on three microporous carbons, *viz.* Carbosieve B (Carb B), and two charcoal cloths, CC1 and CC2. The log V_g values recorded by Cao

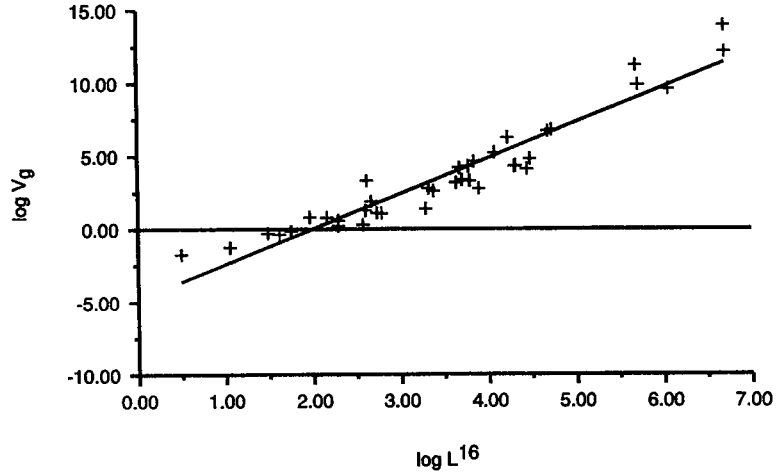

Fig. 3. Log V_g *vs.* log L^{16} for compounds on Carbotrap at 293 K.

TABLE II

SPECIFIC RETENTION VOLUMES (V_g, l/g) FOR ORGANIC COMPOUNDS ON VARIOUS ADSORBENTS AT 293 K, AND COMPOUND PARAMETERS

Compound	log V_g (293 K) (l/g)[a]			R_2	Log L^{16}
	Carbosieve B	CC1	CC2		
Methane	−0.92	−0.89	−1.30	0.000	−0.323
Ethane	0.76	0.04	0.08	0.000	0.492
Propane	2.52	1.70	1.72	0.000	1.050
n-Butane	4.28	3.71	3.26	0.000	1.615
n-Pentane	5.70	5.23	4.45	0.000	2.162
2-Methylbutane	5.36	4.57	4.62	0.000	2.013
n-Hexane	6.88	6.79	6.08	0.000	2.668
2-Methylpentane	6.45	6.52	5.41	0.000	2.503
2,2-Dimethylbutane		6.34	5.20	0.000	2.352
n-Heptane	9.60	8.59	7.62	0.000	3.173
n-Octane		10.26		0.000	3.677
n-Nonane		13.18		0.000	4.182
Cyclohexane	5.41	6.00	5.08	0.305	3.007
Ethene	−0.10	−0.17	−0.21	0.107	0.289
Propene	1.65	1.52	1.53	0.103	0.946
But-1-ene	3.08	3.04	3.00	0.100	1.491
Benzene	5.45	5.96	5.30	0.610	2.786

[a] Data obtained from Cao [9].

at 293 K, together with the corresponding solute R_2 and log L^{16} values, are in Table II. With no data exclusion at all, we can construct the following equations:

$$\log V_g(\text{Carb B}) = -0.41 - 4.46R_2 + 2.82 \log L^{16} \quad (8)$$

$n = 14$, $\rho = 0.9834$, S.D. = 0.58, $F = 162$

$$\log V_g(\text{Carb B}) = -0.40 + 2.59 \log L^{16} \quad (9)$$

$n = 14$, $\rho = 0.9523$, S.D. = 0.94, $F = 117$

$$\log V_g(\text{CC1}) = -1.05 - 3.35R_2 + 3.06 \log L^{16} \quad (10)$$

$n = 17$, $\rho = 0.9868$, S.D. = 0.66, $F = 260$

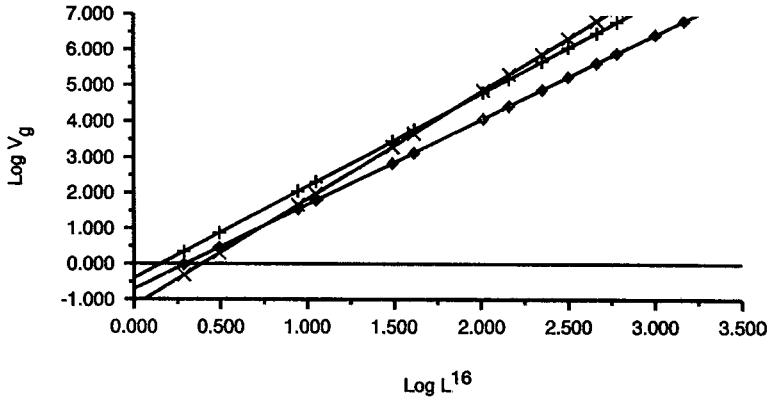

Fig. 4. Log V_g *vs.* log L^{16} for (+) Carbosieve B, (×) CC1 and (◆) CC2 at 293 K.

$$\log V_g\,(CC1) = -1.17 + 3.00 \log L^{16} \quad (11)$$
$$n = 17,\ \rho = 0.9769,\ \text{S.D.} = 0.84,\ F = 313$$

$$\log V_g\,(CC2) = -0.71 - 2.23R_2 + 2.48 \log L^{16} \quad (12)$$
$$n = 15,\ \rho = 0.9897,\ \text{S.D.} = 0.40,\ F = 287$$

$$\log V_g\,(CC2) = -0.70 + 2.38 \log L^{16} \quad (13)$$
$$n = 15,\ \rho = 0.9800,\ \text{S.D.} = 0.53,\ F = 315$$

Bearing in mind the spread of data, some 14 log units for CC1, eqns. 8–13, especially the double regressions in R_2 and log L^{16}, do provide a useful means of estimating further log V_g values.

In addition, eqns. 8–13 are especially valuable in the characterisation of adsorbents. Plots according to eqns. 9, 11 and 13 are shown in Fig. 4 and illustrate how difficult it is to define what is the "best" adsorbent, even for *n*-alkanes. For rather small compounds, *i.e.* those with low log L^{16} values, Carbosieve B is the best adsorbent, but for larger compounds CC1 is the best. For the *n*-alkanes illustrated in Fig. 4 the cross-over point is between ethane and propane for CC1 and CC2 and between hexane and heptane for CC1 and Carbosieve B.

We can also compare Carbotrap with Carbosieve B, through eqns. 3 and 9. It is now clear that V_g values on Carbosieve B are always greater than on Carbotrap by factors upwards of 10^4, no matter what the size of the solute is, *i.e.* no matter what is the solute log L^{16} value.

CONCLUSIONS

Our new solvation equation, eqn. 1, can usefully be applied to analyses of log V_g values for solutes on adsorbents such as Carbotrap, Carbosieve B and charcoal cloths. Not only can log V_g values be estimated to around 0.4 to 0.9 log units when V_g covers a range of up to 15 orders of magnitude, but equations in R_2 and log L^{16}, and particularly the simple equation in log L^{16} can be used to select the adsorbent that will yield the largest V_g value for a solute of a given log L^{16} value.

ACKNOWLEDGEMENTS

We thank Dr. M. J. Wilkinson for his interest in this work, and the Ministry of Defence for support under Agreement No. 2047/140.

REFERENCES

1 M. H. Abraham, G. S. Whiting, R. M. Doherty and W. J. Shuely, *J. Chromatogr.*, 587 (1991) 229.
2 M. H. Abraham, G. S. Whiting, J. Andonian-Haftvan and J. W. Steed, *J. Chromatogr.*, 588 (1991) 361.
3 M. H. Abraham, I. Hamerton, J. B. Rose and J. W. Grate, *J. Chem. Soc., Perkin Trans. 2*, (1991) 1417.
4 M. H. Abraham, G. S. Whiting, R. M. Doherty, W. J. Shuely and P. Sakellariou, *Polymer*, 33 (1992) 2162.
5 M. H. Abraham, G. S. Whiting, R. M. Doherty and W. J. Shuely, *J. Chem. Soc. Perkin Trans. 2*, (1990) 1451.
6 M. H. Abraham, G. S. Whiting, R. M. Doherty and W. J. Shuely, *J. Chromatogr.*, 587 (1991) 213.
7 M. H. Abraham, P. L. Grellier and R. A. McGill, *J. Chem. Soc., Perkin Trans. 2*, (1987) 797.
8 J. F. Pankow, *J. Chromatogr.*, 547 (1991) 488.
9 X.-L. Cao, *J. Chromatogr.*, 586 (1991) 161.

Journal of Chromatography, 627 (1992) 300–304
Elsevier Science Publishers B.V., Amsterdam

CHROM. 24 632

Short Communication

Gas chromatographic method for simultaneous determination of acephate and methamidophos in bark, cone and seed samples of conifers

K. M. S. Sundaram and R. Nott

Forestry Canada, Forest Pest Management Institute, 1219 Queen Street East, P.O. Box 490, Sault Ste. Marie, Ontario P6A 5M7 (Canada)

(First received May 20th, 1992; revised manuscript received September 21st, 1992)

ABSTRACT

A convenient, simple and rapid gas chromatographic method is described to quantify simultaneously acephate and methamidophos from the bark, cones and seeds of black spruce, *Picea mariana* (Mill.), by ethyl acetate solvent extraction, concentration and charcoal–cellulose microcolumn cleanup. Average recoveries from the matrices fortified with 0.10, 1.0 and 5.0 μg/g ranged from 88.8 to 99.0% with overall relative standard deviations of 1.1 to 6.5%. The limits of detection and quantification of the two compounds from the three matrices were 3 and 10 ng/g, respectively.

INTRODUCTION

Acephate (O,S-dimethyl acetylphosphoramidothioate) is the active component of Acecap-97 implants (Creative Sales, Inc., Fremont, NE, U.S.A.) that are used in controlling certain destructive pests of diptera and lepidopterous species in high-volume conifers and seed orchards [1]. Recent studies have shown that trunk implants in black spruce, *Picea mariana* (Mill.), trees with Acecap is effective in controlling cone and seed insects, protecting cone crops from insect attack and increasing the seed procurement to meet regeneration requirements of spruce trees [2].

In plants, acephate is converted into metabolic products, primarily methamidophos (O,S-dimethyl phosphoramidothioate), a potent anticholinesterase agent [3,4]. The insecticidal action of acephate has been related to its conversion to methamidophos or to a combined anticholinesterase effect of the parent and its primary metabolite [5].

As part of studying the efficacy of Acecap implants, we are required to measure the upward mobility of acephate, its accumulation, persistence and metabolic conversion to methamidophos in bark, cones and seeds of black spruce at varying times after implantation. At present, no suitable residue method is available in the literature to analyze acephate and methamidophos from these complex matrixes containing terpenes, hydroxy acids, lipoidal materials and esters. Gas chromatographic (GC) [6–13], GC–mass spectrometric [14] and high-performance liquid chromatographic (HPLC) [15,16] methods have been reported for the analysis of ace-

Correspondence to: K. M. S. Sundaram, Forestry Canada, Forest Pest Management Institute, 1219 Queen Street East, P.O. Box 490, Sault Ste. Marie, Ontario P6A 5M7, Canada.

0021-9673/92/$05.00

phate and methamidophos. Most of these methods are primarily for agricultural commodities, foods, biological samples and formulated products. The procedures by Sundaram and Hopewell [8], Szeto *et al.* [9] and Richmond *et al.* [12], although relevant to our present needs, are somewhat laborious and expensive due to high volume sample extraction followed by evaporation or centrifugation, solvent partition and macrocolumn cleanup consuming time and large quantities of solvents. This paper describes a convenient, simple and rapid method to quantify simultaneously acephate and methamidophos from the bark, cones and seeds of black spruce by using solvent extraction, concentration, microcolumn cleanup and GC analysis of the purified extracts.

EXPERIMENTAL

Chemical standards

Samples of acephate and methamidophos (purity > 98%) were provided, as a free gift, by Chevron (Richmond, CA, USA). Stock solutions of the standards were made accurately in ethyl acetate at 100 μg/ml and stored at 4°C in tightly sealed volumetric flasks. Dilute solutions at 0.10, 1.0 and 5.0 μg/ml in ethyl acetate were made from the standards in amber coloured volumetric flasks and stored similarly at 4°C. These dilute solutions were used for spiking samples and for the preparation of analytical standards to calibrate the GC.

Reagents

Ethyl acetate was pesticide grade supplied by Caledon Labs., Georgetown, Canada. Nuchar SN charcoal, supplied by Fisher Scientific (Cat. No. C-177), Unionville, Canada, was acid washed [17] and used. Whatman CF-11 cellulose powder, supplied by Fisher was used as received. Sodium sulphate (reagent grade) and Pyrex glass wool were obtained from Fisher, cleaned [18] and used.

Apparatus

The gas chromatograph was a Hewlett-Packard (HP) (Analytical Division, Palo Alto, CA, USA) Model 5890A fitted with a nitrogen–phosphorus detector, HP 7673A autosampler and HP 3292A computerized integrator for area and height measurements of the peaks. The column was DB-17, 15 m × 530 μm with 1.0 μm film thickness. The other instrument parameters were: *Gases*: carrier (helium), 15 ml/min; split flow, 80 ml/min; septum purge, 5 ml/min; detector (hydrogen), 3.5 ml/min; air, 120 ml/min; make-up (helium), 15 ml/min. *Temperatures*: capillary injection port 200°C, detector 250°C. *Oven programme*: initial 60°C at 0.5 min, ramp rate 70°C/min; final 190°C at 8 min. *Injection mode*: splitless, inlet purge on at 0.5 min. *Injection volume*: 2 μl for standards and samples. *Retention time*: Methamidophos 5.3 min, acephate 7.4 min.

All other equipment used in the study was similar to the ones described earlier [13].

Bark, cone and seed samples

Bark and cone samples from untreated control spruce trees were sampled from the forest areas in Newfoundland, Canada and stored in plastic bags at 4°C until analysis. All seeds were removed by breaking the cones into small pieces and vigorously shaking them in plastic vials using a mechanical shaker.

Sample preparation and extraction

The bark and cone samples were cut into small pieces using clean hand pruners. Before fortification, the seeds, cones and bark samples were pulverized individually using a Sorvall Omni-mixer. Aliquots (5 g) of each sample were taken in glass jars, fortified with 0.10, 1.0 and 5.0 μg/g acephate and methamidophos, allowed to equilibrate for 30 min and homogenized (Polytron PT-40, speed 6000 rpm) thrice, using 75 ml of ethyl acetate each time. Each homogenate was filtered under suction through a tube funnel plugged with a small wad of glass wool at the bottom topped with sodium sulphate (25 g) to remove the moisture. The crude extract was flash evaporated to a small volume, transferred quantitatively to a graduated centrifuge tube and the volume adjusted to 5.0 ml by a Meyer N-Evap so that 1 g of the matrix was equal to 1 ml of the extract.

Microcolumn cleanup

The packing of the microcolumn (Pasteur pipette 15 cm × 0.8 cm I.D.) consisted of a wad of glass wool at the bottom, 1 cm of anhydrous Na_2SO_4 followed by 3 cm of a mixture containing 20% Nuchar charcoal and 80% cellulose and topped with 1

TABLE I

RECOVERIES OF ACEPHATE AND METHAMIDOPHOS RESIDUES FROM FORTIFIED BLACK SPRUCE SAMPLES

Substrate	Fortification level (μg/g)	No. of replicates	Acephate			Methamidophos		
			Recovery (%)	S.D. (±)	R.S.D. (%)	Recovery (%)	S.D. (±)	R.S.D (%)
Bark	0.10	3	95.6	5.5	5.8	93.6	4.6	4.9
	1.00	3	89.7	3.2	3.6	94.9	5.0	5.3
	5.00	3	92.8	4.9	5.3	90.3	3.0	3.3
	0.10–5.00	9	92.7	4.8	5.2	92.9	4.2	4.5
Cones	0.10	3	91.9	4.3	4.7	91.4	3.8	4.2
	1.00	3	99.0	1.1	1.1	94.1	2.1	2.2
	5.00	3	92.0	5.4	5.9	95.8	2.8	2.9
	0.10–5.00	9	94.3	5.0	5.3	93.8	3.2	3.4
Seeds	0.10	3	91.4	5.9	6.5	88.8	3.6	4.1
	1.00	3	96.6	2.0	2.1	96.4	2.9	3.0
	5.00	3	95.2	4.3	4.5	90.6	3.8	4.2
	0.10–5.00	9	94.4	4.4	4.7	91.9	4.6	5.0

cm of Na_2SO_4. After thoroughly washing the column with 20 ml of ethyl acetate, 1.0 ml of the extract was transferred to the column, eluted with 10.0 ml of ethyl acetate and the eluate concentrated using the N-Evap to 1.0 ml for GC analysis. The sorbent size and elution volume necessary to desorb the analytes were determined by spiking the columns with standards, eluting and analyzing the eluates.

Gas chromatographic analysis

A volume of 2 μl of the final extract was injected into the gas chromatograph and concentrations of acephate and methamidophos were determined by comparing the area counts obtained by the integrator with those obtained by injections of analytical standard solutions. Control samples and reagent blanks did not give any interference peaks corresponding to the analytes.

RESULTS AND DISCUSSION

The solvent for sample extraction was chosen after several options (acetonitrile [11,14], acetone [6], methanol and dichloromethane [15]) were tested. Similarly, the use of different adsorbents (alumina, silica and Florisil) in microcolumn cleanups and eluting solvents and solvent mixtures [3,8,9] were tested. The resultant chromatograms after column cleanups were unsatisfactory due to high background noise, interference peaks and late eluting peaks. Best results were obtained using ethyl acetate as extracting solvent and Nuchar–cellulose microcolumns for cleanup with ethyl acetate as eluent. Occasionally, the excessive amount of lipids in the concentrated crude extracts of spruce seeds, caused the column capacity to exceed altering the elution pattern. In such cases, the crude extracts equivalent to < 1.0 g of the matrix was used or a liquid–liquid (hexane–acetonitrile) partition [8,11] step was introduced to remove the waxy impurities prior to column cleanup.

Table I shows the recovery data of fortified bark, cone and seed samples. The mean recoveries from the three matrixes at three fortification (0.10, 1.0 and 5.0 μg/g) levels were within the range of 88.8–99.0% with overall relative standard deviations (R.S.D.s) of 1.1–6.5%. Considering the complexity of the matrixes, the recovery of the two analytes were quantitative and the low standard deviations (S.D.s) and R.S.D.s indicate that the method is precise.

Using the final extraction volume of 5.0 ml, the limit of detection (LOD) [19] (3 × S.D. of blank

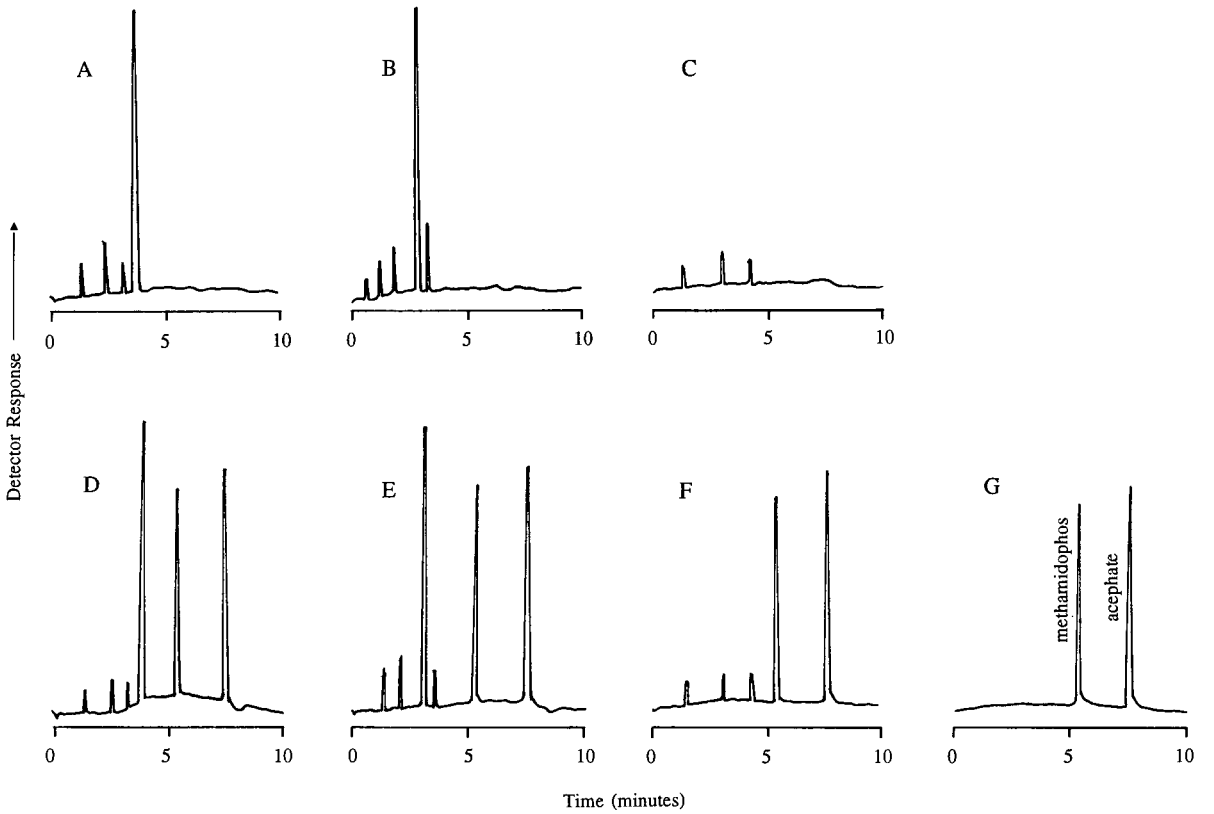

Fig. 1. Typical GC chromatograms of fortified black spruce samples: (A) bark control; (B) seeds control; (C) cones control; (D) bark fortified at 1.0 μg/g; (E) seeds fortified at 1.0 μg/g; (F) cones fortified at 1.0 μg/g; (G) acephate and methamidophos mixed standard solution (2 ng each) at GC conditions used in analysis of black spruce samples (integrator attenuation 2^9 at time 0 min; 2^7 at time 6.5 min).

response) for the three matrixes was 3 ng/g. The limit of quantification (LOQ) (10 × S.D. of blank response) was 10 ng/g. The sensitivity may be improved by using a smaller final extraction volume.

Typical chromatograms obtained for a mixed standard of acephate and methamidophos, unfortified blank samples of bark, cone and seed and the three of them each fortified separately with 1.0 ppm of the mixed standard are given in Fig. 1. The chromatographic peaks are sharp and well resolved with no chromatographic interferences in the vicinity of the retention times of methamidophos (5.3 min) and acephate (7.4 min). The total chromatographic analysis time amounted to 10 min and the total analysis time on average is less than 1.2 h/sample.

The method developed provides the basis for a sensitive, rapid and inexpensive method for the analysis of acephate and methamidophos in conifer bark, cone and seed samples. The high recoveries and low R.S.D.s indicate that the method is applicable to other forestry matrixes.

ACKNOWLEDGEMENTS

The authors thank Dr. Rick J. West of Forestry Canada, Newfoundland and Labrador Region for providing the conifer samples used in the study and J. Palermo for excellent technical assistance.

REFERENCES

1 R. C. Reardon, *For. Ecol. Manage.*, 7 (1984) 183.
2 R. J. West and K. M. S. Sundaram, *Can. Ent.*, 124 (1992) 577.

3 K. M. S. Sundaram, W. W. Hopewell and G. Lafrance, *Chem. Control Res. Inst., Environ. Canada, Ottawa, Inf. Rep. CC-X-139*, (1977).
4 D. L. Bull, *J. Agric. Food Chem.*, 27 (1979) 268.
5 M. A. Hussain, R. B. Mohamad and P. C. Oloffs, *J. Environ. Sci. Health, Part B*, B19 (1984) 355.
6 J. A. Lubkowitz, J. Baruel, A. P. de Revilla and M. M. Cermeli, *J. Agric. Food Chem.*, 27(1) (1973) 143.
7 J. B. Leary, *J. Ass. Offic. Anal. Chem.*, 57 (1974) 189.
8 K. M. S. Sundaram and W. W. Hopewell, *Chem. Control Res. Inst., Environ. Canada, Ottawa, Inf. Rep. CC-X-121*, (1976).
9 S. Y. Szeto, H. R. MacCarthy, P. C. Oloffs and R. F. Shepherd, *J. Environ. Sci. Health, Part B*, B13 (1978) 87.
10 S. Y. Szeto, H. R. MacCarthy, P. C. Oloffs and R. F. Shepherd, *J. Environ. Sci. Health, Part B*, B14 (1979) 635.
11 S. Y. Szeto, J. Yee, M. J. Brown and P. C. Oloffs, *J. Chromatogr.*, 240 (1982) 526.
12 C. E. Richmond, C. E. Crisp, J. E. Larson and G. R. Pieper, *Bull. Environ. Contam. Toxicol.*, 22 (1979) 512.
13 L. Bystricky, M. Michalek and L. Kuruc, *Chem. Zvesti*, 35(1) (1981) 85.
14 A. K. Singh, *J. Chromatogr.*, 301 (1984) 465.
15 M. A. Alawi, *Fresenius Z. Anal. Chem.*, 315 (1983) 358.
16 E. Rodriguez-Gonzalo, M. J. Sánchez-Martin and M. Sánchez-Camazano, *J. Chromatogr.*, 585 (1991) 324.
17 M. J. Brown, *J. Agric. Food Chem.*, 23(2) (1975) 334.
18 K. M. S. Sundaram, *J. Environ. Sci. Health, Part B*, B25 (1990) 357.
19 ACS Committe on Environmental Improvement and Subcommittee on Environmental Analytical Chemistry (1980), *Anal. Chem.*, 52 (1980) 2242.

Author Index

PUBLICATION SCHEDULE FOR 1993

Journal of Chromatography and *Journal of Chromatography, Biomedical Applications*

MONTH	O 1992	N 1992	D 1992	
Journal of Chromatography	623/1 623/2 624	625/1 625/2	626/1 626/2 627/1+2	The publication schedule for further issues will be published later.
Cumulative Indexes, Vols. 601–650				
Bibliography Section				
Biomedical Applications				

INFORMATION FOR AUTHORS

(Detailed *Instructions to Authors* were published in Vol. 609, pp. 439–445. A free reprint can be obtained by application to the publisher, Elsevier Science Publishers B.V., P.O. Box 330, 1000 AH Amsterdam, The Netherlands.)

Types of Contributions. The following types of papers are published in the *Journal of Chromatography* and the section on *Biomedical Applications:* Regular research papers (Full-length papers), Review articles, Short Communications and Discussions. Short Communications are usually descriptions of short investigations, or they can report minor technical improvements of previously published procedures; they reflect the same quality of research as Full-length papers, but should preferably not exceed five printed pages. Discussions (one or two pages) should explain, amplify, correct or otherwise comment substantively upon an article recently published in the journal. For Review articles, see inside front cover under Submission of Papers.

Submission. Every paper must be accompanied by a letter from the senior author, stating that he/she is submitting the paper for publication in the *Journal of Chromatography*.

Manuscripts. Manuscripts should be typed in **double spacing** on consecutively numbered pages of uniform size. The manuscript should be preceded by a sheet of manuscript paper carrying the title of the paper and the name and full postal address of the person to whom the proofs are to be sent. As a rule, papers should be divided into sections, headed by a caption (*e.g.*, Abstract, Introduction, Experimental, Results, Discussion, etc.). All illustrations, photographs, tables, etc., should be on separate sheets.

Abstract. All articles should have an abstract of 50–100 words which clearly and briefly indicates what is new, different and significant. No references should be given.

Introduction. Every paper must have a concise introduction mentioning what has been done before on the topic described, and stating clearly what is new in the paper now submitted.

Illustrations. The figures should be submitted in a form suitable for reproduction, drawn in Indian ink on drawing or tracing paper. Each illustration should have a legend, all the *legends* being typed (with double spacing) together on a *separate sheet*. If structures are given in the text, the original drawings should be supplied. Coloured illustrations are reproduced at the author's expense, the cost being determined by the number of pages and by the number of colours needed. The written permission of the author and publisher must be obtained for the use of any figure already published. Its source must be indicated in the legend.

References. References should be numbered in the order in which they are cited in the text, and listed in numerical sequence on a separate sheet at the end of the article. Please check a recent issue for the layout of the reference list. Abbreviations for the titles of journals should follow the system used by *Chemical Abstracts*. Articles not yet published should be given as "in press" (journal should be specified), "submitted for publication" (journal should be specified), "in preparation" or "personal communication".

Dispatch. Before sending the manuscript to the Editor please check that the envelope contains four copies of the paper complete with references, legends and figures. One of the sets of figures must be the originals suitable for direct reproduction. Please also ensure that permission to publish has been obtained from your institute.

Proofs. One set of proofs will be sent to the author to be carefully checked for printer's errors. Corrections must be restricted to instances in which the proof is at variance with the manuscript. "Extra corrections" will be inserted at the author's expense.

Reprints. Fifty reprints will be supplied free of charge. Additional reprints can be ordered by the authors. An order form containing price quotations will be sent to the authors together with the proofs of their article.

PREP-93

10th INTERNATIONAL SYMPOSIUM ON PREPARATIVE CHROMATOGRAPHY

CALL FOR PAPERS

Abstract Deadline: December 1, 1992
Send Abstracts to:
Prep-93 Symposium Manager
Barr Enterprises
P.O. Box 279
Walkersville, MD 21793 USA
Abstracts received after December 1, 1992 will be considered for poster presentation.

JUNE 14 – 16, 1993

ARLINGTON, VIRGINIA
USA

CHAIRMAN:
Professor Georges Guiochon
Oak Ridge National Laboratory
and University of Tennessee

SYMPOSIUM MANAGER:
Mrs. Janet Cunningham
Barr Enterprises
P.O. Box 279
Walkersville, MD 21793 USA
Phone: (301) 898-3772
Fax: (301) 898-5596

PREP-93